Julius-Maximilians-Universität
Würzburg

VERSATILE USE OF NEUTRAL AND CATIONIC DIORGANO BISMUTH COMPOUNDS:

LIGATION OF TRANSITION METALS, LEWIS ACIDITY, LOW VALENT SPECIES AND CATALYSIS

Dissertation zur Erlangung des
naturwissenschaftlichen Doktorgrades

Jacqueline Ramler
Würzburg 2021

VERSATILE USE OF NEUTRAL AND CATIONIC DIORGANO BISMUTH COMPOUNDS:

LIGATION OF TRANSITION METALS, LEWIS ACIDITY, LOW VALENT SPECIES AND CATALYSIS

Dissertation zur Erlangung
des naturwissenschaftlichen Doktorgrades
der
Julius-Maximilians-Universität Würzburg

vorgelegt von

Jacqueline Ramler
aus
Andernach

Würzburg 2021

Eingereicht bei der Fakultät für Chemie und Pharmazie der Julius-Maximilians-Universität Würzburg am: 07.05.2021

Gutachter der schriftlichen Arbeit:

1. Gutachter: Priv.-Doz. Dr. Crispin Lichtenberg

2. Gutachter: Prof. Dr. Udo Radius

Prüfer des öffentlichen Promotionskolloquiums:

1. Prüfer: Priv.-Doz. Dr. Crispin Lichtenberg

2. Prüfer: Prof. Dr. Udo Radius

3. Prüfer: Prof. Dr. Bernd Engels

Tag des öffentlichen Promotionskolloquiums: 25.06.2021

Doktorurkunde ausgehändigt am:

Die Experimente zur vorliegenden Arbeit wurden in der Zeit von Oktober 2017 bis April 2021 unter Anleitung von Priv.-Doz. Dr. Crispin Lichtenberg am Institut für Anorganische Chemie der Fakultät für Chemie und Pharmazie der Julius-Maximilians-Universität Würzburg durchgeführt.

Et hätt noch immer jot jejange.

Die vorliegende Arbeit wurde auszugweise veröffentlicht unter:

Bismuth Compounds in Radical Catalysis: Transition Metal Bismuthanes Facilitate Thermally Induced Cyclo-Isomerisations

Jacqueline Ramler, Ivo Krummenacher, Crispin Lichtenberg

Angew. Chem. Int. Ed. **2019**, *58*, 12924–12929. *Angew. Chem.* **2019**, *131*, 13056–13062.

https://onlinelibrary.wiley.com/doi/full/10.1002/anie.201904365

Carbon monoxide insertion at a heavy p-block element: unprecedented formation of cationic bismuth carbamoyl

Jacqueline Ramler, Jordi Poater, Florian Hirsch, Benedikt Ritschel, Ingo Fischer, F. Matthias Bickelhaupt, Crispin Lichtenberg

Chem. Sci. **2019**, *10*, 4169–4176.

https://pubs.rsc.org/en/Content/ArticleLanding/2019/SC/C9SC00278B#!divAbstract

Neutral and Cationic Bismuth Compounds: Structure, Heteroaromaticity, and Lewis Acidity of Bismepines

Jacqueline Ramler, Klaus Hofmann, Crispin Lichtenberg

Inorg. Chem. **2020**, *59*, 3367–3376.

https://pubs.acs.org/doi/abs/10.1021/acs.inorgchem.9b03189

Molecular Bismuth Cations: Assessment of Soft Lewis Acidity

Jacqueline Ramler, Crispin Lichtenberg

Chem. Eur. J. **2020**, *26*, 10250–10258.

https://chemistry-europe.onlinelibrary.wiley.com/doi/epdf/10.1002/chem.202001674

Well-defined, Molecular Bismuth Compounds: Catalysts in Photochemically-Induced Radical Dehydrocoupling Reactions

Jacqueline Ramler, Ivo Krummenacher, Crispin Lichtenberg

Chem. Eur. J. **2020**, *26*, 14551–14555.

https://chemistry-europe.onlinelibrary.wiley.com/doi/10.1002/chem.202002219

Methylbismuth: an organometallic bismuthinidene biradical

Deb Pratim Mukhopadhyay, Domenik Schleier, Sara Wirsing, Jacqueline Ramler, Dustin Kaiser, Engelbert Reusch, Patrick Hemberger, Tobias Preitschopf, Ivo Krummenacher, Bernd Engels, Ingo Fischer, Crispin Lichtenberg

Chem. Sci. **2020**, *11*, 7562–7568.

https://pubs.rsc.org/en/content/articlelanding/2020/sc/d0sc02410d

Combined experimental and theoretical studies towards mutual osmium-bismuth donor/acceptor bonding

Jacqueline Ramler, Krzysztof Radacki, Josh Abbenseth, Crispin Lichtenberg

Dalton Trans. **2020**, *49*, 9024–9034.

https://pubs.rsc.org/en/content/articlelanding/2020/dt/d0dt01663b#!divAbstract

Bismuth Atoms in Hydrocarbon Ligands: Bismepines as Rigid, Ditopic Arene Donors in Coordination Chemistry

Jacqueline Ramler, Leonie Wüst, Anna Rempel, Laura Wolz, Crispin Lichtenberg

Organometallics **2021**, *40*, 832–837.

https://pubs.acs.org/doi/10.1021/acs.organomet.1c00020

Bismuth Species in the Coordination Sphere of Transition Metals: Syntheses, Bonding, Coordination Chemistry, and Reactivity of Molecular Complexes

Jacqueline Ramler, Crispin Lichtenberg

Dalton Trans. **2021**, *50*, 7120–7138.

https://pubs.rsc.org/en/content/articlelanding/2021/dt/d1dt01300a#!divAbstract

The Dimethylbismuth Cation: Entry into Dative Bi–Bi Bonding and Unconventional Methyl Exchange

Jacqueline Ramler, Felipe Fantuzzi, Felix Geist, Anna Hanft, Holger Braunschweig, Bernd Engels, Crispin Lichtenberg

Submitted.

Darüber hinaus sind Teile dieser Arbeit in den folgenden Bachelorarbeiten beschrieben worden:

C. M. P. Mihm, **2018**, Synthese und Reaktivität von Übergangsmetallbismutanen mit Olefinfunktionalität.

K. Hofmann, **2019**, Heterozyklische Bismutorganyle mit Olefinfunktionalität: Synthese, Reaktivität und Substituenteneinfluss.

L. Brändler, **2019**, Dibenzobismepine: Reaktivität gegenüber Übergangsmetallkomplexen, Reduktionsmitteln und Lewis-basischen Bismut(III)organylen.

L. Lubczyk, **2020**, Übergangsmetallbismutane: Reaktivität der Übergangsmetall-Bismut-Bindung und Synthese chiraler Cobaltkomplexe.

DANKSAGUNG

Zuallererst möchte ich *Priv.-Doz. Dr. Crispin Lichtenberg* danken. Ich kann mir keinen besseren Chef für das Arbeiten an einer Doktorarbeit vorstellen, wissenschaftlich wie auch menschlich. Du hast mir wahnsinnig viel beigebracht und ich bin sehr froh, dich in deinen ersten Jahren als Arbeitsgruppenleiter begleiten zu dürfen. Ich wünsche dir nur das aller Beste für die Zukunft und eine große wissenschaftliche Karriere.

Anna, auch ich kann mir keine bessere Laborpartnerin als dich vorstellen. Mir hat das Arbeiten mit dir unglaublich viel Spaß gemacht, und man hat sich auch mal in stressigeren Zeiten immer wohlgefühlt und ich war und bin sehr froh, dich richtig kennengelernt zu haben. Ich möchte mich außerdem bei *Kai*, *Malte* und *Felix* bedanken, für das gute und stets lustige Zusammenarbeiten, und dass ihr den Laden doch sehr sicher erfolgreich übernommen habt oder übernehmen werdet. Dem ganzen Labor 02.004 (*Anna*, *Malte*, *Kai*, *Felix*, *Sonja*) danke ich für die angenehme Stimmung im Labor, die die Arbeit doch sehr erträglich gemacht hat.

Ich möchte mich ausdrücklich bei Herrn *Prof. Dr. Holger Braunschweig* für die Unterstützung unseres Arbeitskreises in vielen Belangen, finanzieller und menschlicher Natur, bedanken. Insbesondere *Kai* und *Carina* möchte ich in diesem Zug danken, dass ihr mir immer in chemischen/präparativen Fragen weitergeholfen habt. *Kai*, du bist einfach ein super Typ, und ohne dich würde wirklich was fehlen, du hälst den Laden am Laufen. Und danke dir *Birgit*, dass ich mit allen organisatorischen Problemen zu dir kommen durfte und du dich immer großartig um alles kümmerst.

Bei der ganzen NMR Abteilung, *Laura Wolz*, *Marie-Luise Schäfer* und *Dr. Rüdiger Bertermann* möchte ich mich für die, zum Glück, vielen Messungen bedanken. Es war mir immer ein Vergnügen gerade mit dir, Laura, zusammenzuarbeiten, da man nicht nur seine chemischen Ergebnisse geliefert bekommen hat, sondern auch die neuesten Erkenntnisse zwischenmenschlicher Beziehungen der AC. Zudem möchte ich *Liselotte Michels* und *Sabine Timmroth* für das Anfertigen der Elementaranalysen meinen Dank aussprechen. Auch das teilweise sehr spontane Messen von CHNS war nie ein Problem, was das Leben doch sehr vereinfacht hat. *Christoph Mahler* danke ich für die Aufnahme von hochaufgelösten Massenspektren. *Ivo*, ich danke dir für das Messen der EPR Spektren und für das angenehme Zusammenarbeiten bei der ein oder anderen Publikation. *Berthold Fertig* und *Bernhard Werner* gilt mein Dank für das schnelle Zur-Verfügung-Stellen von gewünschten und zu Bruch gegangenen Glasgeräten, sowie dafür, dass auch spezielle Wünsche erfüllt wurden. *Dr. Krzysztof Radacki* möchte ich für das Lösen aller technischen und kristallographischen Probleme danken. *Merle*, dir danke ich dafür, dass du meine Arbeit Korrektur gelesen hast. An dieser Stelle bedanke ich mich auch bei allen weiteren Korrekturlesern, insbesondere *Valerie*, die neben *Merle* den größten Teil stemmen musste.

Meinen Praktikanten *Christine*, *C. M. P. Mihm*, *Lisa*, *Klaus*, *Konstantin*, *Felix, Leonie, Lukas* und *Johannes* danke ich für die sehr ertragreiche und sehr angenehme Zusammenarbeit mit jedem von euch. Meinen Kooperationspartnern danke ich für die gute Zusammenarbeit und die schönen Ergebnisse, die wir zusammen produzieren konnten. Ich danke außerdem allen anderen Arbeitskreisen des Instituts. Der großen Hilfsbereitschaft, die in unserem Institut untereinander ausgelebt wird, bin ich sehr dankbar.

Darüber hinaus danke ich allen Mitarbeitern des *Arbeitskreises Braunschweig* für die Aufnahme des *AK Lichtenberg* in die Gruppe, die große Hilfsbereitschaft und die überragende Arbeitsatmosphäre, die das ein oder andere Feierabendbier einschließt. In bester Erinnerung bleiben mir der ChemCup Sieg, aber auch die vielen (langen) Abende im Kaffeeraum. Insbesondere der *Truppe* gilt mein Dank, dass ihr einen „alten Hasen" wie mich immer auf dem neusten Stand haltet, auch wenn ich viele Anspielungen schon nicht mehr verstehe.

Besonders dankbar bin ich um all die lieben Menschen, die ich während meiner Doktorarbeit kennenlernen durfte. Besonders die, wahrscheinlich in ganz Würzburg bekannten, „Chemiker" *Valerie, Domi, Uwe, Anna, Marco, Juli, Felix, Katha, Matze, Laura, Lena, Caro, Michel, Brüggi* und *Tatjana*, haben die Abend- und Wochenendgestaltung hervorragend gemeistert. Mit euch ist es immer lustig und ich freue mich auf viele weitere gemeinsame Tage! Außerdem danke ich allen anderen Mädels vom *Stammtisch*, für viele lustige (digitale) Abende und eine sehr sinnvolle Mittwochsbeschäftigung.

Ich danke außerdem meinen Kommilitonen die mich während meines Studiums begleitet haben, insbesondere *Regi*, *Sammy* und *Benn(i)y*, die auch während der Doktorarbeit immer an meiner Seite waren. Ein ganz besonderer Dank gilt *Regi* und *Dave*, ihr seid wunderbare Menschen und ich bin sehr dankbar, euch kennengelernt zu haben. Ihr habt mir immer geholfen, wenn ich Hilfe brauchte. Ihr seid wirklich die aller Besten.

Ich möchte mich auch bei meiner Familie bedanken. Die finanzielle Unterstützung ist ja zum Glück weniger geworden, aber der Hilfe in so zahlreichen Situationen bin ich sehr dankbar. Ein riesen Dank an *Marcel* und *Denise*, dass ihr euch immer um alles kümmert, was zuhause so ansteht! *Eikes Familie* danke ich für das liebevolle Aufnehmen in die Familie und das Unterstützen in allen Lebensbereichen.

Eike (Eik?Eikmän?Eiki?) dir gilt mein größter Dank, dafür, dass du mich immer unterstützt, aber auch mal sagst, wenn was zu viel ist oder falsch läuft. Du bist der beste Partner, den man sich vorstellen kann, und *Schorsch*, der sowieso auch der Beste ist, und ich sind sehr glücklich, dass du es mit uns aushältst. Ihr zwei Mausebeinchen.

List of Abbreviations

Å	Angström = 10^{-10} m
AN	acceptor number
appr.	approximately
Ar	aryl, specified in text
$BArF^{24}$	tetrakis[3,5-bis(trifluormethyl)phenyl]borate, $[\{3,5\text{-}(CF_3)_2C_6H_3\}_4B]^-$
benzil	1,2-diphenylethane-1,2-dione, $C_{14}H_{10}O_2$
bipy	bipyridine, $C_{10}H_8N_2$
br	broad
Bu	butyl, C_4H_9
°C	degree Celsius
$cAAC^{Me}$	*N*-(2,6-di-*iso*-propylphenyl)-3,3,5,5-tetramethylpyrrolidin-2-ylidene, $C_{20}H_{33}N$
CCDC	Cambridge Crystallographic Data Center
CN	coordination number
cod	1,5-cyclooctadiene, C_8H_{12}
coe	*cis*-cyclooctene, C_8H_{14}
Cp	cyclopentadienyl, C_5H_5
Cp*	pentamethylcyclopentadienyl, C_5Me_5
Ct	cation
CV	cyclic voltammetry
d	doublet (NMR); day(s)
DCM	methylene chloride, CH_2Cl_2
DHB	dihydridodicyanoborate, $[BH_2(CN)_2]^-$
Dip	2,6-di-*iso*-propylphenyl, 2,6-$iPr_2C_6H_3$
DFB	difluorobenzene, $C_6H_4F_2$
(TD-)DFT	(time-dependent) density functional theory
E	main group element; energy
e.g.	*exempli gratia*: for example
EMIm	1-ethyl-3-methylimidazolium, $C_6H_{11}N_2^+$
EPR	electron paramagnetic resonance
Eq.	equivalents
equat.	equatorial

Et	ethyl, C_2H_5
et al.	*et alii*: and others
ex.	excess
Fc	ferrocene, $Fe(C_5H_5)_2$
h	Planck constant = $6.62607015 \cdot 10^{-34}$ J · s
h	hour(s)
HOMO	highest occupied molecular orbital
HRMS	high resolution mass spectrometry
Hz	Hertz
i.e.	*id est*: that is
IPr	1,3-bis(2,6-di-*iso*-propylphenyl)imidazol-2-ylidene, $C_{27}H_{36}N_2$
IMes	1,3-dimesitylimidazol-2-ylidene, $C_{21}H_{24}N_2$
IR	infrared
J	coupling constant (NMR)
K	Kelvin
L	neutral ligand
LB	Lewis base
LIFDI	liquid injection field desorption ionization
LUMO	lowest unoccupied molecular orbital
m	multiplet (NMR)
MHB	monohydridotricyanoborate, $[BH(CN)_3]^-$
Me	methyl, CH_3
Mes	1,3,5-trimethylbenzene, C_9H_{12}
Monophos	(3,5-dioxa-4-phosphacyclohepta[2,1-a:3,4-a']dinaphthalen-4-yl)dimethylamine, $C_{22}H_{18}NO_2P$
min	minute(s)
mL	milliliter
mmol	millimol
nbe	norbornene, C_7H_{10}
NBO	natural bond orbital
NHC	*N*-heterocyclic carbene
NMR	nuclear magnetic resonance
o	*ortho*

o-chloranil	3,4,5,6-tetrachloro-1,2-benzoquinone, $C_6Cl_4O_2$
OTf	trifluoromethanesulfonate, $CF_3SO_3^-$
PBN	*N*-*t*Bu-α-phenylnitrone, $C_6H_5CH{=}N(O)C(CH_3)_3$
Ph	phenyl, C_6H_5
phen	phenanthroline, $C_{12}H_8N_2$
py	pyridine, C_5H_5N
R	organic group, specified in text
R^F	(per)fluorinated aryl/alkyl groups
r.t.	ambient temperature
s	singlet (NMR)
t	triplet (NMR)
TBPY	trigonal bipyramidal
TEMPO	(2,2,6,6-tetramethylpiperidin-1-yl)oxyl, $(CH_2)_3(CMe_2)_2NO^{\bullet}$
THF	tetrahydrofuran, C_4H_8O
TM	transition metal
[TM]	transition metal complex fragment
TMEDA	tetramethylethylenediamine, $(CH_3)_2NCH_2CH_2N(CH_3)_2$
TMS	trimethylsilyl, $Si(CH_3)_3$
UV-vis	ultraviolet-visible
VT	variable temperature
vide infra	see below
vide supra	see above
WCA	weakly coordinating anion
δ	chemical shift (NMR) in ppm
Φ_e	radiant power [W]
λ	wavelength [nm]
$\tilde{\nu}$	wavenumber [cm^{-1}]

Table of Contents

I Introduction

Natural bismuth was long considered the heaviest stable element. A low radioactivity of ^{209}Bi was only detected in 2003. However, the half-life of the α-emitter amounts to $1.9 \cdot 10^{19}$ a, which clearly exceeds the estimated age of the universe ($13.8 \cdot 10^{9}$ a), thus practical significance can be ruled out.[1] In fact, bismuth and its compounds are associated with lower toxicities than its neighboring elements such as tin, tellurium, antimony, lead, and polonium.[2]

Group 15 elements in their +III oxidation state bear a lone pair of electrons, which shows an increasing s-orbital character with an increasing atomic number of the pnictogen. This results in a predominant 6s-orbital character for the lone pair of bismuth as the heaviest group 15 element. These electrons are in principle available for bonding,[3–7] but they are energetically low-lying due to relativistic effects and the inert-pair effect.[8,9] Thus, the Lewis basic properties of Bi(III) species are strongly reduced, when compared to their lighter congeners.[10–13]

In contrast to analog compounds of the lighter pnictogens, bismuth(III) species show a pronounced Lewis acidic character, particularly when electronegative groups are the bonding partners for the central bismuth atom.[14–18] The Lewis acidic character of bismuth compounds is ascribed to the presence of vacant σ*-Bi–X molecular orbitals, which become energetically accessible for Lewis basic bonding partners, when the electronegativity of the substituent(s) X is high enough. Consequently, the Lewis acidity of bismuth compounds increases with increasing electronegativity of these substituents.[18] In addition, the enhancement of Lewis acidic properties by cationization of neutral parent compounds is a commonly used tool in main group chemistry. The synthesis of bismuth(III) cations is frequently achieved by salt elimination, halide abstraction,[19] or protonolysis.[20–22] The synthesis of bismuth(III) cations can also be achieved by addition of neutral donor ligands to a bismuth compound with at least one halide ligand,[23–25] as recently shown for Ph_2Bi^+, which was obtained by reaction of $[Ph_2BiCl]_2$ with a carbene to yield the corresponding carbene-stabilized cation.[26] The enhanced Lewis acidity of bismuth cations R_2Bi^+ (R = aryl, allyl, amide) originates from the vacant p-orbital at the bismuth center. However, such species in their isolable forms are either stabilized by intra- or intermolecular coordination of neutral donor ligands, or by interactions between (weakly) coordinating anions and the bismuth center.[19,23,27,28]

The higher Lewis acidity of bismuth cations in comparison with their neutral parent compounds results in drastically changed reactivity patterns, so that unusual reaction pathways become accessible, such as controlled radical polymerization[22] and C–H bond activation.[21] In addition to differences in reactivity, the coordination chemistry, e.g. the coordination number, coordination geometry and degree of aggregation, of cationic species are affected by the enhanced Lewis acidity of such species.[20,22,26,29,30] Several different methods have been introduced for the quantification

of Lewis acidity, e.g. the Child's method,[31] fluoride ion affinity[32] or the Gutmann-Beckett method.[33,34] The latter is frequently applied and is based on the addition of (defined amounts of) $OPEt_3$ as a Lewis base to a solution (of non or weakly coordinating solvents) and the subsequent ^{31}P NMR spectroscopic investigation of the resulting solution. The chemical shift of the ^{31}P NMR spectroscopic resonance is transformed into an acceptor number (AN) by applying equation (1).

$$AN = 2.21 \times \left(\delta(^{31}\text{P NMR})_{\text{Sample}}/_{ppm} - 41.0\right) \qquad \text{(eq. 1)}$$

Only a limited number of AN for bismuth(III) cations have been reported to date. VENUGOPAL and co-workers demonstrated a dependency of the acceptor number on the bite angle α of the ligand, with higher acceptor numbers resulting from smaller bite angles (Figure 1).[35] The acceptor number quantified by the Gutmann-Beckett method for the dicationic bismuth species **III** demonstrates an increase in Lewis acidity with increasing positive charge on the central atom, so that its Lewis acidity becomes similar to species such as $B(C_6F_5)_3$, commonly classified as a strong Lewis acid.[36,37]

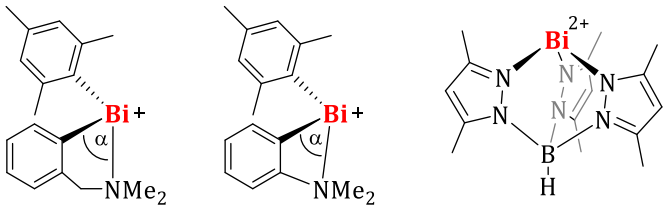

I AN = 55 **II** AN = 69 **III** AN = 75

Figure 1. Bite angle dependent acceptor numbers of monocationic bismuth species **I** and **II**, as well as dicationic **III**, showing an even higher acceptor number.

As mentioned above, the Lewis acidic character of bismuth species often results in the formation of intra- and intermolecular Lewis acid/base adducts, yielding a broad coordination chemistry of bismuth(III) species with a broad variety of different coordination numbers and geometries, however, with a coordination number of four being most common. Cationic bismuth species with a formal coordination number of two are discussed in the literature, but such cations are either stabilized by (weak) cation-anion interactions,[19,28] or intramolecular electrostatic and London dispersion interactions as described for the heavy carbene analog $(2,6\text{-}Mes_2C_6H_3)_2Bi^+$ (Mes = 1,3,5-trimethylphenyl).[38] The introduction of weakly coordinating anions into the chemistry of main group element cations led to the generation of compounds with significantly increased Lewis acidity due to reduced cation···anion interactions.[39] This is made feasible by distributing as little (negative) charge as possible over a large molecule, resulting in low polarizability and nucleophilicity, as was achieved, for example, for anions such as $B(R^F)_4^-$, SbF_6^- or $Al(OR^F)_4^-$ (R^F = (per)fluorinated aryl/alkyl groups).[40–42]

Due to their Lewis acidity, good accessibility and high functional group tolerance, simple bismuth salts of type BiX_3 (X = OTf, Cl) are frequently applied as Lewis acid catalysts in organic transformations such as hydroamination,[43] hydrosilylation, and Diels-Alder reactions,[44] respectively (OTf = trifluoromethanesulfonate).[45,46] In recent years, cationic bismuth organyls have also been used as Lewis acid catalysts in organic transformations. Based on the ligand in **IV** and closely related species **V**, a family of bismuth cations was prepared, which were applied as diastereoselective Lewis acid catalysts in organic transformations such as crossed-condensations of aldehydes and ketones, and Mannich reactions (Figure 2).[47–51]

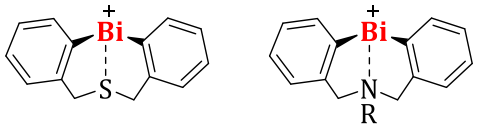

IV **V**

Figure 2. Bismuth cations which were successfully applied in Lewis acid catalysis.

More recently, bismuth dications such as **III**, a species with multiple electrophilic sites, have been applied as efficient and highly selective catalysts in the hydrosilylation of olefins, aldehydes and ketones.[36,52]

Interest in the catalytic activity of bismuth compounds is not limited to species with the pnictogen atom in the oxidation state of +III, but also expands to bismuth compounds with the central atom in low oxidation states. A limited number of bismuth(II) radicals, which are difficult to characterize or to isolate, have been studied spectroscopically to date. While **VIII** is a persistent radical species, **VI** and **VII** are the first examples of isolabe Bi(II)-radicals (Figure 3).[53–56] The bismuth radicals **VI–VIII** are highly reactive species, which have been generated by homolysis of a Bi–Bi single bond, or through reduction of a bismuth(III) halide, and are kinetically stabilized by the introduction of sterically demanding substituents.

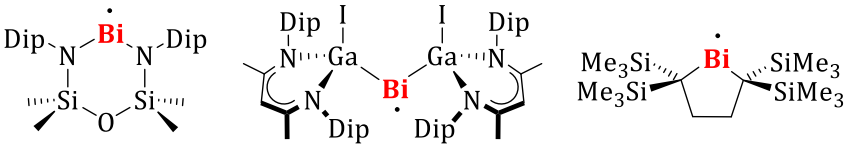

VI **VII** **VIII**

isolable

Figure 3. Isolable and persistent bismuth(II) radicals. Dip = 2,6-di-*iso*-propylphenyl.

The EPR spectroscopic characterization of such species can be hampered due to fast relaxation as a result of large spin-orbit coupling, and enhanced complexity of the resonances, which were (so far) only detectable at very low temperatures (21.5 K).[53–55,57]

COLES and co-workers were able to use the isolable bismuth radical **VI**[54] as catalyst in the oxidative coupling of phenylsilane with TEMPO (TEMPO = (2,2,6,6-tetramethylpiperidin-1-yl)oxyl), in which the Bi(II)-radical and a (putative) Bi(III)-hydride species are involved in the catalytic cycle.[58] Even under harsh reaction conditions only low catalytic activities were obtained, but these reactions exemplify the first applications of a well-defined bismuth radical in catalysis.

Lowering the oxidation state of the bismuth atom by one yields Bi(I)R species, so-called "bismuthinidenes" (R = monoanionic ligand). Bismuthinidenes are highly reactive, electron-deficient species, which are in principle able to adopt a singlet or triplet electronic ground state. Especially for the heavier elements of group 15 (As, Sb, Bi), the synthesis of species ER is challenging, since compounds of this type increasingly undergo degradation reactions, such as oligomerization, disproportionation, and bond activation. To date, only inorganic bismuthinidenes of type BiX (X = H, F, Cl, Br, I, $AlCl_4$) without further Lewis base stabilization are accessible by comproportionation reactions, or by reaction of Bi(0) with reactive species such as Cl_2 in the gas phase.[59–63] The synthesis, characterization and electronic situation of organometallic, Lewis-base-free, bismuthinidenes has not been reported, yet. Instead, the isolation of organometallic bismuthinidenes was accomplished as Lewis base adducts, which show unexceptional singlet electronic ground states (Figure 4a).[64–66] The first example of a cationic bismuthinidene species synthesized by a one-pot reduction of $BiCl_3$ in the presence of a carbene and LiOTf was demonstrated (Figure 4).[67]

a) *neutral bismuthinidenes* b) *cationic bismuthinidene*

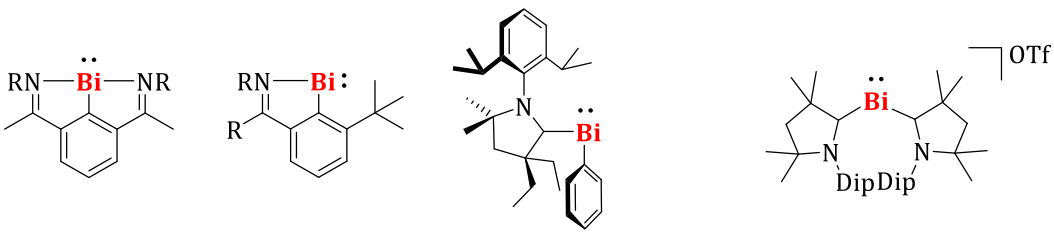

IX **X** **XI** **XII**

Figure 4. Known organometallic, Lewis-base-stabilized bismuthinidenes.

Recently, it has also been shown that the well-defined, Lewis-base-stabilized bismuthinidene **IX** (R = *t*Bu) catalyzes the transfer-hydrogenation of azoarenes and nitroarenes.[68] During the catalytic cycle, **IX** is oxidized by (formal) addition of H_2, which is released from ammonia borane, so that the formation of a dihydride bismuth(III) species may be suggested. Formal transfer of H_2 to a hydrogen acceptor such as an azoarene regenerates **IX** in a formal reductive elimination. Consequently, the redox couple Bi(I)/Bi(III) has been suggested to be operative in the catalytic cycle (Scheme 1).

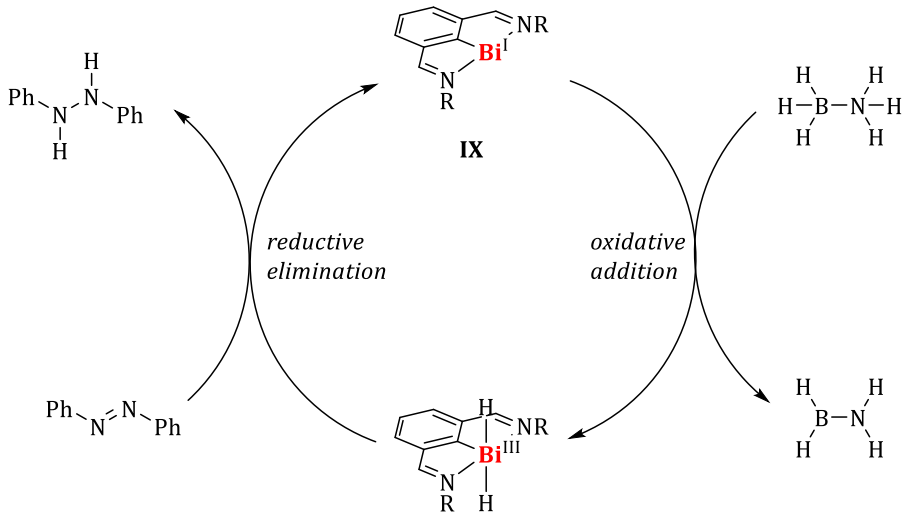

Scheme 1. Suggested catalytic cycle for the transfer-hydrogenation of 1,2-diphenyldiazene.

Although rarely described, bismuth species can also serve as redox catalysts with the redox couple Bi(III)/Bi(V), which is part of the catalytic cleavage of α-glycol,[69,70] as well as the fluorination of arylboronic esters, in which a bismuth(III) species is first fluorinated, followed by reductive elimination of a C–F bond.[71]

Research on molecular bismuth compounds has gained in popularity in recent years, probably also because it represents a non-toxic metal, and suitable starting materials are readily accessible and comparatively inexpensive. Nevertheless, essential questions on well-defined, molecular bismuth compounds regarding their Lewis acidity, catalytic activity in radical reactions and properties as ligands remain unresolved, to date.

II Bismuth Species in the Coordination Sphere of Transition Metals: Syntheses, Bonding, Coordination Chemistry, and Reactivity of Molecular Complexes

When this thesis was submitted to the university of Würzburg, the manuscript was just accepted for publication in *Dalton Transactions*.

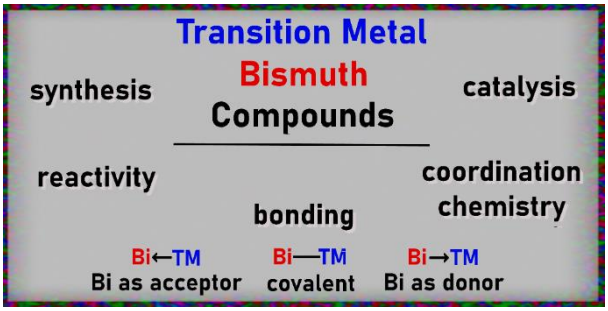

Bismuth Species in the Coordination Sphere of Transition Metals: Syntheses, Bonding, Coordination Chemistry, and Reactivity of Molecular Complexes

Received 00th January 20xx,
Accepted 00th January 20xx

DOI: 10.1039/x0xx00000x

Jacqueline Ramler[a] and Crispin Lichtenberg*[a]

This contribution is focused on bismuth species in the coordination sphere of transition metals. In molecular transition metal complexes, three types of Bi–M bonding are considered, namely dative Bi→M interactions (with Bi acting as a donor), dative Bi←M interactions (with Bi acting as an acceptor) and covalent Bi–M interactions (M = transition metal). Synthetic routes to all three classes of compounds are outlined, the Bi–M bonding situation is discussed, trends in the geometric parameters and in the coordination chemistry of the compounds are addressed, and common spectroscopic properties are summarized. As an important part of this contribution, the reactivity of bismuth species in the coordination sphere of transition metal complexes in stoichiometric and catalytic reactions is highlighted.

1. Introduction

Heterometallic species contain two or more different types of metal atoms. The careful design and detailed analysis of such compounds can grant access to properties, reactivities, and applications that are difficult or even impossible to realize with homometallic species.[1-9] In bismuth chemistry, heterometallic species have been utilized in industrial processes (such as the oxidation/ammoxidation of propene to acrolein/acrylonitrile)[10, 11] and hold promise as less toxic[12] substitutes for lead compounds in double perovskites for optoelectronic applications.[13] Further examples include the fabrication of materials with high oxide ion conductivities,[14] the investigation of diode-like effects in single-ferroelectric-domain $BiFeO_3$ crystals,[15] the development of narrow-bandgap photocatalysts for oxygen evolution,[16] and the identification of high-temperature superconductors.[17, 18]

When bismuth species are considered as ligands in the coordination sphere of molecular transition metal complexes, the understanding of their properties and reactivity as well as their application in catalysis and materials science are clearly underdeveloped compared to those of the lighter group 15 homologs, especially those based on phosphorus.[19-26] Nonetheless, researchers have devoted detailed studies to molecular transition metal complexes with bismuth ligands in the last decades, which were concerned with their synthesis and isolation, the rationalization of their bonding situations, and the exploitation of their reactivity patterns. Within this class of compounds, three different types of compounds may be distinguished: i) species with dative Bi(III)→M bonding, ii) species with dative M→Bi(III) bonding, and iii) species with covalent Bi–M bonding (M = transition metal; Figure 1). Unique properties of bismuth species in the coordination sphere of transition metals have been revealed and have allowed for intriguing stoichiometric and catalytic reactions. Previous valuable review articles on compounds with Bi–M bonds have been focused either on one single bonding mode,[27-29] on specifically one family of compounds,[30] have taken the ligand design at the transition metal as their guideline,[31] or have been devoted to cluster compounds.[32] With this contribution, we aim to conceptualize the possible bonding modes, emphasizing ligand design to selectively target one bonding mode, systematically review the synthetic approaches to such compounds, summarize their reactivity patterns in stoichiometric reactions, and highlight catalytic applications.

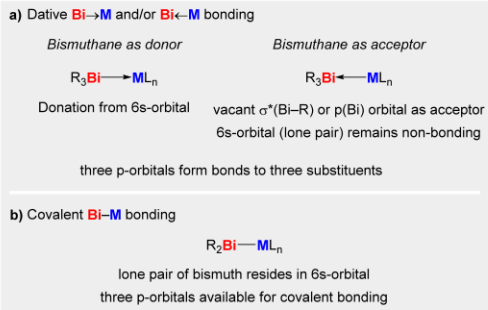

Figure 1. Types of interactions between a transition metal and bismuth covered in this contribution. M = transition metal.

2. Bismuthanes (BiR_3) as L-type Ligands

Bismuth(III) compounds bear a lone pair of electrons in a molecular orbital (MO) that usually shows dominant contributions by the 6s(Bi) atomic orbital (AO). This lone pair is in principle available for bonding interactions with Lewis

[a] Department of Inorganic Chemistry
Julius-Maximilians-Universität Würzburg
Am Hubland, 97074 Würzburg, Germany.
Email: crispin.lichtenberg@uni-wuerzburg.de

acids.[33-36] Due to the inert pair effect and relativistic effects,[37, 38] however, this MO is low in energy and the nature of the substituents R in BiR_3 type compounds will crucially affect their ability to act as an L-type ligand.[36] An electron-donating character of the substituents R is usually necessary to sufficiently increase the electron density at the bismuth atom and facilitate Bi→M bonding (M = transition metal). This is commonly achieved by installing carbon-based substituents (especially alkyl groups) at the bismuth atom. Despite these insights into the design principles of bismuth-based donor ligands, only a limited number of transition metal complexes with bismuthanes BiR_3 acting as a two electron donor ligands has been described in the literature.

2.1 Synthesis of complexes with L-type bismuth ligands

A range of strategies for the synthesis of transition metal complexes featuring bismuthanes as donor ligands has been reported (Scheme 1). When targeting transition metal carbonyl complexes, reactive precursors can be generated by photochemically-initiated exchange of a carbonyl ligand for a substitutionally labile ligand L (such as THF). Subsequent addition of the bismuthane leads to elimination of L and to formation of the target compound (Scheme 1a). For instance, the complexes $[M(CO)_5(BiR_3)]$ (M = Cr, Mo, W) and $[CpV(CO)_3(BiR_3)]$ ($Cp = \eta^5\text{-}C_5H_5$) have been synthesized with this strategy (R = alkyl, aryl).[39-42]

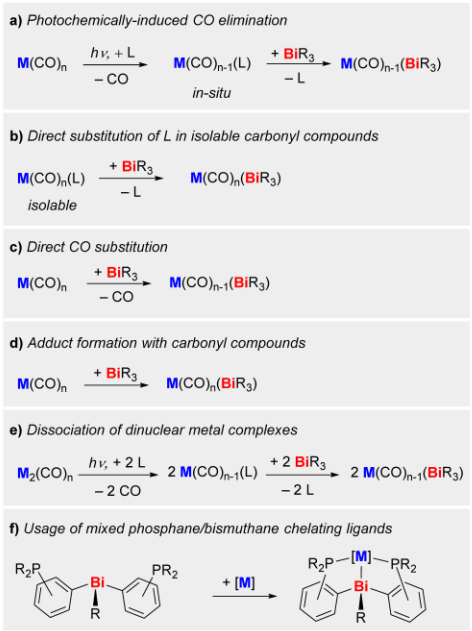

Scheme 1. Synthetic routes to transition metal complexes containing bismuthanes (BiR_3) as a two electron donor ligand.

In addition to neutral complexes, a few ionic carbonyl complexes with BiR_3 ligands have also been described. For example, $[Et_4N][V(CO)_5(BiEt_3)]$ and $[CpFe(CO)_2(BiPh_3)][BF_4]$ have been obtained by photochemically-induced elimination of a carbonyl ligand in $[Et_4N][V(CO)_6]$ and $[CpFe(CO)_3][BF_4]$, respectively, and subsequent addition of BiR_3.[41, 42] In addition to *in-situ* generated compounds of type $[M(CO)_nL]$, isolable species of this kind have also been utilized as starting materials for the substitution of L by BiR_3. The few literature-known examples include carbonyl complexes with carbene,[43] nitrile,[44, 45] or alkyne ligands[46] (carbene = $C(OCH_3)CH_3$); Scheme 1b). In the case of $[Ni(CO)_4]$, an irradiation is not even necessary, since $[Ni(CO)_4]$ directly reacted with $BitBu_3$ to give $[Ni(CO)_3(BitBu_3)]$ (Scheme 1c).[41] Instead of the substitution of CO ligands, coordinatively and electronically unsaturated carbonyl complexes have also been reported to form adducts with BiR_3 (Scheme 1d). Consequently, these reactions proceed with an increase of the coordination number at the transition metal center. This behavior has been reported for $[Nb(CO)_5]$, which reacted with $BiPh_3$ to give the adduct $[Nb(CO)_5(BiPh_3)]$. It should be noted, however, that this compound was only characterized by elemental analysis.[47]

Further synthetic routes to transition metal complexes with Lewis basic bismuth ligands make use of dinuclear metal precursors (Scheme 1e): the iron carbonyl complexes $[Fe(CO)_4(BiR_3)]$ (R = Et, *n*Pr, *n*Bu) were synthesized from dinuclear $[Fe_2(CO)_9]$ by irradiation in THF and subsequent addition of BiR_3. In the case of R = Ph and Me, the target compounds of type $[Fe(CO)_4(BiR_3)]$ could not be obtained, which was attributed to the lack of these carbon-based substituents R to sufficiently enhance the electron density at the bismuth center. In those cases $[Fe_3(CO)_{12}]$ and $[Fe(CO)_5]$ were obtained instead of $[Fe(CO)_4(BiR_3)]$ (R = Me, Ph), indicating, however, a BiR_3-induced dissociation of the starting material $[Fe_2(CO)_9]$.[48] Irradiation of the dinuclear $[Mo(CO)_3Cp]_2$ with a mercury vapor lamp in the presence of $BiPh_3$ and ferrocenium tetrafluoroborate yielded the ionic complex $[Mo(CO)_2(BiPh_3)_2Cp][BF_4]$.[49] The postulated mechanism involves substitution of one CO ligand by $BiPh_3$, followed by photochemically-induced oxidative cleavage of the Mo–Mo bond, and subsequent reaction with a second equivalent of $BiPh_3$. Only recently, the range of synthetic routes to species featuring Bi→M interactions has been extended by the use of bismuth complexes containing phosphane moieties, which allow pre-coordination of late transition metals (Scheme 1f).[50, 51] This approach has granted access to the first examples of complexes bearing a Bi→M functionality for group 10 and 11 transition metals. For example, reaction of transition metal chlorides with the mixed phosphane/bismuthane ligand **1** yielded group 11 metal complexes **2** and **3** (Scheme 2).[51]

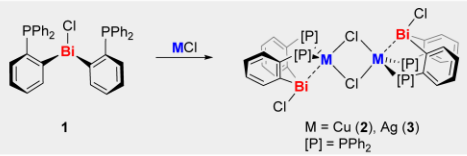

Scheme 2. Reaction of **1** with copper and silver chloride.

However, the coordination of a metal atom in a binding pocket of a bismuthane ligand does not necessarily generate Bi–M interactions. For instance, bismuthanes with pyridyl substituents coordinate copper exclusively via N→Cu interactions, and no Bi→Cu coordination was observed.[52] This demonstrates that Bi→M interactions tend to be weak and that other donor functional groups may easily preferred as L type ligands towards transition metals, if present. In turn, the weak donor character of bismuth atoms may be exploited by using bismuth atoms as coordinatively innocent, structure-directing features in ligand design.[52, 53]

2.2 Stability

Transition metal complexes featuring L-type bismuthane donor ligands tend to be air-sensitive. Exceptions have been reported for compounds of the general formula $[M(CO)_5(BiPh_3)]$, with an increasing stability of the complexes in the order Mo<Cr<W.[39] These compounds have been described to be less stable towards heat or in solution than their P, As, and Sb analogues.[39, 54-56] The choice of the bismuth ligand has a strong impact on the stability of species $[M(CO)_5(BiR_3)]$ (M = Cr, Mo, W): for R = *t*Bu, a limited air-stability of the solid material was noted, while compounds with R = $GeMe_3$, $SnMe_3$ rapidly decompose at ambient temperature. All these compounds were reported to rapidly deposit an ill-defined black residue when solvated in hydrocarbons.[40]

The coordination of bismuthanes to transition metals can significantly increase their stability: the complexes $[Fe(CO)_4(BiR_3)]$ (R = Et, *n*Pr, *n*Bu) are brown liquids, which are stable in solution for several weeks. They show a higher stability towards air than the non-coordinating bismuthanes BiR_3 (R = Et, *n*Pr, *n*Bu) which are spontaneously inflammable upon contact with air.[48]

2.3 Solid-state structure

Single-crystal X-ray diffraction analysis of species of the type $[M(CO)_5(ER_3)]$ (M = Cr, Mo, W, E = P-Bi, R = Ph, Me, Table 1) revealed a correlation between a growing s-orbital character of the lone pair at the group 15 element and increasing M–E–C angles as well as decreasing C–E–C angles.[57-63] In addition, Cr–E and E–C bond lengths in $[Cr(CO)_5EPh_3]$ have been analyzed by subtracting the tetrahedral covalent radii for E. The result revealed little variation (and no clear trend) in the case of E–C and decreasing differences in the case of Cr–E (P>As>Sb>Bi), which was suggested to point towards increasing s-orbital participation in Cr–E bonding along the series P<As<Sb<Bi.[63] The bonding parameters summarized in Table 1 also show that coordination of BiR_3 to a transition metal increases the C–Bi–C angles, and decreases the Bi–C bond lengths compared to non-coordinating bismuthanes (average Bi–C bond length and C–Bi–C angle in $BiMe_3$: 2.26 Å and 92°,[64] in $BiPh_3$: 2.25 Å and 94°),[65] which was attributed to a hybridization with significant p-orbital participation of the bond-forming orbitals of bismuth (Figure 2).[57, 60, 66]

Table 1. Comparison of bond lengths and angles of some $[M(CO)_5(ER_3)]$ species. The listed E–C bond lengths [Å], as well as the M–E–C and C–E–C angles [°] are averaged values.

	E = P		E = As	E = Sb		E = Bi	
M = Cr	Ph	Me	Ph	Ph	Me	Ph	Me
M–E	2.422	2.3664	2.497	2.617	2.610	2.705	2.701
E–C	1.828	1.813	1.947	2.133	2.130	2.216	2.218
M–E–C	115.7	115.8	116.6	117.9	117.2	118.9	118.1
C–E–C	102.6	102.4	101.4	99.2	100.8	98.7	99.5
M = Mo							
M–E	2.560	----	2.612	2.756	----	2.833	----
E–C	1.828	----	1.947	2.132	----	2.22	----
M–E–C	115.6	----	116.5	118.2	----	119.3	----
C–E–C	102.6	----	101.7	99.5	----	98.0	----
M = W							
M–E	2.545	2.516	2.617	2.753	2.759	2.829	2.837
E–C	1.830	1.85	1.950	2.137	2.134	2.225	2.237
M–E–C	115.4	115.6	116.7	118.0	117.1	118.6	118.6
C–E–C	102.9	102.7	101.3	99.8	100.9	98.9	99.0

Ref. for $[M(CO)_5(EMe_3)]$ (M = Cr, W, E = Sb, Bi): 57. Ref. for $[M(CO)_5(BiPh_3)]$ (M = W, Mo): 60. Ref for $[Cr(CO)_5(EPh_3)]$ E = P-Bi: 63. Crystal data for $[W(CO)_5(EPh_3)]$ (E = P-Sb) and $[Mo(CO)_5(EPh_3)]$ (E = As, Sb) from ref. 58. Crystal data for $[Mo(CO)_5(PPh_3)]$ from ref. 59. Crystal data for $[Cr(CO)_5(PMe_3)]$ from ref. 61. Crystal data for $[W(CO)_5(PMe_3)]$ from ref. 62.

The substitution pattern at bismuth in BiR_3 type compounds can have an impact on Bi–M bond lengths, when the BiR_3 group acts as an L-type ligand. This effect is not apparent when comparing the bismuth compounds listed in Table 1 ($BiMe_3$ vs. $BiPh_3$). However, the copper and silver complexes **5** and **6** (synthesized from the bismuthane/phosphane ligand **4**) show shorter Bi–M bond lengths in comparison to **2** and **3** (*cf.* Scheme 2), which was attributed to a greater donor ability of the bismuth ligand due to formal exchange of the chlorine atom for a carbon based substituent (Figure 3a).[50]

Most of the literature-known transition metal compounds with L-type bismuthane ligands are monomeric (i.e. they contain one transition metal), if they do not fall in the category of cluster chemistry. However, the incorporation of electronegative substituents such as a chlorido ligands can result in the formation of dimeric species (*cf.* Scheme 2) or coordination polymers in the solid state. Compounds **7** and **8**, for instance, yield one-dimensional coordination polymers in the solid state through intermolecular Cl···M interactions (Figure 3b).[51]

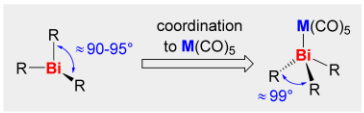

Figure 2. Comparison of bond angles in BiR_3 being either non-coordinating (left) or being bound to a transition metal acting as an L-type ligand (right).

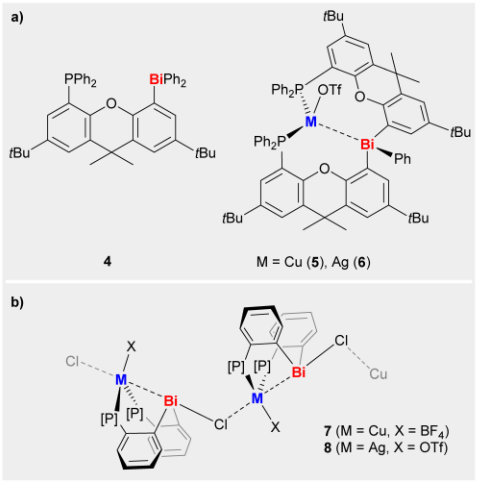

Figure 3. a) Copper and silver complexes **5** and **6** based on the phosphane/bismuthane ligand **4**. b) Coordination polymers of copper and silver complexes **7** and **8**. [P] = PPh_2.

2.4 Spectroscopic properties

For $[W(CO)_5(EPh_3)]$ (E = N-Bi), ^{13}C NMR spectroscopic analyses showed that, as a trend, the $^1J_{WC}$ coupling constants increase along the series N<P<As<Sb<Bi ($^1J_{WC}$ = 140-183 Hz), suggesting only weak σ-donor properties of $BiPh_3$.[60] Only minor differences in IR spectroscopic CO stretching modes between $[M(CO)_5(ER)_3]$ (M = Cr, Mo, W, E = P-Bi) were determined (Table 2). This was explained by the fact that both, the σ-donor strength and the π-acceptor properties, are lowered for ER_3 (E = As, Sb, Bi) in comparison to the phosphane derivatives.[60]

Table 2. IR frequencies $\tilde{\nu}_{CO}$ [cm^{-1}] for $[M(CO)_5L]$ complexes determined in hydrocarbon solutions.

EPh_3	$Cr(CO)_5L$	$Mo(CO)_5$	$W(CO)_5L$
PPh_3	2066, 1943[67]	2075, 1950, 1945[68]	2075, 1944[69]
$AsPh_3$	2068, 1946[69]	2076, 1952, 1945[68]	2076, 1945[60]
$SbPh_3$	2065, 1948[69]	2075, 1955[68]	2070, 1943[67]
$BiPh_3$[60]	2064, 1945	2075, 1954	2074, 1945

Three IR active $\tilde{\nu}_{CO}$ stretches are expected for a $[M(CO)_5L]$ complex with C_{4v} symmetry. For the majority of the complexes listed here only two vibrations are experimentally detected, which was attributed to near coincidence of two stretching modes.

2.5 Density functional theory

Density functional theory (DFT) calculations on $[M(CO)_5(BiMe_3)]$ (M = Cr, W) showed that the bonding situation of the Bi–M bonds in these compounds can be described as donor-acceptor interactions using the Dewar-Chatt-Duncanson model.[57] Charge decomposition analysis (CDA) on these systems indicated that the Bi→M interaction dominates, which is mirrored by donation/back-donation (d/b) ratios of 3.6 (M = Cr) to 4.9 (M = W). The larger d/b ratio in the case of M = W was rationalized by a better orbital overlap. The backbonding in both complexes is weak and less pronounced than in the analogue antimony complexes. An energy decomposition analysis (EDA) showed that the electrostatic contribution to Bi–M bonding is significantly larger than the contribution by orbital interactions. The nature of the Bi···M interactions in **2** and **3** (*cf.* Scheme 2) was also studied computationally. According to natural bond orbital (NBO) population analyses, these interactions are dominated by Bi→M donation, the interaction energy of which is approximately twice as large as that of the Bi←M backdonation.[51] The dominating role of the Bi→M donation is somewhat surprising in view of the electronegative chlorido substituent at bismuth. Substitution of the electronegative chlorido ligand in **2** and **3** for a phenyl group in **5** and **6** led to more pronounced donor/acceptor interactions between the occupied 6s bismuth atomic orbital and the vacant s-orbital of copper and silver, according to NBO analyses. The deletion energies (E_{Del}) associated with Bi→M donation sum up to 30.3 kcal · mol^{-1} and 40.0 kcal · mol^{-1} for **5** and **6**, respectively. In both complexes **5** and **6**, Bi←M backdonation interactions are also present, but only amount to 9.1 kcal · mol^{-1} for **5** and 7.7 kcal · mol^{-1} for **6**.

Starting from the Xantphos-based bismuthane/phosphane ligand **4** (*cf.* Figure 3), the gold and palladium complexes **9** and **10** were obtained (Figure 4).[50, 70] Among the coinage metal complexes **5**, **6**, and **9**, compound **9** is – in contrast to **5** and **6** – an ionic species with a third phosphane bound to Au, which decreases the Lewis acidity of the Au center. Therefore, the Bi···Au interaction is weakened, but still mainly caused through Bi(6s)→Au(6s) interactions according to DFT studies, which revealed a deletion energy of 17.7 kcal · mol^{-1}. The sum of the stabilizing energies from interactions of filled Au orbitals with empty Bi orbitals is 7.1 kcal · mol^{-1}. The nature of the metallophilic Bi···Pd interactions in **10** was studied by NBO analyses, which indicate one dominating donor-acceptor interaction between the filled 6s-orbital of Bi and the empty 5s-orbital of Pd, with deletion energies of 67.1 and 56.8 kcal · mol^{-1} for the two Bi→Pd interactions.[70]

In conclusion, the strength of the Bi→M interaction is drastically influenced by the substituents around bismuth. As a trend, electron-donating substituents at bismuth strengthen the Bi→M donor/acceptor interactions. In turn, the introduction of

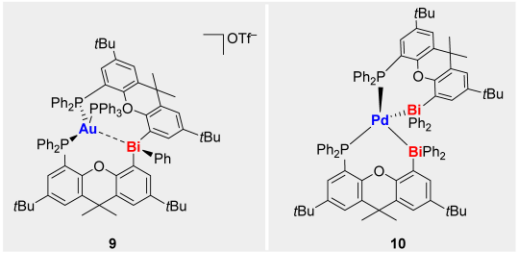

Figure 4. Gold and palladium complexes **9** and **10**.

electronegative substituents R' in compounds of type BiR_2R' reduces the donor strength of bismuthanes and enables the corresponding Bi←M backdonation (see section 3). It should be noted that the exact numbers (rather than the trends) obtained from such theoretical analyses may depend on factors such as the choice of the functional and basis set(s) and the version of the program used for analysis.

2.6 Reactivity and applications

It has been demonstrated that the $BiMe_3$ ligand in $[M(CO)_5(BiMe_3)]$ (M = Cr, W) can be substituted by the addition of $SbMe_3$. The reverse reaction, substitution of $SbMe_3$ by addition of $BiMe_3$, was not successful, illustrating the weaker donor/acceptor character of $BiMe_3$ compared to $SbMe_3$ in these compounds.[57]

The reduced donor ability of the pnictogen atom in $BiPh_3$ in comparison with the lighter congeners also became apparent with cationic ruthenium species as bonding partners: reaction of EPh_3 (E = P-Sb) with $[Ru(MeCN)_3Cp]^+$ quantitatively gave $[Ru(MeCN)_2(EPh_3)Cp]^+$ (Cp = C_5H_5), i.e. compounds with Ru–E bonds. In contrast, the analogue reaction with $BiPh_3$ led to the formation of two products in which exclusively the phenyl moieties of $BiPh_3$ served as donor functionalities, resulting in a mixture of the sandwich complexes $[Ru(\eta^6\text{-}PhBiPh_2)Cp]^+$ (**11**) and $[(RuCp)_2(\mu\text{-}\eta^6,\eta^6\text{-}Ph_2BiPh)]^{2+}$ (**12**, Scheme 3).[71]

The relatively weak donor strength of bismuth-based ligands has also been exploited as a valuable feature in synthetic chemistry. The xanthene-based ligand in complex **10** bears a phosphanyl and a bismuthanyl functional group and can act as a hemilabile ligand: in the presence of O_2, the bismuthanyl groups de-coordinate from the metal center, and the peroxido species **13** is formed. As a catalyst, **10** enabled the oxidation of PPh_3 and 2,4-di-*tert*-butylphenol with O_2 to give $OPPh_3$ and a biphenyl species **14**, respectively (Scheme 4). The hemilabile behavior of the bismuthane/phosphane ligand proved to be advantageous in these reactions, since a structurally related xantphos-ligated palladium complex (with a P,P-chelating ligand) did not show one full catalytic turnover (PPh_3) or no C–C coupling reaction at all (2,4-di-*tert*-butylphenol).

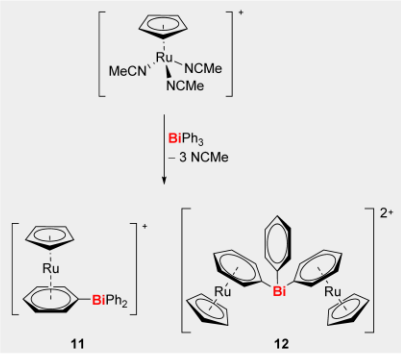

Scheme 3. Reaction of $[RuCp(MeCN)_3]^+$ with $BiPh_3$. The positive charge is balanced by $[PF_6]^-$ counteranions.

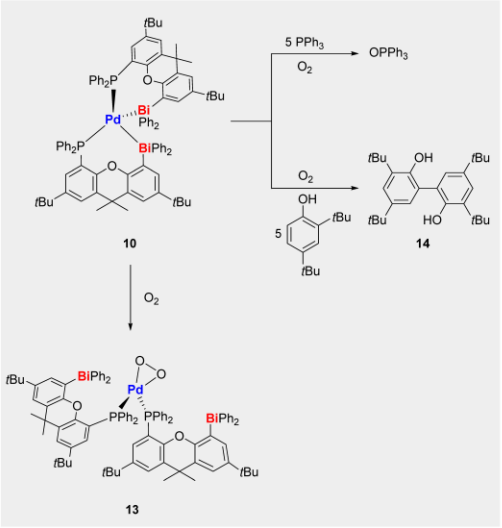

Scheme 4. Palladium(0) complex **10** and its reactions with PPh_3 and 2,4-di-tert-butylphenol in the presence of dioxygen to give $OPPh_3$ and 3,3',5,5'-tetra-tert-butyl-2,4-bisphenol (**14**) (top) and with O_2 (bottom).

3. Bismuthanes (BiR_3) as Z-type ligands

The substituents R in bismuthanes BiR_3 not only influence the bismuth-centered Lewis basicity (section 2), but are also key to controlling the Lewis acidity of these compounds. When these substituents are sufficiently electronegative, the Lewis basicity (based on the 6s atomic orbital of bismuth) can be reduced or even suppressed and the Lewis acidic character becomes more prominent. Antibonding σ*-Bi–R MOs are responsible for bismuth-centered Lewis acidity in bismuthanes BiR_3. Consequently, the Lewis acidity of BiR_3 increases with an increasing electronegativity of R, and the vacant σ*-orbital that is available for bonding interactions with a Lewis base is located in *trans*-position to R.[72-74] While interactions of Lewis acidic bismuth compounds with organic or non-metallic inorganic Lewis bases have frequently been reported,[75-82] the ligation of Lewis-basic transition metal complexes to give metal-only Lewis pairs have only recently been explored.[83] So far, bismuthanes as two electron acceptor ligands (Z-type ligands) in the coordination sphere of transition metals are limited to isolable complexes of palladium, platinum, and gold.

3.1 Synthesis of compounds with BiR_3 as Z-type ligands

The synthetic routes to transition metal complexes with M→Bi interactions as the exclusive or dominating type of M–Bi bonding are so far restricted to bismuth precursors that contain additional donor moieties. These donor functionalities confer a chelating nature to the bismuth ligand and direct the transition metal in close proximity to the bismuth atom. In a straightforward synthetic approach, transition metal complex

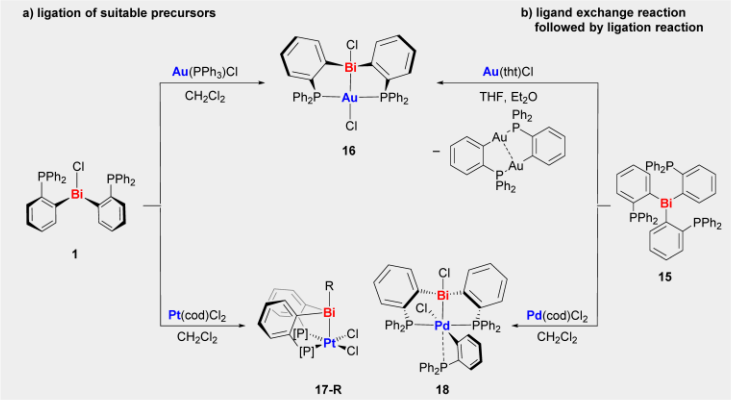

Scheme 5. Synthetic routes to transition metal complexes with M→Bi interactions. tht = tetrahydrothiophene, cod = 1,5-cyclooctadiene, CH_2Cl_2.

fragments such as AuCl or $PtCl_2$ can be liberated from suitable precursors and directly be ligated by a bismuthane such as **1**, which contains a sufficiently electronegative substituent such as Cl (Scheme 5a).[84] Alternatively, homoleptic bismuth precursors BiR_3 such as **15** may be employed, which do not bear sufficiently electronegative substituents. In this case, a ligand exchange reaction (e.g. with a chlorido ligand of the transition metal precursor) is necessary in order to turn the bismuth species into a Z-type ligand, which then coordinates to the transition metal in a second step (Scheme 5b).[85]

The ligand design employed here leads to an orientation of vacant bismuth-centered and occupied metal-centered orbitals, which can even turn triorganobismuth compounds into Z-type ligands (as in compound **17-Me**; for a discussion of the bonding situation see section 3.4).[73]

It has to be noted that suitable transition metal precursors for M = Pd, Pt that have been identified to date must have the metal center in the +II oxidation state, otherwise oxidative addition of the Bi–X bond to M(0) may occur during synthesis (see section 4.1).[86]

3.2 Solid-state structure

Compounds **16**, **17-R** (R = Cl, OTf, Me, C_6F_5), and **18** were investigated by single-crystal X-ray analyses. In compounds **16** and **18** the phosphanyl groups are in *trans* position to each other, in the platinum derivative **17-R** they adopt a *cis* arrangement.[73, 84, 85] The gold center in **16** adopts an unusual distorted square-planar coordination geometry, which was attributed to the unique characteristics of the ligand system.[84] In the platinum and palladium complexes **17-R** and **18** the M–Bi–Cl unit is in an almost linear arrangement, which maximizes the M→Bi interactions (*cf.* section 3.4). The Bi–Cl bonds in **16** (2.62 Å[84]-2.64 Å[85]), **17-Cl** (2.62 Å),[84] and **18** (2.62 Å)[85] are significantly elongated compared to that in bismuth compound **1** (2.56 Å). This is in agreement with population of the σ*(Bi–Cl) orbital in the heterobimetallic complexes by electron density from occupied transition metal-centered orbitals. In the series of compounds **17-R**, one substituent at bismuth is varied (R = OTf, Cl, C_6F_5, Me) and a systematic increase of the Pt–Bi bond length with decreasing electronegativity of this substituent was observed. These results reveal increasingly efficient orbital overlap between the σ*(Bi–R) orbital and the d_z^2(Pt) orbital for increasingly electronegative substituents R.[73]

3.3 Stability and spectroscopic properties

Transition metal compounds featuring Z-type bismuthane ligands were commonly handled under inert conditions.[73, 84] Interestingly, however, the sterically encumbered complex **18** has been reported to be air-stable. NMR spectroscopic analysis of **18** indicated an apparent C_s symmetry in solution.[85] Somewhat counterintuitively, the phosphanyl moieties in compounds **17-Cl** and **17-OTf** give two resonances in their ^{31}P NMR spectra, reflecting a slightly different environment of the phosphorus nuclei in solution.[73, 84] The photophysical properties of **16** were examined, since metal-metal interactions in heterobimetallic gold complexes can modify their photophysical properties. Indeed, **16** shows an absorption band in dichloromethane solution, which peaks at 377 nm and is not due to the monometallic starting materials. However, no emission was detected in static fluorescence measurements.[84]

3.4 DFT Calculations

According to NBO analyses on compounds **16** and **18**, the Bi–Cl bond may be described as a ionic interaction.[85] This leads to a vacant p-atomic orbital of bismuth in these compounds, which is populated by electron density from the chloride ligand and the transition metal center, resulting in three-center-four-electron interactions. However, the deletion energies for the Cl→Bi interactions (**16**: E_{Del} = 90.8 kcal · mol^{-1}; **18**: E_{Del} = 101.3 kcal · mol^{-1}) are significantly higher than those for the M→Bi interactions (**16**: E_{Del} = 16.4 kcal · mol^{-1}; **18**: E_{Del} = 19.2 kcal · mol^{-1}).[85] In compound **16**, backdonation from Bi to Au was determined to have only minor contributions to the overall Bi–

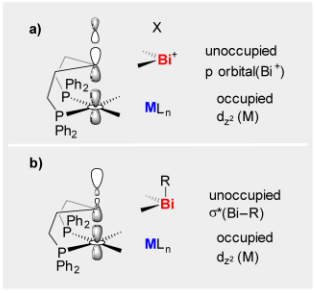

Figure 5. General framework enabling the synthesis of transition metal complexes with M→interaction. R, X = monoanionic ligand.

Au bonding.[84] In complexes **17-R**, NBO analyses indicate an ionic Bi–R interaction for R = OTf, Cl (Figure 5a) and a covalent interaction for R = C_6F_5, Me (Figure 5b).

However, the orbital fragments pointing towards the transition metal look similar in all cases,[73] suggesting that qualitatively similar bonding situations are realized in all cases. Importantly, the ligand framework that was employed for the synthesis of **17-R** (and **18**) effectively aligns the vacant σ*(Bi–R)/p(Bi) orbital with the occupied d_z^2(M) orbital (Figure 5).[84, 85] Deletion energies associated with the 5d(Pt)→Bi interactions in compounds **17-R** unambiguously demonstrated the strong influence of the substituent R (OTf, Cl, C_6F_5, or Me) at the bismuth atom on the M→Bi bond strength: steadily increasing deletion energy values were obtained with increasing electron-withdrawing character of the substituent R (E_{Del} = 25.65 kcal · mol^{-1} (R = Me), 33.42 kcal · mol^{-1} (R = C_6F_5), 54.22 kcal · mol^{-1} (R = Cl), and 74.23 kcal · mol^{-1} (R = OTf)). These investigations show that the following factors increase the potential of bismuth compounds to act as Z-type ligands: i) a high group electronegativity of substituents at bismuth, ii) pre-coordination of an electron-rich transition metal center through additional donor functionalities in the bismuth species, and iii) an ideal (quasi-)linear alignment of a vacant σ*(Bi–R)/p(Bi) orbital with an occupied transition metal-centered orbital. When the latter two design principles are met, even Bi–Me groups with a relatively electron-rich methyl group can act as electron-accepting moieties towards transition metal complex fragments.

3.5 Ambiguous ligands: BiR_3 as donor and acceptor

Theoretical analyses of the bonding situation in transition metal complexes containing bismuthanes have been used to classify these bismuth species either as electron-donating L-type ligands (section 2.5) or as electron-accepting Z-type ligands (section 3.4). In some cases, NBO analyses revealed significant contributions by Bi→M and M→Bi interactions, but one of them is commonly dominating.[57, 66, 84, 85] However, even cases in which both types of interactions are similar in strength are possible: compound **20** with Os–Bi donor/acceptor interactions has been investigated computationally, since steric bulk around the Os center prevented such bonding in the experimentally obtained compound **19** (Figure 6).[87] NBO analyses revealed deletion energies for Os→Bi (49.8 kcal · mol^{-1}) and Bi→Os (66.2 kcal · mol^{-1}) interactions, which are high in absolute numbers and similar in magnitude (differing by a factor of 1.3). This demonstrates that mutual M→Bi and Bi→M bonding can contribute to the stabilization of Bi–M donor/acceptor interactions. This case is especially unusual since a cationic bismuth compound shows electron-donor capabilities in this compound.

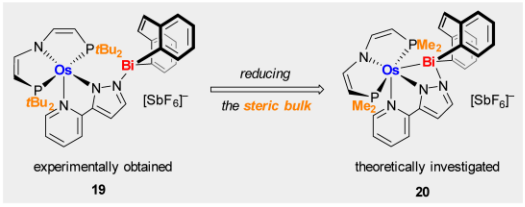

Figure 6. Reducing the steric bulk around Os (by exchange of *t*Bu for Me) enables mutual Bi→Os and Os→Bi donor-acceptor interactions in **20**.

4. Bismuthyl as X-type ligands

The largest group of transition metal complexes containing bismuth-based ligands are transition metal bismuthanes, i.e. compounds featuring one or more covalent Bi–M interactions. The large covalence radius of bismuth allows bonding of at least three transition metal complex fragments to bismuth centers that maintain an occupied 6s(Bi) orbital.[88]

An analysis of the distribution of literature-known transition metal bismuthanes across the periodic table of the elements reveals that there has been a particular focus on compounds featuring transition metals of group 6 to 9. Especially for the early and late transition metals, no or only very few examples of transition metal bismuthanes have been reported (Figure 7).

Sc	Ti	V	Cr	Mn	Fe	Co	Ni	Cu	Zn
Y	Zr	Nb	Mo	Tc	Ru	Rh	Pd	Ag	Cd
La	Hf	Ta	W	Re	Os	Ir	Pt	Au	Hg

Figure 7. Transition metals, for which complexes containing at least one covalent Bi–M interaction are described, are shown with a colored background. Elements highlighted in light green: at least one example of a transition metal bismuthane is known. Elements highlighted in dark green: Five or more species with covalent Bi–M bonds in molecular compounds are described in the literature. The literature research on which this scheme is based was performed with scifinder.cas.org.

4.1 Synthesis of transition metal bismuthanes

General synthetic procedures for the synthesis of transition metal bismuthanes with up to three covalent M–Bi bonds are

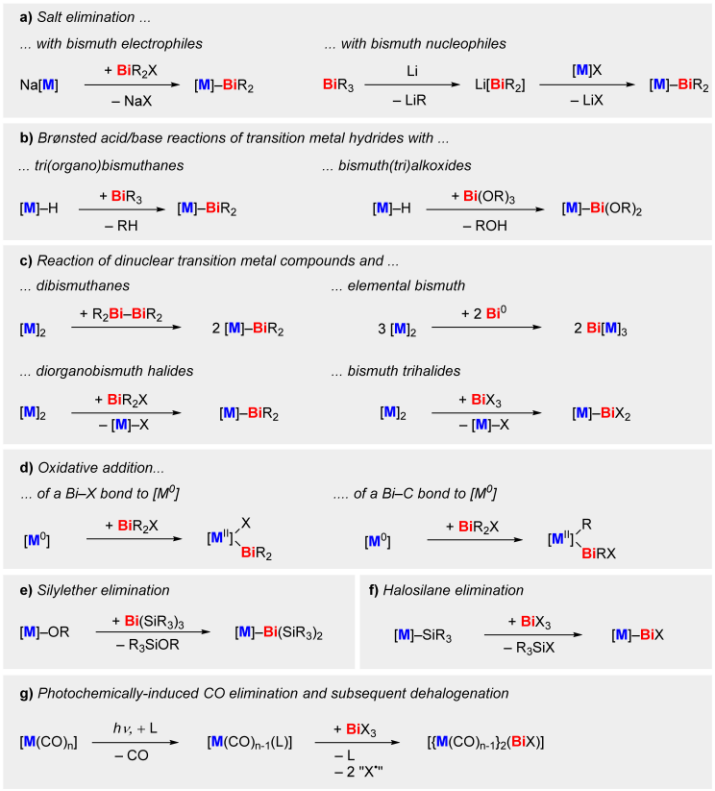

Scheme 6. Synthetic routes to molecular transition metal complexes containing covalent Bi–M bonds.

outlined in this section (Scheme 6). The most frequently used approach for the formation of such complexes is a salt elimination using bismuth halides and alkali metal metallates of the desired transition metal as starting materials (Scheme 6a, left). Examples include group 6 to group 9 metallates such as $[Cr(CO)_3Cp]^-$, $[Mn(CO)_5]^-$, $[Fe(CO)_2Cp]^-$ and $[Co(CO)_4]^-$.[89-93] Bismuth trihalides, [90, 91, 94, 95] organobismuth dihalides,[93] and diorganobismuth halides,[92, 93] are frequently used as bismuth precursors in these metathesis reactions. Mono-, di-, and trimetalated bismuth species can be generated by adjusting the stoichiometry[89, 94, 96] and/or the choice of bismuth precursor. Instead of using bismuth halides as precursors, there are also reports on the successful usage of bismuth nitrates.[97] The salt elimination approach depicted in Scheme 6a (left) makes use of bismuth electrophiles and is mainly limited by the availability of the transition metal nucleophiles. The salt elimination with reverse polarities, i.e. reaction of a bismuth nucleophile with a transition metal electrophile, is also possible (Scheme 6a, right). The reaction of *in-situ* generated (2,5-dimethylbismolyl)lithium ($LiBi(MeCCH)_2$) with $[Mn(CO)_5Br]$ is an example that falls into this category.[98] This strategy is less explored due to difficulties in accessing or even isolating bismuthides of type $[BiR_2]^-$ with alkali metal counter anions.[99] Apart from the limited availability of nucleophiles in salt elimination reactions en route to transition metal bismuthanes, ligand redistribution processes are problematic side reactions in this approach, as observed during the reaction of $Na[M(CO)_3Cp]$ with Me_2BiBr, which did not give the desired $[(M(CO)_3Cp(BiMe_2)]$, but rather gave mixtures of $[(M(CO)_3Cp)_2BiMe]$ and $[(M(CO)_3Cp)_2BiBr]$ along with $BiMe_3$ (M = Mo, W).[100] In an alternative strategy, Brønsted acidic transition metal complexes can be reacted with sufficiently Brønsted basic bismuth compounds such as tri(alkyl)bismuth species, BiR_3,[100] and bismuth(tri)alkoxides, $Bi(OR)_3$ (Scheme 6b).[101-105] The utilization of $BiMe_3$ as a starting material leads to the formation of volatile methane as a by-product, which is an additional driving force for this reaction (Scheme 6b, left). Reactions of $Bi(OR)_3$ with transition metal hydrides have been coined as the "hydride-alkoxide-approach" and have been exploited for the synthesis of a wide range of molybdenum, rhenium, and iron species bearing covalent Bi–M bonds (Scheme 6b, right).[101-106] Furthermore, dinuclear transition metal compounds are suitable precursors for the

synthesis of transition metal bismuthanes in reactions with dibismuthanes,[107, 108] elemental bismuth,[94, 109] diorganobismuth halides, bismuth trihalides[110-112] and bismuth carboxylates (Scheme 6c).[113] While reactions with dibismuthanes proceed with high atom economy (Scheme 6c, top), reactions with halide-containing bismuth precursors generate the corresponding transition metal halide as a by-product which needs to be separated, as described for the reaction of $[Fe(CO)_2Cp]_2$ with $BiCl_3$ to give $[Fe(CO)_2Cp(BiCl_2)]$ and $[Fe(CO)_2CpCl]$.[111, 112] There are a few additional strategies for the synthesis of transition metal bismuthanes (or related species), which have so far only rarely been used but significantly broaden the methodological approaches for the generation of these compounds (Scheme 6d-g). Only recently, the oxidative addition of the Bi–X bond in $BiCl_3$ or R_2BiCl to low-valent late transition metals has been reported (Scheme 6d).[86, 114] In a bismacyclic compound with two endocyclic Bi–C bonds and an exocyclic Bi–Cl bond, the oxidative addition of a Bi–C bond to Pt(0) has been reported to be thermodynamically favored over the kinetically favored oxidative addition of a Bi–Cl bond.[115] These approaches are mainly restricted to precursors with the transition metals in the oxidation state of zero so far (an example of a iridium(I) complex as a precursor has also been reported).[86, 114, 115] Furthermore, an example of a silylether elimination has been shown to allow for Bi–M bond formation (Scheme 6e).[116, 117] Specifically, reaction of $Bi(SiMe_3)_3$ with Cu(O*t*Bu) in the presence of PMe_3 allowed for the isolation of $[(PMe_3)_3Cu(Bi(SiMe_3)_2)]$, the first example of a species bearing a Bi–Cu bond.[116] Halosilane elimination has not been proven to be a key step in the synthesis of species featuring Bi–M bonds, but may be anticipated in the reaction of $[HMn(C_5MeH_4)(SiPh_3)(CO)_2]$ with NaH and $BiCl_3$ to give $[BiCl(Mn(C_5MeH_4)(CO)_2)_2]$ (Scheme 6f).[24] It should be noted, however, that the product of this reaction has been discussed in terms of a bismuthinidene species (i.e. a Bi(I) compound). The same types of compounds have also been synthesized in a photochemical approach: $[Mn(CO)_2(thf)Cp]$ was generated *in-situ* by photochemically-induced CO elimination from $[Mn(CO)_3Cp]$ in THF and subsequently reacted with $BiCl_3$ yielding $[(Mn(CO)_2Cp)_2BiCl]_2$ in a (formal) dehalogenation (Scheme 6g).[117, 118]

4.2 Stability

In most cases, the strongly colored molecular complexes with covalent Bi–M bond are unstable or only moderately stable towards air and moisture.[100, 112, 119, 120] In addition, some transition metal bismuthanes have been reported to degrade in solution under inert conditions.[93, 110] There have also been reports of pronounced heat and light sensitivity to an extent that a full characterization was not possible.[116, 121] In some cases, thermally- or photochemically-induced reactions proceed selectively, and the identification of the resulting products could be achieved (see section 4.6). While these observations speak for the sensitivity of transition metal bismuthanes, there are also reports on $[Bi(Co(CO)_4)_3]$, $[(Mn(CO)_2Cp)_2BiCl]_2$ and related species that have been synthesized from degassed water in excellent yield[109] or have been isolated by column chromatography.[117, 118] Overall, transition metal bismuthanes tend to be unstable towards oxygen, water, heat, and light, but the extent to which this sensitivity is observed varies greatly with the nature of the compound under consideration.

4.3 Solid state structure

The group electronegativity of transition metal complex fragments that have been installed in the coordination sphere of bismuth span a relatively wide range. As a result, the polarity of covalent Bi–M bonds and the energy of antibonding σ*(Bi–M) orbitals show a significant tunability. For the majority of the cases, population of the antibonding σ*(Bi–M) orbital by electron density from an additional donor ligand is not observed. In these cases, tri-coordinate bismuth compounds are obtained, e.g. $[Bi(Mn(CO)_5)_3]$,[96] $[Bi(FeCp(CO)_2)_3]$,[112] $[BiPh_2(Co(CO)_3(PPh_3)]$,[108] and $[Bi(Co(CO)_4)_3]$.[109] In such compounds, the expected trigonal-pyramidal coordination geometry around bismuth is observed, but the M–Bi–M angles are significantly increased from 92-96° in $BiPh_3$[122, 123] to 96-101° in $[BiPh_2(Co(CO)_3(PPh_3)]$,[108] 107° in $[Bi(Co(CO)_4)_3]$,[109] and 108-110° in $[Bi(FeCp(CO)_2)_3]$ (Scheme 7a).[112]

A general rationalization of this phenomenon has not been achieved, yet: in some cases, it has been attributed to steric effects based on comparison to the increase of bond angles in bulky tri(aryl)bismuthanes.[112] In other cases, steric effects have been ruled out as a possible reason because of the large distances between bismuth-bound transition metal complex fragments.[109]

Transition metal bismuthanes with four-coordinate bismuth atoms can also be obtained. This is possible, when one of the ligands in bismuth complexes of type $Bi[M]_2R$ or $Bi[M]R_2$ shows a sufficiently high group electronegativity or when cationic species of type $[Bi[M]_2]^+$ are targeted ([M] = monoanionic transition metal complex fragment, R = sufficiently electronegative monoanionic ligand such as a halide). Either of these complexes or complex fragments may then interact with Lewis bases. In the case of $Bi[M]_2R$ and $Bi[M]R_2$, this can be realized through the formation of coordination oligomers or polymers $(Bi[M]_2R)_n$ and $(Bi[M]R_2)_n$ in the solid state (*vide infra*) or through addition of one equivalent of a Lewis base such as a halide to give species such as $[Bi[M]_2R_2]^-$. In the case of $[Bi[M]_2]^+$, a four-coordinate bismuth atom is obtained upon coordination of two equivalents of a neutral Lewis base L (such as $OP(NMe_2)_3$) to give compounds of type $[Bi[M]_2L_2]^+$.

The structural features of these different types of transition metal bismuthanes with four-coordinate bismuth centers may vary. Examples resulting from the use of sufficiently electronegative transition metal complex fragments bound to bismuth include [cation][Bi(Co(CO)$_4$)$_4$],[124-126] [cation][BiPh$_2$(M(CO)$_5$)$_2$] (M = Cr, Mo, W),[127] [cation][BiPh$_2$(Fe(CO)$_4$)$_2$],[127] [cation][BiPh$_2$(Cr(CO)$_5$)Fe(CO)$_4$)],[127] and [cation][BiPh$_2$(ReH(CO)$_4$)$_2$][128] ([cation]$^+$ = [CoCp$_2$]$^+$, [NMe$_4$]$^+$, [N(*n*Bu)$_4$]$^+$, [K(18-crown-6)]$^+$, [Ph$_3$PNPPh$_3$]$^+$). The bismuth atom in the homoleptic complex anion $[Bi(Co(CO)_4)_4]^-$ shows an unusual tetrahedral coordination geometry, which has been ascribed to steric interactions (Scheme 7b).[126] The exceptionally

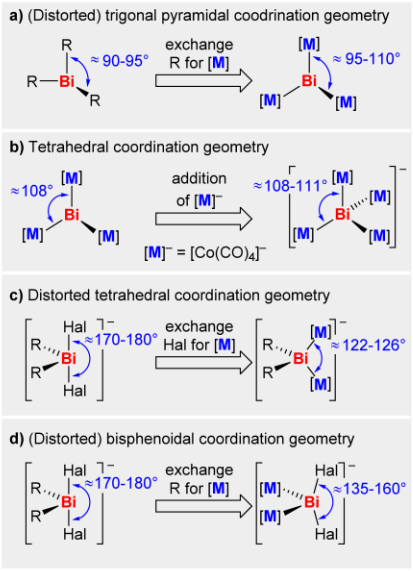

Scheme 7. Influence of transition metal complex fragments on the coordination geometry around bismuth.

long Bi–Co bonds in these compounds have been assigned to the lone pair at bismuth residing in an antibonding a_1* orbital.[126, 129] This is supported by short Bi–Fe bonds in $[Bi(Fe(CO)_4)_4]^{3-}$, which contains a tetrahedrally coordinated bismuth atom without a lone pair.[130] Compound $[CoCp_2][Bi(Co(CO)_4)_4]$ has originally been reported to be paramagnetic,[124] but this was later ascribed to paramagentic impurities formed through adventitious oxidation of the sample.[32]

For the structural properties of heteroleptic, four-coordinate bismuth compounds with Bi–M bonds, two different scenarios may be discussed (Scheme 7c,d). For comparison, it is helpful to recall that transition metal-free bismuth compounds with a coordination number of four commonly adopt bisphenoidal coordination geometries with the angle between ligands in the axial positions and the central atom approaching the ideally expected value of 180° (Scheme 7c,d, left; e.g.: $[BiPh_2Cl]_\infty$ (Cl–Bi–Cl, 176°),[131] $[BiPh_2Cl_2]^-$ (Cl–Bi–Cl, 174°),[132] $[BiPh_2(OP(NMe_2)_3)_2]^+$ (O–Bi–O, 172°)).[133] In contrast, distorted tetrahedral coordination geometries have been ascribed to the bismuth atom in the abovementioned heteroleptic complex anions $[BiPh_2([M])_2]^-$ ([M] = $Cr(CO)_5$, $Mo(CO)_5$), $W(CO)_5$), $Fe(CO)_4$, $ReH(CO)_4$). An sp^3 hybridization has been suggested as an explanation of this phenomenon: comparison of Bi–Cr bond lengths in species $[Cr(CO)_5(BiPh_3)]$ (2.705 Å) and $[BiPh_2(Cr(CO)_5)_2]^-$ (2.750 Å) reveal a longer bond length for the covalent Bi–Cr bond in $[BiPh_2(Cr(CO)_5)_2]^-$, which is counterintuitive when dative vs. covalent bonding situations are compared.[134] However, since the bond length increases as the degree of s-orbital character in the bonding orbitals decreases, a sp^3 hybridization can be assumed for species such as $[BiPh_2(Cr(CO)_5)_2]^-$.[127] Remarkably, the C–Bi–C angles in these compounds remain small (≤ 95°), while the M–Bi–M angles are commonly found in the small range of ca. 122-126° in non-cyclic compounds (Scheme 7c).

Compounds of type $(Bi[M]_2Hal)_n$, $[Bi[M]_2Hal_2]^-$, and $[Bi[M]_2L_2]^+$ also deviate from the ideal bisphenoidal coordination geometry around bismuth (Scheme 7d). The angle between the bismuth atom and ligands in the "axial positions" is significantly smaller than the expected 180° and typically in the range of ca. 135-160° (examples include $[Bi(MoCp(CO)_3)_2Cl]_\infty$ (Cl–Bi–Cl, 142-152°),[89] $[Bi(MoCp(CO)_3)_2Cl_2]^-$ (Cl–Bi–Cl, 138-155°),[135, 136] and $[Bi(FeCp(CO)_2)_2(OP(NMe_2)_3)_2]^+$ (O–Bi–O, 161°)).[137] This has been ascribed to π-donation of transition metal complex fragments into the vacant 6p(Bi) orbital, based on theoretical calculations on Sb analogues.[135]

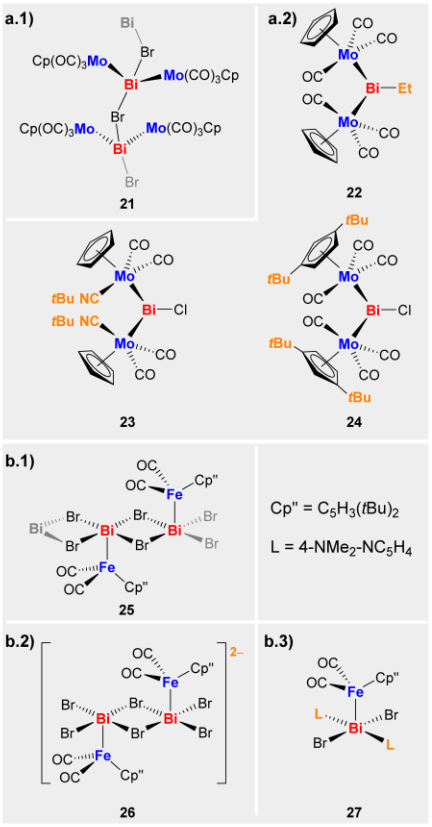

Figure 8. Controlling the degree of aggregation in transition metal bismuthanes. a.1) coordination polymer (cut-out shown); a.2) monomeric species due to electronic (top) or steric effects (bottom); b.1) coordination polymer (cut-out shown); b.2) dimeric species and b.3) monomeric species obtained from addition of an anionic Lewis base (Br^-) and a neutral Lewis base (4-NMe_2-NC_5H_4), respectively. Anionic charge is balanced by $[N(nBu)_4]^+$ countercations.

Aggregation phenomena have frequently been reported for transition metal bismuthanes. Whether or not this phenomenon is observed critically depends on the steric and electronic nature of the substituents at bismuth. The introduction of sufficiently electronegative ligands such as halides or alcoholates facilitates the formation of oligomeric or polymeric species in the solid state. On the other hand, oligomerization can be suppressed by changing the electronic situation at bismuth or increasing the steric bulk in the coordination sphere of bismuth.[109, 119, 138-141] This is exemplified by comparison of $[BiBr(MoCp(CO)_3)_2]$ (**21**),[139] $[BiEt(MoCp(CO)_3)_2]$ (**22**),[138] $[BiCl(MoCp(CNtBu)(CO)_2)_2]$ (**23**),[109, 140] and $[BiCl(Mo(C_5H_3tBu_2)(CO)_3)_2]$ (**24**),[141] which form either a coordination polymer (**21**) or molecular complexes (**22**-**24**) in the solid state (Figure 8a). De-aggregation of transition metal bismuthane coordination polymers can also be achieved by addition of anionic or neutral Lewis bases; examples include the reactions of the coordination polymer $[BiBr_2(Fe(C_5tBu_2H_3)(CO)_2)]_\infty$ (**25**) with $[N(nBu)_4]Br$ or N,N-dimethylaminopyridine, which give dimeric $[[BiBr_3(Fe(C_5tBu_2H_3)(CO)_2)]_2]^{2-}$ (**26**) and monomeric $[BiBr_2(Fe(C_5tBu_2H_3)(CO)_2)(4\text{-}NMe_2\text{-}C_5H_4)_2]_2$ (**27**), respectively (Figure 8b).[110]

Generally, transition metal bismuthanes with at least one sufficiently electronegative ligand bound to Bi can form dimeric, trimeric, and polymeric arrangements in the solid state (for examples see Figure 8a.1,b.1, Figure 9 and Figure 10). As long as the transition metal complex fragments can formally be interpreted as monoanionic ligands, the ligands R (commonly halide, alcoholate or acetate species) are located in bridging positions between two bismuth atoms (Figure 9). When the transition metal and the bismuth atom each form two Bi–M bonds, coordination polymers with $(Bi–M)_\infty$ chains can be obtained (Figure 10).

Figure 9. Compounds which form intermolecular interactions to give dimeric and trimeric species in the solid-state.

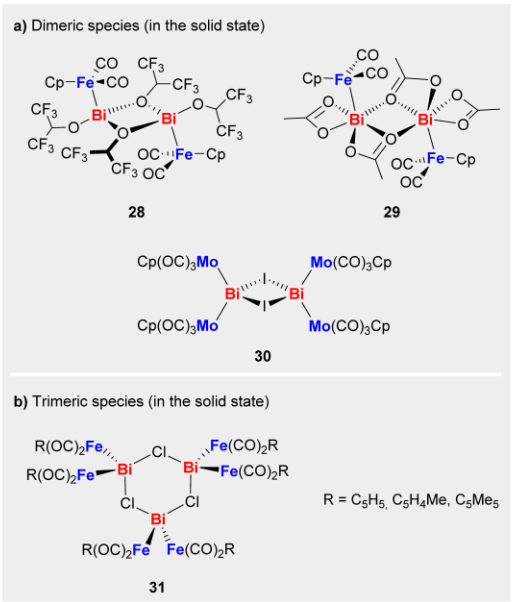

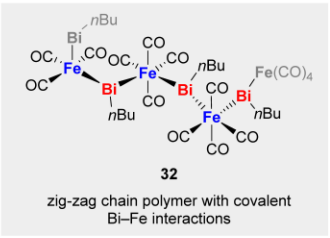

Figure 10. Example of a transition metal bismuthane that forms a coordination polymer with a $(Bi–M)_\infty$ backbone.

4.4 Polarity of covalent Bi–M bonds

The polarity of M–Bi bonds can be expected to depend not only on the nature of the transition metal itself, but also on the ligands bound to M and Bi. For a small series of transition metal bismuthanes $[Bi((C_6H_4CH_2)_2S)(ML_n)]$, the polarity of the Bi–M bond has been investigated in some more detail (ML_n = $Mn(CO)_5$ (**33**), $Fe(CO)_2Cp$ (**34**), $Co(CO)_3(PPh_3)$ (**35**), Figure 11).[92]

The sulfur atom in the ligand backbone is sensitive to the electronic situation of the bismuth center: if an electronegative group X is bound to the bismuth atom, resulting in a polarized $Bi^{\delta+}–X^{\delta-}$ bond, the sulfur atom acts as a donor functionality, which is reflected by a shortened Bi–S distance in the solid state (Figure 11b).[142, 143] Based on distance criteria, such a Bi–S interaction was excluded for the transition metal bismuthanes **33**-**35** in the solid state, hinting towards non- or only weakly polarized Bi–M bonds in compounds **33**-**35**.[92] Analyses of the CO stretching frequencies of compounds **33**-**35** by IR spectroscopy and a comparison with related compounds confirmed essentially non- or very weakly polarized Bi–M interactions for **33** and **34** (Figure 12).[92] For the cobalt derivative **35**, only a polarization towards Co was ruled out.[92]

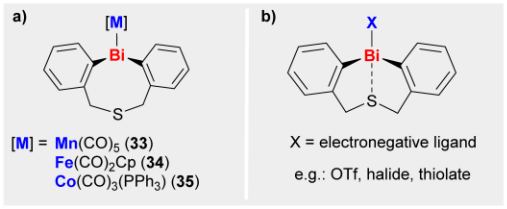

Figure 11. Manganese, iron, and cobalt complexes with a bismuthyl group bearing a thioether moiety in the ligand backbone.

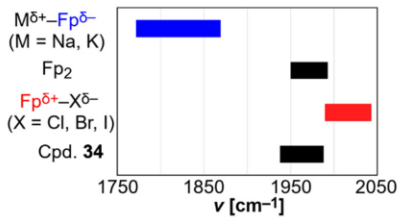

Figure 12. CO stretching frequencies of compounds Fp–E (Fp = $Fe(C_5H_5)(CO)_2$), where E is an electropositive or electronegative binding partner, another Fp moiety or a bismuthyl group. Reproduced with permission of Wiley VCH from reference 92 (colors and compound number have been modified).

4.5 Spectroscopic properties

Transition metal carbonyl complexes with tertiary bismuthanes acting as neutral donor ligand show CO stretching frequencies similar to complexes of the lighter pnictogen congeners, which was ascribed to a concurrent reduction of the σ-donor strength as well as reduced π-acceptor properties of bismuthanes compared to phosphanes, arsanes and stibanes (see section 2.4). An entirely different trend is observed for carbonyl complexes with ER_2 moieties as ligands (E = As-Bi). The CO stretching frequencies of the species $[Co(EPh_2)(CO)_3(PPh_3)]$ decrease in the sequence As > Sb > Bi ($\tilde{\nu}_{CO}$ = 2030, 1967 cm^{-1} for E = As, $\tilde{\nu}_{CO}$ = 2026, 1959 cm^{-1} for E = Sb, $\tilde{\nu}_{CO}$ = 2013, 1957, 1948 cm^{-1} for E = Bi), indicating a significantly higher σ-donor strength of the bismuth derivatives compared to the lighter homologs, thus increasing the electron density on Co and the Co→CO π-backbonding interaction.[108] The related complex $[BiPh(Co(CO)_3(PPh_3))_2]$ with a bridging bismuth unit shows CO stretching frequencies at $\tilde{\nu}_{CO}$ = 1998, 1961 and 1950 cm^{-1}, thus in a similar range as $[Co(CO)_3(PPh_3)(BiPh_2)]$ ($\tilde{\nu}_{CO}$ = 2013, 1957 and 1948 cm^{-1}) according to IR spectroscopy.[138]

The CO stretching frequencies of $[BiMe_2(FeCp(CO)_2]$ are found at lower wavenumbers ($\tilde{\nu}_{CO}$ = 1894 cm^{-1}) compared to the aryl derivative $[Bi((C_6H_4CH_2)_2S)(FeCp(CO)_2)]$ ($\tilde{\nu}_{CO}$ = 1988, 1938 cm^{-1}), indicating stronger σ-donor properties of alkylbismuth species in comparison to arylbismuth species.[92, 120] This parallels the trend that has been found for the behavior of tertiary bismuthanes acting as neutral donor ligands (e.g. section 2.1).[48]

The exact substitution pattern of the aryl substituents in BiR_2 complex fragments does not have a strong impact in their donor/acceptor properties towards transition metals according to IR spectroscopy: similar CO stretching frequencies have been reported for compounds of type $[BiR_2Mn(CO)_5]$ with BiR_2 = $BiPh_2$, $Bi((C_6H_4CH_2)_2S)$ and 2,5-dimethylbismolyl.[92, 93, 98]

For the small series of complexes $[FeCp(CO)(PMe_3)(EMe_2)]$ (E = As-Bi), the influence of E on the ^{31}P NMR spectroscopic resonance of PMe_3 has been investigated.[120] Again, an increasing σ-donor strength is observed in the series As<Sb<Bi, as suggested by a steady high-field shift of the ^{31}P NMR spectroscopic resonances of these compounds in the same order.

In conclusion, IR and NMR spectroscopic studies suggest that the σ-donor strength of transition metal-bound "–BiR_2" and "–(BiR)–" groups can be tuned by the choice of R and exceeds those of the lighter As and Sb congeners.

4.5 DFT Calculations

Detailed bonding analysis of the Bi–M bond on the basis of DFT calculations have been performed for the species $[BiX_2(MCp(CO)_2)]$[144] (M = Fe, Ru, Os, X = Cl, Br, I) and *trans*-$[BiX_2(MX(PMe_3)_2]$[145] (M = Ni, Pd, Pt, X = Cl, Br, I), all of which bear terminally bound dihalobismuth ligands. Both studies conclude that: i) the Bi–M σ-bonds can be interpreted as covalent, electron-sharing bonds that are not considerably polarized (M = Ni, Pd) or (slightly) polarized towards the transition metal (M = Fe, Ru, Os, Pt), ii) upon going from 3d to 4d to 5d transition metals, the orbital overlap between the transition metal and bismuth increases, leading to increasing Bi–M bond strengths, iii) the lone pair at bismuth has high s-orbital character and does not contribute significantly to the Bi–M bond.[144, 145]

4.6 Reactivity and application

Substitution and elimination of CO.

Studies concerning the reactivity of molecular transition metal bismuthanes with covalent Bi–M interaction are rather limited to date. Early reports on reactions that yielded isolable products include the substitution of transition metal-bound carbonyl ligands by phosphanes. In the series of compounds $[BiPh_2(MCp(CO)_3)]$ (M = Cr, Mo, W), the reaction with PPh_3 showed a strong dependency on the transition metal: for the chromium compound no reaction (or only decomposition reactions) have been observed, the molybdenum complex $[BiPh_2(MoCp(PPh_3)(CO)_2)]$ (**37-Mo**) was formed selectively at room temperature in the dark, and the tungsten complex $[BiPh_2(WCp(PPh_3)(CO)_2)]$ (**37-W**) was not generated at room temperature in the dark, but could be isolated after irradiation with a mercury vapor lamp (Scheme 8).[107]

These findings show that ligand exchange reactions in transition metal bismuthanes can be performed at elevated temperature and with irradiation of the sample, while keeping the Bi–M bond intact. They also reflect the trend of 4d transition metals being easier susceptible to selective CO substitution reactions than

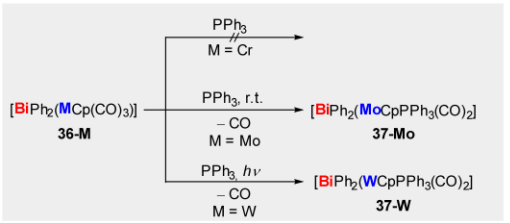

Scheme 8. Transition metal-dependent substitution of a carbonyl ligand by triphenyl phosphane.

Scheme 9 Rates of reaction in ligand exchange reactions of iron complexes containing group 15 complex fragments EMe_2 (E = As, Sb, Bi).

their 3d and 5d counterparts in many cases.[146] The substitution of a carbonyl ligand for PMe_3 in the series of compounds $[EMe_2(FeCp(CO)_2)]$ (E = As, Sb, Bi) shows decreasing rates of reaction with As>Sb>Bi (Scheme 9). This was ascribed to an increasingly stronger fixation of the carbonyl ligands to the iron center (As<Sb<Bi) due to the electronegativity of E decreasing in the same order.[120] Not only the substitution, but also the elimination of carbonyl ligands from transition metal bismuthanes has been reported. Compound **40** features olefin functionalities as potential intramolecular coordination sites. Thus, heating $[Mo(\eta^1\text{-}Bi(CMeCH)_2)(CO)_5]$ (**40**) led to elimination of two equivalents of CO and formation of $[Mo(\eta^5\text{-}Bi(CMeCH)_2)(CO)_3]$ (**41**) through a change of the coordination mode from η^1 to η^5 (Scheme 10).[98] However, **41** was only characterized based on spectroscopic data.[147]

The elimination of CO from transition metal bismuthanes can also lead to the formation of cluster compounds, only some of which are mentioned here since cluster compounds are not in the focus of this contribution. Heating **42** in THF solution gives the heterocubane $[Bi_4(Co(CO)_3)_4]$ (**43**) with the concomitant elimination of CO and formation of Co^0 (Scheme 11a).[125] The same compound **43** was also obtained from irradiation of the transition metal bismuthane $[Bi(Co(CO)_4)_2(FeCp(CO)_2)]$ (**44**) containing two different transition metals and proceeded with the elimination of CO and formation of the byproduct $[FeCp(CO)_2]_2$.[141] Photochemically-induced elimination of CO was also observed in the transformation of $[Bi(FeCp(CO)_2)_3]$ (**45**) to the *closo*-cluster $[Bi(FeCpCO)_3]$ (**46**) (Scheme 11b).[91]

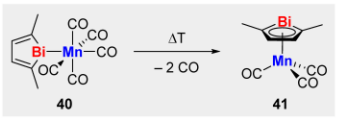

Scheme 10. Thermally induced CO-elimination from **42** with formation of (η^5-2,5-dimethylbismolyl)$Mn(CO)_3$ (**41**).

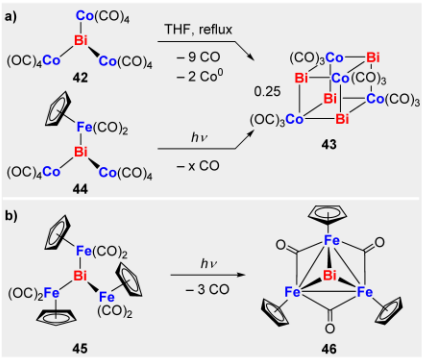

Scheme 11. Examples of CO elimination from transition metal bismuthanes leading to the formation of compounds that may be described as clusters. In part a) (bottom), formation of $[FeCp(CO)_2]_2$ was also observed and the equivalents x of eliminated CO were not determined.

Substitution chemistry at bismuth.

Simple substitution reactions at the bismuth atoms of transition metal bismuthanes, such as halide/alkyl exchange, have only rarely been reported. For instance, reaction of $[BiBr(Fe(CO)_2Cp)_2]$ (**47**) with $AlEt_3$ gave the alkyl analogue $[BiEt(Fe(CO)_2Cp)_2]$ (**48**) (Scheme 12a).[91] In a salt elimination reaction with $Na[Fe(CO)_2Cp]$, the same precursor **47** could be transformed into the homoleptic species $[Bi(Fe(CO)_2Cp)_3]$ (**45**). Further examples of such reactions have been reported.[112] However, these types of salt elimination reactions are not generally reliable transformations, especially when compounds containing different types of transition metals are targeted: for example, the synthesis of mixed-metal compounds **50-M** (M = Mo, Co) could not be achieved by reaction of **49** with one equivalent of $Na[MoCp(CO)_3]$ or $K[CoPPh_3(CO)_3]$, and the homoleptic transition metal bismuthanes **51-M** (M = Mo, Co) were obtained instead (Scheme 12b).[148]

Reactions targeting the controlled cleavage of Bi–M bonds remain relatively rare to date and have been reported in the context of cluster formation and scrambling of bismuth-bound transition metal complex fragments (*vide supra*).[141, 148] Furthermore, reaction of $[Bi(Mn(CO)_5)_3]$ (**52**) with iodine gives $[BiI(Mn(CO)_5)_2]$ (**53**) and $[(MnI(CO)_5)]$ (**54**) (Scheme 13a).[148] Along these lines, transition metal bismuthanes **33** and **34** have been shown to react with CCl_4 to give **55** and with diphenyl dichalcogenides to give compounds **56-EPh** (E = S, Se, Te; Scheme 13b).[92, 143] These reactions have been suggested to proceed via radical pathways.

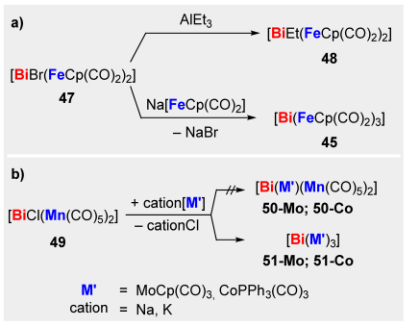

Scheme 12. Approaches targeting the exchange of bismuth-bound halide ligands in transition metal bismuthanes for alkyl groups or transition metal complex fragments.

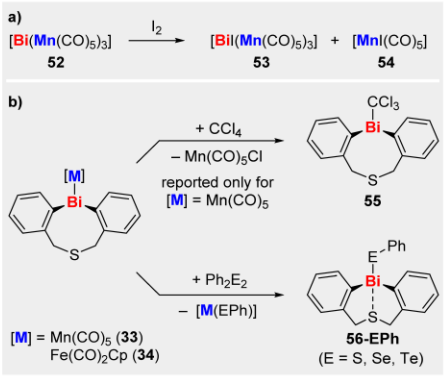

Scheme 13. Cleavage of Bi–M bonds by reaction with I_2, CCl_4, and E_2Ph_2 (E = S, Se, Te).

C–H bond activation

C–H activation has been observed for a range of transition metal bismuth alkoxides.[103, 104] A "complex-induced proximity" between one hydrogen atom of the cyclopentadienide and the alkoxide substituent of the bismuth atom has been identified as a key phenomenon that facilitates these reactions (Scheme 14). A bridging coordination mode of a "BiOR" unit between two transition metal centers is a leading structural feature in these types of compounds that undergo C–H activation. Further studies revealed an impact of the substitution pattern at the cyclopentadienide ligand on the regioselectivity of the reaction: In closely related molybdenum complexes, a C_5H_4Me ligand was twofold activated (**57** → **58**), while the use a C_5H_5 ligands also allowed the single activation of two such ligands (**59** → **60**; Scheme 14a,b).[101, 103] Furthermore, the choice of the alkoxide is also crucial. Sterically demanding and electron-deficient alkoxides such as $OCH(CF_3)_2$, $OSiMe_2tBu$, and $OSiPh_3$ prevent C–H activation (e.g.: Scheme 14c).[102, 106, 149] In reactions with the alkoxide ligand $(OCHMeCHCH_2)^-$, an unusual Bi–Bi bond formation was observed instead of C–H activation.[150]

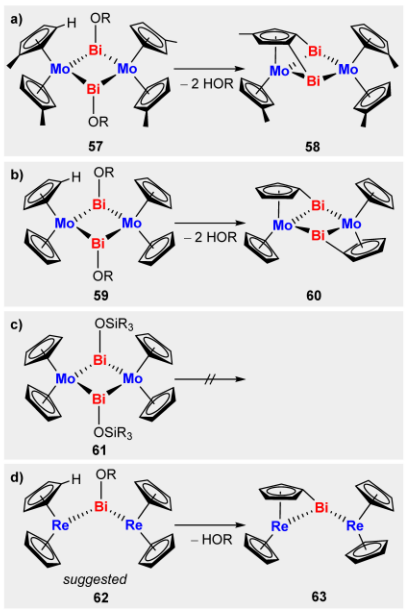

Scheme 14. C–H activation reactions observed for molybdenum and rhenium bismuth alkoxides. a) R = *t*Bu; b) R = *t*Bu; c) R_3 = Me_2tBu, Ph_3; d) R = *t*Bu.

Catalytic applications.

The synthesis of heterometallic rhodium bismuth "paddlewheel" carboxylates and their reactivity towards pyrene have been reported and have already been reviewed (for examples see Scheme 15a).[31, 151-154] More recently, catalytic applications of these types of compounds have been reported with a focus on cyclo-propanation and C–H activation reactions between the carbene precursors and substrates such as styrene (-derivatives) and 1,4-cyclohexadiene. Initial results showed that the heterobimetallic species of type **64-CF$_3$** performed similar to the homobimetallic rhodium complex **65-CF$_3$** when applied as catalysts in these types of reactions (e.g.: Scheme 15b,c).[155] However, in comparison to analogue Rh–Rh complexes, the heterometallic species enhances the electrophilic character of the carbene that is obtained from reactions of paddlewheel complexes with diazo compounds such as those in Scheme b-d. This allows for catalytic cyclo-propanation of electron-deficient alkenes and the activation of chloroalkanes (e.g. Scheme 15d,e).[156] Only recently, the asymmetric cyclo-propanation of styrene derivatives has been accomplished with chiral heterobimetallic bismuth rhodium "paddlewheel" species such as **64-R***.[157] The enantiomeric excess was higher for the heterobimetallic species than for reactions with its homometallic rhodium counterpart **65-R*** (e.g.: Scheme 15f). This was ascribed to the fact that the bismuth center is not catalytically active, but has a larger covalent/ionic radius than Rh, thereby creating a narrower chiral pocket at Rh in **64-R*** than in **65-R***.[157, 158] The structurally related, air-stable paddlewheel complex $[BiPt(SAc)_5]_n$ (SAc = thioacetate) has been exploited as an electrocatalyst in the reduction of CO_2 to CO with a Faradaic efficiency of 92%.[159] According to extended X-ray absorption fine structure analyses and DFT calculations, the Bi–Pt interactions remain intact under catalytic conditions and the bismuth center acts as the active site during the reduction.[159]

The first examples of transition metal bismuthanes (with unsupported Bi–M bonds) showing a bismuth-based catalytic activity have only recently been reported. Simple transition metal bismuthanes such as $[BiPh_2(Mn(CO)_5)]$ (**68**) act as (pre-)catalysts in the cyclo-isomerization of δ-iodo-olefins (e.g.: Scheme 16).[92] These reactions show a good functional group tolerance, are thermally induced, catalytic in the transition metal bismuthane, and proceed via radical pathways, making them complementary or superior to existing methods.[160]

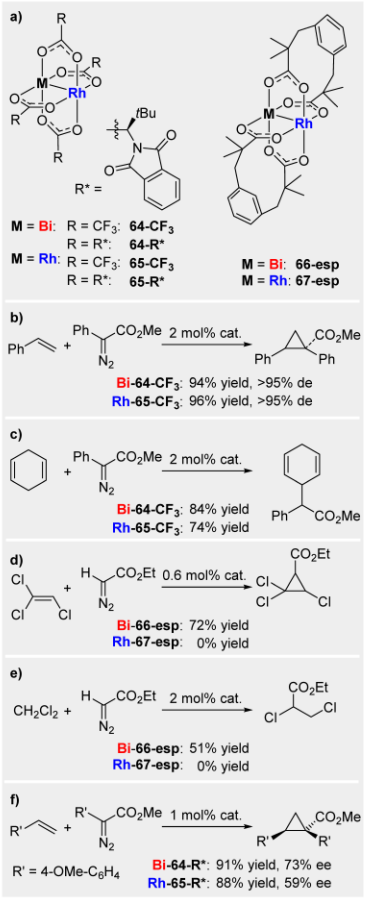

Scheme 15. Catalytic applications of homometallic (Rh/Rh) and heterobimetallic (Bi/Rh) paddlewheel complexes in cyclopropnation, C–H acdtivation, and C–Cl activation reactions.

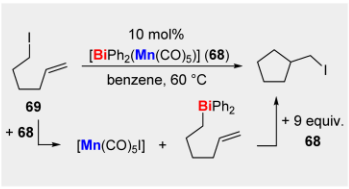

Scheme 16. Transition metal bismuthane-catalyzed cyclo-isomerization of 6-iodo-1-hexene and identified intermediate species.

5. Conclusion

The variety of bismuth compounds containing Bi–M interactions has a long tradition in organometallic chemistry and has significantly been expanded in recent years (M = transition metal). Three types of interaction can be distinguished: dative Bi→M with Bi acting as a donor, dative Bi←M bonding with Bi acting as an acceptor, and covalent Bi–M bonding interactions. A considerable variety of strategies to synthetically access compounds with Bi–M interactions have been summarized. Trends in the structural parameters resulting from all three types of bonding scenarios have been obtained and give guidelines for complex design. Factors influencing the nature and strength of Bi–M bonding have been delineated in some cases and help to evaluate existing and predict future reactivity patterns of compounds featuring Bi–M interactions. The intrinsic properties of Bi–M interactions have been exploited for remarkable catalytic applications including C–H activation, CO_2 reduction, cyclo-isomerization reactions, and stereoselective cyclo-propanation reactions. However, the reactivity of compounds with Bi–M functional groups in stoichiometric and catalytic transformations remains largely unexplored to date. It is anticipated that this contribution will inspire the design, detailed characterization, and synthetic application of existing and new molecules containing Bi–M bonds.

Conflicts of interest

There are no conflicts to declare.

Acknowledgements

Funding through the FCI, the DFG (LI 2860/3-1, LI 2860/5-1), and the Universitätsbund Würzburg is gratefully acknowledged.

Notes and references

1. N. Wheatley and P. Kalck, *Chem. Rev.*, 1999, **99**, 3379-3420.
2. E. Bodio, M. Picquet, P. Le Gendre, *Top. Organomet. Chem.*, 2016, **59**, 139-186.
3. D. Das, S. S. Mohapatra and S. Roy, *Chem. Soc. Rev.*, 2015, **44**, 3666-3690.
4. H.-C. Yu and N. P. Mankad, *Synthesis*, 2021, **53**, 1409-1422.
5. V. Ritleng and M. J. Chetcuti, *Chem. Rev.*, 2007, **107**, 797-858.
6. S. D. Robertson, M. Uzelac and R. E. Mulvey, *Chem. Rev.*, 2019, **119**, 8332-8405.
7. J. M. Gil-Negrete and E. Hevia, *Chem. Sci.*, 2021, **12**, 1982-1992.
8. R. E. Mulvey, F. Mongin, M. Uchiyama and Y. Kondo, *Angew. Chem. Int. Ed.*, 2007, **46**, 3802-3824.
9. R. E. Mulvey, *Organometallics*, 2006, **25**, 1060-1075.
10. T. A. Hanna, *Coord. Chem. Rev.*, 2004, **248**, 429-440.
11. C. Limberg, *Angew. Chem. Int. Ed.*, 2003, **42**, 5932-5954.
12. R. Mohan, *Nature Chem.*, 2010, **2**, 336-336.
13. B. Yang, J. Chen, S. Yang, F. Hong, L. Sun, P. Han, T. Pullerits, W. Deng and K. Han, *Angew. Chem.*, 2018, **130**, 5457-5461.
14. R. Punn, A. M. Feteira, D. C. Sinclair and C. Greaves, *J. Am. Chem. Soc.*, 2006, **128**, 15386-15387.
15. T. Choi, S. Lee, Y. J. Choi, V. Kiryukhin and S.-W. Cheong, *Science*, 2009, **324**, 63-66.

16. H. Liu, R. Nakamura and Y. Nakato, *ChemPhysChem*, 2005, **6**, 2499-2502.
17. M. A. Subramanian, C. C. Torardi, J. C. Calabrese, J. Gopalakrishnan, K. J. Morrissey, T. R. Askew, R. B. Flippen, U. Chowdhry and A. W. Sleight, *Science*, 1988, **239**, 1015-1017.
18. H. Maeda, *Bismuth-based high-temperature superconductors*, CRC Press, Tsukuba, Ibaraki, Japan, 1996.
19. T. Li, S. Kaercher and P. W. Roesky, *Chem. Soc. Rev.*, 2014, **43**, 42-57.
20. C. A. Tolman, *Chem. Rev.*, 1977, **77**, 313-348.
21. S. Lühr, J. Holz and A. Börner, *ChemCatChem*, 2011, **3**, 1708-1730.
22. S. Castillón, C. Claver and Y. Díaz, *Chem. Soc. Rev.*, 2005, **34**, 702-713.
23. W. Tang and X. Zhang, *Chem. Rev.*, 2003, **103**, 3029-3070.
24. I. M. Dixon, E. Lebon, P. Sutra and A. Igau, *Chem. Soc. Rev.*, 2009, **38**, 1621-1634.
25. P. B. Dias, M. E. M. de Piedade and J. A. M. Simões, *Coord. Chem. Rev.*, 1994, **135-136**, 737-807.
26. J. Ansell and M. Wills, *Chem. Soc. Rev.*, 2002, **31**, 259-268.
27. V. K. Greenacre, W. Levason and G. Reid, *Coord. Chem. Rev.*, 2021, **432**, 213698.
28. S. L. Benjamin and G. Reid, *Coord. Chem. Rev.*, 2015, **297-298**, 168-180.
29. N. R. Champness and W. Levason, *Coord. Chem. Rev.*, 1994, **133**, 115-217.
30. S. Roggan and C. Limberg, *Inorg. Chim. Acta*, 2006, **359**, 4698-4722.
31. H. Braunschweig, P. Cogswell and K. Schwab, *Coord. Chem. Rev.*, 2011, **255**, 101-117.
32. K. H. Whitmire, *J. Cluster Sci.*, 1991, **2**, 231-258.
33. A. Kuczkowski, S. Schulz and M. Nieger, *Eur. J. Inorg. Chem.*, 2001, 2605-2611.
34. A. Kuczkowski, F. Thomas, S. Schulz and M. Nieger, *Organometallics*, 2000, **19**, 5758-5762.
35. A. Kuczkowski, S. Fahrenholz, S. Schulz and M. Nieger, *Organometallics*, 2004, **23**, 3615-3621.
36. A. Kuczkowski, S. Schulz, M. Nieger and P. R. Schreiner, *Organometallics*, 2002, **21**, 1408-1419.
37. P. Pyykkö, *Annu. Rev. Phys. Chem.*, 2012, **63**, 45-64.
38. P. Pyykkö, *Chem. Rev.*, 1988, **88**, 563-594.
39. R. A. Brown and G. R. Dobson, *J. Inorg. Nucl. Chem.*, 1971, **33**, 892-894.
40. H. Schumann and H. J. Breunig, *J. Organomet. Chem.*, 1975, **87**, 83-92.
41. N. J. Holmes, W. Levason and M. Webster, *J. Organomet. Chem.*, 1999, **584**, 179-184.
42. R. Talay and D. Rehder, *Chem. Ber.*, 1978, **111**, 1978-1988.
43. E. O. Fischer and K. Richter, *Chem. Ber.*, 1976, **109**, 1140-1157.
44. P. K. Baker, S. G. Fraser and T. M. Matthews, *Inorg. Chim. Acta*, 1988, **150**, 217-221.
45. P. K. Baker and S. G. Fraser, *J. Coord. Chem.*, 1987, **16**, 97-100.
46. E. Bayram and S. Özkar, *J. Organomet. Chem.*, 2006, **691**, 3267-3273.
47. J. Desnoyers and R. Rivest, *Can. J. Chem.*, 1965, **43**, 1879-1880.
48. H. J. Breunig and U. Gräfe, *Z. Anorg. Allg. Chem.*, 1984, **510**, 104-108.
49. H. Schumann, *J. Organomet. Chem.*, 1987, **323**, 193-197.
50. K. Materne, S. Hoof, N. Frank, C. Herwig and C. Limberg, *Organometallics*, 2017, **36**, 4891-4895.
51. C. Tschersich, B. Braun, C. Herwig and C. Limberg, *J. Organomet. Chem.*, 2015, **784**, 62-68.
52. A. J. Plajer, A. L. Colebatch, F. J. Rizzuto, P. Pröhm, A. D. Bond, R. García-Rodríguez and D. S. Wright, *Angew. Chem. Int. Ed.*, 2018, **57**, 6648-6652.
53. J. Ramler, L. Wüst, A. Rempel, L. Wolz and C. Lichtenberg, *Organometallics*, 2021, **40**, 832-837.
54. T. A. Magee, C. N. Matthews, T. S. Wang and J. H. Wotiz, *J. Am. Chem. Soc.*, 1961, **83**, 3200-3203.
55. D. Benlian and M. Bigorgne, *Bull. Soc. Chim. Fr.*, 1963, 1583.
56. G. Bouquet and M. Birgogne, *Bull. Soc. chim. Fr*, 1962, 433.
57. H. J. Breunig, T. Borrmann, E. Lork, O. Moldovan, C. I. Raț and R. P. Wagner, *J. Organomet. Chem.*, 2009, **694**, 427-432.
58. M. J. Aroney, I. E. Buys, M. S. Davies and T. W. Hambley, *J. Chem. Soc., Dalton Trans.*, 1994, 2827-2834.
59. F. A. Cotton, D. J. Darensbourg and W. H. Ilsley, *Inorg. Chem.*, 1981, **20**, 578-583.
60. N. J. Holmes, W. Levason and M. Webster, *J. Organomet. Chem.*, 1997, **545**, 111-115.
61. K. J. Lee and T. L. Brown, *Inorg. Chem.*, 1992, **31**, 289-294.
62. F. A. Cotton, D. J. Darensbourg and B. W. S. Kolthammer, *Inorg. Chem.*, 1981, **20**, 4440-4442.
63. A. J. Carty, N. J. Taylor, A. W. Coleman and M. F. Lappert, *J. Chem. Soc., Chem. Commun.*, 1979, 639-640.
64. S. Schulz, A. Kuczkowski, D. Bläser, C. Wölper, G. Jansen and R. Haack, *Organometallics*, 2013, **32**, 5445-5450.
65. L. Bučinský, D. Jayatilaka and S. Grabowsky, *J. Phys. Chem. A*, 2016, **120**, 6650-6669.
66. H. J. Breunig, E. Lork, C. I. Raț and R. P. Wagner, *J. Organomet. Chem.*, 2007, **692**, 3430-3434.
67. E. O. Fischer, W. Bathelt and J. Müller, *Chem. Ber.*, 1971, **104**, 986-992.
68. D. J. Darensbourg and T. L. Brown, *Inorg. Chem.*, 1968, **7**, 959-966.
69. R. A. Brown and G. R. Dobson, *Inorg. Chim. Acta*, 1972, **6**, 65-71.
70. K. Materne, B. Braun-Cula, C. Herwig, N. Frank and C. Limberg, *Chem. Eur. J*, 2017, **23**, 11797-11801.
71. E. Becker, C. Slugovc, E. Rüba, C. Standfest-Hauser, K. Mereiter, R. Schmid and K. Kirchner, *J. Organomet. Chem.*, 2002, **649**, 55-63.
72. J. Ramler, K. Hofmann and C. Lichtenberg, *Inorg. Chem.*, 2020, **59**, 3367-3376.
73. C. Tschersich, S. Hoof, N. Frank, C. Herwig and C. Limberg, *Inorg. Chem.*, 2016, **55**, 1837-1842.
74. C. Lichtenberg, *Chem. Commun.*, 2021, DOI: doi.org/10.1039/D1CC01284C.
75. C. Silvestru, H. J. Breunig and H. Althaus, *Chem. Rev.*, 1999, **99**, 3277-3328.
76. S. L. Benjamin, W. Levason, G. Reid, M. C. Rogers and R. P. Warr, *J. Organomet. Chem.*, 2012, **708**, 106-111.
77. S. C. James, N. C. Norman and A. G. Orpen, *J. Chem. Soc., Dalton Trans.*, 1999, 2837-2843.
78. B. Ritschel, J. Poater, H. Dengel, F. M. Bickelhaupt and C. Lichtenberg, *Angew. Chem. Int. Ed.*, 2018, **57**, 3825-3829.
79. W. Frank, V. Reiland and G. J. Reiß, *Angew. Chem. Int. Ed.*, 1998, **37**, 2983-2985.
80. I. I. Ozturk, C. N. Banti, S. K. Hadjikakou, N. Panagiotou and A. J. Tasiopoulos, *Inorg. Chim. Acta*, 2019, **497**, 119094.

81. X.-H. Zhu, N. Mercier, P. Frère, P. Blanchard, J. Roncali, M. Allain, C. Pasquier and A. Riou, *Inorg. Chem.*, 2003, **42**, 5330-5339.
82. J. Ramler and C. Lichtenberg, *Chem. Eur. J*, 2020, **26**, 10250-10258.
83. J. Bauer, H. Braunschweig and R. D. Dewhurst, *Chem. Rev.*, 2012, **112**, 4329-4346.
84. C. Tschersich, C. Limberg, S. Roggan, C. Herwig, N. Ernsting, S. Kovalenko and S. Mebs, *Angew. Chem. Int. Ed.*, 2012, **51**, 4989-4992.
85. T.-P. Lin, I.-S. Ke and F. P. Gabbaï, *Angew. Chem. Int. Ed.*, 2012, **51**, 4985-4988.
86. C. Tschersich, B. Braun, C. Herwig and C. Limberg, *Organometallics*, 2015, **34**, 3782-3787.
87. J. Ramler, K. Radacki, J. Abbenseth and C. Lichtenberg, *Dalton Trans.*, 2020, **49**, 9024-9034.
88. Cluster compounds and compounds, in which the bismuth center bears a vacant 6s orbital are not covered in this contribution.
89. W. Clegg, N. A. Compton, R. J. Errington, N. C. Norman, A. J. Tucker and M. J. Winter, *J. Chem. Soc., Dalton Trans.*, 1988, 2941-2951.
90. W. Clegg, N. A. Compton, R. J. Errington and N. C. Norman, *J. Chem. Soc., Dalton Trans.*, 1988, 1671-1678.
91. J. M. Wallis, G. Müller and H. Schmidbaur, *J. Organomet. Chem.*, 1987, **325**, 159-168.
92. J. Ramler, I. Krummenacher and C. Lichtenberg, *Angew. Chem. Int. Ed.*, 2019, **58**, 12924-12929.
93. J. M. Cassidy and K. H. Whitmire, *Inorg. Chem.*, 1991, **30**, 2788-2795.
94. W. Clegg, N. A. Compton, R. J. Errington, D. C. R. Hockless, N. C. Norman, M. Ramshaw and P. M. Webster, *J. Chem. Soc., Dalton Trans.*, 1990, 2375-2385.
95. N. C. Norman, N. L. Pickett, W. D. Storr, N. M. Boag and A. J. Goodby, *Polyhedron*, 1994, **13**, 2525-2530.
96. J. M. Wallis, G. Mueller and H. Schmidbaur, *Inorg. Chem.*, 1987, **26**, 458-459.
97. R. J. Errington, L. J. Farrugia, G. A. Fisher, A. Niklaus and N. C. Norman, *J. Chem. Soc., Dalton Trans.*, 1993, 1201-1205.
98. A. J. Ashe, J. W. Kampf and D. B. Puranik, *J. Organomet. Chem.*, 1993, **447**, 197-201.
99. G. Linti, W. Köstler and H. Pritzkow, *Eur. J. Inorg. Chem.*, 2002, 2643-2647.
100. P. Panster and W. Malisch, *J. Organomet. Chem.*, 1977, **134**, C32-C36.
101. S. Roggan, G. Schnakenburg, C. Limberg, S. Sandhöfner, H. Pritzkow and B. Ziemer, *Chem. Eur. J*, 2005, **11**, 225-234.
102. M. Hunger, C. Limberg, E. Kaifer and P. Rutsch, *J. Organomet. Chem.*, 2002, **641**, 9-14.
103. S. Roggan, C. Limberg, B. Ziemer and M. Brandt, *Angew. Chem. Int. Ed.*, 2004, **43**, 2846-2849.
104. R. Schiwon, C. Knispel and C. Limberg, *Organometallics*, 2010, **29**, 1670-1674.
105. R. Schiwon, B. Braun, R. Metzinger and C. Limberg, *Z. Anorg. Allg. Chem.*, 2016, **642**, 1198-1206.
106. R. Schiwon, R. Metzinger, C. Pfirrmann and C. Limberg, *Z. Naturforsch. B*, 2013, **68**, 561-568.
107. F. Calderazzo, A. Juris, R. Poli and F. Ungari, *Inorg. Chem.*, 1991, **30**, 1274-1279.
108. F. Calderazzo, R. Poli and G. Pelizzi, *J. Chem. Soc., Dalton Trans.*, 1984, 2535-2540.
109. G. Etzrodt, R. B. Und and G. Schmid, *Chem. Ber.*, 1979, **112**, 2574-2580.
110. K. Wójcik, P. Ecorchard, D. Schaarschmidt, T. Rüffer, H. Lang and M. Mehring, *Z. Anorg. Allg. Chem.*, 2012, **638**, 1723-1730.
111. W. R. Cullen, D. J. Patmore, J. R. Sams, M. J. Newlands and L. K. Thompson, *J. Chem. Soc., Chem. Commun.*, 1971, 952-953.
112. T. Gröer and M. Scheer, *J. Chem. Soc., Dalton Trans.*, 2000, 647-653.
113. R. Schiwon, F. Schax, B. Braun and C. Limberg, *J. Organomet. Chem.*, 2016, **821**, 71-77.
114. H. Braunschweig, P. Brenner, P. Cogswell, K. Kraft and K. Schwab, *Chem. Commun.*, 2010, **46**, 7894-7896.
115. S. Shimada, X.-B. Wang and M. Tanaka, *Chem. Commun.*, 2020, **56**, 15216-15219.
116. D. Fenske, A. Rothenberger and S. Wieber, *Z. Anorg. Allg. Chem.*, 2003, **629**, 929-930.
117. S. J. Davies, N. A. Compton, G. Huttner, L. Zsolnai and S. E. Garner, *Chem. Ber.*, 1991, **124**, 2731-2738.
118. J. Von Seyerl and G. Huttner, *J. Organomet. Chem.*, 1980, **195**, 207-212.
119. A. M. Caminade, M. Veith, V. Huch and W. Malisch, *Organometallics*, 1990, **9**, 1798-1802.
120. H.-A. Kaul, D. Greissinger, M. Luksza and W. Malisch, *J. Organomet. Chem.*, 1982, **228**, C29-C35.
121. G. I. Nikonov, D. A. Lemenovskii and J. Lorberth, *Polyhedron*, 1996, **15**, 1565-1566.
122. A. Sobolev, I. Romm and N. G. Ko, *Koord. Khim*, 1980, **6**, 945.
123. D. M. Hawley and G. Ferguson, *J. Chem. Soc. A*, 1968, 2059-2063.
124. J. S. Leigh and K. H. Whitmire, *Angew. Chem. Int. Ed.*, 1988, **27**, 396-398.
125. S. Martinengo, A. Fumagalli, G. Ciani and M. Moret, *J. Organomet. Chem.*, 1988, **347**, 413-422.
126. C. J. Carmalt, L. J. Farrugia, N. C. Norman and S. Sunley, *Inorg. Chim. Acta*, 1995, **234**, 189-193.
127. R. E. Bachman and K. H. Whitmire, *Inorg. Chem.*, 1995, **34**, 1542-1551.
128. R. D. Adams and W. C. Pearl, *J. Organomet. Chem.*, 2010, **695**, 937-940.
129. An interpretation in which $[Bi(Co(CO)_4)_3]$ acts as an L-type ligand towards $[Co(CO)_4]^-$ has not been discussed in detail.
130. M. Rowen Churchill, J. C. Fettinger, K. H. Whitmire and C. B. Lagrone, *J. Organomet. Chem.*, 1986, **303**, 99-109.
131. R. Hillwig, F. Kunkel, K. Harms, B. Neumüller and K. Dehnicke, *Z. Naturforsch. B*, 1997, **52**, 149-152.
132. J. P. H. Charmant, A. G. Orpen, S. C. James, N. C. Norman and J. Starbuck, *Acta Cryst. E*, 2002, **58**, m488-m489.
133. C. J. Carmalt, L. J. Farrugia and N. C. Norman, *J. Chem. Soc., Dalton Trans.*, 1996, 443-454.
134. The larger coordination number and the anionic character of $[BiPh_2(Cr(CO)_5)_2]^-$ can also be put forward as arguments for the Bi–Cr bonds in this compound being longer than that in $[Cr(CO)_5(BiPh_3)]$.
135. W. Clegg, N. A. Compton, R. J. Errington, G. A. Fisher, D. C. R. Hockless, N. C. Norman, A. G. Orpen and S. E. Stratford, *J. Chem. Soc., Dalton Trans.*, 1992, 3515-3523.
136. W. Clegg, N. A. Compton, R. J. Errington, G. A. Fisher, D. C. R. Hockless, N. C. Norman and A. G. Orpen, *Polyhedron*, 1991, **10**, 123-126.

137. C. J. Carmalt, L. J. Farrugia and N. C. Norman, *J. Chem. Soc., Dalton Trans.*, 1996, 455-459.
138. W. Clegg, N. A. Compton, R. J. Errington, G. A. Fisher, N. C. Norman and N. Wishart, *J. Organomet. Chem.*, 1990, **399**, C21-C25.
139. W. Clegg, N. A. Compton, R. J. Errington, G. A. Fisher, D. C. R. Hockless, N. C. Norman, N. A. L. Williams, S. E. Stratford, S. J. Nichols, P. S. Jarrett and A. G. Orpen, *J. Chem. Soc., Dalton Trans.*, 1992, 193-201.
140. W. Clegg, N. A. Compton, R. J. Errington and N. C. Norman, *J. Organomet. Chem.*, 1987, **335**, C1-C5.
141. T. Gröer and M. Scheer, *Organometallics*, 2000, **19**, 3683-3691.
142. A. M. Toma, C. I. Raţ, O. D. Pavel, C. Hardacre, T. Rüffer, H. Lang, M. Mehring, A. Silvestru and V. I. Pârvulescu, *Catal. Sci. Technol.*, 2017, **7**, 5343-5353.
143. J. Ramler, I. Krummenacher and C. Lichtenberg, *Chem. Eur. J*, 2020, **26**, 14551-14555.
144. K. K. Pandey, P. Patidar and P. Tiwari, *Polyhedron*, 2012, **34**, 84-91.
145. K. K. Pandey, *Comput. Theor. Chem.*, 2011, **967**, 140-146.
146. I. Wender and P. Pino, *Organic syntheses via metal carbonyls*, Interscience Publishers, New York, 1968.
147. For additional examples of compounds with bismolyl groups in a η^5-coordination mode that have been accessed in salt elimination protocols see: a) A. J. Ashe III, S. Al-Ahmad, S. Pilotek and D. B. Puranik, *Organometallics*, 1995, **14**, 2689; b) A. J. Ashe III, J. W. Kampf, D. B. Puranik and S. M. Al-Taweel, *Organometallics*, 1992, **11**, 2743–2745.
148. N. A. Compton, R. J. Errington, G. A. Fisher, N. C. Norman, P. M. Webster, P. S. Jarrett, S. J. Nicholls, A. G. Orpen, S. E. Stratford and N. A. L. Williams, *J. Chem. Soc., Dalton Trans.*, 1991, 669-676.
149. C. Knispel, C. Limberg and M. Mehring, *Organometallics*, 2009, **28**, 646-651.
150. C. Knispel, C. Limberg and C. Tschersich, *Chem. Commun.*, 2011, **47**, 10794-10796.
151. E. V. Dikarev, T. G. Gray and B. Li, *Angew. Chem.*, 2005, **44**, 1721-1724.
152. E. V. Dikarev, B. Li, A. Y. Rogachev, H. Zhang and M. A. Petrukhina, *Organometallics*, 2008, **27**, 3728-3735.
153. E. V. Dikarev, B. Li and H. Zhang, *J. Am. Chem. Soc.*, 2006, **128**, 2814-2815.
154. T. L. Sunderland and J. F. Berry, *J. Chem. Soc., Dalton Trans.*, 2016, **45**, 50-55.
155. J. Hansen, B. Li, E. Dikarev, J. Autschbach and H. M. L. Davies, *J. Org. Chem.*, 2009, **74**, 6564-6571.
156. L. R. Collins, M. van Gastel, F. Neese and A. Fürstner, *J. Am. Chem. Soc.*, 2018, **140**, 13042-13055.
157. L. R. Collins, S. Auris, R. Goddard and A. Fürstner, *Angew. Chem. Int. Ed.*, 2019, **58**, 3557-3561.
158. For further examples of bismuth atoms influencing substrate binding without direct bismuth-substrate interactions see: a) A. J. Plajer, A. L. Colebatch, F. J. Rizzuto, P. Pröhm, A. D. Bond, R. García-Rodríguez and D. S. Wright, *Angew. Chem. Int. Ed.*, 2018, **57**, 6648-6652; b) J. Ramler, L. Wüst, A. Rempel, L. Wolz and C. Lichtenberg, *Organometallics*, 2021, **40**, 832-837.
159. T. Yoshida, H. M. Ahsan, H.-T. Zhang, D. C. Izuogu, H. Abe, H. Ohtsu, T. Yamaguchi, B. K. Breedlove, A. J. W. Thom and M. Yamashita, *J. Chem. Soc., Dalton Trans.*, 2020, **49**, 2652-2660.
160. C. Lichtenberg, *Chem. Eur. J.*, 2020, **26**, 9674-9687.

III Bismuth Compounds in Radical Catalysis: Transition Metal Bismuthanes Facilitate Thermally Induced Cyclo-Isomerizations

This chapter was published in: Jacqueline Ramler, Ivo Krummenacher, Crispin Lichtenberg, *Angew. Chem. Int. Ed.* **2019**, *58*, 12924–12929. Reprinted from ref. 72 with permission from 2019 WILEY-VCH Verlag GmbH.

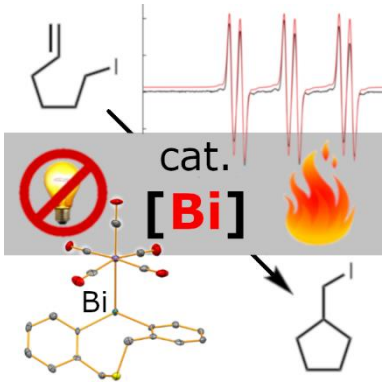

GDCh Communications Angewandte International Edition Chemie

Check for updates

Radical Reactions

International Edition: DOI: 10.1002/anie.201904365
German Edition: DOI: 10.1002/ange.201904365

Bismuth Compounds in Radical Catalysis: Transition Metal Bismuthanes Facilitate Thermally Induced Cycloisomerizations

*Jacqueline Ramler, Ivo Krummenacher, and Crispin Lichtenberg**

Abstract: *The controlled radical chemistry of bismuth compounds is still in its infancy. Further developments are fueled by the properties of these complexes (e.g., low toxicity, high functional group tolerance, low homolytic bond dissociation energies, and reversible homolytic bond dissociations), which are highly attractive for applications in synthetic chemistry. Here we report the first catalytic application of transition metal bismuthanes (i.e. compounds with a Bi–TM bond; TM = transition metal). Using the catalyzed radical cyclo-isomerization of δ-iodo-olefins as a model reaction, characteristics complementary or superior to known B, Mn, Cu, Zn, Sn, and alkali metal reagents are demonstrated (including a different crucial intermediate), establishing transition metal bismuthanes as a new class of (pre-)catalysts for controlled radical reactions.*

Complexes based on the heavy main group element bismuth have been associated with low homolytic bond dissociation energies of Bi–X bonds (X = H, alkyl, allyl, aryloxide, amide).[1–5] This is due to i) an inefficient orbital overlap of the substituents with large and diffuse bismuth-centered orbitals, ii) a relatively low polarity of the Bi–X bond, and iii) a stabilization of bismuth-centered radical species by relativistic effects.[6] Such homolytic bond dissociations have been exploited in synthetic chemistry, polymerization catalysis, and materials science. Examples include the synthesis of dibismuthanes $[Bi(aryl)_2]_2$ in dehydrogenative coupling reactions from in situ generated $HBi(aryl)_2$,[1a,b] the polymerization of activated olefins,[2] and the deposition of thin films of BiO_x and strontium bismuth tantalate in metal-organic chemical vapor deposition.[1c,d]

Reactive radical species that are generated in the course of such reactions can be extremely difficult or even impossible to detect experimentally. Hence, their existence was often suggested merely based on the analysis of stable diamagnetic products.[2,4,7] Only recently, the first examples of well-defined persistent[8] or even isolable bismuth radical compounds have been reported.[9–11] To date, the only catalytic application of an isolable bismuth radical is the dehydrogenative coupling of $SiPhH_3$ with TEMPO to give $SiPhH_2$(TEMPO) (TEMPO = tetramethylpiperidinyl-*N*-oxide).[12,13] While of great fundamental significance, the bismuth radical showed a low catalytic activity (75 % conversion after 15 d)[14] and the use of the isolable radical TEMPO as a substrate was necessary to facilitate the reaction.

In the context of controlled radical reactions, we became interested in transition metal bismuthanes, that is molecules containing the structural motif R_2Bi–[TM] ([TM] = transition metal complex fragment). This large class of compounds shows a broadly tunable set of properties—an ideal setting for catalytic applications.[15–17] However, the stoichiometric or even catalytic reactivity of Bi–[TM] bonds towards organic substrates is largely unexplored. Using the radical cyclo-isomerization of 6-iodo-1-hexene as a model reaction, we demonstrate here the first catalytic version of this reaction under thermal conditions, revealing the great potential of transition metal bismuthanes to be exploited as a new class of readily tunable catalysts in controlled radical reactions.

Starting from the diaryl bismuth chloride [Bi-{$(C_6H_4CH_2)_2S$}Cl] (**1**)[19] a series of closely related transition metal bismuthanes **2**–**4** was synthesized and isolated in 73–80 % yield (Scheme 1). According to single-crystal X-ray

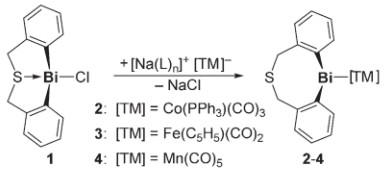

Scheme 1. Synthesis of transition metal bismuthanes **2**–**4**. Compound **2** was synthesized from **1** and $Na[Co(CO)_4]$ in the presence of PPh_3. L = thf.

diffraction analyses,[47] **2**–**4** possess typical molecular structures in the solid state without directed intermolecular interactions (**4** is exemplarily shown in Scheme 2; for details see Supporting Information). The transition metal atoms are found in distorted tetrahedral (**3**), trigonal bipyramidal (**2**; Bi1 and P1 in the axial positions; $\tau_5 = 0.91$), and octahedral (**4**) coordination geometries, respectively. The Bi–C (2.27–2.29 Å) and Bi–TM bond lengths (TM = Co, Fe, Mn: 2.70, 2.69, 2.86 Å) are in the expected ranges.[15–18] Importantly, in all cases, the thioether functionality does not interact with the bismuth center. This type of interaction is observed when the bismuth atom in such complexes is part of a $Bi^{\delta+}$–$X^{\delta-}$ bond which is polarized towards X (e.g. X = Cl, Br, I, NO_3, O_3SCF_3).[19] Thus, the absence of Lewis acid/base interactions between the bismuth atom and the thioether group is a first hint towards non- or only weakly polarized Bi–TM bonds in compounds **2**–**4**.

[*] J. Ramler, Dr. I. Krummenacher, Dr. C. Lichtenberg
Institute of Inorganic Chemistry
Julius-Maximilians-University Würzburg
Am Hubland, 97074 Würzburg (Germany)
E-mail: crispin.lichtenberg@uni-wuerzburg.de
Supporting information and the ORCID identification number(s) for the author(s) of this article can be found under: https://doi.org/10.1002/anie.201904365.

GDCh Communications Angewandte International Edition Chemie

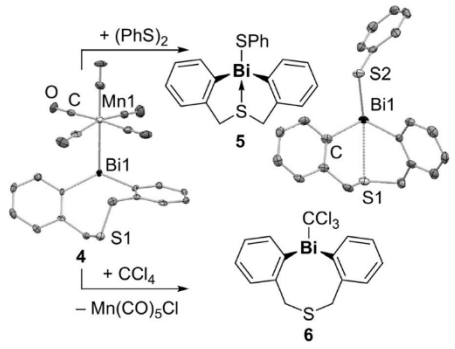

Scheme 2. Reactions of $[Bi\{(C_6H_4CH_2)_2S\}(Mn(CO)_5)]$ (**4**) with $(PhS)_2$ and CCl_4 to give $[Bi\{(C_6H_4CH_2)_2S\}(SPh)]$ (**5**) and $[Bi\{(C_6H_4CH_2)_2S\}(CCl_3)]$ (**6**), respectively. Molecular structures of **4** and **5** in the solid state: selected bond lengths [Å]: Compound **4**: Bi1–Mn1 2.8576(8), Bi1–C 2.275(5)–2.277(5), Mn1–CO(*cis*) 1.844(6)–1.871(6), Mn1–CO(*trans*) 1.818(6); C-Bi1-C 105.56(18), Mn1-Bi1-C 96.73(12)–101.12(12), Bi1-Mn1-CO(*trans*) 176.77(17), Bi1-Mn1-CO(*cis*) 82.19(16)–88.37(15). Compound **5**: Bi1–C 2.254(5)–2.287(5), Bi1–S1 2.9401(15), Bi1–S2 2.6149(16).

Compounds **2**–**4** were analyzed by solution IR spectroscopy. In particular, the CO stretching frequencies were used as a tool for the experimental approximation of the partial charge at the transition metal centers. Thus, the CO stretching frequencies of **2**–**4** were compared to those of $[TM]^{\delta+}$–Cl/Br, $[TM]_2$, and $[Cat]$–$[TM]^{\delta-}$ ($[TM] = Co(CO)_3(PPh_3)$, $Fe(C_5H_5)(CO)_2$, $Mn(CO)_5$; Cat = countercation). This comparison is visualized for the relevant iron compounds in Figure 1.[20,21] Accordingly, the Bi–Fe bond in **3** and the Bi–Mn bond in **4** are essentially non-polar or very weakly polarized, whereas for the Bi–Co bond in **2**, the data analysis only allowed one to rule out a polarization towards Co (for details see Supporting Information).

The reactivity of compound **4** towards the radical scavengers diphenyldisulfide and CCl_4 was investigated (Scheme 2 and Supporting Information). Reactions of **4** with 1 equiv of $(PhS)_2$ resulted in the formation of $[Bi\{(C_6H_4CH_2)_2S\}(SPh)]$ (**6**) in 94% spectroscopic yield, which was isolated and fully characterized. Single-crystal X-ray analysis confirmed an S1→Bi1 donor/acceptor interaction as a result of the polarized $Bi1^{\delta+}$–$S2^{\delta-}$ bond (vide supra; for details see Supporting Information).[47] Reactions of **4** with CCl_4 gave $Mn(CO)_5Cl$ and $[Mn(CO)_4Cl]_2$ (identified by comparison of IR spectra and single-crystal XRD data with the literature data) along with $[Bi\{(C_6H_4CH_2)_2S\}(CCl_3)]$ (**6**) (identified by NMR spectroscopy and HRMS analysis). These results suggest that **4** undergoes radical reactions with suitable substrates.

The cyclo-isomerization of 6-iodo-1-hexene and related compounds is a powerful tool for the synthesis of cyclo-pentane structural motifs while

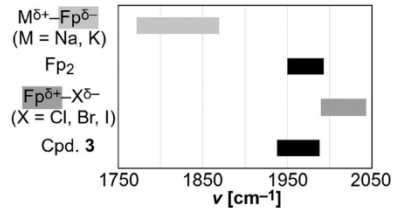

Figure 1. CO stretching frequencies of compounds Fp–E (Fp = Fe-$(C_5H_5)(CO)_2$), where E is an electropositive or electronegative binding partner, another Fp moiety,[21] or a bismuthyl group.

preserving the synthetically valuable iodo functionality (see reaction in Table 1).[22,23] From a mechanistic point of view, radical and polar reaction pathways have been suggested, depending on the reagents used (vide infra). Importantly, the substitution pattern at the substrate also crucially influences the feasibility and mechanistic pathways of this reaction. For the parent substrate, 6-iodo-1-hexene (**S1**), a limited number of protocols is available for the cyclo-isomerization to give iodo-methyl-cyclopentane (**P1**). One stoichiometric reaction relies on Zn and I_2 (along with small amounts of O_2) and proceeds via a radical pathway.[24] A catalytic version was realized with strongly basic/nucleophilic organolithium compounds and most likely proceeds via a polar reaction mechanism.[25a] A catalyzed radical reaction can be considered a standard protocol and is based on toxic organotin species $[SnR_3]_2$.[5,24a,26,27] Photochemical conditions (e.g.: 275 W sunlamp) are necessary to facilitate these reactions. In contrast, there are no reports of the thermally induced

Table 1: Potential catalysts for the radical cyclo-isomerization of **S1** to give **P1**.

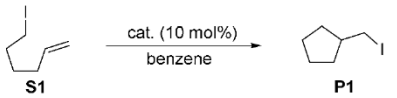

Entry	Catalyst	Conditions	Yield[a]
1	$[Sn(nBu)_3]_2$	20 °C, 1.25 h, h·v[b]	90
2	$[Sn(nBu)_3]_2$	20 °C, 1.0 h, h·v[c]	2
3	$[Sn(nBu)_3]_2$	60 °C, 20 h[d]	<1
4	AIBN	60 °C, 20 h[d]	10
5[e]	CuCl, 2,2′-bipy	60 °C, 20 h[d]	<1
6[e]	CuI, 2,2′-bipy	60 °C, 20 h[d]	<1
7	$[Mn(CO)_5]_2$	60 °C, 20 h[d]	17
8	$[Mn(CO)_5]_2$	60 °C, 20 h[f]	<1
9[g]	BEt_3 (solvent: H_2O)	23 °C, 20 h[d,h]	5
10[i]	BEt_3 (solvent: H_2O/MeOH (97:3))	23 °C, 20 h[d,h]	4
11	BEt_3	23 °C, 20 h[d,h,j]	55
12[k]	$[Bi(C_6H_4CH_2)_2S(Co(CO)_3PPh_3)]$ (**2**)	80 °C, 20 h[d]	4
13	$[Bi(C_6H_4CH_2)_2S(Fe(CO)_2(C_5H_5))]$ (**3**)	60 °C, 20 h[d]	24
14	$[Bi(C_6H_4CH_2)_2S(Mn(CO)_5]$ (**4**)	60 °C, 20 h[d]	73
15	$[BiPh_2(Mn(CO)_5)]$ (**7**)	60 °C, 20 h[d]	96

[a] Given in %, determined by ^1H NMR spectroscopy and/or GC/MS. [b] Hg lamp. [c] 400 nm (LED). [d] Ambient light. [e] The same yield of **P1** was obtained with MeCN as the solvent. [f] In the dark. [g] Water was used as the solvent. [h] Traces of O_2. [i] Water/MeOH (97:3) was used as the solvent. [j] 50% yield at 60 °C (Supporting Information). [k] A yield of <1% was detected, when the reaction was run for 20 h at 60 °C.

catalyzed radical cyclo-isomerization of 6-iodo-1-hexene. This would allow the use of substrates with functional groups that do not tolerate strongly basic/nucleophilic conditions and facilitate this reaction under simplified conditions (i.e. without the need for a photochemical apparatus). We set out to validate the catalytic competence of transition metal bismuthanes in the cyclo-isomerization of 6-iodo-1-hexene (**S1**) under thermal conditions. In order to contribute towards a comprehensive understanding of this reaction, we reproduced the results that were previously reported with 10 mol% $[Sn(n\text{Bu})_3]_2$ as a catalyst (photochemical conditions with $\lambda_{max} < 400$ nm),[24] which resulted in the formation of the cyclo-isomerized product **P1** in 90% yield (Table 1, entry 1).[28] When the wavelength of the light source was set to $\lambda_{max} = 400$ nm (light emitting diode, $P = 3$ W), no significant conversion of **S1** was observed (entry 2). Importantly, $[Sn(n\text{Bu})_3]_2$ also failed to catalyze the formation of **P1** under thermal conditions (60 °C, 20 h; entry 3).[29] Common radical sources such as AIBN were also tested as catalysts under thermal conditions, but gave only low conversions (entry 4; AIBN = azo-bis-isobutyronitrile).[30] Simple Cu^I salts in combination with suitable ligand platforms have recently been shown to effectively catalyze the cyclo-isomerization of activated halo-olefins,[22g] but mixtures of CuCl or CuI with 2,2′-bipyridine did not catalyze the cyclo-isomerization of **S1** (entries 5 and 6). Transition metal carbonyl species such as $[Mn(CO)_5]_2$ have been reported as stoichiometric reagents in a hydro-dehalogenative cyclization of **S1**.[31] $[Mn(CO)_5]_2$ also catalyzes related carboacylations of unactivated iodo-olefins, when pressurized with 10 atm of CO.[32] However, both types of transformations require irradiation of the sample with a sunlamp or ambient light. When 10 mol% of $[Mn(CO)_5]_2$ were reacted with **S1** at 60 °C, only a low yield (17%) of the cyclo-isomerization product **P1** was detected in the presence of ambient light, and no conversion was observed when the reaction was performed in the dark (entries 7 and 8). Triethylborane in combination with traces of O_2 has been introduced as a reagent for the cyclo-isomerization of iodo-olefins in water or water/MeOH as the most suitable solvents.[33a,b] So far, activated and secondary iodides have been reported as substrates.[33] Using these standard protocols, BEt_3 did not effectively catalyze the cyclo-isomerization of **S1** (entries 9 and 10). In contrast to previous reports on other substrates, a higher conversion was obtained with benzene as the solvent. In our hands, moderate yields of up to 55% **P1** were obtained, when **S1** was treated with 10 mol% BEt_3 in benzene for 20 h at 23 °C in the presence of traces of O_2 (entry 11). Finally, the transition metal bismuthanes **2**–**4** were tested as catalysts in the cyclo-isomerization of **S1**. Whereas the cobalt species **2** showed low activity, the iron compound **3** and the manganese compound **4** led to yields of 24% and 73%, respectively (entries 12–14). Focusing on manganese bismuthanes as the most active species, the synthesis of literature-known[15a] $[BiPh_2(Mn(CO)_5)]$ (**7**) was improved (see Supporting Information). In the presence of **7** (10 mol%), **S1** smoothly cyclo-isomerized at 60 °C to give **P1** in 96% yield after 20 h (entry 15; for time-conversion-plot see Supporting Information). The differences in the catalytic activity of **2**, **3**, **4**, and **7** were ascribed to the presence/absence of the thioether bridge in the ligand backbone and to the variation of the transition metal complex fragments, each of which may enter different reaction pathways under catalytic conditions (for details see Supporting Informaiton). The high catalytic competence of **7** in *thermally* induced reactions is in stark contrast to the performance of established reagents (Table 1), offering potential to be exploited in orthogonal synthetic strategies and multi-catalysis. These results provide the first examples for the use of well-defined, molecular transition metal bismuthanes, R_2Bi–[TM], as readily accessible and tunable (pre-)catalysts in an organic transformation ([TM] = transition metal complex fragment).

The remarkable activity of **7** as a (pre-)catalyst in the cyclo-isomerization of **S1** under ambient light was maintained, when the reaction was carried out in the dark (Table 2, entries 1 and 2). This is in contrast to the related $[Mn(CO)_5]_2$-catalyzed carboacylations of non-activated iodo-olefins, which require at least ambient light in order reach significant conversion.[32] The catalyst loading could be lowered to 1 mol%, albeit longer reaction times of 66 h were necessary to reach high yields of 86% (entry 3). To gain further insights into the cyclo-isomerization of **S1** catalyzed by compound **7**, the reaction was carried out in a 1:1 stoichiometry at 60 °C. IR spectroscopic analysis of the reaction mixture indicated the presence of the by-product $[MnI(CO)_5]$ (**8**), which could also be isolated and unequivocally identified by single-crystal X-ray analysis and IR spectroscopy of the isolated sample (Table 2). In agreement with these observations, NMR spectroscopic analyses of the reaction mixture revealed the formation of the (alkyl)(diphenyl)bismuth compound $[BiPh_2((CH_2)_4CH{=}CH_2)]$ (**9**) (Table 2).[34] Addition of 9 equiv **S1** followed by heating to 60 °C for 20 h led to formation of **P1** in near-quantitative yield, demonstrating the catalytic competence of the in situ generated species (Table 2). Compound **9** was also detected as an intermediate by NMR spectroscopy under catalytic conditions (see Supporting Information),

Table 2: Cyclo-isomerization of **S1** catalyzed by $[BiPh_2(Mn(CO)_5)]$ (**7**) and related compounds.

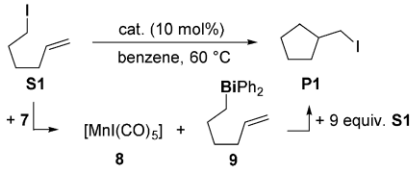

Entry	Catalyst	Conditions	Yield[a] [%]
1	$[BiPh_2(Mn(CO)_5)]$ (**7**)	20 h, ambient light	96
2	$[BiPh_2(Mn(CO)_5)]$ (**7**)	20 h, in the dark	95
3	$[BiPh_2(Mn(CO)_5)]$ (**7**)[b]	56 h, ambient light	86
4	$[MnI(CO)_5]$ (**8**)	20 h, ambient light	7
5	$[Bi((CH_2)_4CH{=}CH_2)_3]$[c]	66 h, ambient light	86
6	$[BiPh_2(Mn(CO)_5)]$ (**7**)	20 h, CCl_4 added	50

[a] Yield of **P1** determined by ^{1}H NMR spectroscopy and/or GC/MS analysis. [b] 1 mol% catalyst was used. [c] $[Bi((CH_2)_4CH{=}CH_2)_3]$ was synthesized via a Mn-free route in 85% purity according to NMR spectroscopic analyses.

demonstrating fundamental differences to related reactions facilitated by tin species under photochemical conditions. The manganese compound **8** was also synthesized via an independent route[35] and tested for its catalytic competence in the cyclo-isomerization reaction, where it led to low conversions of only 7% (entry 4). Attempts to synthesize and isolate **9** via Mn-free routes were unsuccessful so far; however, the structurally related compound $[Bi((CH_2)_4CH{=}CH_2)_3]$ could be obtained in 85% purity by reaction of $BiCl_3$ with in situ generated $[Li(CH_2)_4CH{=}CH_2]$ at −78 °C.[36] Indeed, $[Bi((CH_2)_4CH{=}CH_2)_3]$ showed a significant catalytic activity in the cyclo-isomerization of **S1**, albeit extended reaction times of 66 h were necessary to reach high yields of **P1** (86%; entry 5; cf. entry 3).[37] Thus, the transition metal bismuthane **7** represents a new type of readily available, storable pre-catalyst for the operationally simple generation of bismuth species that are active in the catalyzed cyclo-isomerization of **S1**. The reaction can also be performed on the 1 mmol scale (Supporting Information).

Catalyzed 5-*exo*-trig-cyclizations (such as **S1**→**P1**) may proceed via polar or radical-type pathways, depending on the nature of the substrate, the choice of catalyst, and the reaction conditions. This can have a dramatic influence on the substrate scope and the stereochemical outcome of these reactions. Thus, the cyclo-isomerization of **S1** catalyzed by **7** was carried out in the presence of CCl_4 as a radical scavenger. This led to significantly lower yields of **P1** (50%), suggesting that radical pathways are operative (entry 6 vs. entry 1). To gain direct evidence for radical participation, the cyclo-isomerization of **S1** catalyzed by **7** was performed at 60 °C in the presence of the nitrone **10** as a radical trap and analyzed by EPR spectroscopy at 23 °C. Indeed, an isotropic resonance with $g = 2.006$ and hyperfine couplings of $a(^{14}N) = 41$ MHz, $a(^{1}H) = 8.0$ MHz, and $a(^{13}C) = 15.1$ MHz was detected (Figure 2).[38] These parameters are in good agreement with those expected for radical species **11**,[39,40] indicating the presence of the cyclopentylmethyl radical during cyclo-isomerization of **S1** catalyzed by **7**.

The cyclo-isomerization of 6-iodo-1-heptene (**S2**) gives two diastereomers of **P2**, the *cis*- and *trans*-isomer (Table 3). It has been reported that the diastereoselectivity of this and related cyclizations is significantly affected by the mechanistic pathway that dominates the reaction: whereas polar reactions favor formation of the *trans*-isomer (*cis*/*trans* < 1.0:40),[25b,41–43] the observation of *cis*/*trans* ratios > 2.5:1.0 have been attributed to radical pathways.[24a,44] 10 mol% of **7** smoothly catalyzed the transformation of **S2** into **P2** with > 99% conversion after 3.5 h at 60 °C (Table 3, entry 1). **P2** was formed with a *cis*/*trans* ratio of 3.4:1.0. This is in line with results reported for the same reaction using $[Sn(n\mathrm{Bu})_3]_2$ as a radical catalyst under photochemical conditions,[24a] and thus also points towards **7** operating via radical pathways in this reaction. Polar and strongly basic organometallic compounds such as MeLi or PhLi have been reported to catalyze the cyclo-isomerization of **S1** and **S2**.[25] However, when the allyl ethers **S3** and **S4** were used as substrates, no cyclo-isomerization was observed and compounds $LiO(C_3H_5)$, $CH_2{=}CHR$ (R = H, Me), and MeI/PhI were detected instead (Table 3, entries 2 and 3).[25] These product distributions clearly demonstrate that polar degradation pathways are energetically accessible for **S3** and **S4**. Consequently, these allyl ethers were also tested as substrates towards **7**. Indeed, **S3** and **S4** underwent smooth cyclo-isomerization reactions to give **P3** and **P4** in the presence of 10–20 mol% of compound **7** (Table 3, entries 4 and 5). The slight preference for formation of *cis*-**P4** over *trans*-**P4** (2.7:1.0) is in agreement with a radical intermediate.[44]

Amide functional groups are also tolerated by the transition metal bismuthane (pre-)catalyst, as demonstrated by the smooth quantitative cyclization of **S5** to give pyrrolidinone **P5** within 4.5 h at 60 °C in the presence of 10 mol% **7** (Table 3, entry 6).[45] The more reactive tertiary iodide **S6** cyclo-isomerized to give **P6** in the presence of 10 mol% **7** at ambient temperature in 5 h with a yield of 90% (Table 3, entry 7).[46] Overall, these results further corroborate the applicability of transition metal bismuthane **7** as a (pre)-catalyst in cyclo-isomerization reactions of iodo-olefins, operating via radical pathways.

In conclusion, we have demonstrated that transition metal bismuthanes R_2Bi–[TM] (R = aryl, [TM] = $Fe(C_5H_5)CO_2$,

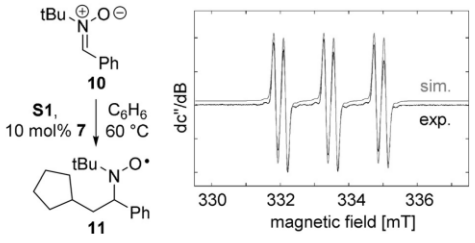

Figure 2. Left: Use of nitrone **10** as a radical trap in the cyclo-isomerization of **S1** catalyzed by **7**. Right: X-band EPR spectrum of **11** in benzene (black = experimental, gray = simulated).

Table 3: Radical cyclo-isomerization catalyzed by **7** (this work) as compared to polar degradation (Bailey et al.).

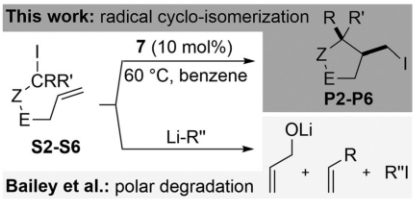

Entry	Substr.	R	R′	Z	E	Li-R″/Cat., Pathway	Yield[a]
1[b]	**S2**	Me	H	CH_2	CH_2	**7, rad. cycl.**	> 99
2[c]	**S3**	H	H	CH_2	O	Li-Me, **polar degr.**	≈ 100
3[d]	**S4**	Me	H	CH_2	O	Li-Ph, **polar degr.**	≈ 100
4[e]	**S3**	H	H	CH_2	O	**7, rad. cycl.**	83
5[f]	**S4**	Me	H	CH_2	O	**7, rad. cycl.**	> 99
6	**S5**	H	H	CO	NC_3H_5	**7, rad. cycl.**	> 95
7[g]	**S6**	Me	Me	CH_2	CH_2	**7, rad. cycl.**	90

[a] yield of **P2–P6** determined by ^{1}H NMR spectroscopy and/or GC/MS analysis. [b] **P2**: *cis*/*trans* = 3.4:1.0. [c] R″ = Me, Ref. [25]. [d] R″ = Ph, Ref. [25]. [e] 20 mol% catalyst. [f] **P4**: *cis*/*trans* = 2.7:1.0. [g] *T* = 23 °C.

$Mn(CO)_5$) undergo highly selective radical reactions. Proof of principle was delivered using the catalyzed cyclo-isomerization of δ-iodo-olefins as a model reaction. For the first time, this catalyzed radical reaction of the parent substrate (6-iodo-1-hexene) was achieved under thermal conditions. This is the first example of transition metal bismuthanes acting as highly selective radical (pre-)catalysts in organic reactions. Thereby, this class of compounds is established as a new type of (pre)-catalyst for radical transformations, with properties complementary or superior to Cu, Zn, Sn, and alkali metal reagents.

Acknowledgements

The authors thank Dr. R. D. Dewhurst for helpful discussions, Prof. H. Braunschweig for continuous support, as well as the FCI (Liebig fellowship) and the DFG for generous financial support.

Conflict of interest

The authors declare no conflict of interest.

Keywords: bismuth · catalysis · cyclo-isomerizations · radical reactions · transition metal bismuthanes

How to cite: *Angew. Chem. Int. Ed.* **2019**, *58*, 12924–12929
Angew. Chem. **2019**, *131*, 13056–13062

[1] a) L. Balázs, H. J. Breunig, E. Lork, *Z. Naturforsch. B* **2005**, *60*, 180–182; b) G. Balázs, L. Balázs, H. J. Breunig, E. Lork, *Organometallics* **2003**, *22*, 2919; c) J.-Y. Hyeon, M. Lisker, M. Silinskas, E. Burte, F. T. Edelmann, *Chem. Vap. Deposition* **2005**, *11*, 213–218; d) M. Vehkamäki, T. Hatanpää, M. Titala, M. Leskelä, *J. Mater. Chem.* **2004**, *14*, 3191–3197.

[2] a) S. Yamago, E. Kayahara, M. Kotani, B. Ray, Y. Kwak, A. Goto, T. Fukuda, *Angew. Chem. Int. Ed.* **2007**, *46*, 1304–1306; *Angew. Chem.* **2007**, *119*, 1326–1328; b) C. Lichtenberg, F. Pan, T. P. Spaniol, U. Englert, J. Okuda, *Angew. Chem. Int. Ed.* **2012**, *51*, 13011–13015; *Angew. Chem.* **2012**, *124*, 13186–13190.

[3] T. A. Hanna, A. L. Rieger, P. H. Rieger, X. Wang, *Inorg. Chem.* **2002**, *41*, 3590–3592.

[4] a) I. J. Casely, J. W. Ziller, M. Fang, F. Furche, W. J. Evans, *J. Am. Chem. Soc.* **2011**, *133*, 5244–5247; b) C. Hering-Junghans, A. Schulz, M. Thomas, A. Villinger, *Dalton Trans.* **2016**, *45*, 6053–6059; c) C. Knispel, C. Limberg, C. Tschersich, *Chem. Commun.* **2011**, *47*, 10794–10796.

[5] The toxicity of bismuth compounds has been reported to be typically low, especially when compared to related Sn, Pb, Sb, or Te species. For example: J. M. Bothwell, S. W. Krabbe, R. S. Mohan, *Chem. Soc. Rev.* **2011**, *40*, 4649–4707, and references therein.

[6] P. Pyykkö, *Chem. Rev.* **1988**, *88*, 563–594.

[7] A low-valent bismuth compound has been generated in situ, suggested to have biradical character based on CASSCF calculations, and trapped by reaction with an alkyne: J. Bresien, A. Hinz, A. Schulz, A. Villinger, *Dalton Trans.* **2018**, *47*, 4433–4436.

[8] S. Ishida, F. Hirakawa, K. Furukawa, K. Yoza, T. Iwamoto, *Angew. Chem. Int. Ed.* **2014**, *53*, 11172–11176; *Angew. Chem.* **2014**, *126*, 11354–11358.

[9] a) R. J. Schwamm, J. R. Harmer, M. Lein, C. M. Fitchett, S. Gramville, M. P. Coles, *Angew. Chem. Int. Ed.* **2015**, *54*, 10630–10633; *Angew. Chem.* **2015**, *127*, 10776–10779; b) C. Ganesamoorthy, C. Helling, C. Wölper, W. Frank, E. Bill, G. E. Cutsail III, S. Schulz, *Nat. Commun.* **2018**, *9*, 87.

[10] C. Lichtenberg, *Angew. Chem. Int. Ed.* **2016**, *55*, 484–486; *Angew. Chem.* **2016**, *128*, 494–496.

[11] For reversible electron transfer at Bi see: J. Ramler, J. Poater, F. Hirsch, B. Ritschel, I. Fischer, F. M. Bickelhaupt, C. Lichtenberg, *Chem. Sci.* **2019**, *10*, 4169–4176.

[12] R. J. Schwamm, M. Lein, M. P. Coles, C. M. Fitchett, *Chem. Commun.* **2018**, *54*, 916–919.

[13] For stoichiometric reactivity studies with bismuth radicals see: a) R. J. Schwamm, M. Lein, M. P. Coles, C. M. Fitchett, *J. Am. Chem. Soc.* **2017**, *139*, 16490–16493; b) R. J. Schwamm, M. Lein, M. P. Coles, C. M. Fitchett, *Angew. Chem. Int. Ed.* **2016**, *55*, 14798–14801; *Angew. Chem.* **2016**, *128*, 15018–15021.

[14] D. J. Liptrot, M. S. Hill, M. F. Mahon, *Angew. Chem. Int. Ed.* **2014**, *53*, 6224–6227; *Angew. Chem.* **2014**, *126*, 6338–6341.

[15] Selected examples of compounds with Bi^{III}–Mn bonds: a) J. M. Cassidy, K. H. Whitmire, *Inorg. Chem.* **1991**, *30*, 2788–2795; b) A. J. Ashe III, J. W. Kampf, D. B. Puranik, *J. Organomet. Chem.* **1993**, *447*, 197–201; c) N. A. Compton, R. J. Errington, G. A. Fisher, N. C. Norman, P. M. Webster, P. S. Jarrett, S. J. Nicholls, A. G. Orpen, S. E. Stratford, N. A. L. Williams, *J. Chem. Soc. Dalton Trans.* **1991**, 669–676; d) J. M. Wallis, G. Müller, H. Schmidbaur, *Inorg. Chem.* **1987**, *26*, 458–459.

[16] Selected examples of compounds with Bi^{III}–Fe bonds: a) R. E. Bachmann, K. H. Whitmire, *Inorg. Chem.* **1995**, *34*, 1542–1551; b) J. M. Wallis, G. Müller, H. Schmidbaur, *J. Organomet. Chem.* **1987**, *325*, 159–168; c) M. Shieh, Y. Liou, M.-H. Hsu, R.-T. Chen, S.-J. Yeh, S.-M. Peng, G.-H. Lee, *Angew. Chem. Int. Ed.* **2002**, *41*, 2384–2386; *Angew. Chem.* **2002**, *114*, 2490–2492; d) R. Schiwon, R. Metzinger, C. Pfirrmann, C. Limberg, *Z. Naturforsch. B* **2013**, *68*, 561–568; e) T. Gröer, M. Scheer, *J. Chem. Soc. Dalton Trans.* **2000**, 647–653; f) T. Gröer, M. Scheer, *Organometallics* **2000**, *19*, 3683–3691; g) R. Schiwon, F. Schax, B. Braun, C. Limberg, *J. Organomet. Chem.* **2016**, *821*, 71–77; h) R. Schiwon, B. Braun, R. Methinger, C. Limberg, *Z. Anorg. Allg. Chem.* **2016**, *642*, 1198–1206; i) G. Bendt, R. Schiwon, S. Salamon, J. Landers, U. Hagemann, C. Limberg, H. Wende, S. Schulz, *Inorg. Chem.* **2016**, *55*, 7542–7549.

[17] Selected examples of compounds with Bi^{III}–Co bonds: a) F. Calderazzo, R. Poli, G. Pelizzi, *J. Chem. Soc. Dalton Trans.* **1984**, 2535–2540; b) S. Martinengo, G. Ciani, *J. Chem. Soc. Chem. Commun.* **1987**, 1589–1591; c) G. Ciani, M. Moret, A. Fumagalli, S. Martinengo, *J. Organomet. Chem.* **1989**, *362*, 291–296; d) also see Ref. [16f].

[18] Compounds of the general formula $[R_2BiFe(C_5H_5)(CO)_2]$ (R = aryl, alkyl) have not been structurally characterized. The Bi–Fe bond length in **3** (2.69 Å) is similar to that in $[Bi(Fe(C_5H_5)(CO)_2)_3]$ (2.72 Å); see Ref. [16e].

[19] a) R. Qiu, S. Yin, X. Zhang, J. Xia, X. Xu, S. Luo, *Chem. Commun.* **2009**, 4759–4761; b) X.-W. Zhang, J. Xia, H.-W. Yan, S.-L. Luo, S.-F. Yin, C.-T. Au, W.-Y. Wong, *J. Organomet. Chem.* **2009**, *694*, 3019–3026; c) A. Toma, C. I. Raţ, A. Silvestru, T. Rüffer, H. Lang, M. Mehring, *J. Organomet. Chem.* **2016**, *806*, 5–11.

[20] a) A. R. Manning, *J. Chem. Soc. A* **1968**, 1319–1324; b) X. Jiang, L. Chen, X. Wang, L. Long, Z. Xiao, X. Liu, *Chem. Eur. J.* **2015**, *21*, 13065–13072; c) K. Inkrott, R. Goetze, S. G. Shore, *J. Organomet. Chem.* **1978**, *154*, 337–342; d) K. H. Pannell, D. Jackson, *J. Am. Chem. Soc.* **1976**, *98*, 4443–4446.

[21] In the discussion of $[Fe(C_5H_5)(CO)_2]_2$, IR spectroscopic data ascribed to the isomer without bridging CO ligands has been used (see Ref. [20]).

[22] a) D. P. Curran, *Synthesis* **1988**, 417 – 439; b) P. A. Baguley, J. C. Walton, *Angew. Chem. Int. Ed.* **1998**, *37*, 3072 – 3082; *Angew. Chem.* **1998**, *110*, 3272 – 3283; c) K. C. Majumdar, G. V. Karunakar, B. Sinha, *Synthesis* **2012**, *44*, 2475 – 2505; d) K. C. Majumdar, P. K. Basu, P. P. Mukhopadhyay, *Tetrahedron* **2005**, *61*, 10603 – 10642; e) B. Giese, B. Kopping, T. Göbel, J. Dickhaut, G. Thoma, K. J. Kulicke, F. Trach, *Org. React.* **1996**, *48*, 301 – 856; f) G. J. Rowlands, *Tetrahedron* **2010**, *66*, 1593 – 1636; g) A. J. Clark, *Chem. Soc. Rev.* **2002**, *31*, 1 – 11.

[23] For the related, stoichiometric radical cyclo-isomerization of δ-alkoxyamino-olefins see: K. Molawi, T. Schulte, K. O. Sigenthaler, C. Wetter, A. Studer, *Chem. Eur. J.* **2005**, *11*, 2335 – 2350.

[24] a) T. Cohen, H. Gibney, R. Ivanov, E. A.-H. Yeh, I. Marek, D. P. Curran, *J. Am. Chem. Soc.* **2007**, *129*, 15405 – 15409; b) C. Meyer, I. Marek, G. Courtemanche, J.-F. Normant, *Synlett* **1993**, 266 – 268; c) C. Meyer, I. Marek, G. Courtemanche, J.-F. Normant, *Tetrahedron Lett.* **1993**, *34*, 6053 – 6056; d) C. Meyer, I. Marek, G. Courtemanche, J.-F. Normant, *Tetrahedron* **1994**, *50*, 11665 – 11692.

[25] a) W. F. Bailey, M. W. Carson, *J. Org. Chem.* **1998**, *63*, 361 – 365; b) W. F. Bailey, M. W. Carson, *J. Org. Chem.* **1998**, *63*, 9960 – 9967.

[26] D. P. Curran, D. Kim, *Tetrahedron Lett.* **1986**, *27*, 5821 – 5824.

[27] Distannanes in radical cyclo-isomerizations of iodo-olefins and iodo-alkynes have been suggested to act as initiators and/or trapping agents for I and I_2 (depending on substrate and conditions): a) D. P. Curran, M.-H. Chen, D. Kim, *J. Am. Chem. Soc.* **1989**, *111*, 6265 – 6276; b) M. Newcomb, D. P. Curran, *Acc. Chem. Res.* **1988**, *21*, 206 – 214; c) A. Studer, D. P. Curran, *Angew. Chem. Int. Ed.* **2016**, *55*, 58 – 102; *Angew. Chem.* **2016**, *128*, 58 – 106.

[28] It has been shown that the radical cyclization step of **S1** proceeds with an *exo*/*endo* selectivity of 50:1 (Ref. [22]); for simplicity, only the major product (**P1**) is shown and discussed throughout this work.

[29] $[SnMe_3]_2$ has been reported to act as a catalyst in the cyclo-isomerization of an activated δ-iodo-olefin under thermal conditions: D. P. Curran, C.-T. Chang, *J. Org. Chem.* **1989**, *54*, 3140 – 3157.

[30] Also see closely related reactions in Ref. [26].

[31] B. Giese, G. Thoma, *Helv. Chim. Acta* **1991**, *74*, 1135 – 1142.

[32] C. M. McMahon, M. S. Renn, E. J. Alexanian, *Org. Lett.* **2016**, *18*, 4148 – 4150.

[33] a) H. Yorimitsu, T. Nakamura, H. Shinokubo, K. Oshima, *J. Org. Chem.* **1998**, *63*, 8604 – 8605; b) H. Yorimitsu, T. Nakamura, H. Shinokubo, K. Oshima, K. Omoto, H. Fujimoto, *J. Am. Chem. Soc.* **2000**, *122*, 11041 – 11047; c) A. Fusano, S. Sumino, S. Nishitani, T. Inouye, K. Morimoto, T. Fukuyama, I. Ryu, *Chem. Eur. J.* **2012**, *18*, 9415 – 9422.

[34] With extended reaction times of 20 h, reaction of **S1** with one equivalent of **7** also gives small amounts of the cyclo-isomerization product **P1**. Larger quantities of **P1** (65%) were detected, when 2 equiv MeI were added to the in situ generated mixture of **8** and **9**.

[35] K. Oshima, *Sci. Synth.* **2003**, *2*, 13 – 89.

[36] The impurities are compounds, in which olefin functionalities have been carbometalated by $Bi((CH_2)_4CH{=}CH_2)$ groups according to NMR spectroscopy and GC/MS analysis after aqueous work-up.

[37] A slow cyclo-isomerization of $[In((CH_2)_4CH{=}CH_2)_3]$ has been reported: T. W. Dolzine, J. P. Oliver, *J. Organomet. Chem.* **1974**, *78*, 165 – 176.

[38] A bismuth radical was not directly detected in reactions of **S1** catalyzed by **7**, which was ascribed to the low concentration and short life-time of such species; fast relaxation times may generally prohibit their detection, even at low temperature (c.f. Ref. [8] and Supporting Information). No resonance could be detected by EPR spectroscopy, when **S1** and **10** were heated to 60 °C in benzene in the absence of **7**.

[39] D. Rehorek, *Z. Chem.* **1980**, *20*, 325 – 332.

[40] Formation of the corresponding nitroxyl radical with a 1-hexene-6-yl substituent rather than **11** cannot be formally ruled out.

[41] a) W. F. Bailey, T. T. Nurmi, J. J. Patricia, W. Wang, *J. Am. Chem. Soc.* **1987**, *109*, 2442 – 2448; b) E. C. Ashby, T. N. Pham, *J. Org. Chem.* **1987**, *52*, 1291 – 1300; c) K. Deng, A. Bensari-Bouguerra, J. Whetstone, T. Cohen, *J. Org. Chem.* **2006**, *71*, 2360 – 2372; d) H. Liu, K. Deng, T. Cohen, K. D. Jordan, *Org. Lett.* **2007**, *9*, 1911 – 1914.

[42] Adding 6-iodo-1-hexene (**S2**) to a solution of *t*BuLi in pentane/Et_2O at −78 °C (rather than the reverse order of addition) gave a *cis*/*trans* product ratio of ca. 1.5–1.9:1.0 with low yields of 11–13% (Ref. [41a,b]).

[43] Grignard reagents generated from 6-chloro-1-hexene also cyclize with a preference for the *trans*-product: a) H. G. Richey, Jr., T. C. Rees, *Tetrahedron Lett.* **1966**, *7*, 4297 – 4301; b) W. C. Kossa, Jr., T. C. Rees, H. G. Richey, Jr., *Tetrahedron Lett.* **1971**, *12*, 3455 – 3458.

[44] a) A. L. J. Beckwith, I. Blair, G. Phillipou, *J. Am. Chem. Soc.* **1974**, *96*, 1613 – 1614; b) D. C. Spellmeyer, K. N. Houk, *J. Org. Chem.* **1987**, *52*, 959 – 974.

[45] For cyclization of **S5** with initiators such as BEt_3, $TiCl_3$, $[Sn(nBu)_3]_2$, organic radical precursors, and related species see: a) M. Ikeda, H. Teranishi, K. Nozaki, H. Ishibashi, *J. Chem. Soc. Perkin Trans. 1* **1998**, 1691 – 1697; b) K. Wakabayashi, H. Yormitsu, H. Shinokubo, K. Oshima, *Bull. Chem. Soc. Jpn.* **2000**, *73*, 2377 – 2378; c) H. Yorimitsu, K. Oshima, *Bull. Chem. Soc. Jpn.* **2002**, *75*, 853 – 854; d) L. Cao, C. Li, *Tetrahedron Lett.* **2008**, *49*, 7380 – 7382; e) D. P. Curran, J. Tamine, *J. Org. Chem.* **1991**, *56*, 2746 – 2750; f) A. G. Hernán, J. Kilburn, *Tetrahedron Lett.* **2004**, *45*, 831 – 834; g) H. Yorimitsu, K. Wakabayashi, H. Shinokubo, K. Oshima, *Bull. Chem. Soc. Jpn.* **2001**, *74*, 1963 – 1970.

[46] Here, **7** is an alternative to initiators like polar and reducing $LiAlH_4$ or toxic $[Sn(nBu)_3]_2$, which requires irradiation conditions: a) E. C. Ashby, C. O. Welder, *J. Org. Chem.* **1998**, *63*, 7707 – 7714; b) see Ref. [26].

[47] CCDC 1884682, 1884683, 1884684, and 1884685 contains the supplementary crystallographic data for this paper. These data can be obtained free of charge from The Cambridge Crystallographic Data Centre.

Manuscript received: April 9, 2019
Accepted manuscript online: June 5, 2019
Version of record online: July 25, 2019

IV Well-defined, Molecular Bismuth Compounds: Catalysts in Photochemically-Induced Radical Dehydrocoupling Reactions

This chapter was published in: Jacqueline Ramler, Ivo Krummenacher, Crispin Lichtenberg, *Chem. Eur. J.* **2020**, *26*, 14551–14555. Reprinted from ref. 77 with permission from 2020 WILEY-VCH Verlag GmbH.

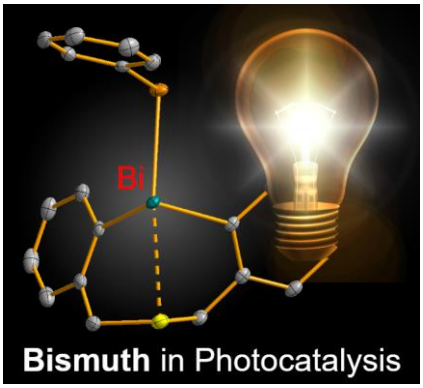

Chemistry–A European Journal | Communication
doi.org/10.1002/chem.202002219
Check for updates
Chemistry Europe
European Chemical Societies Publishing

Homogeneous Catalysis

Well-Defined, Molecular Bismuth Compounds: Catalysts in Photochemically Induced Radical Dehydrocoupling Reactions

Jacqueline Ramler,[a] Ivo Krummenacher,[a, b] and Crispin Lichtenberg*[a]

Abstract: A series of diorgano(bismuth)chalcogenides, [Bi(di-aryl)EPh], has been synthesised and fully characterised (E = S, Se, Te). These molecular bismuth complexes have been exploited in homogeneous *photochemically*-induced radical catalysis, using the coupling of silanes with TEMPO as a model reaction (TEMPO = (tetramethyl-piperidin-1-yl)-oxyl). Their catalytic properties are complementary or superior to those of known catalysts for these coupling reactions. Catalytically competent intermediates of the reaction have been identified. Applied analytical techniques include NMR, UV/Vis, and EPR spectroscopy, mass spectrometry, single-crystal X-ray diffraction analysis, and (TD)-DFT calculations.

Covalent bonds Z–X with a heavy p-block element Z as one of the bonding partners show low homolytic bond dissociation energies due to inefficient spatial and energetic overlap of the relevant atomic orbitals.[1] This allows access to reversible homolytic bond dissociations (Z–X = Z• + X•) under mild reaction conditions, which is a key feature for potential catalytic applications via radical pathways.[2] For instance, equilibrium scenarios have been reported for the homolysis of the Sn ≡ Sn bond in $(SnAr)_2$ and the Pn–Pn bonds in $(Pn(CSiMe_3CH_2)_2)_2$ (Ar = C_6H_3-2,6-(C_6H_3-2,6-*i*Pr_2)$_2$; Pn = Sb, Bi).[3,4] Such findings have paved the way for new catalytic applications of well-defined, molecular complexes of heavy p-block elements in radical reactions.[2c] Among potential catalysts of this kind, bismuth compounds in particular are attractive synthetic targets due to characteristics such as low cost, (relatively) low toxicity, and prospects for recyclability.[5,8a] In this context, the radical dehydrocoupling of $SiPhH_3$ and TEMPO with [Bi(NON^{Dipp})]• and the radical cyclo-isomerisation of δ-iodo-olefins with Ph_2Bi-$Mn(CO)_5$ have recently been reported (Scheme 1; TEMPO = (tetramethyl-piperidin-1-yl)-oxyl; NON^{Dipp} = $O(SiMe_2N^{Dipp})_2$, Dipp = 2,6-*i*$Pr_2C_6H_3$).[6,7] While these reactions are thermally-initiated, photochemically-induced transformations represent an important complementary approach to radical catalysis. Indeed, a range of inorganic bismuth compounds such as (nanostructured) oxides (Bi_2O_3),[8] titanates ($Bi_4Ti_3O_{12}$),[9] vanadates ($BiVO_4$),[10] halide perovskites ($Cs_3Bi_2Br_9$),[11] and an oxybromide ($Bi_{24}O_{31}Br_{10}(OH)_6$)[12] have been exploited in photocatalytic transformations. Catalysed types of reactions include the degradation of organic dyes such as methyl orange,[9] antibiotics such as tetracycline,[10] and biocides such as triclosan,[8b] as well as CH activation of aliphatic and aromatic hydrocarbons,[11] transfer (de)hydrogenation of alcohols/ketones,[12] and olefin polymerisation.[8a] These applications of bismuth compounds in heterogeneous catalysis suggest that photochemical strategies might also be applicable for well-defined, molecular bismuth compounds under homogeneous conditions. Indeed, the light-sensitivity of molecular bismuth complexes such as organobismuthanes, dibismuthanes, bismuth amides, and related species has been phenomenologically reported in some cases.[13] The direct involvement of bismuth functional groups in visible light absorption has been demonstrated through TD-DFT calculations and UV/Vis spectroscopy for the bismuth radical [Bi(NON^{Dipp})]•, a dibismuthane, and a cationic bismuth carbamoyl ($[RBi\text{-}C(O)NR'_2]^+$).[4a,14,15,16] However, applications of well-defined molecular bismuth compounds in photochemically-initiated, catalysed radical reactions have not been reported to date.

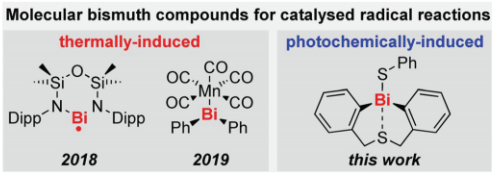

Scheme 1. Well-defined, molecular bismuth compounds for catalysed radical reactions: species applied in thermally- vs. photochemically-induced transformations.

We show here that an easily accessible, storable, molecular organo(bismuth)thiolate is catalytically active in photochemically-induced radical dehydrocoupling reactions.

We recently reported preliminary results on the synthesis of the diorgano(bismuth)thiolate **2-SPh** from transition metal bismuthane **1-Mn(CO)$_5$** and diphenyldisulfide, $(SPh)_2$ (Scheme 2,

[a] J. Ramler, Dr. I. Krummenacher, Dr. C. Lichtenberg
Institute of Inorganic Chemistry, Julius-Maximilians-University Würzburg
Am Hubland, 97074 Würzburg (Germany)
E-mail: crispin.lichtenberg@uni-wuerzburg.de
[b] Dr. I. Krummenacher
Institute for Sustainable Chemistry & Catalysis with Boron
Am Hubland, 97074 Würzburg (Germany)
Supporting information and the ORCID identification number(s) for the author(s) of this article can be found under: https://doi.org/10.1002/chem.202002219.

Chemistry–A European Journal | Communication doi.org/10.1002/chem.202002219 | Chemistry Europe European Chemical Societies Publishing

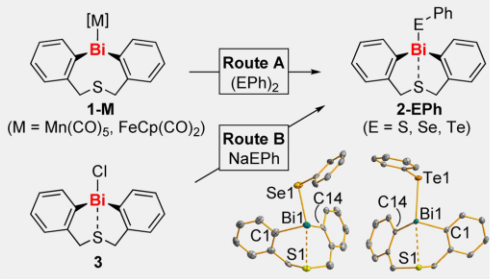

Scheme 2. Synthesis of compounds **2-EPh** via routes A and B and molecular structures of **2-SePh** and **2-TePh** in the solid state. Cp = C_5H_5. Displacement parameters are drawn at the 50% probability level. Selected bond lengths (Å) and angles (°): **2-SePh**: Bi1–C1, 2.284(11); Bi1–C14, 2.303(10); Bi1–Se1, 2.7285(11); Bi1–S1, 2.966(3); C1-Bi1-C14, 97.9(3); C1-Bi1-Se1, 90.0(3); S1-Bi1-Se1, 157.23(6). **2-TePh**: Bi1–C1, 2.288(3); Bi1–C14, 2.289(3); Bi1–Te1, 2.9296(3); Bi1–S1, 3.0007(7); C1-Bi1-C14, 96.98(9); C1-Bi1-Te1, 93.92(7); S1-Bi1-Te1, 161.818(14).

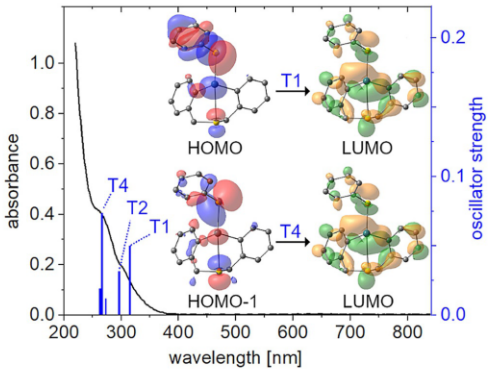

Figure 1. Experimental UV/Vis spectrum of **2-SPh** in THF (solid black line), five lowest energy calculated transitions (blue bars), and molecular orbitals involved in the two calculated absorptions with highest intensity (A1 and A4). Isovalue = 0.03.

Route A).[6] Here, we extend this approach to the heavier homologues **2-SePh** and **2-TePh**, which could be obtained in high yields (>90%, Supporting Information). In addition, compounds **2-EPh** were also synthesised in a straightforward, transition-metal-free salt elimination protocol via Route B and fully characterised (Scheme 2, Supporting Information, E = S, Se, Te). Single-crystal X-ray diffraction analysis of **2-SePh** and **2-TePh** confirmed Bi1–Se1 and Bi1–Te1 bond length in the expected ranges[17] and bonding interactions between Bi1 and the sulfur atom of the ligand backbone, S1, as recently reported for the sulfur analogue **2-SPh**.[6,18] According to NBO analyses, these Bi1···S1 interactions are realised through n(S1)→σ*(Bi-EPh) bonding with the corresponding deletion energies ranging from 18.2 to 21.3 kcal mol^{-1} (Supporting Information). In order to evaluate the potential of compounds **2-EPh** to be applied in photochemical reactions, they were analysed by UV/Vis spectroscopy and (TD)-DFT calculations. The results are qualitatively identical and discussed here for **2-SPh** (for details see Supporting Information). The experimental UV/Vis spectrum of **2-SPh** in THF shows two absorption features centred around 307 and 264 nm with an onset at ca. 380 nm (Figure 1). These absorption bands were correlated with five singlet–singlet transitions T1–T5, three of which show larger oscillator strengths (T1 (315 nm), T2 (296 nm), T4 (266 nm)). T1, T2, and T4 correspond to a HOMO/LUMO (T1, 88%), HOMO/LUMO+1 (T2, 78%), and HOMO−1/LUMO (T4, 59%) transition, respectively (Figure 1 and Supporting Information). While the HOMO and the HOMO−1 show contributions to Bi–SPh σ-bonding,[19] the LUMO and LUMO+1 show contributions to Bi–SPh σ*-antibonding interactions. These analyses suggest that compounds **2-EPh** should be susceptible to photochemical Bi-EPh bond cleavage, rendering them candidates for photocatalytic applications.

We thus turned our attention towards the dehydrocoupling of phenylsilane (**S1**) with TEMPO to give siloxides **P1** and **P1′** (see reaction scheme in Table 1). This reaction has recently been investigated as a model reaction for *thermally*-initiated radical catalysis with main group compounds in pivotal studies by the groups of Hill[20] and Coles.[7] In benzene solution at 23 °C with a reaction time of 1 d, 10 mol% of compounds **2-EPh** proved to be not catalytically active (entries 1–3). At an elevated temperature of 80 °C, small amounts of the coupling

Table 1. Bismuth species in the catalysed dehydrocoupling reaction of TEMPO with $PhSiH_3$ (**S1**) or Ph_2SiH_2 (**S2**).

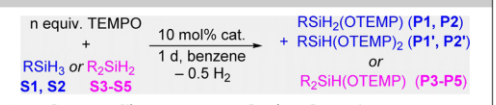

#	Cat.	Silane (R or R_2)	*n*	Cond.	Conversion [%][a]
1	**2-SPh**	**S1** (Ph)	1	23 °C	<1 (**P1**)
2	**2-SePh**	**S1** (Ph)	1	23 °C	<1 (**P1**)
3	**2-TePh**	**S1** (Ph)	1	23 °C	<1 (**P1**)
4	**2-SPh**	**S1** (Ph)	1	80 °C	3 (**P1**)
5	**2-SePh**	**S1** (Ph)	1	80 °C	9 (**P1**)
6	**2-TePh**	**S1** (Ph)	1	80 °C	9 (**P1**)
7	None	**S1** (Ph)	1	*hv*	10 (**P1**)
8	**2-SPh**	**S1** (Ph)	1	*hv*	93 (53% **P1**, 20% **P1′**)
9	**2-SePh**	**S1** (Ph)	1	*hv*	65 (39% **P1**, 13% **P1′**)
10	**2-TePh**	**S1** (Ph)	1	*hv*	13 (**P1**)
11	**2-SPh**	**S1** (Ph)	2	*hv*	94 (13% **P1**, 87% **P1′**)
12	**2-SPh**	**S3** (Ph_2)	1	*hv*	63 (**P3**)
13	**2-SPh**	**S3** (Ph_2)	2	*hv*	97 (**P3**)[b]
14	**2-SPh**	**S2** (*n*Hex)	2	*hv*	64 (69% **P2**, 29% **P2′**)
15	**2-SPh**	**S4** (Ph/Me)	2	*hv*	54 (**P4**)[b]
16	**2-SPh**	**S5** (tBu_2)	2	*hv*	0 (**P5**)
17	**4**	**S1** (Ph)	1	23 °C	4 (**P1**)
18	**4**	**S1** (Ph)	1	*hv*	>99 (52% **P1**, 24% **P1′**)[c]
19	**5**	**S1** (Ph)	1	23 °C	<1 (**P1**)
20	**5**	**S1** (Ph)	1	*hv*	48 (**P1**)

[a] Conversion of TEMPO, determined by ^{1}H NMR spectroscopic analysis of silanes **S1–S5** and **P1–P4** (also see Supporting Information).[20] [b] Conversion of **S3** and **S4** to **P3** and **P4**. [c] The TEMPO that is part of **4** is also fully converted (Supporting Information).

Chemistry–A European Journal | Communication doi.org/10.1002/chem.202002219 | Chemistry Europe European Chemical Societies Publishing

product **P1** were detected, but the product formations are in agreement with stoichiometric regimes (entries 4–6). Following our UV/Vis spectroscopic and (TD-)DFT analyses of compounds **2-EPh**, these bismuth chalcogenides were also tested as dehydrocoupling catalysts under *photochemical* conditions. Indeed, **2-EPh** proved to be catalytically active under irradiation with a mercury vapour lamp (entries 7–10). While the background reaction and the tellurium compound **2-TePh** only led to low yields of the desired coupling products, good (65%) and excellent conversions (93%) could be obtained with the homologous selenium (**2-SePh**) and sulfur species (**2-SPh**). This trend was ascribed to the photosensitivity of **2-EPh**, which increases with increasing atomic numbers of E, and to the higher reactivity of selenium and tellurium containing by-products (with the potential to undergo unselective side reactions).[21] The by-product dihydrogen, H_2, was detected by ^{1}H NMR spectroscopy. With **2-SPh** as a catalyst and two equivalents of TEMPO, 94% conversion was obtained in 1 d reaction time, necessarily with a clear preference for the double substitution product **P1′** (entry 11). **2-SPh** is also active as a catalyst for dehydrocoupling of the less reactive substrate Ph_2SiH_2 (**S3**): with one equivalent of TEMPO, 63% yield of **P3** were obtained under standard photochemical conditions (entry 12). Near-quantitative conversion of **S3** to **P3** in 1 d was obtained by using $n=$ 2 equivalents of TEMPO (entry 13). These results demonstrate for the first time the high potential of well-defined molecular bismuth compounds for the exploitation in photochemically-induced catalytic bond forming events via radical pathways. In terms of catalytic activity, the bismuth thiolate **2-SPh** clearly outperforms the bismuth radical compound [Bi(NON^{Dipp})]$^\bullet$, which was recently reported to catalyse the reaction of **S1** with TEMPO in a thermally-induced transformation (e.g.: 10 mol% [Bi(NON^{Dipp})]$^\bullet$, 70 °C, 1.7 d reaction time, 10% conversion (formation of **P1**);[22] (*cf.* entries 8, 11).[7] Furthermore, the catalytic activity of **2-SPh** can compete with that of the magnesium amide $Mg\{N(SiMe_3)_2\}_2(thf)_2$, which has been shown to catalyse thermally-initiated dehydrocoupling reactions of **S1** and **S3** with TEMPO: while $Mg\{N(SiMe_3)_2\}_2(thf)_2$ is catalytically more selective in addressing only one Si–H bond of $PhSiH_3$, that is, reaction of **S1** with 1 equiv TEMPO (10 mol% cat., 60 °C 1 d, 99% yield of **P1**; *cf.* entry 8), **2-SPh** is catalytically more active in addressing Si–H bonds of secondary silanes, that is, in the overall reaction of **S1** or **S3** with two equiv TEMPO (**S1**: 10 mol% $Mg\{N(SiMe_3)_2\}_2(thf)_2$, 80 °C, 6 d, 96% yield, **S3**: 10 mol% $Mg\{N(SiMe_3)_2\}_2(thf)_2$, 80 °C, 4 d, 99% yield; *cf.* entries 11, 13). Concerning the mode of initiation of the reaction (thermally vs. photochemically), our approach is complementary to those previously reported for the dehydrocoupling of TEMPO with silanes.[7,20]

Preliminary investigations into the substrate scope of this reaction show reduced catalytic activities for silanes bearing one or more alkyl substituents (entries 14–16 and Supporting Information).

In order to identify potential intermediates of the catalysed reactions, a reaction mixture obtained under our standard catalytic conditions (e.g. entry 8) was analysed by high-resolution mass spectrometry. Signals of $m/z=$578.1922 and 843.1000 were detected (Supporting Information).[23] This corresponds to species with the sum formulae $[C_{23}H_{31}BiNOS]^+$ (calc. $m/z=$578.1925) and $[C_{28}H_{25}Bi_2S_2]^+$ (calc. $m/z=$843.1000), which were assigned to protonated derivatives of the bismuth tempoxide $[Bi(C_6H_4CH_2)_2S(OTEMP)]$ (**4**) and the dibismuthane $[Bi(C_6H_4CH_2)_2S]_2$ (**5**), respectively. Both compounds were synthesised in independent approaches, isolated, and fully characterised (Scheme 3). Compound **4** was obtained as a colourless solid from the reaction of **3** with in situ-generated Na(OTEMP). Single-crystal X-ray diffraction analysis revealed X–O1 bond lengths (Bi1–O1, 2.18 Å; N1–O1, 1.46 Å) and an angle sum around N1 (333.9°), which point towards this complex being best described as a bismuth tempoxide species (Scheme 3b).[3b,7,24,25] This is also in agreement with the presence of a Bi1···S1 bonding interaction, which is expected for a sufficiently electronegative anionic substituent X^- bound to $[Bi(C_6H_4CH_2)_2S]^+$.[6,18] EPR spectroscopic investigations revealed a very weak resonance indicating the presence of trace amounts (0.3%) of TEMPO in solution. Since the NMR spectroscopic and elemental analysis of **4** gave no hints at the presence of impurities, the postulation of an equilibrium scenario $[Bi(C_6H_4CH_2)_2S(OTEMP)] \rightleftharpoons [Bi(C_6H_4CH_2)_2S]^\bullet + TEMPO^\bullet$, appeared tempting.[3b,7] However, powder EPR spectra of **4** and the temperature-dependence of the EPR signals of **4** in solution clearly ruled out an equilibrium scenario in the range of −60 to +20 °C,[26] indicating that it is in fact due to trace impurities of TEMPO in the sample, which could not be removed by repeated re-crystallisations (Figure S12, Supporting Information).

Compound **5** was obtained as a red solid from the reaction of **4** with $PhSiH_3$. NMR spectroscopic reaction monitoring revealed the formation of $PhSiH_2(OTEMP)$ and H_2, suggesting a mechanism via the short-lived bismuthane

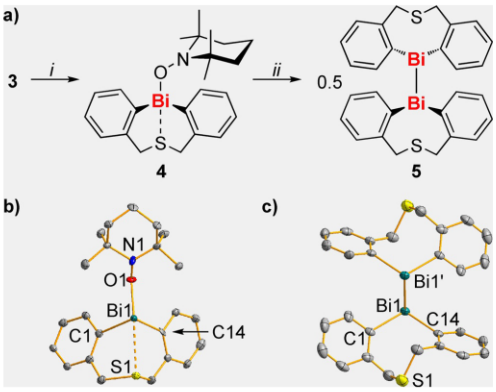

Scheme 3. a) Synthesis of compounds **4** and **5**; i: Na(OTEMP), r.t. THF, 2 h; ii: $PhSiH_3$, 60 °C, benzene, 4 d. b, c) Molecular structures of **4** and **5** in the solid state. Displacement parameters are drawn at the 50% probability level. Selected bond lengths (Å) and angles (°): **4**: Bi1–C1, 2.274(8); Bi1–C14, 2.271(9); Bi1–O1, 2.184(5); Bi1–S1, 2.936(2); N1–O1, 1.459(8); C1-Bi1-C14, 91.5(3); C1-Bi1-O1, 92.3(3); Bi1-O1-N1, 106.1(4); S1-Bi1-O1, 159.76(15); ΣC/O-N1-C/O, 333.9(6). **5**: Bi1–C1, 2.262(7); Bi1–C14, 2.289(7); Bi1–Bi1′, 3.0211(5); C1-Bi1-C14, 104.8(3); C1-Bi1-Bi1′, 91.59(18); C1-Bi1-Bi1′-C1′, 180.

Chemistry–A European Journal | Communication doi.org/10.1002/chem.202002219 | Chemistry Europe European Chemical Societies Publishing

$[HBi(C_6H_4CH_2)_2S]$.[27,28] Once compound **5** is precipitated, its solubility in common organic solvents is very poor. NMR spectroscopic data could only be obtained at elevated temperature in pyridine (Supporting Information).[29] Single-crystal X-ray diffraction analysis confirmed the expected molecular structure with C_i symmetry and a non-polar Bi–Bi bond (3.02 Å), resulting in the absence of Bi1···S1 interactions (Scheme 3 c).[6]

Combined UV/Vis spectroscopic and (TD-)DFT analyses of **4** and **5** suggest that they should be susceptible to photochemically-induced Bi–O/Bi–Bi bond cleavage (Supporting Information). In agreement with these results, isolated compounds **4** and **5** proved to be catalytically competent in the photochemically-induced dehydrocoupling of **S1** with TEMPO (Table 1, entries 17–20). While quantitative yields were obtained with **4**, the lower yield of 48% obtained with **5** was ascribed to the poor solubility of the isolated species. The mechanism of the catalysed reactions presented in this work is certainly complex and potentially involves resting states and parallel reaction pathways. In order to rationalise the catalytic reaction, a tentatively suggested catalytic cycle involving all compounds that were isolated or detected in catalytic experiments is shown in Scheme 4 (for further details, see Supporting Information).

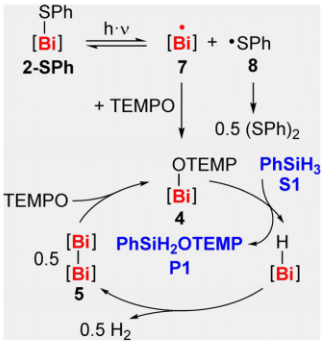

Scheme 4. Tentatively suggested catalytic cycle for dehydrocoupling of **S1** with TEMPO to give **P1**, catalysed by **2-SPh** (for further details see Supporting Information). [Bi] = $[Bi(C_6H_4CH_2)_2S]$.

In summary, we have demonstrated that the easily accessible and storable diorgano(bismuth)thiolate $[Bi(C_6H_4CH_2)_2S(SPh)]$ (**2-SPh**) allows for the first application of a well-defined molecular bismuth compound as a catalyst in a homogeneous *photochemical* approach. In the radical dehydrocoupling of silanes with TEMPO, **2-SPh** shows a much higher catalytic activity than previously reported bismuth compounds and is competitive with a previously reported magnesium species. The new approach is complementary to existing ones in terms of reaction initiation (thermal vs. photochemical), opening up perspectives for orthogonal synthetic strategies. TD-DFT calculations gave insights into the initiating step of the reaction and catalytically competent intermediates have been isolated and characterised.

Experimental Section

Crystallographic data: Deposition numbers 1990330, 1990331, 1990332, and 1990333 contain the supplementary crystallographic data for this paper. These data are provided free of charge by the joint Cambridge Crystallographic Data Centre and Fachinformationszentrum Karlsruhe Access Structures service.

Acknowledgements

Funding through the Fonds der Chemischen Industrie, the Universitätsbund Würzburg, the University of Würzburg, and the Deutsche Forschungsgemeinschaft is gratefully acknowledged. C.L. thanks Prof. Holger Braunschweig for continuous support. Open access funding enabled and organized by Projekt DEAL.

Conflict of interest

The authors declare no conflict of interest.

Keywords: bismuth · chalcogens · dehydrocoupling · photocatalysis · radical reactions

[1] a) "Bond Dissociation Energies": Y.-R. Luo in *CRC Handbook of Chemistry and Physics*, 89th ed. (Ed.: D. R. Lide), CRC/Taylor and Francis, Boca Raton, **2009**; b) S. J. W. Price, A. F. Trotman-Dickenson, *Trans. Faraday Soc.* **1958**, *54*, 1630–1637; c) D. P. Mukhopadhyay, D. Schleier, S. Wirsing, J. Ramler, D. Kaiser, E. Reusch, P. Hemberger, T. Preitschopf, I. Krummenacher, B. Engels, I. Fischer, C. Lichtenberg, *Chem. Sci.* **2020**, *11*, 7562–7568 .

[2] a) A. Studer, D. P. Curran, *Angew. Chem. Int. Ed.* **2016**, *55*, 58–102; b) C. Lichtenberg, *Angew. Chem. Int. Ed.* **2016**, *55*, 484–486; c) C. Lichtenberg, *Chem. Eur. J.* **2020**, *26*, 9674–9687.

[3] a) T. Y. Lai, L. Tao, R. D. Britt, P. P. Power, *J. Am. Chem. Soc.* **2019**, *141*, 12527–12530; b) S. Ishida, F. Hirakawa, K. Furukawa, K. Yoza, T. Iwamoto, *Angew. Chem. Int. Ed.* **2014**, *53*, 11172–11176.

[4] For isolable bismuth radicals see: a) R. J. Schwamm, J. R. Harmer, M. Lein, C. M. Fitchett, S. Granville, M. P. Coles, *Angew. Chem. Int. Ed.* **2015**, *54*, 10630–10633; b) C. Ganesamoorthy, C. Helling, C. Wölper, W. Frank, E. Bill, G. E. Cutsail III, S. Schulz, *Nat. Commun.* **2018**, *9*, 87.

[5] a) J. M. Bothwell, S. W. Krabbe, R. S. Mohan, *Chem. Soc. Rev.* **2011**, *40*, 4649–4707; b) R. Mohan, *Nat. Chem.* **2010**, *2*, 336; c) R. Qiu, Y. Qiu, S. Yin, X. Song, Z. Meng, X. Xu, X. Zhang, S. Luo, C.-T. Au, W.-Y. Wong, *Green Chem.* **2010**, *12*, 1767–1771.

[6] J. Ramler, I. Krummenacher, C. Lichtenberg, *Angew. Chem. Int. Ed.* **2019**, *58*, 12924–12929.

[7] R. J. Schwamm, M. Lein, M. P. Coles, C. M. Fitchett, *Chem. Commun.* **2018**, *54*, 916–919.

[8] a) K. Hakobyan, T. Gegenhuber, C. S. P. McErlean, M. Müllner, *Angew. Chem. Int. Ed.* **2019**, *58*, 1828–1832; b) M. Weber, T. Rüffer, F. Speck, F. Göhler, D. P. Weimann, C. A. Schalley, T. Seyller, H. Lang, M. Mehring, *Inorg. Chem.* **2020**, *59*, 3353–3366; c) L. Zhou, W. Wang, H. Xu, S. Sun, M. Shang, *Chem. Eur. J.* **2009**, *15*, 1776–1782; d) H. Cheng, B. Huang, J. Lu, Z. Wang, B. Xu, X. Qin, X. Zhang, Y. Dai, *Phys. Chem. Chem. Phys.* **2010**, *12*, 15468–15475.

[9] W. F. Yao, X. H. Xu, H. Wang, J. T. Uhou, X. N. Yang, Y. Zhang, S. X. Shang, B. B. Huang, *Appl. Catal. B* **2004**, *52*, 109–116.

[10] M. Tayebi, A. Tayyebi, T. Soltani, B.-K. Lee, *New J. Chem.* **2019**, *43*, 9106–9115.

[11] Y. Dai, C. Pidevin, C. Ochoa-Hernández, A. A. Auer, H. Tüysüz, *Angew. Chem. Int. Ed.* **2020**, *59*, 5788–5796.

[12] Y. Dai, C. Li, Y. Shen, S. Zhu, M. S. Hvid, L.-C. Wu, J. Skibsted, Y. Li, J. W. H. Niemantsverdriet, F. Besenbacher, N. Lock, R. Su, *J. Am. Chem. Soc.* **2018**, *140*, 16711–16719.

Chemistry–A European Journal | Communication doi.org/10.1002/chem.202002219 | Chemistry Europe European Chemical Societies Publishing

[13] a) A. J. Ashe III, E. G. Ludwig, Jr., J. Oleksyszyn, *Organometallics* **1983**, *2*, 1859 – 1866; b) J. Lorberth, W. Massa, S. Wocadlo, I. Sarraje, S.-H. Shin, X.-W. Li, *J. Organomet. Chem.* **1995**, *485*, 149 – 152; c) W. Clegg, N. A. Compton, R. J. Errington, G. A. Fisher, M. E. Green, D. C. R. Hockless, N. C. Norman, *Inorg. Chem.* **1991**, *30*, 4680 – 4682; d) J. M. Wallis, G. Müller, H. Schmidbaur, *J. Organomet. Chem.* **1987**, *325*, 159 – 168; e) . Lichtenberg, F. Pan, T. P. Spaniol, U. Englert, J. Okuda, *Angew. Chem. Int. Ed.* **2012**, *51*, 13011 – 13015.

[14] a) J. Ramler, J. Poater, F. Hirsch, B. Ritschel, I. Fischer, F. M. Bickelhaupt, C. Lichtenberg, *Chem. Sci.* **2019**, *10*, 4169 – 4176; b) B. Ritschel, J. Poater, H. Dengel, F. M. Bickelhaupt, C. Lichtenberg, *Angew. Chem. Int. Ed.* **2018**, *57*, 3825 – 3829.

[15] Also see ref. [3b] for comparison.

[16] K. Y. Monakhov, T. Zessin, G. Linti, *Eur. J. Inorg. Chem.* **2010**, 322 – 332.

[17] a) F. Calderazzo, A. Morvillo, G. Pelizzi, R. Poly, F. Ungari, *Inorg. Chem.* **1988**, *27*, 3730 – 3733; b) P. Šimon, R. Jambor, A. Růžička, L. Dostál, *Organometallics* **2013**, *32*, 239 – 248; c) J. Ramler, C. Lichtenberg, *Chem. Eur. J.* **2020**, *26*, 10250 – 10258.

[18] Also see: A. Toma, C. I. Raț, A. Silvestru, T. Rüffer, H. Lang, M. Mehring, *J. Organomet. Chem.* **2016**, *806*, 5 – 11.

[19] There are also significant contributions of a sulfur-centred lone pair to the HOMO and the HOMO−1.

[20] D. J. Liptrot, M. S. Hill, M. F. Mahon, *Angew. Chem. Int. Ed.* **2014**, *53*, 6224 – 6227.

[21] a) J.-J. Aleman-Lara, E. Block, S. Braverman, M. Cherkinsky, M. B. C. de la Plata, *Sulfur, Selenium, and Tellurium, Science of Synthesis, Vol. 39*, Houben – Weyl, **2014**; b) S. M. Horvat, C. H. Schiesser, *New J. Chem.* **2010**, *34*, 1692 – 1699.

[22] Data read out from Figure S7 of ref. [7].

[23] Bismuth radicals are challenging to detect EPR spectroscopically, which has been ascribed to fast relaxation as a result of large spin–orbit coupling (ref. [2b]). For example, the bismuth radical that is formed in the equilibrium reaction $[Bi(CSiMe_3CH_2)_2]_2 \rightleftharpoons 2\,[Bi(CSiMe_3CH_2)_2]^{\bullet}$ could not be detected by EPR spectroscopy (ref. [2b]). The EPR spectroscopic detection of a bismuth radical that may be a reactive species in the catalytic experiments presented in this work would thus be surprising, since it would be expected to be very short-lived and present only in very low concentrations. Nevertheless, attempts to detect bismuth radical species by irradiating **2-SPh** or **4** during EPR spectroscopic experiments were undertaken, but proved to be unsuccessful (for details see Supporting Information).

[24] G. C. Forbes, A. R. Kennedy, R. E. Mulvey, P. J. A. Rodger, *Chem. Commun.* **2001**, 1400 – 1401.

[25] Z. Turner, *Inorg. Chem.* **2019**, *58*, 14212 – 14227.

[26] This equilibrium scenario may well be accessible at elevated temperatures, since the homolytic cleavage of the Bi–O bond in **4** is only mildly endergonic ($\Delta G = +12.0$ kcal mol^{-1}) according to DFT calculations (Supporting Information).

[27] a) G. Balázs, H. J. Breunig, E. Lork, *Organometallics* **2002**, *21*, 2584 – 2586; b) G. Balázs, H. J. Breunig, E. Lork, *Z. Naturforsch. B* **2005**, *60*, 180 – 182; c) R. J. Schwamm, M. Lein, M. P. Coles, C. M. Fitchett, *Angew. Chem. Int. Ed.* **2016**, *55*, 14798 – 14801.

[28] A sole example of an isolable secondary bismuthane has been reported: N. J. Hardman, B. Twamley, P. P. Power, *Angew. Chem. Int. Ed.* **2000**, *39*, 2771 – 2773.

[29] A poor solubility of the related species $[Bi(C_6H_4CH_2)_2NMe]_2$ is suggested by the use of 100 mL THF for the extraction of 59 mg of this compound: S. Shimada, J. Maruyama, Y.-K. Choe, T. Yamashita, *Chem. Commun.* **2009**, 6168 – 6170.

Manuscript received: May 5, 2020
Revised manuscript received: June 8, 2020
Accepted manuscript online: June 23, 2020
Version of record online: October 14, 2020

V Transition Metal Bismuthanes

1 Homolytic Bismuth–Transition Metal Bond Cleavage

In 2019, our group demonstrated the catalytic activity of transition metal bismuthanes (i.e. compounds with a Bi–TM bond, TM = transition metal) in the cyclo-isomerization of δ-iodo-olefins (see Chapter III). In the course of this work, further results addressing homolytic Bi–TM bond cleavage were obtained and are presented in this chapter.

1.1 Cyclo-Isomerization: Catalyst Loading-dependent Formation of Cyclopentane or Cyclohexane Derivatives

Transition metal bismuthane [$Ph_2Bi\{Mn(CO)_5\}$] (**1**) catalyzes the cyclo-isomerization of 2-iodo-2-methyl-6-heptene to give 2-(iodomethyl)-1,1-dimethylcyclopentane in 90% yield.[72] A catalyst loading of 10 mol% was used for this reaction. If only 1 mol% of the catalyst is used, the reaction time increases from 5 h to 2 d and, more importantly, the main product obtained isn't 2-(iodomethyl)-1,1-dimethylcyclopentane, but rather the 6-membered ring, 3-iodo-1,1-dimethylcyclohexane according to ^1H and ^{13}C NMR spectroscopy (Scheme 2).

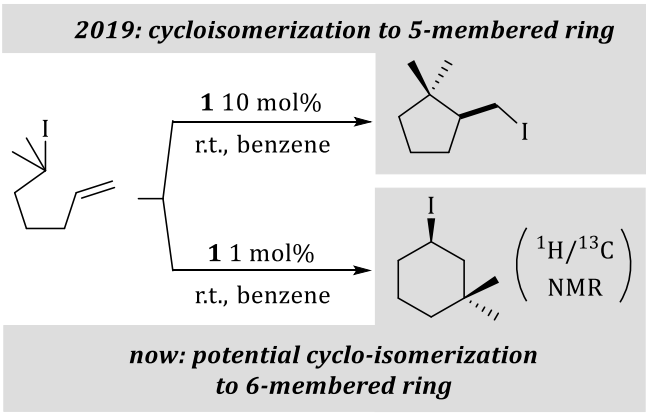

Scheme 2. Catalyst loading-dependent cyclo-isomerization of 2-iodo-2-methyl-6-heptene to give either the five-membered or the six-membered ring as the main product.

The reaction of 2-iodo-2-methyl-6-heptene with 1 mol% of **1** was monitored by ^1H NMR spectroscopy. Complete conversion of the starting material was observed after two days at ambient temperature, whereby the obtained ^1H and ^{13}C NMR spectroscopic data indicate the formation of 3-iodo-1,1-dimethylcyclohexane as the main product. The formation of the 5-membered ring as a by-product is also observed, with a product ratio of 9:1 (Figure 5). A complete separation of the two compounds by column chromatography (eluent: *n*-pentane), as well as a full characterization of the main product, could not be achieved, yet.

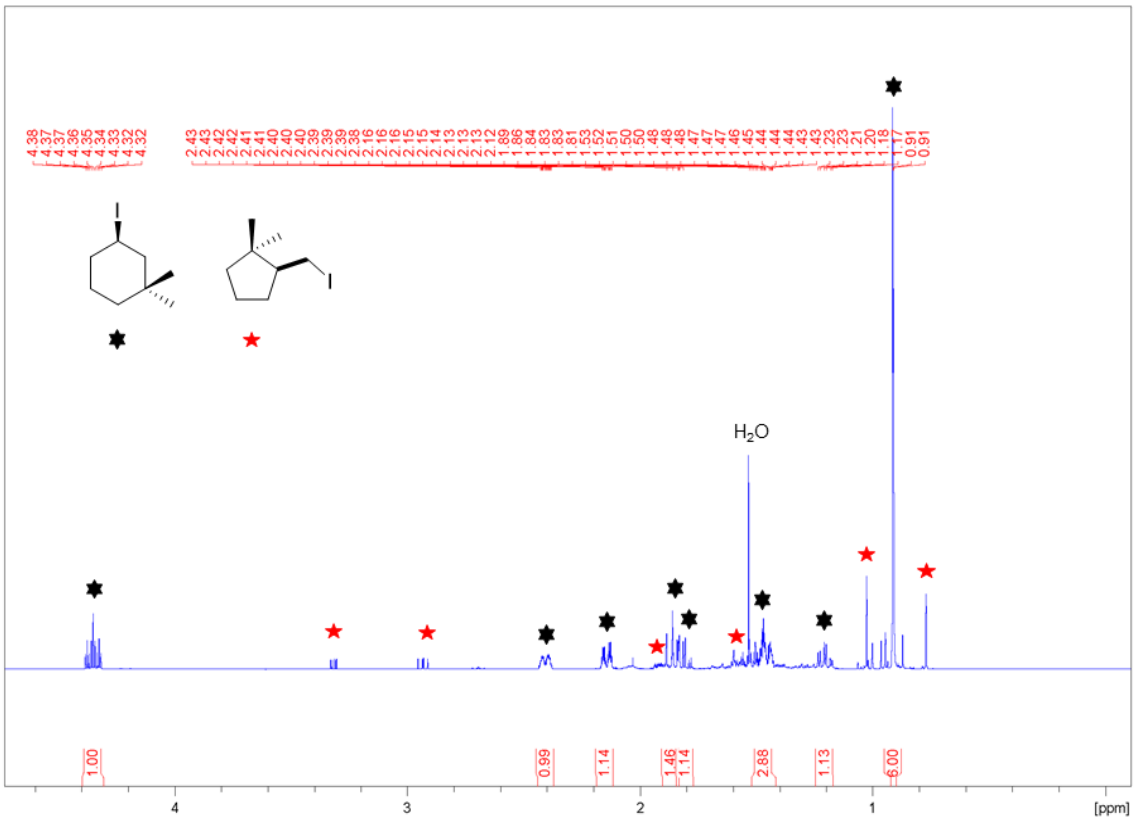

Figure 5. Aliphatic region of the ^{1}H NMR spectrum of the catalytic cyclo-isomerization of 2-iodo-2-methyl-6-heptene with a catalyst loading of 1 mol%. Black, hexagonal stars: 6-membered product. Red pentagonal stars: 5-membered product. The product ratio is 9:1.

The mechanism of the ring-closure of 5-hexenyl-radicals was investigated in detail in the early 1980s. The 1,6-ring closure of such radicals is less favored than the 1,5-ring closure, partly due to steric effects, which is rationalized by considering the transition states for both ring types/geometries (Figure 6).[73–75]

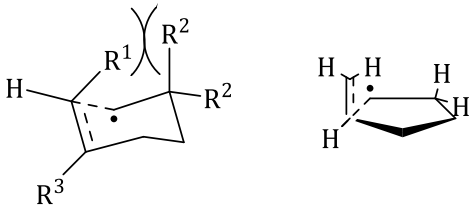

1,6-ring closure 1,5-ring closure

Figure 6. Transition states for the 1,6- and 1,5-ring closure of 5-hexenyl-radicals.

Thus, formation of the 6-membered ring is very uncommon. In addition, differences in catalyst loading normally lead to an increase/decrease in yields and lengthening/shortening of reaction times. Excluding heterocatalysis, changes in product distribution remains scarce. A dependence of the ring size formed on the catalyst loading has not been described for the cyclo-isomerization

of δ-iodo-olefins and might be considered an important tool for the formation of synthetically valuable, organic building blocks.

As part of this work, the isolable antimony radical **2** was also tested as a catalyst in the cyclo-isomerization of δ-iodo-olefins (Figure 7). The cyclo-isomerization of 6-iodo-1-hexene in benzene only reached a low conversion of 16% after 20 h at 60 °C. Due to poor solubility of the catalyst in benzene, the solvent was changed to more polar THF, which led to a conversion of 32% after 20 h at 60 °C. Using the activated iodo-olefin 2-iodo-2-methyl-6-heptene as a substrate and a 10:1 benzene/THF mixture as solvent, a conversion of 75% was observed after 1 d at ambient temperature and a 2:1 product mixture of the 5- and 6-membered rings, respectively, was obtained (catalyst loading: 10 mol%). In conclusion, the use of antimony radical **2** as a catalyst in the cyclo-isomerization leads to lower conversion (substrates 6-iodo-1-hexene and 2-iodo-2-methyl-6-heptene) as well as lower selectivity (2-iodo-2-methyl-6-heptene) compared to transition metal bismuthane **1**.

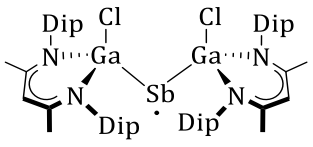

2

Figure 7. Stable antimony radical **2**.

1.2 Reactivity towards Benzoquinones

The homolytic Bi–Mn bond cleavage in [{($C_{14}H_{12}$)S}Bi{$Mn(CO)_5$}] (**3**) was demonstrated by selective reaction with Ph_2S_2 and CCl_4 (see Chapter III). Further results were obtained when **3** was reacted with 1,4-benzoquinone derivatives. The reaction of **3** with the parent compound 1,4-benzoquinone in benzene led to the immediate formation of a dark precipitate. Attempts to dissolve the precipitate in polar solvents (pyridine, THF, 1,2-difluorobenzene) in order to carry out spectroscopic analyses, as well as attempts to obtain single crystals of the product by layering a THF solution of **2** with a THF solution of 1,4-benzoquinone did not succeed. Similar results, accompanied by gas evolution, were obtained by the reaction of **3** with 2,3-dichloro-5,6-dicyano-1,4-benzoquinone (DDQ).

The reaction of **3** with 2,5-di-*tert*-butyl-1,4-benzoquinone at 60 °C led to a light orange solution and small amounts of a black, insoluble precipitate which was removed by filtration (Scheme 3). Due to signal broadening and signal overlap in the ^1H NMR spectrum of the reaction mixture in C_6D_6, the consumption of starting material could not be quantified. Single-crystals of the product **4** suitable for single-crystal X-ray diffraction analysis were obtained by filtration, layering the filtrate with *n*-pentane and storage of the (initially) biphasic system at ambient temperature.

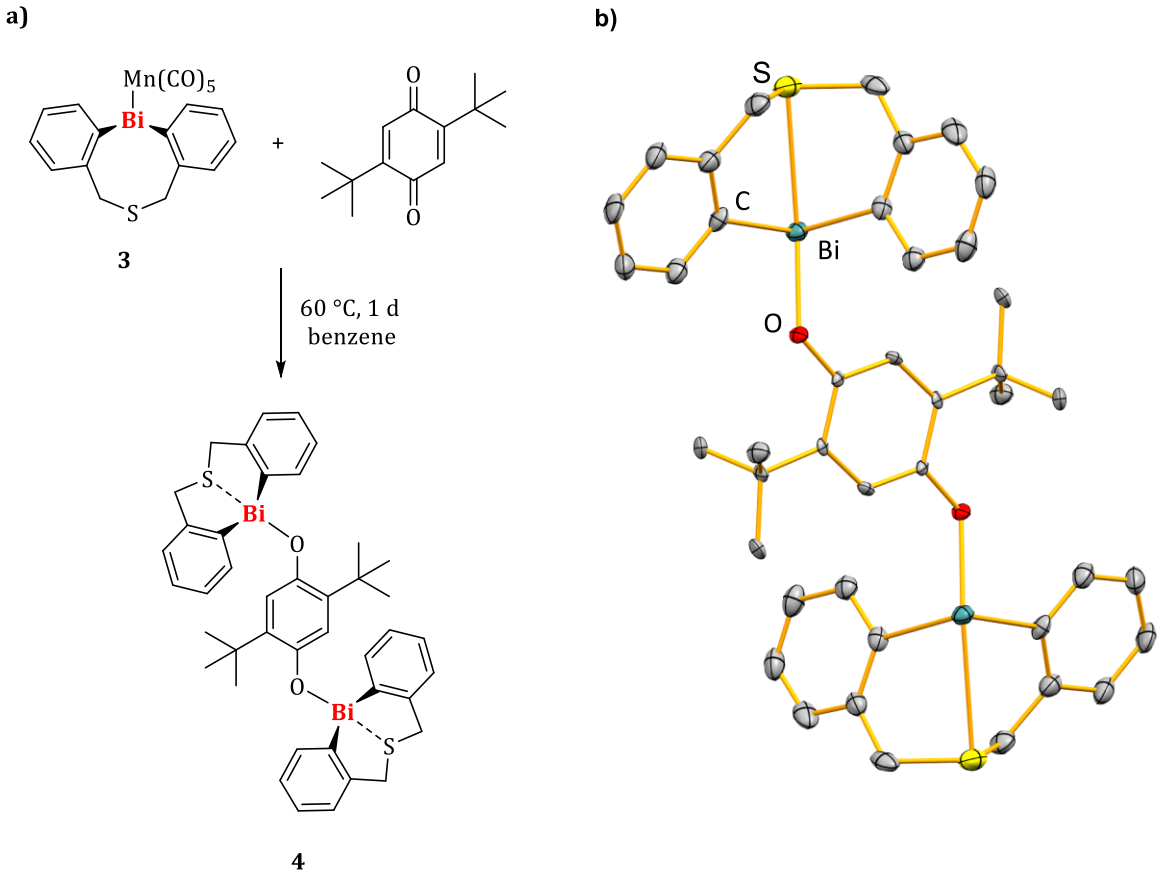

Scheme 3. a) Reaction of **3** with 2,5-di-*tert*-butyl-1,4-benzoquinone. b) Molecular structure of **4** in the solid state. Displacement ellipsoids are shown at the 50% probability level. Hydrogen atoms are omitted for clarity. Selected bond lengths (Å) and angles (°): Bi–C, 2.269(7)–2.299(7); Bi–O, 2.159(4), Bi–S, 3.012(3); C–Bi–C, 95.1(3), C–Bi–O, 81.1(2)–93.1(2); S–Bi–C, 73.16(19)–73.89(19); S–Bi–O, 154.90(13).

The solid-state structure of **4** revealed the formation of two Bi–O bonds and is centrosymmetric (monoclinic space group $P2_1/c$ with $Z = 2$, Scheme 3). The bismuth center adopts a bisphenoidal coordination geometry with the sulfur and oxygen atoms in axial positions and angles of 154.90(13)° for S–Bi–O and 73.16(19)–73.89(19)° for C–Bi–S. The Bi–O bond in **4** (2.159(5) Å) is significantly shorter than the corresponding Bi–O bonds in the salts [{$(C_6H_4)_2S$}Bi][ONO_2] (2.431(9) Å) and [{$(C_6H_4)_2S$}Bi][OSO_2CF_3] (2.571(5) Å)[76] and in the same range as in [{$(C_6H_4)_2S$}Bi{OTEMP}] (2.184(5) Å, TEMP = NC_9H_{18}).[77] In combination with the elongated Bi–S bond in **4** (3.012(3) Å) compared to the above-mentioned salts ([{$(C_6H_4)_2S$}Bi][ONO_2]: 2.764(3) Å; [{$(C_6H_4)_2S$}Bi][OSO_2CF_3]: 2.6741(17) Å) this is indicative for a lower ionic character of the Bi–O bond in **4** and a bonding situation similar to [{$(C_6H_4)_2S$}Bi{OTEMP}] (Bi–S: 2.936(2) Å). The difference in polarity of the (non- or weakly polar) Bi–Mn bond in **3** versus the more polar $Bi^{\delta+}$–$O^{\delta-}$ bond in **4** leads to the additional coordination of the sulfur atom from the ligand backbone to the bismuth center in **4**, which is expected for a sufficiently electronegative substituent X, as in

{$(C_6H_4)_2S$}BiX.[72,76] The electron donation from the sulfur to the bismuth atom is owed to the increased electropositivity of the metal center in **4** as opposed to **3**. In order to balance the reaction shown in Scheme 3, it is conceivable that two $Mn(CO)_5^{\bullet}$ radicals recombine to give $Mn_2(CO)_{10}$. To verify this, an IR spectrum of the reaction mixture was recorded. CO stretching frequencies were observed at $\tilde{\nu}_{CO}$ = 2089, 2066, 2029m 1972 and 1944 cm^{-1}, which are similar, but not equal to the values for $Mn_2(CO)_{10}$ found in the literature ($\tilde{\nu}_{CO}$ = 2046, 2014, 1988 cm^{-1}).[78] Furthermore, the presence of five instead of three carbonyl stretching frequencies for $Mn_2(CO)_{10}$ indicates the formation of by-products. Due to the small amount of isolated substance, the yield of **4** and possible manganese-containing by-products could not be determined, hence the exact course of the reaction of **4** with 2,5-di-*tert*-butyl-1,4-benzoquinone could not be clarified.

1.3 Reactivity towards Tetraphenyl Dibismuthane

As described above, the non-polar Bi–TM bond enables homolytic bond dissociation under mild conditions. A $[R_2Bi]^{\bullet}$ radical generated this way could react with dibismuthanes,[79] i.e. compounds of the general formula $R'_2Bi–BiR'_2$, in order to form hitherto unknown unsymmetrically substituted dibismuthanes $R_2Bi–BiR'_2$. The corresponding transition metal bismuthane $R'_2Bi–[TM]$ would be expected as a by-product of this reaction ([TM] = transition metal complex fragment). In order to test this hypothesis, the manganese bismuthane **3** was combined with stoichiometric amounts of tetraphenyl dibismuthane in benzene solution (Scheme 4). A ^1H NMR spectroscopic analysis of the reaction mixture revealed the formation of $[Ph_2Bi\{Mn(CO)_5\}]$ (**1**)[72] and one set of signals for an unknown {$(C_6H_4)_2S$}Bi species in a 1:0.5 ratio. In addition, traces of other species bearing phenyl and thioether groups were observed. Filtration of the reaction mixture and layering the orange filtrate with *n*-pentane yielded small amounts of a red, crystalline solid suitable for single-crystal X-ray diffraction analysis. The resulting solid-state structure revealed the formation of dibismuthane **5** (Scheme 4). Dibismuthane **5** had also been obtained from the reaction of [{$(C_6H_4)_2S$}Bi{OTEMP}] with $PhSiH_3$, and fully characterized (see Chapter IV for a detailed analysis of **5**). While the reaction did not yield the expected unsymmetrical dibismuthane, it provides a synthetic pathway to a dibismuthane, which had otherwise proved inaccessible by standard reduction attempts of the chloro-precursor **6** in earlier studies (Scheme 4).[80,81]

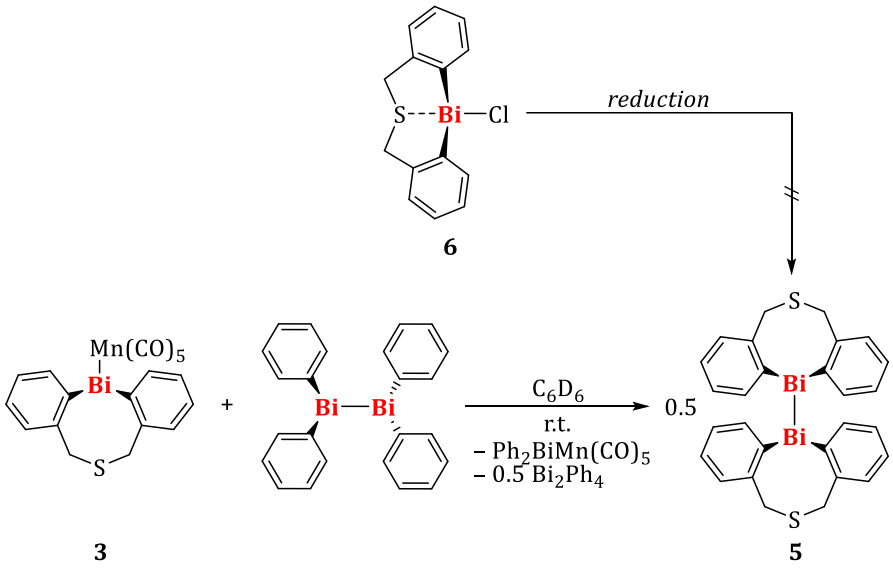

Scheme 4. Reaction of manganese bismuthane **3** with tetraphenyl dibismuthane to give **5**. The synthesis of **5** by reduction of precursor **6** was not successful.[80]

2 Dibenzobismepine as a Hemilabile Ligand: Photochemically-Induced CO-Elimination

Recently, our group described the synthesis of the halo-dibenzobismepine species **8-X** (X = Cl, Br, I) from dinuclear bismepine **7** (Scheme 5, for details see Chapter VI, for attempts to synthesize **7** in other ways than described in Chapter VI, see Table 6 in Experimental Part).[82]

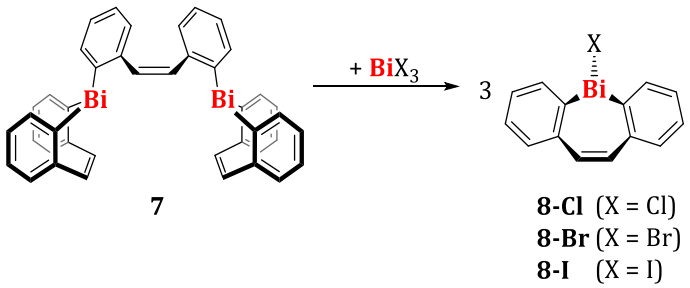

Scheme 5. Synthesis of halobismepines **8-X** starting from dinuclear bismepine **7**.

In the following, the properties of a dibenzobismepinyl group as ligand in transition metal complexes are examined. One focus of these investigations was to verify whether the olefin functionality of the dibenzobismepinyl ligand can participate in a chelating interaction with transition metal centers. The synthesis of transition metal bismuthanes takes place via various synthetic routes: a) The reaction of a triorganobismuthane with a transition metal hydride complex under elimination of RH; b) the reaction of a dibismuthane with dinuclear transition metal complexes to form two equivalents of the transition metal bismuthane; c) invers salt elimination with an alkali metal bismuthide (formed *in situ*) and a transition metal complex

bearing at least one halogen ligand; d) salt elimination of a diorganobismuth halide with a transition metallate; and e) reaction of a bismuth halide with dinuclear transition metal complexes to eliminate transition metal halides (Scheme 6, for further synthetic routes see Chapter II).[83–86]

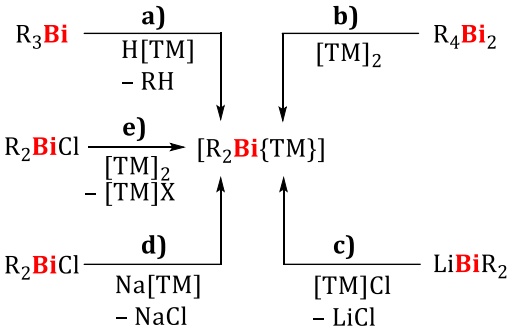

Scheme 6. Synthetic routes frequently used to access transition metal bismuthanes. [TM] = transition metal complex fragment.

Besides other transition metals, manganese, iron and cobalt complexes were the main precursors investigated (for results with other bismepine precursors and/or transition metals see Table 7 in Experimental Part). The initial approach was to react the dinuclear transition metal complexes $[Mn(CO)_5]_2$, $[Fe(CO)_2Cp]_2$ and $[Co(CO)_4]_2$ with chlorobismepine **8-Cl**. However, these reactions led either to i) decomposition with formation of phenanthrene, ii) formation of dinuclear bismepine **7**, iii) generation of $[Bi\{TM\}_3]$, or iv) no conversion under several conditions.[87] In contrast, the salt elimination of chlorobismepine **8-Cl** with sodium metallates (Scheme 6d) proved to be a powerful tool for the generation of transition metal bismuthanes. The complexes synthesized through this way are discussed in more detail below.

2.1 Synthesis and Characterization of Manganese and Iron Complexes

Chlorobismepine **8-Cl** was reacted with $Na(thf)_3[Mn(CO)_5]$ in a mixture of benzene and THF at ambient temperature. $[(C_{14}H_{10})Bi\{Fe(CO)_2Cp\}]$ (**10**) was synthesized in a similar manner at –78 °C (Scheme 7). ^1H NMR spectroscopic analysis of the reaction mixtures showed full conversion of the starting materials in both cases.

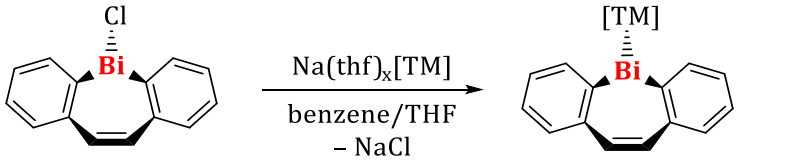

8-Cl

9 ([TM] = $Mn(CO)_5$)
10 ([TM] = $Fe(CO)_2Cp$)

Scheme 7. Synthesis of transition metal bismuthanes **9** and **10** via salt elimination; $Na(thf)_x[TM]$ = $Na(thf)_3[Mn(CO)_5]$, $Na(thf)[Fe(CO)_2Cp]$; Cp = cyclopentadienyl.

In the case of $[\{C_{14}H_{10}\}Bi\{Mn(CO)_5\}]$ (**9**) full characterization of the product was not possible due to decomposition in the solid state as well as in benzene solution. $[Bi\{Mn(CO)_5\}_3]$ and $[Mn(CO)_5]_2$ were identified as decomposition products by single-crystal X-ray diffraction analysis in several samples.[88,89] The decomposition of **9** was also monitored by ^{1}H NMR spectroscopy, revealing dinuclear bismepine **7** as a further decomposition product. The decomposition of **9** can be expressed as three equivalents of **9** reacting to one equivalent of **7** and one equivalent of $[Bi\{Mn(CO)_5\}_3]$. The additional formation of $[Mn(CO)_5]_2$ can be explained by the fact that $[Bi\{Mn(CO)_5\}_3]$ decomposes further, whereby low-valent bismuth species could be formed. Nevertheless, complex **9** was characterized *in situ* by ^{1}H and ^{13}C NMR spectroscopy. The NMR spectra of **9** show the expected set of signals for the bismepine unit, with the resonances for the olefin unit at $\delta(^1H)$ = 6.92 ppm and $\delta(^{13}C)$ = 134.44 ppm, respectively. This indicates no interaction between the manganese center and the olefin backbone, since the resonances for this functionality are found at similar values for **8-Cl** and other non-coordinating bismepine species ($\delta(^1H)$ = 6.49–6.65 ppm and $\delta(^{13}C)$ = 131.19–136.07 ppm for **7** and **8-X** (X = Cl, Br, I)). The ^{13}C NMR resonance for the carbonyl groups is found at $\delta(^{13}C)$ = 203.99 ppm showing a significant upfield shift compared to the carbonyl resonances in **1** ($\delta(^{13}C)$ = 218.96 ppm) and **3** ($\delta(^{13}C)$ = 213.73 ppm).[72] The differences in the ^{13}C NMR spectroscopic resonances for the carbonyl ligands is accompanied by weaker π-backdonation from the metal to the carbonyl in the case of **9**. One reason for this could be the decrease of electron density at the manganese center due to the introduction of the bismepinyl ligand. Such a significant difference in the chemical shifts (^{13}C) for the carbonyls in $[Ph_2Bi\{TM\}]$, $[(C_{14}H_{12}S)Bi\{TM\}]$ and $[\{C_{14}H_{10}\}Bi\{TM\}]$ only occurs for the manganese species (see below).

$[\{C_{14}H_{10}\}Bi\{Fe(CO)_2Cp\}]$ (**10**) was synthesized according to Scheme 7 at –78 °C in 63% yield. **10** was analyzed by single-crystal X-ray diffraction and crystallized in the triclinic space group $\bar{P}1$ with Z = 4[1] (Figure 8).

[1] Indications of a higher symmetry of the space group were not found.

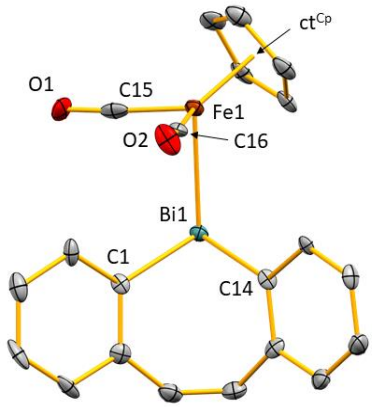

Figure 8. Molecular structure of **10** in the solid state. Displacement ellipsoids are shown at the 50% probability level. Hydrogen atoms are omitted for clarity; ct^{Cp} represents the centroid of the cyclopentadienide ligand. The asymmetric unit contains two chemically identical but crystallographically independent formula units of **10**, only one of which is discussed because the bonding parameters do not differ significantly. Selected bond lengths (Å) and angles (°): Bi1–C1, 2.6645(14); Bi1–C14, 2.259(8); Bi1–Fe1, 2.6645(14); Fe1–C15, 1.772(10); Fe1–C16, 1.754(11); Fe1–ct^{Cp}, 1.720; Fe1–Bi1–C1, 105.1(2); Fe1–Bi1–C14, 103.4(2); C1–Bi1–C14, 86.5(3), C16–Fe1–C15, 94.9(4); Bi1–Fe1–ct^{Cp}, 117.75; C15–Fe1–ct^{Cp}, 127.48; C16–Fe1–ct^{Cp}, 127.13.

The asymmetric unit contains two crystallographically distinct molecules of **10**, only one of which is discussed herein because the bonding parameters do not differ significantly. The bismuth center is found in a trigonal pyramidal coordination geometry with a C–Bi–C angle of 86.5(3)° and C–Bi–Fe angles of 103.4(2)–105.1(2)°, respectively. The iron atom adopts a distorted tetrahedral coordination geometry with angles around Fe1 of 94.9(4)–127.13°. The Bi–Fe bond length of 2.6645(14) Å is in the range of reported bismuth iron bonds.[90–98] The ^{1}H and ^{13}C NMR spectra of compound **10** in benzene solution show the expected signal pattern for the bismepine unit and the cyclopentadienide ligand. Remarkably, the ^{1}H NMR resonances of the bismepine protons are shifted significantly to low field ($\Delta\delta$ = 0.26–0.86 ppm) for complex **10** compared to manganese complex **9**. The ^{13}C NMR spectroscopic resonance for the carbonyl ligands at $\delta(^{13}C)$ = 212.49 ppm is very similar to those in $[Ph_2Bi\{Fe(CO)_2Cp\}]$ ($\delta(^{13}C)$ = 210.11 ppm)[80] and $[\{(C_{14}H_{12})S\}Bi\{Fe(CO)_2Cp\}]$ ($\delta(^{13}C)$ = 212.03 ppm). Compound **10** was also characterized by IR and UV-vis spectroscopy. The IR spectrum of **10** shows two CO stretching modes at $\tilde{\nu}_{CO}$ = 1972 cm^{-1} and 1926 cm^{-1}, as expected for tetrahedral iron complexes with C_s symmetry and a non-polar Bi–Fe bond. The UV-vis spectrum of **10** shows an absorption maximum at 362 nm.

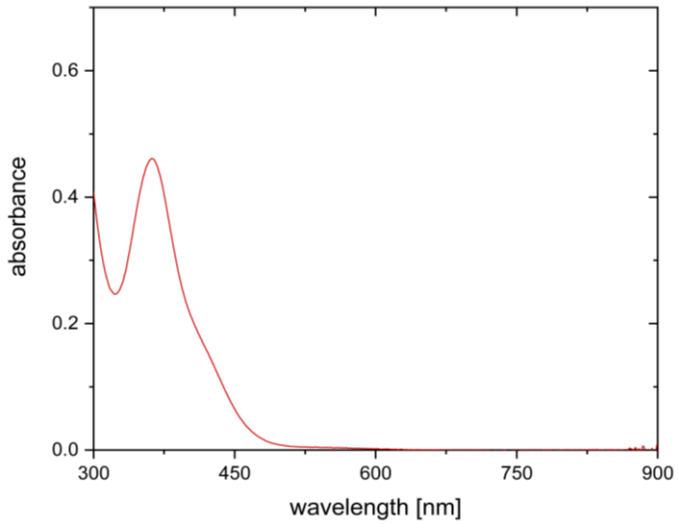

Figure 9. Experimental UV-vis spectrum of **10** (0.34 mM) in THF.

Irradiation of **10** for 5 h at a wavelength of 525 nm in benzene solution led to full conversion to a new bismepine species as observed by ^{1}H NMR spectroscopy (Scheme 8a). The new species shows a ^{1}H NMR spectroscopic signal pattern as expected for a chiral, tetrahedral iron complex: all protons of the bismepine group show a single resonance. The resonances for the protons of the olefin backbone (δ(^{1}H) = 4.66 and 5.03 ppm) show a strong high-field shift compared to the chemical shift of the same protons in **10** (δ(^{1}H) = 6.91 ppm). These results speak for the elimination of one carbonyl ligand upon irradiation with simultaneous π-coordination between the olefin functionality and the iron center. The iron center would thus bear four different ligands and present a stereocenter. Suitable material for single crystal X-ray diffraction of **11** were obtained by layering a THF solution of **11** with *n*-pentane and storage at –30 °C. **11** crystallized in the orthorhombic non-centrosymmetric space group $P2_12_12_1$ with Z = 4 and one molecule in the asymmetric unit (Scheme 8b).

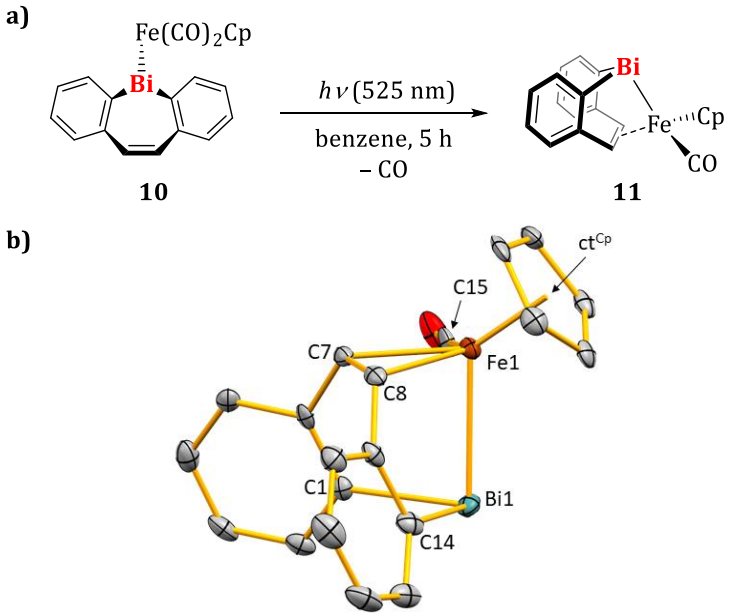

Scheme 8. a) Synthesis of **11** by irradiation of **10**. b) Molecular structure of **11** in the solid state. Displacement ellipsoids are shown at the 50% probability level. Hydrogen atoms and the lattice bound THF molecule are omitted for clarity; ct^{Cp} represents the centroid of the cyclopentadienide ligand. Selected bond lengths (Å) and angles (°): Bi1–C1, 2.271(6); Bi1–C14, 2.258(7); Bi1–Fe1, 2.6465(10); Fe1–C7, 2.137(7); Fe1–C8, 2.128(7); Fe1–C15, 1.762(8); Fe1–ct^{Cp}, 1.728; Fe1–Bi1–C1, 86.71(17); Fe1–Bi1–C14, 89.23(16); C1–Bi1–C14, 84.0(2); Bi1–Fe1–ct^{Cp}, 126.67; C15–Fe1–ct^{Cp}, 120.74.

Due to the bite angle of the bismepine chelate ligand the iron center adopts a more distorted tetrahedral coordination geometry than in starting material **10**, with angles around Fe1 of 86.71(17)–126.67°. The bismuth atom is found in a trigonal pyramidal coordination geometry with a C–Bi–C bond angle of 84.0(2)°. While the central heterocycle of the bismepine framework in **10** is still pointing away from the transition metal center, it now points towards the iron atom in **11** and the olefin functionality occupies the fourth coordination site with a distance of 2.013(7) Å between Fe1 and the center of the C7–C8 bond. Concomitantly, the C7–C8 bond in **11** is significantly longer (1.415(10) Å) than in **10** (1.343(13) Å) and thus in the range of a partial double bond.[99] The Bi–Fe bond length (2.6465(19) Å) is similar to that in **10** (2.6645(14) Å). Crystallization of **11** resulted in obtaining one enantiomer, however, no bulk analysis of the obtained crystalline material was performed. Thus, it cannot be excluded that the other enantiomer of **11** was also obtained by crystallization. Hence, whether crystallization can serve as a separation method for obtaining enantiomerically pure material has not been conclusively clarified.

The IR spectrum of compound **11** shows one CO stretching mode at $\tilde{\nu}_{CO}$ = 1930 cm^{-1}. The UV-vis spectrum of the dark red solid in THF shows an absorption maximum at 353 nm and a very low intensity secondary maximum at 604 nm (Figure 10).

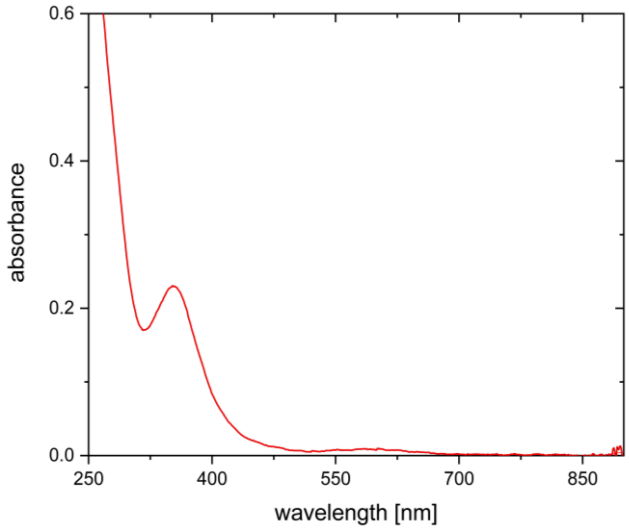

Figure 10. Experimental UV-vis spectrum of **11** (0.30 mM) in THF.

It was also possible to show a partial reversibility of the reaction shown in Scheme 8 by exposing a solution of complex **11** to an atmosphere of 0.5 bar CO. ^{1}H NMR spectroscopic analysis showed a 1:3 mixture of **10** and **11**, respectively (Scheme 9).

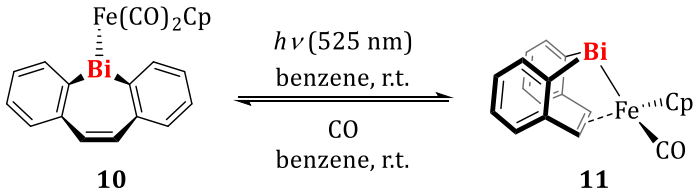

Scheme 9. Reversible formation of chelate complex **11**.

Based on the synthesis of the doubly substituted iron complex $[(Ph_2Bi)_2Fe(CO)_4]$,[83] the bismepinyl analog **12** was prepared according to Scheme 10 and isolated in 53% yield as a yellow solid.

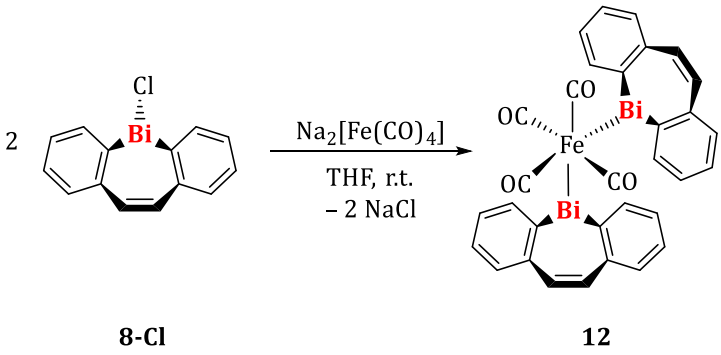

Scheme 10. Synthesis of bis-bismepinyl substituted iron complex **12** (Collman's reagent washed with small amounts of THF and dried *in vacuo* prior to use to remove decomposition products).

The solid-state structure of **12** was determined by X-ray diffraction analysis (triclinic space group $\bar{P}1$ with $Z = 2$, Figure 11). The quality of the data does not allow for a discussion of the bonding parameters due to twinning, that could not be adequately modelled, and insufficient scattering. However, analog to the parent compound $[(Ph_2Bi)_2Fe(CO)_4]$,[83] **12** shows a *cis*-arrangement of the bismepinyl ligands around the octahedrally coordinated iron atom in the solid state. The olefin functionalities of the bismepine ligands are bent towards the iron center, which could allow CO elimination and formation of a chelate complex.

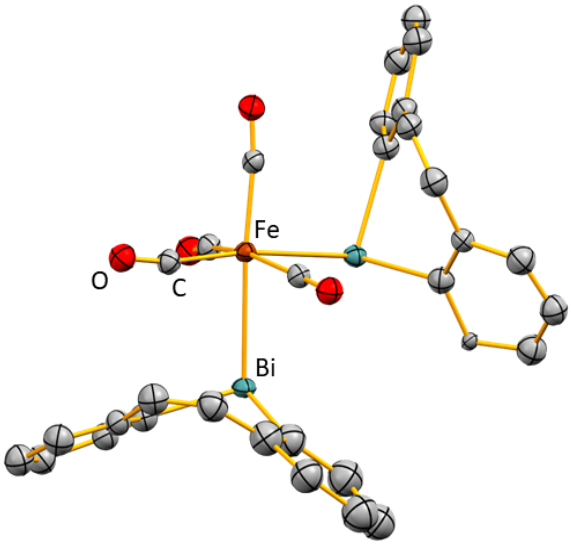

Figure 11. Molecular structure of **12** in the solid state. Displacement ellipsoids are shown at the 50% probability level. Hydrogen atoms are omitted for clarity.

In contrast to literature known $[(Ph_2Bi)_2Fe(CO)_4]$, which shows rapid decomposition in solution,[83] **12** is stable in benzene solution for at least 24 h. Compound **12** shows four bands for the CO stretching modes, as to be expected for compounds of the type *cis*-$[Fe(CO)_4L_2]$. However, literature reports list three CO stretching modes in the range of 2081–1973 cm^{-1} for $[(Ph_2Bi)_2Fe(CO)_4]$ in methylene chloride solution and five in *n*-hexane solution, respectively. These findings are not discussed in detail, but are possibly due to decomposition.[83] The absorption bands observed for **12** at $\tilde{\nu}_{CO}$ = 2040, 1981, 1961 and 1933 cm^{-1} are in the same range as the analog absorptions for $[\{C_{14}H_{10}\}Bi\{Fe(CO)_2Cp\}]$ (**10** ($\tilde{\nu}_{CO}$ = 1972, 1920 cm^{-1}) and $[\{\kappa^2C,\kappa^1Bi\text{-}(C_{14}H_{10})Bi\}FeCp(CO)_2]$ (**11**) ($\tilde{\nu}_{CO}$ = 1930 cm^{-1}), with a somewhat higher frequency for one CO ligand. However, a clear comparison of the carbonyl stretching frequencies between these compounds is hampered by their different symmetries.

The UV-vis spectrum of **12** shows two absorption maxima at 288 and 362 nm, with an onset at approximately 460 nm (Figure 12).

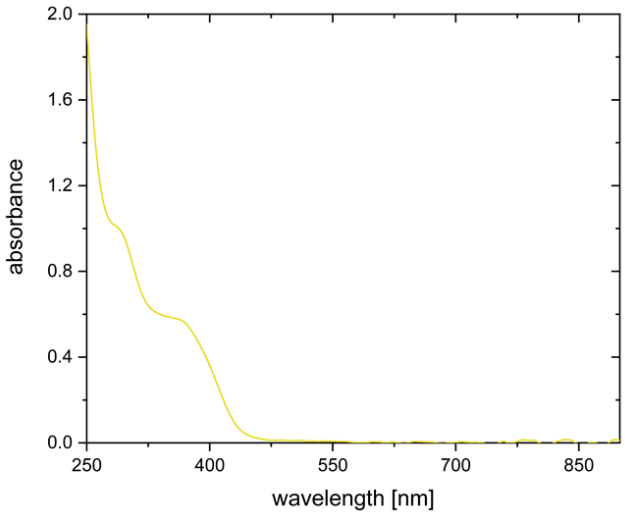

Figure 12. Experimental UV-vis spectrum of **12** (0.10 mM) in THF.

In light of its solid-state structure and the successful synthesis of chelate complex **11**, compound **12** was irradiated at a wavelength of 365 nm. After 5 h of irradiation, the selective formation of a new product was detected by ^{1}H NMR spectroscopy (ca. 20% conversion). Further irradiation for several hours did not result in further conversion to this unknown product. The new species shows two ^{1}H NMR resonances at $\delta(^1H)$ = 3.57 and 4.27 ppm, indicating the formation of a coordinated olefin complex. Since no further conversion of **12** could be achieved under these conditions, the reaction mixture was put under an atmosphere of CO gas to check whether this was due to an equilibrium. Under a CO atmosphere, no conversion of the new species back to starting material **12** was observed by ^{1}H NMR spectroscopy. These observations point to either an irreversible CO elimination under formation of cluster species, or a reaction in which CO elimination does not take place. No attempt was made to isolate the unknown reaction product, due to the small amount of substance.

2.2 Synthesis and Characterization of Chiral Cobalt Complexes

Other transition metal bismuthanes investigated in this work were trigonal bipyramidal cobalt complexes of the type [{($C_{14}H_{10}$)Bi}Co(CO)$_n$L$_{4-n}$] with L as a neutral donor ligand. The parent compound [{($C_{14}H_{10}$)Bi}Co(CO)$_4$] (**13**) was synthesized according to Scheme 11. In accordance with the literature-known compound [{Ph_2Bi}Co(CO)$_4$], it was only possible to characterize the product in solution due to decomposition during attempts to isolate this species.[84] The slow and selective conversion (10% conversion after 5 h) of **13** into a single new species in benzene solution was also observed. The product was identified as the chelate complex [{κ^2*C*,κ^1*Bi*-($C_{14}H_{10}$)Bi}Co(CO)$_3$] (**14**), the selective synthesis and characterization of which will be discussed in more detail later.

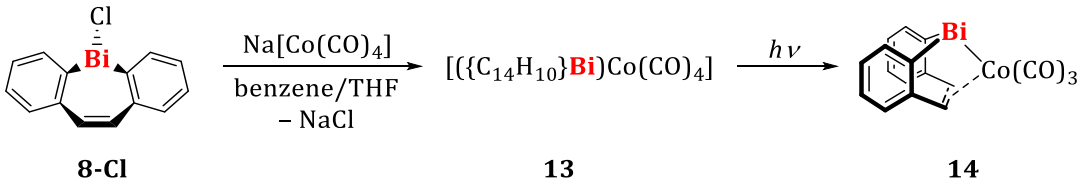

8-Cl **13** **14**

Scheme 11. Synthesis of transition metal bismuthane **13** via salt elimination.

As described in the literature, one equivalent of a neutral donor ligand (PPh_3, PCy_3 or *t*BuNC) was added to the reaction mixture to stabilize the product, so that the transition metal bismuthanes **13-L** could be obtained in moderate yields (32%–62%, Scheme 12). In the synthesis of **13-PCy$_3$**, the transition metal bismuthane [Bi{Co(CO)$_3$(PCy$_3$)}$_3$] by-product was identified by X-ray diffraction analysis (the data quality does not allow a discussion of the bonding parameters).

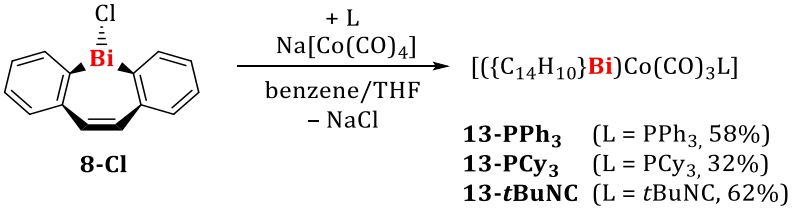

8-Cl

Scheme 12. Synthesis of transition metal bismuthanes **13-PPh$_3$**, **13-PCy$_3$** and **13-*t*BuNC**.

The ^{1}H NMR spectra of **13(-L)** each show one doublet for the α-proton, i.e. the proton in *ortho*-position to the bismuthyl-substituted carbon atom, at $\delta(^1H)$ = 8.47 (**13**), 8.92 (**13-PPh$_3$**), 8.90 (**13-PCy$_3$**), and 8.82 (**13-*t*BuNC**) ppm, respectively, which represents a pronounced downfield shift of the resonances compared to the resonances of the analog protons in the iron (**10**, $\delta(^1H)$ = 8.13 ppm) and manganese complexes (**9**, $\delta(^1H)$ = 7.58 ppm). This trend has also been observed in the series [{($C_{14}H_{12}$)S}Bi[TM]] with [TM] = $Mn(CO)_5$ (**3**, $\delta(^1H)$ = 7.16 ppm), $Fe(CO)_2Cp$ ($\delta(^1H)$ = 7.78 ppm) and $Co(CO)_3(PPh_3)$ ($\delta(^1H)$ = 8.47 ppm). The resonances for the protons of the olefin backbone are in the range of $\delta(^1H)$ = 6.72–6.89 ppm, which indicates that there is no coordination of the olefin to the transition metal center in **13(-L)**. The ^{13}C NMR spectroscopic resonances for the carbonyl ligands are found at $\delta(^{13}C)$ = 200.99 (**13**), 201.61 (**13-PPh$_3$**), 202.95 (**13-PCy$_3$**) and 203.67 (**13-*t*BuNC**) ppm, with the resonance for **13-PPh$_3$** splitting into a doublet with a $^2J_{PC}$ coupling constant of 16.3 Hz. The phosphine containing complexes show resonances at $\delta(^{31}P)$ = 68.22 (**13-PPh$_3$**) and 78.55 (**13-PCy$_3$**) ppm, respectively, in their ^{31}P NMR spectra. The related compound [{($C_{14}H_{12}$)S}Bi{Co(CO)$_3$(PPh$_3$)}] ($\delta(^{31}P)$ = 68.89) shows a very similar resonance in the ^{31}P NMR spectrum, indicating no significant differences in *trans*-influence of the bismuthyl ligands. Thus, the resonance for **13-PCy$_3$** at higher chemical shift can be attributed to the stronger donor influence of the PCy_3 ligand compared to PPh_3.

The IR spectra of **13(-L)** show the expected four (**13**) or three (**13-L**) CO stretching vibrations, with the modes for **13** appearing at higher wavenumbers ($\tilde{\nu}_{CO}$ = 2075, 2036, 2019, 1989 cm^{-1}), which is consistent with results from the literature for $[(Ph_2Bi)Co(CO)_4]$.[84] The relevant IR frequencies for the substituted derivatives are summarized in Table 1. The CO stretching frequencies for **13-PPh$_3$** are in the same range as those for $[\{(C_{14}H_{12})S\}Bi\{Co(CO)_3(PPh_3)\}]$.[72] For **13-PCy$_3$** and **13-*t*BuNC**, the CO stretching frequencies are slightly shifted to lower wavenumbers compared to those of **13-PPh$_3$**, which might be due to stronger σ-donor capabilities of the former two ligands. The IR spectrum of **13-*t*BuNC** shows an additional band at $\tilde{\nu}_{NC}$ = 2167 for the *t*BuNC moiety.

Table 1. CO (and NC) stretching frequencies of compounds **13-L**.

Entry	Compound	$\tilde{\nu}_{CO}$ [cm^{-1}]			$\tilde{\nu}_{NC}$ [cm^{-1}]
1	**13-PPh$_3$**	2010	1944	1927	–
2	**13-PCy$_3$**	1998	1932	1913	–
3	**13-*t*BuNC**	1984	1934	1923	2167

Because of the instability of **13** in the solid state, no crystalline material was obtained from this compound. For **13-L**, however, it was possible to obtain crystals suitable for X-ray diffraction analyses (**13-PPh$_3$**: monoclinic space group $P2_1/c$ with Z = 4; **13-PCy$_3$**: triclinic space group $\bar{P}1$ with Z = 2; **13-*t*BuNC**: monoclinic space group $P2_1/m$ with Z = 2, Figure 13).

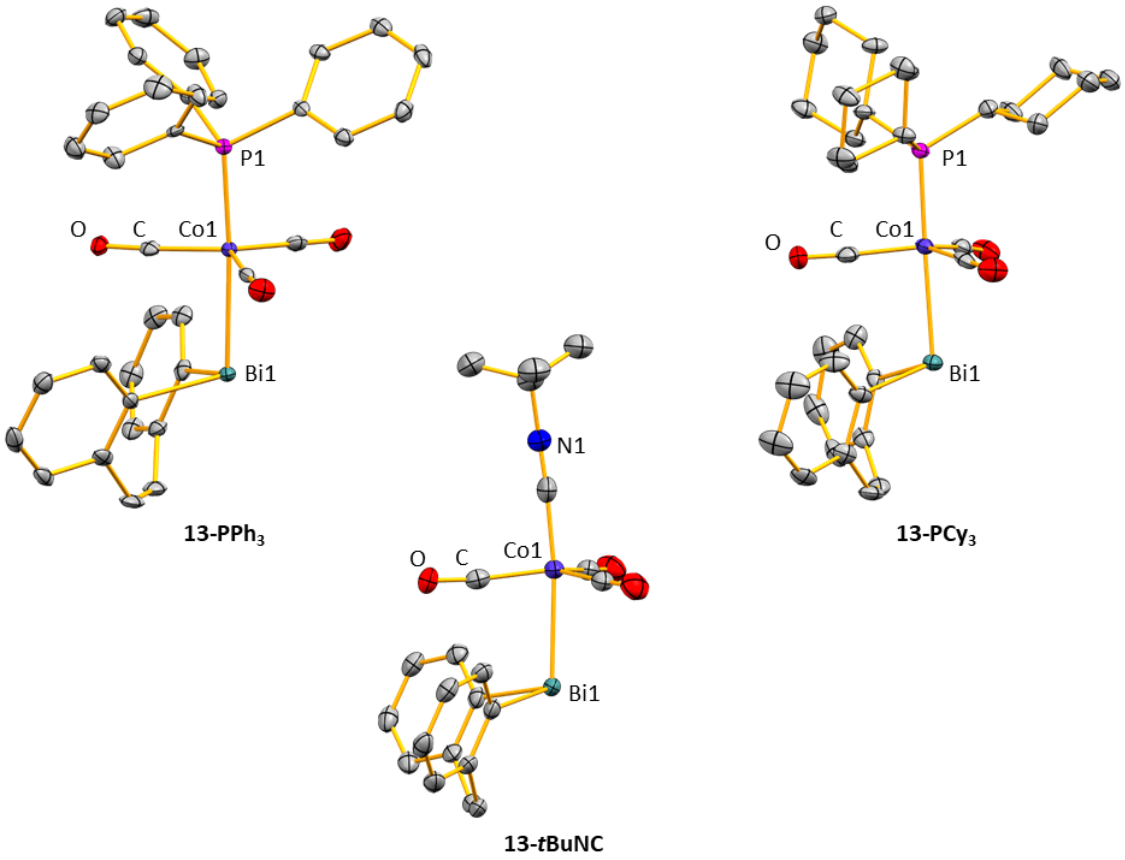

Figure 13. Molecular structures of [{($C_{14}H_{10}$)Bi}Co(CO)$_3$(PPh_3)] (**13-PPh$_3$**), [{($C_{14}H_{10}$)Bi}Co(CO)$_3$(PCy_3)] (**13-PCy$_3$**), and [{($C_{14}H_{10}$)Bi}Co(CO)$_3$(*t*BuNC)] (**13-*t*BuNC**), in the solid state. Displacement ellipsoids are drawn at the 50% probability level. Hydrogen atoms and lattice bound solvent molecules are omitted for clarity. Selected bond lengths (Å) and angles (°): Compound **13-PPh$_3$**: Bi1–Co1, 2.6741(4), Bi1–C, 2.252(3)–2.262(3); Co1–C_{CO}, 1.765(4)–1.783(3); Co1–P1, 2.2045(9); C_{olefin}–C_{olefin}, 1.317(5); C–Bi1–C, 89.37(12); C–Bi1–Co1, 99.32(9)–100.76(9); Bi1–Co1–C_{cis}, 84.61(11)–86.34(11); Bi1–Co1–P1, 176.13(3); C_{CO}–Co1–C_{CO}, 114.93(15)–123.54(15). Compound **13-PCy$_3$**: Bi1–Co1, 2.6877(10), Bi1–C, 2.253(6)–2.256(7); Co1–C_{CO}, 1.768(7)–1.784(7); Co1–P1, 2.2292(18); C_{olefin}–C_{olefin}, 1.338(10); C–Bi1–C, 88.6(2); C–Bi1–Co1, 101.52(17)–102.88(16); Bi1–Co1–C_{CO}, 81.8(2)–87.6(2); Bi1–Co1–P1, 176.15(6); C_{CO}–Co1–C_{CO}, 116.9(3)–121.9(3). Compound **13-*t*BuNC**: Bi1–Co1, 2.7276(8); Bi1–C, 2.258(4); Co1–C_{CO}, 1.785(7)–1.789(5), Co1–C_{NC}, 1.859(7); C_{olefin}–C_{olefin}, 1.336(10); C–Bi1–C, 89.3(2); C–Bi1–Co1, 100.25(10); Bi1–Co1–C_{cis}, 82.18(19)–85.79(14); Bi1–Co1–C_{trans}, 173.7(2); Co1–C_{NC}–N1, 176.7(6); C_{CO}–Co1–C_{CO}, 114.5(3)–121.39(15).

Compounds **13-L** possess typical molecular structures in the solid state without directed intermolecular interactions. The cobalt centers are found in trigonal bipyramidal coordination geometries (τ_5 = 0.88 (**13-PPh$_3$**), 0.90 (**13-PCy$_3$**), 0.87 (**13-*t*BuNC**)) with phosphanes (**13-PPh$_3$** and **13-PCy$_3$**) or the isonitrile (**13-*t*BuNC**), respectively, and bismuthyl units in the axial positions. The bismuth atoms are found in trigonal pyramidal geometries with Bi–C (2.252(3)–2.262(3) Å) and Bi–Co (2.6741(4)–2.7276(8) Å) bond lengths in the expected ranges.[72,84,100,101] However, the Bi–Co bond length in **13-*t*BuNC** is significantly longer than those in the phosphane analogs due to the good σ-donating ability of the isonitrile ligand in *trans*-position.[102] The olefins in the ligand

backbones do not coordinate to the transition metal centers, and their C–C bond lengths (1.317(5)–1.338(10) Å) are in the range for classic C–C double bonds.[99]

UV-vis spectroscopic experiments were carried out on compounds **13** (orange in THF solution), **13-PPh$_3$** (orange solid), **13-PCy$_3$** (orange solid) and **13-*t*BuNC** (red solid). Additionally, (TD)-DFT studies were performed with the Gaussian programme[103] on compounds **13(-L)** (Figure 14). The results presented here were obtained with the functionals B3LYP[104] for optimizations and frequency calculations, and CAM-B3LYP for TD-DFT calculations,[105] Grimme D3 dispersion corrections,[106] and 6-31G(d,p)[107] [H, C, N, O, P] and LANL2DZ[108–110] [Co, Bi] basis sets. All transitions discussed here are singlet-singlet transitions.

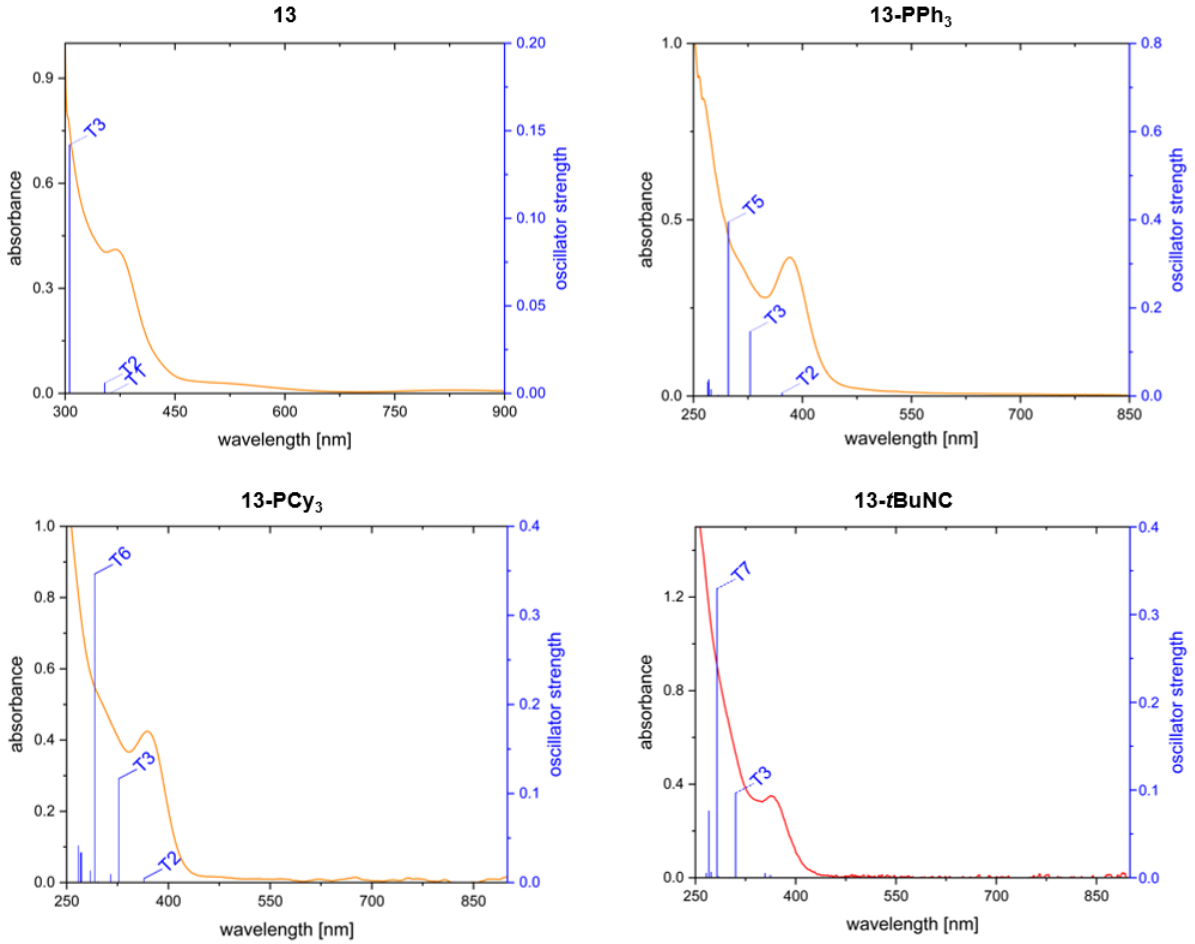

Figure 14. Experimental UV-vis spectra of **13** (0.04 mM), **13-PPh$_3$** (0.03 mM), **13-PCy$_3$** (0.08 mM), and **13-*t*BuNC** (0.07 mM), in THF (**13**: orange, λ_{max} = 369 nm, onset at 530 nm; **13-PPh$_3$**: orange, λ_{max} = 382 nm, onset at ca. 540 nm; **13-PCy$_3$**: orange, λ_{max} = 369 nm, onset at ca. 430 nm; **13-*t*BuNC**: red, λ_{max} = 362 nm, onset at ca. 450 nm) and calculated transitions (blue).

The experimental UV-vis spectrum of the parent compound **13** in THF shows an absorption maximum at 369 nm. The absorptions were correlated with three singlet-singlet transitions T1–T3, one of which shows a larger oscillator strength (T3: 306 nm). The difference between the calculated and experimentally determined value of 63 nm is large. This could be due to the level

of theory used in the DFT calculations. T1, T2 and T3 correspond to a range of transitions, but mainly to HOMO–5→LUMO (T1, 66%), HOMO–4→LUMO (T2, 63%), and HOMO–1→LUMO (T3, 31%) transitions, respectively. While the HOMO–5 and the HOMO–4 show contributions to Co–C_{CO} σ-bonding, the HOMO–1 shows contributions to Bi–Co σ-bonding and the LUMO shows contributions to Co–C_{CO} σ*-antibonding interactions to all four carbonyl ligands and Co–Bi σ*-antibonding interactions (Figure 15).

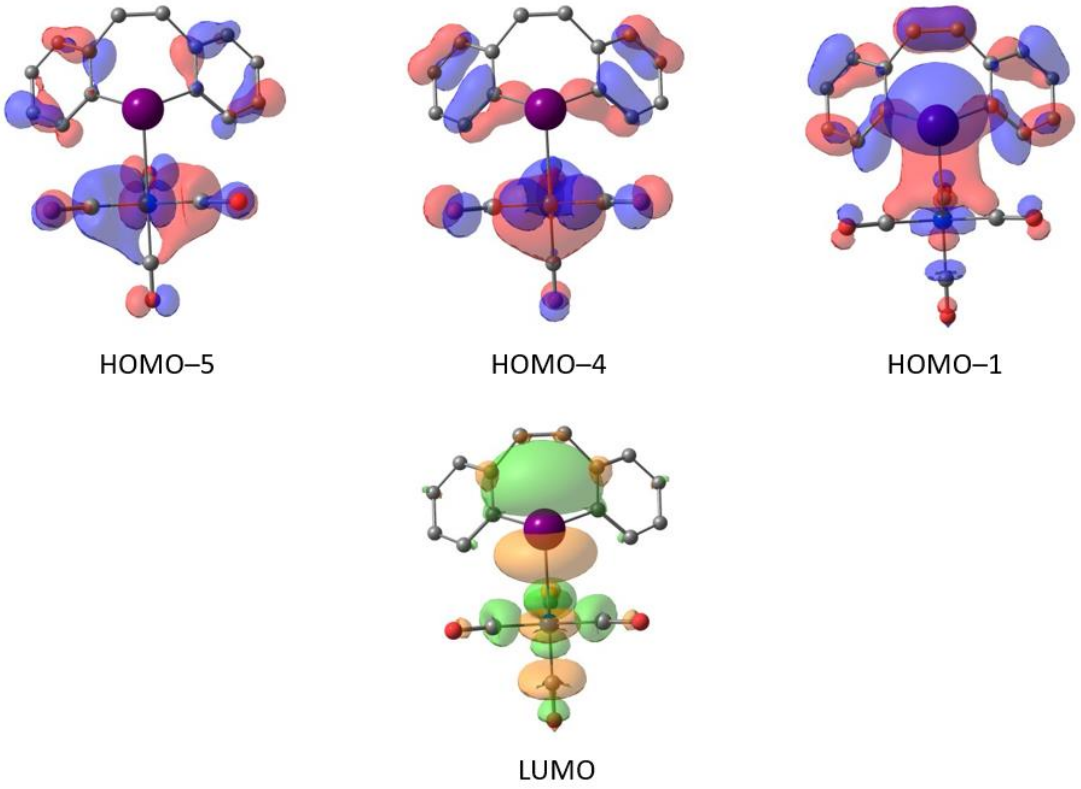

Figure 15. Frontier orbitals of compound **13** (isovalues = 0.03) with main contributions to transitions T1, T2 and T3.

For compound **13-PPh$_3$**, the experimental UV-vis spectrum in THF shows an absorption maximum at 382 nm with an onset at ca. 540 nm. These absorptions were correlated with five singlet-singlet transitions T1–T5, two of which show larger oscillator strengths (T3: 328 nm; T5: 297 nm). T3 and T5 correspond to a range of transitions, but mainly to HOMO→LUMO (T3, 32%; T5, 42%) transitions. The HOMO shows contributions of Co–C_{CO}, as well as Co–Bi σ-bonding interactions, and the LUMO shows contributions of Co–C_{CO} σ*-antibonding interactions (Figure 16).

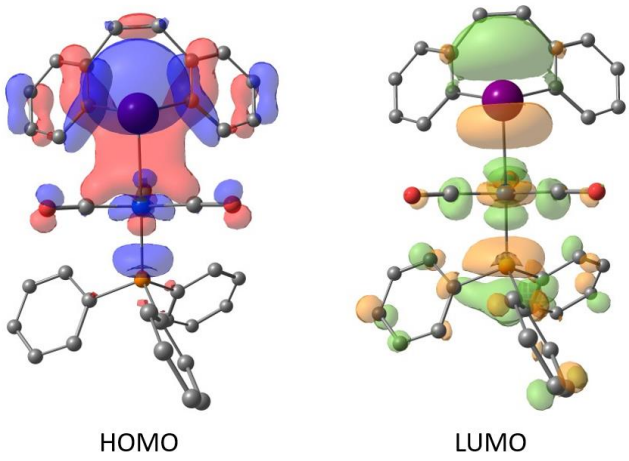

Figure 16. Frontier orbitals of compound **13-PPh$_3$** (isovalues = 0.03) with main contributions to transitions T3 and T6.

The experimental UV-vis spectrum of **13-PCy$_3$** in THF shows an absorption maximum at 369 nm. Here, the absorptions correlate with six singlet-singlet transitions T1–T6, two of which show larger oscillator strengths (T3: 327 nm; T6: 291 nm). As for **13-PPh$_3$**, T3 and T6 show a high proportion of HOMO→LUMO transitions (T3, 30%; T6, 44%). The HOMO shows contributions of Co–C_{CO}, as well as Co–Bi σ-bonding interactions, and the LUMO shows contributions of Co–C_{CO} σ*-antibonding interactions, similarly (and optically identical) to **13-PPh$_3$**.

The experimental UV-vis spectrum of **13-*t*BuNC** in THF shows an absorption maximum at 362 nm. The absorptions were correlated with seven singlet-singlet transitions T1–T7, three of which show larger oscillator strengths (T3: 310 nm; T7: 282 nm; T9: 270 nm). T3, T7 and T9 correspond mainly to HOMO–10→LUMO (T3, 37%), HOMO→LUMO (T7, 43%), HOMO–1→LUMO+1 (T9, 26%) and HOMO→LUMO+2 (T9, 19%) transitions, respectively. While the HOMO–10 shows contributions to Co–C_{CO} σ-bonding, the HOMO–1 and HOMO show contributions to Bi–Co σ-bonding, and the LUMO, LUMO+1 and LUMO+2 show contributions to Co–C_{CO} σ*-antibonding interactions to all three (LUMO and LUMO+1), or only two (LUMO+2) carbonyl ligands, respectively (Figure 17).

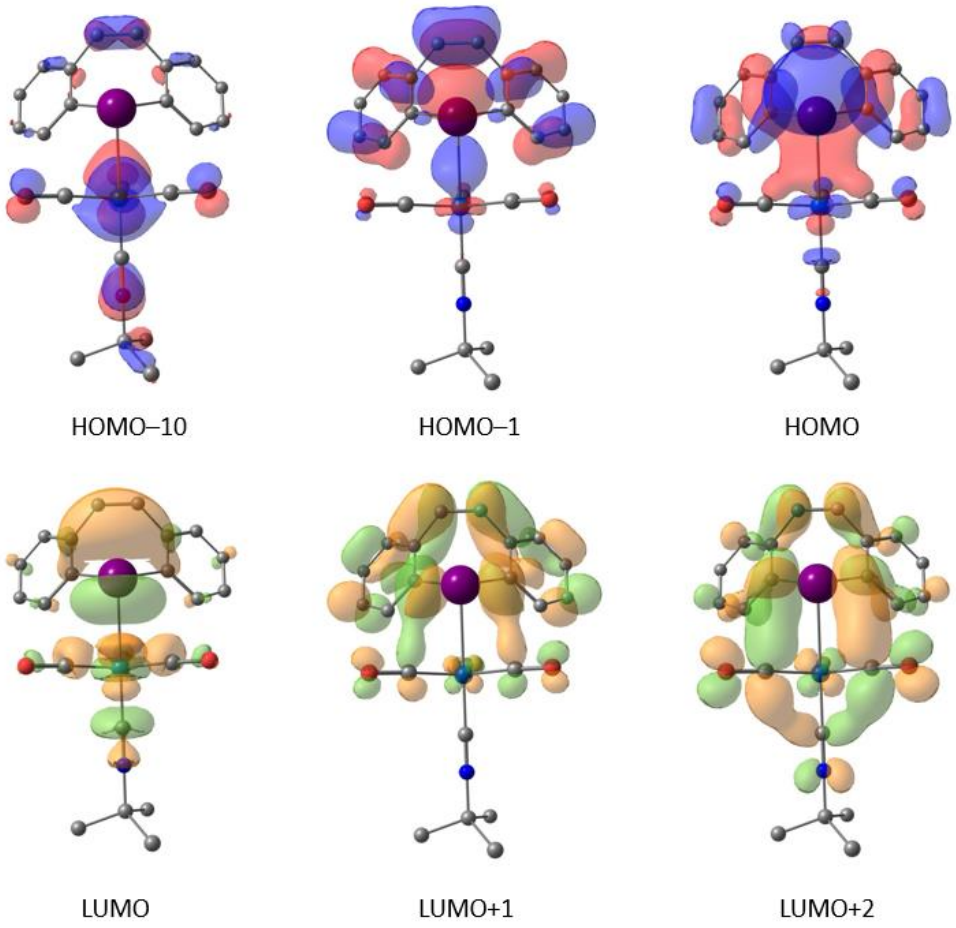

Figure 17. Frontier orbitals of compound **13-*t*BuNC** (isovalues = 0.03) with main contributions to transitions T3, T7 and T9.

The fact that compounds **13(-L)** all show LUMOs with Co-C_{CO} σ*-antibonding interactions suggest that they should be susceptible to photochemical Co–CO bond cleavage. Analog to the synthesis of **11**, this should lead to the olefin backbone coordinating to the transition metal. Since the cobalt centers in **13(-L)** carry further CO ligands, it should be possible to form chiral cobalt complexes of the form [{κ²*C*,κ¹*Bi*-($C_{14}H_{10}$)Bi}Co(CO)LL'] by alternating olefin-coordination and olefin-dissociation cycles (Scheme 13).

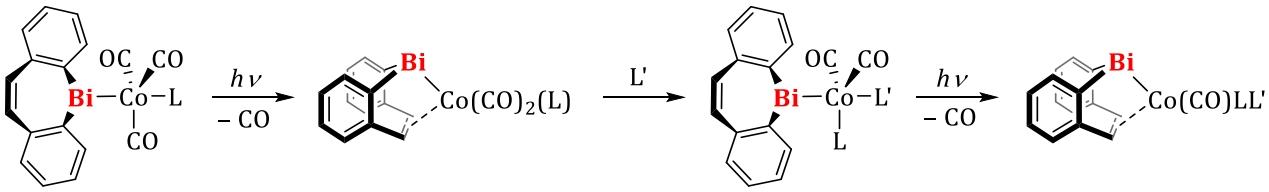

Scheme 13. Proposed synthesis of chiral cobalt complexes by alternating olefin-coordination and olefin-dissociation steps.

Parent compound **13** showed low conversion (10% after 5 h) to an unknown species **14** in solution under ambient light. When irradiated with light at a wavelength of 535 nm, a 1:1 equilibrium was established between **13** and a new species, **14**, after 30 h, as determined by ^{1}H NMR spectroscopy. Gas evolution was observed during the reaction, which is attributed to the dissociation of CO. ^{1}H NMR spectroscopic analysis of the reaction mixture suggests that the ligand backbone of the bismepinyl ligand in **14** coordinates to the transition metal center via the olefin moiety, as indicated by a strong upfield shift of the olefin proton resonances, compared to the starting material **13** ($\Delta\delta$ = –1.61 ppm) (Table 2, Entry 1). Complete conversion to **14** was achieved by the exchange of the atmosphere above the reaction solution at least twice during the reaction. The reverse reaction, i.e. the formation of **13** by placing **14** under an atmosphere of CO gas, resulted in high conversion of the starting material (80%) to selectively one species (**13**, as determined by ^{1}H NMR spectroscopy) after 5 h at ambient temperature.

Irradiation of **13-PPh$_3$**, **13-PCy$_3$** and **13-*t*BuNC** with light at 455 nm (**13-PPh$_3$**) and 365 nm (**13-PCy$_3$** and **13-*t*BuNC**), respectively, led to the formation of **14-PPh$_3$**, **14-PCy$_3$** and **14-*t*BuNC** in moderate to high yields (Table 2). The presence of the phosphane or isonitrile donor ligands *trans* to the bismepinyl ligands seems to have a favorable influence on the formation of the chelate complexes **14-L**, which, unlike that of **14**, don't require an exchange of the atmosphere during the reaction. The chelate complexes **14(-L)** are soluble in toluene, benzene, THF, 1,2-diflourobenzene and methylene chloride. **14-*t*BuNC** is also slightly soluble in *n*-pentane, while **14-PCy$_3$** is the least soluble, requiring polar solvents like THF and $CHCl_3$ for a quantitative solubility.

Table 2. Synthesis of chelate complexes **14(-L)** with the associated reaction conditions.

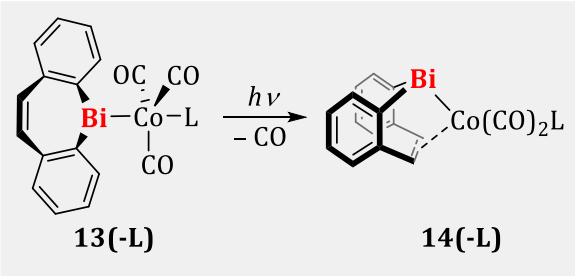

13(-L) **14(-L)**

Entry	starting material	ligand L	*hν* [nm]	reaction time [h]	solvent	yield[a] [%]
1	**13**	CO	525	45	toluene/THF[b]	39
2	**13-PPh$_3$**	PPh_3	455	5	benzene	50
3	**13-PCy$_3$**	PCy_3	365	7.5	benzene	74
4	**13-*t*BuNC**	*t*BuNC	365	2.5	benzene	79

a. isolated yield after work-up. b. in a 20:1 ratio.

The ^{1}H NMR spectra of the isolated complexes **14(-L)** in benzene solution show upfield shifts of $\Delta\delta$ = 1.08–1.20 ppm for the resonances of the α-protons of the bismepinyl ligand in comparison with starting materials **13(-L)**. Furthermore, the resonances of the olefin moieties are strongly upfield shifted in **14(-L)** ($\Delta\delta$ = 1.34–2.27 ppm) compared to **13(-L)** (δ(^{1}H) = 6.72–6.89 ppm). The

phosphane analogs show $^{3}J_{PH}$ coupling constants of 7.0 Hz (**14-PPh$_3$**) and 5.6 Hz (**14-PCy$_3$**) for the olefin resonances. The ^{13}C NMR spectroscopic resonances of the carbonyl ligands for **14(-L)** are found at $\delta(^{13}C)$ = 203.35–207.00 ppm, which corresponds to a downfield shift of $\Delta\delta$ = 6.01 (**14**), 3.54 (**14-PPh$_3$**) and 2.88 (**14-PCy$_3$**) ppm compared to their respective starting materials. This might be due to the olefin moiety and the carbonyls competing for π-electrons from the metal, which is why the metal carbonyl bonds are weakened, although a clear comparison is hampered by different symmetries. Only **14-*t*BuNC** shows a similar chemical shift for the ^{13}C NMR spectroscopic signal for CO of $\delta(^{13}C)$ = 203.35 ppm compared to its starting material **13-*t*BuNC** ($\delta(^{13}C)$ = 203.67 ppm). The ^{31}P NMR spectroscopic resonances for the phosphanes are found at $\delta(^{31}P)$ = 73.94 (**14-PPh$_3$**), and 68.49 (**14-PCy$_3$**) ppm, which corresponds to a downfield shift of 5.72 ppm for **13-PPh$_3$** ($\delta(^{31}P)$ = 68.22 ppm) and an upfield shift of –10.06 ppm for **13-PCy$_3$** ($\delta(^{31}P)$ = 78.55 ppm).

The change in the electronic situation compared to **13(-L)**, especially in complexes **14** and **14-PPh$_3$**, but also in complex **14-PCy$_3$**, is evident not only from the ^{13}C NMR spectroscopic shifts of the CO ligands but also from the IR CO stretching frequencies. The IR spectra for **14** ($\tilde{\nu}_{CO}$ = 2003 cm^{-1}) and **14-PPh$_3$** ($\tilde{\nu}_{CO}$ = 1975, 1923 cm^{-1}) show stretching frequencies for the carbonyl ligands at lower wavenumbers than the starting materials **13** ($\tilde{\nu}_{CO}$ = 2075–1989 cm^{-1}) and **13-PPh$_3$** ($\tilde{\nu}_{CO}$ = 2010–1927 cm^{-1}), suggesting stronger M–CO bonds in **14** and **14-PPh$_3$** than in their respective starting materials. For **14-PCy$_3$** they are in a slightly lower or similar wavenumber range ($\tilde{\nu}_{CO}$ = 1969–1933 cm^{-1}) as for starting material **13-PCy$_3$** ($\tilde{\nu}_{CO}$ = 1998–1913 cm^{-1}). Only the isonitrile analogs show extremely small differences in both the CO stretching frequencies ($\tilde{\nu}_{CO}$ = 1983–1930 (**14-*t*BuNC**); 1984–1923 (**13-*t*BuNC**) cm^{-1}), and the NC stretching frequencies ($\tilde{\nu}_{NC}$ = 2163 (**14-*t*BuNC**); 2167 (**13-*t*BuNC**) cm^{-1}), which is in accordance with the ^{13}C NMR spectroscopic resonances for the carbonyl carbon in that complex.

The solid-state structures of **14(-L)** were determined by single-crystal X-ray diffraction analyses. **14** crystallized in the orthorhombic space group *Pnma* with Z = 4, **14-PPh$_3$** crystallized in the triclinic space group $P\bar{1}$ with Z = 4,[2] **14-PCy$_3$** crystallized in the monoclinic space group $P2_1/c$ with Z = 4, and **14-*t*BuNC** crystallized in the orthorhombic space group $Pna2_1$ with Z = 4 (Figure 18).

[2] Indications of higher symmetry of the space group were not found.

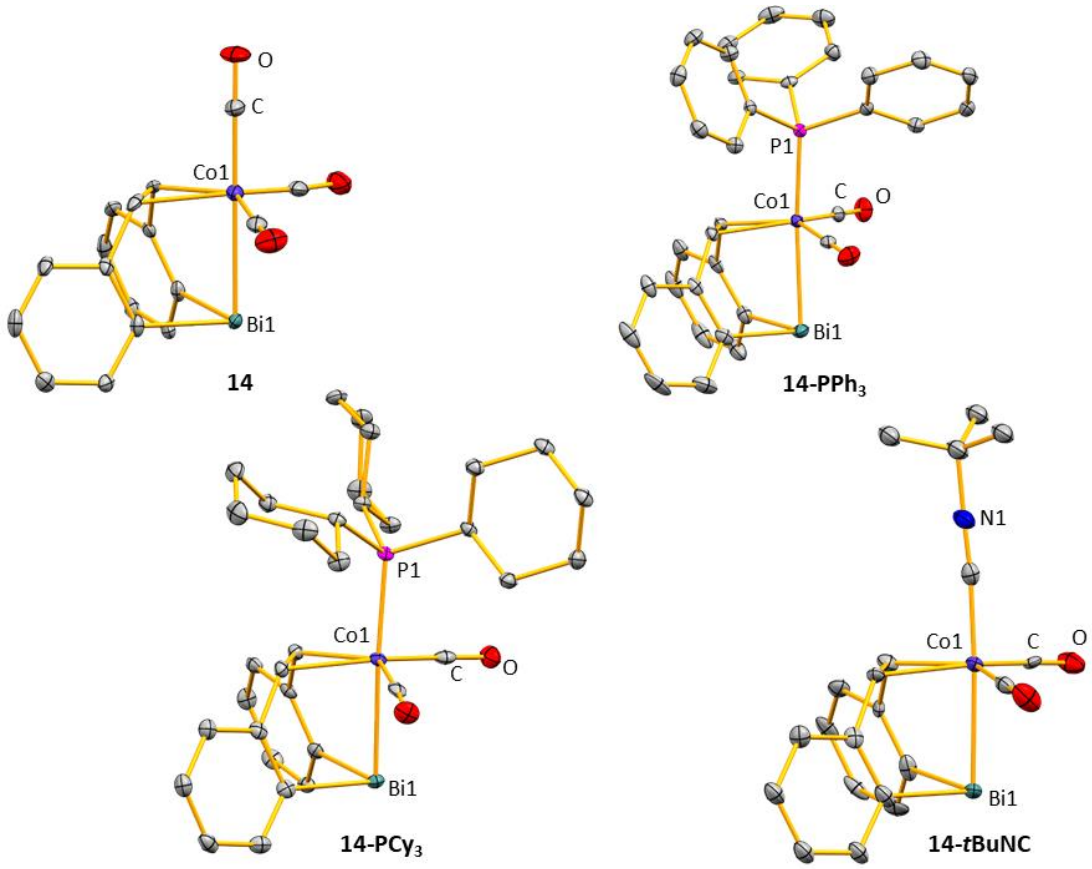

Figure 18. Molecular structures of [{κ²*C*,κ¹*Bi*-($C_{14}H_{10}$)Bi}Co(CO)$_3$] (**14**), [{κ²*C*,κ¹*Bi*-($C_{14}H_{10}$)Bi}Co(CO)$_2$(PPh_3)] (**14-PPh$_3$**), [{κ²*C*,κ¹*Bi*-($C_{14}H_{10}$)Bi}Co(CO)$_2$(PCy_3)] (**14-PCy$_3$**), and [{κ²*C*,κ¹*Bi*-($C_{14}H_{10}$)Bi}Co(CO)$_2$(*t*BuNC)] (**14-*t*BuNC**), in the solid state. Displacement ellipsoids are drawn at the 50% probability level. Hydrogen atoms and lattice bound solvent molecules are omitted for clarity. For compound **14-PPh$_3$**, the asymmetric unit contains two formula units of **14-PPh$_3$**, the bonding parameters of which are very similar to each other, so that only one of them is discussed. Selected bond lengths (Å) and angles (°): Compound **14**: Bi1–Co1, 2.7308(9); Bi1–C, 2.253(4); Co1–C_{olefin}, 2.083(4); Co1–C_{CO}, 1.788(5)–1.805(6); C_{olefin}–C_{olefin}, 1.371(9); C–Bi1–C, 83.4(2); C–Bi1–Co1, 86.16(11); Bi1–Co1–C_{trans}, 179.92(19); Bi1–Co1–C_{cis}, 82.83(14)–85.04(12); C_{equat}–Co1–C_{equat}, 101.16(19)–138.75(18). Compound **14-PPh$_3$**: Bi1–Co1, 2.6904(4); Bi1–C, 2.2250(2), 2.246(2); Co1–P1, 2.2442(6); Co1–C_{olefin}, 2.097(2)–2.100(2); Co1–C_{CO}, 1.765(2)–1.774(2); C_{olefin}–C_{olefin}, 1.412(3); C–Bi1–C, 87.58(8); C–Bi1–Co1, 86.26(6), 86.54(6); Bi1–Co1–C_{cis}, 81.16(7)–86.01(7); Bi1–Co1–P1, 173.979(19); C_{equat}–Co1–C_{equat}, 95.20(9)–141.30(9). Compound **14-PCy$_3$**: Bi1–Co1, 2.6839(4); Bi1–C, 2.252(3), 2.256(3); Co1–P1, 2.2814(8); Co1–C_{olefin}, 2.069(3)–2.073(3); Co1–C_{CO}, 1.771(3)–1.772(3); C_{olefin}–C_{olefin}, 1.431(4); C–Bi1–C, 87.71(11); C–Bi1–Co1, 86.52(8), 87.31(8); Bi1–Co1–C_{cis}, 82.62(10)–85.15(8); Bi1–Co1–P1, 175.00(3); C_{equat}–Co1–C_{equat}, 94.67(13)–149.53(13). Compound **14-*t*BuNC**: Bi1–Co1, 2.688(2); Bi1–C, 2.249(14), 2.259(13); Co1–C_{NC}, 1.893(15); Co1–C_{olefin}, 2.077(14)–2.107(13); Co1–C_{CO}, 1.762(15)–1.775(15); C_{olefin}–C_{olefin}, 1.440(17); C_{NC}–N1, 1.158(18); C–Bi1–C, 87.3(5); C–Bi1–Co1, 86.8(4), 87.0(4); Bi1–Co1–C_{cis}, 83.5(5)–86.4(4); Bi1–Co1–C_{NC}, 175.8(4); Co1–C_{NC}–N1, 175.6(13); C_{equat}–Co1–C_{equat}, 99.5(5)–143.7(5).

Due to the η²-coordination mode of the olefin moieties the cobalt centers adopt (distorted) trigonal bipyramidal geometries with the bismuth atom and one carbonyl ligand (**14**: Bi1–Co1–C_{trans}, 179.92(19)°, τ = 0.99), the phosphanes (**14-PPh$_3$**: Bi1–Co1–P1, 173.979(19)°,

τ = 0.83; **14-PCy$_3$**: Bi1–Co1–P1, 175.00(3)°, τ = 0.75), or the isonitrile (**14-*t*BuNC**: Bi1–Co1–C_{NC}, 175.8(4)°, τ = 0.86) in the axial positions, respectively. The bismuth–cobalt bond lengths of ca. 2.68–2.73 Å are in the same range as in **13-PPh$_3$**, **13-PCy$_3$** and **13-*t*BuNC**. Reported π-coordinated C–C bond lengths in cobalt complexes are approximately in the range of 1.38–1.41 Å,[111–113] and are in good agreement with C_{olefin}–C_{olefin} bond lengths in **14** (1.371(9) Å), and **14-PPh$_3$** (1.412(3) Å), respectively. Compounds **14-PCy$_3$** and **14-*t*BuNC** show longer C_{olefin}–C_{olefin} bond lengths of 1.431(4) Å and 1.440(17) Å, probably because PCy_3 and *t*BuNC may be classified as strong σ-donor ligands. This corresponds to a bond length expansion of non-coordinating (in **13-L**) to coordinating olefin (in **14-L**) of 6.9–7.8%. The bismuth centers display trigonal pyramidal coordination geometries with Bi–C bond lengths (2.2250(2)–2.259(13) Å) in the same way as the corresponding starting materials. Compared to **13-PPh$_3$**, **13-PCy$_3$**, and **13-*t*BuNC** (C–Bi–C: 88.6(2)–89.37(12)°; C–Bi–Co: 99.32(9)–102.88(16)°), the C–Bi–C/Co angles in **14**, **14-PPh$_3$**, **14-PCy$_3$** and **14-*t*BuNC** are reduced to 86.16(11)–87.71(11)° due to the bite angle of the chelating bonding mode of the bismepinyl ligand. Compound **14** shows the smallest C–Bi–C bond angle with 83.4(2)°. In the cobalt complexes reported herein without a coordinating olefin, the central heterocycle of the bismepinyl ligand points away from the transition metal center, therefore a inversion of this ligand is required in order for the olefin to coordinate to the transition metal center.

The UV-vis spectra of compounds **14(-L)** show absorption maxima at λ_{max} = 346 nm (**14**), 360 nm (**14-PPh$_3$**), 350 nm (**14-PCy$_3$**), and 338 nm (**14-*t*BuNC**), respectively. Compound **14-PCy$_3$** shows a second absorption maximum at 430 nm. All absorption maxima, except the second absorption maximum for **14-PCy$_3$**, are at lower wavelengths compared to precursors **13(-L)**, which correlates to higher energies for excitations.

Due to the poor isolated yield (39%) of compound **14**, the latter was not used in further reactions for the synthesis of chiral cobalt compounds. The three complexes **14-PPh$_3$**, **14-PCy$_3$** and **14-*t*BuNC**, however, were deemed suitable for further reactivity.

Reactions of **14-PPh$_3$** with other donor ligands such as *t*BuNC and the N-heterocyclic carbene 1,3-bis(2,6-di-*iso*-propylphenyl)imidazol-2-ylidene (IPr) led to unselective or incomplete conversions. Disadvantages of using **14-PCy$_3$** as starting material for follow up reactivity were i) the low isolated yield of the precursor **13-PCy$_3$**, ii) that in an *in situ* synthesis of **14-PCy$_3$** from **8-Cl**, PCy_3 and $Na[Co(CO)_4]$ the by-product $[Bi\{Co(CO)_3(PCy_3)\}]$ had been obtained in a yield of 63%,[114] and iii) that the reaction of **14-PCy$_3$** with *t*BuNC also led to an unselective reaction. Hence subsequent studies focused mainly on **14-*t*BuNC** as a starting compound for a reaction sequence to yield a chiral cobalt complex. Another advantage of using **14-*t*BuNC** is its reproducibly good isolated yield of 79%, as well as its storability at ambient temperature for several weeks under an atmosphere of purified argon. Accordingly, **14-*t*BuNC** was combined with stoichiometric amounts

of PCy_3 in benzene, and after 3 h at 60 °C full conversion to **15** was determined by ^1H NMR spectroscopy (Scheme 14).

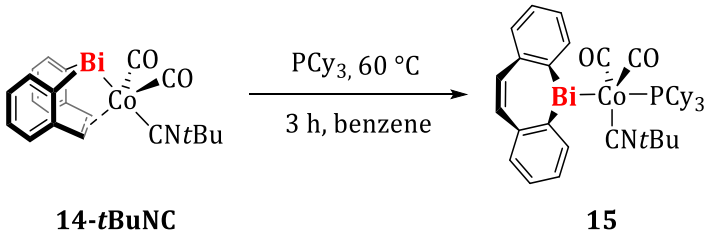

14-*t*BuNC **15**

Scheme 14. Synthesis of **15** by reaction of **14-*t*BuNC** and PCy_3.

A ^1H NMR spectroscopic analysis of the product revealed a significant downfield shift of the resonance for the α-protons of the bismepinyl ligand to $\delta(^1H)$ = 8.95 ppm in comparison with the starting material **14-*t*BuNC** ($\delta(^1H)$ = 7.63 ppm). Combined with the fact that the signal for the olefin protons appears at $\delta(^1H)$ = 6.90 ppm compared to the resonance at $\delta(^1H)$ = 5.44 ppm for **14-*t*BuNC**, this clearly indicate a dissociation of the olefin from the transition metal center. At the same time, the 1:1:1 ratio of the resonance integrals of the bismepinyl, the cyclohexylphosphane and the *tert*-butylisonitrile ligands clearly supports the formation of **15**. The ^{31}P NMR spectroscopic resonance found at $\delta(^{31}P)$ = 83.60 ppm is shifted by 5 ppm to the lower field compared to the resonance of **13-PCy$_3$** ($\delta(^{31}P)$ = 78.55 ppm). The ^{13}C NMR spectrum shows a resonance for the carbonyl groups at $\delta(^{13}C)$ = 204.24 ppm, with a $^2J_{CP}$ coupling of 14.6 Hz. In comparison with **13-*t*BuNC** ($\delta(^{13}C)$ = 203.67 ppm) and **13-PCy$_3$** ($\delta(^{13}C)$ = 202.95 ppm) this represents a slightly downfield shift of the ^{13}C NMR spectroscopic carbonyl resonance. The signals for the isonitrile carbon show a clearer difference in the chemical shift, with $\delta(^{13}C)$ = 154.83 ppm for **15** and $\delta(^{13}C)$ = 150.80 ppm for **13-*t*BuNC**, which corresponds to a difference of $\Delta\delta$ = 4.03 ppm.

By layering the reaction mixture with hexamethyldisiloxane (HMDSO) and storage at ambient temperature, it was possible to isolate the product in 68% yield as a crystalline solid with crystals suitable for X-ray diffraction analysis (orthorhombic space group $Pca2_1$ with Z = 4, Figure 19).

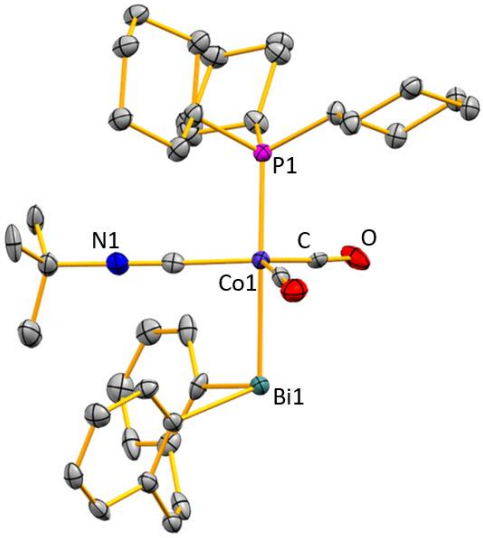

Figure 19. Molecular structure of [{($C_{14}H_{10}$)Bi}Co(CO)$_2$(*t*BuNC)(PCy_3)] (**15**) in the solid state. Displacement ellipsoids are drawn at the 50% probability level. Hydrogen atoms are omitted for clarity. Selected bond lengths (Å) and angles (°): Bi1–C, 2.253(13), 2.262(13); Bi1–Co1, 2.6636(17); Co1–C_{CO}, 1.757(14), 1.772(17); Co1–C_{NC}, 1.839(14); Co1–P1, 2.228(4); C_{olefin}–C_{olefin}, 1.328(19); C–Bi1–C, 87.9(5); C–Bi1–Co1, 100.4(4), 103.6(3); Bi1–Co1–C_{cis}, 81.7(4)–89.7(4); Bi1–Co1–P1, 169.47(12); Co1–C_{NC}–N1, 178.5(12); $C_{equat.}$–Co1–$C_{equat.}$, 111.0(6)–124.4(6).

The cobalt center adopts a distorted trigonal bipyramidal coordination geometry (τ = 0.75), with the bismepinyl and phosphane ligands in axial positions (Bi1–Co1–P1, 169.47(12)°). The Bi–Co bond length of 2.6636(17) Å is at the lower limit of those found in the other cobalt complexes reported here (Bi–Co, appr. 2.67–2.73 Å). The Co–P bond length is, within limits of error, identical to that in **13-PCy$_3$**. The Co–C_{NC} bond (1.839(14) Å), on the other hand, is somewhat shorter than in [{($C_{14}H_{10}$)Bi}Co(CO)$_3$(*t*BuNC)] (**13-*t*BuNC**, 1.859(7) Å), which might be due to the change of the isonitrile ligand from the axial position in **13-*t*BuNC** to the equatorial position in **15**. The bismuth atom possesses a distorted trigonal pyramidal coordination geometry with Bi–C bond lengths (2.253(13)–2.262(13) Å) and angles around Bi1 (87.9(5)–103.6(3)°) similar to bonding parameters in other complexes without olefin coordination reported in this thesis.

The CO stretching frequencies of **15** obtained by IR spectroscopy are shifted to significantly lower wavenumbers ($\tilde{\nu}_{CO}$ = 1932, 1881 cm^{-1}) compared to the other cobalt complexes reported in this work, which is due to the isonitrile ligand being a stronger σ-donor than CO, resulting in more pronounced π-M–CO backbonding.[115] The N≡C stretching frequency of the isonitrile ligand is found at $\tilde{\nu}_{NC}$ = 2116 cm^{-1} and is thus strongly blue-shifted compared to the frequencies in complexes **13-*t*BuNC** ($\tilde{\nu}_{NC}$ = 2167 cm^{-1}) and **14-*t*BuNC** ($\tilde{\nu}_{NC}$ = 2163 cm^{-1}), as well as free *tert*-butylisonitrile ($\tilde{\nu}_{NC}$ = 2136 cm^{-1}),[116] which corresponds to strong π-backbonding from cobalt, probably because of the presence of the σ-donor PCy_3.[117,118]

Compound **15** is obtained as an orange solid of which UV-vis measurements were carried out in THF solution. Additionally, (TD)-DFT studies were performed with the Gaussian programme[103] on compound **15** (Figure 20). The results presented here were obtained with the functionals B3LYP[104] for optimizations and CAM-B3LYP for TD-DFT calculations,[105] Grimme D3 dispersion corrections,[106] and 6-31G(d,p)[107] [H, C, N, O, P] and LANL2DZ[108–110] [Co, Bi] basis sets. All transitions discussed here are singlet-singlet transitions.

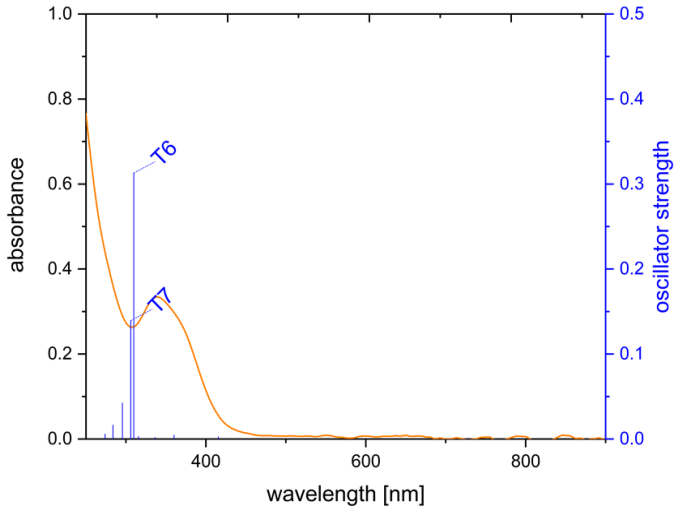

Figure 20. Experimental UV-vis spectrum of **15** (0.06 mM) in THF (orange, absorption maximum at 340 nm) and calculated transitions (blue).

The experimental UV-vis spectrum of compound **15** in THF shows an absorption maximum at 340 nm with an onset at ca. 430 nm. These absorptions were correlated with seven singlet-singlet transitions T1–T7, two of which show larger oscillator strengths (T6: 301 nm; T7: 297 nm). T6 and T7 correspond mainly to HOMO→LUMO+1 (T6, 52%), HOMO–1→LUMO+2 (T7, 9%), HOMO→LUMO (T7, 10%), HOMO→LUMO+1 (T7, 24%), and HOMO→LUMO+2 (T7, 8%) transitions, respectively. While the HOMO–1 shows contributions to Co–C_{CO} π-bonding and the HOMO shows contributions to Co–Bi σ-bonding as well as Co–P σ*-antibonding, the LUMO consists of a bismepinyl ligand centered molecular orbital, while the LUMO+1 shows contributions to Co–L σ*-antibonding to all ligands, and the LUMO+2 shows contributions to Co–C_{CO} σ*-antibonding interactions to both carbonyl ligands (Figure 21). These findings result in a more complex picture than for compounds **13(-L)**, with the risk that irradiation could lead to the loss of a ligand other than a carbonyl.

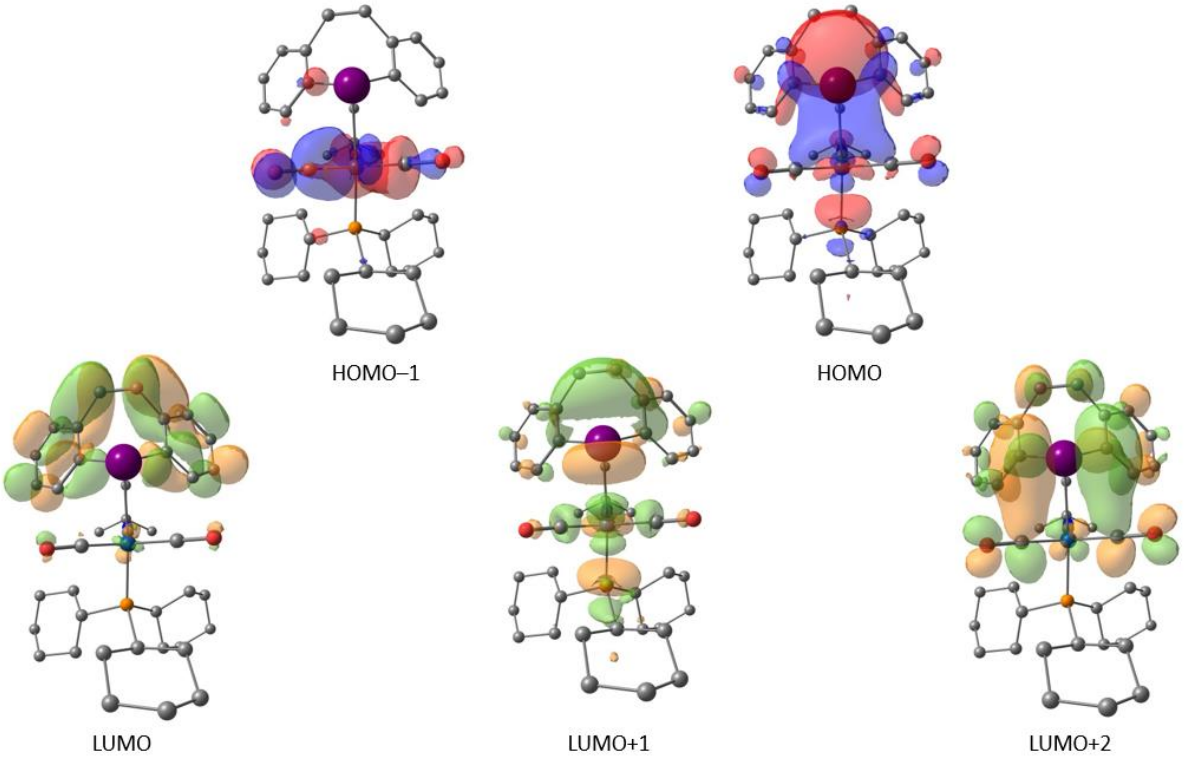

Figure 21. Frontier orbitals of compound **15** (isovalues = 0.03) with main contributions to transitions T6 and T7.

Nevertheless, a solution of **15** in benzene was irradiated at a wavelength of 365 nm for 12 h (Scheme 15).

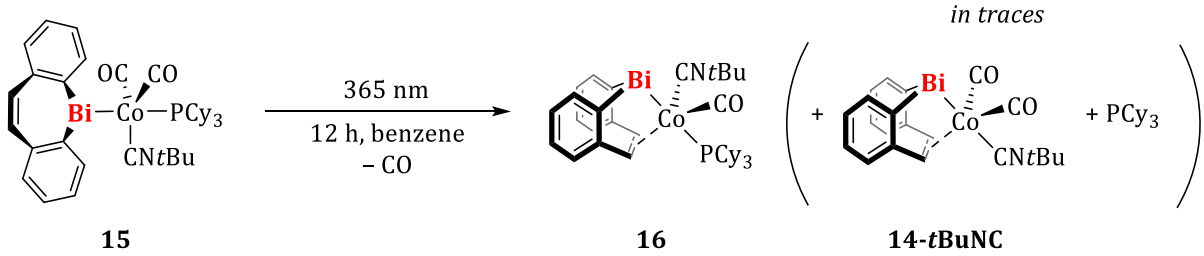

15 **16** **14-*t*BuNC**

Scheme 15. Synthesis of **16** accompanied with the formation of **14-*t*BuNC** and PCy_3 as by-products according to ^1H and ^{31}P NMR spectroscopy.

The course of the reaction was regularly monitored by ^1H and ^{31}P NMR spectroscopy. After 12 h complete conversion of the starting material **15** was observed both in the ^1H and in the ^{31}P NMR spectrum. At the same time the formation of **14-*t*BuNC** and of free tricyclohexylphosphane was unambiguously identified by ^1H NMR and ^{31}P NMR spectroscopy, respectively. The main product (80%), however, is the chiral compound **16**. The ^{31}P NMR spectrum of the reaction mixture shows a new signal at $\delta(^{31}P)$ = 68.89 ppm, which was assigned to the desired chiral complex. The ^1H NMR spectrum shows the expected upfield shift of the α-protons of the bismepinyl ligand ($\Delta\delta$ = –1.01 and –1.04 ppm), as well as for the olefin bridge ($\Delta\delta$ = –1.68 and –2.02 ppm) compared to the

corresponding resonances of **15**. Due to the diastereotopicity of **16**, all sets of protons, which were previously chemically and magnetically equivalent, now split into two signals each. An isolation of **16** in sufficient amounts for full characterization was not possible due to the good solubility of the compound in polar (THF, 1,2-difluorobenzene, pyridine, chloroform), as well as weakly or non-polar (benzene, toluene, methylene chloride, *n*-pentane, *n*-hexane and HMDSO) solvents, rendering a separation from the by-products unsuccessful to date. Nonetheless, it was possible to obtain small amounts of crystalline material suitable for X-ray diffraction analysis by layering the reaction mixture in 1,2-difluorobenzene with *n*-pentane and storage at –30 °C for several days (triclinic space group $\bar{P}1$ with $Z = 2$).

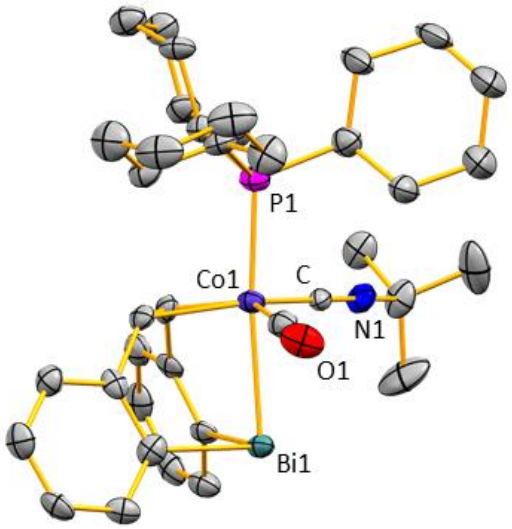

Figure 22. Molecular structure of [{κ²*C*,κ¹*Bi*-($C_{14}H_{10}$)Bi}Co(CO)(*t*BuNC)(PCy_3)] (**16**) in the solid state. Displacement ellipsoids are drawn at the 50% probability level. Hydrogen atoms and lattice bound solvent molecules are omitted for clarity. Selected bond lengths (Å) and angles (°): Bi1–C, 2.249(7), 2.254(8); Bi1–Co1, 2.6638(11); Co1–C_{CO}, 1.740(8); Co1–C_{NC}, 1.850(7); Co1–P1, 2.280(2); C_{NC}–N1, 1.166(9); C_{olefin}–C_{olefin}, 1.430(10); Co1–C_{olefin}, 2.066(7)–2.084(7); C–Bi1–C, 87.7(3); C–Bi1–Co1, 85.8(2), 87.40(12); Bi1–Co1–P1, 173.76(7); Bi1–Co1–$C_{equat.}$, 81.1(3)–85.7(2); Co1–C_{NC}–N1, 176.8(7).

Compound **16** forms a mixture of enantiomers, which could not be separated through crystallization under the conditions used herein, since space group $\bar{P}1$ is a centrosymmetric space group. The bismuth atom in **16** adopts a trigonal pyramidal coordination geometry with C–Bi–C/Co angles of 85.8(2)–87.7(3)°. A reduction in the angles around Bi1 due to the olefin–cobalt interaction also occurs in this case. The Bi–Co (2.6638(11) Å), as well as the Bi–C (2.249(7), 2.254(8) Å) bonds are, within limits of error, equal to those in precursor **15**. The cobalt center possesses a distorted trigonal bipyramidal coordination geometry (Bi–Co–P, 173.76(7)°, Bi–Co–$C_{equat.}$, 81.1(3)–85.7(2)°, $\tau = 0.79$). The C_{olefin}–Co bond lengths of 2.066(7) and 2.084(7) Å are in the same range as the other Co–C_{olefin} bond lengths reported in this work (ca. 2.06–2.11 Å, see above). Due to coordination to the metal center, the C–C bond length of the olefin backbone is

elongated to 1.430(10) Å, which is equivalent to an elongation of 7.7% compared to the corresponding bond length in **15**.

The reaction shown in Scheme 15 led to a racemic mixture of complex **16**. This serves as proof of principle that the introduction of a bismepinyl ligand, with its property of being able to function as a hemilabile ligand, allows access to chiral cobalt complexes through olefin-coordination/dissociation cycles. By adding a chiral ligand during the reaction sequences, the product should be a mixture of diastereomers that should be separable using simpler methods (due to (mostly) different physical properties). Once the two diastereomers have been separated, the stereogenic ligand could be replaced by an achiral ligand while retaining, provided that the substitution proceeds while retaining the stereo information, the chirality at cobalt, enabling the isolation of enantiomerically pure compounds.

Consequently, in a one-pot synthesis, **13-*t*BuNC** was combined with the chiral phosphane (*S*)-Monophos ((*S*)-(+)-(3,5-dioxa-4-phosphacyclohepta[2,1-a;3,4-a']dinaphthalene-4-yl)-dimethyl-amine) in benzene and irradiated at a wavelength of 365 nm (Scheme 16).

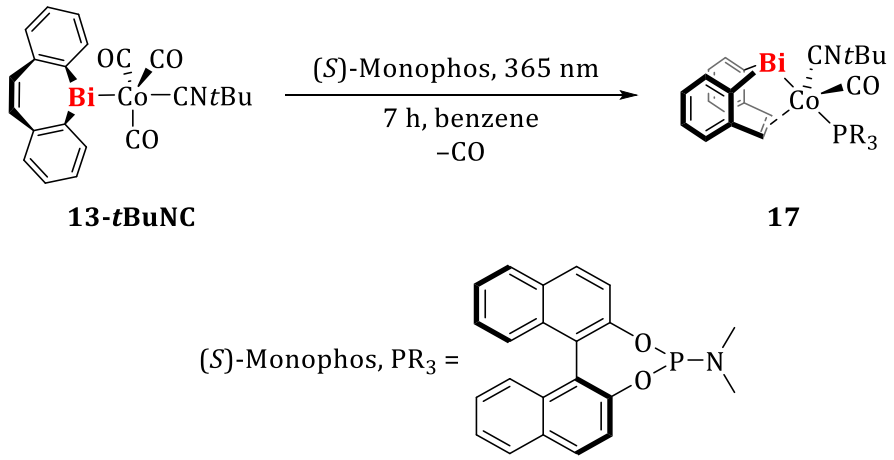

13-*t*BuNC **17**

Scheme 16. Formation of **17** in a one-pot synthesis starting from **13-*t*BuNC**.

Complex **13-*t*BuNC** was treated with (*S*)-Monophos and, after no further gas evolution was observed (1 h), irradiated for 7 h. ^{1}H NMR spectroscopic analysis of the reaction product showed a rather complex situation: five resonances in the chemical shift range for olefinic protons were observed, of which two sets of two resonances were assigned to one diastereomer **17**, respectively, based on their integrations. The remaining signal was assigned to **14-*t*BuNC** by comparison with spectra of the isolated compound. This suggests that the desired mixture of diastereomers **17** was formed, while **14-*t*BuNC** appears as by-product. The integration ratio is 0.5:1:1.7, whereby **14-*t*BuNC** is the minor species and one diastereomer is formed preferentially. Analysis of the ^{1}H NMR resonance integrations in the aromatic region showed that a fourth species must be present in a 1:1 ratio with the minor diastereomer. Further analysis of the corresponding

resonances in the aliphatic proton chemical shift range suggests the composition [({$C_{14}H_{10}$}Bi)Co(*t*BuNC)$(CO)_2$((*S*)-monophos)]. The ^{31}P NMR spectrum shows two resonances ($\delta(^{31}P)$ = 221.95 and 221.39 ppm) in a ca. 3:1 ratio. Assuming that the resonances for both diastereomers of **17** coincide, this supports the observations from the ^{1}H NMR spectroscopic analysis.

A separation of the reaction products did not succeed within the timeframe of this thesis. However, it was possible to obtain small amounts of crystalline material suitable for X-ray diffraction analysis of **17** (triclinic space group *P*1 with *Z* = 4, Figure 23). The quality of the data obtained does not allow a discussion of the bonding parameters due to the presence of multiple twinning domains, for which suitable models could not be established, as well as insufficient scattering.

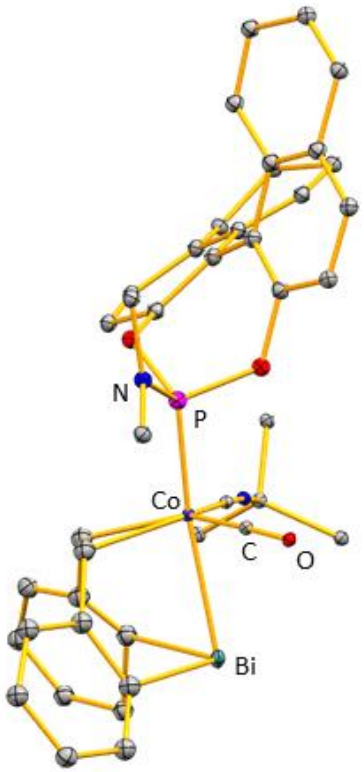

Figure 23. Molecular structure of [{κ²*C*,κ¹*Bi*-($C_{14}H_{10}$)Bi}Co(CO)(*t*BuNC)((*S*)-monophos)] (**17**) in the solid state. Displacement ellipsoids are drawn at the 50% probability level. Hydrogen atoms are omitted for clarity. The asymmetric unit contains four crystallographically distinct formula units of **17**, the bonding situation of which are very similar to each other, so that only one of them is depicted.

The cobalt center adopts a distorted trigonal bipyramidal coordination geometry with the bismuth and the phosphorous atoms in the axial positions. The asymmetric unit contains four formula units of **17**, all of which show the same substitution pattern and chirality. Thus, the material consists of one diastereoisomer with an TBPY-12-C-configuration at Co and an *S*-

configuration at P, crystallizing in the chiral space group *P*1. Consequently, fractional crystallization seems to be a suitable separation method for the two diastereomers of **17**.

In summary, the reaction shown in Scheme 16 was successful but still requires optimization to enable selective access to the diastereomer mixture of **17**. Further analytical data for **17** could not be obtained, yet. In further work, the synthesis of **17** should be investigated in more detail, for example by varying the chiral phosphane or using other chiral donor ligands. Particular attention should be paid to the separation of the diastereoisomeric mixtures, or in the case of racemic **16**, to the isolation and complete characterization of this species and the separation of the enantiomers. First reactivity studies on a possible catalytic application of **16** are discussed below (see Chapter V.2.4).

2.3 Reaction Kinetics for the Formation of 11, 14 and 14-PPh$_3$

The reaction kinetics for the formation of the model compounds **11**, **14** and **14-PPh$_3$** were investigated. The photochemical elimination of CO can be described by the relaxation of an electronically excited molecule A* under transition metal carbon bond cleavage. For example, the release of CO could occur via a reaction of the excited starting material A* with a coordinating solvent, which kinetically corresponds to a pseudo-first-order reaction in each case.[119] The vast excess of solvent compared to [A] allows for the concentration of the solvent to be considered constant. Since the bismepinyl ligand remains bound to the transition metal complex during excitation, the concentration of the backbone remains constant throughout, so that the reaction from metal complex with non-coordinating olefin to the metal complex with coordination of the olefin to the transition metal center should follow first-order kinetics. In this case, the reaction rate is proportional to the concentration of the excited molecule A*. Since it is assumed that the excitation of A to A* is much faster than the subsequent step (CO elimination), it can be assumed that [A] = [A*], and consequently the rate law of a first-order reaction is defined as:

$$\frac{d[\mathrm{A}]}{d\mathrm{t}} = -\,\mathrm{k}[\mathrm{A}] \qquad (2)$$

where the change in concentration over time $\frac{d[\mathrm{A}]}{d\mathrm{t}}$ of a molecule A is defined as a linear function of concentration [A] and a rate constant k.[120] Solving the differential equation (2) using variable separation gives the linear relationship of the reaction time t depending on the initial concentration $[\mathrm{A}]_0$ of the molecule A as

$$\ln\left(\frac{[\mathrm{A}]}{[\mathrm{A}]_0}\right) = -\,\mathrm{kt} \qquad (3).$$

The concentration ratio was determined by monitoring the reaction course by ^{1}H NMR spectroscopy. From the representation of the logarithmic concentration ratio as a function of the

irradiation time according to equation (3), the rate constant *k* can be determined as the slope of a linear fit for the CO elimination reaction.[120]

It must be noted that for compound **14**, as described in Chapter V.2.2, in addition to the photochemically induced CO elimination, a thermally induced CO release also takes place at ambient temperature. To obtain the reaction kinetics for the photochemically-induced reaction only, it was assumed that the photochemically- and thermally-induced reactions proceed independently from one another. Thus, two reactions were carried out in parallel, one reaction being irradiated the other not. For the irradiated sample, the kinetics of the overall reaction with both thermal and photochemical components were obtained. These results do not follow a classic reaction order. In parallel, the second reaction, which was not irradiated and started at the same time as the irradiated one, served to determine the proportion of the solely thermally-induced CO release at any given time. By subtracting the latter from the overall kinetics of the irradiated sample the proportion of solely photochemical CO elimination was viewed in isolation. A second hindrance to determining the reaction kinetics for the formation of **14** is the fact that the conversion proceeds via an equilibrium reaction between **13** and **14**. However, since the reverse reaction of the cobalt complex **13** and CO is a second-order reaction, it could not be mathematically taken into account in the experiment. In a simplified form it was rather assumed that the influence of the reverse reaction path at the start of the reaction, due to only a low concentration of CO in the atmosphere, can be neglected for conversions of up to 30%. Thus, within the first 10 hours of the experiment, first-order kinetics with a rate constant of $(2.09 \pm 0.13) \cdot 10^{-5}\ s^{-1}$ were determined for the forward reaction after thermal correction (Figure 24). After 24 hours, the influence of the reverse reaction became too large to use the approximations mentioned.

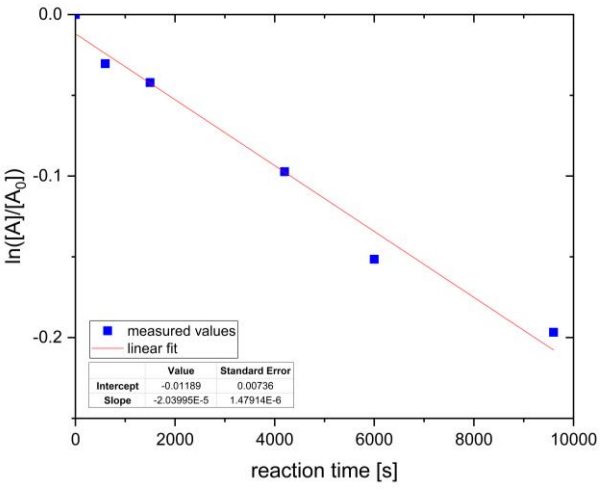

Figure 24. Thermally corrected logarithmic plots of equation (3) to determine the rate constant for the CO elimination reaction to form **14** by linear fit analysis.

For **11** and **14-PPh$_3$**, for which the above mentioned problems do not arise, first-order kinetics with rate constants of (2.69 ± 0.09) · 10^{-4} s^{-1} and (1.98 ± 0.11) · 10^{-4} s^{-1} were obtained (Figure 25).

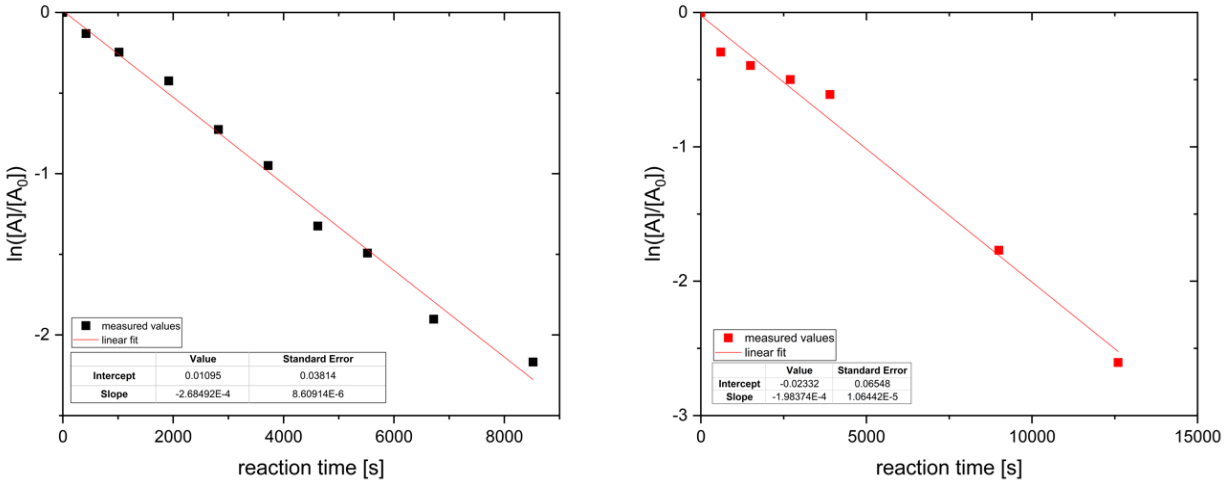

Figure 25. Logarithmic plot of equation (3) to determine the rate constant for the CO elimination reaction for the formation of **11** (left) and **14-PPh$_3$** (right) by linear fit analysis.

When the CO elimination reactions of **11**, **14** and **14-PPh$_3$** are compared, the photochemical reaction of **14** shows the smallest conversion rate constant. This, among other things, is reflected in the longer reaction time of 45 hours for this reaction. If the calculated concentration profile is plotted for all three complexes as a function of the reaction time, the curve profile for **14** demonstrates that the formation of **14** is a much slower reaction compared to the formation of **11** and **14-PPh$_3$** (Figure 26).

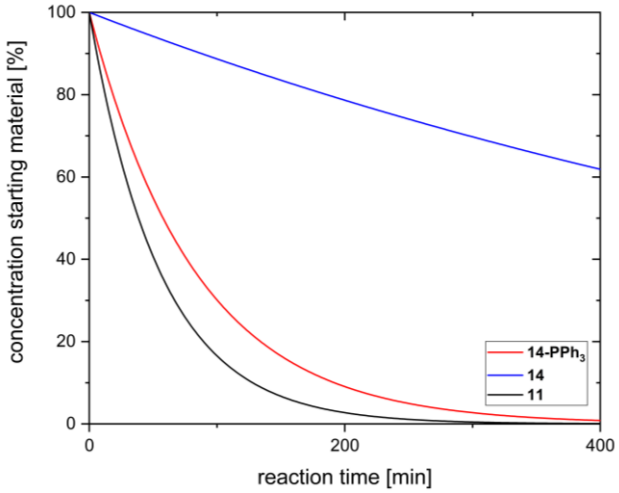

Figure 26. Time-dependent concentration of the respective transition metal bismuthanes calculated from the rate constants for the CO elimination reaction.

The irradiation of the iron complex **11** and cobalt complex **14-PPh$_3$**, on the other hand, show a similar efficiency for the respective selected wavelength. The comparability of the two reactions

is, however, restricted due to the different irradiation wavelengths. The results are summarized in Table 3. In conclusion, kinetic investigations monitored by ^{1}H NMR spectroscopy of the formation of **11**, **14** and **14-PPh$_3$** from **10**, **13** and **13-PPh$_3$**, respectively, showed a first-order reaction in each case.

Table 3. Overview of the kinetic data of the CO elimination reactions in benzene/THF solutions

Entry	complex	λ [nm]	rate constant k [s^{-1}]	reaction half-life ($t_{1/2}$) [min]
1	**11**	525	$(2.69 \pm 0.09) \cdot 10^{-4}$	43
2	**14-PPh$_3$**	455	$(1.98 \pm 0.11) \cdot 10^{-4}$	58
3	**14**	525	$(2.09 \pm 0.13) \cdot 10^{-5}$	553

2.4 Reactivity of Compounds 11, 13-PPh$_3$, 14, 14-PPh$_3$ and 16

In the following, selected reactivities of individual complexes are discussed, whereby three questions in particular were investigated: the redox properties of the selected complexes, the possibility of converting the covalent bismuth transition metal bond into a dative interaction, and initial investigations regarding a potential catalytic activity.

2.4.1 Electrochemical Behavior of Cobalt Complexes 13-PPh$_3$, 14-PPh$_3$ and 14

The redox behavior of compounds **13-PPh$_3$**, **14-PPh$_3$** and **14** was investigated by cyclic voltammetry in THF/0.1 mM [N(nBu)$_4$][PF$_6$] at ambient temperature.

For compound **13-PPh$_3$** two irreversible reduction waves were found at E_{pc} = –2.14 and –2.49 V vs $Fc^{+/0}$, while two irreversible oxidation waves were found at E_{pa} = –0.95 and –2.00 V vs $Fc^{+/0}$ (Fc = $Fe(C_5H_5)_2$, Figure 27, left). A somewhat more complex picture emerges for the chelate complex **14-PPh$_3$**. In addition to two irreversible reductive events at E_{pc} = –2.34 and –2.77 V vs $Fc^{+/0}$, a series of irreversible oxidation waves are observed at E_{pa} = –0.79, –1.88, –2.34 and –2.79 V vs $Fc^{+/0}$, of which the oxidation wave at –0.79 V vs $Fc^{+/0}$ shows the highest intensity (Figure 27, right).

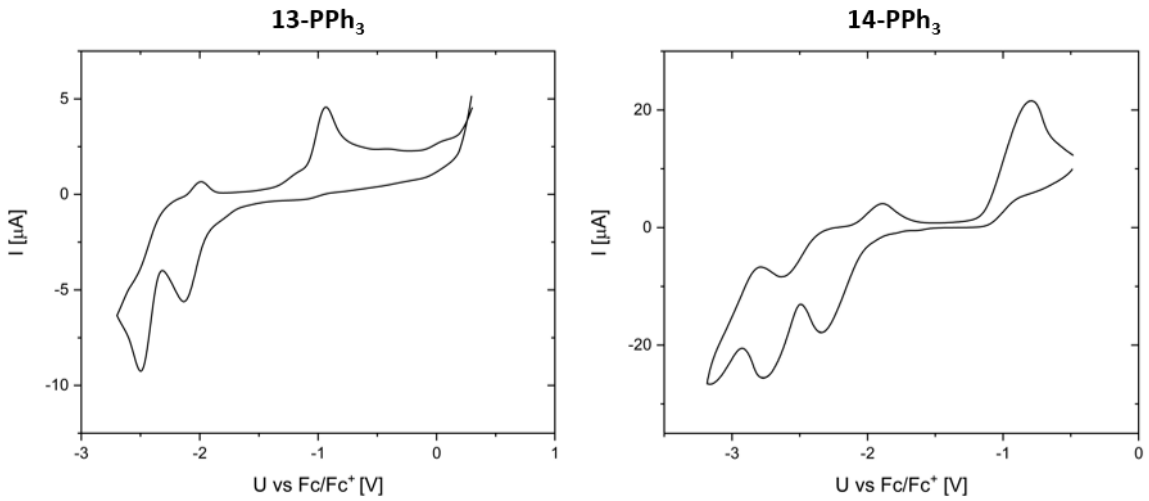

Figure 27. Cyclic voltammogram of **13-PPh$_3$** (left) and **14-PPh$_3$** (right) in THF/0.1 mM [N(*n*Bu)$_4$][PF$_6$] at 23 °C with a scan rate of 250 mV · s^{-1}, Fc = Fe(C$_5$H$_5$)$_2$.

The cyclic voltammometric analysis of the parent compound **14** presents a much simpler picture with an oxidation wave at –0.37 V vs Fc$^{+/0}$ and a reduction wave at –2.17 V vs Fc$^{+/0}$ (Figure 28). Since the oxidation and reduction waves are clearly separated (ΔE = 1.8 V), it can be assumed that a chemical reaction ensues from the reduction of the complex.

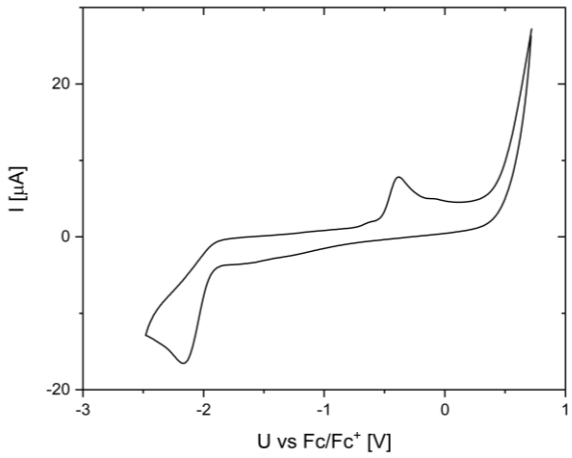

Figure 28. Cyclic voltammogram of **14** in THF/0.1 mM [N(*n*Bu)$_4$][PF$_6$] at 23 °C with a scan rate of 250 mV · s^{-1}, Fc = Fe(C$_5$H$_5$)$_2$.

Based on these results, a first attempt was made to reduce the cobalt complex **14** with decamethyl cobaltocene (Scheme 17).

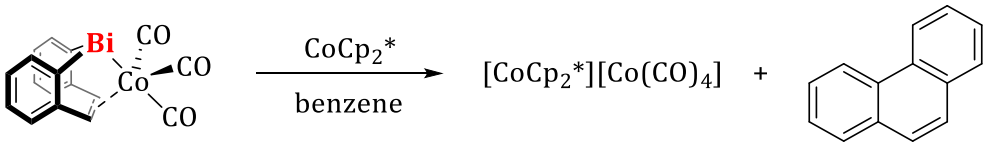

14

Scheme 17. Reaction of **14** with decamethyl cobaltocene in benzene. Cp* = C_5Me_5.

After 2 h at ambient temperature, the formation of a precipitate was observed and a full conversion of the transition metal bismuthane was indicated by ^{1}H NMR spectroscopy (only resonances with minor intensity were detected). The precipitate was filtered off and re-dissolved in THF, whereby a black solid, presumably "bismuth black",[16] remained insoluble. The ^{1}H NMR spectrum of the THF phase revealed the formation of phenanthrene as the main product, and several species containing aromatic protons. By layering the THF solution with *n*-pentane and storage at –30 °C a yellow crystalline solid was obtained. Single-crystal diffraction analysis revealed the formation of the salt $[CoCp_2^*][Co(CO)_4]$ (monoclinic space group $P2_1/n$ with Z = 4, Figure 29, Cp* = C_5Me_5).

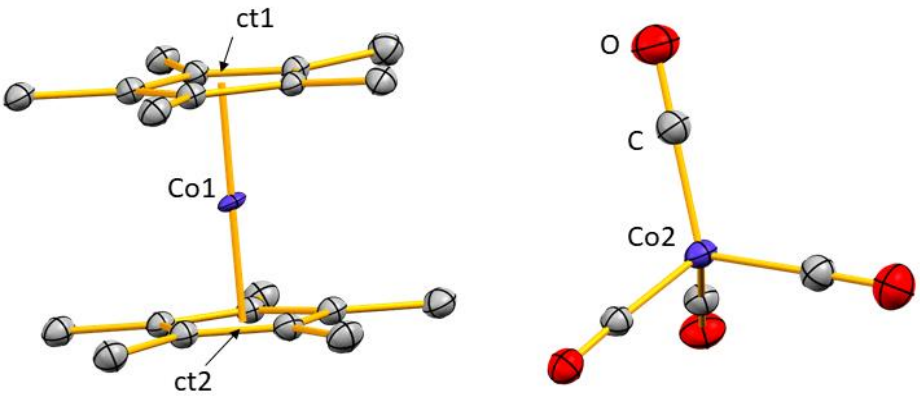

Figure 29. Molecular structure of $[CoCp_2^*][Co(CO)_4]$ in the solid state. Displacement ellipsoids are drawn at the 50% probability level. Hydrogen atoms are omitted for clarity. ct1 represents the centroid of C(1-5) and ct2 represents the centroid of C(11-15). Selected bond lengths (Å) and angles (°): Co1–ct, 1.646, 1.651; Co2–C_{CO}, 1.757(6), 1.774(6); C–O, 1.145(7)–1.162(7); ct1–Co1–ct2; 179.57; C_{CO}–Co2–C_{CO}, 105.0(3)–113.2(3).

The bonding parameters obtained for $[CoCp_2^*][Co(CO)_4]$ are similar to those described for such ion pairs in the literature, which is why they will not be discussed at this point.[121,122] The observation of a black, insoluble precipitate formed during the reaction, as well as the formation of $[CoCp_2^*][Co(CO)_4]$, suggests that a reduction under Bi–Co bond cleavage has taken place.

In the following, **14** was oxidized with AgOTf (Scheme 18). This reaction also leads (partially) to the formation of "bismuth black"[16] and the formation of phenanthrene, as determined by ^{1}H NMR spectroscopy for the latter species. A complete consumption of starting material **14** was not

observed. The fate of the transition metal complex fragment could not be clarified, but the formation of a silver mirror was not observed.

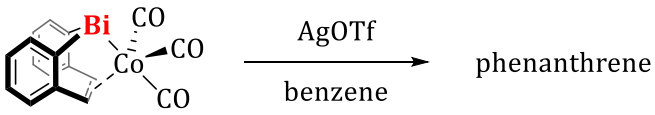

14

Scheme 18. Reaction of **14** with silver triflate in benzene solution.

From the results obtained it can be concluded that both the reduction of **14** with $CoCp_2^*$ and the oxidation with AgOTf lead to cleavage of the Bi–Co bond and no radical or ionic transition metal bismuthane species was accessible.

2.4.2 The Transition Metal Bismuth Bond: Conversion into a dative Interaction

Recently, LIMBERG and GABBAI simultaneously reported on the first complexes with Bi–TM donor-acceptor bonding through Lewis acidic bismuth moieties (Figure 30).[14,18,123–125] The use of a P–Bi–P pincer ligand in these complexes facilitates the Bi–TM interaction.

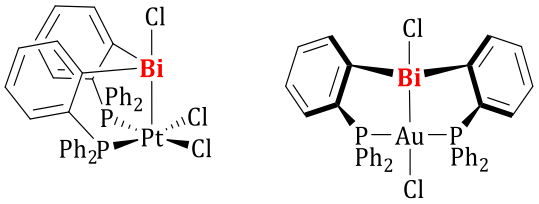

Figure 30. First examples of TM→Bi dative bonds with the bismuth moieties acting as electron acceptors.

By adding a further, electronegative substituent to the bismuth atom in chelate complexes **11** and **14-PPh$_3$**, complexes featuring a dative TM→Bi bond, with bismuth as an electron acceptor, should be accessible. This could be achieved by the 1,2-addition of X–R to the TM–Bi bond (Scheme 19). At the same time, the olefin–Fe/Co bond must remain intact in order to prevent dissociation of the bismepine.

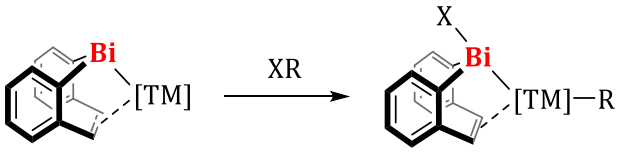

X = electronegative substituent

Scheme 19. Schematic representation of the generation of a dative transition metal bismuth bond based on chelate complexes **11** and **14-PPh$_3$**.

Accordingly, complex **11** was reacted with HOTf, and MeOTf, respectively (Scheme 20).

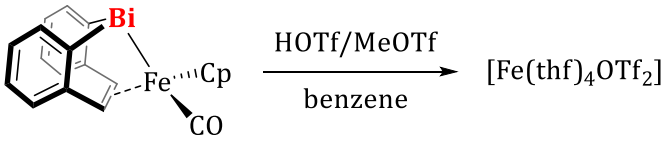

11

Scheme 20. Reaction of **11** with HOTf, and MeOTf, respectively.

First, **11** was combined with HOTf in benzene solution at ambient temperature. Immediately after the addition of HOTf, the reaction mixture turned dark brown and a large amount of black solid precipitated. ^{1}H NMR spectroscopic analysis of the suspension showed complete conversion of **11**. However, the identification of new products was not successful due to strong signal broadening and signal overlap. The black solid was isolated by filtration, re-dissolved in THF and recrystallized by solvent diffusion with *n*-pentane. Single-crystal X-ray diffraction analysis revealed the formation of $[Fe(thf)_4(OTf)_2]$ (orthorhombic space group $P2_12_12_1$ with Z = 4, Figure 31).

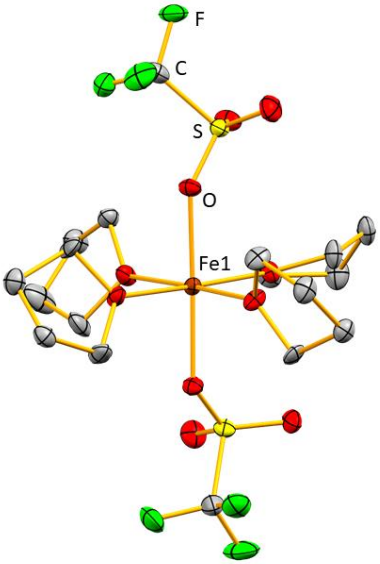

Figure 31. Molecular structure of $[Fe(thf)_4(OTf)_2]$ in the solid state. Displacement ellipsoids are drawn at the 50% probability level. Hydrogen atoms are omitted for clarity. Selected bond lengths (Å) and angles (°): Fe1–C_{thf}, 2.096(4)–2.119(4); Fe1–O_{OTf}, 2.134(4)–2.122(4); O_{OTf}–Fe1–O_{OTf}, 177.50(15); O_{thf}–Fe1–O_{thf}, 87.94(15)–177.65(16); O_{thf}–Fe1–O_{OTf}, 87.94(15)–92.48(14).

The iron center adopts an octahedral coordination geometry with the triflates in *trans* position (177.50(15)°). The four thf ligands coordinate through the oxygen atom with Fe1–O bond lengths of 2.096(4)–2.119(4) Å, identical to those reported by LUTZ *et al.*.[126] $[Fe(thf)_4(OTf)_2]$ was isolated in 86% yield, indicating that this reaction is not suitable for the generation of a dative Fe→Bi bond.

The analog reaction of **11** with MeOTf in benzene led to the formation of a dark precipitate. ^{1}H NMR spectroscopic analysis of the reaction mixture showed incomplete conversion of the starting material **11** after 4 d at ambient temperature. After 5.5 h at 60 °C complete conversion was observed by ^{1}H NMR spectroscopy. The precipitate was filtered off and re-dissolved in THF. The benzene phase was layered with *n*-pentane, and after 16 h at ambient temperature small amounts of a crystalline solid were obtained by filtration and identified by X-ray diffraction analysis as starting material **11**. The THF phase was layered with *n*-pentane and after 16 h at –30 °C small amounts of a black solid were obtained, which could not be analyzed due to insufficient amount of substance. Since similar observations were made in the reaction of **11** with HOTf, it is assumed that $[Fe(thf)_4(OTf)_2]$ is also formed here.

A second approach was to react cobalt complex **14-PPh$_3$** with iodine at –78 °C in the hope that iodine atoms would be transferred to both the bismuth atom and the cobalt center, while maintaining the olefin–cobalt bond (Scheme 21).

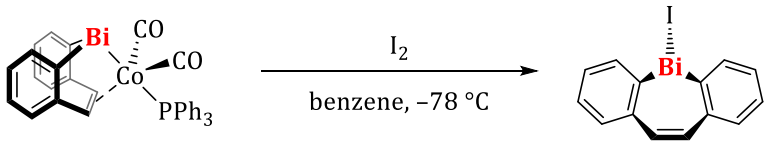

14-PPh$_3$ **8-I**

Scheme 21. Formation of **8-I** by reaction of **14-PPh$_3$** with iodine.

A toluene solution of **14-PPh$_3$** was treated with a solution of iodine in toluene at –78 °C then ambient temperature. Small amounts of a black solid precipitated, which was filtered off. The toluene solution was layered with *n*-pentane. After 16 h at –30 °C a crystalline solid was obtained by filtration, and X-ray diffraction analysis revealed the formation of **8-I**. In conclusion, the transfer of iodine to the bismuth center succeeded. However, the bismepine also dissociates from the transition metal complex fragment, possibly because the olefin cobalt interaction is too weak. The remaining cobalt complex was not identified.

In conclusion, it seems like the 1,2-addition of R–X species to the TM–Bi bonds occurs, but the olefin–transition metal interaction is too weak, and thus the bismepinyl ligands dissociate from the transition metal centers.

2.4.3 Investigations Concerning a Potential Catalytic Activity

In the course of this thesis the reactivity of transition metal bismuthanes towards various small molecule substrates was investigated in order to determine their suitability as potential catalysts. The preliminary results of these are summarized in Table 4.

According to ^{1}H NMR spectra, the reactions of **11** with five equivalents of dimethylamine borane (entry 1), as well as the reactions of **16** with diphenylacetylene (entry 4), catecholborane (entry 5), and hydrogen (entry 6) did not result in any conversion of the transition metal bismuthanes, or in the case of **11**, the reactions led to decomposition if harsh photochemical conditions were applied.

The reaction of **14-PPh$_3$** with ten equivalents of $HPPh_2$ did not lead to the formation of the homo-coupled product $[PPh_2]_2$ under elimination of H_2, but rather to an unselective reaction generating at least four new species according to the ^{31}P NMR spectrum (entry 2).

The reaction of **14-PPh$_3$** with $\frac{1}{8}$ S_8 in benzene at 60 °C led to the formation of the sulfur-bridged bis(bismuthane) **18**, which was isolated as a crystalline material suitable for X-ray diffraction analysis by layering the reaction mixture with *n*-pentane, storage at ambient temperature and subsequent filtration (monoclinic space group $P2_1/m$, Figure 32). However, the quality of the data is not sufficient to discuss bond parameters and only serves as proof of connectivity. The fate of the transition metal complex fragment in this reaction remained unclear as two pathways are possible: i) **14-PPh$_3$** could decompose first to an unknown transition metal complex and the corresponding dibismuthane, which then undergoes insertion of the sulfur atom,[127] or ii) the sulfur atom could insert into the Bi–Co bond with subsequent decomposition to **18**.

Table 4. Reactivity of transition metal bismuthanes towards a range of substrates.

Entry	bismuthane	substrate	reaction conditions	result[a]
1	**11**	5 eq. Me_2NHBH_3	benzene/THF i) r.t.→60 °C, ii) *hν*[b]	i) no conversion ii) decomposition to phenanthrene
2	**14-PPh$_3$**	10 eq. $HPPh_2$	benzene, r.t.	unselective reaction, no coupling product $[PPh_2]_2$
3	**14-PPh$_3$**	S_8	benzene, 60 °C	unselective reaction, small amounts of **18**
4	**16**[c]	1 eq. tolane	benzene i) r.t.→60 °C, ii) *hν*[d] benzene	no conversion
5	**16**[c]	1 eq. catecholborane	i) 60 °C→80 °C, ii) *hν*[d]	no conversion
6	**16**[c]	excess H_2	benzene i) 60 °C ii) *hν*[d]	no conversion
7	**16**[c]	2.5 eq. S_8	benzene, r.t.	full consumption of **16**, $\delta(^{31}P)$ = 61.2 ppm ($SPCy_3$)[128]

a. The conversion of starting materials was monitored by ^{1}H and ^{31}P NMR spectroscopy. b. *hν* = 455 nm. c. **16** was synthesized *in situ* and used as a raw product in these reactions. d. *hν* = 365 nm or mercury vapor lamp.

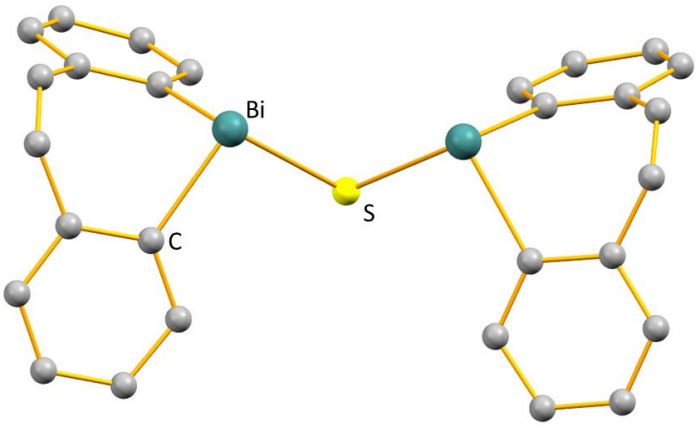

Figure 32. Molecular structure of **18** in the solid state. Hydrogen atoms are omitted for claritiy.

In conclusion, the reactivity of novel transition metal bismuthanes with a chelating bismepinyl ligand towards several catalysis-relevant substrates was investigated. While these preliminary results have failed to provide evidence for selective and useful reactivity, further studies are required in order to determine whether complexes with hemilabile bismepinyl ligands could be applied as catalysts in organic transformations, in particular of olefins or alkynes.

VI Neutral and Cationic Bismuth Compounds: Structure, Hetero-Aromaticity, and Lewis Acidity of Bismepines

This chapter was published in: Jacqueline Ramler, Klaus Hofmann, Crispin Lichtenberg, *Inorg. Chem.* **2020**, *59*, 3367–3376. Reproduced from ref. 82 with permission from the American Chemical Society.

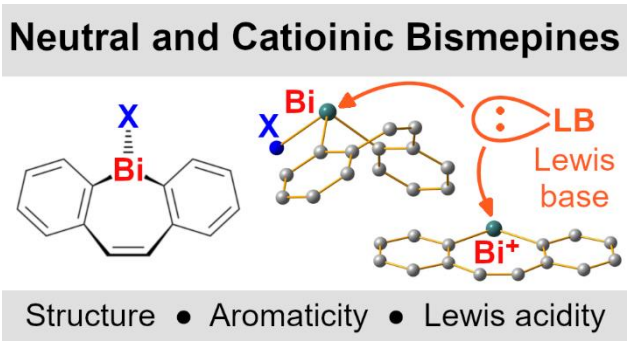

Inorganic Chemistry
Cite This: Inorg. Chem. 2020, 59, 3367−3376
Forum Article
pubs.acs.org/IC

Neutral and Cationic Bismuth Compounds: Structure, Heteroaromaticity, and Lewis Acidity of Bismepines

Jacqueline Ramler, Klaus Hofmann, and Crispin Lichtenberg*

Institute of Inorganic Chemistry, Julius-Maximilians-University Würzburg, Am Hubland, 97074 Würzburg, Germany

Supporting Information

ABSTRACT: Bismepines are 3-fold unsaturated seven-membered rings containing one bismuth atom. A set of dibenzobismepine complexes have been synthesized and isolated, among them a dinuclear bismepine, halobismepines, and cationic bismepines. They were investigated with respect to the structural properties, olefin−bismuth interactions, heteroaromaticity, and Lewis acidity (including a comparison with a range of simple bismuth and group 13 Lewis acids). Applied analytical techniques include NMR spectroscopy, single-crystal X-ray analysis, elemental analysis, and density functional theory calculations.

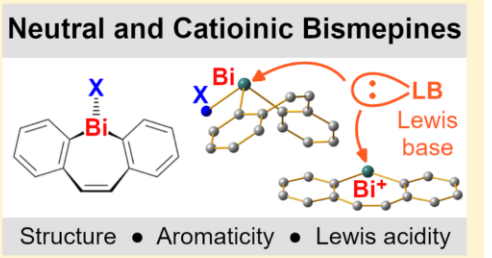

INTRODUCTION

The transformation of neutral bismuth compounds into cationic derivatives can drastically change the reactivity patterns of these compounds. This has recently been exploited in order to realize unusual stoichiometric reactions and enhanced catalytic activities. Examples include diastereoselective Mannich reactions in water,[1] the hydrosilylation of alkenes,[2] controlled radical polymerization of activated olefins,[3] CH activation of diarylamines,[4,5] and insertion reactions with carbon monoxide.[6] The cationic nature of bismuth(III) compounds may also affect their transformation into low-valent bismuth(II) and bismuth(I) species.[7]

In some cases, attempts have been undertaken to rationalize the differences in the reactivity of cationic species and their neutral parent compounds. In this respect, the higher Lewis acidity of the charged species is one of the key parameters: it can significantly affect properties such as the coordination number, coordination geometry, degree of aggregation, solubility, and ability to precoordinate and Lewis-acid-activate a substrate.[1−5,8]

Lewis acidic bismuth(III) compounds may be separated into three different classes, A−C (Scheme 1). One extreme is represented by class A compounds, which are not classified as cationic species.[9,10] Their Lewis acidity is due to an antibonding σ^*(Bi−X) orbital, which commonly becomes energetically accessible for interactions with Lewis bases if X shows a sufficiently high electronegativity.[10,11] At the other extreme, there are compounds of class C, which are cationic species without direct bonding interactions between the anion and the cation.[12] In most cases, these compounds can only be isolated as Lewis base adducts.[13] The main interactions with Lewis bases are realized via the empty 6p orbital of the $(R_2Bi)^+$ complex fragment.[8] Compounds of type B are intermediate

Scheme 1. Three Classes of Bismuth Lewis Acids, A−C (Isolable As Shown or Stabilized by Interactions with Lewis Bases), with Their Orbitals Most Relevant for the Binding of Lewis Bases[a]

	Class A	Class B	Class C
	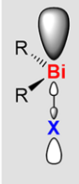		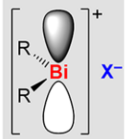
Bi–X bond (strength, type)	regular, polar covalent	weak, polar covalent	none
orbital for interaction with Lewis base	σ* (Bi–X)	σ* (Bi···X)	6p (Bi)
typical X	halide	OTf, $AlCl_4$	SbF_6, $B(Ar^F)_4$

[a]OTf = O_3SCF_3; Ar^F = aryl group with substituents that are or contain fluorine atoms.

Special Issue: Bismuth - The Magic Element
Received: October 31, 2019
Published: December 31, 2019

DOI: 10.1021/acs.inorgchem.9b03189
Inorg. Chem. 2020, 59, 3367−3376

between types A and C in the sense that there are Bi···X bonding interactions, which are weak because of delocalization of the negative charge in X (e.g., for X = O_3SCF_3, $AlCl_4$).[14−16]

The Lewis acidic character of bismuth compounds usually results in the formation of σ-type interactions with one or more Lewis bases. A recent report on the first isolable bismabenzene derivative **I**, however, demonstrated that bismuth-centered p orbitals can also engage in the formation of π bonds with carbon-centered p-type orbitals (Scheme 2a).[17] Thus, cationic bismuth compounds, in which the bismuth center is in conjugation with a π-electron system, could potentially also show partial Bi−C multiple-bond character. This also raises the question of whether, for cationic bismuth species $(R_2Bi)^+$, the formation of intramolecular Bi−C π bonds can compete with the formation of intermolecular Bi−LB σ bonds (LB = Lewis base). In the case of cationic bismepines **II**, this goes along with potential heteroaromatic character (Scheme 2b). While a small number of neutral bismepines **III** that bear annelated aromatic substituents at the bismepine core are known for R = Ph (but have not been fully characterized),[18] derivatives thereof and cationic species **II** in particular are unknown.

Scheme 2. (a) First Isolable Bismabenzene I and (b) Cationic Bismepine II (a Potentially Heteroaromatic Compound) and a Neutral Parent Compound III

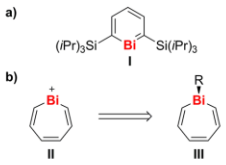

Here we report the synthesis, isolation, and characterization of a range of neutral and cationic bismepine compounds, along with an evaluation of their Lewis acidity and heteroaromaticity.

RESULTS AND DISCUSSION

Synthesis of Bismepines. For the small number of literature-known bismepines **III**, a strong impact of the substitution pattern at the bismepine core on their stability has been reported. Some complexes showed half-lives of only <1 min in a toluene solution at 50 °C.[18b] With the aim of synthesizing new Lewis acidic bismepines (R ≠ Ph), a dibenzobismepine core was chosen as the synthetic target in order to generate species that are sufficiently stable to be isolated. Using the literature-known dilithium species **1** as an isolable starting material,[19] the dinuclear bismepine **2** was synthesized in a salt elimination reaction with $BiCl_3$ and isolated in quantitative yield as a colorless solid (Scheme 3). In atom economic approaches, comproportionation reactions of **2** with bismuth halides BiX_3 gave the first examples of halobismepines **3-X** as colorless solids in 67−88% yield (X = Cl, Br, I).[20]

Salt elimination reactions of **3-Cl** with AgOTf, $AgBF_4$, and $AgSbF_6$ gave access to the first examples of cationic bismepines **3-OTf**, **3-BF_4**, and [**3-thf$_2$**][**SbF_6**], which were isolated as colorless (**3-OTf** and [**3-thf$_2$**][**SbF_6**]) and yellow (**3-BF_4**) solids in 56−92% yield (OTf = O_3SCF_3; Scheme 4). While **3-OTf** and **3-BF_4** could be isolated free of neutral donor ligands, [**3-thf$_2$**][**SbF_6**] was obtained as a bis(tetrahydrofuran) [bis(thf)] adduct. The thf ligands in [**3-thf$_2$**][**SbF_6**] could not be removed upon exposure to vacuum (10^{-3} mbar) at temperatures of up to 40 °C,[21,22] but are substitutionally labile according to NMR spectroscopic analysis. A signal of m/z 387.0572, which corresponds to the donor-free cation $[Bi(C_6H_4)_2C_2H_2]^+$ (calcd m/z 387.0581), was detected by high-resolution electrospray ionization mass spectrometry (ESI-MS).

Scheme 4. Synthesis of Cationic Bismepines 3-OTf, 3-BF_4, and [3-thf$_2$][SbF_6]

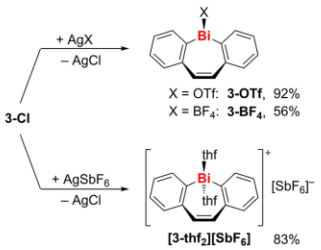

NMR Spectroscopic Analysis of Bismepines. ^{1}H NMR spectra of the dinuclear bismepine **2** show two sets of signals with an intensity ratio of 1:2, each of which contains resonances typical of a benzo group plus a singlet in the olefinic region. This suggests an apparent C_{2v} symmetry in solution. ^{1}H NMR spectra of the mononuclear bismepines **3-X** (X = Cl, Br, I, OTf) and [**3-thf$_2$**][**SbF_6**] display resonances typical of a benzo group and a singlet in the olefinic region, suggesting apparent C_s symmetry in solution.[23] The ^{13}C NMR spectra of all compounds are in agreement with the suggested structures. The resonances of the *ipso*-carbon atoms in the bismepines are sensitive spectroscopic handles for the group electronegativity of the BiX moiety. Their chemical shift steadily increases from X = aryl (δ = 152 ppm) via X = halide [δ = 157 (I), 167 (Br), 173 (Cl) ppm] to X = weakly coordinating anion [δ = 191 (OTf), 193 (SbF_6) ppm].

Single-Crystal X-ray Analysis. Compound **2** crystallized in the triclinic space group $P\bar{1}$ with Z = 2. It represents a

Scheme 3. Synthesis of Dinuclear Bismepine 2 and Halobismepines 3-X (X = Cl, Br, I)

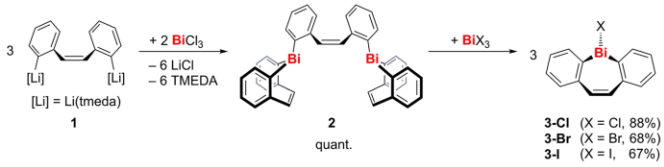

DOI: 10.1021/acs.inorgchem.9b03189
Inorg. Chem. 2020, 59, 3367−3376

typical molecular structure without directed intermolecular interactions in the solid state. The two bismepine units of the dinuclear compound are crystallographically independent but show highly similar bonding parameters, so only one of them is discussed. The bismuth atom Bi1 shows the expected trigonal-pyramidal coordination geometry. The C−Bi−C angle of the chelating ligand (88.3°) is smaller than those involving carbon atoms of the bridging hydrocarbon moiety (92.2−94.7°). All Bi−C bond lengths amount to 2.26 Å, which is in the typical range of Bi(aryl)$_3$-type compounds.[24] In the bismepine heterocycle, the C6−C7 and C8−C9 bond lengths (1.48 Å) indicate single-bond character, while the C7−C8 bond length (1.34 Å) is in agreement with a typical C═C double bond. The bismepine core shows a boat conformation, with the bismuth atom and the olefin unit pointing toward each other (Figure 1b).

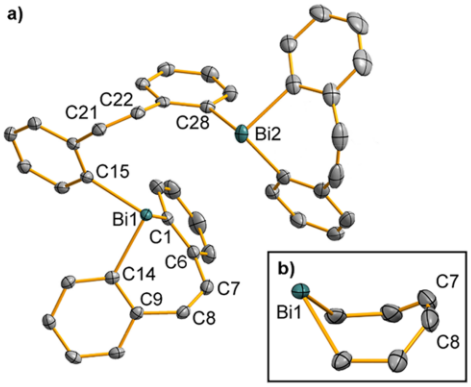

Figure 1. (a) Molecular structure of **2·tol** in the solid state. Displacement ellipsoids are drawn at the 50% probability level; hydrogen atoms and lattice-bound toluene molecules are omitted for clarity. Selected bond lengths (Å) and angles (deg): Bi1−C1, 2.257(3); Bi1−C14, 2.261(3); Bi1−C15, 2.255(3); C1−C6, 1.399(4); C6−C7, 1.483(4); C7−C8, 1.338(4); C8−C9, 1.480(4); C9−C14, 1.400(4); C21−C22, 1.330(4); C1−Bi1−C14, 88.30(9); C15−Bi1−C1, 94.68(10); C15−Bi1−C14, 92.21(9); angle[plane-(C1−C6)]/[plane(C9−C14)], 106.3. (b) Cutout showing the boat conformation of a seven-membered BiC_6 ring in the side view.

Compounds **3-Cl**, **3-Br**, and **3-I** crystallized in the monoclinic space group $P2_1/c$ with $Z = 4$ and are isostructural (Figure 2; for details, see the Supporting Information). Molecular units of the halobismepines adopt boat conformations and show bismuth atoms in trigonal-pyramidal coordination geometries (Figure 2a). Weak intermolecular interactions between bismuth centers and benzo groups of neighboring bismepine units lead to the formation of one-dimensional coordination polymers in the solid state [Bi1···ct(C1′−C6′), 3.38−3.44 Å; ct indicates the centroid of a benzo group]. These interactions can be expected to be mainly dispersive, as reported for $BiPh_3$ or Bi(3,5-tBu$_2$C$_6$H$_3$)$_2$Cl.[10c] Notably, there are no intermolecular Bi···halide interactions in **3-Cl**,[25] **3-Br**, and **3-I**, which is in contrast to the bonding situation in other diarylbismuth halides such as $BiPh_2Cl$, Bi(3,5-tBu$_2$C$_6$H$_3$)$_2$Cl, $BiMes_2Br$, and $BiPh_2I$(4-MeNC$_6$H$_4$).[10c,26,27] This may be rationalized by the fact that the

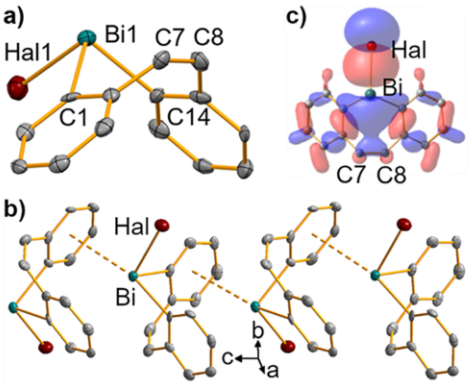

Figure 2. (a) Molecular structures of **3-Cl**, **3-Br**, and **3-I** and (b) arrangement as one-dimensional coordination polymers in the solid state (shown for **3-Br**). Displacement ellipsoids ar·e drawn at the 50% probability level. Hydrogen atoms are omitted for clarity. Selected bond lengths (Å), bond angles (deg), and interatomic distances (Å). **3-Cl**: Bi1−Cl1, 2.5127(13); Bi1−C1, 2.240(5); Bi1−C14, 2.240(5); Bi1···ct(C1′−C6′), 3.444(5); Bi1···C7, 3.247(5); Bi1···C8, 3.227(5); C1−Bi1−C14, 85.94(17); C1−Bi1−Cl1, 93.68(13); C14−Bi1−Cl1, 93.39(14); angle(C1−C6)/(C9−C14), 100.2. **3-Br**: Bi1−Br1, 2.6407(9); Bi1−C1, 2.254(7); Bi1−C14, 2.245(7); Bi1···ct(C1′−C6′), 3.382(7); Bi1···C7, 3.199(7); Bi1···C8, 3.204(7); C1−Bi1−C14, 85.5(3); C1−Bi1−Br1, 94.72(19); C14−Bi1−Br1, 92.77(19); angle(C1−C6)/(C9−C14), 91.3. **3-I**: Bi1−I1, 2.7845(11); Bi1−C1, 2.242(12); Bi1−C14, 2.254(11); Bi1···ct(C1′−C6′), 3.410(12); Bi1···C7, 3.211(12); Bi1···C8, 3.212(12); C1−Bi1−C14, 85.7(4); C1−Bi1−I1, 93.4(3); C14−Bi1−I1, 96.8(3); angle(C1−C6)/(C9−C14), 91.9. (c) HOMO−9 of **3-Hal** (shown for **3-Br** with an isovalue of 0.024) revealing an overlap between the π(C7−C8) and σ(Bi−Hal) orbitals.

antibonding σ^*(Bi−Hal) orbitals of the halobismepines point toward the olefin functionality of their ligand backbones. Weak Bi···olefin interactions are supported by Bi···C7 and Bi···C8 distances of 3.20−3.25 Å, which is 14−15% below the sum of the van der Waals radii (3.77 Å).[28] In agreement with these distance criteria, natural bond orbital (NBO) analyses indicate weak interactions between the π(C7−C8) and σ^*(Bi−Hal) orbitals with deletion energies of 2.6−2.9 kcal mol^{-1} (for details, see the Supporting Information). A molecular orbital analysis revealed an overlap between the π(C7−C8) and σ(Bi−Hal) orbitals in HOMO−9 (Figure 2c). These results suggest that compounds **3-Cl**, **3-Br**, and **3-I** show the first examples of (weak and intramolecular) bismuth−olefin bonding interactions.

The bismepine triflate **3-OTf** crystallized in the monoclinic space group $P2_1/c$ with $Z = 4$ as a contact ion pair (Figure 3). The bismuth atom is found in a bisphenoidal coordination geometry. Oxygen atoms of the OTf anion (O1) and the OTf anion of a neighboring formula unit (O3′) occupy the axial positions. The bridging coordination mode of the triflate anion leads to the formation of a one-dimensional coordination polymer in the solid state (Figure 3b). The equatorial positions in the coordination sphere of the bismuth center are occupied by the hydrocarbon ligand. The Bi−O and Bi−C bond lengths in **3-OTf** are similar to those in $BiPh_2OTf$.[29] The bismepine core in **3-OTf** is significantly flattened compared to **3-Cl**, **3-Br**,

DOI: 10.1021/acs.inorgchem.9b03189
Inorg. Chem. 2020, 59, 3367−3376

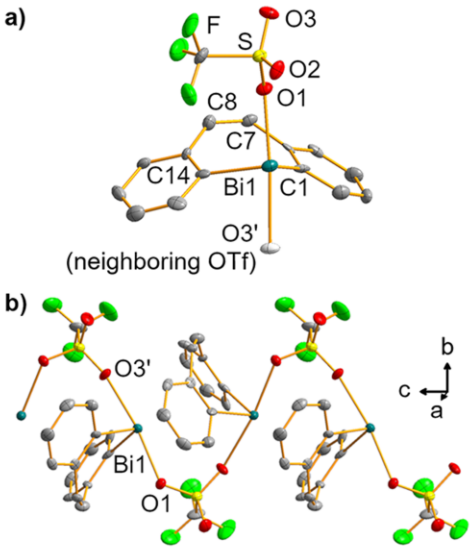

Figure 3. (a) Molecular structure of **3-OTf** and (b) arrangement as one-dimensional coordination polymers in the solid state. Displacement ellipsoids are drawn at the 50% probability level. Hydrogen atoms are omitted for clarity. The atom exceeding one formula unit in part a is shown as a colorless ellipsoid. Selected bond lengths (Å) and angles (deg): Bi1−C1, 2.191(10); Bi1−C14, 2.217(10); Bi1−O1, 2.381(6); Bi1−O3′, 2.525(6); C1−Bi1−C14, 95.1(4); O1−Bi1−O3′, 172.1(2); angle(C1−C6)/(C9−C14), 126.1. O3 and O3′ are related by symmetry code x, 0.5 − y, 0.5 + z.

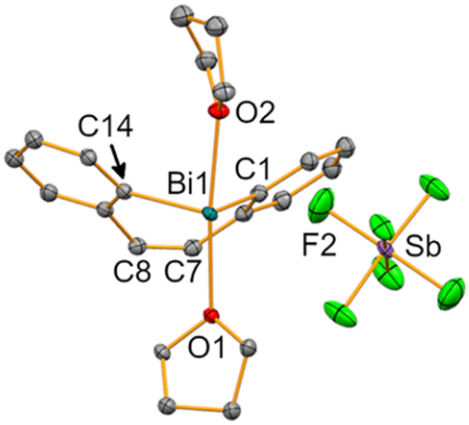

Figure 4. Molecular structure of [**3-thf$_2$**][**SbF$_6$**] in the solid state. Displacement ellipsoids are drawn at the 50% probability level. Hydrogen atoms and lattice-bound solvent molecules are omitted for clarity. Selected bond lengths (Å), bond angles (deg), and interatomic distances (Å): Bi1−C1, 2.223(5); Bi1−C14, 2.238(5); Bi1−O1, 2.432(3); Bi1−O2, 2.433(3); Bi1···F2, 3.228(4); C1−Bi1−C14, 93.67(19); O1−Bi1−O2, 173.81(12); angle(C1−C6)/(C9−C14), 124.0.

and **3-I**. This is reflected by **3-OTf** showing a larger C1−Bi1−C14 angle (95.1° vs 85.5−85.9°) and a larger angle between the mean planes of the benzo groups (126° vs 91.3−100.2°). These observations may be rationalized by the fact that the bismuth-centered p orbital, which is not involved in Bi−C bond formation, is occupied by two triflate donors in **3-OTf**.[30] This orbital is thus unavailable for interactions with the olefin moiety of the ligand backbone, which bends less toward the bismuth atom. In addition, steric interactions between the triflate anions and olefin moiety would also disfavor Bi···olefin interactions in **3-OTf**. A closely related structure was determined for **3-BF$_4$** (Figure S4).

The cationic bismepine [**3-thf$_2$**][**SbF$_6$**] crystallized in the monoclinic space group $P2_1/c$ with Z = 4 as a solvent-separated ion pair (Figure 4).[31] The bismuth center adopts a bisphenoidal coordination geometry with two thf ligands in the axial and hydrocarbon ligands in the equatorial positions. The same type of coordination geometry has been reported for diarylbismuth cations such as [$BiPh_2L_2$][anion] (L = neutral donor ligand).[12a,32] The Bi−O bond lengths (2.43 Å) are similar to those in the bis(allyl)bismuth cation [Bi-$(C_3H_5)_2$(thf)$_2$][B(3,5-$Cl_2C_6H_3)_4$],[3,33] while the Bi−C bond lengths (2.22−2.24 Å) are close to those in **3-OTf** and other diarylbismuth cations.[12a,32] The occupation of the bismuth-centered p orbital by two thf ligands prohibits Bi···olefin interactions and leads to considerable flattening of the bismepine core (C1−Bi1−C14, 93.7°; angle between mean planes defined by benzo groups, 124°), as observed for **3-OTf** and **3-BF$_4$**.

Aromaticity of Cationic Bismepines. Recently, the first isolable bismabenzene compound has been reported (cf. **I** in Scheme 2).[17] Exchange of two CH groups in benzene [2 × 5 valence electrons (VEs)] for one Bi$^+$ moiety (4 VEs) and one NH group (6 VEs) also yielded a moderately aromatic compound, as shown by density functional theory (DFT) calculations on [$Bi(C_6H_4)_2NH$][OTf].[4] In this contribution, the potential of cationic bismepines to show heteroaromaticity was investigated by DFT calculations. The cationic dibenzobismepine [$Bi(C_6H_4)_2C_2H_2$(thf)$_2$]$^+$ ([**3-thf$_2$**]$^+$) bears 14 π electrons in a cyclic conjugated π-electron system. However, its nonplanar structure and the presence of thf ligands (as determined for [**3-thf$_2$**][**SbF$_6$**]) speak against a heteroaromatic character.[34] DFT calculations on [**3-thf$_2$**]$^+$ revealed two minima on the potential energy surface (for details, see the Experimental Section). One of them corresponds to the slightly bent bismepine geometry [**3-thf$_2$**]$^+$**-bent**, which was also found experimentally in the solid state (Figure 5a). The second structure, [**3-thf$_2$**]$^+$**-planar**, shows a perfectly planar bismepine core and is only marginally higher in energy by 1.6 kcal mol^{-1} (Figure 5b).[35] Aided by a relaxed potential energy surface scan, a low-energy transition state between [**3-thf$_2$**]$^+$**-bent** and [**3-thf$_2$**]$^+$**-planar** was located ($\Delta G^{\ddagger}$ = +2.9 kcal mol^{-1}), supporting the facile transformation between these two conformations (see the Supporting Information). This is equivalent to an almost barrierless inversion of the boat conformation in [**3-thf$_2$**]$^+$**-bent**. Slightly positive nucleus-independent chemical shift (NICS) values of [**3-thf$_2$**]$^+$**-planar** demonstrate the nonaromatic character of the cationic bismacycle [NICS(0) = +0.9 ppm, NICS(1) = +1.0 ppm, and $NICS(1)_{zz}$ = +2.9 ppm]. Removal of the thf ligands from the cationic bismepine changed the preferred conformation of

DOI: 10.1021/acs.inorgchem.9b03189
Inorg. Chem. 2020, 59, 3367−3376

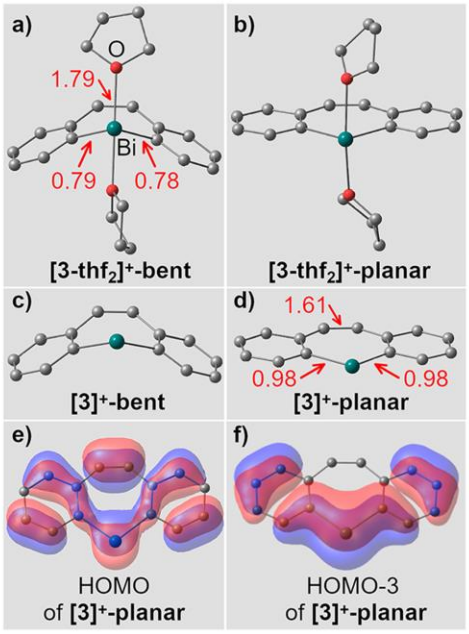

Figure 5. Molecular structures of cationic bismepines (a-d) and selected molecular orbitals of $[\mathbf{3}]^+$-**planar** (e and f) as determined by DFT calculations. Selected WBIs are shown in red.

the bismepine cation: analysis of $[Bi(C_6H_4)_2C_2H_2]^+$ ($[\mathbf{3}]^+$; as detected by mass spectrometry; vide supra) revealed that the planar conformer $[\mathbf{3}]^+$-**planar** is by 7.9 kcal mol^{-1} lower in energy than the bent isomer $[\mathbf{3}]^+$-**bent** (Figure 5c,d).[35,36] Negative NICS values of NICS(0) = −1.5 ppm, NICS(1) = −3.8 ppm, and $NICS(1)_{zz}$ = −8.0 ppm suggest a moderate heteroaromaticity for $[\mathbf{3}]^+$-**planar**. This is further supported by a molecular orbital analysis, which revealed Bi−C π bonding involving the bismuth-centered p orbital orthogonal to the bismepine plane (Figure 5e,f). In agreement with this, the Bi−C Wiberg bond indices (WBIs) in $[\mathbf{3}]^+$-**planar** (WBI_{Bi-C} = 0.98) are significantly larger than those in $[\mathbf{3\text{-}thf_2}]^+$-**bent** ($WBI_{Bi-C}$ = 0.78−0.79), while the reverse trend is observed for the C−C WBIs of the C_2H_2 linker ($[\mathbf{3}]^+$-**planar**, WBI_{C-C} = 1.61; $[\mathbf{3\text{-}thf_2}]^+$-**bent**, WBI_{C-C} = 1.79; see the red numbers in Figure 5a,d).[37] The addition of two thf ligands to $[\mathbf{3}]^+$-**planar** to give $[\mathbf{3\text{-}thf_2}]^+$-**bent** is exergonic by ΔG = −28.5 kcal mol^{-1}, underlining the Lewis acidic character of cationic bismuth species. The isolation of donor-free bismepine cations $[Bi(C_6H_4)_2C_2H_2]^+[anion]^-$ and related compounds[13] will be an intriguing future challenge for synthetic chemists.

Lewis Acidity of Bismuth Compounds. Bismuth compounds such as $BiCl_3$ and $Bi(OTf)_3$ are frequently applied as Lewis acids with a high functional group tolerance in organic reactions. Examples include Sakurai reactions, Mannich reactions, hydroamination of olefins, alkynes, and dienes, as well as cycloisomerizations of enynes to name a few.[38] In contrast to these frequent applications, quantification of the Lewis acidity of bismuth compounds has only rarely been reported. For instance, monocationic diarylbismuth complexes with NMe_2-donor moieties and a dicationic bismuth tris(pyrazolyl)borate have been investigated using the Gutmann−Beckett method.[2,39] In this method, the ^{31}P NMR chemical shift of $OPEt_3$ is measured in the presence of a Lewis acid under investigation.[40,41] An acceptor number (AN) can be calculated according to eq 1

$$AN = 2.21[\delta(^{31}PNMR)_{sample}/ppm - 41.0] \quad (1)$$

where AN = 0 corresponds to $OPEt_3$ in hexane and AN = 100 corresponds to $OPEt_3{\cdot}SbCl_5$ in dichloroethane.[40a,42] The bismepines presented in this work were investigated using the Gutmann−Beckett method along with a range of fundamental bismuth aryl and halide compounds and related species (Table 1). Quantification was performed in dichloromethane (DCM), which shows only a weak donor ability and guaranteed sufficient solubility of the bismuth compounds. Expectedly, the arylbismuth compounds **2** and $BiPh_3$ showed only a weak Lewis acidity with ANs of 19−20 (entries 1 and 2). Among the halobismepines, **3-Cl** and **3-Br** with their energetically low-lying σ^*(Bi−X) acceptor orbitals showed ANs of 26, while that of **3-I** was slightly lower (AN = 23; entries 3−5). Homoleptic bismuth halides $BiCl_3$ and $BiBr_3$ are generally more Lewis acidic than the halobismepines, while BiI_3 is only weakly Lewis acidic [AN = 49 (X = Cl), 30 (X = Br), and 22 (X = I); entries 6−8]. The cationic bismepines **3-OTf** and $[\mathbf{3\text{-}thf_2}][\mathbf{SbF_6}]$ show ANs of 59−64 (entries 9 and 10). This is in the same range as the AN of the literature-known diphenylbismuth cation $BiPh_2(OTf)$ (AN = 63, entry 11), which was determined for comparison.[29] These values range between those reported for classical Lewis acids such as BPh_3 (AN = 58),[43] on the one hand, and $B(C_6F_5)_3$ (AN = 77)[43] or $AlCl_3$ (AN = 81),[44] on the other hand (entries 13−15). Cationic diarylbismuth complexes with NMe_2-donor groups have been reported to show ANs of 55−69 (depending on the ligand bite angle),[39] while a dicationic bismuth tris(pyrazolyl)borate is associated with AN = 75.[45] The commercially available and frequently used bismuth triflate

Table 1. Analysis of Bismuth Compounds and Related Species by the Gutmann−Beckett Method Using $OPEt_3$ as the Lewis Base[a]

entry	compound	δ $^{31}P\{^1H\}$ [ppm]	AN
1	**2**	49.4	19
2	$BiPh_3$	50.5	20
3	**3-Cl**	52.8	26
4	**3-Br**	52.8	26
5	**3-I**	51.2	23
6	$BiCl_3$	63.1	49
7	$BiBr_3$	54.6	30
8	BiI_3	51.0	22
9	**3-OTf**[b]	67.5	59
10	$[\mathbf{3\text{-}thf_2}][\mathbf{SbF_6}]$	70.0	64
11	$BiPh_2(OTf)$[b]	69.3	63
12	$Bi(OTf)_3$	88.5	105
13	BPh_3[43]	67.2	58
14	$B(C_6F_5)_3$[43]	75.9	77
15	$AlCl_3$[44]	77.8	81

[a]A total of 1 equiv of $OPEt_3$ per bismuth atom was added to a solution of the respective Lewis acid in DCM. [b]Solvent = CH_2Cl_2/THF (25:1, v/v).

DOI: 10.1021/acs.inorgchem.9b03189
Inorg. Chem. 2020, 59, 3367−3376

shows an exceptionally high AN of 105 (entry 12), which is in the same range as that of the extraordinarily strong Lewis acids $SbCl_5$ (AN = 100) and BBr_3 (AN = 105).[43]

CONCLUSIONS

A set of dibenzobismepines were synthesized and characterized, including the first examples of a dinuclear bismepine, halobismepines, and cationic bismepines. The first single-crystal X-ray diffraction studies of bismepines were performed. These revealed boat conformations for the neutral species. Supported by DFT calculations, unprecedented (weak and intramolecular) Bi−olefin interactions were located in halobismepines. In the cationic compounds, the boat conformation of the bismepine core was considerably flattened and a planar conformer was only marginally higher in energy (ΔG = +1.6 kcal mol^{-1}), as determined by DFT calculations. Molecular orbital analysis and calculated NICS values revealed a heteroaromatic character for the donor-free cationic dibenzobismepine $[Bi(C_6H_4)_2C_2H_2]^+$, which is diminished upon coordination of neutral donor ligands to the bismuth center; i.e., in the cationic bismepines investigated here, Bi−C π bonding is, in principle, possible but cannot compete with the formation of intermolecular Lewis pair formation. The Lewis acidity of a broad range of common bismuth(III) compounds, halobismepines, and cationic bismepines has been evaluated with the Gutmann−Beckett method. The Lewis acidity of the cationic species ranges between that of the classical group 13 Lewis acids BPh_3 and $B(C_6F_5)_3$ or $AlCl_3$. Commercially available $Bi(OTf)_3$ showed an exceptional Lewis acidity in the range of BBr_3 and $SbCl_5$. It is anticipated that the findings disclosed in this work will contribute to an understanding of the bonding situation in Lewis acidic bismuth compounds, the design of new bismuth Lewis acids, and their application in synthesis and catalysis.

EXPERIMENTAL SECTION

General Considerations. All air- and moisture-sensitive manipulations were carried out using standard vacuum-line Schlenk techniques or in gloveboxes containing an atmosphere of purified argon. Solvents were degassed and purified according to standard laboratory procedures. NMR spectra were recorded on Bruker instruments operating at 400 or 500 MHz with respect to ^{1}H. ^{19}F and ^{31}P NMR spectra were recorded with proton decoupling. All chemical shifts (δ) are reported in parts per million (ppm). ^{1}H and ^{13}C NMR chemical shifts are reported relative to $SiMe_4$ using the residual ^{1}H and ^{13}C chemical shifts of the solvent as a secondary standard. ^{19}F and ^{31}P NMR chemical shifts are reported relative to $CFCl_3$ and 85% aqueous H_3PO_4, respectively, as external standards. NMR spectra were recorded at ambient temperature (typically 23 °C). Single crystals suitable for X-ray diffraction were coated with perfluorinated polyether oil in a glovebox, transferred to a nylon loop, and then transferred to the goniometer of a diffractometer equipped with a molybdenum X-ray tube (λ = 0.71073 Å). The structures were solved using intrinsic phasing methods (*SHELXT*) completed by Fourier synthesis and refined by full-matrix least-squares procedures. CCDC 1961394−1961400, 1961403, 1961404, and 1961408−1961411 contain the crystallographic information for this work.

DFT Calculations. DFT calculations were performed with the *Gaussian* program[46] using the 6-31G(d,p)[47] (hydrogen, carbon, and oxygen atoms) or LanL2DZ[48] (chlorine, bromine, iodine, and bismuth atoms) basis set and the B3LYP functional.[49] The D3 version of Grimme's dispersion model with the original D3 damping function was applied.[50] Frequency analyses of the reported structures showed no imaginary frequencies for ground states and one imaginary frequency for transition states. The thermodynamic parameters were calculated at a temperature of 298.15 K and a pressure of 1.00 atm for single-phase systems; i.e., they are standard parameters according to IUPAC.[51] NBO analyses were performed using the program version *NBO 7*.[52]

The following labeling scheme was used for reporting NMR chemical shifts:

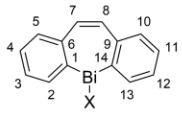

(*Z*)-1,2-Bis[2-(5*H*-dibenzo[*b*,*f*]bismepin-5-yl)phenyl]ethene (2). At −78 °C, a solution of **1** (150 mg, 0.35 mmol) in THF (2 mL) was added dropwise to a suspension of bismuth(III) chloride (74.3 mg, 0.24 mmol) in THF (2 mL). The resulting suspension was stirred for 2 h at −78 °C and then for 16 h at ambient temperature. All volatiles were removed under reduced pressure, and the residue was extracted with toluene (5 mL). The light-yellow filtrate was layered with *n*-pentane (5 mL) and stored at −30 °C. Colorless crystals were obtained after 16 h, isolated by filtration, and dried in vacuo. Yield: 120 mg, 0.12 mmol, quant.

^{1}H NMR (500 MHz, 6:1 C_6D_6/CD_2Cl_2): δ 6.65 (s, 4H, H-7, H-8), 6.89 (ddd, 2H, $^3J_{HH}$ = 7.5 Hz, $^3J_{HH}$ = 7.5 Hz, $^2J_{HH}$ = 1.3 Hz, H-3^{bridge}, H-12^{bridge}), 6.91 (s, 2H, H-7^{bridge}, H-8^{bridge}), 6.94 (ddd, 4H, $^3J_{HH}$ = 7.5 Hz, $^3J_{HH}$ = 7.5 Hz, $^2J_{HH}$ = 1.3 Hz, H-3, H-12), 7.02 (ddd, 4H, $^3J_{HH}$ = 7.5 Hz, $^3J_{HH}$ = 7.5 Hz, $^2J_{HH}$ = 1.3 Hz, H-4, H-11), 7.10 (ddd, 2H, $^3J_{HH}$ = 7.5 Hz, $^3J_{HH}$ = 7.5 Hz, $^2J_{HH}$ = 1.3 Hz, H-4^{bridge}, H-11^{bridge}), 7.16−7.18 (m, 4H, H-5, H-10, overlapping with solvent resonance), 7.23 (dd, 4H, $^3J_{HH}$ = 7.5 Hz, $^2J_{HH}$ = 1.3 Hz, H-2, H-13), 7.31 (dd, 2H, $^3J_{HH}$ = 7.5 Hz, $^2J_{HH}$ = 1.3 Hz, H-5^{bridge}, H-10^{bridge}), 7.83 (dd, 2H, $^3J_{HH}$ = 7.5 Hz, $^2J_{HH}$ = 1.3 Hz, H-2^{bridge}, H-13^{bridge}).

^{1}H NMR (400 MHz, THF-d_8): δ 6.77 (s, 4H, C_2H_2), 7.02 (m, 4H, C_2H_2, C_6H_4), 7.09−7.20 (m, 12H, C_6H_4), 7.26−7.38 (m, 8H, C_6H_4), 7.83 (d, 2H, $^3J_{HH}$ = 7.4 Hz, C_6H_4).

^{1}H NMR (400 MHz, C_6D_6): δ 6.68 (s, 4H, C_2H_2), 6.84−6.88 (m, 4H, C_2H_2, C_6H_4), 6.96−7.10 (m, 10H, C_6H_4), 7.18−7.24 (m, 4H, C_6H_4), 7.35−7.38 (m, 6H, C_6H_4), 7.94 (dd, 2H, $^3J_{HH}$ = 7.5 Hz, $^4J_{HH}$ = 1.0 Hz, C_6H_4).

^{1}H NMR (400 MHz, CD_2Cl_2): δ 6.81 (s, 4H, C_2H_2), 7.06−7.09 (m, 4H, C_2H_2, C_6H_4), 7.13−7.22 (m, 12 H, C_6H_4), 7.31−7.39 (m, 8H, C_6H_4), 7.82 (d, 2H, $^3J_{HH}$ = 7.3 Hz, C_6H_4).

^{13}C NMR (126 MHz, 6:1 C_6D_6/CD_2Cl_2): δ 127.35 (s, C-4, C-11), 128.49 (s, C-3^{bridge}, C-12^{bridge}), 129.99 (s, C-2^{bridge}, C-13^{bridge}), 130.29 (s, C-5, C-10), 130.51 (s, C-3, C-12), 131.13 (s, C-4^{bridge}, C-11^{bridge}), 133.39 (s, C-7, C-8), 136.07 (s, C-7^{bridge}, C-8^{bridge}), 137.21 (s, C-2, C-13), 142.62 (s, C-6, C-9), 142.71 (s, C-5^{bridge}, C-10^{bridge}), 145.51 (s, C-6^{bridge}, C-9^{bridge}), 152.27 (s, C-1, C-14), 159.39 (s, C-1^{bridge}, C-14^{bridge}).

Elem anal. Calcd for $C_{42}H_{30}Bi_2$ (952.66 g mol^{-1}): C, 52.95; H, 3.17. Found: C, 53.29; H, 3.57.

5-Chloro-5*H*-dibenzo[*b*,*f*]bismepine (3-Cl). A solution of $BiCl_3$ (54.6 mg, 0.17 mmol) and **2** (165.0 mg, 0.17 mmol) in THF (5 mL) was stirred at 60 °C for 16 h. All volatiles were removed under reduced pressure, and the residue was extracted with toluene (3 × 1 mL). The colorless solution was layered with *n*-pentane (5 mL) and stored at −30 °C. After 16 h, a colorless solid had precipitated, which was isolated by filtration and dried in vacuo. Yield: 190.1 mg, 0.45 mmol, 88%.

^{1}H NMR (400 MHz, C_6D_6): δ 6.49 (s, 2H, H-7, H-8), 6.92 (dd, 2H, $^3J_{HH}$ = 7.6 Hz, $^4J_{HH}$ = 1.3 Hz, H-4, H-11), 7.17 (d, 2H, $^4J_{HH}$ = 1.1 Hz, H-5, H-10, overlapping with solvent resonance), 7.35 (dd, 2H, $^3J_{HH}$ = 7.6 Hz, $^4J_{HH}$ = 1.3 Hz, H-3, H-12), 8.72 (d, 2H, $^3J_{HH}$ = 7.2 Hz, H-2, H-13).

^{1}H NMR (400 MHz, THF-d_8): δ 6.89 (s, 2H, C_2H_4), 7.12 (ddd, 2H, $^3J_{HH}$ = 7.5 Hz, $^3J_{HH}$ = 7.5 Hz, $^4J_{HH}$ = 1.1 Hz, C_6H_4), 7.45 (d, 4H, $^3J_{HH}$ = 7.6 Hz, C_6H_4), 7.52 (dd, 2H, $^3J_{HH}$ = 7.4 Hz, $^3J_{HH}$ = 7.4 Hz, C_6H_4), 8.51 (d, 2H, $^3J_{HH}$ = 7.7 Hz, C_6H_4).

DOI: 10.1021/acs.inorgchem.9b03189
Inorg. Chem. 2020, 59, 3367−3376

^{13}C NMR (101 MHz, C_6D_6): δ 127.64 (s, C-4, C-11), 131.19 (s, C-7, C-8), 132.16 (s, C-5, C-10), 133.45 (s, C-3, C-12), 134.38 (s, C-2, C-13), 139.61 (s, C-6, C-9), 172.88 (br, C-1, C-14).

Elem anal. Calcd for $[C_{14}H_{10}BiCl]$ (422.66 g mol^{-1}): C, 39.78; H, 2.38. Found: C, 39.93; H, 2.02.

LIFDI-MS (positive mode). Calcd for $[C_{14}H_9]^+$: m/z 178.0783. Found: m/z 178.0774 (100%). Calcd for $[C_8H_8BiO]^+$: m/z 281.0373. Found: m/z 281.0368 (30%). Calcd for $[C_8H_{16}BiO_2]^+$: m/z 353.0949. Found: m/z 353.0941 (20%). Calcd for $[C_{18}H_{18}BiO]^+$: m/z 459.1156. Found: m/z 459.1147 (20%). Calcd for $[C_{22}H_{26}BiO_2]^+$: m/z 531.1721. Found: m/z 531.1722 (10%). Calcd for $[C_{14}H_{11}Bi]^+$: m/z 388.0659. Found: m/z 388.0629 (<1%). Calcd for $[Bi]^+$: m/z 208.9798. Found: m/z 208.9794 (<1%).

5-Bromo-5*H*-dibenzo[*b*,*f*]bismepine (3-Br). A solution of $BiBr_3$ (53.8 mg, 0.12 mmol) and **2** (100 mg, 0.10 mmol) in THF (3 mL) was stirred at 60 °C for 16 h. All volatiles were removed under reduced pressure, and the residue was extracted with toluene (3 × 1.5 mL). The light-yellow solution was layered with *n*-pentane (5 mL) and stored at −30 °C. After 16 h, a colorless solid had precipitated, which was isolated by filtration and dried in vacuo. Yield: 95.0 mg, 0.20 mmol, 68%.

^{1}H NMR (500 MHz, C_6D_6): δ 6.51 (s, 2H, H-7, H-8), 6.94 (ddd, 2H, $^3J_{HH}$ = 7.4 Hz, $^3J_{HH}$ = 7.5 Hz, $^4J_{HH}$ = 1.3 Hz, H-4, H-11), 7.15 (dd, 2H, $^3J_{HH}$ = 7.7 Hz, $^4J_{HH}$ = 1.1 Hz, H-5, H-10), 7.30 (ddd, 2H $^3J_{HH}$ = 7.4 Hz, $^3J_{HH}$ = 7.5 Hz, $^4J_{HH}$ = 1.3 Hz, H-3, H-12), 8.90 (dd, 2H, $^3J_{HH}$ = 7.4 Hz, $^4J_{HH}$ = 1.1 Hz, H-2, H-13).

^{1}H NMR (400 MHz, THF-d_8): δ 6.95 (s, 2H, C_2H_4), 7.24 (ddd, 2H, $^3J_{HH}$ = 7.6 Hz, $^3J_{HH}$ = 7.6 Hz, $^4J_{HH}$ = 1.3 Hz, C_6H_4), 7.49 (dd, 2H, $^3J_{HH}$ = 7.7 Hz, $^4J_{HH}$ = 1.0 Hz, C_6H_4), 7.54 (ddd, 2H, $^3J_{HH}$ = 7.4 Hz, $^3J_{HH}$ = 7.4 Hz, $^4J_{HH}$ = 1.3 Hz, C_6H_4), 8.64 (dd, 2H, $^3J_{HH}$ = 7.6 Hz, $^4J_{HH}$ = 1.1 Hz, C_6H_4).

^{1}H NMR (500 MHz, CD_2Cl_2): δ 7.05 (s, 2H, C_2H_2), 7.33 (ddd, 2H, $^3J_{HH}$ = 7.5 Hz, $^3J_{HH}$ = 7.4 Hz, $^4J_{HH}$ = 1.3 Hz, C_6H_4), 7.52 (d, 2H, $^3J_{HH}$ = 7.7 Hz, C_6H_4), 7.65 (ddd, 2H, $^3J_{HH}$ = 7.5 Hz, $^3J_{HH}$ = 7.5 Hz, $^4J_{HH}$ = 1.3 Hz, C_6H_4).

^{13}C NMR (126 MHz, C_6D_6): δ 127.75 (s, C-4, C-11), 131.48 (s, C-7, C-8), 131.80 (s, C-5, C-10), 133.81 (s, C-3, C-12), 136.24 (s, C-2, C-13), 139.61 (s, C-6, C-9), 166.9 (br, C-1, C-14, detected via ^{13}C and ^{1}H HMBC experiments).

Elem anal. Calcd for $[C_{14}H_{10}BiBr]$ (567.12 g mol^{-1}): C, 36.00; H, 2.12. Found: C, 36.36; H, 2.12.

LIFDI-MS (positive mode). Calcd for $[C_{14}H_9]^+$: m/z 178.0783. Found: m/z 178.0774 (100%). Calcd for $[C_8H_8BiO]^+$: m/z 281.0373. Found: m/z 281.0367 (20%). Calcd for $[C_8H_{16}BiO_2]^+$: m/z 353.0949. Found: m/z 353.0941 (10%). Calcd for $[C_{18}H_{18}BiO]^+$: m/z 459.1156. Found: 459.1147 (10%). Calcd for $[C_{22}H_{26}BiO_2]^+$: m/z 531.1721. Found: m/z = 531.1723 (5%). Calcd for $[Bi]^+$: m/z 208.9798. Found: m/z = 208.9795 (<1%).

5-Iodo-5*H*-dibenzo[*b*,*f*]bismepine (3-I). A solution of BiI_3 (55.7 mg, 0.09 mmol) and **2** (75.0 mg, 0.08 mmol) in THF (2 mL) was stirred at 60 °C for 16 h. All volatiles were removed under reduced pressure, and the residue was extracted with toluene (3 × 0.5 mL). The colorless solution was layered with *n*-pentane (1.5 mL) and stored at −30 °C. After 16 h, a colorless solid had precipitated, which was isolated by filtration and dried in vacuo. Yield: 81.0 mg, 0.20 mmol, 67%.

^{1}H NMR (500 MHz, C_6D_6): δ 6.56 (s, 2H, H-7, H-8), 6.96 (ddd, 2H, $^3J_{HH}$ = 7.4 Hz, $^3J_{HH}$ = 7.6 Hz, $^4J_{HH}$ = 1.3 Hz, H-4, H-11), 7.10 (dd, 2H, $^3J_{HH}$ = 7.3 Hz, $^4J_{HH}$ = 1.3 Hz, H-5, H-10), 7.18 (ddd, 2H, $^3J_{HH}$ = 7.4 Hz, $^3J_{HH}$ = 7.4 Hz, $^4J_{HH}$ = 1.3 Hz, H-3, H-12), 9.19 (dd, 2H, $^3J_{HH}$ = 7.6 Hz, $^4J_{HH}$ = 1.3 Hz, H-2, H-13).

^{1}H NMR (400 MHz, CD_2Cl_2): δ 7.08 (s, 2H, C_2H_2), 7.34 (dd, 2H, $^3J_{HH}$ = 7.2 Hz, $^3J_{HH}$ = 7.2 Hz, C_6H_4), 7.45 (d, 2H, $^3J_{HH}$ = 7.6 Hz, C_6H_4), 7.52 (dd, 2H, $^3J_{HH}$ = 7.7 Hz, $^3J_{HH}$ = 7.7 Hz, C_6H_4), 9.03 (d, 2H, $^3J_{HH}$ = 7.4 Hz, C_6H_4).

^{1}H NMR (400 MHz, THF-d_8): δ 7.01 (s, 2H, C_2H_2), 7.27 (dd, 2H, $^3J_{HH}$ = 7.4 Hz, $^3J_{HH}$ = 7.4 Hz, C_6H_4), 7.45 (m, 4H, C_6H_4), 8.93 (d, 2H, $^3J_{HH}$ = 7.0 Hz, C_6H_4).

^{13}C NMR (126 MHz, C_6D_6): δ 128.59 (s, C-4, C-11), 131.05 (s, C-5, C-10), 132.07 (s, C-7, C-8), 134.26 (s, C-3, C-12), 139.57 (s, C-6, C-9), 140.10 (s, C-2, C-13), 157.08 (br, C-1, C-14, detected via ^{13}C and ^{1}H HMBC experiments).

Elem anal. Calcd for $[C_{14}H_{10}BiI]$ (514.12 g mol^{-1}): C, 32.71; H, 1.96. Found: C, 32.84; H, 1.84.

5*H*-Dibenzo[*b*,*f*]bismepine-5-yl Triflate (3-OTf). A solution of **3-Cl** (35.0 mg, 80.6 μmol) in THF (1 mL) was added to a solution of AgOTf (20.7 mg, 80.6 μmol) in THF (1 mL). The colorless suspension was filtered. The solvent was removed from the filtrate under reduced pressure, and the residue was recrystallized from toluene/*n*-pentane (1 mL, 1 mL) at −30 °C. A colorless solid precipitated after 16 h, was isolated by filtration, and was dried in vacuo. Yield: 39.7 mg, 74.0 μmol, 92%.

^{1}H NMR (500 MHz, THF-d_8): δ 6.72 (s, 2H, H-7, H-8), 7.39 (ddd, 2H, $^3J_{HH}$ = 7.5 Hz, $^3J_{HH}$ = 7.5 Hz, $^4J_{HH}$ = 1.2 Hz, H-4, H-11), 7.67 (ddd, 2H, $^3J_{HH}$ = 7.4 Hz, $^3J_{HH}$ = 7.4 Hz, $^4J_{HH}$ = 1.2 Hz, H-3, H-12), 7.92 (d, 2H, $^3J_{HH}$ = 7.6 Hz, H-5, H-10), 8.30 (d, 2H, $^3J_{HH}$ = 7.5 Hz, H-2, H-13).

^{13}C NMR (126 MHz, THF-d_8): δ 129.41 (s, C-4, C-11), 129,47 (br, CF_3), 130.83 (s, C-3, C-12), 131.42 (s, C-7, C-8), 136.33 (s, C-5, C-10), 136.62 (s, C-2, C-13), 144.98 (s, C-6, C-9), 191.17 (s, C-1, C-14, detected via ^{13}C and ^{1}H HMBC experiments).

^{19}F NMR (470 MHz, THF-d_8): δ −78.93 (s, OTf).

LIFDI-MS (positive mode). Calcd for $[C_4H_8BiO]^+$: m/z 281.0373. Found: m/z 281.0367 (100%). Calcd for $[C_{22}H_{26}BiO_2]^+$: m/z 531.1721. Found: m/z 531.1721 (75%). Calcd for $[C_{18}H_{18}BiO]^+$: m/z 459.1156. Found: m/z 459.1146 (50%). Calcd for $[C_8H_{16}BiO_2]^+$: m/z 353.0949. Found: m/z 353.0941 (40%). Calcd for $[C_{14}H_9]^+$: m/z 178.0783. Found: m/z 178.0774 (35%). Calcd for $[Bi]^+$: m/z 208.9798. Found: m/z 208.9794 (10%). Calcd for $[C_{14}H_{10}Bi]^+$: m/z 387.0581. Found: m/z 387.0566 (<1%).

5*H*-Dibenzo[*b*,*f*]bismepine-5-yl Tetrafluoroborate (3-BF_4). To a solution of **3-Cl** (50 mg, 0.12 mmol) in CH_2Cl_2 (1 mL) was added a suspension of $AgBF_4$ (22.8 mg, 0.12 mmol) in DCM (1 mL). The bright-yellow suspension was immediately filtered. The product crystallized from the filtrate as yellow crystals. After 16 h, the solid was isolated by filtration and dried in vacuo. Yield: 32 mg, 67.5 μmol, 56%.

The solubility of **3-BF_4** in weakly coordinating solvents was insufficient for ^{1}H and ^{13}C NMR spectroscopic investigations.[23]

^{11}B NMR (129 MHz, CD_2Cl_2): δ −0.88 (s, BF_4).

^{19}F NMR (376 MHz, CD_2Cl_2): δ −150.66 (br s, BF_4).

Elem anal. Calcd for $[C_{14}H_{10}BiBF_4]$ (474.02 g mol^{-1}): C, 35.47; H, 2.13. Found: C, 35.32; H, 2.33.

IR (neat): $\tilde{\nu}$ 3041 (w), 3005 (w), 2960 (w), 2923 (w), 2866 (w), 1577 (w), 1550 (w), 1470 (m), 1421 (m), 1293 (m), 1264 (w), 1099 (s), 1058 (s) cm^{-1}.

5*H*-Dibenzo[*b*,*f*]-bis(tetrahydro-1λ^3-furan-1-yl)-bismepine-5-yl Hexafluoroantimonate ([3-thf$_2$][SbF_6]). To a solution of **3-Cl** (100 mg, 0.24 mmol) in THF (1 mL) was added $AgSbF_6$ (81.0 mg, 0.24 mmol). The colorless suspension was filtered. All volatiles were removed from the filtrate to give a colorless solid, which was dried in vacuo. Yield: 150 mg, 0.20 mmol, 83%.

^{1}H NMR (400 MHz, THF-d_8): δ 6.76 (s, 2H, H-7, H-8), 7.48 (ddd, 2H, $^3J_{HH}$ = 7.5 Hz, $^3J_{HH}$ = 7.5 Hz, $^4J_{HH}$ = 1.2 Hz, H-4, H-11), 7.76 (ddd, 2H, $^3J_{HH}$ = 7.4 Hz, $^3J_{HH}$ = 7.4 Hz, $^4J_{HH}$ = 0.9 Hz, H-3, H-12), 8.02 (dd, 2H, $^3J_{HH}$ = 7.8 Hz, $^4J_{HH}$ = 0.9 Hz, H-5, H-10), 8.32 (dd, 2H, $^3J_{HH}$ = 7.5 Hz, $^4J_{HH}$ = 1.1 Hz, H-2, H-13).

^{1}H NMR (400 MHz, CD_2Cl_2): δ 1.80 (s, 8H, β-thf), 3.62 (s, 8H, α-thf), 6.75 (s, 2H, C_2H_2), 7.55 (dd, 2H, $^3J_{HH}$ = 7.6 Hz, $^3J_{HH}$ = 7.6 Hz, C_6H_4), 7.82 (dd, 2H, $^3J_{HH}$ = 7.8 Hz, $^3J_{HH}$ = 7.8 Hz, C_6H_4), 8.07 (d, 2H, $^3J_{HH}$ = 7.9 Hz, C_6H_4), 8.20 (d, 2H, $^3J_{HH}$ = 7.5 Hz, C_6H_4).

^{13}C NMR (126 MHz, CD_2Cl_2): δ 25.66 (s, β-thf), 69.34 (s, α-thf), 130.49 (s, C-4, C-11), 130.72 (s, C-3, C-12), 130.85 (s, C-7, C-8), 135.87 (s, C-2, C-13), 137.30 (s, C-5, C-10), 144.20 (s, C-6, C-9), 190.00 (s, C-1, C-14).

^{13}C NMR (101 MHz, THF-d_8): δ 130.34 (s, C-4, C-11), 130.89 (s, C-3, C-12), 131.50 (s, C-7, C-8), 136.85 (s, C-2, C-13), 137.51 (s, C-5, C-10), 145.32 (s, C-6, C-9), 193.90 (s, C-1, C-14).

DOI: 10.1021/acs.inorgchem.9b03189
Inorg. Chem. 2020, 59, 3367−3376

The ^{1}H and ^{13}C NMR spectra of [**3-thf$_2$**][**SbF$_6$**] in THF-d_8 were obtained from a compound generated in situ from **3-Cl** and $AgSbF_6$ in THF-d_8 (precipitated AgCl was filtered off); therefore, resonances for coordinating THF-d_8 ligands were not detected.

^{19}F NMR (470 MHz, CD_2Cl_2): δ −132.01 (s, SbF_6).

Elem anal. Calcd for $[C_{14}H_{10}BiSbF_6](thf)_2$ (767.18 g mol^{-1}): C, 34.44; H, 3.42. Found: C, 34.53; H, 3.38.

LIFDI-MS (positive mode). Calcd for $[C_{14}H_9]^+$: m/z 178.0783. Found: m/z 178.0776 (100%). Calcd for $[C_8H_{16}BiO_2]^+$: m/z 353.0949. Found: m/z 353.0945 (25%). Calcd for $[C_{22}H_{26}BiO_2]^+$: m/z 531.1721. Found: m/z 531.1731 (15%). Calcd for $[C_{14}H_{11}Bi]^+$: m/z 388.0659. Found: m/z 388.0633 (15%). Calcd for $[C_4H_8BiO]^+$: m/z 281.0373. Found: m/z 281.0369 (10%).

ESI-MS (positive mode). Calcd for $[C_{18}H_{18}BiO]^+$: m/z 459.1156. Found: m/z 459.1147 (100%). Calcd for $[C_{14}H_{10}Bi]^+$: m/z 387.0581. Found: m/z 387.0572 (90%). Calcd for $[Bi]^+$: m/z 208.9798. Found: m/z 208.9795 (60%). Calcd for $[C_4H_8BiO]^+$: m/z 281.0373. Found: m/z 281.0369 (30%). Calcd for $[C_{14}H_{11}Bi]^+$: m/z 388.0659. Found: m/z 388.0605 (20%).

Diphenylbismuthyl Triflate Triethylphosphine Oxide Adduct. This compound was generated in situ. Diphenylbismuth chloride (10 mg, 0.03 mmol) was dissolved in DCM/THF (0.5 mL/0.02 mL), and AgOTf (6.4 mg, 0.03 mmol) was added. The suspension was filtered, and $OPEt_3$ (3.4 mg, 0.03 mmol) was added. The ^{19}F and ^{31}P NMR spectra were measured without isolation of the product.

^{31}P NMR (162 MHz, DCM): δ 69.3 (br, $OPEt_3$).

^{19}F NMR (376 MHz, DCM): δ −78.4 (s, OTf).

General Procedure for the Gutmann−Beckett Method. If not otherwise noted, equimolar amounts of the potential Lewis acid and the Lewis base $OPEt_3$ were dissolved in DCM. One of the following three different methods was used for the determination of accurate ^{31}P NMR chemical shifts: (i) the use of CD_2Cl_2 as the solvent, so that locking and shimming was possible; (ii) the use of CH_2Cl_2 as the solvent along with a capillary containing deuterated acetone, so that locking and shimming was possible; (iii) the use of CH_2Cl_2 as the solvent along with a capillary containing an 85% aqueous solution of H_3PO_4 as a reference. The three methods gave identical results, when applied to identical samples.

■ ASSOCIATED CONTENT

Supporting Information

The Supporting Information is available free of charge at https://pubs.acs.org/doi/10.1021/acs.inorgchem.9b03189.

Additional experimental and theoretical details (PDF)

Coordinates of calculated structures (XYZ)

Accession Codes

CCDC 1961394−1961400, 1961403, 1961404, and 1961408−1961411 contain the supplementary crystallographic data for this paper. These data can be obtained free of charge via www.ccdc.cam.ac.uk/data_request/cif, or by emailing data_request@ccdc.cam.ac.uk, or by contacting The Cambridge Crystallographic Data Centre, 12 Union Road, Cambridge CB2 1EZ, UK; fax: +44 1223 336033.

■ AUTHOR INFORMATION

Corresponding Author

*Email: crispin.lichtenberg@uni-wuerzburg.de.

ORCID

Crispin Lichtenberg: 0000-0002-0176-0939

Notes

The authors declare no competing financial interest.

■ ACKNOWLEDGMENTS

Financial support by the Fonds der Chemischen Industrie (Liebig scholarship to C.L.) and Deutsche Forschungsgemeinschaft is gratefully acknowledged. Experimental contributions by Christine Sternstein are gratefully acknowledged. The authors thank Prof. Holger Braunschweig for continuous support.

■ REFERENCES

(1) Qiu, R.; Yin, S.; Zhang, X.; Xia, J.; Xu, X.; Luo, S. Synthesis and structure of an air-stable cationic organobismuth complex and its use as a highly efficient catalyst for the direct diastereoselective Mannich reaction in water. *Chem. Commun.* **2009**, 4759−4761.

(2) Balasubramaniam, S.; Kumar, S.; Andrews, A. P.; Varghese, B.; Jemmis, E. D.; Venugopal, A. A Dicationic Bismuth(III) Lewis Acid: Catalytic Hydrosilylation of Olefins. *Eur. J. Inorg. Chem.* **2019**, *2019*, 3265−3269.

(3) Lichtenberg, C.; Pan, F.; Spaniol, T. P.; Englert, U.; Okuda, J. The Bis(allyl)bismuth Cation: A Reagent for Direct Allyl Transfer by Lewis Acid Activation and Controlled Radical Polymerization. *Angew. Chem., Int. Ed.* **2012**, *51*, 13011−13015.

(4) Ritschel, B.; Poater, J.; Dengel, H.; Bickelhaupt, F. M.; Lichtenberg, C. Double CH Activation of a Masked Cationic Bismuth Amide. *Angew. Chem., Int. Ed.* **2018**, *57*, 3825−3829.

(5) Ritschel, B.; Lichtenberg, C. Cationic Bismuth Compounds in Organic Synthesis and Catalysis: New Prospects for CH Activation. *Synlett* **2018**, *29*, 2213−2217.

(6) Ramler, J.; Poater, J.; Hirsch, F.; Ritschel, B.; Fischer, I.; Bickelhaupt, F. M.; Lichtenberg, C. Carbon Monoxide Insertion at a Heavy p-Block Element: Unprecedented Formation of a Cationic Bismuth Carbamoyl. *Chem. Sci.* **2019**, *10*, 4169−4176.

(7) Lichtenberg, C. Well-Defined, Mononuclear Bi^{I} and Bi^{II} Compounds: En Route to Transition-Metal-Like Behavior. *Angew. Chem., Int. Ed.* **2016**, *55*, 484−486.

(8) Dengel, H.; Lichtenberg, C. Cationic Bismuth Amides: Accessibility, Structure, and Reactivity. *Chem. - Eur. J.* **2016**, *22*, 18465−18475.

(9) For example, see: (a) Tschersich, C.; Limberg, C.; Roggan, S.; Herwig, C.; Ernsting, N.; Kovalenko, S.; Mebs, S. Gold− and Platinum−Bismuth Donor−Acceptor Interactions Supported by an Ambiphilic PBiP Pincer Ligand. *Angew. Chem., Int. Ed.* **2012**, *51*, 4989−4992. (b) Lin, T.-P.; Ke, I.-S.; Gabbaï, P. σ-Accepting Properties of a Chlorobismuthine Ligand. *Angew. Chem., Int. Ed.* **2012**, *51*, 4985−4988. (c) Tschersich, C.; Hoof, S.; Frank, N.; Herwig, C.; Limberg, C. The Effect of Substituents at Lewis Acidic Bismuth(III) Centers on Its Propensity to Bind a Noble Metal Donor. *Inorg. Chem.* **2016**, *55*, 1837−1842. (d) Schwamm, R.; Fitchett, C. M.; Coles, M. P. Intramolecular Metal···π-Arene Interactions in Neutral and Cationic Main Group Compounds. *Chem. - Asian J.* **2019**, *14*, 1204−1211. (e) Bresien, J.; Hering-Junghans, C.; Schulz, A.; Thomas, M.; Villinger, A. Reactivity of $TerN(SiMe_3)BiCl_2$ − Synthesis of an Aminobismuthenium Cation and $TerN(SiMe_3)Bi(N_3)_2$. *Organometallics* **2018**, *37*, 2571−2580. (f) Bresien, J.; Schulz, A.; Thomas, M.; Villinger, A. A Bismuth-Arene σ-Complex − on the Edge of Menshutkin-type Complexes. *Eur. J. Inorg. Chem.* **2019**, *2019*, 1279−1287. (g) Hanft, A.; Lichtenberg, C. Aminotroponiminates: ligand-centred, reversible redox events under oxidative conditions in sodium and bismuth complexes. *Dalton Trans.* **2018**, *47*, 10578−10589.

(10) (a) Krasowska, M.; Fritzsche, A.-M.; Mehring, M.; Auer, A. A. Balancing Donor − Acceptor and Dispersion Effects in Heavy Main Group Element π Interactions: Effect of Substituents on the Pnictogen···π Arene Interaction. *ChemPhysChem* **2019**, *20*, 2539−2552. (b) Krasowska, M.; Schneider, W. B.; Mehring, M.; Auer, A. A. High-Level Ab Inition Calculations of Intermolecular Interactions: Heavy Main-Group Element π-Interactions. *Chem. - Eur. J.* **2018**, *24*, 10238−10245. (c) Preda, A.-M.; Krasowska, M.; Wrobel, L.; Kitschke, P.; Andrews, P. C.; MacLellan, J. G.; Mertens, L.; Korb,

DOI: 10.1021/acs.inorgchem.9b03189
Inorg. Chem. 2020, 59, 3367−3376

M.; Rüffer, T.; Lang, H.; Auer, A. A.; Mehring, M. Evaluation of dispersion type metal···π arene interaction in arylbismuth compounds − an experimental and theoretical study. *Beilstein J. Org. Chem.* **2018**, *14*, 2125−2145. (d) Frank, W.; Schneider, J.; Müller-Becker, S. The Layer Polymer $\{[Bi(C_6H_6)Cl_3]_2\}_\infty$: Very Weak Bismuth-Arene Bonding in the Parent Compound of the Bismuth Analogue of Menshutkin Complexes. *J. Chem. Soc., Chem. Commun.* **1993**, 799−800. (e) Müller-Becker, S.; Frank, W.; Schneider, J. The Chain Polymers $_\infty[(1,2\text{-}CH_3)_2C_6H_4BiCl_3)_2]$, $_\infty[(1,3\text{-}CH_3)_2C_6H_4BiCl_3)_2]$ and $_\infty[(1,4\text{-}CH_3)_2C_6H_4BiCl_3)_2]$. *Z. Anorg. Allg. Chem.* **1993**, *619*, 1073−1082.

(11) For bimetallic complexes containing triarylbismuth moieties, predominantly Bi → M-type donor acceptor interactions have been reported (M = Cu, Ag, Au): Materne, K.; Hoof, S.; Frank, N.; Herwig, C.; Limberg, C. In Situ Formation of PBiP Ligands upon Complexation of a Mixed Phosphane/Bismuthane with Group 11 Metal Ions. *Organometallics* **2017**, *36*, 4891−4895.

(12) For example, see: (a) Carmalt, C. J.; Norman, N. C.; Orpen, A. G.; Stratford, S. E. A cationic, four-coordinate, ten-electron bismuth(III) complex: synthesis and structure of $[BiPh_2(HMPA)_2][BF_4]$ (HMPA = hexamethylphosphoramide). *J. Organomet. Chem.* **1993**, *460*, C22−C24. (b) Lehmann, M.; Schulz, A.; Villinger, A. Cyclic Distiba- and Dibismadiazenium Cations. *Angew. Chem., Int. Ed.* **2012**, *51*, 8087−8091. (c) Also see refs 3, 8, and 16.

(13) For a dicoordinated cationic bismuth compound, see: Olaru, M.; Duvinage, D.; Lork, E.; Mebs, S.; Beckmann, J. Heavy Carbene Analogues: Donor-Free Bismuthenium and Stibenium Ions. *Angew. Chem., Int. Ed.* **2018**, *57*, 10080−10084.

(14) For example, see: (a) Schwamm, R. J.; Day, B. M.; Coles, M. P.; Fitchett, C. M. Low-Coordinate Bismuth Cations. *Inorg. Chem.* **2014**, *53*, 3778−3787. (b) Veith, M.; Bertsch, B.; Huch, V. The Element-Nitrogen Double Bond in Cations of Cyclic Bis(amino)phospha-, -arsa-, -stiba-, and bismuthines. *Z. Anorg. Allg. Chem.* **1988**, *559*, 73−88. (c) Also see refs 4, 6, 9a, and 9c.

(15) (a) Frank, W.; Weber, J.; Fuchs, E. $[CH_3C_6H_3BiCl_2][AlCl_4]$ and $[(CH_3)_6C_6BiCl_2][AlCl_4]$-Compounds containing η^6-Arene-Complexed $BiCl_2^+$ Units. *Angew. Chem., Int. Ed. Engl.* **1987**, *26*, 74−75. (b) Conrad, E.; Burford, N.; McDonald, R.; Ferguson, M. J. Bismuthenium-pnictonium dications $[R'BiPnR_3]^{2+}$ (Pn = As, Sb) containing carbenoid bismuth centers and rare Bi−Sb bonds. *Chem. Commun.* **2010**, *46*, 4598−4600. (c) Schwamm, R. J.; Coles, M. P.; Fitchett, C. M. Neutral and cationic bismuth compounds supported by bis(amidodimoethyl)disiloxane ligands. *Dalton Trans.* **2017**, *46*, 4066−4074.

(16) Hering-Junghans, C.; Thomas, M.; Villinger, A.; Schulz, A. Synthesis of Elusive Chloropnictenium Ions. *Chem. - Eur. J.* **2015**, *21*, 6713−6717.

(17) Ishii, T.; Suzuki, K.; Nakamura, T.; Yamashita, M. An Isolable Bismabenzene: Synthesis, Structure, and Reactivity. *J. Am. Chem. Soc.* **2016**, *138*, 12787−12790.

(18) (a) Yasuike, S.; Ohta, H.; Shiratori, S.; Kurita, J.; Tsuchiya, T. Syntheses of the Group 15 1-Benzoheteroepines, Dibenzo[b,d]-heteroepines and Dibenzo[b,f]heteroepines involving the First Isolated Example of Arsepines and Bismepines. *J. Chem. Soc., Chem. Commun.* **1993**, 1817−1819. (b) Yasuike, S.; Kiharada, T.; Kurita, J.; Tsuchiya, T. A versatile synthesis of the group 15 and 16 3-benzoheteroepines involving the first isolated examples of several C-unsubstituted 3-benzoheteropines. *Chem. Commun.* **1996**, 2183−2184. (c) Yasuike, S.; Nakashima, F.; Kurita, J.; Tsuchiya, T. Syntheses of Novel Dithieno[2,3-b; 3′,2′-f]- and Dithieno[3,4-b; 3′,4′f]Heteroepines Containing Group 14, 15 and 16 Heavier Elements. *Heterocycles* **1997**, *45*, 1899−1902.

(19) Quillian, B.; Wang, Y.; Wei, P.; Wannere, C. S.; Schleyer, P. v. R.; Robinson, G. H. Neutral Gallium Analogues of the Tropylium Ion: Synthesis Structure and Aromaticity. *J. Am. Chem. Soc.* **2007**, *129*, 13380−13381.

(20) Attempts to directly synthesize **3-X** from **1** and BiX_3 were unsuccessful because of the formation of **2** as a side product (X = Cl, Br, I).

(21) The beginning of decomposition was detected at higher temperatures.

(22) Bismuth-bound thf ligands in $[\mathbf{3\text{-}thf_2}][\mathbf{SbF_6}]$ and free THF molecules exchange rapidly in solution, as indicated by NMR spectroscopic experiments.

(23) $\mathbf{3\text{-}BF_4}$ was poorly soluble in weakly coordinating solvents such as benzene, dichloromethane, or difluorobenzene. NMR spectroscopic analysis in donor solvents such as THF-d_8 indicated first signs of decomposition, even when the samples were analyzed immediately after solvation. This explains the relatively low yield of $\mathbf{3\text{-}BF_4}$ (compared to **3-OTf**, for instance) and precluded a solution NMR spectroscopic analysis of $\mathbf{3\text{-}BF_4}$ (only ^{11}B and ^{19}F NMR spectroscopic data in CD_2Cl_2 could be acquired with sufficient signal intensities).

(24) For example, see: (a) Bučinský, L.; Jayatilaka, D.; Grabowsky, S. Importance of Relativistic Effects and Electron Correlation Factors and Electron Density of Diphenyl Mercury and Triphenyl Bismuth. *J. Phys. Chem. A* **2016**, *120*, 6650−6669. (b) Jones, P. G.; Blaschette, A.; Henschel, D.; Weitze, A. Redetermination of the crystal structure of triphenylbismuth, $(C_6H_5)_3Bi$. *Z. Kristallogr.* **1995**, *210*, 377−378. (c) Hawley, D. M.; Ferguson, G. The Stereochemistry of Some Organic Derivatives of Group V_B Elements. The Crystal and Molecular Structure of Triphenylbismuth. *J. Chem. Soc. A* **1968**, 2059−2063.

(25) A polymorph of **3-Cl** was obtained (compound **3-Cl′**), which shows intermolecular Bi···Cl interactions that do not involve σ^*(Bi−Cl) orbitals (see the Supporting Information).

(26) (a) Hillwig, R.; Kunkel, F.; Harms, K.; Neumüller, B.; Dehnicke, K. Die Kristallstrukutren von Trimethylbleiiodid und Diphenylbismutchlorid. *Z. Naturforsch., B: J. Chem. Sci.* **1997**, *52*, 149−152. (b) Ebert, K. H.; Schulz, R. E.; Breunig, H. J.; Silvestru, C.; Haiduc, I. Syntheses and structures of dimesitylbismuth(III) bromide, Mes_2BiBr and bis(diphenyldithiophosphinato)mesitylbismuth(III), $MesBi(S_2PPh_2)_2$. *J. Organomet. Chem.* **1994**, *470*, 93−98. (c) James, S. C.; Norman, N. C.; Orpen, A. G. Pyridine adducts of arylbismuth(III) halides. *J. Chem. Soc., Dalton Trans.* **1999**, 2837−2843.

(27) $Bi(2,4,6\text{-}(CF_3)_3C_6H_3)_2Cl$ is an example of a sterically crowded diarylbismuth chloride without intermolecular Bi···Cl interactions in the solid state: Whitmire, K. H.; Labahn, D.; Roesky, H. W.; Noltemeyer, M.; Sheldrick, G. M. Sterically crowded aryl bismuth compounds: synthesis and characterization of bis{2,4,6-tris-(trifluoromethyl)phenyl}bismuth chloride and tris{2,4,6-tirs-(trifluoromethyl)phenyl}bismuth. *J. Organomet. Chem.* **1991**, *402*, 55−66.

(28) Mantina, M.; Chamberlin, A. C.; Valero, R.; Cramer, C. J.; Truhlar, D. G. Consistent van der Waals Radii for the Whole Main Group. *J. Phys. Chem. A* **2009**, *113*, 5806−5812.

(29) Beckmann, J.; Bolsinger, J.; Duthie, A.; Finke, P.; Lork, E.; Lüdtke, C.; Mallow, O.; Mebs, S. Mesityltellurenyl Cations Stabilized by Triphenylpnictogens $[MesTe(EPh_3)]^+$ (E = P, As, Sb). *Inorg. Chem.* **2012**, *51*, 12395−12406.

(30) Ionic interactions are expected to play an important role in Bi··· triflate bonding. The fact that the bismuth atom in **3-OTf** adopts a bisphenoidal coordination geometry (with triflate anions in the axial positions) suggests that covalent contributions are nonnegligible in this case.

(31) Single crystals of a species with an additional, weakly bound thf ligand, $[\mathbf{3\text{-}thf_3}][\mathbf{SbF_6}]$, were also obtained (for details, see the Supporting Information).

(32) Carmalt, C. J.; Farrugia, L. J.; Norman, N. C. Cationic, arylbismuth(III) complexes of the form $[BiR_2L_2]^+$ and $[BiR_2L_2]^{2+}$ where L is a neutral two-electron donor ligand. *J. Chem. Soc., Dalton Trans.* **1996**, 443−454.

(33) Lichtenberg, C.; Okuda, J. Structurally Defined Allyl Compounds of Main Group Metals: Coordination and Reactivity. *Angew. Chem., Int. Ed.* **2013**, *52*, 5228−5246.

(34) It should be noted that a significant degree of aromaticity may also be observed in nonplanar molecules, e.g.: (a) Antić, M.; Furtula, B.; Radenković, S. Aromaticity of Nonplanar Fully Benzeoid

DOI: 10.1021/acs.inorgchem.9b03189
Inorg. Chem. 2020, 59, 3367−3376

Hydrocarbons. *J. Phys. Chem. A* **2017**, *121*, 3616−3626. (b) Zhang, B.; Manning, G. P.; Dobrowolski, M. A.; Cyrański, M. K.; Bodwell, G. J. Nonplanar Aromatic Compounds. 9. Synthesis, Structure, and Aromaticity of 1:2,13:14-Dibenzo[2]paracyclo[2](2,7)-pyrenophane-1,13-diene. *Org. Lett.* **2008**, *10*, 273−276.

(35) Energy value corresponds to free reaction enthalpy ΔG.

(36) All attempts to obtain a minimum structure of $[\mathbf{3}]^+$ with a nonplanar geometry from geometry optimization were unsuccessful. The structure of $[\mathbf{3}]^+$**-bent** was obtained by a single-point calculation with the atomic coordinates of the bismepine core taken from the experimentally determined structure of $[\mathbf{3\text{-}thf_2}][\mathbf{SbF_6}]$.

(37) NBO analysis revealed polar Bi−C bonds in $[\mathbf{3}]^+$**-planar** with 72% and 28% contributions from carbon and bismuth atomic orbitals, respectively. Judging from these values, the degree of bond polarization in $[\mathbf{3}]^+$**-planar** is significantly smaller than that in lanthanoid and actinoid carbene complexes with σ and π contributions to M−C bonding (74−90% contributions from carbon atomic orbitals): Wu, Q.-Y.; Cheng, Z.-P.; Lan, J.-H.; Wang, C.-Z.; Chai, Z.-F.; Gibson, J. K.; Shi, W.-Q. Insight into the nature of M-C bonding in the lanthanide/actinide-biscarbene complexes: a theoretical perspective. *Dalton Trans.* **2018**, *47*, 12718−12725.

(38) (a) Ollevier, T. Bismuth-Mediated Organic Reactions. *Top. Curr. Chem.* **2012**, *311*, 1−270. (b) Hua, R. Recent Advances in Busmuth-Catalyszed Organic Synthesis. *Curr. Org. Synth.* **2008**, *5*, 1−27. (c) Ollevier, T. New trends in bismuth-catalyzed synthetic transformations. *Org. Biomol. Chem.* **2013**, *11*, 2740−2755. (d) Bothwell, J. M.; Krabbe, S. W.; Mohan, R. S. Applications of bismuth(III) compounds in organic synthesis. *Chem. Soc. Rev.* **2011**, *40*, 4649−4707.

(39) Kannan, R.; Kumar, S.; Andrews, A. P.; Jemmis, E. D.; Venugopal, A. Consequence of Ligand Bite Angle on Bismuth Lewis Acidity. *Inorg. Chem.* **2017**, *56*, 9391−9395.

(40) (a) Mayer, U.; Gutmann, V.; Gerger, W. The Acceptor Number − A Quantitative Empirical Parameter for the Electrophilic Properties of Solvents. *Monatsh. Chem.* **1975**, *106*, 1235−1257. (b) Beckett, M. A.; Strickland, G. C.; Holland, J. R.; Sukumar Varma, K. A convenient n.m.r. method for the measurement of Lewis acidity at boron centres: correlation of reaction rates of Lewis acid initiated epoxide polymerizations with Lewis acidity. *Polymer* **1996**, *37*, 4629−4631.

(41) Lack of efficient Lewis pair formation between $OPEt_3$ and the Lewis acid under investigation has been reported as a (potential) limitation of this method: Ashley, A. E.; Herrington, T. J.; Wildgoose, G. G.; Zaher, H.; Thompson, A. L.; Rees, N. H.; Krämer, T.; O'Hare, D. Separating Electrophilicity and Lewis Acidity: The Synthesis, Characterization, and Electrochemistry of the Electron Deficient Tris(aryl)boranes $B(C_6F_5)_{3-n}(C_6Cl_5)_n$ (n = 1−3). *J. Am. Chem. Soc.* **2011**, *133*, 13727−14740. (b) Chitnis, S. S.; Robertson, A. P. M.; Burford, N.; Patrick, B. O.; McDonald, R.; Ferguson, M. J. Bipyridine, complexes of E^{3+} (E = P, As, Sb, Bi): strong Lewis acids, sources of $E(OTf)_3$ and synthons for E^{I} and E^{V} cations. *Chem. Sci.* **2015**, *6*, 6545−6555.

(42) For examples of limitations of NMR-based methods for evaluation of the Lewis acidity, see: Gilhula, J. C.; Radosevich, A. T. Tetragonal phosphorus(v) cations as tunable and robust catalytic Lewis acids. *Chem. Sci.* **2019**, *10*, 7177−7182. and references cited therein.

(43) ANs of 52.9, 77.5, and 105.2 have previously been determined for BPh_3, $B(C_6F_5)_3$, and BBr_3, respectively, in $CDCl_3$: Soltani, Y.; Adams, S. J.; Börger, J.; Wilkins, L. C.; Newman, P. D.; Pope, S. J. A.; Melen, R. L. Charge Transfer Fluorescence in Imine Borane Adducts Towards a Vapochromic Litmus Test. *Dalton Trans.* **2018**, *47*, 12656−12660.

(44) Under slightly different experimental conditions (Et_2O as the solvent, excess of the Lewis acid), an AN of 87 has been determined for $AlCl_3$: Beckett, M. A.; Brassington, D. S.; Coles, S. J.; Hursthouse, M. B. Lewis acidity of tris(pentafluorophenyl)borane: crystal and molecular structure of $B(C_6F_5)_3{\cdot}OPEt_3$. *Inorg. Chem. Commun.* **2000**, *3*, 530−533.

(45) Calculated from a ^{31}P NMR chemical shift of 74.8 ppm reported for a solution of the bismuth dication with 0.25 equiv of $OPEt_3$ in 1,2-Cl_2-C_6D_4: see ref 2.

(46) For the full reference, see the Supporting Information.

(47) Hariharan, P. C.; Pople, J. A. The influence of polarization functions on molecular orbital hydrogenation energies. *Theor. Chim. Acta* **1973**, *28*, 213−222.

(48) (a) Dunning, T. H., Jr.; Hay, P. J. In *Modern Theoretical Chemistry*; Schaefer, H. F., III, Ed.; Plenum: New York, 1977; Vol. 3, pp 1−28. (b) Hay, P. J.; Wadt, W. R. Ab initio effective core potentials for molecular calculations. Potentials for the transition metal atoms Sc to Hg. *J. Chem. Phys.* **1985**, *82*, 270−283. (c) Hay, P. J.; Wadt, W. R. Ab initio effective core potentials for molecular calculations. Potentials for K to Au including the outermost core orbitals. *J. Chem. Phys.* **1985**, *82*, 299−310.

(49) Becke, A. D. Density-functional thermochemistry. III. The role of exact exchange. *J. Chem. Phys.* **1993**, *98*, 5648−5652.

(50) Grimme, S.; Antony, J.; Ehrlich, S.; Krieg, H. A consistent and accurate ab initio parametrization of density functional dispersion correction (DFT-D) for the 94 elements H-Pu. *J. Chem. Phys.* **2010**, *132*, 154104−154119.

(51) Mills, I.; Cvitaš, T.; Homann, K.; Kallay, N.; Kuchitsu, K. *Quantities, Units and Symbols in Physical Chemistry*, 2nd ed.; Blackwell Science, 1993; pp 51−53.

(52) Glendening, E. D.; Badenhoop, J. K.; Reed, A. E.; Carpenter, J. E.; Bohmann, J. A.; Morales, C. M.; Karafiloglou, P.; Landis, C. R.; Weinhold, F. *NBO 7*; Theoretical Chemistry Institute, University of Wisconsin: Madison, WI, 2018.

DOI: 10.1021/acs.inorgchem.9b03189
Inorg. Chem. 2020, 59, 3367−3376

VII Molecular Bismuth Cations: Assessment of Soft Lewis Acidity

This chapter was published in: Jacqueline Ramler, Crispin Lichtenberg, *Chem. Eur. J.* **2020**, *26*, 10250–10258. Reprinted from ref. 137 with permission from 2020 WILEY-VCH Verlag GmbH.

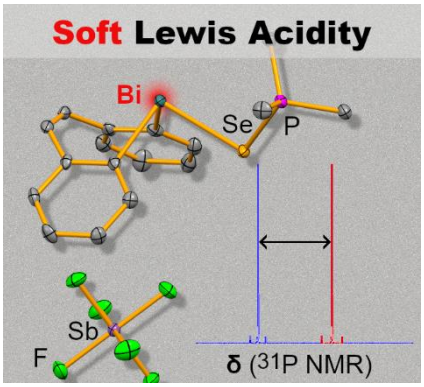

Chemistry–A European Journal | Full Paper
doi.org/10.1002/chem.202001674

Lewis Acids | *Very Important Paper*

VIP Molecular Bismuth Cations: Assessment of Soft Lewis Acidity

Jacqueline Ramler and Crispin Lichtenberg*[a]

Abstract: Three-coordinate cationic bismuth compounds [Bi(diaryl)($EPMe_3$)][SbF_6] have been isolated and fully characterized (diaryl = $[(C_6H_4)_2C_2H_2]^{2-}$, E = S, Se). They represent rare examples of molecular complexes with Bi···EPR_3 interactions (R = monoanionic substituent). The ^{31}P NMR chemical shift of $EPMe_3$ has been found to be sensitive to the formation of LA···$EPMe_3$ Lewis acid/base interactions (LA = Lewis acid). This corresponds to a modification of the Gutmann–Beckett method and reveals information about the hardness/softness of the Lewis acid under investigation. A series of organobismuth compounds, bismuth halides, and cationic bismuth species have been investigated with this approach and compared to traditional group 13 and cationic group 14 Lewis acids. Especially cationic bismuth species have been shown to be potent soft Lewis acids that may prefer Lewis pair formation with a soft (S/Se-based) rather than a hard (O/N-based) donor. Analytical techniques applied in this work include (heteronuclear) NMR spectroscopy, single-crystal X-ray diffraction analysis, and DFT calculations.

Introduction

Bismuth(III) compounds are frequently applied as Lewis acids in stoichiometric and catalytic organic and organometallic transformations.[1] Various types of reactions have been realized with this strategy. The long (and non-exhaustive) list of examples includes pericyclic reactions (such as Diels–Alder reactions),[1b,2] addition reactions (such as hydroamination, hydrosilylation, and carbo/amino-bismuthation),[1a–c,3] addition-elimination sequences (such as aldol and Mannich reactions),[1a–c,4] electrophilic aromatic substitution reactions (such as Friedel Crafts alkylations and acylations),[1a–c,2b,5] S_Ni type reactions (such as dehydro-halogenation reactions),[1c,6] CH activation (such as the metalation of $(C_5H_5)^-$, $(C_5H_4Me)^-$, $(NAr_2)^-$),[7] and small-molecule activation (such as carbon monoxide insertion).[8] The utilization of bismuth Lewis acids can lead to selectivities and activities that are difficult or impossible to obtain with other reagents.[1b,2a,3a,9] In other cases bismuth compounds show advantages in terms of affordability, stability towards air and moisture, or functional group tolerance.[1,7d,e] In addition, prospects for catalyst recyclability have been demonstrated.[4b,10]

While the abovementioned applications make use of Lewis acid/base interactions between bismuth compounds and organic substrates, the coordination of metal-centered Lewis bases to Lewis acidic bismuth components has also been reported. This has been exploited for the design of bismuth-containing Z-type (donor/acceptor) ligands, in which the bismuth atom is responsible for the electron-accepting character of the overall ligand.[11]

We have recently suggested a scheme for the classification of bismuth Lewis acids.[12] Distinctions are made between three types of compounds: class A) R_2Bi-X with an electronegative ligand X; class B) R_2Bi···X′ with ligands X′ such as $(O_3SCF_3)^-$ or $(AlCl_4)^-$, which lead to a weak Bi···X′ interaction; and class C) cationic species $[R_2Bi(L)_n][WCA]$ without any directional bonding interactions between bismuth and the weakly coordinating counteranion (WCA), for which $[SbF_6]^-$ or $[B(C_6F_5)_4]^-$ are typical examples. While σ*(Bi-X/X′)-orbitals are responsible for the Lewis acidic character of class A and B compounds, an empty bismuth-centered p-orbital will accept electron density from Lewis basic bonding partners in the case of class C complexes. For all three classes of bismuth Lewis acids, the orbitals involved in the formation of interactions with Lewis bases are large and diffuse, which is why they may be expected to be soft Lewis acids. This is supported by the fact that interactions with typical soft Lewis bases such as arene moieties, stibanes, and telluroethers have been reported.[13–17] It can be anticipated that the expectedly soft character of bismuth-based Lewis acidity is integral to some of the observed properties and reactivity patterns of bismuth species. Examples include their relatively high tolerance towards (hard) oxygen-based functional groups and their ability to efficiently coordinate and activate (soft) arene and olefin donor groups.[1,3–5,7d,e,13–15]

In contrast to the frequent application of bismuth Lewis acids in synthesis and catalysis, efforts to quantify bismuth-

[a] J. Ramler, Priv.-Doz. Dr. C. Lichtenberg
Institute of Inorganic Chemistry, Julius-Maximilians-University Würzburg
Am Hubland, 97074 Würzburg (Germany)
E-mail: crispin.lichtenberg@uni-wuerzburg.de
Supporting information and the ORCID identification number(s) for the author(s) of this article can be found under: https://doi.org/10.1002/chem.202001674.

Chemistry–A European Journal | Full Paper doi.org/10.1002/chem.202001674 | Chemistry Europe European Chemical Societies Publishing

based Lewis acidity have only scarcely been reported.[3b,12,18] More specifically, there are no detailed studies available that deal with the quantification of the hard or soft character of bismuth Lewis acids.

Here we report Lewis acid/base pair formation between well-defined bismuth compounds and soft Lewis bases $EPMe_3$ (E = S, Se) and suggest an operationally simple method to establish trends in the softness of Lewis acidity.

Results and Discussion

Cationic bismuth compounds show an enhanced Lewis acidity when compared with their neutral parent compounds. Cationic diaryl bismuth compounds are the most prominent subgroup of this family of compounds. They usually bind two equivalents of a Lewis base through their empty bismuth-centered 6p-orbital. We aimed at diaryl bismuth cations that preferentially bind one equivalent of a donor in order to allow direct comparison with archetypical examples of Lewis acids based on group 13 elements. Recently reported cationic bismepines such as compound **1** appeared to be promising candidates, because the olefin bridge in the ligand backbone reduces the flexibility of the aryl groups and provides moderate steric shielding of the bismuth center (Scheme 1).[12] While two equivalents of Lewis bases with a low steric profile (such as thf) interact with the bismuth atom in **1**, sterically more demanding Lewis bases should make the generation of Lewis acid/base adducts with a 1:1 stoichiometry possible. In order to test for the potential of the Lewis acidic bismuth center in **1** to bind soft donors by substitution of the hard thf ligands, compound **1** was reacted with one equivalent of the phosphane chalcogenides $EPMe_3$ (E = S, Se; Scheme 1). Indeed, compounds **2-SPMe$_3$** and **2-SePMe$_3$** could be isolated in excellent yields of 87–91% as pale yellow solids. Adducts of bismuth compounds and phosphane sulfides or selenides are extremely rare: compounds $[Bi(SC_6F_5)_3(SPPh_3)]$ and $[BiX_3(SeP(4\text{-}F\text{-}C_6H_4)_3)]$ (X = Cl, Br) have been reported.[19] NMR spectroscopic data is not available for the former compound and only ^{31}P NMR chemical shifts (without $^1J_{PSe}$ coupling constants) are given for the latter two species, indicating a minor up-field shift of up to 3.7 ppm with respect to the free phosphane selenide, $SeP(4\text{-}F\text{-}C_6H_4)_3$.[20] For compounds **2-SPMe$_3$** and **2-SePMe$_3$**, the ^1H NMR spectra display resonances typical of a benzo group, plus a singlet in the olefinic region and a doublet for the methyl groups bound to phosphorus. In ^{13}C NMR spectra, the resonances of the *ipso*-carbon atoms (**2-SPMe$_3$**: 176.9 ppm; **2-SePMe$_3$**: 162.9 ppm) are significantly up-field-shifted compared to **1** (δ = 193.9 ppm) and close to those of the corresponding chlorobismepine $Bi((C_6H_4)_2C_2H_2)Cl$ (δ = 172.9 ppm),[12] suggesting considerable Bi···S/Se bonding interactions in solution. This is further supported by large down-field shifts of the ^{31}P and ^{77}Se NMR spectroscopic resonances of these compounds when compared to the free phosphane chalcogenides (^{31}P NMR: **2-SPMe$_3$**: 44.2 ppm; **2-SePMe$_3$**: 21.1 ppm; $SPMe_3$: 29.2 ppm; $SePMe_3$: 7.8 ppm; ^{77}Se NMR: **2-SePMe$_3$**: −44.2 ppm; $SePMe_3$: −234.9 ppm).[21] A significant decrease of the $^1J_{PSe}$ coupling constant from 689 Hz in free $SePMe_3$[21] to 488 Hz in the bismuth complex **2-SePMe$_3$** indicates weakening of the P–Se bond[22,23] and is—to the best of our knowledge—the largest decrease reported for metal complexes of $SePMe_3$.[24,25]

Single-crystal X-ray analyses were carried out for compounds **2-SPMe$_3$** and **2-SePMe$_3$**, revealing an isostructural relationship (monoclinic space group $P2_1/c$ with Z = 4 in both cases; Figure 1). The complexes crystallize as separated ion pairs (i.e., without strong directional bonding interactions between cation and anion). The bismepine ligands adopt bent conformations with angles of 88.7° and 76.5° between the mean planes of the benzo groups, as recently reported for bismepines with three-coordinate bismuth atoms.[12] The bismuth atoms are found in pyramidal coordination geometries with bond angles around Bi1 ranging from 85.1–90.6° and 87.8–92.1° for **2-SPMe$_3$** and **2-SePMe$_3$**, respectively. A coordination number of three is extremely unusual for diorganobismuth cations, which commonly adopt coordination numbers of four with the empty 6p-orbital of bismuth being involved in bonding interactions with two ligands.[3d,4,10,12,18,26–28] The Bi1–S1/Se1

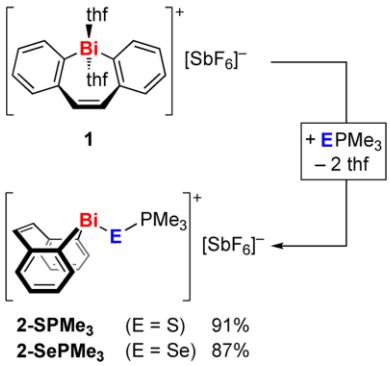

Scheme 1. Reaction of cationic bismepine **1** with soft donors $EPMe_3$ to give compounds **2-EPMe$_3$** through thf elimination (E = S, Se).

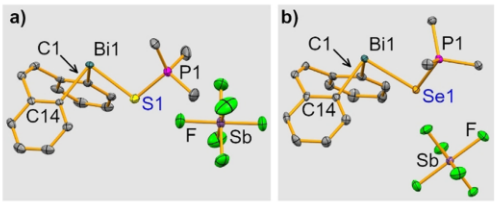

Figure 1. Molecular structures of $[Bi(C_6H_4)_2C_2H_2(EPMe_3)][SbF_6]$ in the solid state: a) E = S: **2-SPMe$_3$**; b) E = Se: **2-SePMe$_3$**). Displacement ellipsoids are drawn at the 50% probability level. Hydrogen atoms and a lattice-bound CH_2Cl_2 molecule in the structure of **2-SPMe$_3$** are omitted for clarity. Selected bond lengths (Å) and bond angles (°): **2-SPMe$_3$**: Bi1–C1, 2.248(6); Bi1–C14, 2.246(5); Bi1–S1, 2.6105(16); P1–S1, 2.026(2); C1–Bi1–C14, 85.1(2); C1–Bi1–S1, 90.59(15); C14–Bi1–S1, 88.81(14); Bi1–S1–P1, 106.12(8). **2-SePMe$_3$**: Bi1–C1, 2.237(4); Bi1–C14, 2.240(4); Bi1–Se1, 2.7222(4); P1–Se1, 2.1889(11); C1–Bi1–C14, 87.77(13); C1–Bi1–Se1, 91.24(10); C14–Bi1–Se1, 92.08(10); Bi1–Se1–P1, 100.31(3).

Chemistry–A European Journal | Full Paper doi.org/10.1002/chem.202001674 | Chemistry Europe European Chemical Societies Publishing

bond length of 2.61 Å and 2.72 Å are 31–33% below the sum of the van der Waals radii (S, 1.80 Å; Se, 1.90 Å; Bi, 2.07 Å).[29] They are much shorter than the corresponding bonds in the literature-known adducts $[Bi(SC_6F_5)_3(SPPh_3)]$ (Bi-SPPh$_3$, 3.01 Å) and $[BiX_3(SeP(4\text{-}F\text{-}C_6H_4)_3)]$ (X = Cl, Br; Bi-Se, 3.35–3.37 Å).[19] In fact, they are in the range of values reported for regular covalent Bi–S/Se bonds in compounds of type Bi(aryl)$_2$(EPh) (E = S: 2.54–2.63 Å; E = Se: 2.70–2.73 Å).[30–32] In agreement with these findings, the P1–S1/Se1 bonds in **2-SPMe$_3$** (2.03 Å) and **2-SePMe$_3$** (2.19 Å) are significantly elongated as compared to those in SPMe$_3$ (1.97 Å, Supporting Information) and SePMe$_3$ (2.12 Å, Supporting Information).[33] This effect is more pronounced in **2-SPMe$_3$** than in literature-known metal complexes with terminal SPMe$_3$ ligands that have been crystallographically characterized (M = Cr, Fe, Cu, In);[34] **2-SePMe$_3$** is the first complex of the SePMe$_3$ ligand that has been crystallographically characterized so that no direct comparison is possible.

The spectroscopic and structural analyses of **2-EPMe$_3$** revealed considerable bonding interactions between the Lewis acidic bismuth atoms in these compounds and the soft Lewis bases EPMe$_3$ (E = S, Se). With its large, diffuse, and polarizable atomic orbitals, bismuth can indeed be expected to generate a soft Lewis acidity in its molecular complexes. Differences in the hardness/softness of Lewis acids have previously been discussed for small series of compounds such as $B(C_6F_5)_n(OC_6F_5)_{3-n}$ (n = 0–3), where the choice of the method for quantification can strongly affect the outcome of the measurement (e.g., OPEt$_3$ as a donor in the Gutmann–Beckett (GB)[35–37] method vs. crotonaldehyde as a donor in Childs[38] method).[39] To the best of our knowledge, however, attempts to assess the softness of a broader range of bismuth Lewis acids have not been reported to date. We suggest here a modification of the GB method in order to compare the softness of Lewis acids in an operationally simple approach. In the original GB method, a sample containing OPEt$_3$ and a (potential) Lewis acid is analyzed by ^{31}P NMR spectroscopy. An acceptor number (AN) can be calculated according to Equation (1):

$$\mathrm{AN}\ (\mathrm{OPEt_3}) = 2.21 \times (\delta(^{31}\mathrm{P\,NMR})_{\mathrm{Sample}}/\mathrm{ppm} - 41.0) \quad (1)$$

where AN = 0 corresponds to OPEt$_3$ in hexane and AN = 100 corresponds to OPEt$_3$·SbCl$_5$ in dichloroethane.[35a] We have exchanged the hard, oxygen-based donor in the original GB method for the softer donors SPMe$_3$ and SePMe$_3$.[40] In analogy with the original GB method, acceptor numbers AN (SPMe$_3$) and AN (SePMe$_3$) may be determined according to Equations (2) and (3):

$$\mathrm{AN}\ (\mathrm{SPMe_3}) = 6.41 \times (\delta(^{31}\mathrm{P\,NMR})_{\mathrm{Sample}}/\mathrm{ppm} - 29.2) \quad (2)$$

$$\mathrm{AN}\ (\mathrm{SePMe_3}) = 5.71 \times (\delta(^{31}\mathrm{P\,NMR})_{\mathrm{Sample}}/\mathrm{ppm} - 7.8) \quad (3)$$

where AN = 0 corresponds to EPMe$_3$ in CH_2Cl_2 and AN = 100 corresponds to EPMe$_3$ with one equiv GaI$_3$ in CH_2Cl_2 (E = S, Se). GaI$_3$ was chosen as a reference point out of a range of potential candidates, because it is a simple, readily available, strong and soft Lewis acid that reacts with EPMe$_3$ in simple and predictable Lewis pair formations in a 1:1 ratio ($SbCl_5$, SbF_5, and Bi(OTf)$_3$, for instance, had to be ruled out due to side reactions; see Supporting Information).

With SPMe$_3$ as a Lewis base, aryl bismuth compounds and halobismepines showed no or only minor interactions according to acceptor numbers of AN (SPMe$_3$) = 0–12 (Table 1, entries 2–6). BiCl$_3$, BiBr$_3$, and BiI$_3$ showed moderate to minor interactions with AN (SPMe$_3$) = 26, 17, and 13, respectively (entries 7–9). For compounds of type BiR$_2$X and BiX$_3$, the acceptor numbers increase with increasing electronegativity of the halide X. Stronger interactions were detected for the bismepine triflate Bi(diaryl)(OTf) (**3**) and Bi(OTf)$_3$ (AN (SPMe$_3$) = 44–52; entries 10, 11; diaryl = $[(C_6H_4)_2C_2H_2]^{2-}$).[41] Very high acceptor numbers of AN (SPMe$_3$) = 85–96 were obtained for the bismepine cation **1**, its corresponding SPMe$_3$ adduct **2-SPMe$_3$**, and the diphenyl bismuth cation $[BiPh_2(thf)_2][SbF_6]$ (**4**), all of which bear $[SbF_6]^-$ counteranions (entries 12–14). The slightly lower acceptor number of **4** is ascribed to the freely accessible bismuth-centered empty 6p-orbital in the complex fragment $[BiPh_2]^+$, which allows binding of two equivalents of a Lewis base[42] rather than only one as in **2-SPMe$_3$**. This is further supported by a single-crystal X-ray analysis of $[BiPh_2(SPMe_3)_2][SbF_6]$, obtained from reaction of **4** with one equiv SPMe$_3$ (Supporting Information).

Table 1. Investigations of potential Lewis acids with the modified Gutmann–Beckett method, using SPMe$_3$ as a donor.

Entry	Compound	δ ^{31}P [ppm][a]	AN (SPMe$_3$)[b]
1	SPMe$_3$	29.2	0 (by definition)
2	BiPh$_3$	30.2	6
3	Bi$_2$(diaryl)$_3$[a]	29.2	0
4	Bi(diaryl)Cl[a]	31.0	12
5	Bi(diaryl)Br[a]	30.3	7
6	Bi(diaryl)I[a]	29.2	0
7	BiCl$_3$	33.2	26
8	BiBr$_3$	31.8	17
9	BiI$_3$	31.2	13
10	Bi(OTf)$_3$	37.3	52
11	Bi(diaryl)(OTf) (3)[c,d]	36.1	44
12	**1**	**44.0**	**95**
13	**2-SPMe$_3$**	**44.2**[e]	**96**
14	$[BiPh_2(thf)_2][SbF_6]$ (4)	42.5	85
15	Me$_3$SiOTf	29.3	1
16	B(C$_6$F$_5$)$_3$	35.8	42
17	AlCl$_3$	41.3	78
18	GaI$_3$	44.8	100 (by definition)
19	B(C$_6$F$_5$)$_3$(thf)	29.4	1
20	AlCl$_3$(thf)	29.7	3
21	GaI$_3$(thf)	43.4	91
22	GaI$_3$(py)[f]	30.2	6
23	2-SPMe$_3$ + py[f]	40.8	74
24	2-SPMe$_3$ + 2 py[f]	35.8	42

[a] If not otherwise noted, CD_2Cl_2 solutions of equimolar amounts of the potential Lewis acid and SPMe$_3$ were investigated at 23 °C (for details see experimental part). [b] determined according to equation 2 (see text). [c] diaryl = $[(C_6H_4)_2C_2H_2]^{2-}$ as in compound **1**; that is, $[Bi(diaryl)]^+$ corresponds to a cationic dibenzobismepine complex fragment.[12] [d] small amounts of THF were added to fully solubilize **3** (CD_2Cl_2/THF = 25:1, v/v). [e] obtained from NMR spectroscopic analysis of isolated **2-SPMe$_3$** in CD_2Cl_2. [f] py = pyridine.

Chemistry–A European Journal | Full Paper doi.org/10.1002/chem.202001674 | Chemistry Europe European Chemical Societies Publishing

In order to allow a discussion of Bi-$SPMe_3$ interactions in the broader context of Lewis acidity, Me_3SiOTf, $B(C_6F_5)_3$, and $AlCl_3$ were chosen as typical examples of frequently applied, (relatively) hard Lewis acids and investigated with the modified GB method (for further examples see Supporting Information). It should be noted that for cationic Me_3SiOTf an extraordinarily high acceptor number towards $OPEt_3$ of AN ($OPEt_3$) = 116 was determined (Supporting Information). In contrast, an acceptor number of only AN ($SPMe_3$) = 1 was found for the softer donor $SPMe_3$ (entry 15), demonstrating that the exceptional Lewis acidity of cationic bismuth species towards soft donors is not only due to their ionic character, but also to the shape, energy, and accessibility of their LUMO. Acceptor numbers AN ($SPMe_3$) of 42 and 78 were obtained for the boron and the aluminum compound, respectively (entries 16, 17), which are significantly lower than those of the cationic bismuth species **1**, **2-SPMe$_3$**, and **4** (entries 12–14). It should be noted that compound **1** contains two equivalents of thf and that the addition of 1 equiv $SPMe_3$ to a solution of **1** gave an acceptor number which is virtually identical to that of isolated **2-SPMe$_3$** (entries 12, 13). In other words, the softer donor $SPMe_3$ can efficiently displace two equivalents of the harder donor thf from the coordination sphere of the bismuth atom in **1**. In order to evaluate the preference of the harder Lewis acids $B(C_6F_5)_3$ and $AlCl_3$ for either thf or $SPMe_3$, samples containing one equivalent of the Lewis acid, one equivalent of thf, and one equivalent of $SPMe_3$ were investigated. Acceptor numbers AN ($SPMe_3$) of 1 and 3 were obtained (entries 19, 20), demonstrating that the softer donor $SPMe_3$ cannot compete with the harder donor thf for the relatively hard binding sites in $B(C_6F_5)_3$ and $AlCl_3$.

The preference to bind a soft donor $SPMe_3$ or a hard donor such as pyridine was also compared for compound **2-SPMe$_3$** and GaI_3. While GaI_3 showed only a minor acceptor number of 6 in the presence of one equivalent of pyridine, significant acceptor numbers of 74 and 42 were obtained for compound **2-SPMe$_3$** in the presence of one and two equivalents of pyridine, respectively (entries 22–24). Only with a large (⩾20-fold) excess of pyridine, values of AN ($SPMe_3$) <10 were obtained for compound **2-SPMe$_3$** (for titration experiments see Supporting Information).

With $SePMe_3$ as a Lewis base, the trends were similar to those observed for $SPMe_3$. Aryl bismuth compounds, halobismepines, and in this case even all bismuth halides BiX_3 (X = Cl–I) showed acceptor numbers suggesting weak or even negligible Lewis acid/base interactions (AN ($SePMe_3$) = 0–14; Table 2, entries 2–9). For the bismuth triflates $Bi(OTf)_3$ and **3**, acceptor numbers of AN ($SePMe_3$) = 46 and 61 demonstrate significant Bi···$SePMe_3$ bonding (entries 10, 11).[41] For $Bi(OTf)_3$, extended reaction times led to the appearance of an additional resonance in the ^{31}P NMR spectrum, which is not due to a simple 1:1 adduct and is tentatively ascribed to the formation of $[Bi(SePMe_3)_6][OTf]_3$ (Supporting Information). High acceptor numbers of 65–76 were obtained for cationic bismuth compounds **1**, **2-SePMe$_3$**, and **4**, indicating considerable interactions with $SePMe_3$ (entries 12–14).[43]

Table 2. Investigations of potential Lewis acids with the modified Gutmann–Beckett method, using $SePMe_3$ as a donor.

Entry	Compound	δ ^{31}P [ppm][a]	AN ($SePMe_3$)[b]
1	$SePMe_3$	7.8	0 (by definition)
2	$BiPh_3$	8.9	6
3	$Bi_2(diaryl)_3$[c]	7.8	0
4	Bi(diaryl)Cl[c]	9.0	7
5	Bi(diaryl)Br[c]	8.4	3
6	Bi(diaryl)I[c]	8.0	1
7	$BiCl_3$	10.3	14
8	$BiBr_3$	9.7	11
9	BiI_3	9.5	10
10	$Bi(OTf)_3$	15.8[d]	46
11	Bi(diaryl)(OTf) (3)[d,e]	18.5	61
12	**1**	19.2	65
13	**2-SePMe$_3$**	**21.1**[f]	**76**
14	$[BiPh_3(thf)_2][SbF_6]$ (4)	20.5	73
15	Me_3SiOTf	7.9	1
16	$B(C_6F_5)_3$	13.0	30
17	$AlCl_3$	20.5	73
18	GaI_3	25.3	100 (by definition)
19	$B(C_6F_5)_3(thf)$	7.9	1
20	$AlCl_3(thf)$	8.0	1
21	$GaI_3(thf)$	24.2	94
22	$GaI_3(py)$[g]	9.0	7
23	2-$SePMe_3$ + py[g]	16.5	50
24	2-$SePMe_3$ + 2 py[g]	15.3	43

[a] If not otherwise noted, CD_2Cl_2 solutions of equimolar amounts of the potential Lewis acid and $SPMe_3$ were investigated at 23 °C (for details see experimental part). [b] determined according to equation 3 (see text). [c] diaryl = $[(C_6H_4)_2C_2H_2]^{2-}$ as in compound **1**; that is, $[Bi(diaryl)]^+$ corresponds to a cationic dibenzobismepine complex fragment.[12] [d] An additional resonance is detected after extended reaction times (for discussion see text and Supporting Information). [e] small amounts of THF were added to fully solubilize **3** (CD_2Cl_2/THF = 25:1, v/v). [f] obtained from NMR spectroscopic analysis of isolated **2-SePMe$_3$** in CD_2Cl_2. [g] py = pyridine.

Analysis of Me_3SiOTf, $B(C_6F_5)_3$, and $AlCl_3$ with the modified GB method revealed that the Si species shows a negligible acceptor number, while the B and the Al compound show moderate to high acceptor numbers towards the soft donor $SePMe_3$ (entries 15–17). But in contrast to the bismuth cation **1** (entries 12, 13), the presence of one equivalent of the hard donor thf leads to negligible B/Al···$SePMe_3$ interactions, as judged from acceptor numbers of only 1 in both cases (entries 19, 20). Similar results were obtained for competition experiments with GaI_3 and **2-SePMe$_3$** as Lewis acids and pyridine and $SePMe_3$ as Lewis bases. GaI_3 showed a minor acceptor number of 7 in the presence of pyridine, while acceptor numbers of 50 and 43 indicate significant Bi···$SePMe_3$ interactions for **2-SPMe$_3$** in the presence of one and two equivalents of pyridine, respectively (entries 22–24). A large (⩾20-fold) excess of pyridine was necessary to lower the acceptor number AN ($SePMe_3$) to an insignificant value of 2 for compound **2-SePMe$_3$** (for titration experiments see Supporting Information).

Major findings from our studies of bismuth-centered Lewis acidity based on the GB method (previous work[12] and Supporting Information) and modified versions thereof (this work) are summarized in Figure 2. As a trend it is apparent that bismuth Lewis acids of class A[12] with a σ^*(Bi-X) acceptor orbital (*cf.* introduction)[12] show moderate Lewis acidities towards the

Chemistry–A European Journal | Full Paper doi.org/10.1002/chem.202001674 | Chemistry Europe European Chemical Societies Publishing

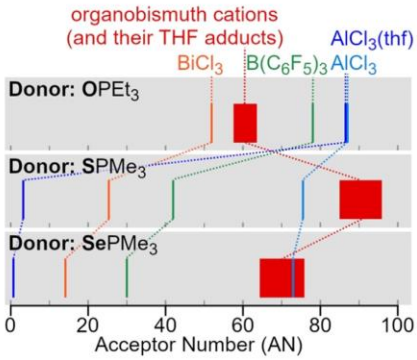

Figure 2. Comparison of acceptor numbers for selected Lewis acids obtained from the Gutmann–Beckett method (top, previous results[12] and this work) and modified versions (middle and bottom, this work). "Organobismuth cations" refers to class C compounds (cf. introduction and ref. [12]) without strong directional cation···anion interactions.

strong and hard donor $OPEt_3$, but only relatively low Lewis acidities towards weaker and softer donors $SPMe_3$ and $SePMe_3$. In contrast, bismuth Lewis acids of class C[12] with an empty 6p(Bi) acceptor orbital show a considerable Lewis acidity towards all three types of donors. It is especially remarkable that (in contrast to Me_3SiOTf, $B(C_6F_5)_3$, and $AlCl_3$) cationic bismuth compounds of class C maintain an extraordinary Lewis acidity towards the soft donors $SPMe_3$ and $SePMe_3$ even in the presence of a hard donor such as thf and pyridine.

DFT calculations and natural bond orbital (NBO) analyses were performed in order to characterize the Bi–S/Se interactions in compounds **2-EPMe$_3$** in more detail (E = S, Se; for details see experimental and Supporting Information). The bismuth Lewis acidic component in these complexes is the (so far non-isolable) low-valent bismepine cation $[Bi((C_6H_4)_2C_2H_2)][SbF_6]$. A frontier orbital analysis of this species was carried out, with its conformation fixed to that found in the optimized structure of the adduct **2-SePMe$_3$**. The LUMO of $[Bi((C_6H_4)_2C_2H_2)][SbF_6]$ is best described as an empty bismuth 6p-orbital with only minor contributions from other atomic orbitals (Figure 3a). The bent conformation of the bismepine core results in steric protection of one lobe of the LUMO by the olefinic functional group of the ligand backbone. This should favor adduct formation in a 1:1 stoichiometry with donors that have at least a moderate steric load, as experimentally observed for **2-SPMe$_3$** and **2-SePMe$_3$**. Theoretical analysis of **2-SPMe$_3$** and **2-SePMe$_3$** indicate that the Bi–S/Se interactions can be interpreted as regular covalent bonds, the NBOs of which are mainly composed of bismuth 6p atomic orbitals and 3/4p S/Se atomic orbitals and strongly polarized towards the chalcogen (S: 79.9%; Se: 78.0%).[44] The molecular orbitals with significant Bi–S/Se bonding contributions are the HOMO−5 (only for **2-SePMe$_3$**) as well as the HOMO−6 and HOMO−7 (for **2-SPMe$_3$** and **2-SePMe$_3$**), which are mainly composed through linear combinations of NBOs associated with Bi–S/Se (5–25%) and Bi–C bonds (8–29%) as well as Bi (10%) and S/Se lone pairs (7–32%) (Figure 3b and Supporting Information). In agreement with these results, natural resonance theory (NRT) revealed exclusively resonance structures featuring R_2Bi-(S/Se)-P^+Me_3 structural motifs (with mesomeric effects

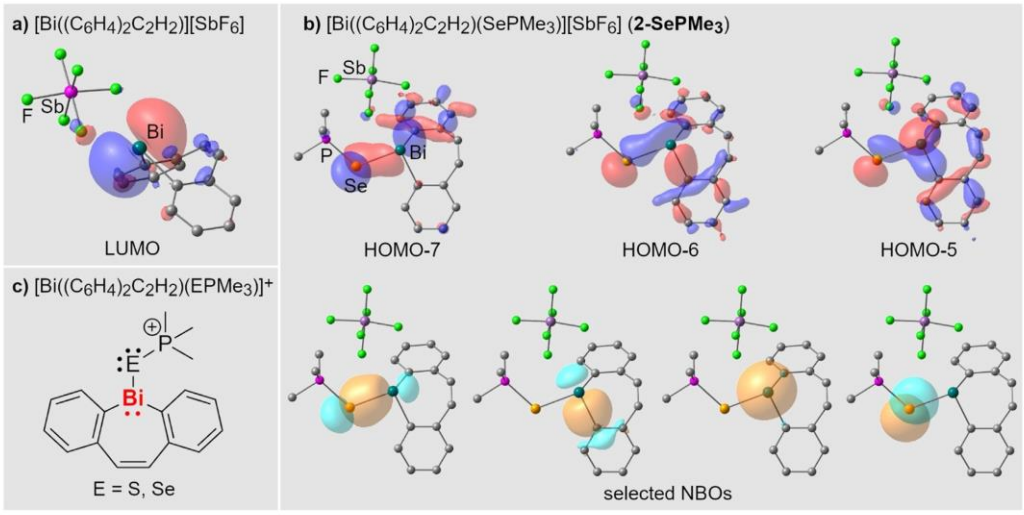

Figure 3. a) LUMO of $[Bi(C_6H_4)_2C_2H_2][SbF_6]$ with its conformation fixed to that found in the optimized structure of **2-SePMe$_3$**. b) Selected molecular orbitals (top) and NBOs (bottom) of **2-SePMe$_3$** with isovalues of 0.04. c) Resonance structure of the **2-EPMe$_3$** according to NRT (E = S, Se; $[SbF_6]^-$ omitted for clarity; only one (out of many) resonance structures of the bismepine core is depicted (see text)).

Chemistry–A European Journal | Full Paper doi.org/10.1002/chem.202001674 | Chemistry Europe European Chemical Societies Publishing

being relevant only within the bismepine core and the $(SbF_6)^-$ anion; resonance structure of the cations shown in Figure 3c). According to NRT, the Bi–S/Se single bonds are generated through 40%/44% covalent and 60%/56% ionic contributions. This is in agreement with large Wiberg bond indices of 0.61 (Bi–S) and 0.65 (Bi–Se) for these bonds.

Thermodynamic parameters of adduct formations between $EPMe_3$ and Lewis acids based on bismuth and group 13 elements (B–Ga) were determined (E = O, S, Se; Table 3 (ΔG values) and Supporting Information (ΔH values and additional examples)). Starting from coordinatively unsaturated Lewis acids, the adduct formations are strongly exergonic ($\Delta G = -20$ to -45 kcal mol^{-1}) for all compounds but $B(C_6F_5)_3$, which shows a mildly exergonic reaction with $OPMe_3$ and endergonic reactions with $S/SePMe_3$ (entries 1–6, for ΔH values see Supporting Information).[45] Most importantly, reactions of all the group 13 compounds become less exergonic (or even endergonic) upon changing the Lewis base from $OPMe_3$ to $S/SePMe_3$ (entries 1–5). The opposite behavior is observed for the cationic bismuth species (entry 6), underlining its soft character according to the HSAB principle.

In order to evaluate trends in the ability of donors $EPMe_3$ to displace one or two thf ligands from the coordination sphere of coordinatively saturated Lewis acids (from a thermodynamic point of view), reactions with compounds [LA]-$(thf)_n$ were investigated ([LA] = Lewis acid; $n = 1$–2). With the exception of $B(C_6F_5)_3$ (entry 7), exergonic reactions are observed for the group 13 compounds with $OPMe_3$ ($\Delta G = -10$ to -11 kcal mol^{-1}, $n = 1$; entries 8–11), while those with bismuth compounds are clearly exergonic for $n = 1$ and marginally endergonic for $n = 2$ ($\Delta G = -12.4$ and $+0.3$ kcal mol^{-1}; entries 12,13). Ligand substitutions with $S/SePMe_3$ at the hard aluminum center are endergonic by 8 to 9 kcal mol^{-1} (entry 8). For the softer gallium compounds, substitution of thf by $S/SePMe_3$ is only slightly endergonic ($\Delta G = +3$ to $+5$ kcal mol^{-1}, $n = 1$; entries 9–11). For the bismuth cations, these reactions are clearly exergonic for $n = 1$ ($\Delta G = -17$ to -19 kcal mol^{-1}, entry 12) and still slightly exergonic for $n = 2$ ($\Delta G = -5$ to -6 kcal mol^{-1}, entry 13). These trends are in good agreement with experimental results obtained from the modified GB method.[45]

Table 3. Calculated free reaction enthalpy of Lewis pair formation with varying Lewis acids and donors $EPMe_3$ (E = O, S, Se) in the presence of 0–2 equivalents of thf.

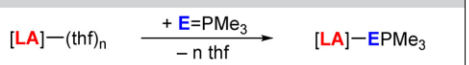

Entry	[LA]	n	ΔG [kcal mol^{-1}] E = O	E = S	E = Se
1	$B(C_6F_5)_3$	0	−0.7	+16.7	+18.3
2	$AlCl_3$	0	−41.8	−23.0	−22.0
3	$GaCl_3$	0	−39.6	−25.0	−24.4
4	$GaBr_3$	0	−37.7	−24.3	−23.8
5	GaI_3	0	−32.7	−19.5	−19.6
6	[Bi(diaryl)][SbF_6][a]	0	−38.6	−43.6	−44.8
7	$B(C_6F_5)_3$	1	+8.8	+26.3	+27.9
8	$AlCl_3$	1	−10.8	+8.1	+9.1
9	$GaCl_3$	1	−10.4	+4.2	+4.8
10	$GaBr_3$	1	−10.9	+2.5	+3.0
11	GaI_3	1	−10.3	+2.9	+2.8
12	[Bi(diaryl)][SbF_6][a]	1	−12.4	−17.4	−18.6
13	[Bi(diaryl)][SbF_6][a]	2	+0.3	−4.7	−5.9

[a] diaryl = $[(C_6H_4)_2C_2H_2]^{2-}$; that is, [LA] = [Bi(diaryl)][SbF_6] with two thf ligands ($n = 2$) corresponds to compound **1**.

Conclusions

The ability of bismuth(III) compounds to form Lewis acid/base adducts with the soft donors $EPMe_3$ has been investigated (E = S, Se). Cationic bismuth compounds $[BiR_2(EPMe_3)][SbF_6]$ featuring rare Bi···EPR_3 interactions were isolated and fully characterized. The bismuth atoms in these compounds show coordination numbers of three, which is extremely unusual for cationic bismuth species without directional Bi···counteranion interactions. Detailed experimental and theoretical analyses revealed significant Bi···EPR_3 bonding with strong covalent contributions that persists in the solid state and in solution. The ^{31}P NMR chemical shift of $EPMe_3$ in the presence of a compound "LA" may be used as an easily accessible experimental parameter to investigate the Lewis acidity of LA. In specific, we suggest the utilization of soft donors such as $EPMe_3$ in order to assess the *hardness/softness* of a Lewis acid. This is equivalent to an extension of the Gutmann–Beckett method. We have investigated bismuth compounds of type BiR_3, BiR_2X, BiX_3, and $[BiR_2]^+$ with this approach, delivering experimental evidence for their soft Lewis acidity. Especially cationic bismuth species $[BiR_2]^+$ that interact with the donor through an empty p-orbital (not through a σ*-orbital) are potent soft Lewis acids. In contrast to well-established, relatively hard Lewis acids such as Me_3SiOTf, $B(C_6F_5)_3$, and $AlCl_3$ and the softer Lewis acid GaI_3, they can still efficiently activate soft donors in the presence of hard donors such as thf and pyridine (*cf.* Figure 2). Future research efforts will be directed towards the exploitation of these findings in the activation of substrates with soft donor functionalities for stoichiometric and catalytic transformations.

Experimental Section

General considerations

All air- and moisture-sensitive manipulations were carried out using standard vacuum line Schlenk techniques or in gloveboxes containing an atmosphere of purified argon. Solvents were degassed and purified according to standard laboratory procedures. NMR spectra were recorded on Bruker instruments operating at 400 or 500 MHz with respect to ^1H. ^1H and ^{13}C NMR chemical shifts are reported relative to $SiMe_4$ using the residual ^1H and ^{13}C chemical shifts of the solvent as a secondary standard. ^{31}P and ^{77}Se NMR chemical shifts are reported relative to H_3PO_4 (85% aqueous solution) and $SeMe_2$ (plus 5% C_6D_6) as external standards. NMR spectra were recorded at ambient temperature (typically 23 °C), if not otherwise noted. Elemental analyses were performed on a Leco or a Carlo Erba instrument. Single-crystals suitable for X-ray diffraction were coated with polyisobutylene or perfluorinated polyether oil in a glovebox, transferred to a nylon loop and then transferred to the goniometer of a diffractometer equipped with a molybdenum X-ray tube ($\lambda = 0.71073$ Å). The structures were solved using intrin-

Chemistry–A European Journal | Full Paper doi.org/10.1002/chem.202001674 | Chemistry Europe European Chemical Societies Publishing

sic phasing methods (SHELXT) completed by Fourier synthesis and refined by full-matrix least-squares procedures.

Deposition Numbers 1961401, 1961402, 1961405, 1961406, 1961407, and 1994719, 1994720, 1994721 contain the supplementary crystallographic data for this paper. These data are provided free of charge by the joint Cambridge Crystallographic Data Centre and Fachinformationszentrum Karlsruhe Access Structures service www.ccdc.cam.ac.uk/structures.

DFT calculations were performed with the Gaussian program[46] using the 6-31G(d,p)[47] [H, C, N, O, F], 6–311G(d,p)[48] [Al, P, S], and the LANL2DZ[49] [Ga, In, Se, Sb, Bi, Br, I] basis set and the B3LYP functional.[50] The D3 version of Grimme's dispersion model with the original D3 damping function was applied.[51] Frequency analyses of the reported structures showed no imaginary frequencies for ground states. Thermodynamic parameters were calculated at a temperature of 298.15 K and a pressure of 1.00 atm. NBO analyses were performed using the program version NBO 7.[52]

The following labeling Scheme has been used for the assignment of atoms to resonances detected in NMR spectroscopic experiments:

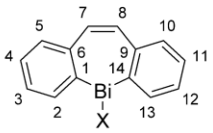

$[Bi((C_6H_4)_2C_2H_2)(SPMe_3)][SbF_6]$ (2-SPMe$_3$): To a solution of $[Bi((C_6H_4)_2C_2H_2)(thf)_2][SbF_6]$ (**1**) (30.0 mg, 39.1 μmol) in CH_2Cl_2 (0.7 mL) was added $SPMe_3$ (4.2 mg, 39.1 μmol) at ambient temperature. The light yellow solution was layered with *n*-pentane (0.7 mL) and stored at −30 °C. A pale yellow solid had precipitated after 1 d, was isolated by filtration, and dried in vacuo. Yield: 26.0 mg, 35.6 μmol, 91 %. ^{1}H NMR (400 MHz, CD_2Cl_2): δ = 2.21 (d, 9H, $^2J_{PH}$ = 13.3 Hz, PMe_3), 7.09 (s, 2H, H-7, H-8), 7.43 (t, 2H, $^3J_{HH}$ = 7.7 Hz, C_6H_4), 7.71 (m, 4H, C_6H_4), 8.41 (m, 2H, C_6H_4) ppm. ^{1}H NMR (500 MHz, [D$_8$]THF): δ = 1.94 (d, 12H, $^2J_{PH}$ = 13.7 Hz, PMe_3), 6.75 (s, 2H, H-7, H-8), 7.40 (ddd, 2H, $^4J_{HH}$ = 1.1 Hz, $^3J_{HH}$ = 7.4 Hz, $^3J_{HH}$ = 7.7 Hz, H-4, H-11) 7.59 (ddd, 2H, $^4J_{HH}$ = 1.3 Hz, $^3J_{HH}$ = 7.4 Hz, $^3J_{HH}$ = 7.4 Hz, H-3, C-12), 7.84 (dd, 2H, $^4J_{HH}$ = 1.1 Hz, $^3J_{HH}$ = 7.7 Hz, H-5, H-10), 8.18 (dd, 2H, $^4J_{HH}$ = 1.3 Hz, $^3J_{HH}$ = 7.4 Hz, H-2, H-13) ppm. ^{13}C NMR (126 MHz, [D$_8$]THF): δ = 19.15 (d, $^1J_{CP}$ = 53.8 Hz, PMe_3), 129.76 (s, H-4, H-11), 130.15 (s, C-3, C-12), 132.95 (s, C-7, C-8), 135.91 (s, C-5, C-10), 136.95 (s, C-2, C-13), 146.21 (s, C-6, C-9), 176.86 (br, C-1, C-14, detected via ^{13}C, ^{1}H HMBC experiments) ppm. ^{31}P NMR (202 MHz, CD_2Cl_2): δ = 44.2 (s) ppm. ^{31}P NMR (202 MHz, [D$_8$]THF): δ = 41.4 (s) ppm.

Elemental analysis: Anal. calc. for: $[C_{17}H_{19}BiPSSbF_6]$ (731.10 g mol^{-1}): C 27.93, H 2.62, S 4.39; found: C 28.19, H 2.58, S 4.36.

$[Bi((C_6H_4)_2C_2H_2)(SePMe_3)][SbF_6]$ (2-SePMe$_3$): To a solution of $[Bi((C_6H_4)_2C_2H_2)(thf)_2][SbF_6]$ (**1**) (20.0 mg, 26.1 μmol) in CH_2Cl_2 (0.5 mL) was added $SePMe_3$ (4.2 mg, 26.1 μmol) at ambient temperature. The light yellow solution was layered with *n*-pentane (0.7 mL) and stored at −30 °C. A pale yellow solid had precipitated after 1 d, was isolated by filtration, and dried in vacuo. Yield: 18.0 mg, 23.1 μmol, 87 %. ^{1}H NMR (500 MHz, CD_2Cl_2): δ = 2.23 (d, 9H, $^2J_{PH}$ = 13.4 Hz, PMe_3), 7.01 (s, 2H, H-7, H-8), 7.43 (ddd, 2H, $^4J_{HH}$ = 1.2 Hz, $^3J_{HH}$ = 7.6 Hz, $^3J_{HH}$ = 7.7 Hz, H-4, H-11) 7.63 (ddd, 2H, $^4J_{HH}$ = 1.3 Hz, $^3J_{HH}$ = 7.5 Hz, $^3J_{HH}$ = 7.5 Hz, H-3, C-12), 7.72 (dd, 2H, $^4J_{HH}$ = 1.2 Hz, $^3J_{HH}$ = 7.6 Hz, H-5, H-10), 8.43 (dd, 2H, $^4J_{HH}$ = 1.2 Hz, $^3J_{HH}$ = 7.5 Hz, H-2, H-13) ppm. ^{13}C NMR (126 MHz, CD_2Cl_2): δ = 19.48 (d, $^1J_{CP}$ = 47.8 Hz, PMe_3), 129.61 (s, H-4, H-11), 132.24 (s, C-3, C-12), 133.49 (s, C-7, C-8), 133.81 (s, C-5, C-10), 136.77 (s, C-2, C-13), 143.49 (s, C-6, C-9), 162.89 (br, C-1, C-14) ppm. ^{31}P NMR (202 MHz, CD_2Cl_2): δ = 21.1 (s, $^1J_{PSe}$ = 488.2 Hz) ppm. ^{31}P NMR (202 MHz, THF): δ = 19.1 (s) ppm. ^{77}Se NMR (100 MHz, CD_2Cl_2): δ = −44.2 (br, detected via ^{1}H, ^{77}Se HMBC experiments) ppm.

Elemental analysis: Anal. calc. for: $[C_{17}H_{19}BiPSeSbF_6]$ (778.01 g mol^{-1}): C 26.24, H 2.46; found: C 25.88, H 2.48.

$[BiPh_2(thf)_2][SbF_6]$ (4): To a solution of diphenylbismuth chloride (50.0 mg, 0.13 mmol) in THF (1 mL) was added a solution of $AgSbF_6$ (43.1 mg, 0.13 mmol) in THF (0.5 mL). The colorless suspension was filtered. The filtrate was layered with *n*-pentane (1.5 mL) and stored at −30 °C. The product was obtained after 2 d by filtration, and dried in vacuo. Yield: 83 mg, 0.11 mmol, 86 %. ^{1}H NMR (500 MHz, CD_2Cl_2): δ = 1.82 (m, 4H, β-thf), 3.70 (m, 4H, α-thf), 7.56–7.69 (m, 2H, *p*-C_6H_5), 8.02 (dd, 4H, $^3J_{HH}$ = 6.6, $^3J_{HH}$ = 6.6 Hz, *o*-C_6H_5), 8.47 (d, 4H, $^3J_{HH}$ = 6.9 Hz, *m*-C_6H_5) ppm. ^{13}C NMR (126 MHz, CD_2Cl_2): δ = 26.03 (s, β-thf), 71.12 (s, α-thf), 130.86 (s, *p*-C_6H_5), 133.63 (s, *o*-C_6H_5), 137.64 (s, *m*-C_6H_5) 198.46 (s, *ipso*-C_6H_5) ppm.

Elemental analysis: Anal. calc. for: $[C_{12}H_{10}BiSbF_6](OC_4H_8)_2$ (743.16 g mol^{-1}): C 32.32, H 3.53; found: C 32.42, H 3.64.

General procedure for modified Gutmann–Beckett method

If not otherwise noted, equimolar amounts of the potential Lewis acid and the Lewis base $EPMe_3$ were dissolved in dichloromethane (E = S, Se). In competition experiments, the required amount of another Lewis base was added (the sequence of addition was not relevant; see Supporting Information). One of the following three different methods was used for the determination of accurate ^{31}P NMR chemical shifts: i) the use of CD_2Cl_2 as the solvent, so that locking and shimming was possible; ii) the use of CH_2Cl_2 as the solvent along with a capillary containing deuterated acetone, so that locking and shimming was possible; iii) the use of CH_2Cl_2 as the solvent along with a capillary containing an 85 % aqueous solution of H_3PO_4 as a reference. The three methods gave identical results, when applied to identical samples. For details see Supporting Information.

Acknowledgements

Generous funding through the Deutsche Forschungsgemeinschaft (DFG), the Fonds der Chemischen Industrie (FCI), and the University of Würzburg is gratefully acknowledged. The authors thank Prof. Holger Braunschweig for continuous support. Open access funding enabled and organized by Projekt DEAL.

Conflict of interest

The authors declare no conflict of interest.

Keywords: bismuth · bonding analysis · cationic species · HSAB principle · Lewis acids

[1] a) T. Ollevier, *Org. Biomol. Chem.* **2013**, *11*, 2740–2755; b) J. M. Bothwell, S. W. Krabbe, R. S. Mohan, *Chem. Soc. Rev.* **2011**, *40*, 4649–4707; c) T. Ollevier, *Bismuth-Mediated Organic Reactions, Topics in Current Chemistry*, Springer, **2012**, Vol. 311; d) A. Gagnon, J. Dansereau, A. Le Roch, *Synthe-*

Chemistry–A European Journal | Full Paper doi.org/10.1002/chem.202001674 | Chemistry Europe European Chemical Societies Publishing

sis **2017**, *49*, 1707 – 1745; e) R. Hua, *Curr. Org. Synth.* **2008**, *5*, 1 – 27; f) H. R. Kricheldorf, *Chem. Rev.* **2009**, *109*, 5579 – 5594.

[2] E.g.: a) G. Sabitha, E. V. Reddy, C. Maruthi, J. S. Yadav, *Tetrahedron Lett.* **2002**, *43*, 1573 – 1575; b) S. Solyntjes, B. Neumann, H.-G. Stammler, N. Ignat'ev, B. Hoge, *Chem. Eur. J.* **2017**, *23*, 1568 – 1575.

[3] E.g.: a) H. Qin, N. Yamagiwa, S. Matsunaga, M. Shibasaki, *J. Am. Chem. Soc.* **2006**, *128*, 1611 – 1614; b) S. Balasubramaniam, S. Kumar, A. P. Andrews, B. Varghese, E. D. Jemmis, A. Venugophal, *Eur. J. Inorg. Chem.* **2019**, 3265 – 3269; c) Y. Nishimoto, M. Takeuchi, M. Yasuda, A. Baba, *Chem. Eur. J.* **2013**, *19*, 14411 – 14415; d) C. Lichtenberg, F. Pan, T. P. Spaniol, U. Englert, J. Okuda, *Angew. Chem. Int. Ed.* **2012**, *51*, 13011 – 13015; *Angew. Chem.* **2012**, *124*, 13186 – 13190; e) H. Dengel, C. Lichtenberg, *Chem. Eur. J.* **2016**, *22*, 18465 – 18475.

[4] E.g.: a) R. Qiu, S. Yin, X. Zhang, J. Xia, X. Xu, S. Luo, *Chem. Commun.* **2009**, 4759 – 4761; b) R. Qiu, Y. Qiu, S. Yin, X. Song, Z. Meng, X. Xu, X. Zhang, S. Luo, C.-T. Au, W.-Y. Wong, *Green Chem.* **2010**, *12*, 1767 – 1771.

[5] E.g.: S. Ghosh, L. K. Kinthada, S. Bhunia, A. Bisai, *Chem. Commun.* **2012**, *48*, 10132 – 10134.

[6] E.g.: E. M. Keramane, B. Boyer, J.-P. Roque, *Tetrahedron* **2001**, *57*, 1909 – 1916.

[7] E.g.: a) S. Roggan, C. Limberg, B. Ziemer, M. Brandt, *Angew. Chem. Int. Ed.* **2004**, *43*, 2846 – 2849; *Angew. Chem.* **2004**, *116*, 2906 – 2910; b) S. Roggan, G. Schnakenburg, C. Limberg, S. Sandhöfner, H. Pritzkow, B. Ziemer, *Chem. Eur. J.* **2005**, *11*, 225 – 234; c) C. Knispel, C. Limberg, C. Tschersich, *Chem. Commun.* **2011**, *47*, 10794 – 10796; d) B. Ritschel, J. Poater, H. Dengel, F. M. Bickelhaupt, C. Lichtenberg, *Angew. Chem. Int. Ed.* **2018**, *57*, 3825 – 3829; *Angew. Chem.* **2018**, *130*, 3887 – 3891; e) B. Ritschel, C. Lichtenberg, *Synlett* **2018**, *29*, 2213 – 2217.

[8] J. Ramler, J. Poater, F. Hirsch, B. Ritschel, I. Fischer, F. M. Bickelhaupt, C. Lichtenberg, *Chem. Sci.* **2019**, *10*, 4169 – 4176.

[9] S. W. Krabbe, R. S. Mohan, *Environmentally Friendly Organic Synthesis Using Bismuth(III) Compounds in Topics in Current Chemistry* (Ed.: T. Ollevier), Springer, **2012**, vol. 311, pp. 50 – 52.

[10] a) X. Zhang, S. Yin, R. Qiu, J. Xia, W. Dai, Z. Yu, C.-T. Au, W.-Y. Wong, *J. Organomet. Chem.* **2009**, *694*, 3559 – 3564; b) N. Tan, S. Yin, Y. Li, R. Qiu, Z. Meng, X. Song, S. Luo, C.-T. Au, W.-Y. Wong, *J. Organomet. Chem.* **2011**, *696*, 1579 – 1583; c) R. Qiu, Y. Qiu, S. Yin, X. Xu, S. Luo, C.-T. Au, W.-Y. Wong, S. Shimada, *Adv. Synth. Catal.* **2010**, *352*, 153 – 162; d) X. Zhang, R. Qiu, N. Tan, S. Yin, J. Xia, S. Luo, C.-T. Au, *Tetrahedron Lett.* **2010**, *51*, 153 – 156.

[11] a) C. Tschersich, C. Limberg, S. Roggan, C. Herwig, N. Ernsting, S. Kovalenko, S. Mebs, *Angew. Chem. Int. Ed.* **2012**, *51*, 4989 – 4992; *Angew. Chem.* **2012**, *124*, 5073 – 5077; b) T.-P. Lin, I.-S. Ke, F. P. Gabbaï, *Angew. Chem. Int. Ed.* **2012**, *51*, 4985 – 4988; *Angew. Chem.* **2012**, *124*, 5069 – 5072; c) C. Tschersich, S. Hoof, N. Frank, C. Herwig, C. Limberg, *Inorg. Chem.* **2016**, *55*, 1837 – 1842.

[12] J. Ramler, K. Hofmann, C. Lichtenberg, *Inorg. Chem.* **2020**, *59*, 3367 – 3376.

[13] a) M. Krasowska, A.-M. Fritzsche, M. Mehring, A. A. Auer, *ChemPhysChem* **2019**, *20*, 2539; b) M. Krasowska, W. B. Schneider, M. Mehring, A. A. Auer, *Chem. Eur. J.* **2018**, *24*, 10238 – 10245; c) A.-M. Preda, M. Krasowska, L. Wrobel, P. Kitschke, P. C. Andrews, J. G. MacLellan, L. Mertens, M. Korb, T. Rüffer, H. Lang, A. A. Auer, M. Mehring, *Beilstein J. Org. Chem.* **2018**, *14*, 2125 – 2145; d) W. Frank, J. Schneider, S. Müller-Becker, *J. Chem. Soc. Chem. Commun.* **1993**, 799 – 800; e) S. Müller-Becker, W. Frank, J. Schneider, *Z. Anorg. Allg. Chem.* **1993**, *619*, 1073 – 1082; f) A. Schier, J. M. Wallis, G. Müller, H. Schmidbaur, *Angew. Chem. Int. Ed. Engl.* **1986**, *25*, 757 – 759; *Angew. Chem.* **1986**, *98*, 742 – 744.

[14] a) W. Frank, J. Weber, E. Fuchs, *Angew. Chem. Int. Ed. Engl.* **1987**, *26*, 74 – 75; *Angew. Chem.* **1987**, *99*, 68 – 69; b) E. Conrad, N. Burford, R. McDonald, M. J. Ferguson, *Chem. Commun.* **2010**, *46*, 4598 – 4600; c) R. J. Schwamm, M. P. Coles, C. M. Fitchett, *Dalton Trans.* **2017**, *46*, 4066 – 4074.

[15] C. Hering-Junghans, M. Thomas, A. Villinger, A. Schulz, *Chem. Eur. J.* **2015**, *21*, 6713 – 6717.

[16] W. Levason, N. J. Hill, G. Reid, *J. Chem. Soc. Dalton Trans.* **2002**, 4316 – 4317.

[17] For bismuth(III) compounds, dispersion interactions through the lone pair at bismuth and the π electrons of arenes have been investigated, which is not in the focus of this contribution and are therefore not discussed in detail (e.g.: I. Caracelli, I. Haiduc, J. Zukerman-Schpector, E. R. T. Tiekink, *Coord. Chem. Rev.* **2013**, *257*, 2863 – 2879; also see ref. [13a – c]).

[18] a) R. Kannan, S. Kumar, A. P. Andrews, E. D. Jemmis, A. Venugopal, *Inorg. Chem.* **2017**, *56*, 9391 – 9395; b) J. A. Johnson, A. Venugopal, *J. Chem. Sci.* **2019**, *131*, 114.

[19] a) L. J. Farrugia, F. J. Lawlor, N. C. Norman, *J. Chem. Soc. Dalton Trans.* **1995**, 1163 – 1171; b) F. B. Alhanash, N. A. barnes, A. K. Brisdon, S. M. Godfrey, R. G. Pritchard, *Dalton Trans.* **2012**, *41*, 10211 – 10218.

[20] The observation of an up-field rather than the expected down-field shift upon coordination of $SeP(4\text{-}F\text{-}C_6H_4)_3$ to $BiCl_3$ and $BiBr_3$ is not discussed in ref. [19b] and may be due to ring current effects of the aromatic substituents.

[21] a) A. Cogne, A. Grand, J. Laugier, J. B. Robert, L. Wiesenfeld, *J. Am. Chem. Soc.* **1980**, *102*, 2238 – 2242; b) W. McFarlane, D. S. Rycroft, *J. Chem. Soc. Dalton Trans.* **1973**, 2162 – 2166.

[22] S. O. Grim, E. D. Walton, L. C. Satek, *Can. J. Chem.* **1980**, *58*, 1476 – 1479.

[23] It should be noted that no correlation between the magnitude of $^1J_{PSe}$ and the calculated homolytic P–Se bond dissociation energy could be found in a series of free phosphane selenides: S. R. Alvarado, I. A. Shortt, H.-J. Fan, J. Vela, *Organometallics* **2015**, *34*, 4023 – 4031.

[24] $^1J_{PSe} = 549$ Hz has been reported for $[Fe(C_5H_5)(CO)_2(SePMe_3)][BF_4]$ (see ref. [25]).

[25] N. Kuhn, H. Schumann, *J. Organomet. Chem.* **1986**, *304*, 181 – 193.

[26] a) C. J. Carmalt, N. C. Norman, A. G. Orpen, S. E. Stratford, *J. Organomet. Chem.* **1993**, *460*, C22 – C24; b) C. J. Carmalt, D. Walsh, A. H. Cowley, N. C. Norman, *Organometallics* **1997**, *16*, 3597 – 3600; c) C. J. Carmalt, L. J. Farrugia, N. C. Norman, *J. Chem. Soc. Dalton Trans.* **1996**, 443 – 454; d) M. Bao, T. Hayashi, S. Shimada, *Organometallics* **2007**, *26*, 1816 – 1822.

[27] Higher coordination numbers may be observed, for example in the presence of intramolecular donors or when counteranions such as NO_3^- interact with the central atom, for example: a) I. J. Casely, J. W. Ziller, B. J. Mincher, W. J. Evans, *Inorg. Chem.* **2011**, *50*, 1513 – 1520; b) H. J. Breunig, M. G. Nema, C. Silvestru, A. P. Soran, R. A. Varga, *Dalton Trans.* **2010**, *39*, 11277 – 11284.

[28] One example of a two-coordinate diorganobismuth cation has been reported: M. Olaru, D. Duvinage, E. Lork, S. Mebs, J. Beckmann, *Angew. Chem. Int. Ed.* **2018**, *57*, 10080 – 10084; *Angew. Chem.* **2018**, *130*, 10237 – 10241.

[29] M. Mantina, A. C. Chamberlin, R. Valero, C. J. Cramer, D. G. Truhlar, *J. Phys. Chem. A* **2009**, *113*, 5806 – 5812.

[30] For example, the following compounds have been reported: $BiPh_2(SPh)$, $Bi(2,6\text{-}Me_2\text{-}C_6H_3)_2(SPh)$, $Bi((C_6H_4CH_2)_2NtBu)(SPh)$ (ref. [31]) and $BiPh_2(SePh)$, $Bi(2\text{-}(CHNDipp)\text{-}C_6H_4)_2(SePh)$ (Bi–Se, 2.70–2.73 Å) (Dipp = 2,6-iPr_2-C_6H_3) (ref. [32]). It has to be noted that intermolecular Bi···SPh bonding interactions appear, for instance, in $BiPh_2(SPh)$.

[31] a) G. G. Briand, A. Decken, N. M. Hunter, G. M. Lee, J. A. Melanson, E. M. Owen, *Polyhedron* **2012**, *31*, 796 – 800; b) S. Shimada, O. Yamazaki, T. Tanaka, Y. Suzuki, M. Tanaka, *J. Organomet. Chem.* **2004**, *689*, 3012 – 3023.

[32] a) F. Calderazzo, A. Morvillo, G. Pelizzi, R. Poli, F. Ungari, *Inorg. Chem.* **1988**, *27*, 3730 – 3733; b) P. Šimon, R. Jambor, A. Růžička, L. Dostál, *Organometallics* **2013**, *32*, 239 – 248.

[33] The single-crystal X-ray analysis of $SePMe_3$ reported in the literature (ref. [21a]) was carried out at ambient temperature. We repeated the analysis at a temperature of 100 K for better comparison (Supporting Information).

[34] a) E. N. Baker, B. R. Reay, *J. Chem. Soc. Dalton Trans.* **1973**, 2205 – 2208; b) Y. Ohki, K. Tanifuji, N. Yamada, R. E. Cramer, K. Tatsumi, *Chem. Asian J.* **2012**, *7*, 2222 – 2224; c) P. W. R. Corfield, *Acta Crystallogr. Sect. E* **2014**, *70*, 281 – 285; d) W. T. Robinson, C. J. Wilkins, Z. Zeying, *J. Chem. Soc. Dalton Trans.* **1988**, 2187 – 2192.

[35] a) U. Mayer, V. Gutmann, W. Gerger, *Monatsh. Chem.* **1975**, *106*, 1235 – 1257; b) M. A. Beckett, G. C. Strickland, J. R. Holland, K. S. Varma, *Polymer* **1996**, *37*, 4629 – 4631.

[36] Effects such as a lack of efficient Lewis pair formation between $OPEt_3$ and the Lewis acid under investigation and magnetic anisotropy of the Lewis acid have been reported as (potential) limitations of this method: a) A. E. Ashley, T. J. Herrington, G. G. Wildgoose, H. Zaher, A. L. Thompson, N. H. Rees, T. Krämer, D. O'Hare, *J. Am. Chem. Soc.* **2011**, *133*, 14727 – 14740; b) S. S. Chitnis, A. P. M. Robertson, N. Burford, B. O. Patrick, R. McDonald, M. J. Ferguson, *Chem. Sci.* **2015**, *6*, 6545 – 6555;

Chemistry–A European Journal | Full Paper doi.org/10.1002/chem.202001674 | Chemistry Europe European Chemical Societies Publishing

c) J. C. Gilhula, A. T. Radosevich, *Chem. Sci.* **2019**, *10*, 7177 – 7182 and references therein.
[37] It should be noted that the Gutmann–Beckett method (and modifications thereof) provide an estimate of the Lewis acidity of the compound under investigation by assessing the polarizability of the $E=PR_3$ bond through ^{31}P NMR spectroscopic measurements (E = O (original method); S, Se (modifications)). Being based on NMR spectroscopy, effects such as magnetic anisotropy of the Lewis acid (or substituents R in EPR_3) may influence the results (see ref. [36]).
[38] R. F. Childs, D. L. Mulholland, A. Nixon, *Can. J. Chem.* **1982**, *60*, 801 – 808.
[39] G. J. P. Britovsek, J. Ugolotti, A. J. P. White, *Organometallics* **2005**, *24*, 1685 – 1691.
[40] Compounds $B(C_6F_5)_n(OC_6F_5)_{3-n}$ ($n=0$–3) have previously been reacted with $SPEt_3$, where only for $B(C_6F_5)_3$ a significant interaction could be determined by ^{31}P NMR spectroscopy: see ref. [39].
[41] Note that small amounts of THF had to be added in order to fully solubilize compound **3**. The nature of the solvents used may have an impact of the acceptor numbers AN($SPMe_3$) and AN($SePMe_3$).
[42] It should be noted that entropic effects, which are relevant in reactions "$[LA](thf)_n + EPMe_3 \rightarrow [LA](EPMe_3) + n\,thf$" for $n=0$ and $n=2$, but not for $n=1$, may be overestimated by DFT methods. For ΔH values of these reactions see Supporting Information.
[43] Even solutions of compound **2-SePMe$_3$** in THF gave an acceptor number of AN ($SePMe_3$) = 65.
[44] NBO analyses indicate that olefin → Bi donor/acceptor interactions are present in **2-SPMe$_3$** and **2-SePMe$_3$** and realized through π(C=C) → σ^*(Bi-S/Se) interactions. The corresponding deletion energies amount to 2.9 kcal mol^{-1} for **2-SPMe$_3$** and 3.1 kcal mol^{-1} for **2-SePMe$_3$**, which is in the range of those reported for the corresponding halobismepines (E_{del} = 2.6–2.9 kcal mol^{-1}; ref. [12]).
[45] It should be noted that entropic effects, which are relevant in reactions "$[LA](thf)_n + EPMe_3 \rightarrow [LA](EPMe_3) + n\,thf$" for $n=0$ and $n=2$, but not for $n=1$, may be overestimated by DFT methods. For ΔH values of these reactions see Supporting Information.
[46] For full reference see Supporting Information.
[47] P. C. Hariharan, J. A. Pople, *Theor. Chim. Acta* **1973**, *28*, 213 – 222.
[48] a) A. D. McLean, G. S. Chandler, *J. Chem. Phys.* **1980**, *72*, 5639 – 5648; b) R. Krishnan, J. S. Binkley, R. Seeger, J. A. Pople, *J. Chem. Phys.* **1980**, *72*, 650.
[49] a) T. H. Dunning, Jr., P. J. Hay, *Modern Theoretical Chemistry* (Ed.: H. F. Schaefer III), Vol. 3, Plenum, New York, **1977**, pp. 1 – 28; b) P. J. Hay, W. R. Wadt, *J. Chem. Phys.* **1985**, *82*, 270 – 283; c) P. J. Hay, W. R. Wadt, *J. Chem. Phys.* **1985**, *82*, 299 – 310.
[50] A. D. Becke, *J. Chem. Phys.* **1993**, *98*, 5648 – 5652.
[51] S. Grimme, J. Antony, S. Ehrlich, H. A. Krieg, *J. Chem. Phys.* **2010**, *132*, 154104 – 154119.
[52] E. D. Glendening, J. K. Badenhoop, A. E. Reed, J. E. Carpenter, J. A. Bohmann, C. M. Morales, P. Karafiloglou, C. R. Landis, F. Weinhold, Theoretical Chemistry Institute, University of Wisconsin, Madison, **2018**.

Manuscript received: April 7, 2020
Revised manuscript received: May 10, 2020
Accepted manuscript online: May 19, 2020
Version of record online: July 28, 2020

VIII The Dimethylbismuth Cation: Entry into Dative Bi–Bi Bonding and Unconventional Methyl Exchange

This chapter was submitted on 05.05.2021. When this thesis was submitted to the university of Würzburg, the manuscript was still in the review process.

Jacqueline Ramler,[1] Felipe Fantuzzi,[1,2] Felix Geist,[1] Anna Hanft,[1] Holger Braunschweig,[1] Bernd Engels,[2] and Crispin Lichtenberg[1,*]

1 Institute of Inorganic Chemistry, Julius-Maximilians-University Würzburg, Am Hubland, 97074 Würzburg, Germany.

2 Institute of Physical and Theoretical Chemistry, Julius-Maximilians-University Würzburg, Emil-Fischer-Str. 42, 97074, Würzburg, Germany.

Abstract

The isolation of simple, fundamentally important, and highly reactive organometallic compounds remains among the most challenging tasks in synthetic chemistry. The detailed characterization of such compounds is key to the discovery of novel bonding scenarios and reactivity. The dimethylbismuth cation, $[BiMe_2(SbF_6)]$ (**1**), has been isolated and characterized. Its reaction with $BiMe_3$ gives access to an unprecedented dative bond, a Bi→Bi donor/acceptor interaction. The exchange of methyl groups (arguably the simplest hydrocarbon moiety) between different metal atoms is among the most principal types of reactions in organometallic chemistry. The reaction of **1** with $BiMe_3$ enables an S_E2(back) type methyl exchange, which is for the first time investigated in detail for isolable, (pseudo-)homoleptic main group compounds. Analytical techniques applied in this work include (VT) NMR and UV/vis spectroscopy, line shape analysis, single-crystal X-ray diffraction analyses, and (TD-)DFT calculations.

Introduction

Contributions towards a detailed and profound understanding of bonding interactions between heavier p-block elements have revived the field of main group chemistry in the last decades.[1-2] Great advances have been achieved in the rationalization of E–E multiple bonding, which may include mutual E→E (and E←E) donor-acceptor interactions (E = heavier main group element).[3-4] Generally, dative bonding in main group compounds has recently been investigated in great detail with experimental and theoretical approaches[5-6] and sometimes been discussed controversially.[7-8] For heavier main group species in particular, unusual E→E unidirectional donor-acceptor bonding has also been reported, where one atom E only serves as a donor while the other atom E only acts as an acceptor (*vide infra*).[9-16]

E–E bonding interactions tend to become weaker with an increasing principal quantum number of E, because the relevant atomic orbitals become larger and more diffuse. In this respect, the investigation of species with bonding interactions between bismuth (the heaviest element without significant radioactivity) is especially challenging. While the first species with a Bi–Bi single bond, $Me_2Bi–BiMe_2$ (**A**), was generated as early as 1935,[17] its isolation and detailed re-investigation was achieved only about 50 years later (Figure 1a).[18-19] Following these pioneering contributions, different types of compounds featuring Bi–Bi multiple bonds have

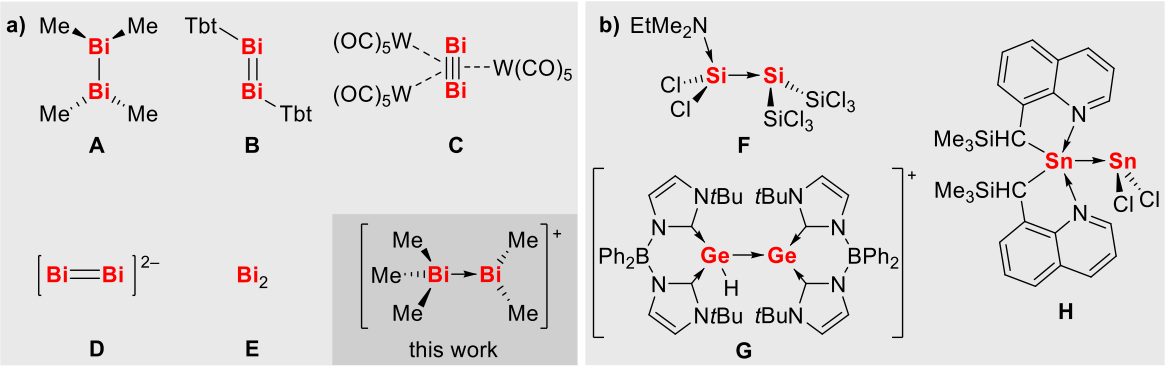

Figure 1. Compounds with a) different types of bismuth-bismuth bonding and b) unidirectional E→E bonding (positive charge in **G** is balanced by $[B(C_6F_5)_4]^-$).

been reported more recently. These include dibismuthenes such as the pivotal TbtBi=BiTbt (**B**) (Tbt = 2,4,6-$[CH(SiMe_3)_2]_3$-C_6H_2),[20] Bi_2 units in the coordination sphere of transition metals (as in $Bi_2(W(CO)_5)_3$ (**C**)),[21] $[K(222\text{-crypt})]_2[Bi_2]$ containing naked $[Bi_2]^{2-}$ anions (**D**),[22] and free Bi_2 (**E**), which has been generated and analyzed in the gas phase and in noble gas matrices (Figure 1a).[23]

In contrast, compounds featuring unidirectional Bi→Bi donor/acceptor interactions have not been reported to date. Unsupported E→E bonding has recently been documented, for instance, in

the low-valent silicon(II), germanium(II), and tin(II) compounds $[Me_2EtN{\rightarrow}SiCl_2{\rightarrow}Si(SiCl_3)_2]$ (**F**), $[R^BHGe{\rightarrow}GeR^B]^+$ (**G**), and $[R^N{}_2Sn{\rightarrow}SnCl_2]$ (**H**), in which the central atoms bear one lone pair and one empty p-orbital (R^B = *bis*(NHC)borate, R^N = $CH(SiMe_3)(C_9H_6N\text{-}8)$; Figure 1b).[9-11,25] In the chemistry of group 15 compounds, unidirectional E→E bonding can be realized by combining a cationic complex fragment $[PnR_2]^+$, which contains one empty p-orbital at Pn, with a trivalent species PnR_3, which bears one lone pair at Pn (Pn = P-Bi).[12-16,24] In fact, E→E bonding has been achieved for all group 15 elements but bismuth.[14] So why is the generation of E→E dative bonding especially challenging in the case of the heaviest congener? On the one hand, the accessibility of (e.g. nitrogen- and aryl-substituted) bismuth cations is well-documented,[26] and they have recently been established as potent soft Lewis-acids.[27] On the other hand, $[BiR_2]^+$ cations without excessive steric stabilization or considerable Bi···anion bonding remain elusive.[26] In addition, compounds of type BiR_3 are poor donors due to the inert pair effect and relativistic effects.[28] Further complications may arise from bismuth compounds being susceptible to ligand scrambling, which may lead to mixtures of compounds, when targeting species of type $R_3Bi{\rightarrow}BiR'_2$.[29]

Herein, we report the first example of a mononuclear alkylbismuth cation, $[BiMe_2(SbF_6)]$, and its reactivity towards $BiMe_3$, revealing unprecedented donor/acceptor interactions and unconventional methyl exchange.

Results and discussion

Reaction of $BiMe_2Cl$ with $AgSbF_6$ in dichloromethane (DCM) gave $[BiMe_2(SbF_6)]$ (**1**) after workup as a yellow, light-sensitive crystalline material in 75% yield (Figure 2a). Solution NMR spectroscopic analyses revealed one singlet in the ^1H (δ = 2.28 ppm) and the ^{13}C NMR spectrum (δ = 64.4 ppm), respectively. Compared to the neutral parent compound $BiMe_3$, these resonances experience a dramatic down-field shift of $\Delta\delta$ = +1.17 ppm (^1H) and $\Delta\delta$ = +71.2 ppm (^{13}C), which reflects the electron-deficient nature of **1**. The light-sensitivity of **1** prompted us to perform UV/vis spectroscopic analyses. In DCM solution, a broad absorption band with its maximum at 321 nm was observed, which stretches well into the visible region of λ > 400 nm (Supp. Inf.).

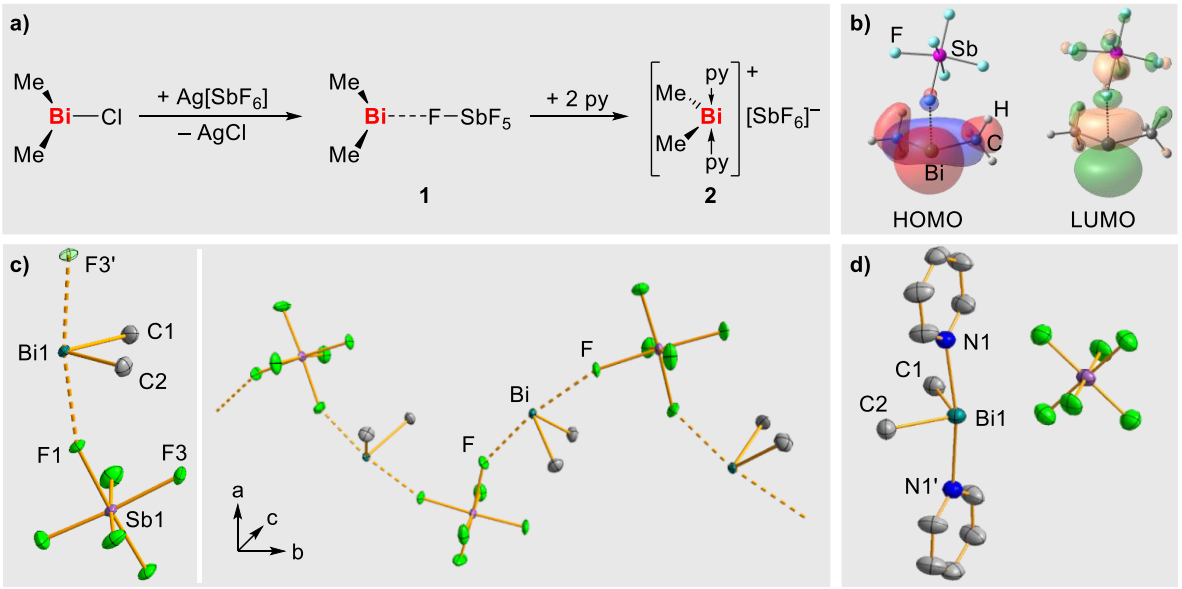

Figure 2. a) Synthesis of **1** and **2**. b) Frontier orbitals of **1** at isovalues of 0.04, as determined by DFT calculations. c) Molecular structure of $[BiMe_2(SbF_6)]$ (**1**) in the solid state. Left: cutout of coordination polymer, F3' exceeds one formula unit and is shown as a transparent ellipsoid. Right: arrangement of **1** as a coordination polymer in the solid state. Displacement ellipsoids are shown at the 50% probability level. Hydrogen atoms are omitted for clarity. Selected bond lengths (Å) and angles (°): Bi1–C1, 2.215(5); Bi1–C2, 2.223(5); Bi1–F1, 2.451(3); Bi1–F3', 2.452(3); C1–Bi1–C2, 93.0(2); F1–Bi1–F3', 169.73(11). d) Molecular structure of $[BiMe_2(py)_2][SbF_6]$ (**2**) in the solid state. Displacement ellipsoids are shown at the 50% probability level. Bi1–C1, 2.235(12); Bi1–C2, 2.223(12); Bi1–N1, 2.519(7); C1–Bi1–C2, 92.3(5); N1–Bi1–N1', 169.1(3).

In good agreement with these data, CAM-B3LYP-based calculations revealed a first electronically excited state (S_1) with dominant contributions by a HOMO→LUMO transition (72%) at λ_{calc} = 333 nm. The HOMO is associated with the occupied in-plane bismuth p-orbital, which is partially delocalized into the Bi–C σ bonds, while the LUMO is represented by an empty bismuth-centered p-orbital (Figure 2b). Geometry optimization of the S_1 state leads to a separation of the $BiMe_2^+$ and the SbF_6^- moieties, as a consequence of populating the bismuth p-orbital oriented along the Bi–F axis. In congruency with these findings, coordination of pyridine to $[BiMe_2]^+$ blocks this transition, leading to the colorless compound $[BiMe_2(py)_2][SbF_6]$ (**2**), which was isolated in 84% yield and fully characterized (Figure 2a, py = pyridine).

Single-crystal X-ray diffraction analysis of **1** revealed the formation of a contact ion pair in the solid state with Bi···F distances of 2.45 Å (Figure 2c, orthorhombic space group *Pbca* with Z = 8). Each $[BiMe_2]^+$ unit interacts with two fluorine atoms of neighboring $[SbF_6]^-$ moieties, leading to a one-dimensional coordination polymer along the crystallographic b-axis in the solid state (Figure 2c, right). The bismuth atom adopts a bisphenoidal coordination geometry with the fluorine atoms in axial (F–Bi–F, 169.7°) and the carbon atoms in equatorial positions (C–Bi–C, 93.0°). The Bi–C bonds (2.22 Å) are shorter than those in neutral $BiMe_3$ (2.23-2.29 Å) or in the trinuclear complex

$[(BiMe_2)_3(Tm^{tBu})_2]^+$ (2.24-2.27 Å; Tm^{tBu} = hydro*tris*(2-mercapto-1-*tert*-butylimidazolyl)borate),[30,31] and marginally shorter than those in **2** (2.22-2.24 Å) (Figure 2d). Compounds **1** and **2** are the first examples of well-defined mononuclear cationic bismuth alkyl complexes.

The soft Lewis acidic nature of compound **1**, the absence of neutral donor ligands, and its lack of steric (over-)protection prompted us to investigate its behavior towards the potential soft Lewis base $BiMe_3$, thereby targeting the formation of the hitherto unknown Bi→Bi donor/acceptor bond. Reaction of **1** with $BiMe_3$ in DCM gave pale yellow solutions, from which light yellow crystals of the composition $[BiMe_2(BiMe_3)(SbF_6)]$ (**3**) were isolated in 88% yield (Figure 3a). UV/vis spectroscopy in DCM solution revealed a broad absorption band peaking at 302 nm and reaching slightly into the visible region of λ > 400 nm (Supp. Inf.). Based on TD-DFT calculations and the natural transition orbital (NTO) analysis using CAM-B3LYP, the $S_0 \rightarrow S_1$ excitation (λ_{calc} = 289 nm) was ascribed to an n(Bi2)→σ^*(Bi1–Bi2) transition with additional σ(Bi2–Me)→σ^*(Bi1–Bi2) contributions (Figure 3b and Supp. Inf.). In line with these results, geometry optimization of the S_1 state leads to dissociation of the Bi–Bi bond as a consequence of populating the σ*(Bi1–Bi2) orbital.

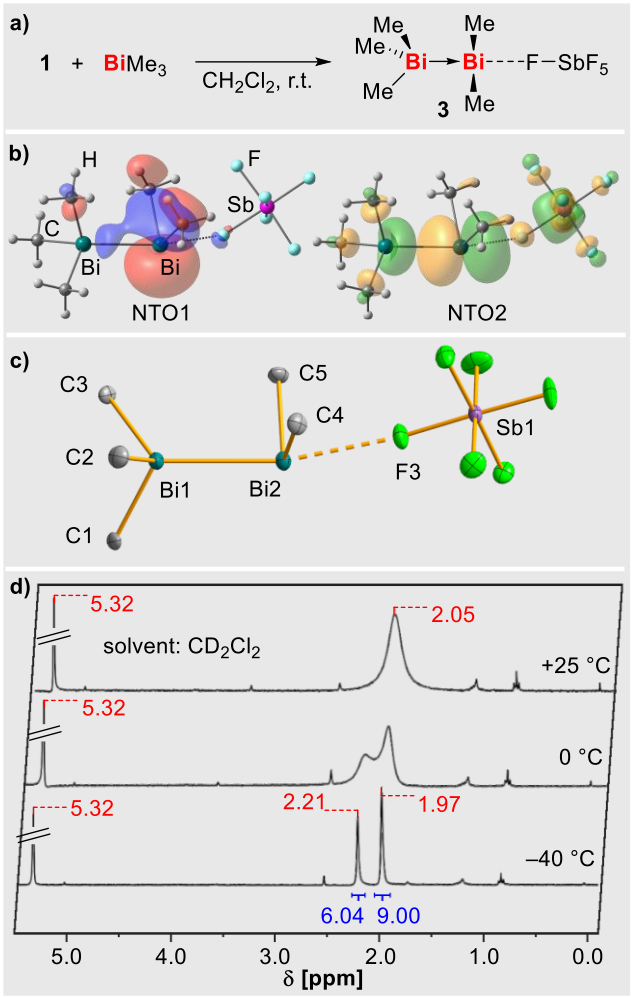

Figure 3. a) Synthesis of $[BiMe_2(BiMe_3)(SbF_6)]$ (**3**). b) Natural transition orbitals of the $S_0 \rightarrow S_1$ excitation of **3** at isovalues of 0.04, as determined by (TD-)DFT calculations. c) Molecular structure of **3** in the solid state. Displacement ellipsoids are shown at the 50% probability level. Hydrogen atoms are omitted for clarity. Selected bond lengths (Å) and angles (°): Bi1–C1, 2.219(18); Bi1–C2, 2.21(2); Bi1–C3, 2.223(18); Bi2–C4, 2.24(2); Bi2–C5, 2.24(2); Bi1–Bi2, 3.0005(11); Bi2···F3, 2.809; C1–Bi1–C2, 97.7(7); C2–Bi1–C3, 103.1(8); C1–Bi1–C3, 101.6(7); C4–Bi2–C5, 94.2(8). d) ^{1}H VT-NMR spectra of **3** in CD_2Cl_2; red (blue) numbers indicate chemical shift (integrals) of the respective signals.

Single-crystal X-ray diffraction analysis of compound **3** unambiguously confirmed the formation of an adduct between $BiMe_3$ and $[BiMe_2(SbF_6)]$ (Figure 3c, monoclinic space group $P2_1/c$, $Z = 4$). The Bi→Bi bond length amounts to the remarkably small value of only 3.00 Å. This is well within the range of Bi–Bi bond lengths that have been reported for dibismuthanes with unsupported, covalent Bi–Bi single bonds, such as Bi_2Et_4, Bi_2Ph_4, and Bi_2Mes_4 (2.98-3.09 Å).[32-34] All Bi–C bond lengths are in the range of 2.21-2.24 Å, ranging between those reported for the single components of this compound (i.e. **1** and $BiMe_3$). Both bismuth atoms in **3** show a coordination number of four. Bi1 shows a distorted tetrahedral coordination geometry. This is

unusual for bismuth^{III} main group compounds,[35-37] in which the bismuth center commonly acts as a Lewis acid resulting in bisphenoidal coordination geometries. $BiMe_3$ in particular has so far only been coordinated as a donor to transition metal complex fragments in $[M(CO)_5(BiMe_3)]$ (M = Cr, W).[28] The angle sums C–Bi–C in these compounds (297.0-298.7°) are larger than in non-coordinate $BiMe_3$ (276.6°), but even larger in compound **3** (302.4°), suggesting a remarkably large degree of hybridization between 6s and 6p bismuth atomic orbitals in the $BiMe_3$ unit of **3**. The Bi2 atom in **3** shows the expected bisphenoidal coordination geometry with $[SbF_6]^-$ (Bi–F, 2.809 Å) and $BiMe_3$ in the axial positions. In line with these results, natural bond orbital (NBO) analyses of **3** reveal an unusually large hybridization between the 6s and 6p orbitals in Bi1 to give a hybrid orbital with 37% s- and 63% p-character (atom labeling is as in Figure 3). This occupied hybrid orbital of Bi1 and a vacant ("non-hybridized") p-orbital of Bi2 form the Bi→Bi donor-acceptor interaction, which is strongly polarized towards Bi1 (localization at Bi1: 79%). A Wiberg bond index (WBI) of 0.52 is associated with this Bi→Bi interaction, which is reasonably large compared to the WBIs of 0.24 that were found for the dative N→Bi interactions in **2** (a WBI of 0.95 is obtained for the regular Bi–Bi single bond in $Me_2Bi–BiMe_2$). The description of the Bi–Bi interaction in **3** as a Bi→Bi dative bond is further corroborated by the intrinsic bond orbital (IBO) analysis and the energy decomposition analysis combined with the natural orbitals for chemical valence (EDA-NOCV) method, the latter excluding the electron-sharing bond scenario due to its larger orbital interaction (ΔE_{orb}) component in comparison to that obtained for a Bi→Bi dative bond (Supp. Inf.). Furthermore, inspection of the NOCV deformation densities reveals that ΔE_{orb} is dominated by σ donation from Bi1 to Bi2 ($\Delta E_{orb\text{-}\sigma}$ = –29.9 kcal mol^{-1}, 87% of ΔE_{orb}), and accounts for ca. 50% of all stabilizing contributions between the $BiMe_3$ and $[BiMe_2][SbF_6]$ fragments in **3**.

^{1}H NMR spectroscopic analysis of **3** in CD_2Cl_2 at 25 °C gave one broad resonance (FWHM = 42 Hz) for all five methyl groups of the compound (Figure 3d (top)). Cooling led to gradual sharpening of the resonances. A coalescence temperature of 16 °C was determined, and splitting of the broad resonance into two sharp signals with an intensity ratio of 2:3 was observed at –40 °C with chemical shifts of δ = 1.97 (9H) and 2.21 (6H) ppm. In line with the ^{1}H NMR data, the ^{13}C NMR spectrum at –40 °C shows two resonances at δ = 26.1 ($BiMe_3$) and 73.5 ($BiMe_2$). That is, the ^{13}C NMR chemical shifts in **3** experience a considerable to strong down-field shift in the case of the $BiMe_2$ group ($\Delta\delta$ = 9.1 ppm) and the $BiMe_3$ moiety ($\Delta\delta$ = 32.9 ppm), when compared to those of compounds **1** and free $BiMe_3$, respectively. These findings demonstrate that at low temperature in solution, **3** shows a quasi-static bonding situation as indicated by the Lewis formula in Figure 3a with a Bi→Bi bonding interaction. At ambient temperature in solution, however, all methyl groups of compound **3** exchange rapidly on the time scale of the NMR spectroscopic experiment. The VT NMR spectroscopic data were subjected to line-shape analysis, revealing activation parameters of $\Delta H^{\ddagger}$ = 8.5 kcal·mol^{-1}, $\Delta S^{\ddagger}$ = –16.7 cal·mol^{-1}, $\Delta G^{\ddagger}(298\ K)$ = 13.5 kcal·mol^{-1}, and

k (298 K) = 1010 s^{-1} (Supp. Inf.). These results may be compared to bonding situations in lighter group 15 homologs of compound **3**. [Me_3P–PMe_2][OTf] and related species are stable in solution, where they show a static bonding situation without exchange reactions at room temperature.[15-16] Compounds such as [$PhMe_2As$–AsPhMe][OTf] are stable in solution, but the exchange of $AsPhMe_2$ ligands (without exchange of the hydrocarbon ligands) takes place at room temperature in solution.[12] [Me_3Sb–$SbMe_2$][$SbMe_2Br_2$] has been structurally characterized in the solid state, but decomposes into mixtures of mononuclear starting materials in solution, so that characteristic spectroscopic features in solution have not been reported.[13] Similarly, the structure of [$(Me_2Sb)_3$][$SbMe_2Br_2$] has been reported not to be preserved in solution.[38] Compound [Me_3Sb–$SbMe_2$][$GaCl_4$] was obtained in very small amounts and not as a pure substance, which complicated its detailed spectroscopic characterization.[39] Thus, the heaviest congener of this series, [$BiMe_2(BiMe_3)(SbF_6)$] (**3**), shows a remarkable combination of being sufficiently stable in solution due to the pronounced and soft Lewis acidity of cationic bismuth species[26-27] such as $[BiMe_2]^+$ and a dynamic bonding situation due to rapid methyl exchange reactions in solution.

Methyl exchange reactions in organometallic main group species have been reported in some detail for compounds such as $(AlMe_3)_2$, for its Lewis base adducts, and for its mixtures with other organometallic compounds such as $GaMe_3$, $InMe_3$, $ZnMe_2$, and LiMe.[40-46] Intra- as well as intermolecular exchange mechanisms have been discussed, sometimes controversially, as in the case of $(AlMe_3)_2$. We performed DFT calculations in order to elucidate the mechanism of methyl exchange in compound **3** (Figure 4a). A reaction pathway with an sp^3-hybridized methyl group bridging two cationic bismuth centers (reminiscent of methyl exchange discussed for compounds such as Al_2Me_6) was first considered (Figure 4a and SI). Surprisingly, a local minimum structure **4** with a three-membered Bi_2C ring as a key structural motif was located on the potential energy surface (PES). According to the IBO analysis, the Bi–(μ_2-sp^3-CH_3)–Bi motif can be described as a three-center-two-electron bond with Bi–C (2×) and Bi–Bi bonding interactions (Supp. Inf.). However, the free energy, ΔG, for the reaction **3** → **4** is +20.7 kcal·mol^{-1}. This value does not yet include an (expectedly small) kinetic barrier and is thus unlikely to solely account for the experimentally observed process. Alternatively, Bi→Bi bond dissociation was considered as the initiating step of the methyl exchange reaction. This bond scission proceeds barrierless to give the starting materials **1** and $BiMe_3$ in a slightly endergonic reaction (ΔG = +1.9 kcal·mol^{-1}). While an electrophilic attack of **1** at the bismuth-centered lone pair of $BiMe_3$ regenerates the adduct **3**, an electrophilic attack of **1** at the methyl group of $BiMe_3$ was also considered. It proceeds via a van der Waals intermediate **5** located 6.9 kcal·mol^{-1} above **3**, with the corresponding transition state (**TS1**) lying 14.2 kcal·mol^{-1} above **3**. These results are in excellent agreement with the experimentally determined value of $\Delta G^{\ddagger}$*(298 K)* = 13.5 kcal·mol^{-1},

and the associative character of the reaction **1** + $BiMe_3$ → **5** → **TS1** is in congruency with the negative activation entropy delineated from line-shape analyses ($\Delta S^{\ddagger}$ = –16.7 cal·mol^{-1}).

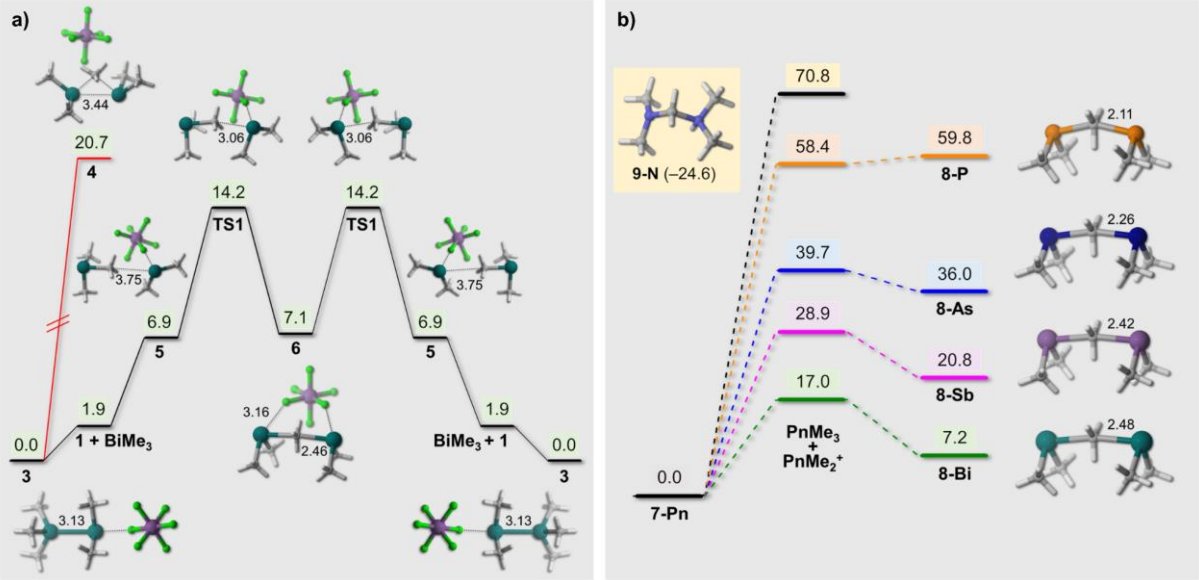

Figure 4. a) Free energy (ΔG) profile of the proposed methyl exchange reaction mechanism of **3**. Disfavored reaction pathway is shown in red. Selected calculated interatomic distances are given in Å. b) Free energies (ΔG) of reactions **7-Pn** → $PnMe_3$ + $PnMe_2^+$ and $PnMe_3$ + $PnMe_2^+$ → **8-Pn** (Pn = N-Bi). All ΔG values (kcal·mol^{-1}) are given with respect to the corresponding **7-Pn** compounds. The structure of **9-N** and the free energy of reaction **7-N** → **9-N** is also shown. Calculated Pn–(sp^2 CH_3) bond lengths are given in Å.

Remarkably, the resulting compound **6** was identified as a local minimum on the PES. It shows an sp^2-hybridized methyl group with a coordination number of five, which is best described as a methyl anion according to its natural charge of –1.20, bridging two bismuth atoms in a (quasi-)linear Bi–(μ_2-sp^2-CH_3)–Bi structural motif. Accordingly, NBO and IBO calculations on **6** indicate a Bi–(μ_2-sp^2-CH_3)–Bi three-center-two-electron bond and a lone pair at each bismuth center, which leads to a closed-shell singlet system with a calculated HOMO–LUMO gap of ca. 4.28 eV (Supp. Inf.). The reaction **3** → **6** is endergonic by only 7.1 kcal·mol^{-1}. Our findings suggest that the exchange of methyl groups between the two bismuth atoms in **1** proceeds via a species featuring an unusual methyl anion with an sp^2-hybridized carbon atom bridging two Bi centers. These findings are in agreement with the previously calculated low inversion barrier of the methyl anion (1.50 kcal·mol^{-1})[47] and demonstrate its practical relevance in methyl anion exchange reactions of organometallic p-block compounds. The methyl exchange reaction

$$BiMe_2SbF_6 + BiMe_2\mathbf{Me^*} \rightarrow \mathbf{6} \rightarrow BiMe\mathbf{Me^*}SbF_6 + BiMe_3 \quad \text{(eq. 1)}$$

corresponds to a bimolecular electrophilic substitution reaction (S_E2 (back)), i.e. the electrophilic analog of the well-known nucleophilic S_N2 substitution reaction in organic chemistry. Methyl exchange along this pathway has rarely been discussed to date, but has been suggested or shown for heterobimetallic systems of transition metal compounds such as "Hg^{2+} +

[$Co(dmg)_2Me(H_2O)$]", "[$PtMe_2$(dmpe)] + [$M(PMe_3)]^+$" (dmg = dimethylglyoxime, dmpe = bis(dimethylphosphino)ethane, M = Cu, Au)[48-52] and for hypothetical systems such as [$Li_2Me]^+$ (based on theoretical investigations).[53-54] To the best of the authors' knowledge, the relevance of backside S_E2-type methyl exchange is now for the first time demonstrated for a simple, isolable, (pseudo-)homoleptic, and homometallic compound. The isolation of compounds featuring Al–(μ_2-sp^2-CH_3)–Al structural motifs suggests that this may well be a more general phenomenon.[55-57]

In order to investigate the role of the pnictogen atom in the methyl exchange reactions presented here, compounds [$Pn_2Me_5]^+$ (**7-Pn**) were investigated by DFT calculations (Pn = N-Bi; Figure 4b). The bond dissociation energies associated with the reactions **7-Pn** → $PnMe_3$ + $PnMe_2^+$ constantly decrease, when going down the group from N (ΔG = 70.8 kcal·mol^{-1}) to Bi (ΔG = 17.0 kcal·mol^{-1}). For Pn = N, a compound of type Me_2Pn–(μ_2-sp^2-CH_3)–$PnMe_2^+$ (**8-Pn**) could not be located as an energy minimum on the PES and the migration of a proton from the bridging methyl group to a nitrogen atom was observed instead to give compound **9-N**. Compound **8-P** corresponds to a saddle point on the PES and is slightly higher in energy than the dissociated species PMe_3 + PMe_2^+. Only for the elements Pn = As-Bi, the reactions $PnMe_3$ + $PnMe_2^+$ → **8-Pn** are exergonic (ΔG = –3.7 (As), –8.1 (Sb), –9.8 (Bi) kcal·mol^{-1}). Thus, the electrophilic attack of cationic pnictogen atoms at a methyl group is most favorable for complexes of the heaviest element bismuth. These results also shed light on the role of the counteranion in methyl exchange reactions. Expectedly, the dissociation of **7-Bi** (without a counteranion) to give $BiMe_2^+$ and $BiMe_3$ is more endergonic than the analogous reaction of **3** (with an SbF_6^- counteranion). As a consequence, the re-association of $BiMe_2^+$ and $BiMe_3$ to give compound **8-Bi** is exergonic by –9.8 kcal·mol^{-1}, while the corresponding reaction with an SbF_6^- counteranion (i.e. **1** + $BiMe_3$ → **6**) is endergonic. This suggests that compounds with a (quasi-)linear Bi–(μ_2-sp^2-CH_3)–Bi structural motif may be isolable, if suitable substitution patterns and sufficiently weakly coordinating counteranions can be identified.

Conclusions

In summary, [$BiMe_2(SbF_6)$] (**1**) has been synthesized, isolated, and fully characterized and represents the first example of a mononuclear dialkyl bismuth cation. Reaction of **1** with $BiMe_3$ gives [$BiMe_2(BiMe_3)(SbF_6)$] (**3**) featuring the unprecedented structural motif of a Bi^{III}→Bi^{III} donor-acceptor interaction. Methyl exchange in **3** is rapid at room temperature in solution and is suggested to proceed via an initial Bi→Bi bond dissociation followed by formation of an intermediate with a trigonal planar (sp^2-hybridized) methyl anion. This corresponds to an S_E2 (back) mechanism, which has been described for heterobimetallic late transition metal

complexes, but rarely been considered or even been pinpointed as a concept for methyl exchange in main group chemistry to date and may be more common than previously anticipated. These findings highlight the unusual properties of cationic bismuth species as Lewis acids, which we aim to exploit in future synthetic applications.

References

1. Power, P. P. Main-group elements as transition metals. *Nature* **463**, 171-177 (2010).

2. Weetman, C. & Inoue, S. The Road Travelled: After Main-Group Elements as Transition Metals. *ChemCatChem* **10**, 4213-4228 (2018).

3. Fischer, R. C. & Power, P. P. π-Bonding and the Lone Pair Effect in Multiple Bonds Involving Heavier Main Group Elements: Developments in the New Millennium. *Chem. Rev.* **110**, 3877-3923 (2010).

4. Power, P. P. An Update on Multiple Bonding between Heavier Main Group Elements: The Importance of Pauli Repulsion, Charge-Shift Character, and London Dispersion Force Effects. *Organometallics* (2020).

5. Zhao, L., Hermann, M., Holzmann, N. & Frenking, G. Dative bonding in main group compounds. *Coord. Chem. Rev.* **344**, 163-204 (2017).

6. Haaland, A. Covalent versus Dative Bonds to Main Group Metals, a Useful Distinction. *Angew. Chem. Int. Ed.* **28**, 992-1007 (1989).

7. Frenking, G. Dative Bonds in Main-Group Compounds: A Case for More Arrows! *Angew. Chem. Int. Ed.* **53**, 6040-6046 (2014).

8. Himmel, D., Krossing, I. & Schnepf, A. Dative Bonds in Main-Group Compounds: A Case for Fewer Arrows! *Angew. Chem. Int. Ed.* **53**, 370-374 (2014).

9. Schweizer, J. I., Scheibel, M. G., Diefenbach, M., Neumeyer, F., Würtele, C., Kulminskaya, N., Linser, R., Auner, N., Schneider, S. & Holthausen, M. C. A Disilene Base Adduct with a Dative Si–Si Single Bond. *Angew. Chem. Int. Ed.* **55**, 1782-1786 (2016).

10. Leung, W.-P., Kwok, W.-H., Xue, F. & Mak, T. C. W. Synthesis and Crystal Structure of an Unprecedented Tin(II)−Tin(II) Donor−Acceptor Complex, $R^{N2}Sn{\rightarrow}SnCl_2$ [R^N = $CH(SiMe_3)C_9H_6N$-8]. *J. Am. Chem. Soc.* **119**, 1145-1146 (1997).

11. Xiong, Y., Szilvási, T., Yao, S., Tan, G. & Driess, M. Synthesis and Unexpected Reactivity of Germyliumylidene Hydride $[:GeH]^+$ Stabilized by a Bis(N-heterocyclic carbene)borate Ligand. *J. Am. Chem. Soc.* **136**, 11300-11303 (2014).

12. Kilah, N. L., Weir, M. L. & Wild, S. B. Tertiary arsine-stabilised arsenium salts: syntheses and comparisons with phosphine analogues. *Dalton Trans.*, 2480-2486 (2008).

13. Althaus, H., J. Breunig, H. & Lork, E. Crystal structure of $[Me_3Sb–SbMe_2]_2[(MeSbBr_3)_2]$, a trimethylstibine adduct of the dimethylstibenium ion or a stibinostibonium salt? *Chem. Commun.*, 1971-1972 (1999).

14. Robertson, A. P. M., Gray, P. A. & Burford, N. Interpnictogen Cations: Exploring New Vistas in Coordination Chemistry. *Angew. Chem. Int. Ed.* **53**, 6050-6069 (2014).

15. Weigand, J. J., Riegel, S. D., Burford, N. & Decken, A. Prototypical Phosphorus Analogues of Ethane: General and Versatile Synthetic Approaches to Hexaalkylated P–P Diphosphonium Cations. *J. Am. Chem. Soc.* **129**, 7969-7976 (2007).

16. Chitnis, S. S., MacDonald, E., Burford, N., Werner-Zwanziger, U. & McDonald, R. P–P Menschutkin preparation of prototypical phosphinophosphonium salts. *Chem. Commun.* **48**, 7359-7361 (2012).

17. Paneth, F. A. & Loleit, H. 81. Free organic radicals in the gaseous state. Part IV. Synthesis of antimony cacodyl and related substances by the use of free methyl and free ethyl. *J. Chem. Soc.*, 366-371 (1935).

18. Ashe, A. J. & Ludwig, E. G. A reinvestigation of Paneth's violet compound. The synthesis of tetramethyldibismuthine. *Organometallics* **1**, 1408-1408 (1982).

19. Ashe III, A. J., Ludwig, E. G. & Oleksyszyn, J. Preparation and properties of dibismuthines. *Organometallics* **2**, 1859-1866 (1983).

20. Tokitoh, N., Arai, Y., Okazaki, R. & Nagase, S. Synthesis and Characterization of a Stable Dibismuthene: Evidence for a Bi-Bi Double Bond. *Science* **277**, 78-80 (1997).

21. Huttner, G., Weber, U. & Zsolnai, L. Bi_2, the Bismuth Homologue of Dinitrogen as a Ligand in $Bi_2[W(CO)_5]_3$. *Z. Naturforsch.* **37b**, 707-710 (1982).

22. Xu, L., Bobev, S., El-Bahraoui, J. & Sevov, S. C. A Naked Diatomic Molecule of Bismuth, $[Bi_2]^{2-}$, with a Short Bi–Bi Bond: Synthesis and Structure. *J. Am. Chem. Soc.* **122**, 1838-1839 (2000).

23. Eberle, B., Sontag, H. & Weber, R. Optical spectroscopy of bismuth clusters isolated in rare-gas matrices. *Chem. Phys.* **92**, 417-422 (1985).

24. Chitnis, S. S., Robertson, A. P. M., Burford, N., Patrick, B. O., McDonald, R. & Ferguson, M. J. Bipyridine complexes of E^{3+} (E = P, As, Sb, Bi): strong Lewis acids, sources of $E(OTf)_3$ and synthons for EI and EV cations. *Chem. Sci.* **6**, 6545-6555 (2015).

25. Hill, M. S., Hitchcock, P. B. & Pongtavornpinyo, R. Dimerization of Indanediyl Fragments: An Alkene Analogue for Group 13? *Angew. Chem. Int. Ed.* **44**, 4231-4235 (2005).

26. Lichtenberg, C. Molecular Bismuth(III) Monocations: Structure, Bonding, Reactivity, and Catalysis. *Chem. Commun.* (2021).

27. Ramler, J. & Lichtenberg, C. Molecular Bismuth Cations: Assessment of Soft Lewis Acidity. *Chem. Eur. J.* **26**, 10250-10258 (2020).

28. Breunig, H. J., Borrmann, T., Lork, E., Moldovan, O., Raț, C. I. & Wagner, R. P. Syntheses, crystal structures and DFT studies of $[Me_3EM(CO)_5]$ (E=Sb, Bi; M=Cr, W), *cis*-$[(Me_3Sb)_2Mo(CO)_4]$, and $[t Bu_3BiFe(CO)_4]$. *J. Organomet. Chem.* **694**, 427-432 (2009).

29. Louis-Goff, T., Rheingold, A. L. & Hyvl, J. Investigation into the Organobismuth Dismutation and Its Use for Rational Synthesis of Heteroleptic Triarylbismuthanes, $Ar^1{}^2Ar^2Bi$. *Organometallics* **39**, 778-782 (2020).

30. Bao, M., Hayashi, T. & Shimada, S. Synthesis and structural characterisation of a cationic trinuclear organobismuth complex with an unprecedented coordination mode of hydrotris(2-mercaptoimidazolyl)borate ligands. *Dalton Trans.*, 2055-2056 (2004).

31. Schulz, S., Kuczkowski, A., Bläser, D., Wölper, C., Jansen, G. & Haack, R. Solid-State Structures of Trialkylbismuthines BiR_3 (R = Me, *i*-Pr). *Organometallics* **32**, 5445-5450 (2013).

32. Calderazzo, F., Morvillo, A., Pelizzi, G. & Poli, R. Synthesis and crystal and molecular structure of tetraphenyldibismuthine, Bi_2Ph_4, the first crystallographically characterized tetraorganyl derivative of bismuth(II). *J. Chem. Soc., Chem. Commun.*, 507-508 (1983).

33. Balázs, L., Breunig, H. J. & Lork, E. Synthesis and Crystal Structure of Tetramesityldibismuthane. *Z. Naturforsch.* **60b**, 180-182 (2005).

34. Kuczkowski, A., Heimann, S., Weber, A., Schulz, S., Bläser, D. & Wölper, C. Structural Characterization of Et_4Sb_2 and Et_4Bi_2. *Organometallics* **30**, 4730-4735 (2011).

35. Kuczkowski, A., Fahrenholz, S., Schulz, S. & Nieger, M. Reactions of Distibines Sb_2R_4 and Dibismuthine Bi_2Et_4 with Trialkyltrieles MR_3. *Organometallics* **23**, 3615-3621 (2004).

36. Kuczkowski, A., Schulz, S. & Nieger, M. Synthesis, X-ray Crystal Structure, and Stability of Novel Trialkylalane−Triorganylbismuthane Adducts. *Eur. J. Inorg. Chem.* **2001**, 2605-2611 (2001).

37. Kuczkowski, A., Thomas, F., Schulz, S. & Nieger, M. Synthesis and X-ray Crystal Structures of Novel Al−Bi and Ga−Bi Compounds. *Organometallics* **19**, 5758-5762 (2000).

38. Breunig, H. J., Denker, M. & Lork, E. A Trinuclear Organoantimony Cation: Structure of $[Me_2Sb–Sb(Me_2)–SbMe_2][Me_2SbBr_2]$. *Angew. Chem. Int. Ed.* **35**, 1005-1006 (1996).

39. Hering, C., Lehmann, M., Schulz, A. & Villinger, A. Chlorine/Methyl Exchange Reactions in Silylated Aminostibanes: A New Route To Stibinostibonium Cations. *Inorg. Chem.* **51**, 8212-8224 (2012).

40. Muller, N. & Pritchard, D. E. Proton Magnetic Resonance Spectrum of Aluminum Trimethyl Dimer. *J. Am. Chem. Soc.* **82**, 248-249 (1960).

41. Laubengayer, A. W. & Gilliam, W. F. The Alkyls of the Third Group Elements. I. Vapor Phase Studies of the Alkyls of Aluminum, Gallium and Indium. *J. Am. Chem. Soc.* **63**, 477-479 (1941).

42. Poole, C. P., Swift, H. E. & Itzel, J. F. ^{27}Al Nuclear Magnetic Resonance of Trialkyl Aluminum Compounds. I. Room-Temperature Studies. *J. Chem. Phys.* **42**, 2576-2580 (1965).

43. Williams, K. C. & Brown, T. L. Organometallic Exchange Reactions. V. Proton Magnetic Resonance Study of Methyl Group Exchanges among the Trimethyl Derivatives of Group III. The Cage Effect in Organometallic Dissociations. *J. Am. Chem. Soc.* **88**, 5460-5465 (1966).

44. Smith, M. B. The monomer-dimer equilibria of liquid aluminum alkyls: IV. Triethylaluminum in mesitylene. *J. Organomet. Chem.* **46**, 211-217 (1972).

45. Brown, T. L. & Murrell, L. L. Methyl group exchanges in Lewis acid-base adducts of Group III trimethyl compounds. *J. Am. Chem. Soc.* **94**, 378-384 (1972).

46. Kieft, R. L. & Brown, T. L. ^{1}H and ^{7}Li NMR observations of exchange processes in alkyllithium-ate complexes. *J. Organomet. Chem.* **77**, 289-298 (1974).

47. Dykstra, C. E., Hereld, M., Lucchese, R. R., III, H. F. S. & Meyer, W. Molecular structure of the methyl anion CH^{-}_{3}. An investigation of the effects of electron correlation using the theory of self-consistent electron pairs (SCEP). *J. Chem. Phys.* **67**, 4071-4075 (1977).

48. Adin, A. & Espenson, J. H. De-alkylation reactions of alkylcobaloxime complexes with mercury(II). *J. Chem. Soc., Chem. Commun.*, 653-654 (1971).

49. Fritz, H. L., Espenson, J. H., Williams, D. A. & Molander, G. A. Inversion at carbon in the cleavage of cobalt-carbon bonds by mercuric ion. *J. Am. Chem. Soc.* **96**, 2378-2381 (1974).

50. Köbrich, G. Electrophilic Substitutions at Saturated Carbon Atoms. *Angew. Chem. Int. Ed.* **1**, 382-393 (1962).

51. Serra, D., Moret, M.-E. & Chen, P. Transmetalation of Methyl Groups Supported by PtII–AuI Bonds in the Gas Phase, in Silico, and in Solution. *J. Am. Chem. Soc.* **133**, 8914-8926 (2011).

52. Moret, M.-E., Serra, D., Bach, A. & Chen, P. Transmetalation Supported by a PtII–CuI Bond. *Angew. Chem. Int. Ed.* **49**, 2873-2877 (2010).

53. Jemmis, E. D., Chandrasekhar, J. & Schleyer, P. v. R. Stabilization of D_{3h} pentacoordinate carbonium ions. Linear three-center-two-electron bonds. Implications for aliphatic electrophilic substitution reactions. *J. Am. Chem. Soc.* **101**, 527-533 (1979).

54. Fernández, I., Uggerud, E. & Frenking, G. Stable Pentacoordinate Carbocations: Structure and Bonding. *Chem. Eur. J.* **13**, 8620-8626 (2007).

55. Ihara, E., Young, V. G. & Jordan, R. F. Cationic Aluminum Alkyl Complexes Incorporating Aminotroponiminate Ligands. *J. Am. Chem. Soc.* **120**, 8277-8278 (1998).

56. Stuhl, C., Maichle-Mössmer, C. & Anwander, R. Magnesium Stung by Nonclassical Scorpionate Ligands: Synthesis and Cone-Angle Calculations. *Chem. Eur. J.* **24**, 14254-14268 (2018).

57. Chen, E. Y. X. & Abboud, K. A. Unusual Weakly Coordinating Anion Reactivity in Metallocene Chemistry. Formation of Tantalocene Cation−Dinuclear Anion Pairs. *Organometallics* **19**, 5541-5543 (2000).

Methods

General considerations. All air- and moisture-sensitive manipulations were carried out using standard vacuum line Schlenk techniques or in gloveboxes containing an atmosphere of purified argon. Solvents were degassed and purified according to standard laboratory procedures.

[$BiMe_2SbF_6$] (1). A solution of $AgSbF_6$ (0.22 g, 0.63 mmol) in methylene chloride (DCM) (3 mL) was added to a solution of $BiMe_2Cl$ (0.17 g, 0.63 mmol) in DCM (2 mL). The precipitate was filtered off. All volatiles were removed from the yellow filtrate under reduced pressure to give a yellow powder, which was dried in vacuo. Yield: 0.22 g, 0.47 mmol, 75%.
^{1}H NMR (400 MHz, C_6D_6): δ = 1.47 (s, 6H, CH_3) ppm. **^{1}H NMR** (400 MHz, CD_2Cl_2): δ = 2.28 (s, 6H, CH_3) ppm. **^{13}C NMR** (101 MHz, C_6D_6): δ = 66.72 (br, CH_3) ppm. **^{13}C NMR** (101 MHz, CD_2Cl_2): δ = 64.38 (br, CH_3) ppm. **^{19}F NMR** (376 MHz, C_6D_6): δ = –123.02 (s, SbF_6) ppm. **^{19}F NMR** (376 MHz, CD_2Cl_2): δ = –128.44 (s, SbF_6) ppm. **Elemental analysis:** Anal. calc. for: $C_2H_6BiSbF_6$ (474.84 g/mol): C 5.06, H 1.27, found: C 5.45, H 1.40.

[$BiMe_2(py)_2$][SbF_6] (2). [$BiMe_2(SbF_6)$] (**1**) (85.6 mg, 0.18 mmol) was dissolved in DCM (2 mL), and pyridine (28.5 mg, 0.36 mmol, 30 µl) was added. The colorless solution was layered with *n*-pentane (2 mL). After 1 d at –30 °C a colorless crystalline solid had precipitated, was isolated by filtration, and dried in vacuo. Yield: 97 mg, 0.15 mmol, 84%.
^{1}H NMR (400 MHz, CD_2Cl_2): δ = 1.79 (s, 6H, CH_3), 7.60 (t, 4H, $^3J_{HH}$ = 6.92 Hz, H2/H6), 8.05 (t, 2H, $^3J_{HH}$ = 7.75 Hz, H4), 8.64 (d, 4H, $^3J_{HH}$ = 4.67 Hz, H3/H5) ppm. **^{13}C NMR** (125 MHz, CD_2Cl_2): δ = 33.86 (CH_3), 126.86 (s, C2/C6), 140.58 (s, C4), 149.75 (s, C3/C5) ppm. A signal for the $[SbF_6]^-$ anion in a ^{19}F NMR experiment could not be detected due to signal broadening. **Elemental analysis:** Anal. calc. for: $C_2H_6BiF_6Sb(C_5H_5N)_2$ (633.00 g/mol): C 22.77, H 2.55, N 4.43 found: C 22.96, H 2.32, N 4.77.

[$BiMe_2(BiMe_3)(SbF_6)$] (3). [$BiMe_2(SbF_6)$] (**1**) (20 mg, 42.2 µmol) was dissolved in DCM (2 mL) and a solution of $BiMe_3$ (11.2 mg, 42.2 µmol) in DCM (1 mL) was added. The light yellow solution was stored at –30 °C. After 1 d light yellow crystals were obtained, isolated by filtration, and dried in vacuo. Yield: 27 mg, 37.0 µmol, 88%.
^{1}H NMR (500 MHz, 298.15 K, CD_2Cl_2): δ = 2.05 (br, 15H, CH_3) ppm. **^{1}H NMR** (300 MHz, 298.15 K, CD_2Cl_2): δ = 2.05 (br, 15H, CH_3) ppm. **^{1}H NMR** (300 MHz, 233.15 K, CD_2Cl_2): δ = 1.97 (s, 9H, $Bi(CH_3)_3$), 2.21 (s, 6H, $Bi(CH_3)_2$) ppm. **^{13}C NMR** (126 MHz, 233.15 K, CD_2Cl_2): δ = 26.07 (s, CH_3), 73.46 (s, CH_3) ppm. **^{19}F NMR** (470 MHz, 233.15 K, CD_2Cl_2): δ = –124.39 (SbF_6) ppm. **Elemental analysis:** Anal. calc. for: $C_5H_{15}Bi_2F_6Sb$ (728.89 g/mol): C 8.24, H 2.07, found: C 8.39, H 1.89.

Computational details. DFT calculations were performed with the Gaussian 16, Revision B.01 program package[58] using the B3LYP[59-62] functional and the 6-311++G(d,p)[63,64] (H, C, F) and LanL2DZ/ECP[65] (Bi) basis sets. The D3 version of Grimme's dispersion model with the original D3 damping function was applied.[66] Frequency analyses of the reported structures showed no imaginary frequencies for minimum energy structures and only one imaginary frequency for transition states. In order to assess the connectivity between the obtained transition states and the corresponding intermediates, further geometry optimizations along the imaginary modes and additional intrinsic reaction coordinate (IRC)[67] calculations were performed. Thermodynamic parameters were calculated at a temperature of 298.15 K and a pressure of 1.00 atm. NBO analyses were performed using the program version NBO 7.[68,69] To investigate the role of the pnictogen atom in the methyl exchange reactions, $[Pn_2Me_5]^+$ (**7-Pn**), their bond dissociation to $PnMe_3$ + $PnMe_2^+$, and the $Me_2Pn–(\mu^2\text{-}sp^2\text{-}CH_3)–PnMe_2^+$ (**8-Pn**) systems were investigated using B3LYP-D3 and the 6-31G(d,p)[70,71] (H, C, N, P) and LANL2DZ/ECP (As, Sb, Bi) basis sets. All calculations, including geometry optimizations, were performed with the PCM[72] solvent model and dichloromethane (ε = 8.93) as solvent. A concentration correction of $\Delta G^{0\rightarrow *}$ = RTln(24.46) = 1.89 kcal mol^{-1} (T = 298.15 K) was added to the free energies of all calculated species to change the 1.00 atm gas phase values to the condensed phase standard state concentration of 1 M, which leads to a proper description of associative/dissociative steps.[73] TD-DFT calculations were performed using the CAM-B3LYP[74] functional at the B3LYP optimized geometries. For **3**, the $S_0 \rightarrow S_1$ vertical excitation was analyzed using the natural transition orbitals (NTO)[75] method. Finally, the bonding situation of selected systems was investigated using the intrinsic bond orbital (IBO)[76] and the energy decomposition analysis based on natural orbitals for chemical valence (EDA-NOCV)[77] methods. The EDA-NOCV calculations on **3** were done considering two distinct scenarios, where the Bi–Bi bond was described either as electron-sharing or donor-acceptor interaction. These investigations, which were performed using the ADF 2019 software,[78] were conducted at the B3LYP-D3/QZ4P level, with relativistic effects considered using the zeroth order regular approximation (ZORA) method.[79,80]

Data availability

The data supporting the findings of this study are available within the paper and its Supplementary Information files.

Acknowledgements

Funding through the FCI, DFG (LI 2860/3-1, LI 2860/5-1), and DECHEMA is gratefully acknowledged. F. F. thanks the Coordenação de Aperfeiçoamento de Pessoal de Nível Superior (CAPES) and the Alexander von Humboldt (AvH) Foundation for a Capes-Humboldt postdoctoral fellowship.

Author contributions

J. R. performed the main experimental work. F. G. contributed to the synthesis of Lewis base adducts of **1**. A. H. contributed to single-crystal X-ray analyses. J. R. and C. L. contributed to theoretical analysis. F. F. performed main parts of the theoretical analyses. C. L. conceived, oversaw, and directed the project. J. R., F. F. and C. L. prepared the manuscript. All authors discussed the results and commented on the manuscript.

Competing interests

The authors declare no competing interests.

References

58. Frisch, M. J. *et al. Gaussian 16, Revision B.01*. (Gaussian, Inc., 2016).
59. Vosko, S. H., Wilk, L. & Nusair, M. Accurate spin-dependent electron liquid correlation energies for local spin density calculations: a critical analysis. *Can. J. Phys.* **58**, 1200–1211 (1980).
60. Lee, C., Yang, W. & Parr, R. G. Development of the Colle-Salvetti correlation-energy formula into a functional of the electron density. *Phys. Rev. B* **37**, 785–789 (1988).
61. Becke, A. D. Density-functional thermochemistry. III. The role of exact exchange. *J. Chem. Phys.* **98**, 5648–5652 (1993).
62. Stephens, P. J., Devlin, F. J., Chabalowski, C. F. & Frisch, M. J. Ab Initio Calculation of Vibrational Absorption and Circular Dichroism Spectra Using Density Functional Force Fields. *J. Phys. Chem.* **98**, 11623–11627 (1994).
63. Krishnan, R., Binkley, J. S., Seeger, R. & Pople, J. A. Self-consistent molecular orbital methods. XX. A basis set for correlated wave functions. *J. Chem. Phys.* **72**, 650–654 (1980).
64. Clark, T., Chandrasekhar, J., Spitznagel, G. W. & Schleyer, P. V. R. Efficient diffuse function-augmented basis sets for anion calculations. III. The 3-21+G basis set for first-row elements, Li-F. *J. Comput. Chem.* **4**, 294–301 (1983).
65. Wadt, W. R. & Hay, P. J. Ab initio effective core potentials for molecular calculations. Potentials for main group elements Na to Bi. *J. Chem. Phys.* **82**, 284–298 (1985).
66. Grimme, S., Antony, J., Ehrlich, S. & Krieg, H. A consistent and accurate ab initio parametrization of density functional dispersion correction (DFT-D) for the 94 elements H-Pu. *J. Chem. Phys.* **132**, 154104 (2010).
67. Ishida, K., Morokuma, K. & Komornicki, A. The intrinsic reaction coordinate. An *ab initio* calculation for HNC→HCN and $H^- + CH_4 \rightarrow CH_4 + H^-$. *J. Chem. Phys.* **66**, 2153–2156 (1977).

68. Weinhold, F., Landis, C. R. & Glendening, E. D. What is NBO analysis and how is it useful? *Int. Rev. Phys. Chem.* **35**, 399–440 (2016).
69. Glendening, E. D., Landis, C. R. & Weinhold, F. NBO 7.0 : New vistas in localized and delocalized chemical bonding theory. *J. Comput. Chem.* jcc.25873 (2019).
70. Gordon, M. S., Binkley, J. S., Pople, J. A., Pietro, W. J. & Hehre, W. J. Self-consistent molecular-orbital methods. 22. Small split-valence basis sets for second-row elements. *J. Am. Chem. Soc.* **104**, 2797–2803 (1982).
71. Francl, M. M. *et al.* Self-consistent molecular orbital methods. XXIII. A polarization-type basis set for second-row elements. *J. Chem. Phys.* **77**, 3654–3665 (1982).
72. Scalmani, G. & Frisch, M. J. Continuous surface charge polarizable continuum models of solvation. I. General formalism. *J. Chem. Phys.* **132**, 114110 (2010).
73. Sparta, M., Riplinger, C. & Neese, F. Mechanism of Olefin Asymmetric Hydrogenation Catalyzed by Iridium Phosphino-Oxazoline: A Pair Natural Orbital Coupled Cluster Study. *J. Chem. Theory Comput.* **10**, 1099–1108 (2014).
74. Yanai, T., Tew, D. P. & Handy, N. C. A new hybrid exchange–correlation functional using the Coulomb-attenuating method (CAM-B3LYP). *Chem. Phys. Lett.* **393**, 51–57 (2004).
75. Martin, R. L. Natural transition orbitals. *J. Chem. Phys.* **118**, 4775–4777 (2003).
76. Knizia, G. Intrinsic Atomic Orbitals: An Unbiased Bridge between Quantum Theory and Chemical Concepts. *J. Chem. Theory Comput.* **9**, 4834–4843 (2013).
77. Mitoraj, M. P., Michalak, A. & Ziegler, T. A Combined Charge and Energy Decomposition Scheme for Bond Analysis. *J. Chem. Theory Comput.* **5**, 962–975 (2009).
78. te Velde, G. *et al.* Chemistry with ADF. *J. Comput. Chem.* **22**, 931–967 (2001).
79. Lenthe, E. van, Baerends, E. J. & Snijders, J. G. Relativistic regular two-component Hamiltonians. *J. Chem. Phys.* **99**, 4597–4610 (1993).
80. van Lenthe, E., Baerends, E. J. & Snijders, J. G. Relativistic total energy using regular approximations. *J. Chem. Phys.* **101**, 9783–9792 (1994).

IX Molecular, Lewis Acidic Bismuth Compounds

1 Unusual Coordination Geometry of Cationic Bismuth Halide: Synthesis and Structure of $[BiCl_2(py)_5][BArF^{24}]$

Bismuth salts are Lewis acidic compounds which are frequently applied as Lewis acid catalysts in organic and organometallic transformations.[45,46,129–131] Due to the electron deficiency of bismuth salts, the formation of Lewis acid/base adducts in the chemistry of such compounds is a common phenomenon.[132] For bismuth cations without strong bonding interactions between anion and cation, Lewis bases interact via the vacant 6p orbital of the bismuth complex fragment. For compounds with distinct Bi–X bonding interactions, the Lewis acidity is based on an energetically accessible antibonding σ*(Bi–X) orbital, if X shows a sufficiently high electronegativity.[82,124,133–137] As a result, it can act as an acceptor orbital for neutral donor ligands.[132] The metal-centered lone pair of electrons of Bi(III) compounds is localized in a non-hybridized 6s orbital. Due to relativistic effects and the inert pair effect,[8,9] it is low in energy. Consequently examples for Bi→M coordination are scarce and limited to compounds with strongly Lewis acidic metal centers.[3–7,12,138–140] For bismuth(III) halides, such interactions are unprecedented to date.[3]

There are numerous examples of neutral (organometallic) bismuth halides BiX_nR_{3-n} (n = 1–3) acting as Lewis acids towards organic molecules.[141–146] Representatives of such Lewis acid/base adducts with high coordination numbers (CN > 6) of the central bismuth atom are pyridine[146] and crown ether adducts.[25,147–151] Bismuth cations with high coordination numbers (CN > 6) have been described for Bi(III) species, with the coordination number eight being most common followed by the coordination numbers of 7, 9 and 10.[19] Species such as $Bi(H_2O)_9^{3+}$,[152,153] $Bi(dmso)_8^{3+}$,[153–155] $Bi(SePMe_3)_6^{3+}$,[137] and $Bi(dmf)_8^{3+}$, respectively, are mononuclear, cationic compounds, without strong bonding interactions between cation and anion.[154,156,157] Related to this work, molecular bismuth halide cations and their structural characteristics, such as a typically adopted *cis*-conformation of the monoanionic ligands, are described in the literature.[24,158–161] Here, we report the synthesis and solid-state structure of $[BiCl_2(py)_5][BArF^{24}]$ (**19-Cl**), and the solid-state structure of its parent compound $[BiCl_3(py)_2]_2$ (**20**) ($[BArF^{24}]^- = [B(3,5\text{-}C_6H_3(CF_3)_2)_4]^-$, py = pyridine).

$[BiCl_2(py)_5][BArF^{24}]$ (**19-Cl**) was obtained by reaction of $BiMeCl_2$ with two equivalents of $Tl[BArF^{24}]$ in pyridine solution in 50% yield as a colorless solid (Scheme 22a). **19-Cl** was also obtained in a rational synthesis from reaction of $BiCl_3$ with one equivalent of $Tl[BArF^{24}]$ in

[3] In this context it may be noted that bismuth(I) halides can act as Lewis bases towards transition metal complex fragments. See also: J. von Seyerl, G. Huttner, *J. Organomet. Chem.* **1980**, 207-212; S. J. Davies, N. A. Compton, G. Huttner, L. Zsolnai, S. E. Garner, *Chem. Ber.* **1991**, 124, 2731-2738.

pyridine. This route also allowed access to $[BiX_2(py)_5][BArF^{24}]$ (**19-X**, X = Br, I) in high yields (85–86%, Scheme 22b).

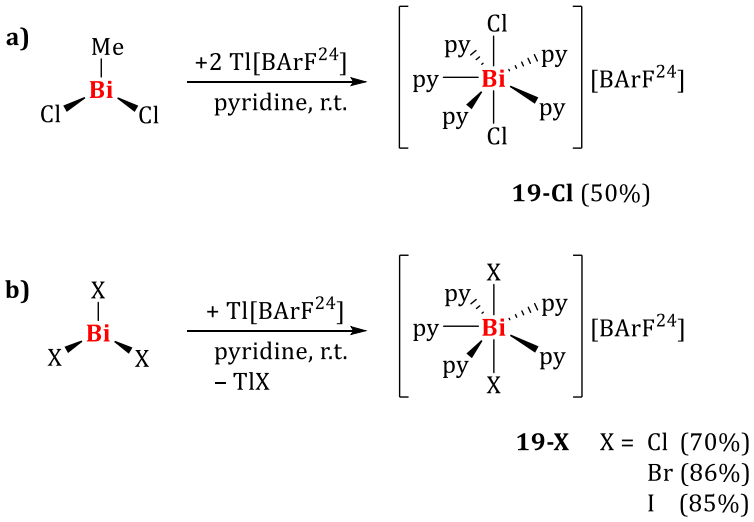

Scheme 22. a) Reaction of $BiMeCl_2$ with $Tl[BArF^{24}]$. b) Reaction of BiX_3 with $Tl[BArF^{24}]$. X = Cl, Br, I. $[BArF^{24}]^- = [B(3,5\text{-}C_6H_3(CF_3)_2)_4]^-$. py = pyridine.

The ^1H NMR spectra of **19-X** in methylene chloride show the expected signal pattern for the bismuth bound pyridine ligands, with significantly downfield shifted resonances ($\Delta\delta$ = 0.17–0.25 (**19-Cl**), 0.17–0.36 (**19-Br**), and 0.08–0.29 ppm (**19-I**)) compared to non-coordinating pyridine. The ^1H, ^{11}B, and ^{19}F NMR spectra also indicate the presence of the $[BArF^{24}]^-$ anion without strong directional bonding interactions between cation and anion.

Material suitable for single-crystal X-ray diffraction analysis was obtained for **19-Cl** by layering a pyridine solution of **19-Cl** with toluene and storage at –30 °C. **19-Cl** crystallized in the monoclinic space group $P2_1/n$ with Z = 4 (Figure 33).

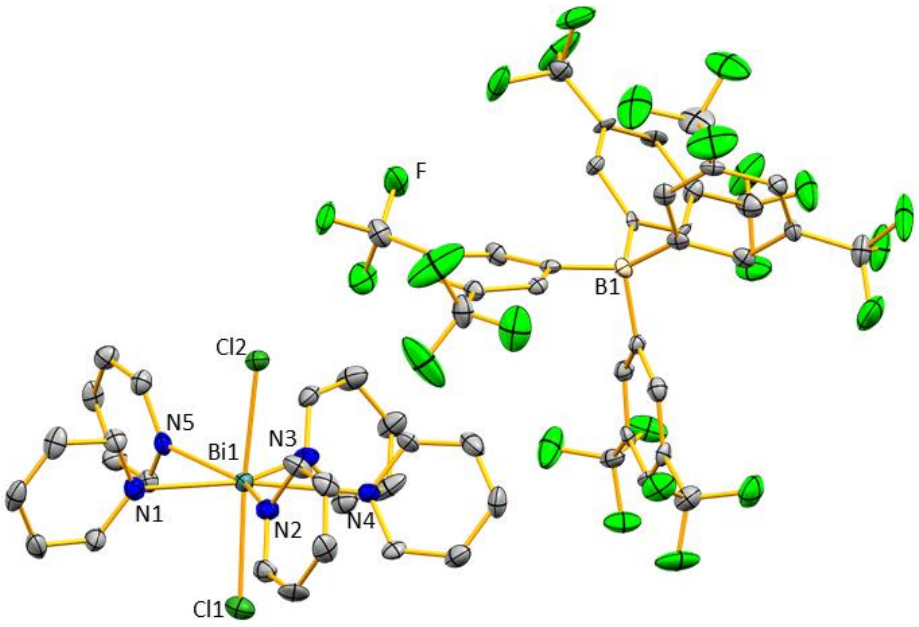

Figure 33. Molecular structure of **19-Cl** in the solid state. Displacement ellipsoids are shown at the 50% probability level. Hydrogen atoms and split positions are omitted for clarity. Selected bond lengths (Å) and angles (°): Bi1–Cl1, 2.626(2); Bi1–Cl2, 2.666(2); Bi1–N1, 2.539(7); Bi1–N2, 2.606(6); Bi1–N3, 2.611(6); Bi1–N4, 2.621(7); Bi1–N5, 2.547(7); Cl1–Bi1–Cl2, 174.35(7); N1–Bi–N2, 73.7(2); N1–Bi1–N3, 143.6(2); N1–Bi1–N4, 146.1(2); N1–Bi1–N5, 75.2(2); N2–Bi1–N3, 69.9(2); N2–Bi1–N4, 140.2(2); N2–Bi1–N5, 148.0(2); N3–Bi1–N4, 70.3(2); N3–Bi1–N5, 140.9(2); N4–Bi1–N5, 71.0(2); Cl1–Bi1–N1, 91.00(16); Cl1–Bi1–N2, 89.92(15); Cl1–Bi1–N3, 88.78(15); Cl1–Bi1–N4, 91.09(16); Cl1–Bi1–N5, 97.62(16); Cl2–Bi1–N1, 90.90(16); Cl2–Bi1–N2, 85.51(15); Cl2–Bi1–N3, 86.53(15); Cl2–Bi1–N4, 90.30(16); Cl2–Bi1–N5, 88.01.

The central bismuth atom adopts a distorted pentagonal bipyramidal coordination geometry with the chlorine atoms in its apical positions (174.35°) with Bi–Cl distances of 2.62-2.67 Å similar to other bismuth chloro species.[17,49] N–Bi–N angles involving neighboring pyridine ligands in the equatorial plane amounts to 69.9–75.2°. The Cl1–Bi–N bond angles (88.8–97.6°) are on average significantly smaller than the Cl2–Bi–N bond angles (85.5–90.9°). Accordingly the Cl1–Bi1–Cl2 angle (174.4°) slightly deviates from the ideally expected 180°. This may indicate some stereoactivity of the lone pair at the bismuth center. The Bi–N distances of 2.53–2.62 Å are in the range of reported Lewis acid/base adducts of bismuth cations and N-donor ligands.[21,30,162] The pentagonal bipyramidal coordination geometry of bismuth atoms is scarce, with only a limited number of examples for bismuth halides, with the neutral parent compound of **19-Cl**, $BiCl_3(py)_4$ as only example for a species with solely monodentate ligands.[144,163–166] The bismuth atom in $[Ph_3SbBiCl(C_6H_6)][AlCl_4]$ also adopts a pentagonal bipyramidal coordination geometry in the solid state,[167] however, it has to be noted that all examples mentioned, except neutral $BiCl_3(py)_4$, are complexes containing at least one chelating ligand (or chelating anion in the case of $[Ph_3SbBiCl(C_6H_6)(\kappa^2\mathit{Cl}\text{-}AlCl_4)_2]$) resulting in **19-Cl** being the first example for a mononuclear, pentagonyl bipyramidal bismuth halide cation with solely monodentate ligands. The bonding

mode of chelating ligands in such species leads to a strong distortion of the pentagonal bipyramidal coordination geometry of the bismuth centers. Solid-state structures of bismuth halide cations in which the halides are in *trans*-position to each other are described in the literature, e.g. $[BiI_2(py)_3(dppom)][BiI_4(py)_2]$ (dppom = $Ph_2P(O)CH_2OPPh_2$).[23] The structural parameters of this compound are similar to **19-Cl**, although the dppom ligand is bidentate.[23] In both compounds, $[BiI_2(py)_3(dppom)][BiI_4(py)_2]$ and **19-Cl**, the regularity of the pentagonal bipyramidal geometry is notable, since the ligands in the equatorial plane are nearly coplanar (maximum deviation from the mean plane: 0.13 Å in $[BiI_2(py)_3(dppom)][BiI_4(py)_2]$; 0.10 Å in **19-Cl**). The related halide cations $[BiX_2(18\text{-crown-}6][BiX_4]$ show structures of *cis*-BiX_2 units coordinated by six oxygen atoms of the crown ether ligands (X = Cl, Br).[24,161] It was not possible to obtain suitable material for single-crystal X-ray diffraction analyses for **19-Br** and **19-I**, so the investigation of a possible dependency of the coordination geometry on the halide substituent is subject for further research. However, the ^{1}H NMR spectroscopic data obtained indicate the presence of five pyridine ligands in **19-X** (X = Br, I).

Although similarities in their coordination chemistry between Ln^{3+} and Bi^{3+} can be expected based on their electronegativity and ionic radii,[168,169] the analog lanthanide (Ln) compounds $LnCl_2(py)_5^+$ are unprecendented to date. The only reported $LnCl_2^+$ complexes containing pyridine based chelating ligands have coordination numbers of 9 (Ln = Nd, Gd),[170,171] and 10 (Ln = La), respectively.[172]

19-Cl may be described as a chloride abstraction product of compound $BiCl_3(py)_4$, which also shows a trigonal bipyramidal coordination geometry around bismuth, the coordination site of the third chlorine atom being saturated by the coordination of a further pyridine ligand in **19-Cl**.[144] However, in the course of this investigation, the solid-state structure of the bis-pyridine adduct of $BiCl_3$ was obtained, which is not reported to date. $[BiCl_3(py)_2]_2$ (**20**) crystallized in the monoclinic space group $C2/m$ with $Z = 2$ (Figure 34).

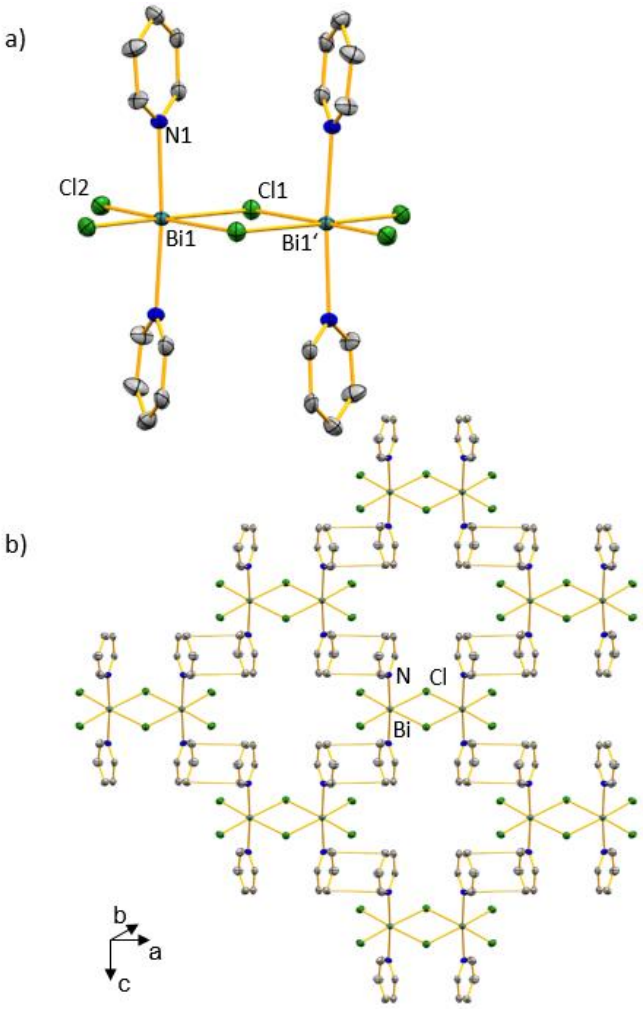

Figure 34. a) Molecular structure of $[BiCl_3(py)_2]_2$ (**20**) in the solid state. Displacement ellipsoids are shown at the 50% probability level. Hydrogen atoms are omitted for clarity. b) Cut out of coordination polymer $[\{BiCl_3(py)_2\}_2]_\infty$. Selected bond lengths (Å) and angles (°): Bi1−Cl1, 2.897(2); Bi1−N1, 2.530(8); Bi1−Cl2, 2.559(2); Cl1−Bi1−$Cl2_{cis}$, 90.79(7); Cl1−Bi−$Cl2_{trans}$, 175.86(7); Cl1−Bi1−Bi1', 85.08(9); Cl2−Bi1−Cl2', 93.35(12), Cl−Bi1−N1, 88.11(18)−91.93(18); N1−Bi1−N1', 175.2(3).

In the solid state, **20** forms dimeric structures via two short intermolecular Bi···Cl contacts with neighboring species, which is in accordance to the analog antimony compound.[173] The bismuth atoms possess octahedral coordination geometries with four equatorial chlorine atoms and two pyridine ligands in apical positions (N−Bi−N, 175.2°). The terminal Bi−Cl bond lengths (2.56 Å) are considerably shorter than the Bi−Cl distances of bridging moieties (2.89 Å). These distances are in the range of reported Bi−Cl bond lengths for bridging and terminal chlorido ligands. However, it may be noted that only a limited number of species $[BiCl_3L_2]_2$ with L trans to each other are described in the literature.[174–176] The Bi−N bond lengths (2.53 Å) are in the range of Bi–N distances observed in other Lewis acid/base adducts with N-donor ligands.[21,143] A bismuth-bismuth interaction is not observed based on distance criteria (the Bi···Bi distance (4.27 Å)

exceeds the sum of the van-der-Waals radii (4.14 Å) by 3%). π-Stacking between pyridine ligands of neighboring formula units is present, resulting in a two-dimensional coordination polymer in the solid state.

For a better understanding of the coordination geometries of neutral and cationic bismuth chlorides, DFT calculations were performed with the Gaussian program[103] using the 6-31G(d,p)[107] (H, B, C, N, F, Cl) and the LanL2DZ[108–110] (Bi) basis set and the B3LYP functional.[104] The D3 version of Grimme's dispersion model with the original D3 damping function was applied.[106] Frequency analyses of the reported structures showed no imaginary frequencies for ground states. Thermodynamic parameters were calculated at a temperature of 298.15 K and a pressure of 1.00 atm. NBO analyses were performed using the program version NBO 7.[177] All calculations were performed with a pyridine solvent model (PCM).

Species $[BiCl_2(py)_n][BArF^{24}]$ (n = 0–6)[4] were subjected to geometry optimizations (Figure 35). In the following, only the cationic fragments $[BiCl_2(py)_n]^+$ are discussed, but the optimizations were carried out in the presence of the $BArF^{24}$ anion. During the optimization of $[BiCl_2(py)_6][BArF^{24}]$, one pyridine ligand dissociated away from the metal center, yielding the same results as obtained for $[BiCl_2(py)_5][BArF^{24}]$, plus one pyridine ligand in the periphery without directional Bi–N interactions. The enthalpies and the free energies of the reactions shown in Figure 36 were determined. Plotting these energy values versus the number of pyridine molecules n used in the reaction shows an increasingly exothermic/exergonic reaction with an increasing number of pyridine ligands (Figure 36).

[4] Optimization of $[BiCl_2][BArF^{24}]$ without constraints resulted in fluoride abstraction from the $BArF^{24}$ anion by the $BiCl_2^+$ fragment. Fixation of angles in CF_3 groups, optimization, and subsequent constraint release and re-optimization resulted in obtaining the minimum structure discussed here.

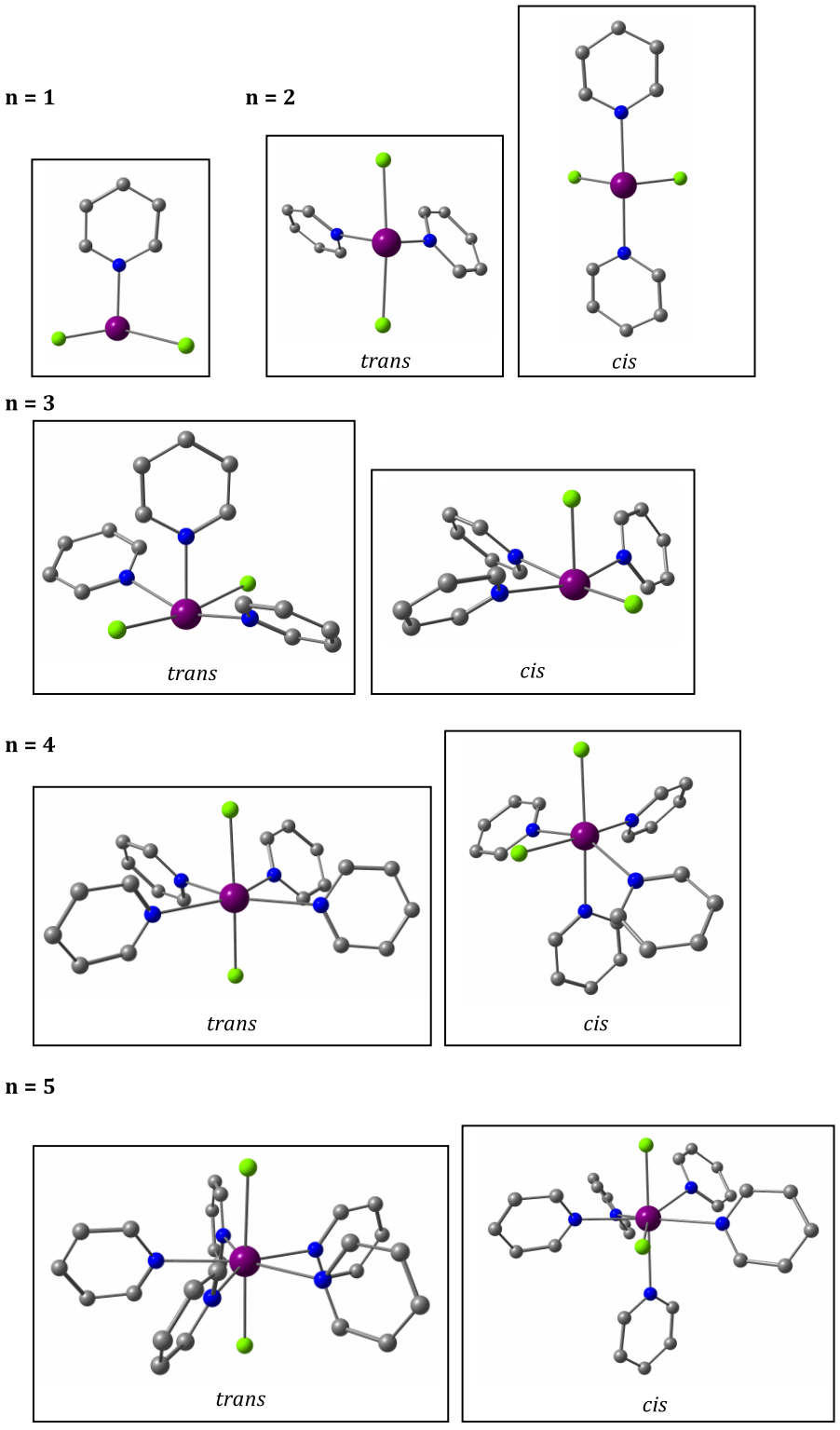

Figure 35. Geometries of optimized $[BiCl_2(py)_n][BArF^{24}]$ (n = 1–5) species. Only the cationic part is shown.

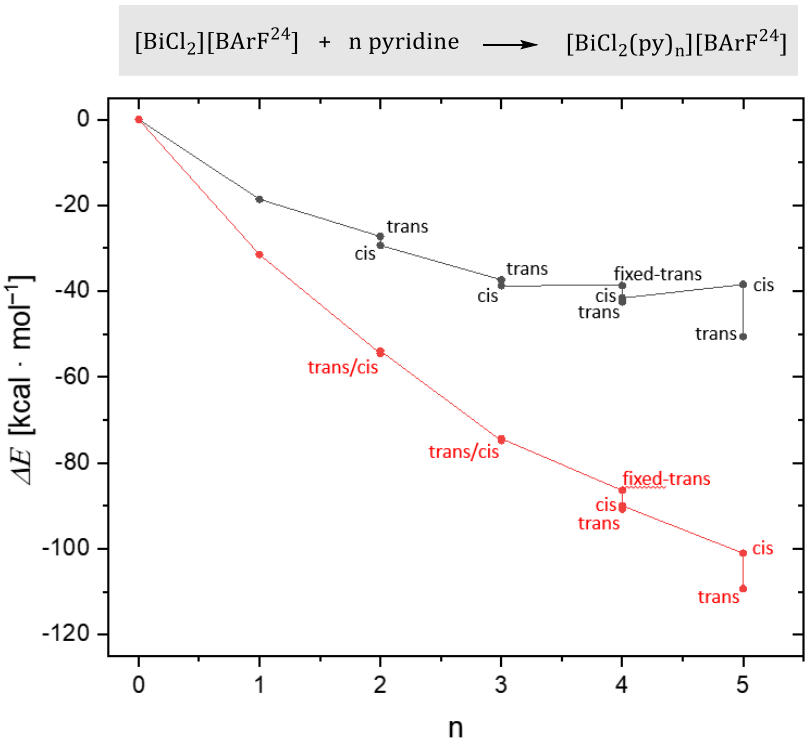

Figure 36. Energy plot of cationic species $[BiCl_2(py)_n][BArF^{24}]$ with n = 0–5. *ΔG* values are depicted in black, and *ΔH* values are depicted in red.

For species with n = 4, both isomers (*cis*/*trans*) show distorted octahedral coordination geometries with one large N–Bi–N/Cl angle (135.9/116.5°), and three small angles (73.5–76.0°/83.9–87.4°) for the pyridine/chlorido ligands in the equatorial plane. The distortion is less pronounced for the *cis*-isomer. In both isomers, the structural parameters indicate a stereoactive lone pair of electrons at the bismuth center. An optimization of the *trans*-isomer with fixed angles (90°) between the ligands in the equatorial plane yielded a structure with a Cl–Bi–Cl angle of 178.1°, which is only slightly higher in energy (ΔG = +2.91/+3.82 kcal · mol^{-1}) than the optimized *cis*-/*trans*-isomers without constraints. For compounds with n = 2 (bisphenoidal), and 3 (square pyramidal), isomers with the chlorido ligands in *cis*-positions are thermodynamic favorable. This changes for n = 4 (octahedral) and 5 (pentagonal bipyramidal), resulting in energetical favored isomers, in which the chlorido ligands are situated in *trans*-positions to each other, by ΔG = 0.8 kcal · mol^{-1} (n = 4) and ΔG = 8.3 kcal · mol^{-1} (n = 5). The gain in free energy per step $\Delta\Delta G$ amounts to 8.1 to 10.8 kcal · mol^{-1}, with the exception of the step going from species with n = 3 to n = 4, in which the energy values are decreased to $\Delta\Delta G$ = –2.9 kcal · mol^{-1} for the *cis*-species, and $\Delta\Delta G$ = –5.1 kcal · mol^{-1} for the *trans*-isomers.

The same trends were obtained for the neutral analogs $BiCl_3(py)_n$ (n = 1–4). In our hands, crystallization attempts of $BiCl_3$ from pyridine yielded the dimeric structure **20**, so that an optimization with subsequent frequency analysis was carried out, too (Figure 37).

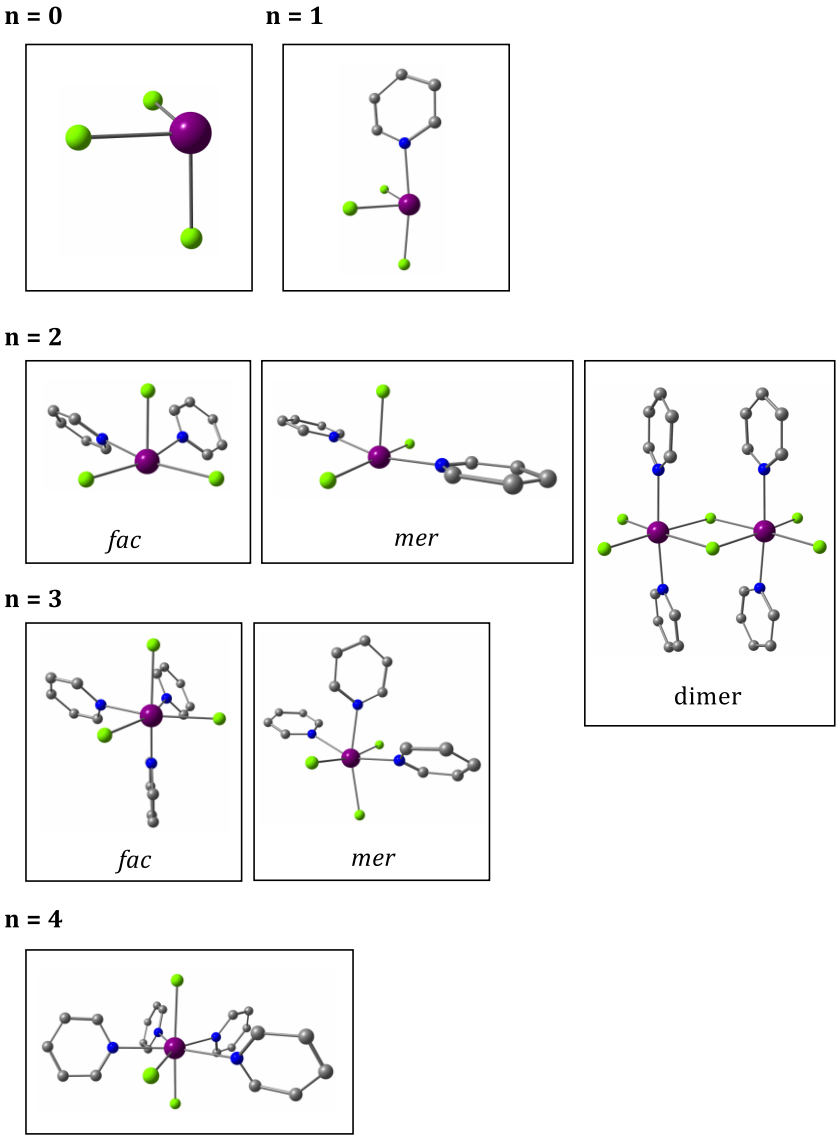

Figure 37. Geometries of optimized $BiCl_3(py)_n$ (n = 0–4) species.

Plotting the enthalpy and free-energy values of the obtained optimized structures versus the number of pyridine molecules n used in the reaction shown in Figure 38 results in energy plots showing that the energy decreases steadily with the addition of pyridine, with the dimeric structure we found representing the absolute minimum in both ΔG and ΔH (Figure 38).

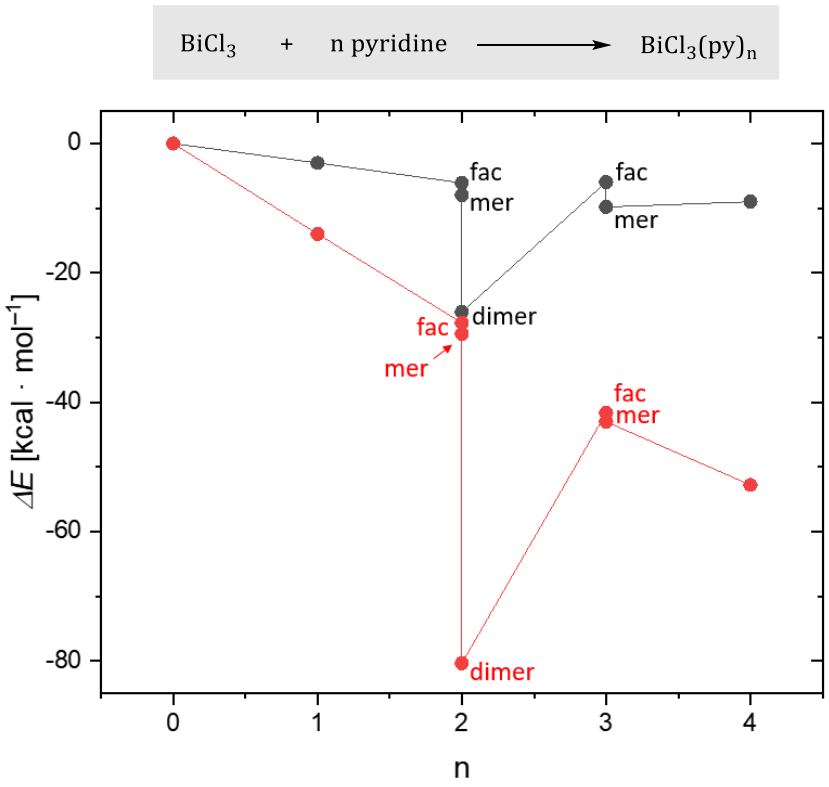

Figure 38. Energy plot for species $BiCl_3(py)_n$ with n = 0–4. ΔG values are depicted in black, and ΔH values are depicted in red.

The differences between the *fac*-/*mer*-isomers of $BiCl_3(py)_n$ with n = 2 (square pyramidal), and 3 (octahedral) are small, but the *mer*-isomers are energetically favored by 1.9 (n = 2) and 3.9 kcal · mol^{-1} (ΔG), respectively. Again, it provides an energetic gain to incorporate additional pyridine ligands. Per step these are $\Delta\Delta G$ = –3.0 to –5.0 kcal · mol^{-1} (the dimer excluded). The incorporation of an additional pyridine ligand starting from *fac*-$BiCl_3(py)_2$, however, is associated with no significant change in energy ($\Delta\Delta G$ = –0.13 kcal · mol^{-1}). When these values are compared to those obtained for the cationic species, the energetic gain per additional pyridine ligand is significantly higher for the cations , illustrating the higher electron deficiency of such species.

To evaluate the Bi–Cl bond strength in **19-Cl** and its neutral analog $BiCl_3(py)_4$, deletion energies (E_{Del}) were calculated. For **19-Cl**, all interactions py→Bi and Cl→Bi, respectively, were considered at once, resulting in E_{Del} = 260.5 kcal · mol^{-1} for the N→Bi interaction, and E_{Del} = 197.1 kcal · mol^{-1} for the Cl→Bi interaction. This corresponds to 52.1 kcal · mol^{-1} for each pyridine ligand, and 98.5 kcal · mol^{-1} for each chlorido ligand in **19-Cl**. For $BiCl_3(py)_4$, the chlorido ligands were grouped into those in axial positions (E_{Del} = 177.6 kcal · mol^{-1}), and the one in an equatorial position (E_{Del} = 83.9 kcal · mol^{-1}), resulting in E_{Del} = 88.8 kcal · mol^{-1} for each chlorine atom in an axial position. The E_{Del} for the each pyridine ligand amounts to 43.6 kcal · mol^{-1}. These results illustrate a bond strengthening for the py→Bi, as well as the Cl→Bi interactions going from neutral to cationic bismuth species.

Finally, a scarce representative of a pentagonal bipyramide of a main group element has been synthesized and fully characterized. According to DFT calculations. the uptake of five neutral donor ligands in the form of pyridine is thermodynamically favored compared to the formation of analog adducts with other coordination numbers. Additionally, the calculations show a strengthening of the Bi–Cl bond, as well as of the Bi–py interaction in **19-Cl**, when compared to the neutral $BiCl_3(py)_4$ analog. Further investigations concerning both the Bi–Cl bond strength, e.g. based on raman spectroscopy, and the potential stereoactivity of the lone pair of electrons at the bismuth centers in the calculated and experimentally obtained compounds are worthwhile to be investigated in future research projects.

2 Solid-State Structures of Simple Bismuth Salts

Bismuth halides BiX_3 are classified as Lewis acids and can therefore accept electron density through coordination of neutral donor ligands. Due to the electropositivity of bismuth, the σ*-antibonding orbital of the Bi−X bond is energetically lowered and thus capable of acting as an acceptor orbital for neutral donor ligands. Bismuth Lewis acids are widley used as catalysts in organic and organometallic transformations,[45,46,129,178,179] as model compounds for perovskites for optoelectronic applications,[147] and as materials in solar cells.[156,180]

The coordination chemistry of neutral (organometallic) bismuth halides has been widely studied.[141–146,181,182] However, only a few Lewis acid/base adducts of (dihalo)alkylbismuthanes BiX_2R have been characterized by X-ray diffraction.[183,184] As part of this work, the solid-state structure of $BiMeCl_2(py)_2$ was added to this class of compounds.

$BiMeCl_2(py)_2$ crystallized in the monoclinic space group $P2_1/c$ with $Z = 4$ (Figure 39). Similarly to $BiMeX_2(tmeda)$ (X = Cl Br), $BiMeBr_2$(2,2'-bipy), $BiMeBr_2$(1,10-phen)[143] and $BiMeBr_2(thf)_2$,[183] $BiMeCl_2(py)_2$ forms a mononuclear structure in the solid state, with the bismuth atom adopting a square pyramidal coordination geometry with the methyl group in axial position (τ = 0.00, tmeda = tetramethylethylenediamine, 2,2'-bipy = 2,2'-bipyridine, phen = phenanthroline). In contrast to the afore mentioned compounds with chelating donor ligands, as well as to the bromine analog $BiMeBr_2(thf)_2$, the chlorine atoms in $BiMeCl_2(py)_2$ are *trans* to each other, and the Cl−Bi−Cl (172.31(2)°) and N−Bi−N angles (172.13(8)°) are close to the ideal 180°. The C−Bi−C/N angles in $BiMeCl_2(py)_2$ are in the range of 84.28(8)−88.15(8)°, and the Bi−C distance of 2.222(3) Å is similar to other Bi–CH_3 bond lengths in related compounds.[143,183] π-Stacking between pyridine ligands of neighboring formula units is present (C−C, ca. 3.38−3.83 Å), resulting in a one-dimensional coordination polymer in the solid state, which extends along the crystallographic a-axis (Figure 39b).

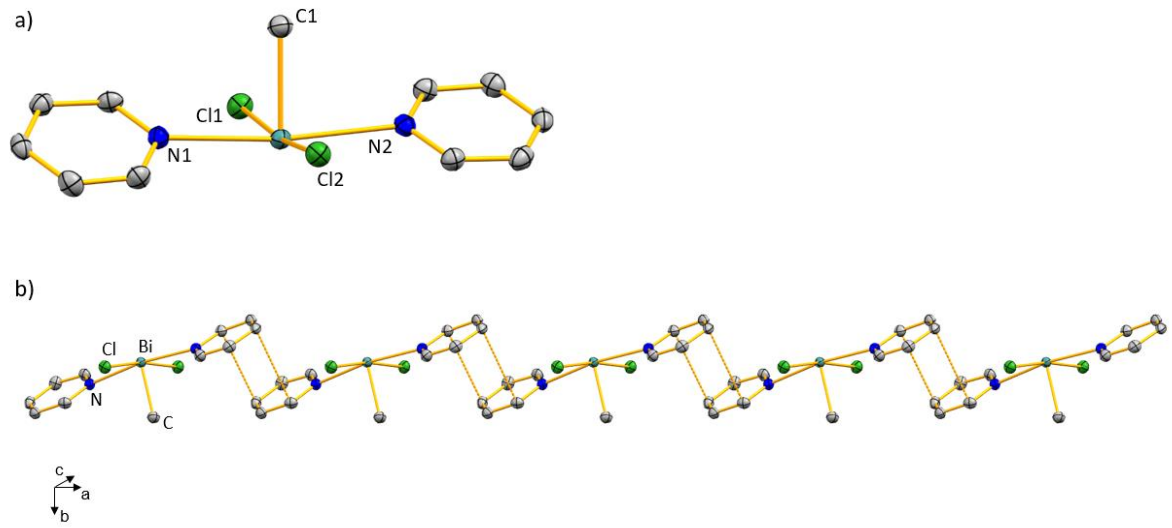

Figure 39. a) Molecular structure of $BiMeCl_2(py)_2$ in the solid state. Displacement ellipsoids are shown at the 50% probability level. Hydrogen atoms are omitted for clarity. b) Representation of the one-dimensional coordination polymer $[BiMeCl_2(py)_2]_\infty$ in the solid state. Selected bond lengths (Å) and angles (°): Bi1–C1, 2.222(3); Bi1–N2, 2.504(2); Bi1–N1, 2.513(2); Bi1–Cl1, 2.6795(9); Bi1–Cl2, 2.6840(9); C1–Bi1–N, 86.19(10)–86.45(10); N1–Bi1–N2, 172.13(8); C1–Bi1–Cl, 84.28(8), 88.15(8); Cl–Bi1–N, 87.73(6)–91.58(6); Cl1–Bi1–Cl2, 172.31(2).

Besides the solid-state structure of $BiMeCl_2(py)_2$, it was also possible to obtain the first structural data for $BiCl_3(SePMe_3)_n$ (n = 2, 3) by combining $BiCl_3$ with $SePMe_3$ in DCM solution (Figure 40). In both cases, the quality of the data obtained does not allow a discussion of bond lengths and angles, and the data only serves as proof of connectivity. This is due to twinning, that could not be adequately modelled, and insufficient scattering. The bis-$SePMe_3$ adduct of $BiCl_3$ crystallized in the orthorhombic space group $P2_12_12_1$ with $Z = 4$ (Figure 40a). Similarly to dimeric $[BiCl_3(py)_2]_2$ (see Chapter IX.1), $BiCl_3(SePMe_3)_2$ forms a dimeric structure in the solid state via two short intermolecular Bi···Cl interactions with neighboring species, with the $SePMe_3$ ligands in the axial positions, resulting in a distorted octahedral coordination geometry of the bismuth atoms. In $BiCl_3(SePMe_3)_3$, the sixth coordination site is occupied by the third phosphane selenide ligand, so that $BiCl_3(SePMe_3)_3$ forms a typical mononuclear structure in the solid state without directional intermolecular interactions, with two chlorine atoms *trans* to each other, and one chlorine atom *trans* to one $SePMe_3$ ligand (triclinic space group $P\bar{1}$ with $Z = 8$[5], Figure 40b).

[5] Indications for a higher symmetry were not observed. Since the quality of data obtained was poor, more suitable crystalline material might reveal a space group of higher symmetry for this compound.

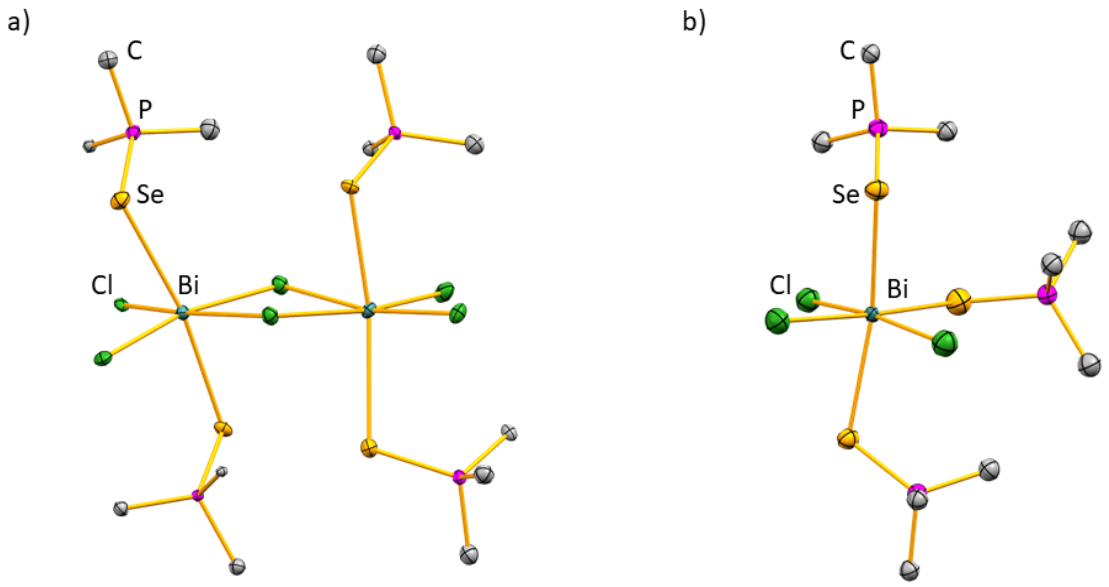

Figure 40. Molecular structures of $BiCl_3(SePMe_3)_2$ (a) and $BiCl_3(SePMe_3)_3$ (b) in the solid state. Displacement ellipsoids are shown at the 50% probability level. Hydrogen atoms are omitted for clarity.

Remarkably, compounds $BiCl_3(SePMe_3)_n$ are yellow solids, which lose their color in THF solution. Layering the colorless solutions with *n*-pentane leads to a yellow boundary phase, and yellow crystals of $BiCl_3(SePMe_3)_n$ (n = 2, 3) are obtained after 16 h at –30 °C. These observations suggest that the phosphane selenide ligands are displaced by coordination of thf ligands in THF solution. Unfortunately, several attempts to obtain more suitable single crystals of $BiCl_3(SePMe_3)_n$ (n = 2, 3) enabling a discussion of bonding parameters did not succeed. Additionally, a separation of the products was unsuccessful. The targeted synthesis of one of the products was not performed.

3 The Dimethylbismuth Cation

Recently, the synthesis of the contact ion pair $[BiMe_2(SbF_6)]$ (**21**), its solvent-separated pyridine adduct $[BiMe_2(py)_2][SbF_6]$ (**21-py**) as well as the first dinuclear bismuth species with Bi→Bi donor/acceptor interactions in form of $[BiMe_2(BiMe_3)][SbF_6]$ were described (see Chapter VIII). Further results on the subject of the chemistry of $[BiMe_2(SbF_6)]$ are discussed below.

3.1 Synthesis and Characterization of $BiMe_2L_2SbF_6$

Following the synthesis of the pyridine adduct $[BiMe_2(py)_2][SbF_6]$ (**21-py**), a range of other Lewis acid/base adducts of $BiMe_2^+$ were synthesized (Scheme 23).

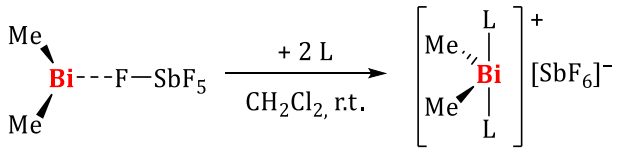

21 **21-L**

Scheme 23. Synthesis of Lewis acid/base adducts **21-L**. L = MeCN (**21-MeCN**), thf (**21-thf**), benzaldehyde (**21-benzaldehyde**).

As described for **21-py**, the reaction solution undergoes an instant color change from yellow to colorless upon the addition of the neutral donor ligands, which was ascribed to the occupation of the p-orbital in parent compound **21**.[185] The isolation of **21-L** succeeded in good yields for L = MeCN (64%) and L = benzaldehyde (63%), while **21-thf** was isolated in only 38% yield. This is because **21-thf**, which is a crystalline solid at –30 °C, begins to melt after 5 min at ambient temperature, thereby hampering its isolation. The ^{1}H NMR spectra of **21-L** show the expected signal pattern with a singlet for the methyl groups at $\delta(^{1}H)$ = 2.03 (**21-benzaldehyde**), 1.87 (**21-thf**), and 1.75 ppm (**21-MeCN**), respectively. This corresponds to a significant upfield shift of the methyl protons in comparison to contact ion pair **21** ($\delta(^{1}H)$ = 2.28 ppm), as adduct formation leads to a more electron rich bismuth center. For **21-thf**, it is possible to remove one thf ligand *in vacuo* to give **21-thf$_1$**. The ^{13}C NMR spectra for **21-thf$_1$** and **21-benzaldehyde** show significant downfield shifts of the methyl resonances (**21-thf$_1$**: $\delta(^{13}C)$ = 48.73 ppm; **21-benzaldehyde**: $\delta(^{13}C)$ = 53.14) compared to **21-py** ($\delta(^{13}C)$ = 33.86 ppm), in line with the increasing donor strengths of the ligands in the order of benzaldehyde < THF < pyridine (Figure 41).[186,187]

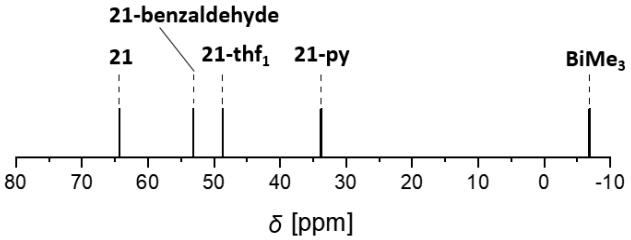

Figure 41. Comparison of ^{13}C NMR methyl shifts of **21**, **21-L** and $BiMe_3$ (added for comparison with a complex with an electron-rich bismuth center).

The ^{19}F NMR spectroscopic resonances for the SbF_6 counteranions are found at $\delta(^{19}F)$ = –121.9 ppm (**21-benzaldehyde**) and $\delta(^{19}F)$ = –132.0 ppm (**21-thf$_1$**). A clear dependence of the resonance on the strength of the Bi···[A]$^-$ interaction is not found, as the resonance for **21** is found at $\delta(^{19}F)$ = –128.4 ppm. Since **21-thf** melts at ambient temperature and melting is also observed for **21-MeCN** and **21-benzaldehyde** under the crystal oil Krytox (during crysal

picking),[6] X-ray diffraction analyses of these species proved difficult. The crystallographic data obtained for **21-thf** and **21-benzaldehyde** only serves as proof of connectivity in both cases due to poor data quality (**21-benzaldehyde**: monoclinic space group, $P2_1/c$ with Z = 8; **21-thf**: monoclinic space group $P2_1/n$ with Z = 16; Figure 42). It was also possible to obtain structural data for the mono-thf adduct of **21-thf$_1$** (triclinic space group $\bar{P}1$ with Z = 2, Figure 42c). In all three cases, in addition to melting, the crystals turned black during mounting on the goniometer. The data presented here was obtained by reducing the time needed for crystal picking and mounting to a minimum rather than cooling the equipment used for these working steps.

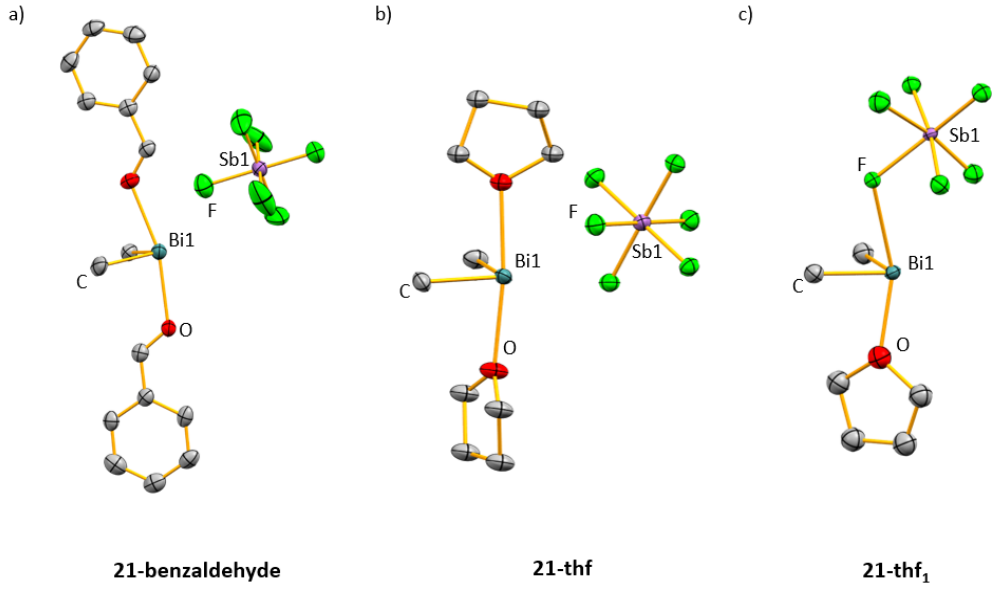

Figure 42. Molecular structures of a) **21-benzaldehyde** (only one of the two units of **21-benzaldehyde** present in the asymmetric unit shown), b) **21-thf** (only one of the four units of **21-thf** present in the asymmetric unit shown, and only one part of the disordered $BiMe_2$ and SbF_6 groups shown), and c) **21-thf$_1$** in the solid state. Displacement ellipsoids are drawn at the 50% probability level. Hydrogen atoms are omitted for clarity.

The solid-state structures of **21-L** show the bismuth atom in bisphenoidal coordination geometries with two ligands (**21-benzaldehyde**, **21-thf**) or thf and the SbF_6 counteranion (**21-thf$_1$**), respectively, occupying the axial positions, similarly as in **21-py** (see Chapter VIII).

Furthermore, the stability of parent compound **21** was examined. Storage of **21** at ambient temperature under an atmosphere of purified argon for several days (>7 d) led to partial discoloration of the yellow compound. Dissolving the solid in pyridine, filtration, and recrystallization (by layering the filtrate with *n*-pentane), afforded colorless crystals, X-ray diffraction analysis of which revealed the decomposition product $[BiMeF(py)_3]_2{\cdot}2[SbF_6]$ (**22**) (monoclinic space group $P2_1/n$ with Z = 2, Figure 43).

[6] However, a melting point of 115 °C was determined for isolated and dried **21-benzaldehyde**.

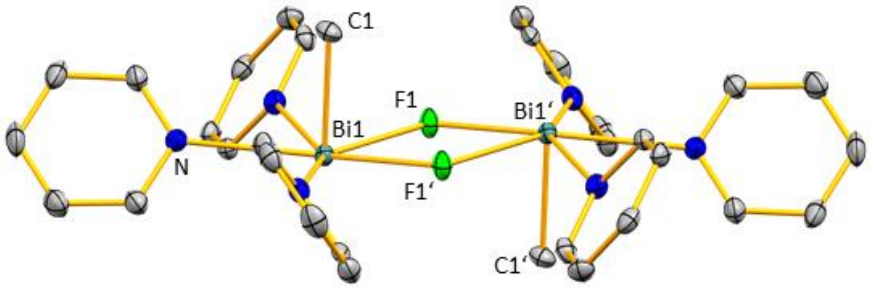

Figure 43. Molecular structure of $[BiMeF(py)_3]_2 \cdot 2[SbF_6]$ (**22**) in the solid state. Displacement ellipsoids are shown at the 50% probability level. Hydrogen atoms and the SbF_6^- anions are omitted for clarity. Selected bond lengths (Å) and angles (°): Bi1–F, 2.295(2), 2.342(2); Bi1–C, 2.215(4); Bi1–N, 2.532(3)–2.600(3); C–Bi–N/F, 72.03(10)–87.89(14).

The solid-state structure of the decomposition product shows a centrosymmetric dimer of $[BiMeF(py)_3]^+$ with short Bi···F bridges (Bi1−F1, 2.295(2) Å; Bi···F1', 2.342(2) Å) and no directional interactions between cation and anion. The bismuth atoms adopt pentagonal pyramidal coordination geometries with the methyl groups in apical position (interactions between the SbF_6^- anion and the bismuth atom are not present, based on Bi–F distances of 3.689(3) Å which is 5% above the sum of the van-der-Waals radii of 3.54 Å). Further pentagonal pyramidal coordination geometries of bismuth atoms are described for phenylbismuth bis(carboxylate), diketonate, and bis(salicylato) derivatives.[188–190] The pyridine ligands in **22** occupy the equatorial positions with Bi–N bond lengths (2.532(3)–2.600(3) Å) equal to those of $BiCl_2(py)_5^+$ (**19-Cl**$^+$, 2.539(7)–2.621(7) Å, see Chapter IX.1). Alkyl- and arylbismuthanes with fluoride ligands are extremely rare, with reported intramolecular Bi–F bond lengths in the range of 2.12–2.26 Å.[191–194] Both Bi–F interactions in **22** (2.295(2), 2.342(2) Å) are significantly longer, which might be due to the bridging bonding mode of the fluorine atoms, as well as to the higher coordination number of six in **22** compared to the literature-known species with coordination numbers of three or four. It should be noted that the Bi1···Bi1' distance of 3.87 Å is 7% below the sum of the van-der-Waals radii (4.14 Å), which could be attributed to the bridging coordination mode of the fluorine atoms. To the best of our knowledge, compound **22** is the first example of a crystallographically characterized cationic (fluoro)organobismuthane. A possible degradation path from **21** to **22** is postulated in Scheme 24.

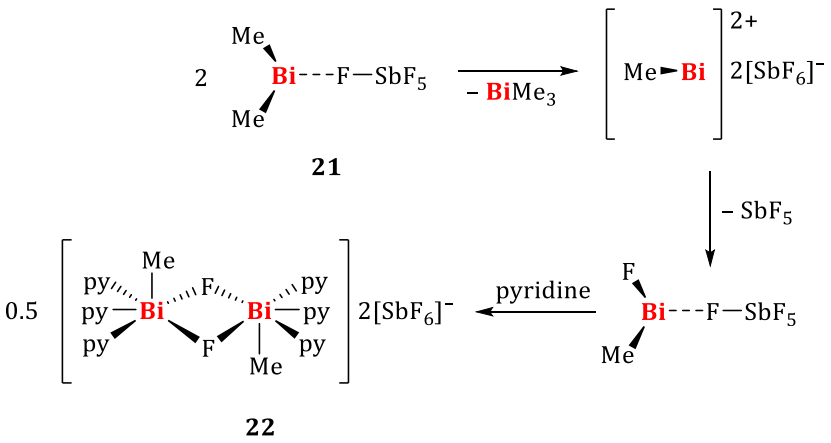

Scheme 24. Tentatively suggested degradation path of **21**. py = pyridine

The high Lewis acidity of parent compound **21** might lead to methyl group abstraction from a second dimethylbismuth cation, resulting in the formation of the expectedly highly Lewis acidic methyl bismuth dication and trimethylbismuth as a by-product. Next the $BiMe^{2+}$ cation abstracts a fluoride ligand from the SbF_6^- anion, leading (after adduct formation with pyridine) to the unusual degradation product **22** and SbF_5. The degradation of SbF_6^- was already described in the literature.[195] One driving force of this fluoride abstraction reaction might be the differences in bond dissociation energies: The bond dissociation energy of the Sb–F bond (96 kcal · mol^{-1}) is slightly lower than the one of the Bi–F bond (103.8 kcal · mol^{-1}).[196] However, a ^1H and ^{19}F NMR spectroscopic monitoring of the degradation reaction has not been performed, yet, so that the by-products, $BiMe_3$ and SbF_5, of the postulated degradation pathway have not yet been identified.

However, several attempts to reproduce the formation of **22** by storing **21** at ambient temperature under an atmosphere of purified argon and evaluate whether **22** is formed in larger quantities all resulted in recovery of the pyridine adduct **21-py** in nearly quantitative yield. This suggests that the formation of $[BiMeF(py)_3]_2{\cdot}2[SbF_6]$ from **21** appears to play a subordinate role under these reaction conditions. However, in the future, the thermal stability of **21** should be further investigated to study the decomposition pathway to **22** in more detail. For this purpose, **21** should be heated to different temperatures and then recrystallized from pyridine. In addition, a differential scanning calorimetry analysis of **21** appears to be useful.

In conclusion, a range of dimethylbismuth cation adducts **21-L** have been successfully synthesized and isolated. Melting of crystalline material hampered their crystallographic characterization. The generation of dimethylbismuth cation adducts with stronger donors than the ones used herein seemed to have positive effects on properties like melting point and stability, as was successfully demonstrated in the case of **21-py**.[185]

3.2 Cyanoborates: Counterions with Tunable Donor Strengths towards $[BiMe_2]^+$

Borate anions are classified as non- or weakly coordinating anions.[40] Especially fluorinated borates like $[B(C_6F_5)_4]^-$, $[B(2,4\text{-}CF_3\text{-}C_6H_3)_4]^-$ and related anions are widely used, e.g. to enhance the Lewis acidity of main group element cations by reduced interaction between cation and anion, as co-catalysts in olefin polymerization,[197] or in the deprotection of acetals.[198] Already in 1951, WITTIG and RAFF described the stabilizing effect of cyano groups on borate anions as similar to CF_3 groups,[199,200] but it was not until twenty years ago that the first tetracyanoborate salt was synthesized and fully characterized.[201,202] There is now a wide variety of cyanoborates with varying properties, including alkyl-, chloro-, perfluoroalkyl- and alkoxycyanoborates.[203] Cyanoborates are often used in the synthesis of ionic liquids, mainly via salt metathesis.[203] For the purposes of this thesis, the focus was limited to cyanohydridoborates of the general formula $[BH_n(CN)_{4-n}]^-$ and the synthesis of the first representatives of aryl- or alkylbismuth salts containing these anions. Except $Ag[B(CN)_4]$, which was synthesized independently, all of the cyanoborate salts used herein were kindly provided by the research group of PROF. MAIK FINZE.

DFT studies carried out by DR. CRISPIN LICHTENBERG showed that the strength of bonding interactions between cyanoborates $[BH_n(CN)_{4-n}]^-$ and the $BiMe_2^+$ can be varied smoothly through the series of cyanohydridoborates. The higher the number of cyano groups, the weaker the interactions between anion and cation, leading to considerable bonding in the trihydridomonocyanoborate salt, similar to salts with the coordinating triflate anion (Figure 44).

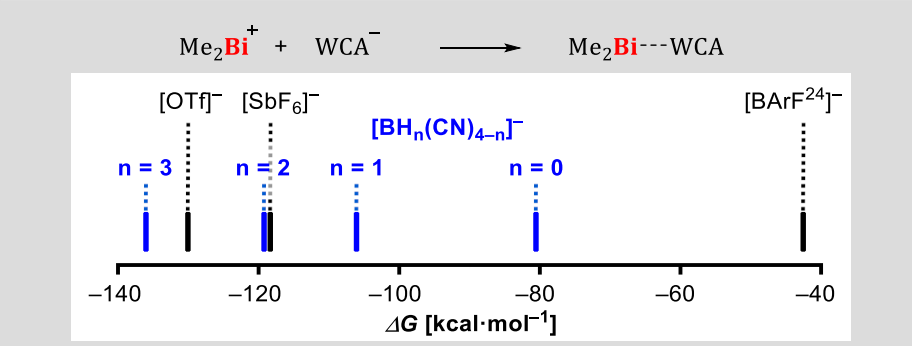

Figure 44. Gibbs energy values for the coordination of WCA^- to Me_2Bi^+. WCA = weakly coordinating anion. Calculations were conducted in the gas phase with the B3LYP functional, the 6-31G(d,p) [H, B, C, N, F], 6-311G(d,p) [S, Cl], and the LANL2DZ [Sb, Bi] basis sets. A dispersion correction (gd3) was applied.

Unsuccessful attempts to generate species of the general formula $[R_2Bi][BH_n(CN)_{4-n}]$ are summarized in Table 8 in the Experimental Part. They will not be discussed in detail, but enabled the establishment of several general principles: i) Diaryl bismuth halides (Ph_2BiCl and Ph_2BiI) do not seem to be suitable for salt eliminations with MHB salts (MHB = tricyanomonohydridoborate), even at elevated temperatures of 60–80 °C, ii) the driving force of reactions with cyanoborate salts

of the lighter and harder alkali metal salts (Na–K) is not sufficient for metathesis with bismuth halides, iii) if the cyanoborate salt shows enhanced reducing properties, other reaction pathways than metatheses are followed. Nonetheless, the synthesis of two cyanoborate salts of the dimethyl bismuth cation succeeded (Scheme 25).

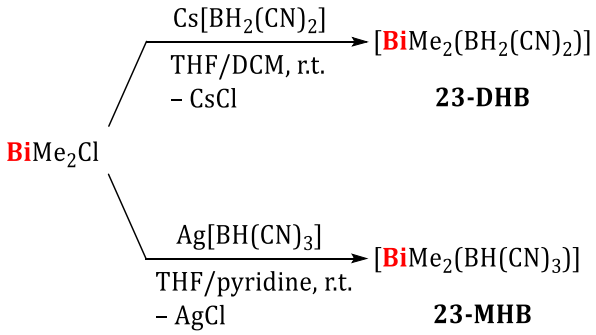

Scheme 25. Formation of the first cyanohydridoborate salts of a bismuth cation. MHB = tricyanomonohydridoborate $[BH(CN)_3]$. DHB = dicyanodihydridoborate $[BH_2(CN)_2]$.

Addition of DCM to an initially colorless solution of CsDHB and $BiMe_2Cl$ in THF led to the formation of a precipitate (DHB = $[BH_2(CN)_2]^-$). Filtration and layering the solution with *n*-pentane led to the formation of colorless crystals after 16 h at –30 °C. These were isolated by filtration and drying *in vacuo*, providing **23-DHB** in 96% yield. **23-MHB** was obtained by reaction of $BiMe_2Cl$ with AgMHB in a mixture of THF and pyridine (10:1), filtration of the precipitate, and layering the colorless filtrate with *n*-pentane. After 16 h at –30 °C colorless crystals of **23-MHB** were obtained by filtration, and dried *in vacuo*, affording **23-MHB** in 72% yield. In repeated syntheses of **23-MHB**, the product was obtained as an oily precipitate, requiring multiple washing cycles with *n*-pentane or recrystallization from THF for purification. Nonetheless, it was possible to obtain pure material of **23-MHB** (according to ^{1}H NMR spectroscopy) in several attempts.

23-DHB and **23-MHB** were crystallographically characterized. **23-DHB** crystallized in the monoclinic space group $P2_1/c$ with $Z = 4$ as a pseudo-merohedral twin with two domains in a 99.8:0.2 ratio which are related by a 177° rotation about the reciprocal [010] axis (Figure 45). The bismuth center adopts a bisphenoidal coordination geometry with the methyl groups in equatorial, and the cyano groups in axial positions (N1–Bi1–N2', 167.0(3)°). Both cyano groups of the anion coordinate to bismuth centers, resulting in infinite chains of $[(BiMe_2)(BH_2(CN)_2)]_\infty$ in the solid state, which extend along the crystallographic b-axis. Other intermolecular interactions are not present. The bismuth carbon bonds (2.238(10)–2.244(10) Å) are within limits of error in the same range as for $[BiMe_2(SbF_6)]$ (2.215(5)–2.223(5) Å).[185] Since **23-DHB** and **23-MHB** are the first bismuth cyanoborates, a comparison of the Bi–N bond lengths with other bismuth cyanoborates is not possible and the Bi–N bond lengths in **23-DHB** (2.480(8)–2.496(8) Å) are compared to nitrile adducts of bismuth complexes. In the latter the Bi–N bonds tend to be longer

(ca. 2.45–2.67 Å).[189,204–207] The bonding parameters within the anion show no irregularities compared to those reported in the literature.[208–210]

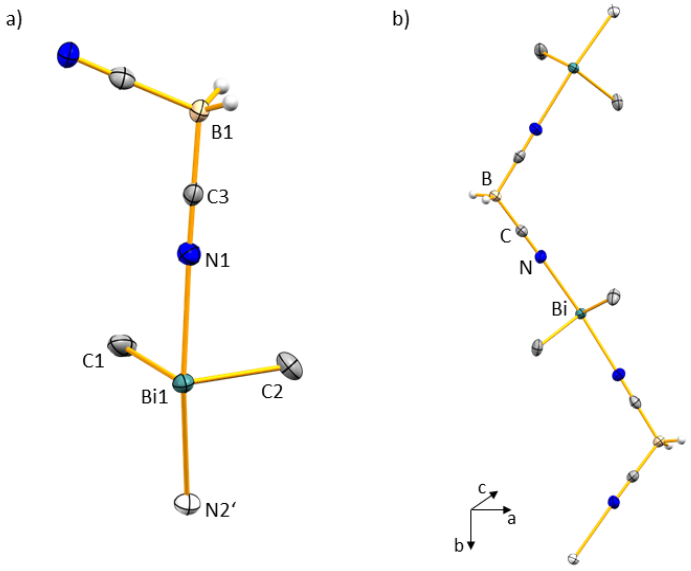

Figure 45. a) Molecular structure of **23-DHB** in the solid state. Displacement ellipsoids are drawn at the 50% probability level. Atoms from secondary molecular units are displayed as white ellipsoids. Hydrogen atoms of methyl groups are omitted for clarity. Selected bond lengths (Å) and angles (°): Bi1–C1, 2.238(10); Bi1–C2, 2.244(10); Bi1–N1, 2.480(8); Bi1–N2', 2.496(8); N1–C3, 1.142(13); B1–C3, 1.580(14); C1–Bi1–C2, 94.0(4); C1–Bi1–N1, 85.1(3); C1–Bi1–N2', 86.6(3); C2–Bi1–N1, 85.8(3); C2–Bi1–N2', 84.8(3); N1–Bi1–N2', 167.0(3); C3–B1–C4; 109.7(9); H–B1–C, 109.7. b) Cut out of coordination polymer $[\{BiMe_2\}\{BH_2(CN)_2\}]_\infty$ in the solid state.

23-MHB crystallized in the monoclinic space group $P2_1/c$ with $Z = 4$ as a pseudo-merohedral twin with two domains in a ratio 80:20 which are related by a 180° rotation about the reciprocal [001] axis (Figure 46).

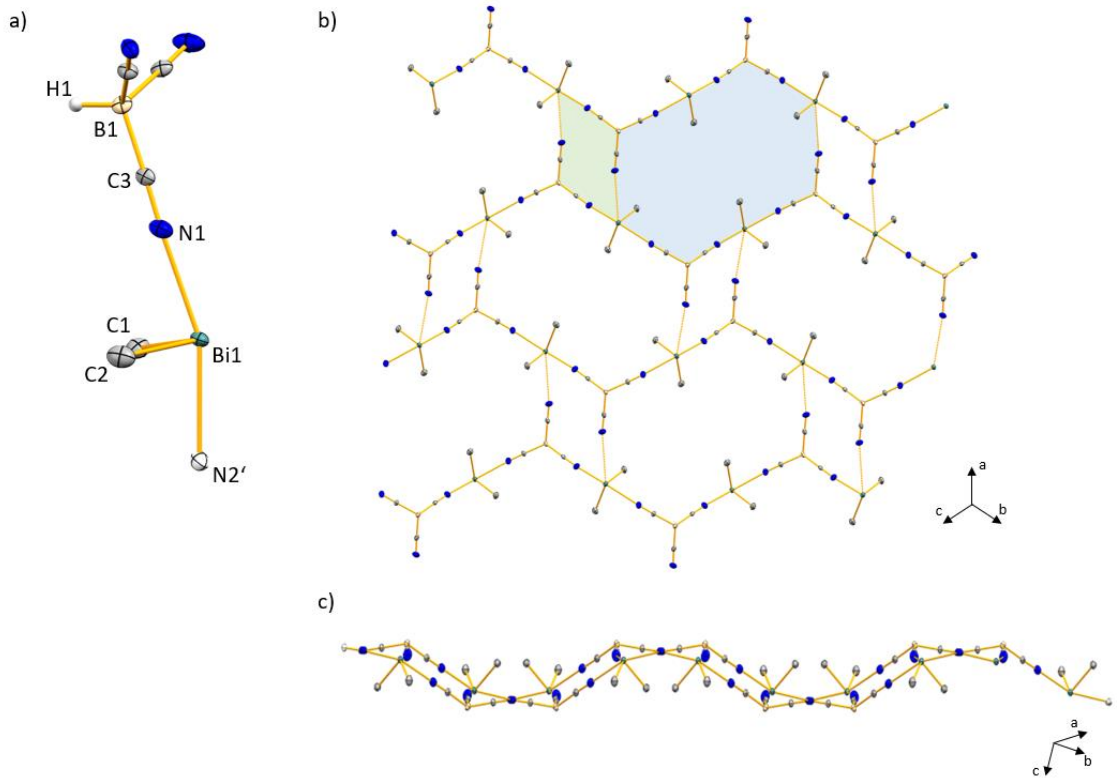

Figure 46. a) Molecular structure of **23-MHB** in the solid state. Displacement ellipsoids are drawn at the 50% probability level. Atoms exceeding one molecular unit are displayed as white ellipsoids. Hydrogen atoms of methyl groups are omitted for clarity. Selected bond lengths (Å) and angles (°): Bi1–C1, 2.203(11); Bi1–C2, 2.239(12); Bi1–N1, 2.442(9); Bi1–N2, 2.550(10); Bi1···N3, 3.435; N1–C3, 1.137(14); B1–C3, 1.584(15); C1–Bi1–C2, 95.9(4); C1–Bi1–N1, 84.9(4); C1–Bi1–N2, 81.3(4); C2–Bi1–N1, 83.9(4); C2–Bi1–N2, 83.9(4); N1–Bi1–N2, 160.5(3); C–B1–C; 109.6(9)–112.2(9); B1–C–N, 177.4(12)–178.1(12); H–B1–C, 108.4. b) and c) Partial view of the 2D coordination polymer $\{[BiMe_2]\{BH(CN)_3\}]_\infty$.

In the solid-state structure of **23-MHB**, all three cyano groups coordinate to bismuth centers, with two shorter Bi–N interactions (2.442(9), 2.550(10) Å), and a longer one (3.44 Å, 5% under the sum of the van-der-Waals radii of 3.62 Å). Considering only the two Bi–C and the two shortest Bi–N interactions, the bismuth atom adopts a bisphenoidal coordination geometry (Figure 46a). As in **23-DHB**, the cyano groups occupy the axial positions (N1–Bi1–N2, 160.5(3)°), and the methyl groups the equatorial positions (C1–Bi1–C2, 95.9(4)°). The bismuth carbon bond situated *trans* to the third cyano group is significantly longer (2.239(12) Å) than the other one (2.203(11) Å). Similarly short Bi–C bonds as the shorter one in **23-MHB** are described for **21**,[185] $[\{BiMe_3\}Cr(CO)_5]$ (2.208(12) Å),[12] an iron bismuth polymer (ca. 2.20 Å),[98] and for an aminobismuthenium cation (2.219(2) Å), respectively.[211] Coordination of the bismuth cation by a third cyano group leads to the formation of a 2D coordination polymer in the solid state, composed of larger and smaller ring systems (Figure 46b and c, rings are marked in green and blue). The bonding parameters within the anion show no irregularities compared to those reported in the literature.[208,212]

Unexpectedly, the solid-state structures of **23-DHB** and **23-MHB** show no coordination of the solvent molecules THF or pyridine, respectively, although the compounds were recrystallized from these solvents. This is in contrast to species like $[BiMe_2(SbF_6)]$ (**21**) and $[BiPh_2(X)]$,[23] which form adducts species of the general formula $[BiR_2L_2][X]$, when exposed to the neutral ligands L (L = neutral ligand, X = counteranion).

The lack of coordination of solvent molecules was also demonstrated by ^{1}H and ^{13}C NMR spectroscopy of both compounds in THF-d_8. Compared to **21-thf**, which shows a ^{1}H NMR resonance for the methyl groups at $\delta(^{1}H)$ = 1.87 ppm and a ^{13}C NMR resonance at $\delta(^{13}C)$ = 48.73 ppm, the resonances for the methyl groups in **23-DHB** and **23-MHB** are shifted to higher field, both in the ^{1}H NMR spectrum, as well as in the ^{13}C NMR spectrum ($\delta(^{1}H)$ = 1.51 (**23-DHB**), 1.58 ppm (**23-MHB**); $\delta(^{13}C)$ = 40.35 (**23-DHB**), 36.46 ppm (**23-MHB**)). In agreement with the DFT studies mentioned above, the chemical shifts obtained for **23-DHB** and **23-MHB** tend to suggest a stronger interaction between the anion and cation in **23-DHB** than in **23-MHB**. Also, NMR spectroscopic analyses suggest that the anion-cation interactions in these borate salts are significantly stronger than in **21**, since the ^{1}H and ^{13}C NMR spectrocoscopic resonances for the methyl groups are downfield shifted in the case of **21** ($\delta(^{1}H)$ = 2.28, $\delta(^{13}C)$ = 64.40 ppm). The ^{1}H NMR spectroscopic resonances for the BH moieties are found at $\delta(^{1}H)$ = 1.22 (**23-DHB**) and 1.88 (**23-MHB**) ppm in the $^{1}H\{^{11}B\}$ NMR spectra. The ^{11}B NMR spectra show resonances at $\delta(^{11}B)$ = –42.1 (**23-DHB**, triplet) and –39.8 (**23-MHB**, doublet) ppm, both with a coupling constant of $^{1}J_{BH}$ = 98 Hz. Whereas the ^{11}B NMR spectroscopic resonance for [EMIm][DHB] (EMIm = 1-ethyl-3-methylimidazolium) stays the same ($\delta(^{11}B)$ = –41.8 ppm), the coupling constant of 94.3 Hz is clearly different than that for **23-DHB**.[212] Similar parameters as for [EMIm][DHB] are obtained for H[DHB], which shows a $^{1}J_{BH}$ coupling constant of 94.3 Hz, and a ^{11}B NMR spectroscopic resonance at $\delta(^{11}B)$ = –41.4 ppm.[208] An IR spectroscopic analysis of **23-DHB** revealed the C–N stretching mode ($\tilde{\nu}_{CN}$ = 2195 cm^{-1}) to be close to that of [EMIm][DHB] ($\tilde{\nu}_{CN}$ = 2192 cm^{-1}), but significantly shifted compared to the corresponding stretching mode for H[DHB] ($\tilde{\nu}_{CN}$ = 2256 cm^{-1}). However, the BH stretching frequency shows a blueshift of almost 20 cm^{-1} in **23-DHB** ($\tilde{\nu}_{BH}$ = 2393 cm^{-1}) compared to the value reported in the literature for [EMIm][DHB] ($\tilde{\nu}_{BH}$ = 2377 cm^{-1}).[212] These spectroscopic results suggest that the ^{11}B NMR, but more pronounced the IR spectroscopy, may be sensitive to changes in the electronic situation within the anion for DHB salts, when the coordination mode of the counter ion remains the same as in the case of H[DHB].

For both **23-DHB** and **23-MHB**, respectively, satisfactory elemental analyses could not be obtained, yet, perhaps due to contamination with CsCl and AgCl, respectively. Future attempts to synthesize **23-DHB** and **23-MHB** should therefore focus on improving yields and purity so that **23-DHB** and **23-MHB** can be isolated and fully characterized. It would also be worthwhile to make

additional attempts to synthesize the other cyanohydridoborates to complete the series $[BiR_2][BH_n(CN)_{4-n}]$ with n = 1–4 and investigate their properties.

3.3 Catalytic Dimerization of 1,2-di-*tert*-butyl-iminoborane

Iminoboranes RB≡NR are isoelectronic to acetylenes, but due to the polarized B–N bond usually more reactive than the latter. It was demonstrated that **21** catalyzes the (unselective) tri-, and oligomerization of 1-pentyne (16 h, ambient temperature), however, with unstatisfactory yields of the trimer 1,3,5-tripropylbenzene. Nonetheless, motivated by this result, the catalytic activity of **21** in the oligomerization of *t*BuN≡B*t*Bu (**24**) was investigated.

The reaction of **24** with 10 mol% of **21** led to the immediate formation of 1,3,2,4-diazadiboretidine $[t\text{BuBN}t\text{Bu}]_2$ as observed by ^{11}B NMR spectroscopy (Scheme 26). The catalytic dimerization of iminoboranes with isonitriles as catalysts has been described by PAETZOLD *et al.*, but the mechanism of the reaction has not been discussed in detail.[213,214] However, it is very likely that the reaction with Lewis acidic **21** as catalyst proceeds by a different mechanism than that reported by PEATZOLD, since they use Lewis basic isonitriles as catalysts.

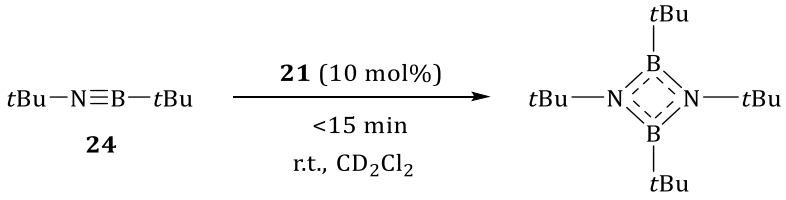

Scheme 26. Reaction of iminoborane **24** with 10 mol% **21**.

Since **21** showed a catalytic activity in the oligomerization of 1-pentyne, an attempt was made to incorporate an organic building block in the form of 1-pentyne into the reaction. For this purpose, stoichiometric amounts of iminoborane **24** and 1-pentyne were reacted with 10 mol% **21** (Scheme 27).

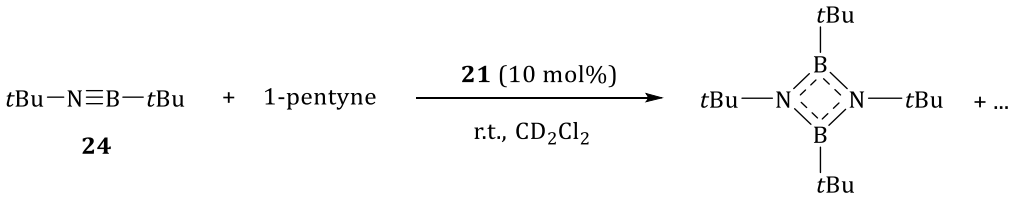

Scheme 27. Reaction of iminoborane **24** with stoichiometric amounts of 1-pentyne and 10 mol% **21**.

The ^{11}B NMR spectrum of the reaction mixture revealed the formation of boroxine,[215] which was confirmed by GCMS analysis. The ^{1}H NMR spectrum indicated the consumption of 1-pentyne,

although no defined products could be assigned to the newly formed set of signals (these resonances do not correspond to the 1-pentyne oligomer). X-ray diffraction analyses of several samples obtained by vapor diffusion crystallization allowed the identification of three decomposition products [*t*BuNH$_3$][*t*BuBF$_3$], [{*t*BuBN*t*Bu}$_2$H][SbF$_6$] and [BiMe$_2$(*t*BuNH$_2$)(SbF$_6$)].

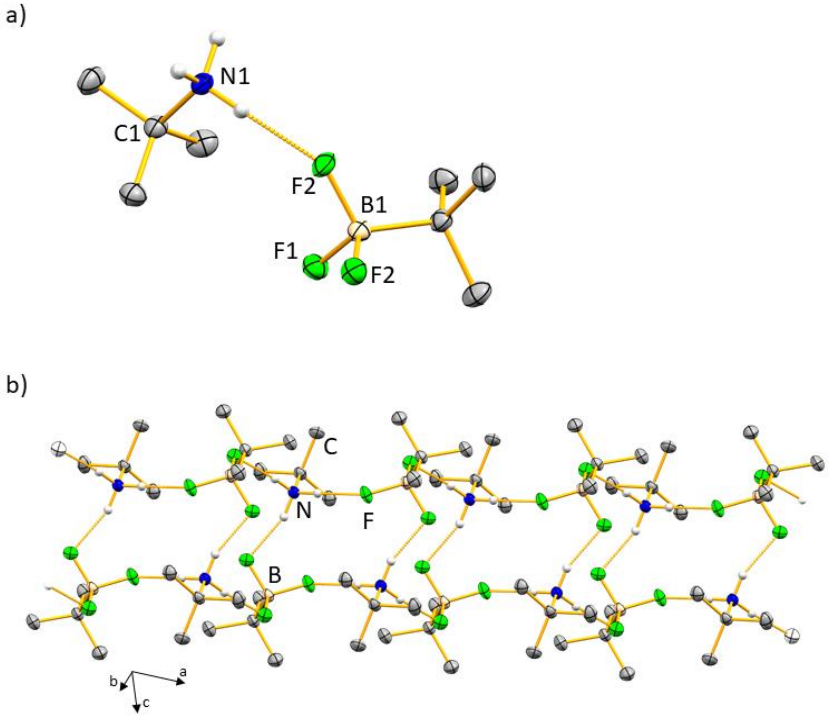

Figure 47. a) Molecular structure of [*t*BuNH$_3$][*t*BuBF$_3$] in the solid state. Displacement ellipsoids are shown at the 50% probability level. Hydrogen atoms of *t*Bu groups are omitted for clarity. Selected bond lengths (Å) and angles (°): B1–F, 1.426(3)–1.434(3); B1–C5, 1.606(3); N1–C1, 1.510(3); F···H, 1.88; C5–B1–F, 112.91(18)–112.94(17); F–B1–F, 104.96(17)–106.60(17); H–N1–C1, 107.9(16)–113.0(15). b) Cut out of coordination polymer [{*t*BuNH$_3$}{*t*BuBF$_3$}]$_\infty$.

The borate salt [*t*BuNH$_3$][*t*BuBF$_3$] crystallized in the triclinic space group $\bar{P}1$ with Z = 2 (Figure 47). Hydrogen bonds between the ammonium cation and fluorides of the borate anion are present (F···H, 1.88 Å), resulting in a two-stranded coordination polymer with cross-links extending through the third F···H interaction. The generation of RBF$_3^-$ indicates the decomposition of the SbF$_6^-$ anion. However, this borate salt was only detected in trace amounts by ^{11}B NMR spectroscopy during the reactions.

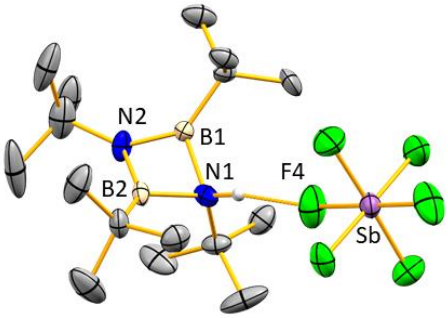

Figure 48. Molecular structure of [{*t*BuBN*t*Bu}$_2$H][SbF_6] in the solid state. Displacement ellipsoids are shown at the 50% probability level. Hydrogen atoms of *t*Bu groups are omitted for clarity. The asymmetric unit contains two chemically identical but crystallographically independent formula units of [{*t*BuBN*t*Bu}$_2$H][SbF_6], only one of which is discussed because the bonding parameters are highly similar. Selected bond lengths (Å) and angles (°): B1–N1, 1.567(16); B1–N2, 1.423(16); B2–N1, 1.570(17); B2–N2, 1.444(19); N–C, 1.518(17)–1.533(13); C–B, 1.549(18)–1.576(15); F···H, 1.99; N–B–N, 92.8(10)–93.7(9); B1–N1–B2, 78.2(9); B1–N2–B2, 87.2(10); H–N1–C, 113.3; B–N1–C, 115.5(9)–118.7(9).

The protonated iminoborane dimer crystallized in the monoclinic space group *Cc* with $Z = 4$ (Figure 48). The asymmetric unit contains two chemically identical but crystallographically independent formula units of [{*t*BuBN*t*Bu}$_2$H][SbF_6], only one of which is discussed because the bonding parameters are highly similar. The protonated diazadiboretidine forms hydrogen bonds with the SbF_6^- anion. PAETZOLD et al. reported the selective coordination of metal chlorides $ZnCl_2$ and $AlCl_3$ to one nitrogen atom of diazadiboretidines.[216] They also reported protolytic ring opening reactions of the four-membered ring upon treatment with protic alcohols, which they attribute to the hydrolysis sensitivity of diazaboretidines.[216] Obtaining the solid-state structure of [{*t*BuBN*t*Bu}$_2$H][SbF_6] now shows for the first time that the protonated form of diazadiboretidines are accessible, and at least stable enough to perform X-ray diffraction analysis. In contrast to the parent compound 1,3-di-*tert*-butyl-2,4-di-*tert*-butyl-diazadiboretidine,[217] the protonated form shows significant differences in the N–B distances. The N–B bonds (1.567(16)–1.570(17) Å) to the ammonium nitrogen are elongated and correspond to B–N single bonds (1.56 Å).[218] The B1/2–N2 bond lengths of 1.423(16) and 1.444(19) Å lie between B–N single and double bonds (B=N, ca. 1.38 Å).[219] The BNBN torsion angle in [{*t*BuBN*t*Bu}$_2$H][SbF_6] (22°) is somewhat larger than in the neutral analog (18°).

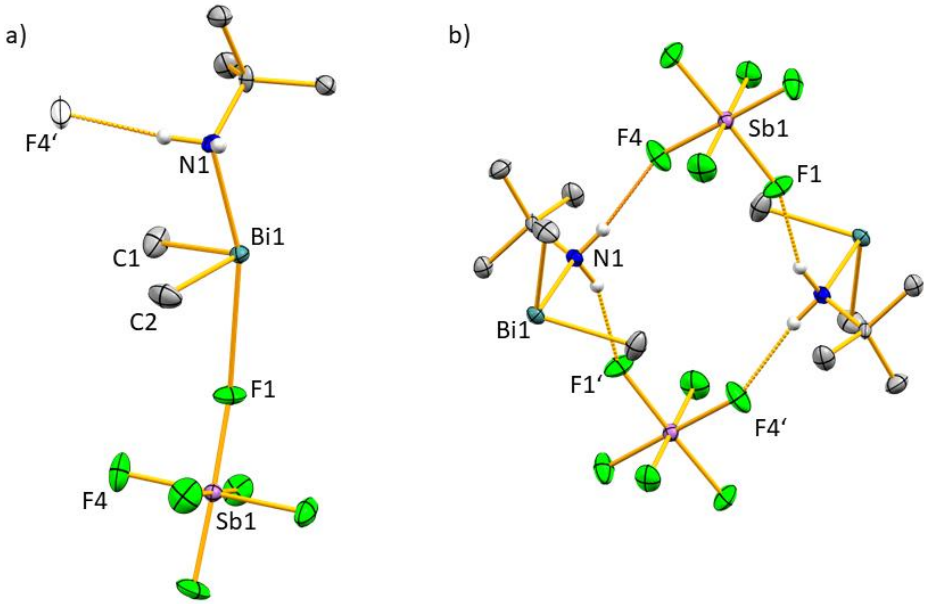

Figure 49. a) Molecular structure of [$BiMe_2$(*t*$BuNH_2$)(SbF_6)] in the solid state. Displacement ellipsoids are shown at the 50% probability level. Hydrogen atoms of *t*Bu and Me groups are omitted for clarity. Selected bond lengths (Å) and angles (°): Bi1–C1, 2.220(5), Bi1–C2, 2.233(5); Bi1–N1, 2.339(3); Bi1–F1, 2.826(3); N1–Bi1–F1, 162.57(11); C1–B1–C2; 93.8(2); N1–B1–C1, 90.51(16); N1–Bi1–C2, 85.13(16); F1–Bi1–C1, 80.04(15); F1–Bi1–C2, 80.95(15). b) Eight-membered rings formed by hydrogen bonds between amine and hexafluoroantimonate.

[$BiMe_2$(*t*$BuNH_2$)(SbF_6)] crystallized in the monoclinic space group $P2_1/n$ with Z = 4 (Figure 49). The bismuth atom adopts a distorted bisphenoidal coordination geometry with the SbF_6^- anion and *t*$BuNH_2$ in the axial positions (162.6°), and methyl groups in equatorial positions with angles around bismuth ranging from 80.0 to 93.8°. The Bi–F distance (2.826(3) Å) is significantly elongated compared to parent compound [$BiMe_2(SbF_6)$] (**21**, 2.451(3)–2.452(3) Å),[185] which is accompanied by a shortening of the N–Bi bond length (2.339(3) Å) compared to other pyridine or amine adducts of bismuth cations like **21-py** (2.519(7) Å), **22** (2.532(3)–2.600(3) Å) or [$Bi(NMe_2)_2(HNMe_2)(BPh_4)$] (2.419(10) Å),[20] and at the lower limit for reported bismuth cations with amines as neutral donor ligands (2.36–2.59 Å).[21,51,220,221] The Bi–C distances are in the range of those observed for parent compound **21**. The amine forms hydrogen bonds to a further SbF_6 moiety, resulting in the formation of eight-membered rings. [$BiMe_2$(*t*$BuNH_2$)(SbF_6)] is the first example of a primary amine adduct of an organometallic bismuth cation, the only other example of a secondary amine adduct is [$Bi(NMe_2)_2(HNMe_2)(BPh_4)$], which decomposes completely within two days in solution to [$BPh_3(NHMe_2)$] and $BiPh(NMe_2)_2$.[20] Since [$BiMe_2$(*t*$BuNH_2$)(SbF_6)] was only obtained in trace amounts, the stability of that compound was not investigated in detail.

Since all decomposition products, as well as the formation of boroxine, indicate the presence of moisture, 1-pentyne was dried and reacted again with **23** and 10 mol% **21**. Although this prevented the generation of boroxine, this time the only product detected by ^{11}B NMR

spectroscopy was the dimer [*t*BuBN*t*Bu]$_2$. In conclusion, **21** acts as a catalyst in the dimerization of iminoborane **24**, however, the catalytic incorporation of alkyne units into the B,N-oligomers or –heterocycles did not succeed via this approach. This might be due to the longer reaction times needed for the oligomerization of 1-pentyne (16 h) compared to the dimerization of **24** (<15 min).

4 The Diphenylbismuth Cation: Synthesis and Characterization

The synthesis of aryl-substituted bismuth cations is well-established and their stoichiometric reactions[137,221] and catalytic activity in organic transformation, e.g. cross-condensation of ketones and aldehydes[48] or Mannich reactions,[49] are well-documented.[23,51,76,82,222,223]

Bismuth(III) cations are in most cases either stabilized by intra- or intermolecular coordination of neutral donor ligands, or by interactions between (weakly) coordinating anions and the bismuth center.[19,23,27,28] Although the synthesis of diphenylbismuth cations stabilized by donor ligands is well-documented, the generation of the corresponding contact ion pairs beside its triflate salt has not been documented in the literature.[224] Analog to the synthesis of **21**, the synthesis of [BiPh$_2$(SbF$_6$)] (**25**) was carried out by reacting BiPh$_2$Cl with AgSbF$_6$, yielding **25** in 77% yield (Scheme 28).

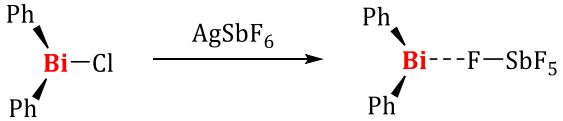

25

Scheme 28. Synthesis of [BiPh$_2$(SbF$_6$)] (**25**).

The addition of a colorless 1,2-difluorobenzene solution of BiPh$_2$Cl to a colorless solution of AgSbF$_6$ in 1,2-difluorobenzene is accompanied by the immediate formation of a colorless precipitate and a color change of the solution to yellow. After filtration and cooling the filtrate to –30 °C for 16 h, **25** was obtained as a yellow solid. The ^{1}H NMR spectrum of **25** in dichloromethane shows the expected resonances for the phenyl groups, as well as significant amounts of benzene. After removing all volatiles *in vacuo* for at least two hours, another ^{1}H NMR spectrum showed an even higher intensity for the benzene resonance. The same observations were also made when working with silanized glassware. This indicates that benzene is formed from the decomposition of the BiPh$_2^+$ cation, although the origin of the hydrogen atom or proton has not been determined. Nevertheless, ^{1}H and ^{13}C NMR spectra of **25** without impurities were obtained by washing the compound with *n*-pentane and drying *in vacuo* for a short period of times (<5 min). The ^{1}H NMR spectroscopic resonances of the phenyl groups in **25** are shifted downfield compared to BiPh$_3$ ($\Delta\delta$ = 0.44–0.76 ppm), as observed for the couple BiMe$_2^+$/BiMe$_3$, owing to the electron deficiency of the bismuth centers in these cations. The ^{13}C NMR spectroscopic resonance for the *ispo*-carbon

of the phenyl groups is found at $\delta(^{13}C)$ = 214.79 ppm, which is an extreme downfield shift compared to neutral parent compound $BiPh_3$ ($\Delta\delta$ = 59.6 ppm). The thf adduct of $BiPh_2^+$ shows a ^{13}C NMR spectroscopic resonance for the same carbon atom at $\delta(^{13}C)$ = 198.46 ppm (**25-thf**) which indicates a significant increase in Lewis acidity of the bismuth atom in **25**.[137] The ^{19}F NMR spectrum shows a resonance for the SbF_6^- anion at $\delta(^{19}F)$ = –122.2 ppm, indicating a strong cation-anion interaction. ^1H NMR spectroscopic monitoring revealed that a dichloromethane solution of **25** decomposes to 20% to biphenyl within 6 h, accompanied by the formation of a black precipitate. It is noteworthy that this decomposition can be prevented by the exclusion of light, and might proceed through a different mechanism than the formation of benzene, which does not occur when **25** is stored in solution.

Crystalline material of **25** was obtained by layering a dichloromethane solution of **25** with *n*-pentane and storage at –30 °C. Several single-crystal X-ray diffraction analyses were performed, however, the crystals that were obtained slowly transformed into an ill-defined oily material during crystal picking,[7] so that the data obtained only serves as proof of connectivity (orthorhombic space group *Pbca* with Z = 8, Figure 50).

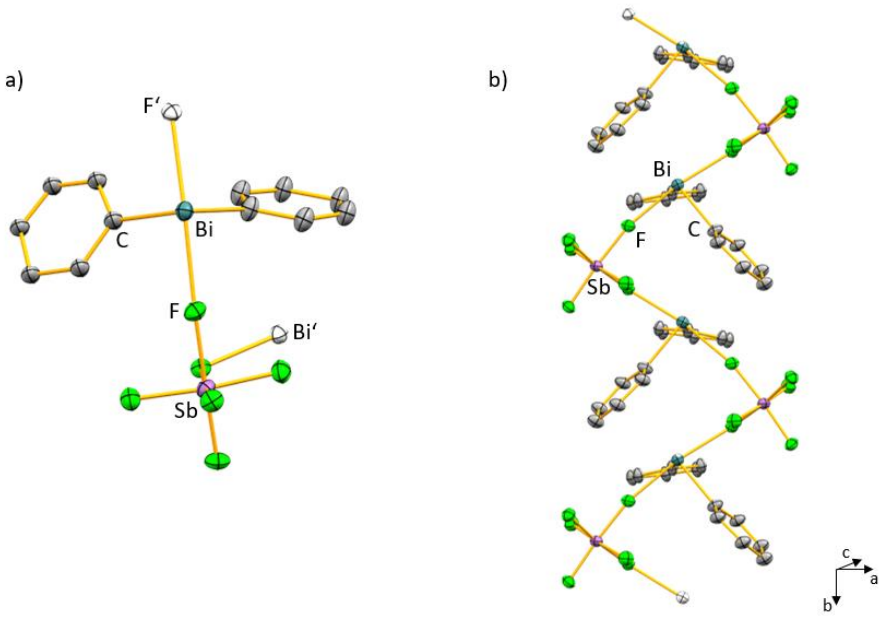

Figure 50. a) Molecular structure of **25** in the solid state. Displacement ellipsoids are shown at the 50% probability level. Hydrogen atoms, a dichloromethane molecule present in the unit cell and disordered phenyl groups are omitted for clarity. Atoms of the next formula unit are depicted as colorless ellipsoids. b) Cut out of coordination polymer $[BiPh_2(SbF_6)]_\infty$ in the solid state.

The bismuth atom adopts a bisphenoidal coordination geometry with the phenyl groups in equatorial positions and the SbF_6^- anion in one of the axial positions. A second SbF_6^- anion of a neighboring formula unit occupies the second axial position, resulting in a polymeric structure

[7] A melting point of 58 °C was determined by visual monitoring of isolated material in the absence of Krytox.

along the crystallographic b-axis in the solid state, analog to the molecular structure of **21**.[185] According to distance criteria, arene···Bi interactions might be present, however, this can only be discussed with better data quality.

During the synthesis of **25**, trace amounts of another colorless crystalline solid were obtained, which were suitable for single-crystal X-ray diffraction analysis. The data revealed the formation of [$BiPh_2$($BiPh_2Cl$)(SbF_6)], an adduct between **25** and the starting material $BiPh_2Cl$ (**25-$BiPh_2Cl$**, triclinic space group $\bar{P}1$ with Z = 2, Figure 51).

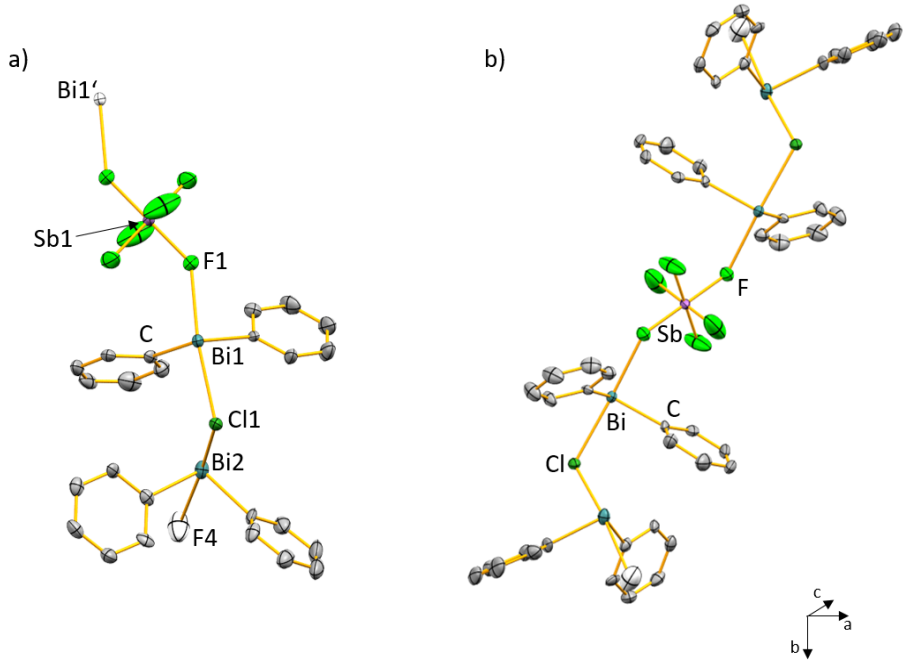

Figure 51. a) Molecular structure of **25-$BiPh_2Cl$** in the solid state. Displacement ellipsoids are shown at the 50% probability level. Hydrogen atoms are omitted for clarity. Atoms of the next formula unit are depicted as colorless ellipsoids. Selected bond lengths (Å) and angles (°): Bi–C, 2.221(9)–2.243(8); Bi–Cl, 2.688(2), 2.706(2); Bi–F, 2.568(6), 2.573(9); C–Bi–C, 97.0(3), 99.1(4); C–Bi–Cl, 87.0(2)–91.6(2); C–Bi–F, 79.1(3)–86.1(3); F–Bi–Cl, 164.7(2)–169.48(15). b) Representation of the one-dimensional coordination polymer [{$BiPh_2$($BiPh_2Cl$)}{SbF_6}]$_\infty$.

As expected, the $BiPh_2Cl$ forms an intermolecular bond to $BiPh_2^+$ through the chloride substituent (a coordination via the bismuth atom in $BiPh_2Cl$ is not to be expected due to the Lewis acidity of bismuth halides, and the good donor ability of chloride ligands). Both bismuth atoms adopt bisphenoidal coordination geometries with the carbon ligands in equatorial (C–Bi–C/F/Cl, 79.1(3)–99.1(4)°), and the chlorine and fluorine atoms of SbF_6^- anions in axial positions (F1–Bi1–Cl1, 169.48(15)°; Cl1–Bi2–F4, 164.7(2)°). The Bi–F and Bi–Cl bonds to each of the two bismuth centers are very similar (Bi–F, 2.568(6), 2.573(9) Å, Bi–Cl, 2.688(2), 2.706(2) Å), indicating a delocalization of the positive charge across both bismuth centers. The Bi–Cl distances in **25-$BiPh_2Cl$** are shortened compared to those in the precursor $BiPh_2Cl$ (ca. 2.74–2.76 Å).[225] The Bi–C distances (2.221(9)–2.243(8) Å)in **25-$BiPh_2Cl$** are significantly longer than those in $BiPh_2Cl$

(ca. 2.12–2.14 Å),[225] somewhat shorter than in $BiPh_3$ (Bi–C, 2.21(2)–2.25(3) Å),[226] and within the range of those found in other diarylbismuth cations.[82,137] Due to the coordination of hexafluoroantimonate to two bismuth centers, a polymeric structure is formed in the solid state, which extends along the crystallographic b-axis.

Like **21**, $[BiPh_2(SbF_6)]$ is a yellow solid, although its adducts with neutral donor ligands are colorless.[23] A UV-vis spectrum of **25** in dichloromethane solution shows a broad absorption band with a maximum at 261 nm, which stretches into the visible region up to $\lambda > 400$ nm.

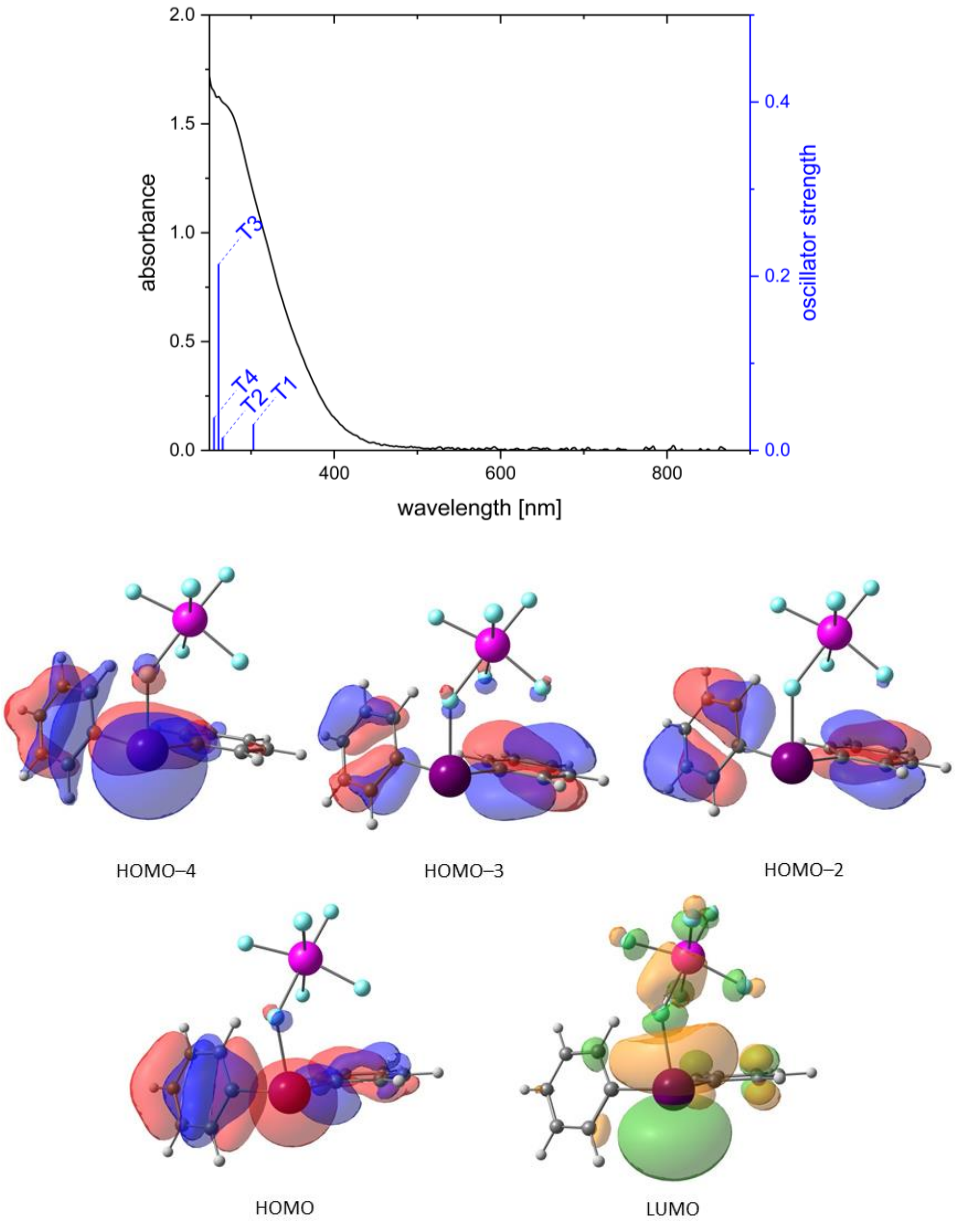

Figure 52. Top: Experimental UV-vis spectrum of **25** (2.4 mM) in dichloromethane (black, absorption maximum at 261 nm) and calculated transitions (blue). Bottom: Frontier molecular orbitals of compound **25** (isovalues = 0.03) with main contributions to transition T3.

Additionally, (TD)-DFT studies were performed with the Gaussian program.[103] The results presented herein were obtained with the functionals B3LYP[104] for optimizations and CAM-B3LYP

for TD-DFT calculations,[105] Grimme D3 dispersion corrections,[106] and 6-31G(d,p)[107] [H, C, F] and LANL2DZ[108–110] [Sb, Bi] basis sets with the PCM solvent model (dichloromethane). In good agreement with the experimental spectrum, a singlet-singlet transition with a pronounced oscillator strength at 261 nm (T3) was obtained (Figure 52). This absorption corresponds to HOMO–4→LUMO (6%), HOMO–3→LUMO (53%), HOMO–2→LUMO (26%), and HOMO→LUMO (10%) transitions. While the HOMO–4 and HOMO are associated with Bi–C σ-bonds, the HOMO–3 and HOMO–2 correspond to ligand-centered orbitals. The LUMO represents the vacant p-orbital of the bismuth center, which has also partial Bi–F σ*-antibonding character (Figure 52).

In the following, an attempt was made to transfer the synthesis of the Bi→Bi adduct $[BiMe_2\{BiMe_3\}][SbF_6]$ to the phenyl analog (Scheme 29, see Chapter VIII). To this end, one equivalent of $BiPh_3$ in dichloromethane solution was combined with one equivalent of **25** in DCM.

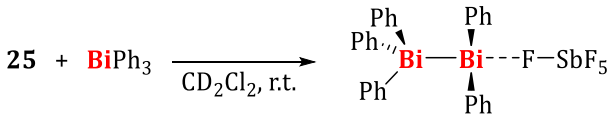

Scheme 29. Reaction of **25** with $BiPh_3$.

Comparison of the ^1H NMR spectrum of the reaction mixture with ^1H NMR spectra of the isolated starting materials shows significant shifts of the resonances, and that all phenyl groups in the product are magnetically equivalent at room temperature, respectively (Figure 53).

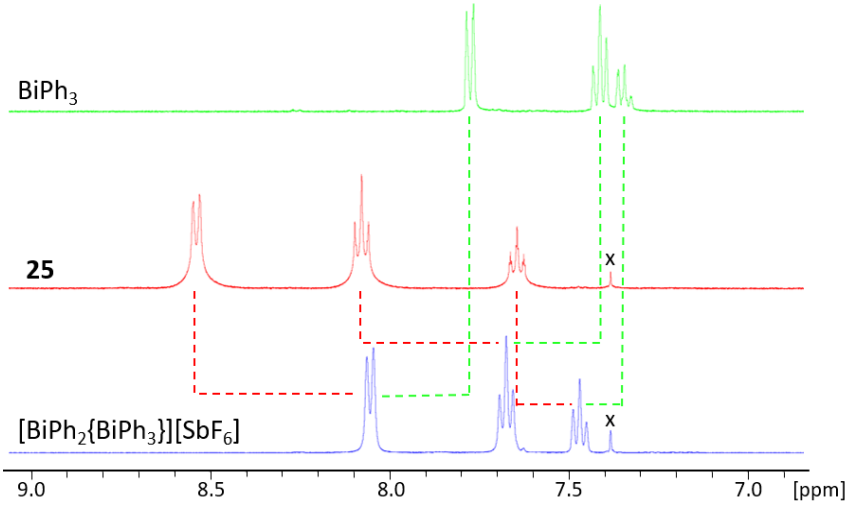

Figure 53. Top: Aromatic region of the ^1H NMR spectrum of $BiPh_3$ in CD_2Cl_2. Middle: Aromatic region of the ^1H NMR spectrum of $[BiPh_2(SbF_6)]$ (**25**) in CD_2Cl_2. Bottom: Aromatic region of the ^1H NMR spectrum of $[BiPh_2\{BiPh_3\}][SbF_6]$ in CD_2Cl_2. Resonances marked with a black x correspond to trace amounts of benzene (see above). Red and green dashed lines illustrate the shifts of the phenyl resonances.

A variable temperature ^{1}H NMR spectroscopic analysis of the reaction mixture did not lead to a splitting of the signals, even at –80 °C, so that a line shape analysis could not be carried out.

However, attempts to crystallize the product out of the reaction mixture by cooling the solution to –30 °C for several days, or layering the solution with *n*-pentane yielded the starting materials $BiPh_3$ or **25** as crystalline solids. Further attempts to isolate the second Bi→Bi adduct in form of $[BiPh_2\{BiPh_3\}][SbF_6]$ were not made in the course of this thesis.

Nonetheless, with the ^{1}H NMR spectra in hand, it seems like a worthwhile goal to test further conditions to isolate the product, or to characterize the Bi→Bi adduct more closely in solution, if isolation fails. In this context, a initial step would be to measure ^{1}H DOSY NMR experiments to confirm adduct formation in solution.

5 Dibenzobismepine Cations: Synthesis, Characterization, and Reactivity towards Platinum(0) Complexes

Recently, our group reported the synthesis of cationic dibenzobismepine species via salt eliminations (Scheme 30, left).[82]

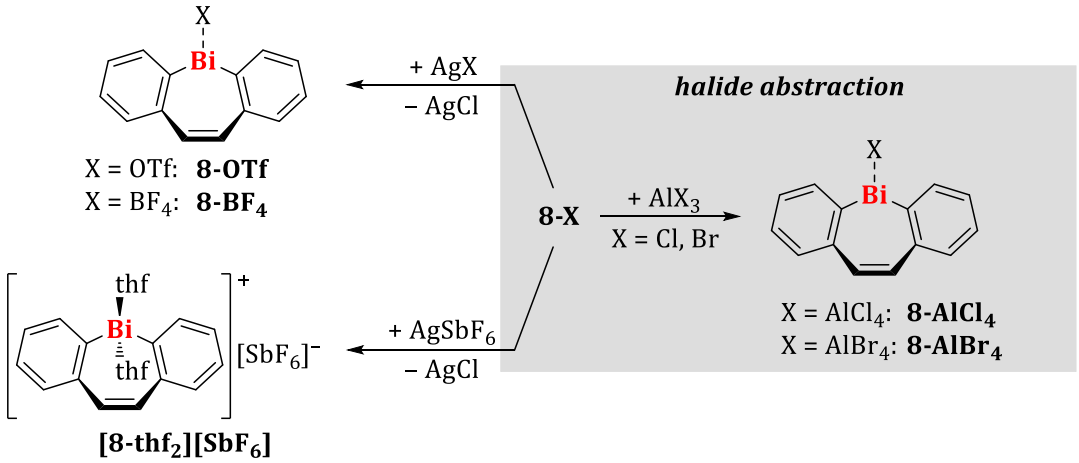

Scheme 30. Synthesis of cationic bismepine species via salt elimination[82] and halide abstraction.

In the course of this thesis, a second pathway to cationic bismepine species was established by halide abstraction reactions with aluminum trihalides (Scheme 30, right). To avoid ligand exchange reactions, the halobismepines were reacted with the aluminum halide carrying the same halide. Reactions of **8-I** with AlI_3 led to decomposition to several unidentified new species containing aromatic moieties, preventing the isolation of **8-AlI$_4$**. The reactions of **8-Cl** with $AlCl_3$, and **8-Br** with $AlBr_3$ in benzene solution, however, led to the formation of the desired cationic bismuth species **8-AlX$_4$**. It was not possible to isolate **8-AlCl$_4$** due to decomposition during work-up. Both reaction mixtures were analyzed by ^{1}H NMR spectroscopy, revealing the full consumption of the starting materials after addition of the aluminum halide at ambient

temperature. In both cases, the α-protons of the bismepine core are shifted upfield by $\Delta\delta$ = 0.14 (**8-AlCl$_4$**) and 0.21 (**8-AlBr$_4$**) ppm, respectively. Compared to **[8-thf$_2$][SbF$_6$]** and **8-BF$_4$**, which also show an upfield shift of these protons in comparison to **8-X** (X = Cl, Br, I), the shift is less pronounced for **8-AlX$_4$**, which might indicate a stronger cation-anion interaction. This is in contrast to the ^{13}C NMR spectrum of **8-AlCl$_4$**, which shows a resonance for the *ipso*-carbon at $\delta(^{13}C)$ = 204.30 ppm. So far, this resonance shows the highest chemical shift for the *ipso*-carbon atoms of cationic dibenzobismepines, suggesting a rather weak interaction between the bismuth atom and the counteranion.[82] No ^{13}C NMR spectrum was collected for **8-AlBr$_4$**. The broad signals in the ^{27}Al NMR spectra of **8-AlCl$_4$** ($\delta(^{27}Al)$ = 103.1 ppm) and **8-AlBr$_4$** ($\delta(^{27}Al)$ = 84.5 ppm) indicate a significant interaction of the aluminate anions with the bismuth atom, which is in accordance with the ^{1}H NMR spectroscopic results. The contradictory results of the ^{1}H and ^{27}Al NMR spectra compared to the data of the ^{13}C NMR spectrum do not allow an exact estimation of the electronic situation at the bismuth center, therefore additional investigations (such as theoretical calculations) will be necessary to generate a better understanding of this class of compounds. However, as the Lewis acidity of the aluminum trihalides increases ($AlCl_3$ < $AlBr_3$ < AlI_3),[227] the stability of the bismepine aluminate complexes appears to decrease, since the anion-cation interactions become increasingly weaker going down the halide group.

Material suitable for single-crystal X-ray diffraction analysis of **8-AlBr$_4$** was obtained by filtration of the reaction mixture, layering the filtrate with *n*-pentane and storage at ambient temperature for 20 h (monoclinic space group $P2_1/c$ with Z = 4, Figure 54).

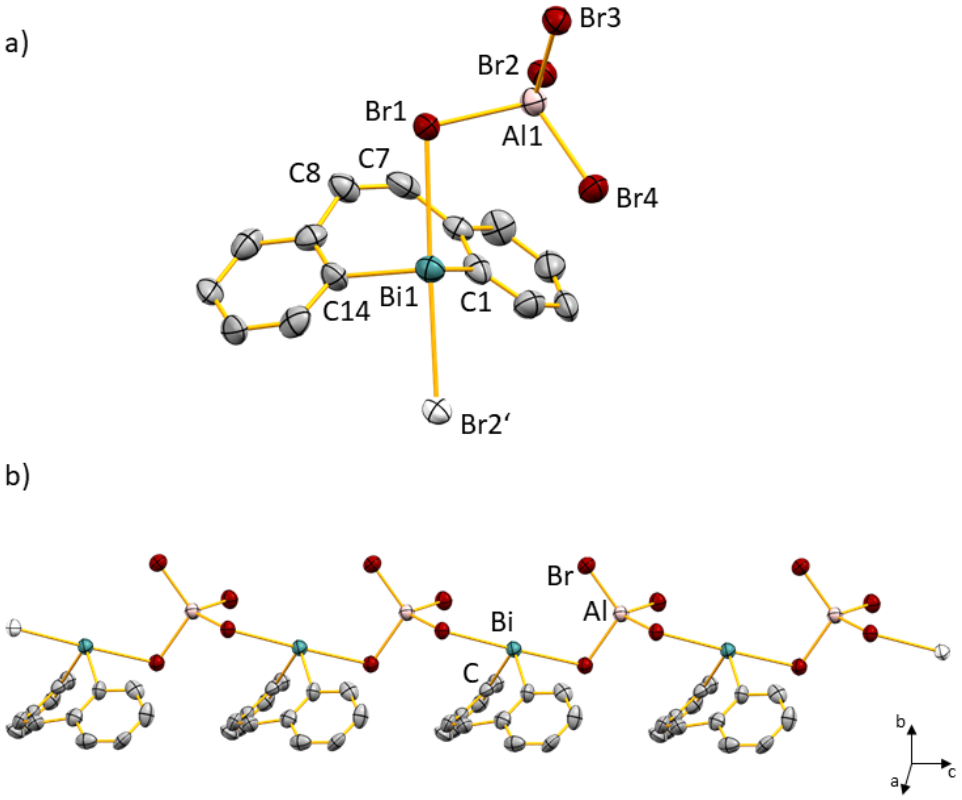

Figure 54. a) Molecular structure of **8-AlBr$_4$** in the solid state. Displacement ellipsoids are shown at the 50% probability level. Hydrogen atoms are omitted for clarity. Atoms of the next formula unit are depicted as colorless ellipsoids. Selected bond lengths (Å) and angles (°): Bi–C1, 2.220(15); Bi1–C14, 2.249(15); Bi1–Br1, 2.9954(16); Bi1–Br2', 3.0138(15); C7–C8, 1.33(2); Al1–Br1, 2.350(4); Al1–Br2, 2.350(4); Al1–Br3, 2.258(4); Al1–Br4, 2.257(4); C1–Bi1–C14, 93.2(6); C1–Bi1–Br1, 87.7(4); C14–Bi1–Br1, 87.1(4); C1–Bi1–Br2', 94.0(4); C14–Bi1–Br2', 93.3(4); Br1–Bi1–Br2', 178.24(5). b) Cut out of coordination polymer $[\{(C_{14}H_{10})Bi\}\{AlBr_4\}]_\infty$ in the solid state.

The bismuth center in **8-AlBr$_4$** adopts a bisphenoidal coordination geometry with bromine atoms in axial positions (178.24(5)°). The solid-state structure of **8-AlBr$_4$** is closely related to that of **8-OTf**, which also shows a flattening of the bismepine core compared to halobismepines **8-X** (X = Cl, Br, I). The angle between the mean planes of the benzo groups in **8-AlBr$_4$** (127°) is significantly larger than those in **8-X** (X = Cl, Br, I, 91.3–100.2°).[82] The Bi–Br bonds in **8-AlBr$_4$** (2.9954(16)–3.0138(15) Å) are significantly longer than in the starting material **8-Br** (2.6407(9) Å), resembling the dative nature of such bonds in **8-AlBr$_4$**.The aluminate anion acts as a bridging counterion with two elongated Al–Br bond lengths of the bridging bromides (ca. 2.35 Å) and two shorter ones of the terminal bromides (ca. 2.25 Å), resulting in the formation of a one-dimensional coordination polymer in the solid state (Figure 54b).

The reactions of **8-X** with AlX_3 (X = Cl, Br, I) appear to be strongly solvent-dependent. Reactions in the electron-donating solvent THF did not lead to consumption of the starting materials,

presumably because of the formation of the aluminum halide thf adducts, which do not react in halide abstractions.

In conclusion, the aluminate complexes **8-AlX$_4$** (X = Cl, Br) show lower stabilities both in solution and in the solid state than the previously described dibenzobismepine salts, which is why further analytical data was not obtained and reactivity studies of these compounds were not performed.

However, in the following the reactivity of **[8-thf$_2$][SbF$_6$]** towards platinum(0) complexes was investigated (for the reactivity of **[8-thf$_2$][SbF$_6$]** towards other transition metal complexes, as well as unsuccessful reactions with platinum complexes see Table 9 in the Experimental Part).

The addition of [Pt(cAAC^{Me})(PCy$_3$)] to a colorless solution of **[8-thf$_2$][SbF$_6$]** in THF-d$_8$ led to a color change to deep red (cAAC^{Me} = *N*-(2,6-di*iso*propylphenyl)-3,3,5,5-tetramethylpyrrolidin-2-ylidene). The ^{1}H NMR spectrum of the reaction mixture revealed an upfield shift of the resonance of the olefin protons from the dibenzobismepine ($\Delta\delta$ = 1.47 ppm). This indicates the presence of an olefin···Pt interaction in solution (see Chapter V). Crystallization attempts led to a red solid, which could not be analyzed in more detail due to insufficient amounts of material and decomposition in the solid state, as well as in solution. However, repeating the reaction in pyridine yielded a yellow solid after crystallization from benzene (Scheme 31, top).

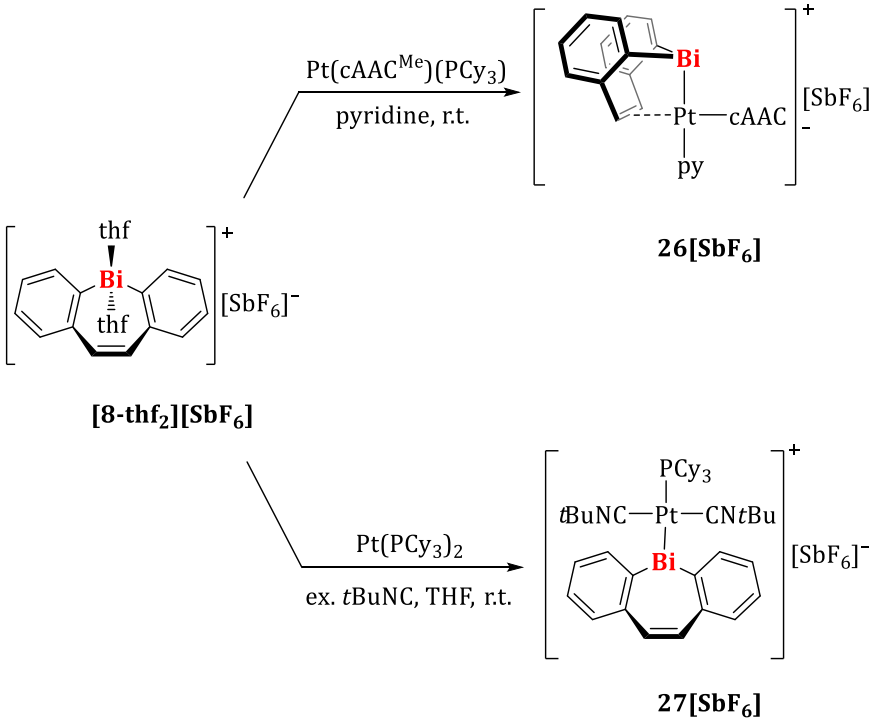

Scheme 31. Reaction of **[8-thf$_2$][SbF$_6$]** with platinum(0) complexes.

Single-crystal X-ray diffraction analysis of the isolated yellow solid revealed the formation of **26[SbF$_6$]** (Figure 55). The compound crystallized in the triclinic space group $\bar{P}1$ with Z = 2. The bismuth atom displays a distorted trigonal pyramidal coordination geometry with C–Bi bonds

(2.259(7)–2.272(8)) significantly elongated compared to the starting material **[8-thf$_2$][SbF$_6$]** (2.223(5)–2.238(5) Å), and a sum of angles around Bi1 of 261°. The PCy_3 ligand in [Pt(cAAC^{Me})(PCy_3)] is replaced by the olefin bridge of the bismepinyl ligand, with an olefin···Pt distance of ca. 2.12 Å. The platinum center adopts a distorted square planar coordination geometry with the bismuth atom and a pyridine ligand in *trans* positions. The Bi–Pt bond in **26[SbF$_6$]** (2.6890(4) Å) is longer than the corresponding bond in [Pt({*o*-$PPh_2C_6H_4$}$_2$Bi)X] (X = Cl, Br, I, 2.6641(13), 2.6491(5), 2.6363(2) Å) reported by LIMBERG *et al.*, and shorter than in [Pt({*o*-$PPh_2C_6H_4$}$_2$BiOTf)Cl_2] (ca. 2.73 Å).[125] The Bi–Pt bond in [Pt({*o*-$PPh_2C_6H_4$}$_2$Bi)X] (X = Cl, Br, I) was described as a covalent interaction between the metal centers, and the longer Bi–Pt bond in [Pt({*o*-$PPh_2C_6H_4$}$_2$BiOTf)Cl_2] was ascribed to a dative interaction between the two metals. Thus, based on distance critera of the Bi–Pt interaction in **26[SbF$_6$]**, an unambiguous classification either as a dative or as a covalent Bi–Pt interaction is not possible. The elongation of the C–Bi bonds in **26[SbF$_6$]** (2.259(7)–2.272(8) Å) compared to those in **[8-thf$_2$][SbF$_6$]** (2.223(5)–2.238(5) Å) rather suggests a covalent nature of the Bi–Pt interaction, due to a reduced electron defiency of the bismuth atom in **26**$^+$ compared to **[8-thf$_2$]**$^+$, which is in accordance with the reported Bi–C distances (ca. 2.27 Å) for the complexes prepared by LIMBERG *et al.* [Pt({*o*-$PPh_2C_6H_4$}$_2$Bi)X] (X = Cl, Br, I).[125] The assumed covalency of the Pt–Bi bond and the presence of the SbF_6^- anion indicates a mono cationic Pt(+II) complex, resulting from the oxidative addition of **[8-thf$_2$][SbF$_6$]** to the Pt(0) precursor. No strong directional bonding interactions between cation and anion were observed based on distance criteria.

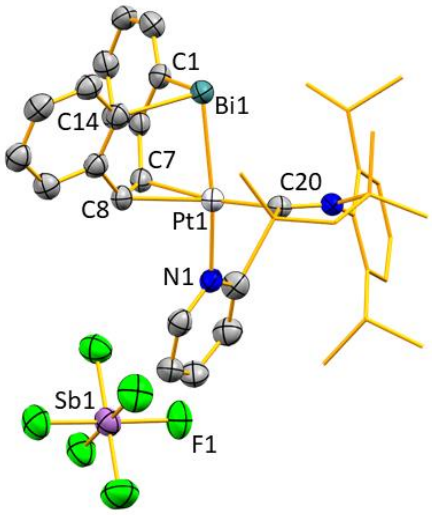

Figure 55. Molecular structure of **[26][SbF$_6$]** in the solid state. Displacement ellipsoids are drawn at the 50% probability level. Hydrogen atoms, lattice bound benzene molecules and ellipsoids of the cAAC^{Me} ligand are omitted for clarity. Selected bond lengths (Å) and angles (°): Bi1–Pt1, 2.6890(4); Bi1–C, 2.259(7), 2.272(8); Pt1–N1, 2.146(6); Pt1–C20, 1.999(7); Pt1–$C_{olefiin}$, 2.199(7), 2.264(7); C7–C8, 1.375(11); C1–Bi1–C14, 86.7(3); C–Bi1–Pt1, 85.8(2), 88.79(19); Bi1–Pt1–N1, 167.76(16); Bi1–Pt1–C20, 90.7(2); N1–Pt1–C20, 100.6(3).

Obtaining larger amounts of substance for isolation and complete characterization of **26[SbF$_6$]** did not succeed. **26[SbF$_6$]** shows full decomposition in solution after 3 h to unidentified substances. However, during the attempted preparation of a larger batch of **26[SbF$_6$]**, small amounts of another crystalline material were obtained in one case. X-ray diffraction analysis revealed the formation of [Pt(cAAC^{Me})(PCy$_3$)(BiCl$_2$)Cl], the oxidative addition product of the bismuth chloride bond of BiCl$_3$ across [Pt(cAAC^{Me})(PCy$_3$)] (monoclinic space group, $P2_1/c$ with Z = 4, Figure 56). The origin of BiCl$_3$, which consequently must have been present in the reaction solution, can be assumed to result from the synthesis of **[8-thf$_2$][SbF$_6$]**.

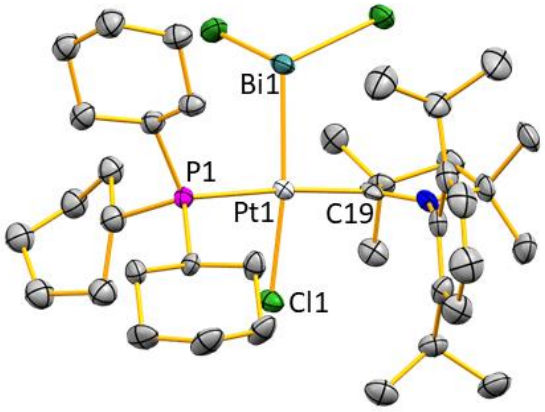

Figure 56. Molecular structure of [Pt(cAAC^{Me})(PCy$_3$)(BiCl$_2$)Cl] in the solid state. Displacement ellipsoids are drawn at the 50% probability level. Hydrogen atoms and lattice bound benzene molecules are omitted for clarity. Selected bond lengths (Å) and angles (°): Bi1–Pt1, 2.6074(6); Bi1–Cl, 2.541(2)–2.5490(19); Pt1–P1, 2.3584(18); Pt1–Cl1, 2.3788(17); Pt1–C19, 2.037(7); Bi1–Pt1–Cl1, 171.08(5); Bi1–Pt1–C19, 94.44(18); Bi1–Pt1–P1, 90.27(5); Cl2–Bi1–Cl3, 91.26(7); Cl–Bi1–Pt1, 100.20(5), 108.55(5); P1–Pt1–C19, 174.33(19).

The bismuth atom adopts a distorted trigonal pyramidal coordination geometry with sum of angles around Bi1 of 300°. Intermolecular interactions, which are present in the related *trans*-[PtCl(PCy$_3$)$_2$(BiCl$_2$)] complex,[228] do not occur in [Pt(cAAC^{Me})(PCy$_3$)(BiCl$_2$)Cl] based on distance criteria. The Pt–Bi bond length (2.6074(6) Å) is in the same range as in *trans*-[PtCl(PCy$_3$)$_2$(BiCl$_2$)] (ca. 2.60 Å), but significantly shorter than that in **26[SbF$_6$]** (2.6890(4) Å), which might reflect the higher electron deficiency of the bismuth atom resulting from the chloride substituents. The platinum center adopts a distorted square pyramidal coordination geometry similar to that in *trans*-[PtCl(PCy$_3$)$_2$(BiCl$_2$)]. Further analytical data for [Pt(cAAC^{Me})(PCy$_3$)(BiCl$_2$)Cl] was not obtained.

26[SbF$_6$] could not be obtained in sufficient quantities in an analytically pure form. However, since the change from THF to pyridine as polar solvents seems to increase the stability of the resulting platinum bismuth complex, the use of even stronger σ-donating ligands to stabilize the system was probed.

The reaction of the bismepine cation **[8-thf$_2$][SbF$_6$]** with [Pt(PCy$_3$)$_2$] in THF solution led to full conversion of the starting materials according to ^{1}H and ^{31}P NMR spectroscopy. The ^{1}H NMR spectrum of the reaction mixture showed an upfield shift of the olefin protons in the bismepinyl ligand ($\Delta\delta$ = –1.01 ppm), indicating the presence of a transition metal-olefin interaction. The ^{31}P NMR spectrum showed a major resonance at δ(^{31}P) = 40.83 ppm and minor amounts of free PCy$_3$. The resonance at δ(^{31}P) = 40.83 ppm showed a $^1J_{PPt}$ coupling constant of 2881.4 Hz, indicating two phosphine ligands in a *trans* conformation. These two structural features, i.e. the presence of an olefin···Pt interaction and two phosphane ligands in *trans* positions, can only be combined in a dinuclear complex (Scheme 32).

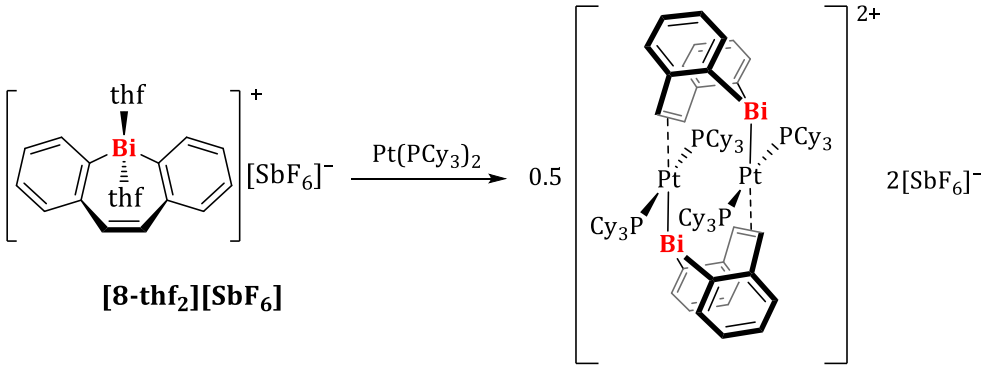

[8-thf$_2$][SbF$_6$]

Scheme 32. Reaction of **[8-thf$_2$][SbF$_6$]** with PCy$_3$ and postulated dinuclear reaction product.

However, attempts to isolate the reaction product led to decomposition and the isolation of a black solid, presumably "bismuth black".[16] LIMBERG *et al.* succeeded in the isolation of a platinum bismuth complex by adding *t*BuNC to the reaction mixture. They presumed an equilibrium between the isolated *tert*-butylisonitrile-free bismuth platinum complex and a complex in which the isonitrile coordinates to the metal center, thus stabilizing the complex. In their hands, only the isonitrile-free complex crystallized from this equilibrium.[18]

Based on these results, **[8-thf$_2$][SbF$_6$]** was reacted with [Pt(PCy$_3$)$_2$] in the presence of one and two equivalents of *t*BuNC, respectively. Both attempts led to decomposition of the reaction product. However, the use of an excess of *t*BuNC yielded a yellow crystalline solid after crystallization from the reaction mixture in THF and *n*-pentane at –30 °C (Scheme 31, bottom). The solid-state structure of the reaction product revealed the formation of [({C$_{14}$H$_{10}$}Bi)Pt(PCy$_3$)(*t*BuNC)$_2$] **27[SbF$_6$]** (monoclinic space group $P2_1$ with Z = 2, Figure 57).

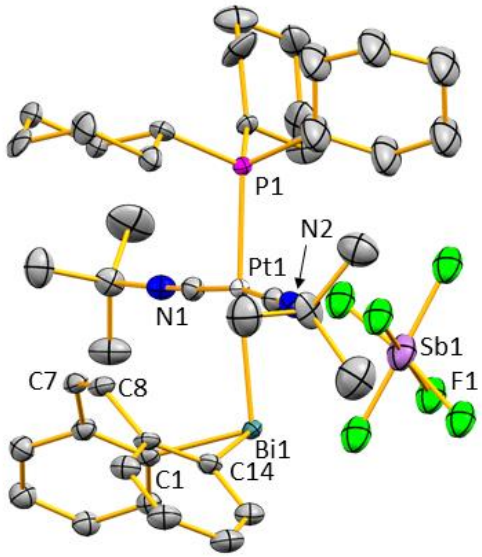

Figure 57. Molecular structure of **[27][SbF$_6$]** in the solid state. Displacement ellipsoids are shown at the 50% probability level. Split positions of disordered *t*Bu groups and SbF_6 anions, hydrogen atoms and THF molecules in the lattice are omitted for clarity. Selected bond lengths (Å) and angles (°): Bi1–Pt1, 2.7417(7); Bi1–C1, 2.250(14); Bi1–C14, 2.250(13); Pt1–C, 1.945(12)–1.960(12); Pt1–P1, 2.351(3); C7–C8, 1.350(18); C1–Bi1–C14, 88.3(5); Bi1–Pt1–P1, 172.93(8); C–Bi1–Pt1, 100.6(3)–100.7(3); C_{NC}–Pt1–C_{NC}, 169.8(5); C_{NC}–Pt1–Bi1, 86.1(4), 87.5(4).

27[SbF$_6$] contains a monocationic platinum complex (**27**$^+$) with two isonitriles, one cyclohexylphosphane and one bismepinyl unit as ligands. The platinum center adopts a distorted square planar coordination geometry with the isonitriles in *trans* positions. In contrast to **26**$^+$, in which the bismepinyl ligand binds through the bismuth atom and the olefin backbone to the transition metal center, a platinum-olefin interaction is not present in **27**$^+$ based on distance criteria. This can also be seen from the C7–C8 bond length of 1.350(18) Å, which is in the range of a C=C double bond.[99] The bismuth atom adopts a trigonal pyramidal coordination geometry with a sum of angles around Bi1 of ca. 289°. The estimated standard deviations of the Bi–C distances in **27**$^+$ are relatively large, which is why these bond lengths cannot be discussed. The Bi–Pt bond length (2.7417(7) Å) is significantly longer than in the related species **26[SbF$_6$]** (2.6890(4) Å), although a direct comparison is hampered by the differing chelating bonding mode of the bismepinyl ligand in **26[SbF$_6$]**. Nonetheless, both bond lengths lie in the range of reported Bi–Pt distances in platinum bismuth compounds (2.6119(14)–2.8373(11) Å).[18,125,229,230]

The ^{1}H NMR spectrum of **27[SbF$_6$]** shows the expected coupling pattern for bismepines in the region of aromatic protons. The chemical shift for the olefin moiety ($\delta(^1H)$ = 6.93 ppm) indicates that the double bond does not coordinate to the platinum center. The resonance in the ^{31}P NMR spectrum at $\delta(^{31}P)$ = 53.93 ppm shows satellites with coupling to ^{195}Pt ($^1J_{PPt}$ = 1810.3 Hz). The $^1J_{PPt}$ couplings constants of 3051.5 Hz and 2789.9 Hz, respectively, in the complex [Pt({*o*-$PPh_2C_6H_4$}$_2$BiOTf)Cl_2], and of 2959–2888 Hz for [Pt({*o*-$PPh_2C_6H_4$}$_2$Bi)X] (X = Cl, Br, I),

synthesized by LIMBERG *et al.* are significantly higher than the value found for **27[SbF$_6$]**, suggesting a weaker P–Pt bond in **27[SbF$_6$]**, although a clear comparison is hampered by different geometries.[125] However, *cis*-Pt(PCy$_3$)$_2$(H)(SiEt$_3$) shows a $^1J_{PPt}$ coupling constant of 2721 Hz for the Pt–P bond *trans* to H, therefore indicating a stronger *trans* influence of the bismepinyl ligand compared to a hydride ligand. The ^{13}C NMR resonance for the *ipso*-carbon atoms of the bismepinyl ligand is shifted upfield ($\delta(^{13}C)$ = 146.10 ppm) compared to the cationic bismepine **[8-thf$_2$][SbF$_6$]** ($\delta(^{13}C)$ = 193.90 ppm).[82] This suggests a significant increase in electron density at the bismuth center. A signal for the platinum atom was not detected in ^{195}Pt NMR spectroscopic experiments. This may be caused by the adjacent ^{209}Bi nucleus with nuclear spin I = 9/2, which induces extreme quadrupolar line broadening, making detection more difficult.

Calculations were carried out on **27[SbF$_6$]**. An NBO analysis suggests the absence of a donor-acceptor bonding situation between platinum and bismuth, which is in contrast to the system [Pt({*o*-PPh$_2$C$_6$H$_4$}$_2$BiCl)Cl$_2$] published by LIMBERG (NBO = Natural Bond Orbitals). In the latter, the Bi–Pt bond is described as a Pt(5d)→Bi(6p) interaction with a stabilizing energy of 24.4 kcal · mol^{-1}.[123] Such an interaction does not occur in **27[SbF$_6$]** according to second-order perturbation analysis. This suggests a covalent nature of the Bi–Pt bond in **27[SbF$_6$]**, which implies a cationic Pt(+II) center, similar to that in **26[SbF$_6$]**. Thus, in both cases, a polarity reversal from a cationic bismuth center in the starting material **[8-thf$_2$][SbF$_6$]** to a neutral bismuth atom in **26**$^+$ and **27**$^+$ took place, which is accompanied by the oxidation from Pt(0) in [Pt(PCy$_3$)$_2$] and [Pt(cAAC^{Me})(PCy$_3$)] to Pt(+II) in **26**$^+$ and **27**$^+$.

In summary, it was possible to gain first results in the chemistry of platinum complexes with bismepinyl ligands. However, it was not possible to obtain full analytical data for **26[SbF$_6$]** and **27[SbF$_6$]**, so that further attempts to stabilize those systems (**26[SbF$_6$]**), or to produce larger amounts of substance (**27[SbF$_6$]**), respectively, have to be made in order to obtain analytically pure substances.

6 Reactions beyond Lewis Acid/Base Reactions

Reactions carried out as part of this thesis, which cannot be directly attributed to the properties of the bismuth compounds as Lewis acids, are briefly presented here.

Inspired by the results concerning the oxidative addition of XeF$_2$ to a bismuth(III) center to form fluorinated bismuth(V) species by the research group of CORNELLA,[231] [BiPh$_2$][OTf] was combined with one equivalent of XeF$_2$. This led to the formation of [BiPh$_3$][OTf]$_2$, as isolated in 37% yield (Scheme 33). The [BiPh$_3$]$^{2+}$ bismuth(V) dication has already been described in the literature.[232]

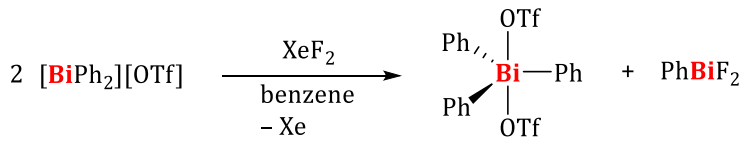

Scheme 33. Reaction of $BiPh_2^+$ with XeF_2 to yield $BiPh_3^{2+}$.

Gas evolution, presumably xenon gas, was observed during the course of the reaction, pointing towards a redox reaction where Bi(III) is partially oxidized to Bi(V) and Xe(II) is reduced to elemental xenon. Accordingly, $PhBiF_2$ must have been formed as a by-product, but could not be identified by ^1H and ^{19}F NMR spectroscopic analyses. However, a dark brown precipitate was formed during the reaction, which might result from the decomposition of $PhBiF_2$. (Difluoro)organobismuth(III) species have not been described in the literature to date, which may be due to their intrinsic instability. Since $[BiPh_3][OTf]_2$ is a fully characterized literature-known compound, no further analyses were performed.

The analog reaction of **21** with XeF_2 at ambient temperature led to gas evolution and at least four new species containing fluorine atoms according to ^{19}F NMR spectroscopy. Since an isolation of one of these species did not succeed, this approach was discarded.

The reaction of **8-Cl** with SbF_3 was intended to result in an exchange of the halide substituent at bismuth, resulting in the formation of **8-F**. Instead of the desired product, the halostibepine $[\{C_{14}H_{10}\}SbCl]$ was isolated and crystallographically characterized (Figure 58).

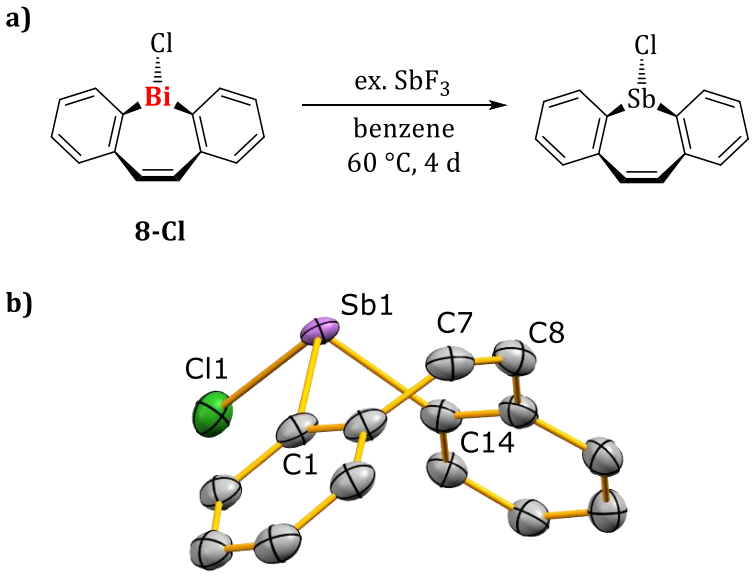

Figure 58. a) Reaction between **8-Cl** and excess SbF_3 (4.3 eq.). b) Molecular structure of $[\{C_{14}H_{10}\}SbCl]$ in the solid state. Displacement ellipsoids are shown at the 50% probability level. Hydrogen atoms are omitted for clarity. Only one of two crystallographically distinct molecules present in the asymmetric unit is shown. Selected bond lengths (Å) and angles (°): Sb1–Cl1, 2.4233(13); Sb1–C1, 2.173(5); Sb1–C14, 2.164(5); C7–C8, 1.337(7); C1–Sb1–Cl1, 94.12(14); C14–Sb1–Cl1, 94.39(14); C1–Sb1–C14, 88.10(18); angle(C1-C6)/(C9-C14), 102.1.

According to ^{1}H NMR spectroscopy, [{$C_{14}H_{10}$}SbCl] represents the major product of the reaction (90%). The ^{1}H NMR spectrum of the halostibepine shows a similar resonance pattern as for **8-Cl** and other halobismepines. A significant difference between **8-Cl** and the halostibepine is the chemical shift of the α-protons, i.e. the protons of the CH unit adjacent to the *ispo*-carbon atom attached to Sb, which is shifted upfield from **8-Cl** ($\Delta\delta$ = –0.8 ppm).

[{$C_{14}H_{10}$}SbCl] crystallized in the monoclinic space group $P2_1/c$ with Z = 8 (Figure 58b). The antimony atom adopts a trigonal pyramidal coordination geometry with slightly larger angles around Sb1 (88.10(18)–94.39(14)°) compared to the solid-state structure of **8-Cl** (85.94(17)–93.68(13)°).[82] Based on distance criteria intermolecular interactions are not present, which is in contrast to the halobismepine species, which forms one-dimensional coordination polymers in the solid state.[82] As described for **8-Cl**, the chlorostibepine adopts a boat conformation in which an Sb1···olefin interaction might be present based on Sb1···C7 and Sb1···C8 distances of ca. 3.19 Å, which is 15% below the sum of the van-der-Waals radii (3.76 Å). DFT studies to investigate this potential interaction have not been performed, yet.

The synthesis of stibepines commonly proceeds via tin-antimony exchange.[233,234] In addition, the synthesis of stibepines via salt eliminations has been described.[235] The access to halostibepines by metal exchange from bismuth to antimony has not been described so far.

X Bismuth Atoms in Hydrocarbon ligands: Bismepines as Rigid, Ditopic Arene Donors in Coordination Chemistry

This chapter was published in: Jacqueline Ramler, Leonie Wüst, Anna Rempel, Laura Wolz, Crispin Lichtenberg, *Organometallics* **2021**, *40*, 832–837. Reproduced from ref. 255 with permission from the American Chemical Society.

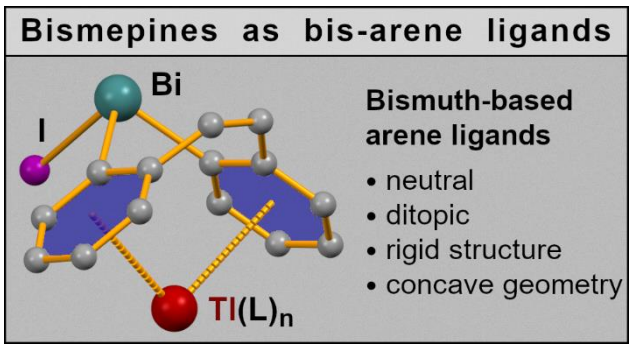

ORGANOMETALLICS

pubs.acs.org/Organometallics Communication

Bismuth Atoms in Hydrocarbon Ligands: Bismepines as Rigid, Ditopic Arene Donors in Coordination Chemistry

Jacqueline Ramler, Leonie Wüst, Anna Rempel, Laura Wolz, and Crispin Lichtenberg*

Cite This: *Organometallics* 2021, 40, 832–837 Read Online

ACCESS | Metrics & More | Article Recommendations | Supporting Information

ABSTRACT: Dibenzobismepines may be described as bismuth heterocycles containing two arene functional groups (see the graphic). The coordination chemistry of mono- and dinuclear bismepines has been investigated in solution and in the solid state, demonstrating that they can act as a new class of rigid, ditopic arene ligands. In contrast to the lighter N, P, and As homologues, the bismuth atom does not directly interact with the metal atom but influences the ligand properties through its energetically low lying 6s orbital, its low electronegativity, and its unusual bond lengths and angles. Analytical techniques applied in this work include (DOSY) NMR spectroscopy, single-crystal X-ray analysis, mass spectrometry, and DFT calculations.

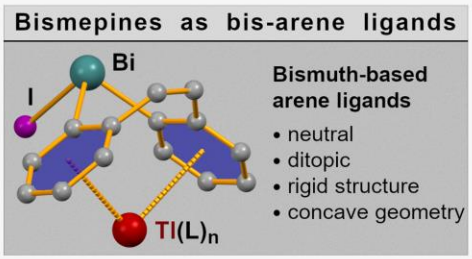

The careful design and skillful choice of arene ligands bound to metals across large sections of the periodic table has aided important advances in a great variety of chemical research disciplines. Selected examples include the fields of coordination chemistry,[1−11] Lewis acidity,[2] CH-activation,[12,13] olefin polymerization catalysis,[3,14] asymmetric catalysis,[15,16] catalyzed CO_2 reduction,[3] and cancer research.[8,17−19] When molecules contain two or more arene groups as coordination sites, their geometry and relative orientation can crucially influence the coordination chemistry of such ligands. This becomes evident in *ansa*-arene,[3,14] corannulene,[20] and cyclophane complexes,[5,21] for instance. Furthermore, the incorporation of heteroatoms into cyclic hydrocarbon frameworks can be employed as a strategy to control the geometry and electronic properties of arene ligands. In this context, we became interested in dibenzoheteropines **1-Pn** (eq 1).

Pn = N, P, As, Sb, Bi
X = monoanionic group (1)

In these ligands, the C−Pn−C angles, the electronegativity of Pn, and the tendency of the lone pair at Pn to interact with a Lewis acid continuously decrease down the group (N−Bi).[22,23] Investigations into the coordination chemistry of these compounds have only rarely been reported. For dibenzoazepines (**1-N**), coordination of the olefin moiety to main-group and transition metals has been investigated (Mg, Ru, Rh, Ir, Pd).[24−29] Theoretical studies suggest that additional coordination modes of dibenzoazepines should be accessible.[30] Complexes of neutral dibenzophosphepines (**1-P**) and dibenzoarsepines (**1-As**) are even more scarce: **1-P** coordinates to Rh via the phosphorus atom and the olefin moiety,[31] while **1-As** coordinates to Au only through its arsenic atom in an adduct with AuCl.[32] For the antimony and bismuth derivatives **1-Sb** and **1-Bi**, their accessibility, derivatization, bonding situations, and chemical properties have been elucidated,[33−36] but coordination compounds remain elusive, to date.[37]

We show here that bowl-shaped dibenzobismepines of the type **1-Bi** can be exploited as new types of rigid, neutral ditopic arene ligands and reveal differences in comparison to their lighter heteropine congeners.

Reaction of the dinuclear bismepine **2**[34] with stoichiometric amounts of Tl[$BArF^{24}$] in dichloromethane gave the adduct **4**[**$BArF^{24}$**] as a colorless solid in 95% isolated yield (Figure 1a; [$BArF^{24}$]$^-$ = [B(3,5-$C_6H_3(CF_3)_2)_4$]$^-$). Similarly, reaction of the iodo-bismepine **3** with Tl[$BArF^{24}$] in a 2:1 stoichiometry led to the formation of the adduct **5**[**$BArF^{24}$**], which was isolated as a colorless solid in 99% yield (Figure 1b).[38] Remarkably, no signs of thallium iodide formation were observed in the latter reaction, demonstrating that the ligation of the soft Lewis acid Tl^+ by a bismepine ligand is favored over salt elimination under these conditions.

Received: January 12, 2021
Published: March 11, 2021

https://dx.doi.org/10.1021/acs.organomet.1c00020
Organometallics 2021, 40, 832–837

Organometallics pubs.acs.org/Organometallics Communication

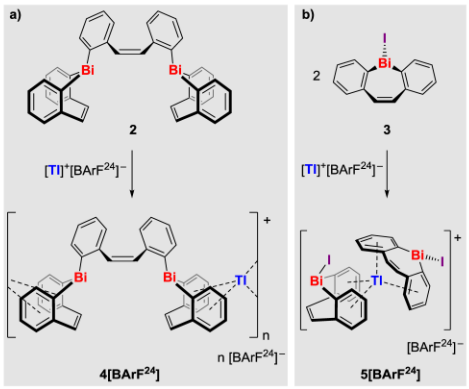

Figure 1. Reactions of **2** and **3** with Tl[BArF^{24}]. [BArF^{24}]$^-$ = [B(3,5-$C_6H_3(CF_3)_2)_4$]$^-$.

The molecular structures of compounds **4**[**BArF^{24}**] and **5**[**BArF^{24}**] in the solid state were investigated by single-crystal X-ray diffraction analyses (Figure 2). No strong directional bonding interactions between cations and anions were observed on the basis of distance criteria (for **5**[**BArF^{24}**], Bi···F distances of 3.21−3.35 Å (5−9% below the sum of the van der Waals radii of 3.54 Å) suggest weak Bi···F interactions in the solid state). In both compounds, the thallium atoms are coordinated by two bismepine units. For the compound **4**[**BArF^{24}**], this results in the formation of a coordination polymer extending along the crystallographic *b* axis, while **5**[**BArF^{24}**] shows a typical molecular structure without strong intermolecular bonding interactions. The thallium atoms in **4**[**BArF^{24}**] and **5**[**BArF^{24}**] show distorted-tetrahedral coordination geometries due to interactions with the benzo groups of the bismepine ligands. The ct−Tl−ct angles are in the ranges 102.1−121.8° (**4**[**BArF^{24}**]) and 98.8−129.1° (**5**[**BArF^{24}**]) with bite angles of the bismepine ligands being highly similar in both cases (100.1−103.3°; ct = centroid of the benzo group). Notably, compounds **4**[**BArF^{24}**] and **5**[**BArF^{24}**] are the first examples of well-defined molecular compounds featuring tetra-arene coordinated thallium cations. The Tl−ct distances of 3.03−3.22 Å (**4**[**BArF^{24}**]) and 3.06−3.24 Å (**5**[**BArF^{24}**]) are well within the range of Tl−ct^{arene} distances of 2.83−3.66 Å that have been reported for thallium species containing arene ligands.[39−47] On the basis of distance criteria, each of the thallium cations in compounds **4**[**BArF^{24}**] and **5**[**BArF^{24}**] shows two η^6- and two η^4-arene interactions. The Bi···Tl distances in both compounds (4.23−4.57 Å) are significantly larger than the sum of the van der Waals radii (4.03 Å), ruling out bonding interactions between these atoms. The trigonal-pyramidal coordination geometry of the bismuth atoms in **4**[**BArF^{24}**] and **5**[**BArF^{24}**][59] and the Bi−C (2.25−2.29 Å) and Bi−I (2.76−2.80 Å) bond lengths are highly similar to those in the thallium-free starting materials **2** and **3** (Bi−C, 2.24−2.26 Å; Bi−I, 2.78 Å).[34] However, a closer

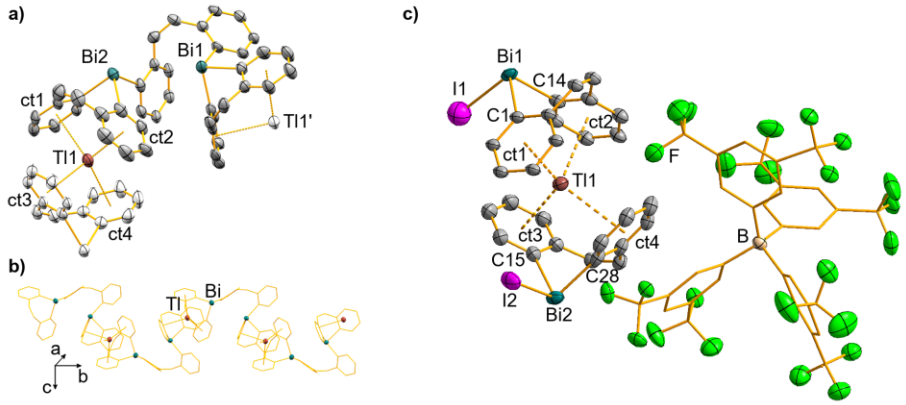

Figure 2. (a) Cutout of the solid-state structure of coordination polymer **4**[**BArF^{24}**]. Displacement ellipsoids are shown at the 50% probability level. Hydrogen atoms, the counteranion, and lattice-bound 1,2-difluorobenzene molecules are omitted for clarity; ct1−ct4 represent the centroids of C(15)−C(20), C(23)−C(28), C(29)−C(34), and C(37)−C(42), respectively. Atoms exceeding one formula unit are shown as white ellipsoids. (b) Arrangement of **4**[**BArF^{24}**] as a one-dimensional coordination polymer in the solid state. Selected bond lengths (Å) and angles (deg): Bi1−C, 2.255(9)−2.277(11); Bi2−C, 2.246(10)−2.252(11); Tl1···ct1, 3.073; Tl1···ct2, 3.033; Tl1···ct3, 3.166; Tl1···ct4, 3.220; C−Bi1−C, 85.1(4)−96.0(4); C−Bi2−C, 83.2(3)−97.8(4); ct1···Tl1···ct2, 102.11; ct1···Tl1···ct3, 106.23; ct1···Tl1···ct4, 118.20; ct2···Tl1···ct3, 103.94; ct3···Tl1···ct4, 102.83; ct2···Tl1···ct4, 121.84. (c) Molecular structure of **5**[**BArF^{24}**] in the solid state. The asymmetric unit contains two chemically identical but crystallographically independent formula units of **5**[**BArF^{24}**], only one of which is discussed because the bonding parameters are highly similar (for details see the Supporting Information). Displacement ellipsoids are shown at the 50% probability level. Hydrogen atoms and split positions are omitted for clarity; ct1−ct4 represent the centroids of C(1)−C(6), C(9)−C(14), C(15)−C(20), and C(23)−C(28), respectively. Selected bond lengths (Å) and angles (deg): Bi1−C1, 2.257(14); Bi1−C14, 2.291(14); Bi1−I1, 2.758(7); Bi2−C15, 2.254(11); Bi2−C28, 2.258(11); Bi2−I2, 2.7985(9); Bi2···F, 3.31; Tl1···ct1, 3.153; Tl1···ct2, 3.074; Tl1···ct3, 3.235; Tl1···ct4, 3.058; C1−Bi1−C14, 84.6(8); I1−Bi1−C1, 95.4(5); I1−Bi1−C14, 94.2(6); C15−Bi2−C28, 87.0(4); I2−Bi2−C15, 95.2(3); I2−Bi2−C28, 92.1(3); ct1···Tl1···ct2, 100.12; ct1···Tl1···ct3, 129.11; ct1···Tl1···ct4, 113.78; ct2···Tl1···ct3, 98.84; ct2···Tl1···ct4, 109.80; ct3···Tl1···ct4, 103.34.[48]

https://dx.doi.org/10.1021/acs.organomet.1c00020
Organometallics 2021, 40, 832−837

analysis reveals that the intracyclic C−Bi−C bond angles in **4**[**BArF**^{24}] are significantly smaller than those in **2**. As a consequence, the angles between the mean planes defined by the carbon atoms of the benzo groups in the bismepine units are also decreased from 106.4−107.3° in **2** to 90.4−100.9° in **4**[**BArF**^{24}]. This suggests that coordination of Tl^+ by **2** requires a slight bending of the bismepine unit, while the geometry of non-coordinated **3** is already very close to that found in the thallium complex **5**[**BArF**^{24}].

The ^{1}H and ^{13}C NMR spectra of **4**[**BArF**^{24}] and **5**[**BArF**^{24}] in CD_2Cl_2 show the expected signal patterns for the bismepine core. Coupling with ^{203}Tl and ^{205}Tl nuclei was not observed, even at a low temperature of −80 °C. In comparison with the thallium-free starting materials **2** and **3**, however, the resonances of **4**[**BArF**^{24}] and **5**[**BArF**^{24}] are shifted significantly. The ^{1}H and ^{13}C NMR spectroscopic resonances of the benzo groups experience downfield shifts of up to 0.14/0.10 ppm (**4**[**BArF**^{24}]/**5**[**BArF**^{24}]) and 2.02/2.14 ppm (**4**-[**BArF**^{24}]/**5**[**BArF**^{24}]), respectively. The ^{1}H, ^{11}B, ^{13}C, and ^{19}F NMR spectra also indicate the presence of $[BArF^{24}]^-$ anions without strong directional bonding interactions. These findings show that the Tl^+ ions of compounds **4**[**BArF**^{24}] and **5**[**BArF**^{24}] remain in the coordination sphere of the bismepine ligands in solution.

^{1}H DOSY NMR spectroscopy of **4**[**BArF**^{24}] and **5**[**BArF**^{24}] in CD_2Cl_2 revealed separate resonances for the bismepine and the borate moieties in the diffusion domain. This supports the absence of close bonding interactions between these molecular units in solution. The diffusion coefficients of thallium-free **2** and **3** are significantly larger than those of the bismepine components in **4**[**BArF**^{24}] and **5**[**BArF**^{24}], indicating bismepine···Tl interactions in solution (Table 1). In the case of

Table 1. Summary of the Results from ^{1}H DOSY NMR Experiments

solvent	compound	av diffusion coefficient D ($m^2\ s^{-1}$)	ratio $D^{Tl\text{-free}}/D^{Tl}$
CD_2Cl_2	**2**	9.171×10^{-10}	1.09
	4[**BArF**^{24}]	8.438×10^{-10}	
	3	1.485×10^{-9}	1.17
	5[**BArF**^{24}]	1.268×10^{-9}	
THF-d_8	**2**	7.407×10^{-10}	1.00
	4[**BArF**^{24}]	7.428×10^{-10}	

4[**BArF**^{24}], these values differ by 9%, suggesting that the mononuclear species $[Tl\{Bi_2(C_{14}H_{10})_3\}]^+$ is the main cationic component in solution. The diffusion coefficient of the bismepine units in **5**[**BArF**^{24}] is 17% smaller than that of its thallium-free bismepine ligand **3**. When the relationship $D \propto (MW)^{-1/3}$ is taken into account,[49−51] these findings suggest that in solution $[Tl\{BiI(C_{14}H_{10})\}_2]^+$ exists in equilibrium with species of type $[Tl\{BiI(C_{14}H_{10})\}L_n]^+$ (L = solvent molecule; see the Supporting Information). For compound **4**[**BArF**^{24}], it was demonstrated that a large excess of the strong σ-donor THF removes the Tl^+ ion from the bismepine binding pocket (Table S1).

ESI-high-resolution mass spectrometric analyses of **4**-[**BArF**^{24}] and **5**[**BArF**^{24}] from CH_2Cl_2 solution further support these results: signals of m/z 1157.1676 and m/z 718.9366 were detected, which correspond to species of the sum formulas $[Tl\{Bi_2(C_{14}H_{10})_3\}]^+$ (calculated m/z 1157.1694) and $[Tl\{BiI(C_{14}H_{10})\}]^+$ (calculated m/z 718.9375), respectively.

Since geometric constraints of the $Bi_2(C_{14}H_{10})_3$ ligand seemed to prohibit a tetrahedral coordination of Tl^+ by four arene groups in a mononuclear species, DFT calculations on the model compound $[Tl\{Bi_2(C_{14}H_{10})_3\}]^+$ (**4**$^+$**-monomer**) were performed in order to get insights into its coordination chemistry. These calculations indicate coordination of the Tl atom by three benzo groups. Interestingly, the olefin moiety of the $C_{14}H_{10}$ linker also binds to the Tl center in an unusual Tl··· olefin interaction (Figure 3). Arene→Tl^+ and olefin→Tl^+

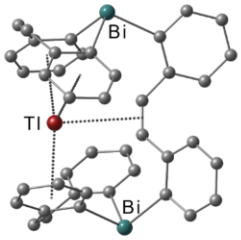

Figure 3. Calculated molecular structure of **4**$^+$**-monomer**.

interactions in this compound are associated with deletion energies of 10.8−15.8 and 9.9 kcal mol^{-1}, respectively, revealing remarkably strong olefin→Tl^+ bonding. The reaction Tl^+ + **2** → **4**$^+$**-monomer** was calculated to be exergonic by ΔG = −64.8 kcal mol^{-1}.

In order to evaluate the influence of the bismuth atom on the properties of bismepine ligands, the complexation of Tl^+ by a series of compounds $Pn(C_{14}H_{10})R$ was investigated by DFT calculations (Table 2; Pn = N−Bi; R = I, Me). Compounds with R = Me were included in order to account for the instability of N−I and P−I bonds. The thermodynamic parameters of the reactions reveal that adduct formation becomes energetically more favorable with an increasing atomic number of Pn for both R = I and R = Me. Despite the ionic nature of the central atom Tl^+, dispersion interactions

Table 2. Calculated Thermodynamic Parameters for the Formation of Coordination Compounds (Pn = N−Bi; R = I, Me)

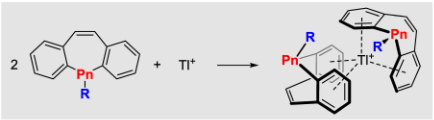

substituent R	element Pn	ΔH^{rel} (kcal mol^{-1})	ΔG^{rel} (kcal mol^{-1})
I	N	−73.81	−54.68
	P	−74.96	−55.76
	As	−77.45	−58.45
	Sb	−83.06	−64.15
	Bi	−87.03	−68.27
Me	N	−59.40	−41.41
	P	−61.39	−42.61
	As	−82.38	−63.06
	Sb	−86.49	−66.45
	Bi	−90.20	−69.84

https://dx.doi.org/10.1021/acs.organomet.1c00020
Organometallics 2021, 40, 832−837

contribute significantly to the stabilization of these complexes: the free reaction enthalpies for adduct formation decrease by 51−56% and range from −26.9 kcal mol^{-1} (Pn = N) to −30.3 kcal mol^{-1} (Pn = Bi) when no dispersion corrections are applied (see the Supporting Information).

Single-point calculations were carried out for the geometries of [Pn($C_{14}H_{10}$)I] and [Pn($C_{14}H_{10}$)Me] as obtained from the optimized geometries in the thallium adducts. The electronic energies without thermal corrections, $E°$, of these species are only 0.4−1.0 kcal mol^{-1} higher than the $E°$ values of the corresponding geometry-optimized structures of the free heteropines. This indicates that electronic parameters rather than geometric constraints account for the differences in heteropine−Tl^+ bonding. In agreement with these findings, NBO analyses show a steady increase in the deletion energies for heteropine→Tl^+ bonding from Pn = N (E_{del} = 45.3 kcal mol^{-1}) to Pn = Sb, Bi (E_{del} = 72.3−71.4 kcal mol^{-1}; see the Supporting Information).

In conclusion, we have demonstrated for the first time that dibenzobismepines can be applied as ligands in coordination chemistry. Specifically, the soft Lewis acid Tl^+ was ligated through arene→Tl^+ and, remarkably, also through olefin→Tl^+ bonding. These interactions persist in solution and lead to molecular complexes or coordination polymers in the solid state. These studies reveal the first examples of tetra-arene coordinated Tl^+ species. DFT calculations indicate that (i) dispersion interactions significantly stabilize the bismepine−Tl complexes and (ii) incorporation of Bi (rather than N−Sb) into the heteropine ligand framework favors the coordination of the soft Lewis acid due to electronic factors. This approach is distinct from previous strategies, which successfully exploited direct Bi→M bonding[36,52−55] and Bi←M back-bonding.[36,56−58] It is anticipated that these findings will stimulate the use of heavy main-group elements such as bismuth in ligand design (including ligand sites that do not directly interact with the central atom), which has been little explored to date.

■ ASSOCIATED CONTENT

Supporting Information

The Supporting Information is available free of charge at https://pubs.acs.org/doi/10.1021/acs.organomet.1c00020.

Experimental details, single-crystal X-ray diffraction analysis, DOSY NMR spectra, DFT calculations, energies of compounds investigated by DFT calculations, and NMR spectra of isolated compounds (PDF)

Cartesian coordinates for the calculated structure (XYZ)

Accession Codes

CCDC 2055286−2055288 contain the supplementary crystallographic data for this paper. These data can be obtained free of charge via www.ccdc.cam.ac.uk/data_request/cif, or by emailing data_request@ccdc.cam.ac.uk, or by contacting The Cambridge Crystallographic Data Centre, 12 Union Road, Cambridge CB2 1EZ, UK; fax: +44 1223 336033.

■ AUTHOR INFORMATION

Corresponding Author

Crispin Lichtenberg − *Julius-Maximilians-University Würzburg, Institute of Inorganic Chemistry, 97074 Würzburg, Germany;* orcid.org/0000-0002-0176-0939; Email: crispin.lichtenberg@uni-wuerzburg.de

Authors

Jacqueline Ramler − *Julius-Maximilians-University Würzburg, Institute of Inorganic Chemistry, 97074 Würzburg, Germany*

Leonie Wüst − *Julius-Maximilians-University Würzburg, Institute of Inorganic Chemistry, 97074 Würzburg, Germany*

Anna Rempel − *Julius-Maximilians-University Würzburg, Institute of Inorganic Chemistry, 97074 Würzburg, Germany*

Laura Wolz − *Julius-Maximilians-University Würzburg, Institute of Inorganic Chemistry, 97074 Würzburg, Germany*

Complete contact information is available at: https://pubs.acs.org/10.1021/acs.organomet.1c00020

Notes

The authors declare no competing financial interest.

■ ACKNOWLEDGMENTS

Continuous support by Prof. Braunschweig and financial support by the DFG (LI2860/3-1 and LI2860/5-1) and the Fonds der Chemischen Industrie are gratefully acknowledged.

■ REFERENCES

(1) Pahl, J.; Friedrich, A.; Elsen, H.; Harder, S. Cationic Magnesium π−Arene Complexes. *Organometallics* **2018**, *37*, 2901−2909.

(2) Schorpp, M.; Krossing, I. Soft interactions with hard Lewis acids: generation of mono- and dicationic alkaline-earth metal arene-complexes by direct oxidation. *Chem. Sci.* **2020**, *11*, 2068−2076.

(3) Dabringhaus, P.; Schorpp, M.; Scherer, H.; Krossing, I. A Highly Lewis Acidic Strontium *ansa*-Arene Complex for Lewis Acid Catalysis and Isobutylene Polymerization. *Angew. Chem., Int. Ed.* **2020**, *59*, 22023−22027.

(4) Schmidbaur, H.; Schier, A. π-Complexation of Post-Transition Metals by Neutral Aromatic Hydrocarbons: The Road from Observations in the 19th Century to New Aspects of Supramolecular Chemistry. *Organometallics* **2008**, *27*, 2361−2395.

(5) Schmidbaur, H. Arene Complexes of Univalent Gallium, Indium, and Thallium. *Angew. Chem., Int. Ed. Engl.* **1985**, *24*, 893−904.

(6) La Pierre, H. S.; Scheurer, A.; Heinemann, F. W.; Hieringer, W.; Meyer, K. Synthesis and characterization of a uranium(II) monoarene complex supported by δ backbonding. *Angew. Chem., Int. Ed.* **2014**, *53*, 7158−7162.

(7) Schwamm, R. J.; Fitchett, C. M.; Coles, M. P. Intramolecular Metal···π-Arene Interactions in Neutral and Cationic Main Group Compounds. *Chem. - Asian J.* **2019**, *14*, 1204−1211.

(8) Pittracher, M.; Frisch, U.; Kopacka, H.; Wurst, K.; Müller, T.; Oehninger, L.; Ott, I.; Wuttke, E.; Scheerer, S.; Winter, R. F.; Bildstein, B. π-Complexes of Tropolone and Its N-Derivatives: Ambidentate [O,O]/[N,O]/[N,N]-Cycloheptatrienyl Pentamethylcyclopentadienyl Ruthenium Sandwich Complexes. *Organometallics* **2014**, *33*, 1630−1643.

(9) Lichtenberg, C. Aminotroponiminates: Alkali Metal Compounds Reveal Unprecedented Coordination Modes. *Organometallics* **2016**, *35*, 894−902.

(10) Hanft, A.; Jürgensen, M.; Bertermann, R.; Lichtenberg, C. Sodium Aminotroponiminates: Ligand-Induced Disproportionation, Mixed-Metal Compounds, and Exceptional Activity in Polymerization Catalysis. *ChemCatChem* **2018**, *10*, 4018−4027.

(11) Hanft, A.; Lichtenberg, C. Rationalizing the Effect of Ligand Substitution Patterns on Coordination and Reactivity of Alkali Metal Aminotroponiminates. *Organometallics* **2018**, *37*, 1781−1787.

(12) Bresien, J.; Schulz, A.; Thomas, M.; Villinger, A. A Bismuth-Arene σ-Complex - On the Edge of Menshutkin-Type Complexes. *Eur. J. Inorg. Chem.* **2019**, *2019*, 1279−1287.

(13) Ritschel, B.; Poater, J.; Dengel, H.; Bickelhaupt, F. M.; Lichtenberg, C. Double CH Activation of a Masked Cationic Bismuth Amide. *Angew. Chem., Int. Ed.* **2018**, *57*, 3825−3829.

https://dx.doi.org/10.1021/acs.organomet.1c00020
Organometallics 2021, 40, 832−837

(14) Lichtenthaler, M. R.; Maurer, S.; Mangan, R. J.; Stahl, F.; Mönkemeyer, F.; Hamann, J.; Krossing, I. Univalent gallium complexes of simple and ansa-arene ligands: effects on the polymerization of isobutylene. *Chem. - Eur. J.* **2015**, *21*, 157−165.
(15) Everaere, K.; Mortreux, A.; Carpentier, J.-F. Ruthenium(II)-Catalyzed Asymmetric Transfer Hydrogenation of Carbonyl Compounds with 2-Propanol and Ephedrine-Type Ligands. *Adv. Synth. Catal.* **2003**, *345*, 67−77.
(16) Ohkuma, T.; Utsumi, N.; Tsutsumi, K.; Murata, K.; Sandoval, C.; Noyori, R. The hydrogenation/transfer hydrogenation network: asymmetric hydrogenation of ketones with chiral η^6-arene/N-Tosylethylenediamine-ruthenium(II) catalysts. *J. Am. Chem. Soc.* **2006**, *128*, 8724−8725.
(17) Caruso, F.; Rossi, M.; Benson, A.; Opazo, C.; Freedman, D.; Monti, E.; Gariboldi, M. B.; Shaulky, J.; Marchetti, F.; Pettinari, R.; Pettinari, C. Ruthenium-arene complexes of curcumin: X-ray and density functional theory structure, synthesis, and spectroscopic characterization, in vitro antitumor activity, and DNA docking studies of (p-cymene)Ru(curcuminato)chloro. *J. Med. Chem.* **2012**, *55*, 1072−1081.
(18) Biancalana, L.; Pratesi, A.; Chiellini, F.; Zacchini, S.; Funaioli, T.; Gabbiani, C.; Marchetti, F. Ruthenium arene complexes with triphenylphosphane ligands: cytotoxicity towards pancreatic cancer cells, interaction with model proteins, and effect of ethacrynic acid substitution. *New J. Chem.* **2017**, *41*, 14574−14588.
(19) Hager, L. A.; Mokesch, S.; Kieler, C.; Alonso-de Castro, S.; Baier, D.; Roller, A.; Kandioller, W.; Keppler, B. K.; Berger, W.; Salassa, L.; Terenzi, A. Ruthenium-arene complexes bearing naphthyl-substituted 1,3-dioxoindan-2-carboxamides ligands for G-quadruplex DNA recognition. *Dalton Trans* **2019**, *48*, 12040−12049.
(20) Siegel, J. S.; Baldridge, K. K.; Linden, A.; Dorta, R. d^8 rhodium and iridium complexes of corannulene. *J. Am. Chem. Soc.* **2006**, *128*, 10644−10645.
(21) Altaf, Y.; Yar, M.; Hashmi, M. A. Main-group metal cyclophane complexes with high coordination numbers. *RSC Adv.* **2020**, *10*, 30796−30805.
(22) Boeyens, J. C. The Periodic Electronegativity Table. *Z. Naturforsch., B: J. Chem. Sci.* **2008**, *63*, 199−209.
(23) See also Table S6 in the Supporting Information.
(24) Frieß, S.; Herrera, A.; Linden, A.; Heinemann, F. W.; Dorta, R. Towards enantiopure macrocyclic trans-dinucleating hemilabile P-Alkene ligands: Syntheses, structures, and Chiral Pd-Complexes. *J. Organomet. Chem.* **2019**, *898*, 120876.
(25) Herrera, A.; Grasruck, A.; Heinemann, F. W.; Scheurer, A.; Chelouan, A.; Frieß, S.; Seidel, F.; Dorta, R. Developing P-Stereogenic, Planar−Chiral P-Alkene Ligands: Monodentate, Bidentate, and Double Agostic Coordination Modes on Ru(II). *Organometallics* **2017**, *36*, 714−720.
(26) Heuermann, I.; Heitmann, B.; Stichauer, R.; Duvinage, D.; Vogt, M. Rh(I) Complex with a Tridentate Pyridine−Amino−Olefin Actor Ligand−Metal−Ligand Cooperative Activation of CO_2 and Phenylisocyanate under C−C and Rh−E (E = O, N) Bond Formation. *Organometallics* **2019**, *38*, 1787−1799.
(27) Mora, G.; van Zutphen, S.; Thoumazet, C.; Le Goff, X. F.; Ricard, L.; Grützmacher, H.; Le Floch, P. A New Bidentate Aminophosphole−Olefin Ligand for the Rhodium-Catalyzed Hydroformylation of Mono- and Disubstituted Olefins. *Organometallics* **2006**, *25*, 5528−5532.
(28) Drinkel, E.; Briceño, A.; Dorta, R.; Dorta, R. Hemilabile P-Alkene Ligands in Chiral Rhodium and Copper Complexes: Catalytic Asymmetric 1,4 Additions to Enones. *Organometallics* **2010**, *29*, 2503−2514.
(29) Freitag, B.; Elsen, H.; Pahl, J.; Ballmann, G.; Herrera, A.; Dorta, R.; Harder, S. s-Block Metal Dibenzoazepinate Complexes: Evidence for Mg−Alkene Encapsulation. *Organometallics* **2017**, *36*, 1860−1866.
(30) Farah, S.; Ababsa, S.; Benhamada, N.; Zouchoune, B. Theoretical investigation of the coordination of dibenzazepine to transition-metal complexes: A DFT study. *Polyhedron* **2010**, *29*, 2722−2730.
(31) Lyaskovskyy, V.; van Dijk-Moes, R. J. A.; Burck, S.; Dzik, W. I.; Lutz, M.; Ehlers, A. W.; Slootweg, J. C.; Bruin, B. de; Lammertsma, K. Dibenzo[b,f]phosphepines: Novel Phosphane−Olefin Ligands for Transition Metals. *Organometallics* **2013**, *32*, 363−373.
(32) Kawashima, I.; Imoto, H.; Ishida, M.; Furuta, H.; Yamamoto, S.; Mitsuishi, M.; Tanaka, S.; Fujii, T.; Naka, K. Dibenzoarsepins: Planarization of 8π-Electron System in the Lowest Singlet Excited State. *Angew. Chem., Int. Ed.* **2019**, *58*, 11686−11690.
(33) Yasuike, S.; Ohta, H.; Shiratori, S.; Kurita, J.; Tsuchiya, T. Syntheses of the group 15 1-benzoheteroepines, dibenzo[b,d]-heteroepines and dibenzo[b,f]heteroepines involving the first isolated examples of arsepines and bismepines. *J. Chem. Soc., Chem. Commun.* **1993**, 1817.
(34) Ramler, J.; Hofmann, K.; Lichtenberg, C. Neutral and Cationic Bismuth Compounds: Structure, Heteroaromaticity, and Lewis Acidity of Bismepines. *Inorg. Chem.* **2020**, *59*, 3367−3376.
(35) Ramler, J.; Lichtenberg, C. Molecular Bismuth Cations: Assessment of Soft Lewis Acidity. *Chem. - Eur. J.* **2020**, *26*, 10250−10258.
(36) Ramler, J.; Radacki, K.; Abbenseth, J.; Lichtenberg, C. Combined experimental and theoretical studies towards mutual osmium-bismuth donor/acceptor bonding. *Dalton Trans* **2020**, *49*, 9024−9034.
(37) For examples of As, Sb, and Bi as bridgehead atoms in tripodal tris(pyridyl) ligands see: Plajer, A. J.; Colebatch, A. L.; Rizzuto, F. J.; Pröhm, P.; Bond, A. D.; García-Rodríguez, R.; Wright, D. S. How Changing the Bridgehead Can Affect the Properties of Tripodal Ligands. *Angew. Chem., Int. Ed.* **2018**, *57*, 6648−6652.
(38) The reaction of **3** with Tl[$BArF^{24}$] in a 1:1 stoichiometry gave **5**[**$BArF^{24}$**] in 79% isolated yield (based on **3**).
(39) Sarazin, Y.; Hughes, D. L.; Kaltsoyannis, N.; Wright, J. A.; Bochmann, M. Thallium(I) sandwich, multidecker, and ether complexes stabilized by weakly-coordinating anions: a spectroscopic, structural, and theoretical investigation. *J. Am. Chem. Soc.* **2007**, *129*, 881−894.
(40) Fernández, E. J.; Laguna, A.; López-de-Luzuriaga, J. M.; Elena Olmos, M.; Pérez, J. [{AuTl(C_6Cl_5)$_2$(toluene)}$_2$(dioxane)]: A striking structure that leads to a blue luminescence. *Chem. Commun.* **2003**, *14*, 1760−1761.
(41) Noirot, M. D.; Anderson, O. P.; Strauss, S. H. A new candidate for the least coordinating anion: preparation and characterization of [TlOTeF_5(mes)$_2$]$_2$.mes (mes = mesitylene) and [Tl(mes)$_2^+$][B(OTeF_5)$_4^-$]. *Inorg. Chem.* **1987**, *26*, 2216−2223.
(42) Frank, W.; Kuhn, D.; Müller-Becker, S.; Razavi, A. Two Modifications of a Cyclopentadienylthallium(I) Complex Linking the Chemistry of the Cp and Arene Complexes of Main Group Elements. *Angew. Chem., Int. Ed. Engl.* **1993**, *32*, 90−92.
(43) Mansaray, H. B.; Kelly, M.; Vidovic, D.; Aldridge, S. Tuning main group redox chemistry through steric loading: subvalent Group 13 metal complexes of carbazolyl ligands. *Chem. - Eur. J.* **2011**, *17*, 5381−5386.
(44) Mathur, R. S.; Drovetskaya, T.; Reed, C. A. Bis(η^6-toluene)thallium(I) 7,8,9,10,11,12-Hexabromo-closo-1-carbadodecaborate: a Halocarborane-Bridged Dimer with Heavy Metal−Arene Interactions. *Acta Cryst. B* **1997**, *53*, 881−883.
(45) Schmidbaur, H.; Bublak, W.; Riede, J.; Müller, G. [{1,3,5-$(CH_3)_3H_3C_6$}$_6$Tl$_4$][$GaBr_4$]$_4^-$ Synthesis and Structure of a Mixed Mono- and Bis(arene)thallium Complex. *Angew. Chem., Int. Ed. Engl.* **1985**, *24*, 414−415.
(46) Strauss, S. H.; Noirot, M. D.; Anderson, O. P. Teflate ($OTeF_5^-$) as a unique ligand for metal complexes: structure of [TlOTeF_5(1,3,5-$(CH_3)_3C_6H_3$)$_2$]$_2$, a thallium(I) complex with neutral arene ligands. *Inorg. Chem.* **1986**, *25*, 3850−3851.
(47) Thomas, J. C.; Peters, J. C. Bis(phosphino)borates: a new family of monoanionic chelating phosphine ligands. *Inorg. Chem.* **2003**, *42*, 5055−5073.
(48) Some atoms were refined in residues, which is indicated by an underscore followed by a number in the atom label (e.g.: Bi1_14). The underscore followed by the number have been omitted for clarity

https://dx.doi.org/10.1021/acs.organomet.1c00020
Organometallics 2021, 40, 832−837

in the main part of the manuscript. For details see the Supporting Information.

(49) It must be noted that the determination of absolute molecular weights is not straightforward for compounds with heavy atoms. Therefore, we only compare the diffusion coefficients of compounds with similar structural features in this work.

(50) Neufeld, R.; Stalke, D. Accurate molecular weight determination of small molecules via DOSY-NMR by using external calibration curves with normalized diffusion coefficients. *Chem. Sci.* **2015**, *6*, 3354−3364.

(51) Li, D.; Kagan, G.; Hopson, R.; Williard, P. G. Formula weight prediction by internal reference diffusion-ordered NMR spectroscopy (DOSY). *J. Am. Chem. Soc.* **2009**, *131*, 5627−5634.

(52) Materne, K.; Hoof, S.; Frank, N.; Herwig, C.; Limberg, C. In Situ Formation of PBiP Ligands upon Complexation of a Mixed Phosphane/Bismuthane with Group 11 Metal Ions. *Organometallics* **2017**, *36*, 4891−4895.

(53) Materne, K.; Braun-Cula, B.; Herwig, C.; Frank, N.; Limberg, C. Bismuthanes as Hemilabile Donors in an O_2-Activating Palladium(0) Complex. *Chem. - Eur. J.* **2017**, *23*, 11797−11801.

(54) Holmes, N. J.; Levason, W.; Webster, M. Triphenylbismuthine complexes of group 6 metal carbonyls: X-ray crystal structures of $[M(CO)_5(BiPh_3)]$ (M = Mo or W). *J. Organomet. Chem.* **1997**, *545*−*546*, 111−115.

(55) Breunig, H. J.; Borrmann, T.; Lork, E.; Moldovan, O.; Raţ, C. I.; Wagner, R. P. Syntheses, crystal structures and DFT studies of $[Me_3EM(CO)_5]$ (E = Sb, Bi; M = Cr, W), cis-$[(Me_3Sb)_2Mo(CO)_4]$, and $[tBu_3BiFe(CO)_4]$. *J. Organomet. Chem.* **2009**, *694*, 427−432.

(56) Tschersich, C.; Hoof, S.; Frank, N.; Herwig, C.; Limberg, C. The Effect of Substituents at Lewis Acidic Bismuth(III) Centers on Its Propensity to Bind a Noble Metal Donor. *Inorg. Chem.* **2016**, *55*, 1837−1842.

(57) Lin, T.-P.; Ke, I.-S.; Gabbaï, F. P. σ-Accepting Properties of a Chlorobismuthine Ligand. *Angew. Chem., Int. Ed.* **2012**, *51*, 4985−4988.

(58) Tschersich, C.; Limberg, C.; Roggan, S.; Herwig, C.; Ernsting, N.; Kovalenko, S.; Mebs, S. Gold- and platinum-bismuth donor-acceptor interactions supported by an ambiphilic PBiP pincer ligand. *Angew. Chem., Int. Ed.* **2012**, *51*, 4989−4992.

(59) DFT calculations on $[Tl\{Bi_2(C_{14}H_{10})_3\}]^+$ (**4$^+$-monomer**) and $[\{Bi(C_{14}H_{10})I\}_2Tl]^+$ (**5$^+$**) suggest weak $\pi(C{=}C){\rightarrow}\sigma^*(Bi{-}C)$ and $\pi(C{=}C){\rightarrow}\sigma^*(Bi{-}I)$ donor−acceptor interactions between the olefin unit and the Bi−C/I moiety with deletion energies of 0.88 and 1.22 kcal mol^{-1} for **4$^+$-monomer** and 2 × 2.74 kcal mol^{-1} for **5$^+$**. Similar interactions have been reported for **3**[34] and cationic derivatives with $EPMe_3$ ligands (E = S, Se[35]).

https://dx.doi.org/10.1021/acs.organomet.1c00020
Organometallics 2021, 40, 832−837

XI Combined Experimental and Theoretical Studies towards Mutual Osmium-Bismuth Donor/Acceptor Bonding

This chapter was published in: Jacqueline Ramler, Krzysztof Radacki, Josh Abbenseth, Crispin Lichtenberg, *Dalton Trans.* **2020**, *49*, 9024–9034. Reproduced from ref. 221 with permission from the Royal Society of Chemistry.

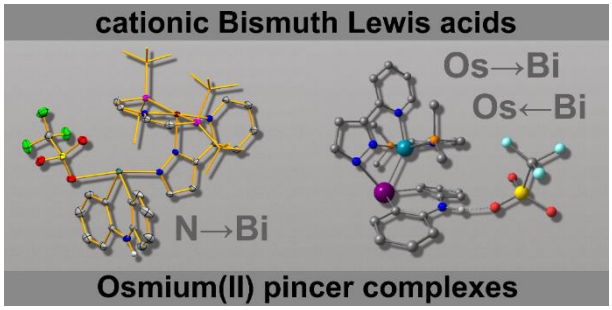

Dalton Transactions

ROYAL SOCIETY OF CHEMISTRY

PAPER

View Article Online
View Journal | View Issue

Check for updates

Cite this: *Dalton Trans.*, 2020, **49**, 9024

Combined experimental and theoretical studies towards mutual osmium–bismuth donor/acceptor bonding†

Jacqueline Ramler,[a] Krzysztof Radacki,[a] Josh Abbenseth *‡[b] and Crispin Lichtenberg *[a]

Received 7th May 2020,
Accepted 12th June 2020

DOI: 10.1039/d0dt01663b

rsc.li/dalton

Osmium(II) PNP pincer complexes bearing a hemilabile pyridyl-pyrazolide (PyrPz) ligand have been synthesised, and their reactivity towards Lewis acidic bismuth compounds has been examined. Reactions with $BiCl_3$ resulted in chlorine-atom-transfer to give an osmium(III) species. Reactions with cationic bismuth species led to adduct formation through N → Bi bond formation *via* the PyrPz ligand. Theoretical analyses revealed that steric interactions hamper Os → Bi bond formation and indicate that such interactions are possible upon reducing the steric profile around the osmium atom. Analytical techniques include NMR, IR, and EPR spectroscopy, cyclic voltammetry, elemental analysis and DFT calculations.

Introduction

Transition metal complexes featuring a terminal M≡N nitrido ligand are a well-studied class of compounds due to their application in important transformations such as C–H functionalization and nitrogen fixation (M = transition metal).[1–5] For the heavier homologues P, As and Sb, terminal pnictide complexes are increasingly difficult to access and mostly restricted to metals of groups 5 and 6 in a d^0 electronic configuration.[6–9] Scheer and co-workers reported the first terminal arsenide and stibide complexes obtained by reaction of the tungsten chloride tris(amido)amine complex [WCl(N{$CH_2CH_2NSiMe_3$}$_3$)] with $LiAs(SiMe_3)_2$ and LiSb(H){$CH(SiMe_3)_2$}, respectively (Scheme 1, top).[10,11] However, this approach has not been exploited for the generation of the corresponding bismuth complexes (yet), most likely due to the relevant bismuth precursors being thermally labile, difficult to access and their reactivity being difficult to control.[12–16] Nevertheless, DFT calculations and gas phase studies suggest that transition metal bismutido species may be isolable, if cleanly generated under suitable experimental conditions.[8,11,17–19] In recent years, heavy cyanate analogues ($PnCO^-$, Pn = P, As) have been introduced as novel "Pn^-" transfer reagents[20–25] and have enabled the syntheses of group 7 complexes with M≡Pn structural motifs (Scheme 1, bottom).[26,27]

With a $[BiCO]^-$ bismide transfer reagent remaining synthetically inaccessible to date,[28] new synthetic approaches are required. Introducing bismuth complex fragments into the coordination sphere of a transition metal through Lewis acid/base interactions would open up reduction and reductive elim-

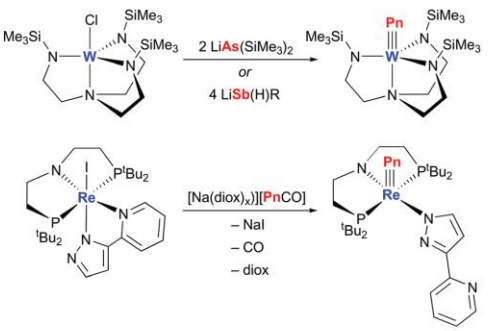

Scheme 1 Top: Syntheses of the first isolated arsenide and stibide complexes. R = $CH(SiMe_3)_2$, Pn = As, Sb. Bottom: Synthesis of terminal pnictide group 7 transition metal complexes using $[PnCO]^-$ as pnictide transfer reagent. Pn = P, As; diox = 1,4-dioxane.

[a]*Department of Inorganic Chemistry, Julius-Maximilians-University Würzburg, Am Hubland, 97074 Würzburg, Germany. E-mail: crispin.lichtenberg@uni-wuerzburg.de*
[b]*Department of Inorganic Chemistry, Georg-August-University Göttingen, Tammanstraße 4, 37077 Göttingen, Germany*

†Electronic supplementary information (ESI) available: Experimental, crystallographic, spectroscopic, cyclic voltammetry, and theoretical details. CCDC 2000260–2000263. For ESI and crystallographic data in CIF or other electronic format see DOI: 10.1039/d0dt01663b

‡Current address: Department of Chemistry, University of Oxford, Chemistry Research Laboratory, 12 Mansfield Road, OX1 3TA, Oxford (UK).

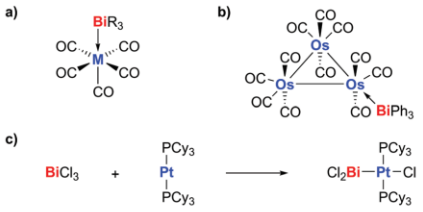

Scheme 2 (a and b) Examples of Lewis acid/base adducts with BiR_3 acting as a (weak) donor; M = Cr, Mo, W; R = Me, aryl. (c) Oxidative addition of $BiCl_3$ at a Pt(0) centre.

ination pathways as promising strategies towards the generation of compounds featuring M–Bi multiple bonding.

Lewis acid/base interactions between bismuth(III) compounds and transition metal complexes have so far mostly been realised through $R_3Bi \rightarrow [M]$ interactions, in which BiR_3 acts as a weak donor ligand (*e.g.*: Scheme 2a and b; [M] = transition metal complex fragment).[29–33] The few publications on such interactions are accompanied by reports on reactions between compounds such as $BiPh_3$ and $Ni(CO)_4$, $Co_3(CO)_8$, or $Fe_2(CO)_9$, which failed to produce Lewis acid/base adducts (in fact, they did not react at all or led to intractable mixtures of products).[34] Previous reports on the successful preparation of such compounds have been questioned in some cases.[34] In the context of Lewis basic bismuth species, it should be noted that isolable and *in situ*-generated bismuth(I) compounds have also been reported to act as Lewis bases towards transition metal complex fragments such as $Mn(CO)_4$, $Fe(CO)_4$, $Co(CO)_3$, and [Au(carbene)][BF_4].[35–41]

Attempts to utilise bismuth halides such as BiX_3 as Lewis acids towards transition metal complexes resulted in an oxidative addition reaction between $BiCl_3$ and the electron-rich late transition metal complex $Pt(PCy_3)_2$ (Scheme 2c; Cy = cyclohexyl).[42,43]

Recently, the first examples of complexes with $[M] \rightarrow BiR_3$ donor/acceptor bonding through Lewis acidic bismuth moieties have been reported by Limberg and Gabbaï (Scheme 3).[44–47] In these compounds, the transition metal complex fragment [M] is arranged in a P–Bi–P-binding pocket created by phosphanyl substituents close to the bismuth centre, thereby facilitating [M]···Bi interactions.

While the Lewis acidity of neutral and cationic bismuth species has been documented and exploited in many synthetic applications,[48–59] only recently it has been quantified for a closely related series of compounds using the Gutmann–Beckett method.[60] These studies highlight the Lewis acidity of cationic bismuth compounds, which ranges between that of classical group 13 Lewis acids such as BPh_3 and $B(C_6F_5)_3$. Subsequently, the potential of cationic bismuth species to act as particularly soft Lewis acids has been demonstrated.[61]

Here we report on the reactivity of osmium PNP pincer complexes towards neutral and cationic bismuth compounds, evaluating their potential for Os → Bi bond formation. Factors that hamper possible donor/acceptor interactions and strategies to overcome these obstacles are revealed.

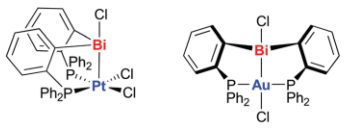

Scheme 3 First examples of Bi–M bonds with the bismuth moiety acting as electron acceptor.

Results and discussion

In order to evaluate synthetic routes to Bi–M Lewis acid/base adducts that may be employed in subsequent reduction or reductive elimination reactions, we focused on osmium(II) complexes based on a PNP pincer ligand (Scheme 4). This unsaturated PNP pincer ligand with bulky $PtBu_2$ substituents has previously been demonstrated to allow for the stabilization of compounds featuring unusual group 8-element multiple bonding.[62–65] The possible linkage isomerism of the PyrPz

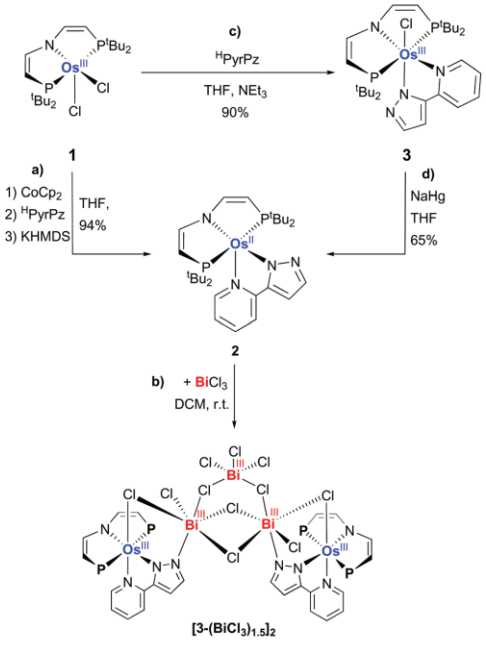

Scheme 4 (a) Synthesis of precursor **2**. (b) Product $[\mathbf{3}\text{-}(BiCl_3)_{1.5}]_2$ from the reaction of **2** with $BiCl_3$. (c) Synthesis of paramagnetic complex **3** from **1** and (d) direct reduction of **3** to form **2**. P = $PtBu_2$. ^{H}PyrPz = 2-(1*H*-pyrazol-5-yl)pyridine. The oxidation states of the metal centres are shown for clarity.

ligand accounts for the expected strong *trans*-influence of the terminal pnictide ligands (*cf.* Scheme 1, bottom).[26]

Synthesis of [Os(PNP)(pyrpz)] and reaction with bismuth-chloro species

The osmium(II) complex [Os(PNP)(pyrpz)] (**2**) was synthesised from [$OsCl_2$(PNP)] (**1**)[66] by the successive addition of $CoCp_2$, 2-(1*H*-pyrazol-5-yl)pyridine (^{H}PyrPz) and K(HMDS), and isolated in 94% yield as a red solid (PNP = $[N(C_2H_2PtBu_2)_2]^-$, Cp = C_5H_5, HMDS = $N(SiMe_3)_2$, Scheme 4a). In the solid state, the osmium centre exhibits a slightly distorted square-pyramidal coordination geometry with the pyridyl-N-atom in the apical position (τ = 0.19, Fig. 1). Out of the three Os–N bonds, Os1–N2 is the shortest one, although the pyridyl group acts as a formally neutral ligand. This was ascribed to the absence of a ligand *trans* to the pyridyl moiety (the C25–C26 bond length of 1.44 Å speaks against major contributions of a resonance structure with a C25=C26 double bond, decreased electron density at N3 and increased electron density at N2; *cf.* Scheme S1 (ESI†)). The Os–N^{PNP} bond length in **2** (2.09 Å) is slightly elongated compared to starting material **1** (1.98 Å) due to the weaker *trans*-influence of the chloride ligand in **1**.[66] In solution, multinuclear NMR-spectroscopic analysis of **2** indicated C_s symmetry on the NMR timescale at room temperature.

Compound **2** was reacted with Lewis acidic $BiCl_3$ [59,60] in a 1 : 1 ratio (Scheme 4b). Monitoring the reaction by ^{1}H NMR spectroscopy revealed two broad resonances at δ = −1.29 and 5.30 ppm besides resonances of precursor **2**.[67] The appearance of the high-field-shifted resonance, the broadness of the new resonances, and the absence of the required number of new resonances in the aromatic region strongly suggested the formation of an open shell species in the reaction. Complete conversion of **2** with the aforementioned species as the main product (according to ^{1}H NMR spectroscopy) was achieved by irradiation with a mercury vapor lamp for 5 h, which was accompanied by the precipitation of a dark solid (presumably "bismuth black").[68] The main product of this reaction was at first presumed to be [OsCl(PNP)(pyrpz)] (**3**), which was therefore synthesised in a rational approach by reaction of **1** with ^{H}PyrPz and addition of NEt_3 in THF (see Scheme 4c).

3 was fully characterized to be an open-shell Os(III) compound with an S = 1/2 ground state as derived from EPR spectroscopy and its magnetic momentum in solution (μ_{eff}^{298K} = 2.1 ± 0.1 μ_B). One-electron reduction by Na/Hg affords **2** in accord with cyclic voltammetry which features an irreversible reductive process at E_{pc} = −1.40 V in THF (for details see experimental part and ESI†).

Single-crystal X-ray diffraction analysis of **3** revealed the expected octahedral coordination geometry of the central atom osmium, accompanied by a switch of the coordination sites occupied by the nitrogen atoms of the pyridyl-pyrazolide ligand (orthorhombic space group *Pnma* with Z = 4, Fig. 2). The Os–N^{PNP} distance in **3** (2.02 Å) is slightly shortened with respect to that in **2** (2.09 Å) due to the increase in oxidation state. In comparison with **1**, the Os–Cl^{apical} (2.38 Å) and the Os–N^{PNP} (2.02 Å) distance are slightly elongated in **3** due to the six-fold coordination environment (Os–Cl^{apical}, 2.32 Å; Os–N^{PNP}, 1.98 Å in **1**).

The ^{1}H NMR spectroscopic signature of paramagnetic **3** showed two intense broad resonances (presumably for the P*t*Bu_2 groups) at δ = −1.24 and +5.40 ppm (for details see experimental part). This is close to, but not identical with the observations made in the NMR spectroscopic monitoring of the reaction between **2** and $BiCl_3$ (*vide supra*), suggesting the formation of a structurally related species.

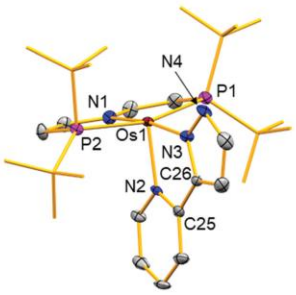

Fig. 1 Molecular structure of [Os(PNP)(pyrpz)] (**2**) in the solid state. Displacement ellipsoids are shown at the 50% probability level. Ellipsoids of *t*Bu groups and hydrogen atoms are omitted for clarity. Selected bond lengths (Å) and angles (°): Os1–N1, 2.087(3); Os1–N2, 2.041(3); Os1–N3, 2.065(3); Os1–P1, 2.3937(9); Os1–P2, 2.3129(9); N3–N4, 1.347(4); C25–C26, 1.444(5); N1–Os1–N2, 93.58(12); N1–Os1–N3, 171.21(12); P1–Os1–P2, 158.92(3); N2–Os1–N3, 77.65(11); N2–Os1–P2, 93.06(8); P2–Os1–N1, 81.12(8).

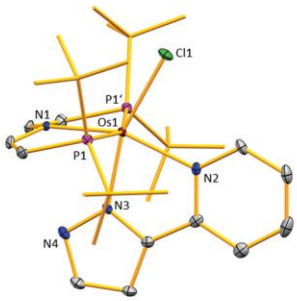

Fig. 2 Molecular structure of [OsCl(PNP)(pyrpz)] (**3**) in the solid state. Heteroatoms are represented by displacement ellipsoids at the 50% probability level. Ellipsoids of *t*Bu groups and hydrogen atoms are omitted for clarity. Selected bond length (Å) and angles (°): Os1–N1, 2.017(3); Os1–N3, 2.063(3); Os1–N2, 2.161(3); Os1–Cl1, 2.3837(9); Os1–P1, 2.4297(6); N1–Os1–N3, 81.46(11); N1–Os1–N2, 157.83(11); N3–Os1–N2, 76.36(12); N1–Os1–Cl1, 116.58(8); N3–Os1–Cl1, 161.95(9); N2–Os1–Cl1, 85.59(8); N1–Os1–P1, 80.297(17); N3–Os1–P1, 92.81(2); N2–Os1–P1, 100.624(15); Cl1–Os1–P1, 90.483(16).

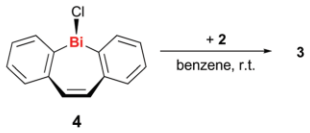

Scheme 5 Reaction of halobismepine **4** with precursor **2**. The slow and incomplete formation of **3** is observed.

Single-crystals suitable for X-ray diffraction analysis from the reaction of $BiCl_3$ with **2** were eventually obtained by layering a solution of **2** in THF with a solution of $BiCl_3$ in THF, followed by storage at −30 °C. Instead of complex **3**, the solid-state structure of the reaction product showed a rather complex connectivity: a Lewis acid/base adduct is formed between **3** and $BiCl_3$ *via* the β-nitrogen of the pyrazolide moiety; two such entities are bridged through Bi···Cl interactions with one another and with an additional $BiCl_3$ unit, resulting in $[\mathbf{3}\text{-}(\mathbf{BiCl_3})_{1.5}]_2$ (Scheme 4d).[69] While the quality of the X-ray crystallographic data is insufficient for the detailed discussion of structural parameters, it provides definite proof of connectivity for complex $[\mathbf{3}\text{-}(\mathbf{BiCl_3})_{1.5}]_2$ (for details see ESI†).

The identification of compound $[\mathbf{3}\text{-}(\mathbf{BiCl_3})_{1.5}]_2$ revealed oxidation reactions and the formation of oligonuclear complexes as potential undesired side reactions when using simple bismuth precursors BiX_3 (X = monoanionic inorganic ligand). As a decreased preference towards chlorine-atom-transfer was expected for halobismepine **4**, this precursor was reacted with **2** (Scheme 5). However, the reaction only resulted in the slow and incomplete formation of **3** according to ^{1}H NMR spectroscopy. Having ruled out compounds of type BiX_3 and $Bi(aryl)_2Cl$ as promising precursors for Bi···Os bond formation with compound **2**, we targeted bismuth Lewis acids that are less prone to undesired atom transfer reactions and have one orbital available for bond formation with a Lewis base.

Reactivity of [Os(PNP)(pyrpz)] towards bismuth cations

In order to form a Lewis acid/base adduct with Os···Bi interactions, cationic bismuthanes **5** and **6** were chosen as highly Lewis acidic species (Scheme 6).[60,61]

The reaction of diorganobismuth cations **5** and **6** with **2** in THF led to the immediate formation of a red precipitate in both cases. Single-crystals of the products **7** and **8** suitable for X-ray diffraction analysis were obtained by layering a THF solution of **2** with a THF solution of **5** or **6** and storage of the (initially) biphasic system at −30 °C. The solid-state structure of **7** revealed coordination of the bismuth centre by the readily accessible β-nitrogen atom of the PyrPz ligand, instead of coordination by the soft Lewis-basic Os(II) centre (monoclinic space group $P2_1/c$ with $Z = 4$; Fig. 3). The bismuth centre adopts a bisphenoidal coordination geometry with the PyrPz and the triflate ligands in the axial positions with bond angles of 171° for N4–Bi1–O1 and 89–91° for C1/12–Bi1–N4. The Bi–C bond lengths (2.21 Å) are similar to those in other diarylbismuth cations.[60,70,71] The Bi–O bond length (2.73 Å) is larger

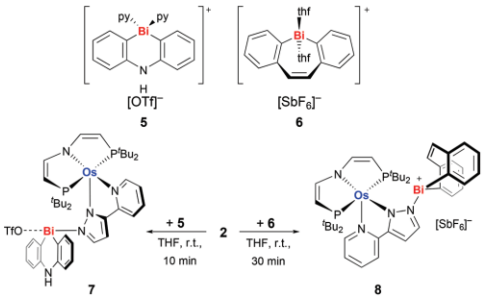

Scheme 6 Cationic organobismuth compounds used in reactions with **2** and isolated products **7** and **8** obtained with **5** and **6**. Py = pyridine; OTf = O_3SCF_3.

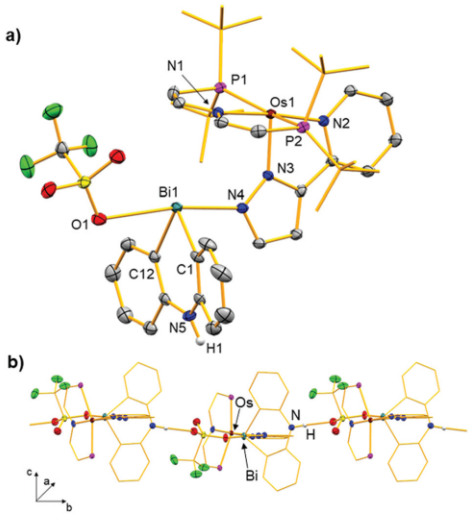

Fig. 3 (a) Molecular structure of **7** in the solid state. Displacement ellipsoids are shown at the 50% probability level. Ellipsoids for *t*Bu units, split positions of disordered *t*Bu groups, hydrogen atoms (except H1) and THF molecules in the lattice are omitted for clarity. (b) Cut out of coordination polymer $(\mathbf{7})_\infty$. Atoms for *t*Bu groups are omitted for clarity. Selected bond lengths (Å) and bond angles (°): Bi1–C1, 2.207(3); Bi1–C12, 2.214(3); Bi1–N4, 2.352(3); Bi1–O1, 2.753(2); Os1–P1, 2.4002(8); Os1–P2, 2.3319(9); Os1–N3, 2.031(3); Os1–N2, 2.100(3); Os1–N1, 2.084(3); C1–Bi1–C12, 88.76(12); C1–Bi1–N4, 90.78(11); C12–Bi1–N4, 89.20(11); N4–Bi1–O1, 171.41(8); C1–Bi1–O1, 84.56(10); C12–Bi1–O1, 83.50(10); N3–Os1–N1, 97.63(10); N3–Os1–N2, 77.61(10); N1–Os1–N2, 175.22(10); N3–Os1–P2, 93.53(8); N1–Os1–P2, 80.87(8); N2–Os1–P2, 98.90(8); N3–Os1–P1, 98.46(8); N1–Os1–P1, 80.40(8); N2–Os1–P1, 100.57(8); P2–Os1–P1, 158.92(3).

than those in $[BiPh_2(OTf)]_\infty$ (2.47–2.53 Å)[72] and $[Bi((C_6H_4)_2C_2H_2)(OTf)]_\infty$ (2.38–2.53 Å),[60] indicating the good σ-donating ability of the β-nitrogen atom of the pyrazolide

ligand in **7**. Indeed, the Bi1–N4 bond length of 2.35 Å is at the lower limit of the range of Bi–N distances observed in structurally related diaryl bismuth cations with pyridine or intramolecular tertiary amine functionalities acting as donors (2.36–2.59 Å).[57,73–75] The osmium centre retains its distorted square-pyramidal coordination enforced by the bite angle of the pincer ligand (τ = 0.27). However, the PyrPz chelate ligand has undergone a rearrangement, which led the pyrazolide moiety into the apical position, thereby directing the bismuth centre away from the osmium atom. The switch of N2 and N3 from the apical to an equatorial coordination site (and *vice versa*) also results in shortening of the Os1–N2 (2.03 Å) and elongation of the Os–N3 bond (2.10 Å) in **7** compared to those in **2** (2.04 Å and 2.07 Å). The Os–N^{PNP} bond length in **7** (2.08 Å) is identical within limits of error to that in precursor **2**. The triflate anion adopts a bridging coordination mode between Bi1 and the NH moiety of the neighbouring formula unit, resulting in the formation of a one-dimensional coordination polymer in the solid state, which extends along the crystallographic *b*-axis (Fig. 3b). IR spectroscopic analysis of **7** confirmed the presence of the NH functionality with a stretching frequency at $\tilde{\nu}$ = 3339 cm^{-1}. This is in accordance with the reported stretching frequency for the same group in **5**, in which hydrogen bonds between NH and the triflate anion are also present.[76] The poor solubility of **7** in common organic solvents of moderate polarity (*e.g.* THF) prohibited its NMR-spectroscopic characterization in solution. In more polar solvents such as pyridine, **7** dissociated into the starting materials **2** and **5**.

The molecular structure of compound **8** (obtained from reaction of **2** with the bismepine cation **6**) also showed coordination of the bismuth atom by the β-nitrogen atom of the pyrazolide ligand (monoclinic space group $P2_1/m$ with Z = 2; Fig. 4). The bismuth atom is found in a trigonal pyramidal coordination geometry with bond angles around the central atom ranging from 88° to 93°. In addition, weak intermolecular interactions with two fluorine atoms of the $[SbF_6]^-$ anion were observed (Bi···F, 3.16 Å, 11% below the sum of the van der Waals radii (3.54 Å)). Due to the weaker Bi···$[A]^-$ interactions in **8** ($[A]^-$ = $[SbF_6]^-$) as compared to **7** ($[A]^-$ = $[OTf]^-$), the Bi1–N4 dative bond in **8** (2.26 Å) is significantly shorter than that in **7** (2.35 Å) and is in fact in the range of covalent Bi–N bond lengths reported for $Bi(N(SiMe_3)_2)_3$ (2.20–2.27 Å).[77] This underlines the strong Lewis acidity of the cationic bismuth complex fragment present in **8**. The Bi–C bond lengths of 2.24 Å are in the range of those reported for related bismepine species.[60] The osmium centre is found in a slightly distorted square pyramidal coordination geometry, without major structural differences compared to the solid-state structure of **2** (τ = 0.18). The Os–N1 bond length in **8** (2.10 Å) is slightly elongated in comparison with **2** (2.07 Å), which was ascribed to the presence of the electron-withdrawing bismepine cation. In contrast to **7**, no rearrangement of the PyrPz ligand occurred in the formation of **8**, which directs the bismuth atom in proximity to the osmium atom. Based on distance criteria, however, there are no directional Os1···Bi1 interactions in **8** due to steric repulsion between the *t*Bu groups and the bismuth complex fragment. As observed for compound **7**, the solution NMR spectroscopic analysis of **8** was hampered by its poor solubility in moderately polar solvents and its fragmentation in polar solvents. In agreement with these observations, heating a suspension of **8** in pyridine for 2 d at 80 °C did not result in the desired migration of the bismuth unit to the osmium centre, but led to slow decomposition.

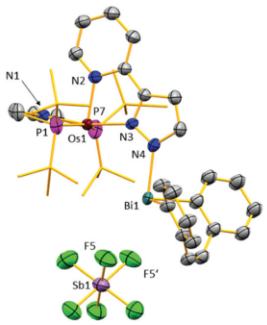

Fig. 4 Molecular structure of **8** in the solid state. Displacement ellipsoids are shown at the 50% probability level. Ellipsoids of *t*Bu units, hydrogen atoms, split positions, the SbF_6 anion and lattice bound THF molecule are omitted for clarity. Selected bond lengths (Å) and bond angles (°): Bi1–C1, 2.244(6); Bi1–C14, 2.245(6); Bi1–N4; 2.258(6); N3–Os1, 2.096(5); N2–Os1, 2.044(6); Os1–N1, 2.088(7); Os1–P1, 2.376(3); Os1–P7, 2.381(4); C1–Bi1–C14, 90.7(3); C1–Bi1–N4, 88.2(5); C14–Bi1–N4, 93.4(4); N2–Os1–N1, 92.1(2); N2–Os1–N3, 77.6(2); N1–Os1–N3, 169.6(2); N2–Os1–P1, 95.9(3); N1–Os1–P1, 80.44(14); N3–Os1–P1, 100.8(2); N2–Os1–P7, 3 94.1(3); N1–Os1–P7, 80.65(14); N3–Os1–P7, 99.5(2); P1–Os1–P7, 158.90(13).

[OsCl(PNP)]: reactivity towards cationic bismuth compounds

In order to avoid adduct formation of bismuth with the readily accessible β-nitrogen atom of the PyrPz ligand, [OsCl(PNP)] (**9**)[66] was chosen as an alternative osmium precursor to be reacted with **5**. The pyridine adduct [OsCl(PNP)(pyr)] (**10**) was obtained as the only isolable product of this reaction (Scheme 7). **10** was formed by transfer of a pyridine ligand from the bismuth atom in **5** to osmium and was characterised by ^{1}H NMR spectroscopy and mass spectrometry with observation of the $[M]^+$ peak at m/z = 662.2 (ESI†). In THF solution,

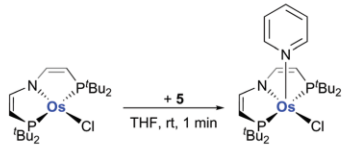

9 **10**

Scheme 7 Reaction of **9** with **5** and isolated pyridine-adduct **10**.

the bismepine cation **6** did not react with **9**. Instead, decomposition of **9** was observed due to its instability in solution.[66]

DFT calculations

Density functional theory (DFT) studies were carried out in order to identify factors that critically influence the potential of compound **2** to realise Os···Bi bonding interactions (for details see experimental and ESI†). So far, Os–Bi bonding has only been described in cluster chemistry and the type of Os···Bi interactions was not investigated in detail.[78–80]

Reactions of **2** with bismuth cations **5** and **6** to give adducts **7** and **8**, respectively, are clearly exothermic and exergonic (**7**: ΔH = −27.2 kcal mol^{-1}; ΔG = −37.8 kcal mol^{-1}; **8**: ΔH = −13.8 kcal mol^{-1}; ΔG = −23.1 kcal mol^{-1}). Natural population analyses (NPA)[81] of Os(II) precursor **2** and products **7** and **8** reveal that the coordination of cationic bismuth compounds by the PyrPz ligand slightly increases the natural charges at the osmium centre (natural charge of Os in **2**: +0.20, **7**: +0.24, **8**: +0.35, Fig. 5a and b). The orientation of the PyrPz ligand in **7** with the pyrazolide unit in the apical position directs the bismuth complex fragment away from the osmium centre. The isomer **7-py-apical** with the pyridyl moiety in the apical position was found to also correspond to a minimum on the potential energy surface and is only slightly higher in energy (**7** → **7-py-apical**: ΔH = +2.9 kcal mol^{-1}; ΔG = +3.1 kcal mol^{-1}).

The structural analysis of compound **8** based on X-ray diffraction data suggested that the steric bulk of the *t*Bu groups hampered potential bonding interactions between the bismuth and the osmium atom. This was verified by analysis of the relevant topographic steric map[82] with the osmium atom in the centre of the sphere, the $N^{pyridyl}$ atom on the *z*-axis, and the N^{PNP} and the P atoms in the *xy*-plane (Fig. 6a and b, left). Relaxed potential energy surface scans, in which the Bi···Os distances in **7-py-apical** and **8** were decreased stepwise, showed an increase in energy, which was ascribed to steric interactions between the *t*Bu groups and the bismuth complex fragments (ESI†). The *t*Bu groups of compound **8** were thus replaced by methyl groups (without geometry optimisation) to give non-optimised compound **8-Me***. The topographic steric map of **8-Me*** revealed a significantly reduced steric hindrance between the osmium and the bismuth atom (Fig. 6b, right).[83] Geometry optimisations of suitable model compounds with PMe_2 instead of $PtBu_2$ groups resulted in the minimum structures **7-Me** and **8-Me** (Fig. 5c and d), in which the bismuth atoms are still coordinated by the β-nitrogen atoms of the PyrPz ligands, but also show significant Bi···Os bonding interactions. Reactions of **2-Me** with **5** and **6** to give **7-Me** and **8-Me**, respectively, were calculated to be exothermal and exergonic (**7-Me**: ΔH = −10.2 kcal mol^{-1}; ΔG = −15.2 kcal mol^{-1}; **8-Me**: ΔH = −13.1 kcal mol^{-1}; ΔG = −22.4 kcal mol^{-1}).

To understand the nature and strength of the Bi···Os interactions in more detail, natural bond orbital (NBO) analyses were carried out. The Wiberg bond indices (WBIs) support the presence of considerable Bi–Os interactions in the methyl ana-

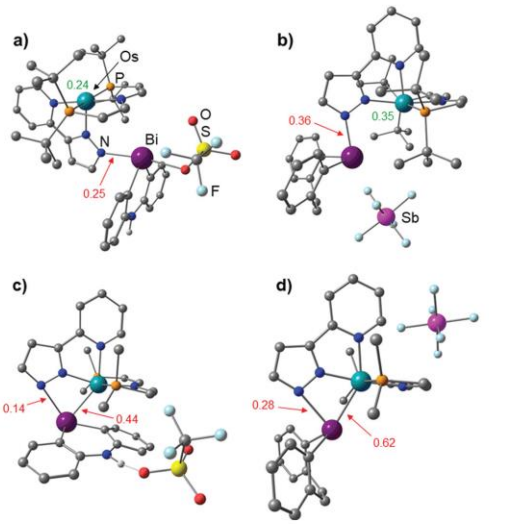

Fig. 5 Calculated molecular structures of **7** and **8** (a and b) and the methyl analogues **7-Me** and **8-Me** (c and d). Selected Wiberg bond indices and natural charges are shown in red and green, respectively.

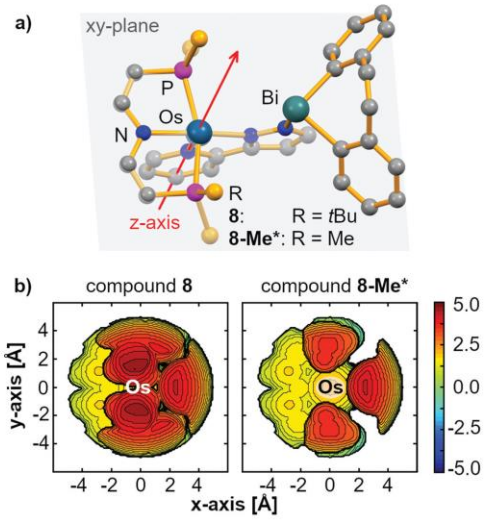

Fig. 6 Analysis of steric interactions around the osmium atom in compounds **8** and **8-Me*** (**8-Me*** has the same geometry as **8**, but the *t*Bu groups have been exchanged for methyl groups). (a) Geometry of **8** and **8-Me*** with coordinate system chosen for steric mapping (hydrogen atoms and counter anions omitted for clarity). (b) Topographic steric maps of compound **8** and **8-Me*** (counter anions omitted for clarity); isocontour curves are given in Å.

Table 1 Deletion energies for selected donor acceptor interactions in **7-Me** and **8-Me** along with NBOs representing the arene donor orbital (left) and the empty acceptor orbitals at bismuth (middle and right) at isovalues of 0.03

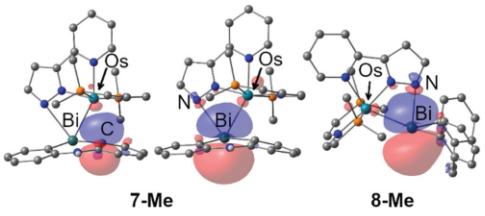

	E_{del} [kcal mol^{-1}]	
Type of E_{del}	**7-Me**	**8-Me**
Os → Bi	48.9	49.8
Os ← Bi	24.3	66.2
N → Bi	20.4	54.3
N ← Bi	1.3	1.5
Arene → Os	22.3	None
Arene ← Os	0.4	None
Sum[a]	121.5	177.4

[a] This also includes minor contributions from the second N atom of the pyrrazolide group (ESI†).

logues **7-Me**/**8-Me** with WBI_{Bi-Os} = 0.44 in **7-Me** and WBI_{Bi-Os} = 0.62 in **8-Me** (Fig. 5). In agreement with these findings, Bi–Os bond formation results in a reduction of the WBIs for Bi–N interactions from 0.25 and 0.36 in **7** and **8** to 0.14 and 0.28 in **7-Me** and **8-Me**, respectively (Fig. 5). Second order perturbation analyses indicate that there is both, Os → Bi donation and Os ← Bi backdonation in **7-Me** and **8-Me**. Dative bonding between nitrogen and bismuth is also relevant in both cases. In addition, arene → Os bonding is significant in **7-Me**. The relevant deletion energies were determined and are summarised in Table 1.

For compound **7-Me**, the deletion energies of Bi–Os interactions sum up to 73.2 kcal mol^{-1} with Os → Bi bonding (E_{del} = 48.9 kcal mol^{-1}) being more pronounced than Os ← Bi backbonding (E_{del} = 24.3 kcal mol^{-1}). Remarkably, the deletion energies for Bi–Os interactions are more than three times larger than those for Bi–N bonding (E_{del}(N → Bi) = 20.4 kcal mol^{-1}; E_{del}(N ← Bi) = 1.3 kcal mol^{-1}), underlining the preference of cationic bismuth species for soft donors.[61] The flat geometry of the aromatic[57] [Bi(C$_6$H$_4$)$_2$NH(OTf)] complex fragment allows for additional dative bonding from a benzo group to the osmium centre with negligible arene ← Os backbonding (E_{del}(arene → Os) = 22.3 kcal mol^{-1}; E_{del}(arene ← Os) = 0.4 kcal mol^{-1}). The most relevant occupied NBO for the arene → Os interaction is best described as a carbon p-orbital (Table 1, top left).

In the case of compound **8-Me**, the sum of Bi–Os deletion energies amounts to 116.0 kcal mol^{-1}, which is somewhat larger than that in **7-Me**, when the arene–Os interactions in **7-Me** are also taken into account (sum: 95.7 kcal mol^{-1}). While, the contribution of Os → Bi donation in **8-Me** is very similar (E_{del} = 49.8 kcal mol^{-1}), the deletion energy for the Os ← Bi backdonation of 66.2 kcal mol^{-1} clearly exceeds that in **7-Me**. These differences can be ascribed to the fact that the NBO, which corresponds to the bismuth 6s-orbital, is polarised away from the carbon atoms attached to bismuth (ESI†). Due to the relative orientation of bismuth and osmium complex fragments in **7-Me** and **8-Me**, this leads to a significantly enhanced overlap of this NBO with osmium-centred NBOs in the case of **8-Me**. It should be noted that especially the large deletion energy for the Os ← 6s(Bi) interactions in **8-Me** are unusual because the Lewis basic character of the 6s(Bi) lone pair is reduced compared to the respective lone pairs of the lighter group 15 homologues due to the inert pair effect and relativistic effects. The Bi–N deletion energies in **8-Me** (E_{del} = 55.8 kcal mol^{-1}) are much larger than those in **7-Me** (E_{del} = 21.7 kcal mol^{-1}) and are almost exclusively due to N → Bi donation. This difference is ascribed to the orientation of the bismuth-centred acceptor orbital in **7-Me** and **8-Me**. According to NBO analysis, this orbital is best described as an empty 6p Bi orbital in both cases. In **7-Me**, this orbital is oriented between the N and the Os atom (Table 1, top middle), while it is primarily oriented towards the N-atom in **8-Me** (Table 1, top right). Steric interactions between the ligand frameworks around Bi and Os prevent the orientation of the bismuth acceptor orbital towards the osmium atom in **8-Me**. It should be pointed out that for **7-Me** and **8-Me** deletion energies for Bi–Os bonding are considerably larger than those for Bi–N interactions due to mutual Os → Bi and Os ← Bi bonding.

Relaxed potential energy surface scans along with subsequent geometry optimizations and frequency analyses show that isomers with weaker Bi···Os interactions also correspond to minima on the potential energy surface (compound **7-Me′** and **8-Me′**; ESI†). While **7-Me′** is higher in energy than **7-Me**, **8-Me′** is lower in energy than **8-Me** (for details see ESI†).

Overall, it is remarkable that even for cationic bismuth species not only strong electron acceptor properties, but also pronounced electron-donating abilities contribute to Lewis pair formation with the Os(II) complex fragment. In contrast, one type of interaction seems to dominate in literature-known related bismuth complexes featuring Bi···M′ interactions (M′ = Cu, Ag, Au, Pd, Pt).[44–47,84] While Bi → M′ interactions dominate when bismuth bears three aryl substituents,[46,84,85] Bi ← M′ bonding is most relevant when one electronegative group X is bound to bismuth (X = Cl, OTf, C$_6$F$_5$) or the M′-centred donor orbital is perfectly aligned with the bismuth centred acceptor orbital (M′ = Pt).[44,45,47,85] The deletion energies calculated for the Bi–Os interactions in **8-Me** (116.0 kcal mol^{-1}) clearly exceed those reported for other Bi–M′ interactions (E_{del} = 16.4–74.2 kcal mol^{-1}).[44–47,85]

Conclusions

Reactions of neutral and cationic bismuth(III) Lewis acids towards osmium(II) compounds [Os(PNP)X] have been investi-

gated (PNP = $[N(C_2H_2PtBu_2)_2]^-$; X = Cl, PyrPz = pyridyl-pyrazolide). It was demonstrated that Lewis acid/base pair formation is hampered by chlorine-atom-transfer from Bi to Os in the case of $BiCl_3$ and Bi(dirayl)Cl. Cationic bismuth species gave Lewis acid/base adducts with the osmium precursor [Os(PNP)(pyrpz)], but were formed through a Bi–N bond between bismuth and a readily accessible, Lewis-basic nitrogen atom of the PyrPz ligand. Structural characterization of these compounds, combined with topographical steric analysis and DFT calculations revealed that steric bulk around the osmium atom prevents Os–Bi bond formation. DFT calculations show that reducing the steric bulk around osmium leads to Os–Bi bonding. Importantly, even for cationic bismuth species, Os–Bi donor/acceptor interactions are realised not only through Os → Bi but also through Os ← Bi bonding. This demonstrates the ability of cationic bismuth species to engage in mutual Lewis acid/base pair formation with complexes of (heavy) transition metals. Future research efforts will focus on the exploitation of transition metal–Bi donor/acceptor bonding for synthetic applications.

Experimental section

General considerations

All air- and moisture-sensitive manipulations were carried out using standard vacuum line Schlenk techniques or in glove-boxes containing an atmosphere of purified argon. Solvents were degassed and purified according to standard laboratory procedures. NMR spectra were recorded on Bruker instruments operating at 300, 400 or 500 MHz with respect to ^{1}H. ^{1}H and ^{13}C NMR chemical shifts are reported relative to $SiMe_4$ using the residual ^{1}H and ^{13}C chemical shifts of the solvent as a secondary standard. ^{31}P NMR chemical shifts are reported relative to 85% aqueous H_3PO_4 as an external standard. NMR spectra were recorded at ambient temperature (typically 23 °C), if not otherwise noted. LIFDI mass spectrometry was performed on a Joel AccuTOF spectrometer under inert conditions. EPR spectra were recorded on a Bruker ELEXSYS-II E500 CW-EPR. Cyclic voltammograms were recorded with a Metrohm Autolab PGSTAT101 using Ag/Ag^+ reference-, glassy-carbon working- and Pt-wire counter electrodes. Elemental analyses were obtained using an Elementar Vario EL 3, a Leco, or a Carlo Erba instrument. Single crystals suitable for X-ray diffraction analysis were coated with polyisobutylene or perfluorinated polyether oil in a glovebox, transferred to a nylon loop and then to the goniometer of a diffractometer equipped with a molybdenum X-ray tube (λ = 0.71073 Å). The data obtained were integrated with SAINT or CrysAlisPro and a semi-empirical absorption correction from equivalents with SADABS or CrysAlisPro was applied. The structure was solved and refined using the Bruker SHELX 2014 software package.[86–88] All non-hydrogen atoms were refined with anisotropic displacement parameters. All hydrogen atoms were refined isotropically on calculated positions by using a riding model with their U_{iso} values constrained to $1.5U_{eq}$ of their pivot atoms for terminal sp^3 carbon atoms and $1.2U_{eq}$ for all other atoms. Crystallographic data have been deposited with the Cambridge Crystallographic Data Centre as supplementary publication no. CCDC 2000260–2000263.†

DFT calculations were performed with the Gaussian program[89] using the 6-31G(d,p)[90] (H, C, N, O, F, P, S) or the LanL2DZ[91–93] (Sb, Os, Bi) basis set and the B3LYP functional.[94] The D3 version of Grimme's dispersion model with the original D3 damping function was applied.[95] Frequency analyses of the reported structures showed no imaginary frequencies for ground states and one imaginary frequency for the transition state. Thermodynamic parameters were calculated at a temperature of 298.15 K and a pressure of 1.00 atm. NBO analyses were performed using the program version NBO 7.[96] Topographic steric maps were generated with the SambVca 2.1 tool.[82] $CoCp_2$ (abcr), $[NBu_4][PF_6]$ (Sigma-Aldrich) and KHMDS (Sigma-Aldrich) were used as purchased. ^{H}PyrPz (TCI) was washed with pentane and dried over-night prior to use. $FeCp_2$ (abcr) was sublimed prior to use.

$[OsCl(PNP)]$[66] (**9**), $[OsCl_2(PNP)]$[66] (**1**), $[Bi(C_6H_4)_2C_2H_2Cl]$[60] (**4**), $[Bi(C_6H_4)_2NH(OTf)(NC_5H_5)_2]$[57] (**5**), $[Bi(C_6H_4)_2C_2H_2(thf)_2(SbF_6)]$[60] (**6**), and NaHg[97] were prepared according to literature procedures.

[Os(PNP)(pyrpz)] (2)

Method A. **1** (200 mg, 323 μmol, 1.00 eq., PNP = $[N(C_2H_2PtBu_2)_2]^-$) and $CoCp_2$ (42.2 mg, 323 μmol, 1.00 eq.) were dissolved in THF (15 mL) and stirred for 2 minutes. 2-(1*H*-pyrazol-5-yl)pyridine (47.0 mg, 323 μmol, 1.00 eq.) was added in small portions over the course of 3 minutes and stirring was continued for 5 minutes. After addition of KHMDS (64.6 mg, 323 μmol, 1.00 eq.) the solution was stirred for 90 minutes. The solvent was removed under reduced pressure, and the solid was extracted with pentane (5 × 10 mL). The solvent was evaporated, and the product was obtained as a red powder (210 mg, 304 μmol, 94%).

Method B. **3** (50 mg, 68.8 μmol, 1.00 eq.) and NaHg (1 w%, 1.66 g, 72.2 μmol, 1.05 eq.) were suspended in THF (10 mL) and stirred for 1 h at room temperature. After removal of the solvent under reduced pressure, the residue was extracted with pentane (4 × 5 mL), the volume was reduced to *ca.* 3 mL and the solution was stored at −40 °C for 2 days. The precipitate was filtered and washed with cold (−35 °C) pentane. Dissolving the red solid in benzene and lyophilization yields [Os(PNP)(pyrpz)] (31 mg, 44.9 μmol, 65%) as a red powder.

^{1}H NMR (500 MHz, THF-d_8): δ = 8.42 (d, $^3J_{HH}$ = 2.1 Hz, 1H, C_1H), 7.98 (ddd, $^3J_{HH}$ = 6.1 Hz, $^4J_{HH}$ = 1.5 Hz, $^5J_{HH}$ = 0.7 Hz, 1H, C_8H), 7.64 ($A_{18}BCXX'A'_{18}B'C'$, $N = |^3J_{CX} + {}^4J_{CX'}|$ = 33.6 Hz, $^3J_{BC}$ = 5.5 Hz, 2H, NC*H*), 7.00 (ddd, $^3J_{HH}$ = 8.0 Hz, $^4J_{HH}$ = 1.5 Hz, $^5J_{HH}$ = 0.7 Hz, C_5H), 6.97 (d, $^3J_{HH}$ = 2.1 Hz, 1H, C_2H), 6.46 (m, $^3J_{HH}$ = 8.0 Hz, $^3J_{HH}$ = 7.3 Hz, 1H, C_5H), 5.87 (m, $^3J_{HH}$ = 7.3 Hz, $^3J_{HH}$ = 6.1 Hz, 1H, C_6H), 4.27 ($A_{18}BCXX'A'_{18}B'C'$, $N = |^2J_{BX} + {}^4J_{BX'}|$ = 5.6 Hz, $^3J_{BC}$ = 5.5 Hz, 2H, PC*H*), 0.64 (m, 18H, $P(C(CH_3)_3)$), 0.57 (m, 18H, $P(C(CH_3)_3)$) ppm. $^{13}C\{^1H\}$ NMR (128.8 MHz, THF-d_8): δ = 163.7 (vt, $N = |^2J_{CP} + {}^3J_{CP}|$ = 7.8 Hz, NCH), 163.5 (t, $^3J_{CP}$ = 1.2 Hz, C_4), 153.9 (s, C_1), 148.3 (s, C_3),

139.3 (s, C_1), 131.2(s, C_6), 117.1 (s, C_7), 116.3(s, C_5), 102.9 (s, C_2), 86.0 (vt, $N = |^1J_{CP} + {}^3J_{CP}| = 19.3$ Hz, P*C*H), 47.7 (vt, $N = |^1J_{CP} + {}^2J_{CP}| = 11.9$ Hz, P(*C*(CH$_3$))), 35.4 (vt, $N = |^1J_{CP} + {}^2J_{CP}| = 10.5$ Hz, P(*C*(CH$_3$)$_3$)), 28.4 (vt, $N = |^2J_{CP} + {}^4J_{CP}| = 2.5$ Hz, P(C(*C*H$_3$)$_3$)), 25.9 (vt, $N = |^2J_{CP} + {}^4J_{CP}| = 1.9$ Hz, P(C(*C*H$_3$)$_3$)) ppm. ^{31}P{^{1}H} NMR (202.5 MHz, THF-d$_8$): δ = 24.6 (s, *P*(C(CH$_3$)$_3$)) ppm. Anal. calc. for $C_{28}H_{46}N_4OsP_2$ (690.88 g mol^{-1}): C, 48.7; H, 6.71; N, 8.11. Found: C, 48.9; H, 7.05; N, 7.95.

[OsCl(PNP)(pyrpz)] (3)

1 (80 mg, 120 µmol, 1.00 eq.) and 2-(1*H*-pyrazol-5-yl)pyridine (19.9 mg, 137 µmol, 1.05 eq.) were dissolved in THF (20 mL). After addition of NEt$_3$ (80 µL, 574 µmol, 4.34 eq.) the solution was stirred for 36 h at room temperature. After removal of all volatiles under reduced pressure, the residue was washed with pentane (3 × 5 mL) at −40 °C. Afterwards the residue was extracted with pentane (8 × 10 mL) at room temperature. The solvent was removed under reduced pressure, and lyophilisation out of benzene yields [OsCl(PNP)(pyrpz)] as a yellow-brown powder (84.5 mg, 116 µmol, 90%).

^{1}H NMR (300 MHz, THF-d$_8$): δ = 49.20 (s br), 43.35 (s br), 21.27 (s br), 12.74 (s br), 9.35 (s br), 5.40 (s br, 18H, P(C(C*H*$_3$)$_3$)), −1.24 (s br, 18H, P(C(C*H*$_3$)$_3$) ppm (only resonances of *t*Bu groups were tentatively assigned due to paramagnetism). EPR (toluene, 150 K): g_1 = 1.498, g_2 = 2.095, g_3 = 2.530. Anal. calc. for $C_{28}H_{46}ClN_4OsP_2$ (726.3 g mol^{-1}): C, 46.3; H, 6.38; N, 7.71. Found: C, 46.7; H, 6.46; N, 7.79.

Reaction of [Os(PNP)(pyrpz)] with 5

A solution of **2** (20.0 mg, 28.9 µmol) in THF (1 mL) was layered with a solution of **5** (15 mg, 28.9 µmol) in THF (1 mL). After 16 h at −30 °C, a red crystalline solid was obtained by filtration and dried *in vacuo*. The product could be identified as **7** by single-crystal X-ray diffraction analysis. Yield: 21.0 mg, 17.3 µmol, 60%.

IR (neat): $\tilde{\nu}$ = 3339 (m), 3192 (w), 3119 (w), 3056 (w), 2963 (m), 2936 (m), 2918 (m), 2895 (m), 2863 (m), 1691 (w), 1605 (m), 1576 (m), 1566(m), 1511 (s), 1477 (m), 1449 (s), 1431 (m), 1395 (m), 1387 (w), 1360 (m), 1336 (m), 1273 (s), 1233 (s), 1208 (s), 1154 (s), 1113 (m), 1092 (m), 1066 (m), 1023 (s) cm^{-1}. Anal. calc. for $C_{41}H_{55}BiF_3N_5O_3SOsP_2(OC_4H_8)$ (1288.24 g mol^{-1}): C, 42.0; H, 4.86; N, 5.44; S, 2.49. Found: C, 42.3; H, 4.57; N, 5.30; S, 2.21.

Reaction of [Os(PNP)(pyrpz)] with 6

2 (7.0 mg, 10.1 µmol) and **6** (7.8 mg, 10.1 µmol) were dissolved in THF (0.5 mL). After 5 h at ambient temperature the obtained dark red solution was filtrated and layered with *n*-pentane (0.8 mL). After 16 h at ambient temperature a dark red solid was obtained by filtration and dried *in vacuo*. To obtain single crystals of **8**, a solution of **1** in THF was layered with a solution of **6** in THF. After 1 d at −30 °C a crystalline, dark red solid was obtained by filtration. Yield: 10.0 mg, 7.22 µmol, 71%.

IR (neat): $\tilde{\nu}$ = 2951.3 (m), 2898.5 (m), 2864.8 (m), 2235 (w), 2082 (w), 1612 (w), 1580 (w), 1514 (s), 1477 (w), 1467 (w), 1458 (w), 1446 (m), 1429 (m), 1390 (w), 1366 (m), 1356 (m), 1336 (w), 1284 (w), 1273 (w), 1230 (s), 1176 (m), 1117 (m), 1097 (m), 1064 (w), 1045 (m), 1021 (m) cm^{-1}. Anal. calc. for $C_{42}H_{56}BiF_6N_4OsP_2Sb(OC_4H_8)$ (1386.29 g mol^{-1}): C, 39.9; H, 4.65; N, 4.04. Found: C, 39.8; H, 4.78; N, 3.74.

[OsCl(py)(PNP)] (10)

1 (18.7 mg, 30.3 µmol, 1.00 eq.) and CoCp$_2$ (5.7 mg, 30 µmol, 1.0 eq.) are dissolved in benzene (3 mL) and stirred for 2 minutes at room temperature. Pyridine (2.4 µL, 30 µmol, 1.0 eq.) is added and the reaction is stirred for 10 minutes. After filtration the solvent is evaporated and the residue is extracted with pentane and evaporated. [OsCl(py)(PNP)] (18.3 mg, 27.7 µmol, 95%) is obtained as a brown solid.

^{1}H NMR (400 MHz, THF-d$_8$): δ = 10.98 (d, $^3J_{HH}$ = 6.0 Hz, 1H, py-*H*$_1$), 7.89 (d, $^3J_{HH}$ = 5.9 Hz, 1H, py-*H*$_5$), 7.30 (A$_{18}$BCXX′A′$_{18}$B′C′, $N = |^3J_{CX} + {}^4J_{CX'}| = 33.3$ Hz, $^3J_{BC}$ = 6.0 Hz, 2H, NC*H*), 6.21–6.14 (m, 1H, py-*H*$_3$), 6.07–6.00 (m, 1H, py-*H*$_4$), 5.96–5.89 (m, 1H, py-*H*$_2$), 4.25–4.18 (br, 2H, P*CH*), 1.03 (A$_{18}$BCXX′A′$_{18}$B′C′, $N = |^3J_{AX} + {}^5J_{AX'}| = 6.3$ Hz, 18H, P(C(C*H*$_3$)$_3$)), 0.65 (A$_{18}$BCXX′A′$_{18}$B′C′, $N = |^3J_{AX} + {}^5J_{AX'}| = 6.3$ Hz, 18H, P(C(C*H*$_3$)$_3$)) ppm. ^{13}C{^{1}H} NMR (128.8 MHz, THF-d$_8$): δ = 165.5 (s, py-*C*$_5$), 164.0 (vt, $N = |^2J_{CP} + {}^3J_{CP}| = 7.7$ Hz, N*C*H), 161.1 (s, py-*C*$_1$), 131.5 (s, py-*C*$_3$), 123.7 (s, py-*C*$_4$), 123.0 (s, py-*C*$_2$), 87.8 (vt, $N = |^1J_{CP} + {}^3J_{CP}| = 18.3$ Hz, P*C*H), 48.2 (vt, $N = |^1J_{CP} + {}^2J_{CP}| = 11.3$ Hz, P(*C*(CH$_3$))), 37.3 (vt, $N = |^1J_{CP} + {}^2J_{CP}| = 10.1$ Hz, P(*C*(CH$_3$)$_3$)), 29.6 (br, P(C(*C*H$_3$)$_3$)), 26.6 (br, P(C(*C*H$_3$)$_3$)) ppm. ^{31}P{^{1}H} NMR (202.5 MHz, THF-d$_8$): δ = 21.7 (s, *P*(C(CH$_3$)$_3$)) ppm. LIFDI-MS, *m*/*z* (%): calcd for $(C_{25}H_{45}ClN_2OsP_2)^+$ 662.2, found: 662.2; $[M^\bullet]^+$.

Conflicts of interest

There are no conflicts to declare.

Acknowledgements

Dr Christian Würtele is acknowledged for his support in crystallography (compounds **2** and **3**). Generous financial support by the Fonds der Chemischen Industrie (PhD fellowship to J. A.; Liebig fellowship to C. L.) and the DFG is gratefully acknowledged. J. A. and C. L. thank Prof. Sven Schneider and Prof. Holger Braunschweig, respectively, for continuous support.

Notes and references

1 R. Eikey, *Coord. Chem. Rev.*, 2003, **243**, 83.
2 Y. Ashida, K. Arashiba, K. Nakajima and Y. Nishibayashi, *Nature*, 2019, **568**, 536.
3 D. V. Yandulov and R. R. Schrock, *Science*, 2003, **301**, 76.

4 V. Vreeken, M. A. Siegler, B. de Bruin, J. N. H. Reek, M. Lutz and J. I. van der Vlugt, *Angew. Chem., Int. Ed.*, 2015, **54**, 7055.
5 I. Klopsch, E. Y. Yuzik-Klimova and S. Schneider, *Top. Organomet. Chem.*, 2017, **60**, 71.
6 J. S. Figueroa and C. C. Cummins, *Angew. Chem., Int. Ed.*, 2004, **43**, 984.
7 J. A. Buss, P. H. Oyala and T. Agapie, *Angew. Chem., Int. Ed.*, 2017, 14502.
8 G. Balázs, L. J. Gregoriades and M. Scheer, *Organometallics*, 2007, **26**, 3058.
9 B. P. Johnson, G. Balázs and M. Scheer, *Coord. Chem. Rev.*, 2006, **250**, 1178.
10 M. Scheer, J. Müller and M. Häser, *Angew. Chem., Int. Ed. Engl.*, 1996, **35**, 2492.
11 G. Balázs, M. Sierka and M. Scheer, *Angew. Chem., Int. Ed.*, 2005, **44**, 4920.
12 A. J. Ashe III, J. W. Kampf and S. M. Al-Taweel, *J. Am. Chem. Soc.*, 1992, **114**, 372.
13 A. J. Ashe III and E. G. Ludwig Jr., *Organometallics*, 1982, **1**, 1408.
14 M. Wieber and I. Sauer, *Z. Naturforsch., B*, 1985, **40**, 1476.
15 G. Linti, W. Köstler and H. Pritzkow, *Eur. J. Inorg. Chem.*, 2002, 2643.
16 O. Mundt, G. Becker, M. Rssler and C. Witthauer, *Z. Anorg. Allg. Chem.*, 1983, **506**, 42.
17 K. Pandey and G. Frenking, *Eur. J. Inorg. Chem.*, 2004, **22**, 4388.
18 J.-Q. Wang, C. Chi, H.-S. Hu, L. Meng, M. Luo, J. Li and M. Zhou, *Angew. Chem., Int. Ed.*, 2018, **57**, 542.
19 B. E. Atkinson, H.-S. Hu and N. Kaltsoyannis, *Chem. Commun.*, 2018, **54**, 11100.
20 J. M. Goicoechea and H. Grützmacher, *Angew. Chem., Int. Ed.*, 2018, **57**, 16968.
21 F. F. Puschmann, D. Stein, D. Heift, C. Hendriksen, Z. A. Gal, H.-F. Grützmacher and H. Grützmacher, *Angew. Chem.*, 2011, **123**, 8420.
22 D. Heift, Z. Benkő and H. Grützmacher, *Chem. – Eur. J.*, 2014, **20**, 11326.
23 A. M. Tondreau, Z. Benkő, J. R. Harmer and H. Grützmacher, *Chem. Sci.*, 2014, **5**, 1545.
24 A. Hinz and J. M. Goicoechea, *Angew. Chem., Int. Ed.*, 2016, **55**, 8536.
25 L. Weber, *Eur. J. Inorg. Chem.*, 2018, 2175.
26 J. Abbenseth, M. Diefenbach, A. Hinz, L. Alig, C. Würtele, J. M. Goicoechea, M. C. Holthausen and S. Schneider, *Angew. Chem., Int. Ed.*, 2019, **58**, 10966.
27 M. Joost, W. J. Transue and C. C. Cummins, *Chem. Commun.*, 2017, **53**, 10731.
28 Y. Lu, H. Wang, Y. Xie, H. Liu and H. F. Schaefer, *Inorg. Chem.*, 2014, **53**, 6252.
29 H. Braunschweig, P. Cogswell and K. Schwab, *Coord. Chem. Rev.*, 2011, **255**, 101.
30 N. J. Holmes, W. Levason and M. Webster, *J. Organomet. Chem.*, 1997, **545–546**, 111.
31 H. J. Breunig, T. Borrmann, E. Lork, O. Moldovan, C. I. Raț and R. P. Wagner, *J. Organomet. Chem.*, 2009, **694**, 427.
32 A. J. Carty, N. J. Taylor, A. W. Coleman and M. F. Lappert, *J. Chem. Soc., Chem. Commun.*, 1979, 639.
33 H. Schumann and L. Eguren, *J. Organomet. Chem.*, 1991, **403**, 183.
34 N. J. Holmes, W. Levason and M. Webster, *J. Organomet. Chem.*, 1999, **584**, 179.
35 J. von Seyerl and G. Huttner, *J. Organomet. Chem.*, 1980, **195**, 207.
36 S. J. Davies, N. A. Compton, G. Huttner, L. Zsolnai and S. E. Garner, *Chem. Ber.*, 1991, **124**, 2731.
37 L. Balazs, H. J. Breunig, E. Lork and C. Silvestru, *Eur. J. Inorg. Chem.*, 2003, 1361.
38 I. Vránová, T. Dušková, M. Erben, R. Jambor, A. Růžička and L. Dostál, *J. Organomet. Chem.*, 2018, **863**, 15.
39 M. Kořenková, V. Kremláček, M. Erben, R. Jirásko, F. de Proft, J. Turek, R. Jambor, A. Růžička, I. Císařová and L. Dostál, *Dalton Trans.*, 2018, **47**, 14503.
40 M. B. Kindervater, K. M. Marczenko, U. Werner-Zwanziger and S. S. Chitnis, *Angew. Chem., Int. Ed.*, 2019, **58**, 7850.
41 I. Vránová, M. Alonso, R. Jambor, A. Růžička, M. Erben and L. Dostál, *Chem. – Eur. J.*, 2016, **22**, 7376.
42 H. Braunschweig, P. Brenner, P. Cogswell, K. Kraft and K. Schwab, *Chem. Commun.*, 2010, **46**, 7894.
43 C. Tschersich, B. Braun, C. Herwig and C. Limberg, *Organometallics*, 2015, **34**, 3782.
44 C. Tschersich, C. Limberg, S. Roggan, C. Herwig, N. Ernsting, S. Kovalenko and S. Mebs, *Angew. Chem., Int. Ed.*, 2012, **51**, 4989.
45 T.-P. Lin, I.-S. Ke and F. P. Gabbaï, *Angew. Chem., Int. Ed.*, 2012, **51**, 4985.
46 K. Materne, S. Hoof, N. Frank, C. Herwig and C. Limberg, *Organometallics*, 2017, **36**, 4891.
47 C. Tschersich, S. Hoof, N. Frank, C. Herwig and C. Limberg, *Inorg. Chem.*, 2016, **55**, 1837.
48 S. Balasubramaniam, S. Kumar, A. P. Andrews, B. Varghese, E. D. Jemmis and A. Venugopal, *Eur. J. Inorg. Chem.*, 2019, 3265.
49 R. J. Schwamm, C. M. Fitchett and M. P. Coles, *Chem. – Asian J.*, 2019, **14**, 1204.
50 R. Kannan, S. Kumar, A. P. Andrews, E. D. Jemmis and A. Venugopal, *Inorg. Chem.*, 2017, **56**, 9391.
51 T. Ollevier, *Org. Biomol. Chem.*, 2013, **11**, 2740.
52 J. M. Bothwell, S. W. Krabbe and R. S. Mohan, *Chem. Soc. Rev.*, 2011, **40**, 4649.
53 S. Solyntjes, B. Neumann, H.-G. Stammler, N. Ignat'ev and B. Hoge, *Chem. – Eur. J.*, 2017, **23**, 1568.
54 C. Lichtenberg, F. Pan, T. P. Spaniol, U. Englert and J. Okuda, *Angew. Chem., Int. Ed.*, 2012, **51**, 13011.
55 R. Qiu, S. Yin, X. Zhang, J. Xia, X. Xu and S. Luo, *Chem. Commun.*, 2009, 4759.
56 J. Ramler, J. Poater, F. Hirsch, B. Ritschel, I. Fischer, F. M. Bickelhaupt and C. Lichtenberg, *Chem. Sci.*, 2019, **10**, 4169.
57 (*a*) B. Ritschel, J. Poater, H. Dengel, F. M. Bickelhaupt and C. Lichtenberg, *Angew. Chem., Int. Ed.*, 2018, **57**, 3825; (*b*) B. Ritschel and C. Lichtenberg, *Synlett*, 2018, **29**, 2213.

58 H. Dengel and C. Lichtenberg, *Chem. – Eur. J.*, 2016, **22**, 18465.
59 J. A. Johnson and A. J. Venugopal, *J. Chem. Sci.*, 2019, **131**, 114.
60 J. Ramler, K. Hofmann and C. Lichtenberg, *Inorg. Chem.*, 2020, **59**, 3367.
61 J. Ramler and C. Lichtenberg, *Chem. – Eur. J.*, 2020, DOI: 10.1002/chem.202001674.
62 J. Abbenseth and S. Schneider, *Z. Anorg. Allg. Chem.*, 2020, **55**, 1690.
63 J. Abbenseth, D. Delony, M. C. Neben, C. Würtele, B. de Bruin and S. Schneider, *Angew. Chem., Int. Ed.*, 2019, **58**, 6338.
64 J. Abbenseth, S. C. Bete, M. Finger, C. Volkmann, C. Würtele and S. Schneider, *Organometallics*, 2018, **37**, 802.
65 A. Glüer, B. Askevold, B. Schluschaß, F. W. Heinemann and S. Schneider, *Z. Anorg. Allg. Chem.*, 2015, **641**, 49.
66 J. Abbenseth, M. Diefenbach, S. C. Bete, C. Würtele, C. Volkmann, S. Demeshko, M. C. Holthausen and S. Schneider, *Chem. Commun.*, 2017, **53**, 5511.
67 The performed ^{1}H NMR spectroscopic analyses only investigated the standard region for diamagnetic compounds.
68 J. Bresien, A. Schulz, M. Thomas and A. Villinger, *Eur. J. Inorg. Chem.*, 2019, 1279.
69 One equivalent of $[\mathbf{3}\text{-}(\mathbf{BiCl_3})]_2$ is also present in the asymmetric unit. For details see ESI.†
70 C. J. Carmalt, D. Walsh, A. H. Cowley and N. C. Norman, *Organometallics*, 1997, **16**, 3597.
71 C. J. Carmalt, L. J. Farrugia and N. C. Norman, *J. Chem. Soc., Dalton Trans.*, 1996, 443.
72 J. Beckmann, J. Bolsinger, A. Duthie, P. Finke, E. Lork, C. Lüdtke, O. Mallow and S. Mebs, *Inorg. Chem.*, 2012, **51**, 12395.
73 X. Zhang, R. Qiu, N. Tan, S. Yin, J. Xia, S. Luo and C.-T. Au, *Tetrahedron Lett.*, 2010, **51**, 153.
74 M. Bao, T. Hayashi and S. Shimada, *Organometallics*, 2007, **26**, 1816.
75 X. Zhang, S. Yin, R. Qiu, J. Xia, W. Dai, Z. Yu, C.-T. Au and W.-Y. Wong, *J. Organomet. Chem.*, 2009, **694**, 3559.
76 In **5** a stretching frequency for the NH functionality is found at 3334 cm^{-1}. See: ref. 57*a*.
77 M. Vehkamäki, T. Hatanpää, M. Ritala and M. Leskelä, *J. Mater. Chem.*, 2004, **14**, 3191.
78 H. G. Ang, C. M. Hay, B. F. G. Johnson, J. Lewis, P. R. Raithby and A. J. Whitton, *J. Organomet. Chem.*, 1987, **330**, C5–C11.
79 R. D. Adams and W. C. Pearl, *Inorg. Chem.*, 2010, **49**, 7170.
80 S. P. Oh, Y.-Z. Li and W. K. Leong, *J. Organomet. Chem.*, 2015, **783**, 46.
81 A. E. Reed, R. B. Weinstock and F. Weinhold, *J. Chem. Phys.*, 1985, **83**, 735.
82 L. Falivene, Z. Cao, A. Petta, L. Serra, A. Poater, R. Oliva, V. Scarano and L. Cavallo, *Nat. Chem.*, 2019, **11**, 872.
83 This is indicated by the empty space between the PMe_2 groups and the bismuth complex fragment located on isocontour curves of >2.5 Å (Fig. 6b, right).
84 K. Materne, B. Braun-Cula, C. Herwig, N. Frank and C. Limberg, *Chem. – Eur. J.*, 2017, **23**, 11797.
85 It should be noted that only Pt → Bi interactions were considered in ref. 46 and only Bi → Pd interactions were considered in ref. 84.
86 G. M. Sheldrick, *Acta Crystallogr., Sect. A: Found. Crystallogr.*, 2008, **64**, 112.
87 G. M. Sheldrick, *Acta Crystallogr., Sect. A: Found. Adv.*, 2014, **70**, C1437.
88 G. M. Sheldrick, *Acta Crystallogr., Sect. A: Found. Adv.*, 2015, **71**, 3.
89 M. J. Frisch, G. W. Trucks, H. B. Schlegel, G. E. Scuseria, M. A. Robb, J. R. Cheeseman, G. Scalmani, V. Barone, G. A. Petersson, H. Nakatsuji, X. Li, M. Caricato, A. V. Marenich, J. Bloino, B. G. Janesko, R. Gomperts, B. Mennucci, H. P. Hratchian, J. V. Ortiz, A. F. Izmaylov, J. L. Sonnenberg, D. Williams-Young, F. Ding, F. Lipparini, F. Egidi, J. Goings, B. Peng, A. Petrone, T. Henderson, D. Ranasinghe, V. G. Zakrzewski, J. Gao, N. Rega, G. Zheng, W. Liang, M. Hada, M. Ehara, K. Toyota, R. Fukuda, J. Hasegawa, M. Ishida, T. Nakajima, Y. Honda, O. Kitao, H. Nakai, T. Vreven, K. Throssell, J. A. Montgomery Jr., J. E. Peralta, F. Ogliaro, M. J. Bearpark, J. J. Heyd, E. N. Brothers, K. N. Kudin, V. N. Staroverov, T. A. Keith, R. Kobayashi, J. Normand, K. Raghavachari, A. P. Rendell, J. C. Burant, S. S. Iyengar, J. Tomasi, M. Cossi, J. M. Millam, M. Klene, C. Adamo, R. Cammi, J. W. Ochterski, R. L. Martin, K. Morokuma, O. Farkas, J. B. Foresman and D. J. Fox, *Gaussian 16, Revision B.01*, Gaussian, Inc., Wallingford, CT, 2016.
90 P. C. Hariharan and J. A. Pople, *Theor. Chim. Acta*, 1973, **28**, 213.
91 T. H. Dunning and P. J. Hay, in *Modern theoretical chemistry*, Plenum Press, New York, 1977, p. 1.
92 P. J. Hay and W. R. Wadt, *J. Chem. Phys.*, 1985, **82**, 299.
93 P. J. Hay and W. R. Wadt, *J. Chem. Phys.*, 1985, **82**, 270.
94 A. D. Becke, *J. Chem. Phys.*, 1993, **98**, 5648.
95 S. Grimme, J. Antony, S. Ehrlich and H. Krieg, *J. Chem. Phys.*, 2010, **132**, 154104.
96 E. D. Glendening, J. K. Badenhoop, A. E. Reed, J. E. Carpenter, J. A. Bohmann, C. M. Morales, P. Karafiloglou, C. R. Landis and F. Weinhold, *NBO 7.0*, Theoretical Chemistry Institute, University of Wisconsin, Madison, 2018.
97 W. B. Renfrow Jr. and C. R. Hauser, *Org. Synth.*, 1939, **19**, 83.

XII Carbon Monoxide Insertion at a Heavy p-Block Element: Unprecedented Formation of a Cationic Bismuth Carbamoyl

This chapter was published in: Jacqueline Ramler, Jordi Poater, Florian Hirsch, Benedikt Ritschel, Ingo Fischer, F. Matthias Bickelhaupt, Crispin Lichtenberg, *Chem. Sci.* **2019**, *10*, 4169–4176. Reproduced from ref. 254 with permission from the Royal Society of Chemistry.

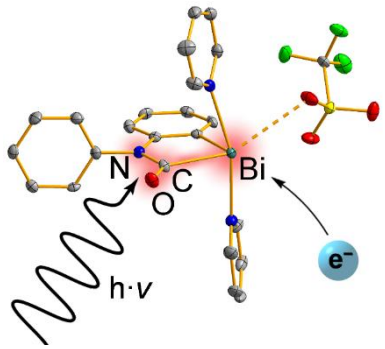

Chemical Science

EDGE ARTICLE

View Article Online
View Journal | View Issue

Check for updates

Cite this: *Chem. Sci.*, 2019, **10**, 4169

All publication charges for this article have been paid for by the Royal Society of Chemistry

Carbon monoxide insertion at a heavy p-block element: unprecedented formation of a cationic bismuth carbamoyl†

Jacqueline Ramler,[a] Jordi Poater,[bc] Florian Hirsch,[d] Benedikt Ritschel,[a] Ingo Fischer,[d] F. Matthias Bickelhaupt[*ef] and Crispin Lichtenberg[*a]

Received 17th January 2019
Accepted 27th February 2019

DOI: 10.1039/c9sc00278b

rsc.li/chemical-science

Major advances in the chemistry of 5th and 6th row heavy p-block element compounds have recently uncovered intriguing reactivity patterns towards small molecules such as H_2, CO_2, and ethylene. However, well-defined, homogeneous insertion reactions with carbon monoxide, one of the benchmark substrates in this field, have not been reported to date. We demonstrate here, that a cationic bismuth amide undergoes facile insertion of CO into the Bi–N bond under mild conditions. This approach grants direct access to the first cationic bismuth carbamoyl species. Its characterization by NMR, IR, and UV/vis spectroscopy, elemental analysis, single-crystal X-ray analysis, cyclic voltammetry, and DFT calculations revealed intriguing properties, such as a reversible electron transfer at the bismuth center and an absorption feature at 353 nm ascribed to a transition involving σ- and π-type orbitals of the bismuth-carbamoyl functionality. A combined experimental and theoretical approach provided insight into the mechanism of CO insertion. The substrate scope could be extended to isonitriles.

Introduction

The traditional distinction between transition metal and main-group compounds according to their physical and chemical properties has recently been challenged.[1] This is due to the fact that researchers are currently in the process of understanding how to design main group compounds with properties including a well-defined one-electron-redox chemistry, small HOMO–LUMO gaps of <4 eV, and remarkable reactivities in the activation of small molecules such as H_2, CO, CO_2, and ethylene.

Among the main group compounds, complexes of the heavy p-block elements with a principal quantum number of $n > 4$ show some inherent characteristics with high potential for applications in synthesis and catalysis. These include low homolytic bond dissociation energies,[2] reversible homolytic bond cleavage/bond forming reactions,[3] and large ionic radii, which allow for the design of cationic species with a considerable soft Lewis acidity. In the case of bismuth, a relatively low toxicity of the element and its complexes should also be noted.[4] For compounds based on elements of the sixth row of the periodic table of the elements, relativistic effects come into play and may affect their physical and spectroscopic properties.[5]

When targeting highly reactive heavy main group species, low-valent compounds, complexes with element–element multiple bonds, and cationic species are promising candidates. However, the synthesis of such compounds may be extremely challenging. This is due to the inherent characteristics of heavy p-block elements, including (i) large ionic and covalent radii, which facilitate (unselective) oligomerization of low-valent species, (ii) relatively low redox potentials, which make over-reduction a serious synthetic problem, (iii) disproportionation reactions of mono-cationic complexes, and (iv) difficulties in accessing extremely Lewis-acidic and Lewis-basic species.

Despite these challenges, considerable efforts in designing heavy main group species that undergo well-defined reactions with small molecules have been crowned with success. The distannyne Sn_2Aryl_2 has been shown to reversibly add two equivalents of ethylene across its Sn≡Sn bond to give the corresponding distannane (Scheme 1a, Aryl = C_6H_3-2,6(C_6H_3-2,6-iPr_2)$_2$).[6,7] This distannyne and closely related derivatives also react with dihydrogen to give a dinuclear tin species with two

[a]Institute of Inorganic Chemistry, Julius-Maximilians Universität Würzburg, Am Hubland, 97074 Würzburg, Germany. E-mail: crispin.lichtenberg@uni-wuerzburg.de
[b]ICREA, Pg. Lluis Companys 23, 08010 Barcelona, Spain
[c]Universitat de Barcelona, Departament de Química Inorgànica i Orgànica & IQTCUB, Martí i Franquès 1-11, 08028 Barcelona, Spain
[d]Institute of Physical Chemistry, Julius-Maximilians Universität Würzburg, Am Hubland, 97074 Würzburg, Germany
[e]Vrije Universiteit Amsterdam, Department of Theoretical Chemistry, Amsterdam Center for Multiscale Modeling (ACMM), The Netherlands. E-mail: f.m.bickelhaupt@vu.nl
[f]Radboud University, Institute for Molecules and Materials, Heyendaalseweg 135, 6525 AJ Nijmegen, The Netherlands

† Electronic supplementary information (ESI) available: Experimental procedures, details of DFT calculations, NMR, IR and UV/vis spectra, cyclic voltammograms, single crystal X-ray analysis data, coordinates of calculated structures. CCDC 1875340–1875343. For ESI and crystallographic data in CIF or other electronic format see DOI: 10.1039/c9sc00278b

bridging hydride ligands, a reaction that has recently been shown to be reversible (Scheme 1b).[8] In an alternative strategy without any E–E multiple bonding, the hypervalent bismuth compound $Bi(C_6H_4CH_2)_2NtBu(OMe)$ with one polar Bi–O bond has been shown to undergo reversible CO_2 fixation under mild reaction conditions (Scheme 1c).[9,10]

Apart from H_2, CO_2, and ethylene, carbon monoxide is an intriguing substrate for insertion chemistry, since it represents an attractive, versatile C1-building block in synthetic chemistry. Traditionally, its utilization for the synthesis of organic molecules such as alcohols, aldehydes, or carboxamides has been realized with transition metal carbonyl species acting as critical intermediates.[11] According to the Dewar–Chatt–Duncanson model, the bond between CO and a transition metal constitutes of ligand-to-metal σ-donation and metal-to-ligand π-back-donation. It has been demonstrated that π-back-donation makes an important or even crucial contribution to the overall bonding energy of most synthetically relevant carbonyl compounds.[12] This renders carbon monoxide an extremely challenging substrate for compounds based on heavy p-block elements, because synthetically accessible species of this kind usually lack occupied orbitals of sufficient symmetry and energy for π-back-donation. As a result, insights in this field of research are very limited.[13,14] Electrochemical sensing of CO at SnO_2 or In_2O_3 surfaces at elevated temperatures has been related to the formation of carbonate and carboxylate species by IR spectroscopy.[15] Matrix isolation techniques allowed for the IR spectroscopic characterization of tin and lead carbonyl species such as SnCO, $Sn(CO)_2$, Sn_nCO, Pb_nCO, and $SnCO^-$ at 7–20 K (n = 1–4).[16] These reports have been complemented by additional purely theoretical studies on these and related compounds.[17] To the best of our knowledge, however, well-defined insertion reactions of carbon monoxide with compounds based on heavy p-block elements showing a principal quantum number of $n > 4$ have not been reported to date.

Cationic bismuth amides combine a considerable Lewis acidity with a good accessibility and a high reactivity, making them promising candidates for small molecule activation.[18–20] Insertion reactions with carbon monoxide in specific would grant direct access to cationic bismuth carbamoyls, an unprecedented structural motif with high potential for the stabilization of (intermediate) radical species (Scheme 1d).[21]

Here we demonstrate that a well-defined cationic bismuth amide undergoes highly selective and facile insertion reactions with carbon monoxide and isonitriles under mild conditions, yielding the first examples of cationic bismuth carbamoyls and amidinoyls, which were isolated and fully characterized.

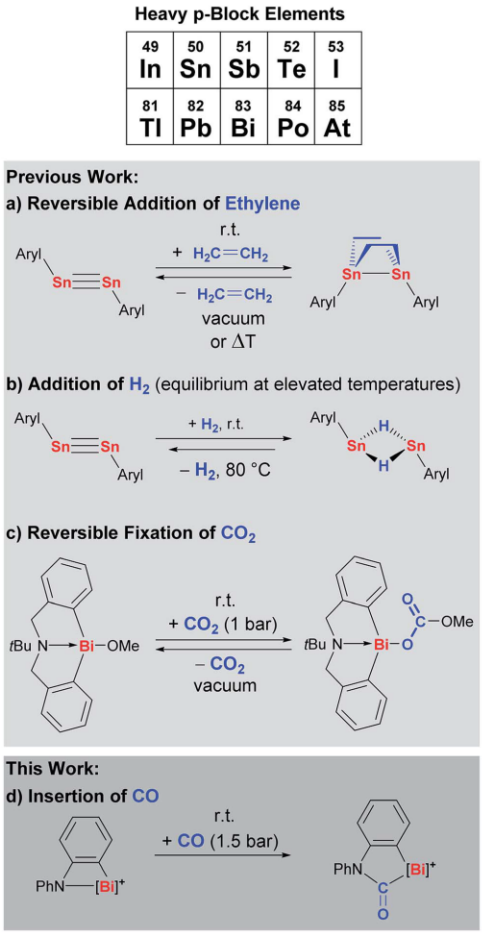

Scheme 1 Examples of well-defined compounds of heavy p-block elements that show unusual reactivity patterns towards small molecules. Aryl = C_6H_3-2,6(C_6H_3-2,6-iPr_2)$_2$.

Results and discussion

The dinuclear cationic bismuth compound $[Bi_2(N(C_6H_4)Ph)_2(OTf)_2(thf)_3]$ (**1**) has recently been reported and was synthesized according to the literature (Scheme 2; Tf = SO_2CF_3).[19a,22] The prominent structural feature of compound **1** is a four-membered C_2NBi ring. The geometric parameters dictated by

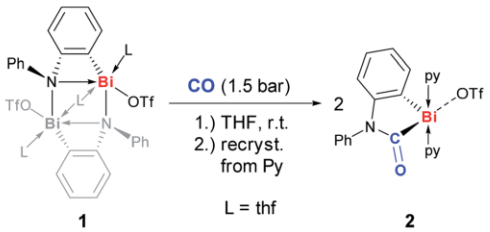

Scheme 2 Insertion of CO into Bi–N bond of (masked) cationic bismuth amide **1** to give cationic bismuth carbamoyl compound **2**; py = pyridine, Tf = SO_2CF_3.

the phenylene unit suggest a considerable ring strain and lead to a significantly elongated Bi–N bond as part of the four-membered ring.[19] These characteristics seem predetermined for compound **1** to be highly active in small molecule activation reactions. Thus, compound **1** was reacted with carbon monoxide, which represents an extraordinarily challenging substrate in the chemistry of heavier group 15 compounds. When a suspension of yellow **1** in THF was exposed to an atmosphere of 1.5 bar CO the precipitation of a pale yellow solid indicated the consumption of the starting materials. Whereas a quantitative reaction monitoring by IR and NMR spectroscopy was hampered by the moderate to poor solubility of the starting material and the product in THF, these methods still indicated significant conversion of **1** after 1 h. However, extended reaction times of 2 d were necessary to reach full conversion of **1**, which was otherwise difficult to separate from the product. Recrystallization of the crude precipitate from pyridine/Et_2O/pentane gave the insertion product **2** in 61% yield (Scheme 2).[23] Compound **2** is moderately soluble in THF, but adequately soluble in pyridine. In pyridine solution, it is stable at ambient temperature and under ambient lighting for at least five weeks and at 80 °C for at least 2 h. NMR spectroscopy indicated the substitutional lability of the pyridine ligands, which can be removed *in vacuo* at 80 °C. ^{1}H and ^{13}C and ^{19}F NMR spectroscopic analyses revealed the expected signal patterns for the functional groups present in **2** (a phenylene and a phenyl group, two pyridine ligands, and a triflate). An unusually large ^{13}C NMR chemical shift of 251 ppm was recorded for the *C*ONR_2 group, which was ascribed to its interaction with the Lewis acidic cationic bismuth center.[24] IR spectroscopic analyses revealed a CO stretching frequency of 1637 cm^{-1} for the carbamoyl functional group. This is close to those reported for carbamoyl compounds of Sn and Pb, which were prepared by classical salt elimination protocols.[25]

The molecular structure of **2** was unambiguously identified by single-crystal X-ray diffraction (monoclinic space group $P2_1/n$ with $Z = 4$; Fig. 1). This confirmed the insertion of CO into the former Bi–N bond, resulting in formation of a bismuth carbamoyl moiety, an unprecedented structural motif.[26] The Bi1–C13 bond is considerably longer than the Bi1–C2 bond ($\Delta = +0.11$ Å). Despite the cationic nature of **2**,[22] the Bi–($CONR_2$) bond length is in the same range as that of electronically stabilized Bi–C bonds in neutral compounds such as $Bi(CH(SiMe_3)_2)_3$, $Bi(\eta^1\text{-2-Me-allyl})_3$, or $Bi(CF_2CF_3)_3$.[27] Accordingly, the C13–N1 distance of 1.38 Å is in agreement with a partial C=N double bond character. According to an energy decomposition analysis (EDA) of **2** and related species, these differences in Bi–C bond lengths are also reflected by the corresponding interaction energies: in homolytic bond dissociations, the interaction energy of the Bi–Aryl bond is 17.9 kcal mol^{-1} larger than that of the Bi–$CONR_2$ bond (ESI†). The covalent character of both types of bonds amounts to 44–49% according to EDA. In the solid state, **2** forms a loosely associated contact ion pair. The Bi1···O2 distance of 3.16 Å is 12% below the sum of the van-der-Waals radii, but significantly elongated compared to the Bi–OTf bond of 2.37 Å in starting material **1**.[19a] The coordination geometry around the bismuth center in **2** is saturated by two

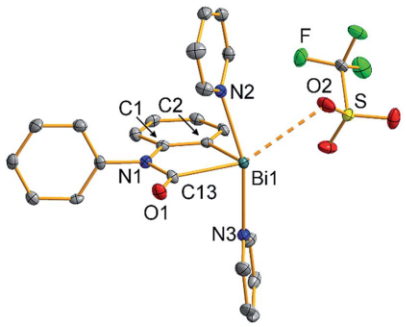

Fig. 1 Molecular structure of [Bi(CONPh(C_6H_4))($NC_5H_5)_2$][OTf] (**2**) in the solid state. Displacement ellipsoids are shown at the 50% probability level. Hydrogen atoms are omitted for clarity. Selected bond lengths (Å) and angles (°): Bi1–C2, 2.227(5); Bi1–C13, 2.335(5); Bi1–N2, 2.520(4); Bi1–N3, 2.471(4); Bi1···O2, 3.164(4); C13–O1, 1.213(5); C13–N1, 1.382(6); C2–Bi1–C13, 76.60(16); C2–Bi1–N2, 84.21(15); C2–Bi1···O2, 103.25(14); N2–Bi1–N3, 163.56(13); C13–Bi1···O2, 153.50(14); τ_5 = 0.17.

pyridine ligands in *trans*-position to each other. Overall, this results in a distorted square pyramidal coordination geometry around bismuth with C2 in the apical position ($\tau_5 = 0.17$).[28]

The electrochemical behavior of **2** was investigated by cyclic voltammetry in THF/0.1 M [N(*n*Bu)$_4$][PF_6] at 23 °C, which revealed a chemically reversible redox event at an only moderately negative potential of −1.66 V *vs.* Fc/Fc^+ (Fig. 2a and ESI;† Fc = $Fe(C_5H_5)_2$). According to DFT calculations, the radical generated upon reduction is free of neutral donor ligands, [Bi(CONPh(C_6H_4))]$^\bullet$ (**2red**). 74% of the spin density are located at the bismuth center, occupying a molecular orbital with dominating contributions from a Bi-6p-type atomic orbital (Fig. 2b and ESI†). The remaining spin density is delocalized over the phenylene and the carbamoyl unit of **2red**, with spin densities of up to 5% at single C, N, and O atoms. This delocalization of spin density is believed to contribute to the stability of this species under the conditions of the

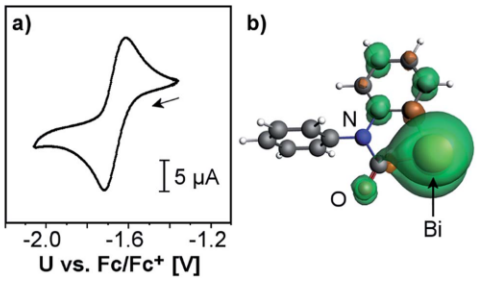

Fig. 2 (a) Cyclic voltammogram of **2** in THF/0.1 M [N(*n*Bu)$_4$][PF_6] at 23 °C with a scan rate of 500 mV s^{-1}; Fc = $Fe(C_5H_5)_2$. (b) Optimized geometry and spin density distribution (iso value = 0.001) of reduced species [Bi(CONPh(C_6H_4))]$^\bullet$ (**2red**).

View Article Online
Chemical Science Edge Article

electrochemical experiment. While two examples of isolable Bi^{II} radical species and one example of a persistent Bi^{II} radical species have recently been reported,[3a,29] this is the first example of a quasi-reversible electron transfer at a mononuclear bismuth compound with the bismuth atom being the major spin carrier, demonstrating the potential of the bismuth carbamoyl functional group for the stabilization of (intermediate) radical species.[30] The pale yellow compound **2** was further investigated by UV/vis spectroscopy in THF solution, which revealed a broad absorption band at $\lambda_{max} = 353$ nm (FWHM = 96 nm; Fig. 3). In dilute solutions, the substitutionally labile pyridine ligands of **2** can presumably be exchanged for thf ligands (ESI†). TD-DFT calculations at the CAMY-B3LYP/TZ2P level of theory on $[Bi(CONPh(C_6H_4))(thf)_2]^+$ indicated a HOMO−1/LUMO singlet–singlet transition at $\lambda = 354$ nm, when spin–orbit-coupling was taken into account using perturbation theory (for details see ESI†). This transition is suggested to correspond to the experimentally observed band at $\lambda_{max} = 353$ nm. The HOMO−1 shows major contributions by orbitals forming the Bi–C and C–N σ-bonds in the carbamoyl group and by an oxygen-centered p-type orbital. The LUMO consists of a bismuth-centered p-orbital and the π*-orbital of the CO group, both of which are orthogonal to the plane defined by the carbamoyl functionality. Thus, the bismuth carbamoyl functional group is directly involved in the electronic transition that is triggered by light in the UV/vis region ($\lambda \approx 310$–400 nm).

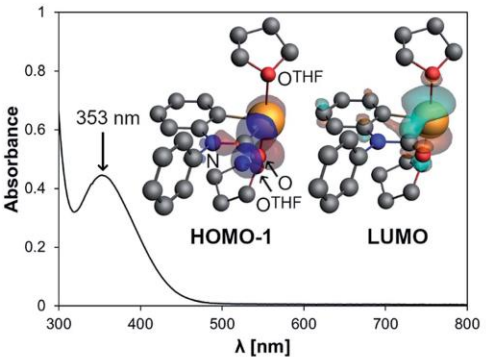

Fig. 3 UV/vis spectrum of **2** (0.4 mM solution in THF) and orbitals involved in the transition at 353 nm according to TD-DFT calculations on $[Bi(CONPh(C_6H_4))(thf)_2]^+$.

The mechanism of CO insertion was investigated by DFT calculations (Scheme 3, for details see ESI†).[31] All values are given in kcal mol^{-1}. We suggest coordination of CO to a Lewis-acidic bismuth center to be the initiating reaction step leading to intermediate **I-1** (ΔH: +9.7; ΔG: +5.9).[32] Insertion of the CO molecule proceeds *via* transition state **TS-1**, in which the CO unit bridges a Bi and an N atom (barrier: $\Delta H^{\neq}$: +8.5; $\Delta G^{\neq}$: +10.5), to give intermediate **I-2** in an almost thermoneutral reaction (ΔH: +0.2; ΔG: +3.0). A similar sequence of CO-coordination (to give **I-3**) and formation of a transition state with a Bi···(CO)···N unit (**TS-2**, barrier: $\Delta H^{\neq}$: +9.3; $\Delta G^{\neq}$: +11.6) and insertion leads to dinuclear intermediate **I-4**. Coordination of THF gives the monomeric compound **I-5**, which is suggested to be the species that precipitates from the reaction mixture, when **1** is reacted with CO in THF (*vide supra*).[23] Up to this point the overall reaction is exothermic and endergonic according to

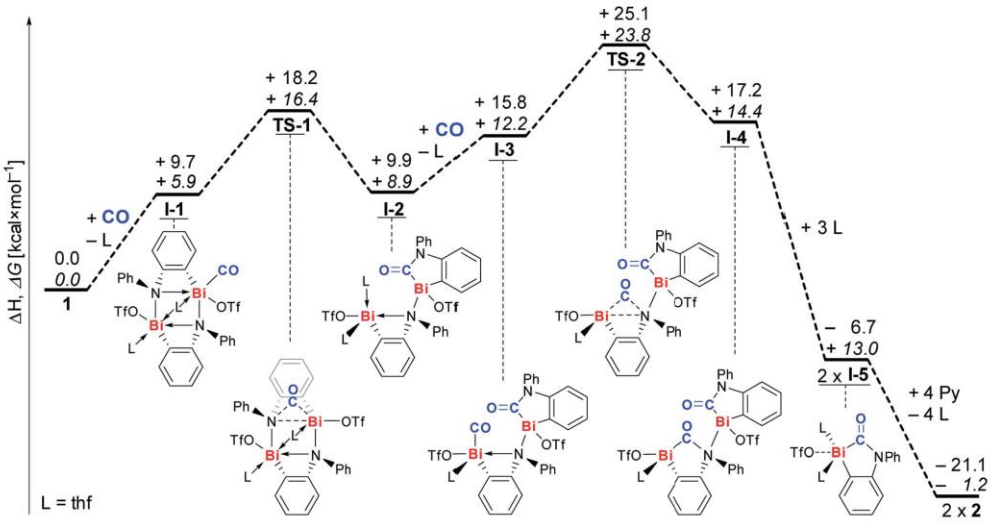

Scheme 3 Proposed mechanism for reaction of **1** with CO to give insertion product **2**; ΔH values (regular font) and ΔG values (italic) are given in kcal mol^{-1}. L = thf.

DFT calculations (ΔH: −6.7; ΔG: +13.0), and the formation of **I-5** is presumably aided by its poor solubility in THF. The exchange of THF for pyridine ligands to give isolated product **2** is exothermal and exergonic, reflecting the Lewis acidity of the bismuth atom (ΔH: −14.4; ΔG: −14.2). Monitoring the reaction by IR spectroscopy indicated the accumulation of **I-5** in solution until its saturation concentration was reached (characteristic band at 1592 cm^{-1}).[23] Whereas intermediates **I-1**, **I-2**, and **I-3** could not unambiguously be identified due to their low concentrations, signal overlapping, or their short-lived character, bands at 1655 and 1669 cm^{-1} were tentatively assigned to intermediate **I-4** (ESI†).

Putting the unusual reactivity of **1** towards carbon monoxide into the broader context of main group chemistry reveals some remarkable points. Compounds of strongly electropositive elements of Groups 1 and 2, as well as light(er) elements of Group 13 (B–Ga) undergo insertion with CO; examples include species such as *n*BuLi, $LiN(iPr)_2$, MgEtBr, or $Al(tBu)_3$.[33,34] These reactivity patterns may be interpreted as a result of the strong polarization of the M–X bond (X = C, N) and the high Lewis acidity of the main-group compound. In addition, compounds of Group 13 and 14 elements with low-valent character or with E–E (single or multiple) bonds have been reported to undergo intriguing insertion reactions with carbon monoxide (E = Group 13/14 element). Examples include diborynes, diboracumulenes, carbenes, germylenes and a disila-Dewar-benzene.[35–37] When it comes to well-defined compounds of the pnictogens P–Bi, selective insertion reactions with CO under mild conditions have only been reported for phosphorous species. Two different strategies have been reported in this context. Frustrated Lewis pairs (FLPs) with a phosphane moiety as the Lewis basic component react with CO under mild conditions to form heterocyclic compounds.[38–43] The second strategy exploits the reactivity of a phosphorus biradicaloid, which inserts CO under harsher conditions to give a P_2N_2C ring motif that maintains the biradicaloid character.[44] Overall, compound **1** represents the first molecular heavy p-block compound ($n > 4$) to undergo a direct and well-defined insertion reaction with carbon monoxide under mild conditions. The Lewis acidity and geometric constraints of **1** play key roles in determining its remarkable reactivity. It may be considered to interpret these driving forces in terms of FLP chemistry with a Lewis basic N and a Lewis acidic Bi site.[45c,d] To the best of our knowledge, this would be the first example of FLP chemistry of molecular compounds being extended to the heavy main group element bismuth.[45–47]

In order to extend the scope of the unusual insertion reactions of **1** with unsaturated small molecules, isonitriles were targeted due to their isoelectronic and isolobal relationship with carbon monoxide. Well-defined insertion reactions of pnictogen compounds with isonitriles are rare. Transition metal-stabilized phosphinidenes and arsinidenes $[E(C_5Me_5)(W(CO)_5)_2]$ (E = P, As) have been reported to coordinate sterically demanding C≡N*t*Bu and to undergo insertion reactions with less bulky isonitriles C≡NR (R = *cyclo*-hexyl, *n*Bu).[48] Only recently, the first example of an insertion reaction between a bismuth compound and an isonitrile has been documented:

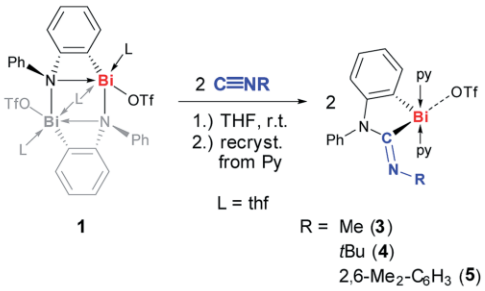

1

R = Me (**3**)
*t*Bu (**4**)
2,6-Me_2-C_6H_3 (**5**)

Scheme 4 Insertion of C≡NR into Bi–N bond of (masked) cationic bismuth amide **1** to give cationic bismuth amidinoyl compounds **3**, **4**, and **5**; py = pyridine, Tf = SO_2CF_3.

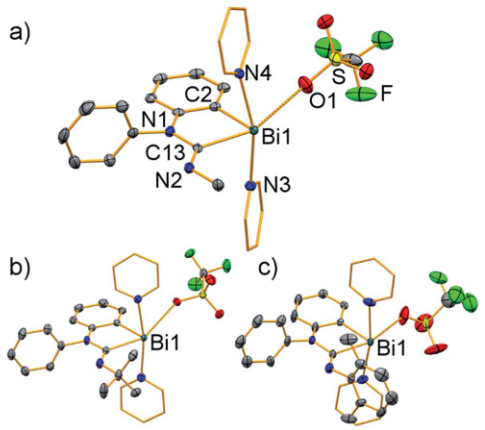

Fig. 4 Molecular structures of $[Bi(CNRNPh(C_6H_4))(NC_5H_5)_2][OTf]$ in the solid state ((a) **3** (R = Me); (b) **4** (R = *t*Bu); (c) **5** (R = 2,6-Me_2-C_6H_3)). Displacement ellipsoids are shown at the 50% probability level; carbon atoms of pyridine ligands are shown as wireframe for clarity. Hydrogen atoms, lattice-bound solvent molecules, and split positions of disordered groups in (c) are omitted for clarity. Atom labelling in (b) and (c) is in analogy with that in (a). Selected bond lengths (Å) and angles (°): (a) Bi1–C2, 2.222(3); Bi1–C13, 2.305(3); Bi1–N3, 2.499(2); Bi1–N4, 2.482(2); Bi1···O1, 3.025(2); C13–N1, 1.402(3); C13–N2, 1.263(3); C2–Bi1–C13, 76.84(10); C2–Bi1–N3, 84.48(8); C2–Bi1···O1, 79.86(9); N3–Bi1–N4, 164.35(7); C13–Bi1···O1, 155.56(8); τ_5 = 0.15. (b) Bi1–C2, 2.225(3); Bi1–C13, 2.331(3); Bi1–N3, 2.485(3); Bi1–N4, 2.525(3); Bi1···O1, 2.997(2); C13–N1, 1.415(4); C13–N2, 1.261(4); C2–Bi1–C13, 77.35(12); C2–Bi1–N3, 87.63(11); C2–Bi1···O1, 80.94(10); N3–Bi1–N4, 169.39(9); C13–Bi1···O1, 153.18(9); τ_5 = 0.27. (c) Bi1–C2, 2.202(4); Bi1–C13, 2.299(4); Bi1–N3, 2.510(4); Bi1–N4, 2.488(4); Bi1···O1, 2.907(15); C13–N1, 1.43(2); C13–N2, 1.269(6); C2–Bi1–C13, 76.89(15); C2–Bi1–N3, 84.96(14); C2–Bi1···O1, 82.0(3); N3–Bi1–N4, 169.41(13); C13–Bi1···O1, 158.8(3); τ_5 = 0.18.

the strongly nucleophilic nature of the boryl group in $[Ph_2Bi(BR_2)]$ allowed for isolation of the insertion product $[Ph_2Bi(C(NPh)BR_2)]$ in 22% yield, when C≡NPh was used as the substrate (BR_2 = 1,2,4,3-triazaborol-3-yl).[49] Remarkably, the

alkyl isonitrile C≡N(*n*Bu) was found to undergo fragmentation with formation of [$BiPh_2$(*n*Bu)], implying that isonitrile insertion is not a general reaction pathway for this bismuth boryl compound.

At ambient temperature, compound **1** readily reacted with isonitriles, C≡NR, that bear alkyl or aryl substituents with a steric profile varying from extremely low (R = Me) to high (R = *t*Bu, 2,6-Me_2-C_6H_3) (Scheme 4). Monitoring the reaction by ^{1}H-NMR spectroscopy in the case of R = *t*Bu revealed full conversion within 10 min and a high spectroscopic yield of >95%. The insertion products **3–5** were isolated in 60–79% yield after recrystallization from pyridine and fully characterized (Scheme 4, Fig. 4). In all cases the bismuth amidinoyl moiety was exclusively formed in its *Z*-configuration according to NMR spectroscopy. Compounds **3–5** show ^{13}C NMR chemical shifts between 210 and 223 ppm and IR bands at 1606–1637 cm^{-1} for the *C*N*R*NR_2 functionality.

Single-crystal X-ray diffraction analyses revealed a very similar coordination behavior for compounds **3–5** (Fig. 4). In each case, the bismuth atom is found in distorted square pyramidal coordination geometry with C2 in the apical position (τ_5 = 0.15–0.27). The Bi–C distances of the amidinoyl unit (Bi1–C13, 2.30–2.33 Å) are significantly larger than those involving the aryl group (Bi1–C2, 2.20–2.23 Å). The N1–C13 bond lengths of 1.40–1.43 Å suggest partial double bond character, albeit they are larger than those in carbamoyl compound **2** (1.38 Å).

Conclusions

In summary, we have reported the facile insertion of carbon monoxide into a bismuth–nitrogen bond, exploiting the Lewis acidity of the cationic bismuth compound and the release of ring strain as driving forces of the reaction. To the best of our knowledge, this is the first example of a molecular compound based on a heavy p-block element with the principal quantum number $n > 4$ to undergo a well-defined insertion reaction with carbon monoxide under mild conditions. This grants access to a novel cationic bismuth carbamoyl species, which allows for the first time to realize a chemically reversible redox process at the bismuth center of a mononuclear molecular compound. The pale yellow color of this compound was attributed to a singlet-singlet-transition that involves the bismuth carbamoyl functionality and is facilitated by spin–orbit coupling. Isonitriles were shown to analogously undergo these unusual insertion reactions. These results reveal the potential of heavy main group compounds in small-molecule activation, reversible electron–transfer reactions at heavy main group elements, and photochemistry targeting the accessibility of excited states with visible light.

Conflicts of interest

There are no conflicts to declare.

Acknowledgements

C. L. thanks Dr R. D. Dewhurst for helpful discussions and Prof. H. Braunschweig for continuous support. Funding by the Fonds der Chemischen Industrie (Liebig fellowship to C. L.), the DFG (funding to C. L. and GRK 2112), the Netherlands Organization for Scientific Research (NWO), the Catalan Government (2017SGR348), and the Spanish MINECO (CTQ2016-77558-R and MDM-2017-0767) is acknowledged.

Notes and references

1 (*a*) P. P. Power, *Nature*, 2010, **463**, 171–177; (*b*) P. P. Power, *Chem. Rev.*, 2003, **103**, 789–809; (*c*) D. Martin, M. Soleilhavoup and G. Bertrand, *Chem. Sci.*, 2011, **2**, 389–399; (*d*) M.-A. Légaré, C. Pranckevicius, H. Braunschweig, *Chem. Rev.* DOI: 10.1021/acs.chemrev.8b00561; (*e*) C. Lichtenberg, *Angew. Chem., Int. Ed.*, 2016, **55**, 484–486; (*f*) C. Weetman, S. Inoue, *ChemCatChem*, 2019, **10**, 4213–4228.

2 *E.g.*: (*a*) L. D. Freedman and G. O. Doak, *Chem. Rev.*, 1982, **82**, 15–57; (*b*) G. P. Smith and R. Patrick, *Int. J. Chem. Kinet.*, 1983, **15**, 167–185 and references therein.

3 *E.g.*: (*a*) S. Ishida, F. Hirakawa, K. Furukawa, K. Yoza and T. Iwamoto, *Angew. Chem., Int. Ed.*, 2014, **53**, 11172–11176; (*b*) D. Dakternieks, D. J. Henry and C. H. Schiesser, *Organometallics*, 1998, **17**, 1079–1084; (*c*) M. Lehnig and K. Dören, *J. Organomet. Chem.*, 1981, **210**, 331–341.

4 *E.g.*: J. M. Bothwell, S. W. Krabbe and R. S. Mohan, *Chem. Soc. Rev.*, 2011, **40**, 4649–4707 and references therein.

5 (*a*) P. Pyykkö, *Chem. Rev.*, 1988, **88**, 563–594; (*b*) P. Pyykkö, *Annu. Rev. Phys. Chem.*, 2012, **63**, 45–64; (*c*) R. J. F. Berger, D. Rettenwander, S. Spirk, C. Wolf, M. Patzschke, M. Ertl, U. Monkowius and N. W. Mitzel, *Phys. Chem. Chem. Phys.*, 2012, **14**, 15520–15524; (*d*) A. Wodyński, O. L. Malkina and M. Pecul, *J. Phys. Chem. A*, 2016, **120**, 5624–5634.

6 Y. Peng, B. D. Ellis, X. Wang, J. C. Fettinger and P. P. Power, *Science*, 2009, **325**, 1668–1670.

7 For the insertion of ethylene into the Sn–C bond of a diarylstannylen see: T. Y. Lai, J.-D. Guo, J. C. Fettinger, S. Nagase and P. P. Power, *Chem. Commun.*, 2019, **55**, 405–407.

8 (*a*) Y. Peng, M. Brynda, B. D. Ellis, J. C. Fettinger, E. Rivard and P. P. Power, *Chem. Commun.*, 2008, 6042–6044; (*b*) S. Wang, T. J. Sherbow, L. A. Berben and P. P. Power, *J. Am. Chem. Soc.*, 2018, **140**, 590–593.

9 S.-F. Yin, J. Maruyama, T. Yamashita and S. Shimada, *Angew. Chem., Int. Ed.*, 2008, **47**, 6590–6593.

10 For reactions of CO_2 with bismuth compounds, also see: (*a*) H. J. Breunig, L. Königsmann, E. Lork, M. Nema, N. Philipp, C. Silvestru, A. Soran, R. A. Varga and R. Wagner, *Dalton Trans.*, 2008, 1831–1842; (*b*) K. Wójcik, T. Rüffer, H. Lang, A. A. Auer and M. Mehring, *J. Organomet. Chem.*, 2011, **696**, 1647–1651; (*c*) D. R. Kindra, I. J. Casely, M. E. Fieser, J. W. Ziller, F. Furche and W. J. Evans, *J. Am. Chem. Soc.*, 2013, **135**, 7777–7787.

11 (*a*) H. T. Luk, C. Mondelli, D. C. Ferré, J. A. Stewart and J. Pérez-Ramírez, *Chem. Soc. Rev.*, 2017, **46**, 1358–1426; (*b*) N. Rajesh, N. Basu and B. Sundararaju, *Tetrahedron Lett.*, 2018, **59**, 862–868; (*c*) A. S. Veige, *Polyhedron*, 2008, **27**, 3177–3189.

12 (*a*) K. Nakashima, X. Zhang, M. Xiang, Y. Lin, M. Lin and Y. Mo, *J. Theor. Comput. Chem.*, 2008, **7**, 639–654; (*b*) G. Bistoni, S. Rampino, N. Scafuri, G. Ciancaleoni, D. Zuccaccia, L. Belpassi and F. Tarantelli, *Chem. Sci.*, 2016, **7**, 1174–1184; (*c*) A. Diefenbach, F. M. Bickelhaupt and G. Frenking, *J. Am. Chem. Soc.*, 2000, **122**, 6449–6458.

13 Iodine reacts with carbon monoxide and water to give carbon dioxide and hydrogen iodide: W. M. MacNevin and W. N. Carson Jr, *J. Am. Chem. Soc.*, 1950, **72**, 42–44.

14 Laser photolysis of HI in a carbon monoxide matrix allows for the detection of the formyl radical: J. A. Brivati, N. Keen and M. C. R. Symons, *J. Chem. Soc.*, 1962, 237–243.

15 (*a*) P. G. Harrison and M. J. Willet, *Nature*, 1988, **332**, 337–339; (*b*) M.-I. Baraton, L. Merhari, H. Ferkel and J.-F. Castagnet, *Mater. Sci. Eng., C*, 2002, **19**, 315–321.

16 (*a*) A. Bos, *J. Chem. Soc., Chem. Commun.*, 1972, 26–27; (*b*) L. N. Zhang, J. Dong and M. F. Zhou, *J. Chem. Phys.*, 2000, **113**, 8700–8705; (*c*) L. Jiang and X. Qiang, *Bull. Chem. Soc. Jpn.*, 2006, **79**, 857–863; (*d*) L. Jiang and Q. Xu, *J. Chem. Phys.*, 2005, **122**, 034506.

17 (*a*) Y. Lu, H. Wang, Y. Xie, H. Liu and H. F. Schaefer, *Inorg. Chem.*, 2014, **53**, 6252–6256; (*b*) C. Gourlaouen, O. Parisel and J.-P. Piquemal, *J. Chem. Phys.*, 2010, **133**, 124310; (*c*) A. J. Bridgeman, *Inorg. Chim. Acta*, 2001, **321**, 27–41.

18 H. Dengel and C. Lichtenberg, *Chem.–Eur. J.*, 2016, **22**, 18465–18475.

19 (*a*) B. Ritschel, J. Poater, H. Dengel, F. M. Bickelhaupt and C. Lichtenberg, *Angew. Chem., Int. Ed.*, 2018, **57**, 3825–3829; (*b*) B. Ritschel and C. Lichtenberg, *Synlett*, 2018, **29**, 2213–2217.

20 (*a*) R. J. Schwamm, B. M. Day, M. P. Coles and C. M. Fitchett, *Inorg. Chem.*, 2014, **53**, 3778–3787; (*b*) R. J. Schwamm, M. P. Coles and C. M. Fitchett, *Dalton Trans.*, 2017, **46**, 4066–4074; (*c*) C. Hering-Junghans, M. Thomas, A. Villinger and A. Schulz, *Chem.–Eur. J.*, 2015, **21**, 6713–6717; (*d*) M. Veith, B. Bertsch and V. Huch, *Z. Anorg. Allg. Chem.*, 1988, **559**, 73–88.

21 For examples of intermediate carbamoyl radical species in synthetic chemistry see: (*a*) F. Minisci, F. Fontana, F. Coppa and Y. M. Yan, *J. Org. Chem.*, 1995, **60**, 5430–5433; (*b*) Q.-F. Bai, C. Jin, J.-Y. He and G. Feng, *Org. Lett.*, 2018, **20**, 2172–2175; (*c*) G. López-Valdez, S. Olguín-Uribe and L. D. Miranda, *Tetrahedron Lett.*, 2007, **48**, 8285–8289.

22 Compounds **1** and **2** represent contact ion pairs in the solid state; the term "cationic species" is used to describe the weak interactions between the triflate anions and the bismuth atoms in these compounds.

23 The solid that precipitated from THF was analyzed by NMR spectroscopy in NC_5D_5. The spectrum showed all resonances for compound **2** (except for those due to NC_5H_5) plus resonances for non-coordinate THF. This supports our results from DFT calculations suggesting that the precipitate is compound **I-5**.

24 A ^{13}C NMR chemical shift of 204.5 ppm has been reported for CO groups in the five-membered cyclic complex anion $[As[C(O)]_2[NDipp]_2]^-$: A. Hinz and J. M. Goicoechea, *Angew. Chem., Int. Ed.*, 2016, **55**, 8536–8541.

25 (*a*) L. C. Willemsens, *J. Organomet. Chem.*, 1971, **27**, 45–51; (*b*) G.-E. Matsubayashi, M. Hiroshima and T. Tanaka, *J. Organomet. Chem.*, 1973, **59**, 207–212.

26 The formation of a bismuth carbamoyl species from $BiCl_3$, DMF and amines has been discussed on the basis of conductance measurements and elemental analysis, but no spectroscopic or structural data has been provided: A. K. Mishra and K. N. Tandon, *Inorg. Chem.*, 1971, **10**, 1896–1899.

27 (*a*) B. Murray, J. Hvoslef, H. Hope and P. P. Power, *Inorg. Chem.*, 1983, **22**, 3421–3424; (*b*) C. Lichtenberg, F. Pan, T. P. Spaniol, U. Englert and J. Okuda, *Angew. Chem., Int. Ed.*, 2012, **51**, 13011–13015; (*c*) S. Solyntjes, J. Bader, B. Neumann, H.-G. Stammler, N. Ignat'ev and B. Hoge, *Chem.–Eur. J.*, 2017, **23**, 1557–1567.

28 A. W. Addison, T. N. Rao, J. Reedijk, J. van Rijn and G. C. Verschoor, *J. Chem. Soc., Dalton Trans.*, 1984, 1349–1356.

29 (*a*) R. J. Schwamm, J. R. Harmer, M. Lein, C. M. Fitchett, S. Granville and M. P. Coles, *Angew. Chem., Int. Ed.*, 2015, **54**, 10630–10633; (*b*) C. Ganesamoorthy, C. Helling, C. Wölper, W. Frank, E. Bill, G. E. Cutsail III and S. Schulz, *Nat. Commun.*, 2018, **9**, 87.

30 For electrochemical studies on dibismuthenes including a ferrocenyl substituted derivative see: (*a*) M. Sakagami, T. Sasamori, H. Sakai, Y. Furukawa and N. Tokitoh, *Chem.–Asian J.*, 2013, **8**, 690–693; (*b*) T. Sasamori, E. Mieda, N. Nagahora, K. Sato, D. Shiomi, T. Takui, Y. Hosoi, Y. Furukawa, N. Takagi, S. Nagase and N. Tokitoh, *J. Am. Chem. Soc.*, 2006, **128**, 12582–12588.

31 Relativistic, dispersion-corrected DFT calculations were carried out at the ZORA-BLYP-D3BJ/TZ2P level of theory using COSMO to simulate solvation in THF, as implemented in the ADF program, see: (*a*) G. te Velde, F. M. Bickelhaupt, E. J. Baerends, C. Fonseca Guerra, S. J. A. van Gisbergen, J. G. Snijders and T. Ziegler, *J. Comput. Chem.*, 2001, **22**, 931–967; (*b*) F. M. Bickelhaupt and E. J. Baerends, in *Reviews in Computational Chemistry*, ed. K. B. Lipkowitz and D. B. Boyd, Wiley-VCH, New York, 2000, vol. 15, pp. 1-86.

32 Substitution of the two terminal thf ligands in **1** for two CO molecules was calculated to be endothermal and endergonic (ΔH: +18.0 kcal mol^{-1}; ΔG: +16.2 kcal mol^{-1}) and is therefore suggested not to be involved in the primary reaction pathway (formation of "**I-1**_2CO", ESI†).

33 (*a*) M. Ryang and S. Tsutsumi, *Bull. Chem. Soc. Jpn.*, 1962, **35**, 1121–1124; (*b*) H. C. Brown and E. Negishi, *J. Am. Chem. Soc.*, 1967, **89**, 5477–5478; (*c*) N. S. Nudelman and A. A. Vitale, *J. Org. Chem.*, 1981, **46**, 4625–4626; (*d*) D. Seyferth and R. M. Weinstein, *J. Am. Chem. Soc.*, 1982, **104**, 5534–5535; (*e*) W. J. J. M. Sprangers and R. Louw, *J. Chem. Soc., Perkin Trans. 2*, 1976, 1895–1901; (*f*) M. D. Anker, C. E. Kefalidis, Y. Yang, J. Fang, M. S. Hill, M. F. Mahon and L. Maron, *J. Am. Chem. Soc.*, 2017, **139**, 10036–10054; (*g*) M. A. Dureen and D. W. Stephan, *J. Am. Chem. Soc.*, 2010, **132**, 13559–13568; (*h*) M. R. Mason, B. Song and K. Kirschbaum, *J. Am. Chem. Soc.*, 2004, **126**, 11812–11813; (*i*) X. Li, C. Ni,

H. Song and C. Cui, *Chem. Commun.*, 2006, 1763–1765; (*j*) M. R. Mason, B. Song, Y. Han and X. Hu, *Inorg. Chim. Acta*, 2008, **361**, 3332–3337; (*k*) C. M. Lindsay and D. A. Widdowson, *J. Chem. Soc., Perkin Trans. 1*, 1988, 569–573.

34 An FLP type reactivity towards CO has recently been reported for a phosphorus ylide with a boryl substituent: M. Radius and F. Breher, *Chem.–Eur. J.*, 2018, **24**, 15744–15749.

35 (*a*) X. Wang, Z. Zhu, Y. Peng, H. Lei, J. C. Fettinger and P. P. Power, *J. Am. Chem. Soc.*, 2009, **131**, 6912–6913; (*b*) Z. D. Brown and P. P. Power, *Inorg. Chem.*, 2013, **52**, 6248–6259.

36 (*a*) H. Braunschweig, T. Dellermann, R. D. Dewhurst, W. C. Ewing, K. Hammond, J. O. C. Jimenez-Halla, T. Kramer, I. Krummenacher, J. Mies, A.-K. Phukan and A. Vargas, *Nat. Chem.*, 2013, **5**, 1025–1028; (*b*) M. Arrowsmith, J. Böhnke, H. Braunschweig and M. A. Celik, *Angew. Chem., Int. Ed.*, 2017, **56**, 14287–14292; (*c*) N. Nakata, T. Oikawa, T. Matsumoto, Y. Kabe and A. Sekiguchi, *Organometallics*, 2005, **24**, 3368–3370; (*d*) H. Zhang, Z. Cao, W. Wu and Y. Mo, *Angew. Chem., Int. Ed.*, 2018, **57**, 13076–13081; (*e*) L. Wallbaum, D. Weismann, D. Löber, C. Bruhn, P. Prochnow, J. E. Bandow and U. Siemeling, *Chem.–Eur. J.*, 2019, **25**, 1488–1497.

37 Carbenes and silylenes also form stable and transient (sila-) ketenes with CO, respectively: (*a*) V. Lavallo, Y. Canac, B. Donnadieu, W. W. Schoeller and G. Bertrand, *Angew. Chem., Int. Ed.*, 2006, **45**, 3488–3491; (*b*) M. Tacke, C. Klein, D. J. Stufkens, A. Oskam, P. Jutzi and E. A. Bunte, *Z. Anorg. Allg. Chem.*, 1993, **619**, 865–868; (*c*) M.-A. Pearsall and R. West, *J. Am. Chem. Soc.*, 1988, **110**, 7228–7229; (*d*) R. Becerra and R. Walsh, *J. Am. Chem. Soc.*, 2000, **122**, 3246–3247.

38 (*a*) M. Sajid, A. Lawzer, W. Dong, C. Rosorius, W. Sander, B. Schirmer, S. Grimme, C. G. Daniliuc, G. Kehr and G. Erker, *J. Am. Chem. Soc.*, 2013, **135**, 18567–18574; (*b*) M. Sajid, L.-M. Elmer, C. Rosorius, C. G. Daniliuc, S. Grimme, G. Kehr and G. Erker, *Angew. Chem., Int. Ed.*, 2013, **52**, 2243–2246; (*c*) L.-M. Elmer, G. Kehr, C. G. Daniliuc, M. Siedow, H. Eckert, M. Tesch, A. Studer, K. Williams, T. H. Warren and G. Erker, *Chem.–Eur. J.*, 2017, **23**, 6056–6068; (*d*) L. Wang, K. Samigullin, M. Wagner, A. C. McQuilken, T. H. Warren, C. Daniliuc, G. Kehr and G. Erker, *Chem.–Eur. J.*, 2016, **22**, 11015–11021; (*e*) K.-Y. Ye, G. Kehr, C. G. Daniliuc, L. Liu, S. Grimme and G. Erker, *Angew. Chem., Int. Ed.*, 2016, **55**, 9216–9219.

39 Also see reaction of $(P(tBu)_3 + 2B(C_6F_5)_3)$ with syngas: R. Dobrovetsky and D. W. Stephan, *J. Am. Chem. Soc.*, 2013, **135**, 4974–4977.

40 For examples of phosphorus compounds reacting with carbonyl ligands see: (*a*) A. Fuchs, D. Gudat, M. Nieger, O. Schmidt, M. Sebastian, L. Nyulaszi and E. Niecke, *Chem.–Eur. J.*, 2002, **8**, 2188–2196; (*b*) L. Weber, K. Reizig and R. Boese, *Angew. Chem., Int. Ed.*, 1986, **25**, 755–757; (*c*) A. Marinetti, J. Fischer and F. Mathey, *J. Am. Chem. Soc.*, 1985, **107**, 5001–5002; (*d*) M. Scheer, E. Leiner, P. Kramkowski, M. Schiffer and G. A. Baum, *Chem.–Eur. J.*, 1998, **4**, 1917–1934; (*e*) M. Finze, E. Bernhardt, H. Willner and C. W. Lehmann, *Inorg. Chem.*, 2006, **45**, 669–678.

41 For examples of metal complexes with phosphorus ligands reacting with CO, see: (*a*) P. G. Edwards, M. B. Hursthouse, K. M. A. Malik and J. S. Parry, *J. Chem. Soc., Chem. Commun.*, 1994, 1249–1250; (*b*) D. M. Roddick, B. D. Santariero and J. E. Bercaw, *J. Am. Chem. Soc.*, 1985, **107**, 4670–4678; (*c*) R. L. De, D. Wolters and H. Vahrenkamp, *Z. Naturforsch.*, 1986, **41b**, 283–291.

42 For an example of Pd-catalyzed synthesis of acylphosphonates using CO as a C1-source see: Y. Masuda, N. Ishida and M. Murakami, *Chem.–Asian J.*, 2015, **10**, 321–324.

43 For an example of reversible coordination of CO to a phosphinidene see: M. Hansmann and G. Bertrand, *J. Am. Chem. Soc.*, 2016, **138**, 15885–15888.

44 A. Hinz, A. Schulz and A. Villinger, *Angew. Chem., Int. Ed.*, 2015, **54**, 2776–2779.

45 (*a*) D. W. Stephan, *J. Am. Chem. Soc.*, 2015, **137**, 10018–10032; (*b*) D. W. Stephan, *Acc. Chem. Res.*, 2015, **48**, 306–316; (*c*) D. W. Stephan and G. Erker, *Chem. Sci.*, 2014, **5**, 2625–2641; (*d*) F.-G. Fontaine and D. W. Stephan, *Philos. Trans. R. Soc., A*, 2017, **375**, 20170004.

46 A 1-phosphane-8-stibonium-naphtalene species with Lewis acidic character has been reported, but no FLP-type reactivity has been described to date: (*a*) R. A. Ugarte, D. Devarajan, R. M. Mushinski and T. W. Hudnall, *Dalton Trans.*, 2016, **45**, 11150–11161; (*b*) R. A. Ugarte and T. W. Hudnall, *Green Chem.*, 2017, **19**, 1990–1998.

47 In the heterogeneously catalyzed photocatalytic reduction of CO_2, the reactivity of frustrated Lewis pairs of $In_2O_{3-x}(OH)_y$ has been modified by isomorphous substitution of In by Bi: Y. Dong, K. K. Ghuman, R. Popescu, P. N. Duchesne, W. Zhou, J. Y. Y. Loh, A. A. Jelle, J. Jia, D. Wang, X. Mu, C. Kübel, L. Wang, L. He, M. Ghoussoub, Q. Wang, T. E. Wood, L. M. Reyes, P. Zhang, N. P. Kherani, C. V. Singh and G. A. Ozin, *Adv. Sci.*, 2018, **5**, 1700743–1700742.

48 M. Seidl, M. Schiffer, M. Bodensteiner, A. Y. Timoshkin and M. Scheer, *Chem.–Eur. J.*, 2013, **19**, 13783–13791.

49 W. Lu, H. Hu, Y. Li, R. Ganguly and R. Kinjo, *J. Am. Chem. Soc.*, 2016, **138**, 6650–6661.

XIII Methylbismuth: an Organometallic Bismuthinidene Biradical

This chapter was published in: Deb Pratim Mukhopadhyay, Domenik Schleier, Sara Wirsing, Jacqueline Ramler, Dustin Kaiser, Engelbert Reusch, Patrick Hemberger, Tobias Preitschopf, Ivo Krummenacher, Bernd Engels, Ingo Fischer, Crispin Lichtenberg, *Chem. Sci.* **2020**, *11*, 7562–7568. Reproduced from ref. 236 with permission from the Royal Society of Chemistry.

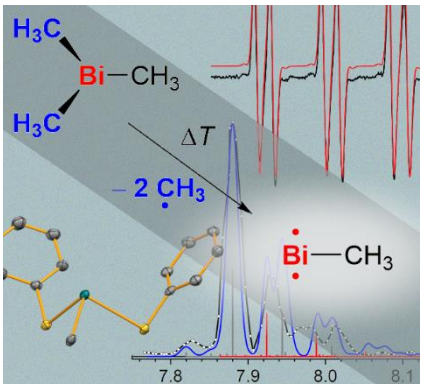

Chemical Science

ROYAL SOCIETY OF CHEMISTRY

EDGE ARTICLE

View Article Online
View Journal | View Issue

Check for updates

Cite this: *Chem. Sci.*, 2020, **11**, 7562

All publication charges for this article have been paid for by the Royal Society of Chemistry

Methylbismuth: an organometallic bismuthinidene biradical†

Deb Pratim Mukhopadhyay,[a] Domenik Schleier,[a] Sara Wirsing,[a] Jacqueline Ramler,[b] Dustin Kaiser,[a] Engelbert Reusch,[a] Patrick Hemberger,[c] Tobias Preitschopf,[a] Ivo Krummenacher,[b] Bernd Engels,*[a] Ingo Fischer*[a] and Crispin Lichtenberg*[b]

Received 28th April 2020
Accepted 2nd June 2020

DOI: 10.1039/d0sc02410d

rsc.li/chemical-science

We report the generation, spectroscopic characterization, and computational analysis of the first free (non-stabilized) organometallic bismuthinidene, BiMe. The title compound was generated *in situ* from $BiMe_3$ by controlled homolytic Bi–C bond cleavage in the gas phase. Its electronic structure was characterized by a combination of photoion mass-selected threshold photoelectron spectroscopy and DFT as well as multi-reference computations. A triplet ground state was identified and an ionization energy (IE) of 7.88 eV was experimentally determined. Methyl abstraction from $BiMe_3$ to give $[BiMe_2]^\bullet$ is a key step in the generation of BiMe. We reaveal a bond dissociation energy of 210 ± 7 kJ mol^{-1}, which is substantially higher than the previously accepted value. Nevertheless, the homolytic cleavage of Me–$BiMe_2$ bonds could be achieved at moderate temperatures (60–120 °C) in the condensed phase, suggesting that $[BiMe_2]^\bullet$ and BiMe are accessible as reactive intermediates under these conditions.

Introduction

Low-valent molecular compounds of group 15 elements, E–R, with the central atom E in the oxidation state of +1 are highly reactive, electron-deficient species (E = N–Bi; R = monoanionic ligand).[1] In principle, they can adopt either singlet or triplet electronic ground states, which strongly influences their physical and chemical properties (Scheme 1). Thus, understanding their (electronic) structures is key to rationalizing the reactivity of these species, which represent important intermediates in fundamental transformations such as insertion and ring expansion reactions.[2] The isolation of such compounds, in which the group 15 atom is bound to only one additional atom, is extremely challenging and has only recently been achieved for the lightest congeners in landmark contributions (E = N, P, Scheme 1a).[2,3] Access to the heavier homologues is increasingly difficult due to their tendency to undergo degradation reactions such as oligomerization, disproportionation, and bond activation processes. For the heaviest group 15 element bismuth, mononuclear organometallic compounds with the metal atom in the oxidation state of +1 (so-called bismuthinidenes) could so far only be accessed by stabilization through adduct formation with Lewis bases (Scheme 1b).[4–9] Very recently, the intriguing properties of such bismuthinidenes have been exploited for (electro-)catalytic and photophysical applications: a Bi^I/Bi^{III} redox couple has been proposed to be a key component in bismuth-catalyzed transfer hydrogenation reactions with ammonia borane.[10] In addition, Bi^I oxalates have been suggested to be involved in the electrochemical reduction of carbon dioxide at bismuth electrodes.[11] When embedded in host materials such as zeolites, $[Bi^I]^+$ centers show intriguing photophysical properties such as ultrabroad near-infrared emission.[12,13] Without any exceptions, the isolable, Lewis-base-stabilized bismuthinidenes reported to date show singlet ground states. This situation changes, when non-stabilized, (so far) non-isolable, electron-deficient molecular bismuthinidenes, Bi–R, are targeted. To date, only inorganic species Bi–X have been reported and were accessed by comproportionation (*e.g.* at high temperature in the melt) or by reaction of Bi atoms with reactive species such as F_2 in the gas phase (X = H, F–I, $AlCl_4$).[14–18] Importantly, these synthetic routes did not allow to study the reactivity of bismuthinidenes, they did not allow to work in conventional solvents at moderate temperature, and they did not allow to access compounds with tunable substituents R, such as organometallic bismuthinidenes Bi–R (R = alkyl, aryl; Fig. 1c).

[a]*Institute of Physical and Theoretical Chemistry, University of Würzburg, Am Hubland, D-97074 Würzburg, Germany. E-mail: bernd.engels@uni-wuerzburg.de; ingo.fischer@uni-wuerzburg.de*

[b]*Institute of Inorganic Chemistry, University of Würzburg, Am Hubland, D-97074 Würzburg, Germany. E-mail: crispin.lichtenberg@uni-wuerzburg.de*

[c]*Laboratory for Femtochemistry and Synchrotron Radiation, Paul Scherrer Institut (PSI), CH-5232 Villigen, Switzerland. E-mail: patrick.hemberger@psi.ch*

† Electronic supplementary information (ESI) available. CCDC 1991253. For ESI and crystallographic data in CIF or other electronic format see DOI: 10.1039/d0sc02410d

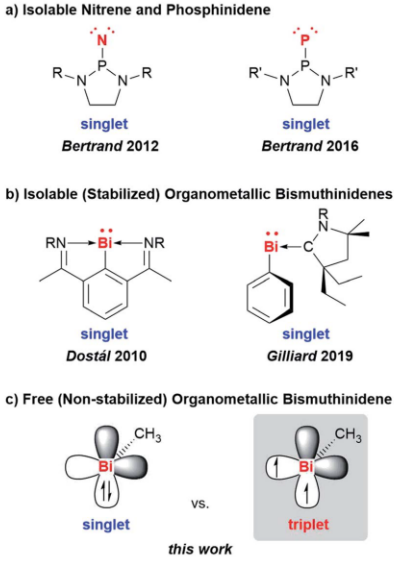

Scheme 1 Low-valent group 15 compounds: (a) isolable nitrene and phosphinidene (singlet ground state). (b) stabilized organometallic bismuthinidenes (singlet ground state; occupied bismuth 6s-orbital omitted for clarity); (c) free (non-stabilized) singlet and triplet species that may be envisaged for BiMe (only two bismuth p-orbitals shown; p-orbital used for Bi–Me bonding and occupied s-orbital are omitted for clarity). R = 2,6-Me_2-C_6H_3; 2,6-iPr_2-C_6H_3; R′ = 2,6-[(4-*t*Bu-C_6H_4)$_2$CH]$_2$-4-Me-C_6H_3.

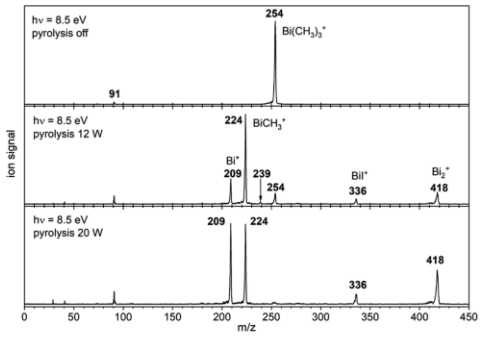

Fig. 1 Photoionization mass spectra recorded at 8.5 eV without pyrolysis (top trace), low pyrolysis power ($T \approx 470$ K, center trace) and medium pyrolysis power ($T \approx 600$ K, bottom trace). The signal at $m/z = 91$ is due to a background signal from previous experiments.

Here we report the generation and characterization of the first free (*i.e.* non-stabilized) organometallic bismuthinidene methylbismuth, BiMe, in a gas-phase reaction with implications for related reactions in condensed phase at moderate temperature. In addition, dimethylbismuth, $[BiMe_2]^\bullet$ was studied to determine the Bi–CH_3 bond dissociation energy in $BiMe_3$.

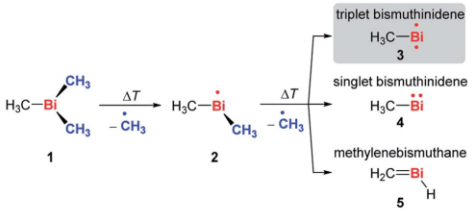

Scheme 2 Controlled, stepwise abstraction of CH_3 radicals from **1** in the gas phase by flash pyrolysis.

Results and discussion

In order to access the elusive class of non-stabilized organometallic bismuthinidenes, we aimed at a "top-down approach", more specifically the homolytic cleavage of Bi–C bonds from the well-defined organometallic precursor $BiMe_3$ (**1**) as shown in Scheme 2. The long-known $BiMe_3$ has been investigated from many different perspectives,[19–21] including its application in chemical vapor deposition, where the abstraction of all its methyl groups is targeted.[22,46]

In a recent study, it was demonstrated that the abstraction of a single methyl group can be achieved by dissociative photoionization of **1**, *i.e.* the Bi–C bond cleavage of the $[BiMe_3]^{\bullet+}$ cation in the gas phase.[23] Under these conditions, only a single methyl group was abstracted, yielding the cation $[BiMe_2]^+$. Here we attempt a thermally-induced, controlled and stepwise abstraction of methyl groups from neutral $BiMe_3$. Thus, a sample of $BiMe_3$ diluted in Ar was pyrolysed in a microreactor and analyzed by photoelectron–photoion coincidence spectroscopy (PEPICO) using synchrotron radiation.[24] This method permits to record photoion mass-selected threshold photoelectron spectra (ms-TPE) for each species by correlating ions and electrons produced in a single photoionization event. Isomer-selective information is then obtained from an analysis of the photoelectron spectrum based on computations.

Fig. 1 shows mass spectra under various pyrolysis conditions. Without pyrolysis (top trace) only the parent ion $\mathbf{1}^{\bullet+}$ is visible, thus dissociative photoionization is irrelevant under our experimental conditions. Already at low pyrolysis power (center trace) a stepwise methyl loss down to atomic Bi occurs, associated with formation of **2** and one of the products **3–5**. The small intensity of $m/z = 239$ ($[Bi(CH_3)_2]^+$) compared to $m/z = 224$ ($[BiCH_3]^{\bullet+}$) indicates that cleavage of the second methyl group is more facile than the first. In addition, Bi_2 is visible at $m/z = 418$, due to dimerization of bismuth atoms (see ESI, Fig. S4†). In some experiments a further peak appeared at $m/z = 478$ and is most likely due to Me_2Bi–$BiMe_2$. Note that CH_3 is not observed due to its ionization energy of 9.83891 eV.[25,26] Traces of BiI from the synthesis are also present in the spectrum.

When the pyrolysis power is further increased (bottom trace) the precursor is fully converted and experimental conditions are suitable for studying the molecule formed after loss of two methyl groups. Three structures are possible for $m/z = 224$, the bismuthinidenes **3** (triplet)/**4** (singlet) or the methylenebismuthane **5**. Threshold photoelectron spectroscopy provides structural isomer-selective information through comparison with Franck–Condon-simulated or reference spectra. Fig. 2 represents the ms-TPE spectrum of a species with the composition $BiCH_3$ at $m/z = 224$. The first major band at 7.88 eV is assigned to the adiabatic ionization energy (IE_{ad}). It is followed by several smaller bands that are *ca.* 40–50 meV apart. Simulations based on DFT and multi-reference calculations were carried out for **3**, **4** and **5**. While DFT often provides very accurate geometries and frequencies even for molecules with complicated electronic structures,[48] it is in many cases less accurate for the computation of energy surfaces or excitation energies.[49] Hence, the ωB97X-D3 [50] functional was employed for frequency computations, but the multi-reference NEVPT2 [51] approach was used to determine geometrical changes and to compute ionization energies as well as the energy difference between the two relevant states of the $[BiCH_3]^{\bullet+}$ cation (*vide infra*). Both methods (DFT and multi-reference) were combined with a scalar relativistic approach and with the SARC-ZORA-TZVP basis set which allows for an all-electron treatment of bismuth[52] (for computational details, see ESI†). Bismuthinidene **3** with a C_{3v} symmetry and an $X\ ^3E$ (T_0) triplet ground state is the lowest-energy structure ($\Delta E = 0$ kJ mol^{-1}). The computations on the NEVPT2-level show a very good agreement with the experimentally determined IE of 7.88 eV ($IE_{calc} = 7.98$ eV for the $X^+\ ^2A'' \leftarrow X\ ^3E$ transition (*vide infra*)), as compared to singlet bismuthinidene **4** ($\Delta E = +0.78$ eV/+75 kJ mol^{-1}; $IE_{calc} = 7.21$ eV) and methylenebismuthane **5** ($\Delta E = +0.91$ eV/+88 kJ mol^{-1}; $IE_{calc} = 8.68$ eV; for energy values obtained through DFT calculations see ESI†). This shows, that the ground state (electronic) structure of species with the sum formula ECH_3 are fundamentally different, depending on the choice of the element E. For E = Bi the triplet bismuthinidene **3** is energetically favored and observed (*vide supra*), whereas for the lighter congeners (E = N, P), the formation of the methylene species $HN{=}CH_2$ and $HP{=}CH_2$ has been determined to be more favorable.[27–32,53]

Upon photoionization of **3**, one electron is removed from either of the two degenerate SOMOs, which correspond in first approximation to the p_x and p_y orbital on the Bi center. The computations for the ionic ground state, $[BiCH_3]^{\bullet+}$ ($\mathbf{3}^{\bullet+}$), yielded a shortening of the Bi–C bond (from 2.27 Å in **3** to 2.21 Å in $\mathbf{3}^{\bullet+}$) and a deformation of the methyl group with a tilt angle of 4° relative to the Bi–C axis. This was ascribed to antibonding interactions between the unpaired electron and the bonding electrons of the two C–H groups, which are approximately aligned with the singly occupied p-type orbital of bismuth (Table S18†). This leads to a loss of the C_3 axis and a reduction to C_s symmetry. As a consequence of this Jahn–Teller distortion, the ^2E state in the C_{3v} symmetric cation splits into a $X^+\ ^2A''$ and a $A^+\ ^2A'$ component. The computations indicate an energy difference of only 50 meV between the two states at the geometry of the $X^+\ ^2A''$. Thus, transitions into both states contribute to the spectrum and have to be included in the simulation in Fig. 2 (blue curve). Transitions from the T_0 ground state of neutral **3** into the $X^+\ ^2A''$ ionic ground state are given as grey bars, while transitions into the $A^+\ ^2A'$ excited state are shown as red bars. In addition, there is a vibrational structure evident in the spectrum with a spacing of around 50 meV, including a hot band transition at 7.83 eV, which is assigned to the Bi–C stretching motion (corresponding to $\nu'' \approx 50$ meV). Vibrational activity is expected due to the reduction of the Bi–C bond lengths in the cation by > 0.06 Å (see ESI† for all geometry parameters). Franck–Condon simulations based on computations of isomer **5** further support the triplet bismuthinidene **3** as the carrier of the spectrum (Fig. S3†). First, the computed IE of **5** is 0.80 eV higher than the experimental value, and second, a more pronounced vibrational progression with a maximum intensity for a transition into an excited vibrational state would be expected for **5**. Thus a contribution of **5** to the spectrum can be ruled out.

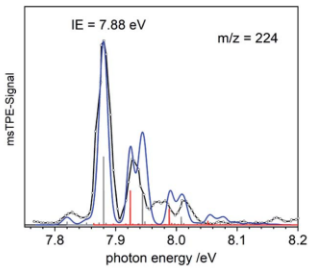

Fig. 2 Mass-selected threshold photoelectron spectrum of $m/z = 224$. The simulation based on **3** as the carrier (blue line) fits the experiment well. Transitions into the $X^+\ ^2A''$ ground state of the ion are given as grey bars, transitions into the $A^+\ ^2A'$ state as red bars.

The computed IE of **3** (for the lowest state of $\mathbf{3}^{\bullet+}$) and the relative energies for the two states of the cation $\mathbf{3}^{\bullet+}$ are in excellent agreement with the corresponding experimental data. This indicates that the neglected spin–orbit effects[33] do not play a key role for the determination of the ionization energies, possibly because they are similar in magnitude for all involved states. While the experimental and calculated IEs nicely agree, deviations were observed in the shape of the spectra and were ascribed to the flatness of the potential energy surface (PES) of the cation. Two factors mainly contribute to the flatness of this PES: (i) the $X^+\ ^2A''$ state is threefold degenerate due to facile rotation around the Bi–C bond. (ii) The shape of the PES going from the equilibrium geometry of the $X^+\ ^2A''$ towards the equilibrium geometry of the $A^+\ ^2A'$ state is expected to be non-harmonic. Efforts to obtain a better description of the surface were so far unsuccessful due to strong correlations of the various internal coordinates, so that high dimensional surfaces would be necessary for an appropriate description.

To gain additional information on the formation of BiMe (**3**) by stepwise abstraction of methyl groups from $BiMe_3$ (**1**), an ms-TPE spectrum of $[BiMe_2]^{\bullet}$ (**2**) ($m/z(2^+) = 239$) was recorded at

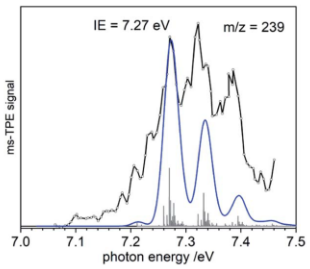

Fig. 3 Ms-TPE spectrum of $Bi(CH_3)_2$, $m/z = 239$. The vibrational progression is due to the symmetric bismuth–carbon stretch and its combination with torsional motion. The blue line represents the simulated spectrum based on **2**.

a low pyrolysis temperature (Fig. 3; *cf.* Fig. 1). Simulations of the spectrum based on DFT calculations indicate C_{2v} symmetry for both **2** and $\mathbf{2}^+$ as well as a $X^+\,{}^1A_1 \leftarrow X\,{}^2B_1$ transition in $[BiMe_2]^\bullet$ (**2**). The first major band at 7.27 eV is assigned to the IE, in excellent agreement with the computed value of 7.35 eV at the NEVTP2 level of theory. A vibrational progression with a spacing of 60 meV is visible and is dominated by the symmetric Bi–C stretching mode in the cation. Additional torsional modes of the CH_3 groups may lead to a broadening of the bands. While there is a good agreement between simulation and experiment, the vibrational intensities (including hot bands) are somewhat underestimated in the simulations. This indicates a slightly larger change of the Bi–C bond length upon ionization than the computed shortening of 0.05 Å (see ESI† for all geometry parameters).

Bond dissociation energies (BDEs) can be determined *via* thermochemical cycles that combine appearance energies (AE) and ionization energies. The zero Kelvin appearance energy AE_{0K} for the abstraction of the first methyl radical from **1** has been determined with very high accuracy, $AE_{0K}(Bi(CH_3)_3, Bi(CH_3)_2^+) = 9.445 \pm 0.064$ eV.[23] According to computations, the methyl loss in the cation is a simple homolytic bond cleavage without a reverse barrier. Combined with the IE of **2**, the $Me_2Bi–CH_3$ bond dissociation energy in **1**, $BDE(Me_2Bi–CH_3)$, can be derived:

$$BDE(Me_2Bi–CH_3) = AE_{0K}(BiMe_3, [BiMe_2]^{\bullet+}) - IE([BiMe_2]^\bullet) \quad (1)$$

From eqn (1) a value of 210 ± 7 kJ mol^{-1} is obtained for $BDE(Me_2Bi–CH_3)$. The bond dissociation energy of the first Bi–CH_3 bond in $BiMe_3$ ($BDE(Me_2Bi–CH_3)$) can be expected to be the highest of the three Bi–CH_3 BDEs in this molecule[34] and is thus crucial for any type of reaction initiation *via* Bi–CH_3 homolysis. However, the value of $BDE(Me_2Bi–CH_3)$ has never been determined explicitly in the primary literature. Based on previous investigations into the thermal decomposition of **1**,[34–36] an estimation of $BDE(Me_2Bi–CH_3)$ can be made, which yields a value of 182 kJ mol^{-1} as the upper limit that would be possible for this parameter.[37] Thus, our results substantially revise the bond dissociation energy of the first Bi–Me bond in **1**, which is key to the radical chemistry of **1** and related bismuth compounds. The calculated isodesmic reaction provides a value of 226 kJ mol^{-1} in good agreement with the experimental findings.

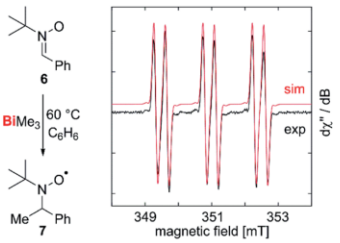

Fig. 4 Abstraction and spin trapping of methyl radicals from $BiMe_3$.

Our correction of the BDE in a fundamentally important organometallic compound such as $BiMe_3$ raised the question, whether homolytic Bi–C bond cleavage is possible at moderate reaction temperatures in the condensed phase, making this process relevant for synthetic chemistry under conventional experimental conditions. To test for methyl radical abstraction from $BiMe_3$, a benzene solution of $BiMe_3$ and the radical trap **6** was heated to 60 °C and subsequently analyzed by EPR spectroscopy (Fig. 4). Indeed, a resonance was detected with $g_{iso} = 2.006$ and $a(^{14}N) = 41.6$ MHz, $a(^1H) = 9.63$ MHz, $a(^{13}C) = 12.9$ MHz, indicating the formation of **7** by methyl radical transfer.[38,54,55]

In order to gain further hints at the generation and subsequent trapping of BiMe in the condensed phase, neat $BiMe_3$ was

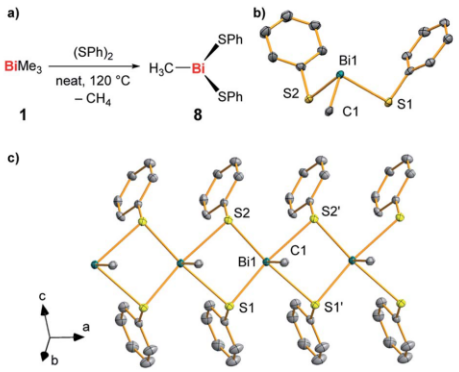

Fig. 5 (a) Synthesis of $BiMe(SPh)_2$ (**8**) from $BiMe_3$ and $(SPh)_2$ with methane as a detected by-product. (b and c) Molecular structure of **8** in the solid state with one formula unit shown in (b) and a cutout of the coordination polymer shown in (c). Displacement ellipsoids are shown at the 50% probability level. Hydrogen atoms and one set of split positions of disordered atoms are omitted for clarity. For detailed discussion of structural parameters see ESI.† Selected bond lengths (Å) and angles (°): Bi1–C1, 2.208(10); Bi1–S1, 2.736(2); Bi1–S2, 2.699(2); C1–Bi1–S1, 89.6(3); C1–Bi1–S2, 89.4(3); S1–Bi1–S2, 93.18(7).

reacted with stoichiometric amounts of $(PhS)_2$ at 120 °C (Fig. 5a). $BiMe(SPh)_2$ (**8**)[39–41] was isolated as the product of this reaction in 41% yield and fully characterized (Fig. 5b and c; for details see ESI†). Methane was detected in the headspace of the reaction by IR spectroscopy (Fig. S5†), suggesting the appearance of methyl radicals in this reaction.

This – together with literature reports[42] – supports the potential of BiMe to act as a transient reactive species in this reaction. The thioether MeSPh was also detected, suggesting that methyl radical attack at sulfur or σ-bond metathesis/disproportionation sequences may also be operative as a parallel reaction pathway.[41] In the solid state, compound **8** forms a coordination polymer through bridging coordination modes of the thiolate ligands (Fig. 5c). This is a unique structural feature within the small number of literature-known compounds $BiR(SR')_2$ (R, R′ = aryl, alkyl; for details see ESI†).[42–45]

Conclusions

In conclusion, we have generated methylbismuth (BiMe), a fundamental organometallic compound and the first example of an organometallic non-stabilized bismuthinidene. BiMe was accessed *via* controlled thermal homolysis in the gas phase. The title compounds shows a triplet (biradical) ground state and an ionization energy of 7.88 eV, as revealed by combination of photoelectron spectroscopy and computations. The homolytic dissociation of the first $Me_2Bi–CH_3$ bond in $BiMe_3$ is crucial to the radical chemistry of this compound (and related species) and is the initiating step in the formation of BiMe. Our results reveal a $Me_2Bi–CH_3$ homolytic bond dissociation energy of 210 ± 7 kJ mol^{-1}, *i.e.* the previously reported value is revised by more than +15% (+28 kJ mol^{-1}). Nevertheless, reactions in the condensed phase demonstrate that the abstraction of methyl radicals from $BiMe_3$ is possible at moderate reaction conditions and suggest that BiMe may act as an intermediate in reactions with suitable trapping reagents. Future research will be directed towards the generation of non-stabilized bismuthinidenes and their exploitation in synthetic chemistry.

Methods and experimental

Details of experimental conditions for synchrotron experiments, for calculations with DFT and multi-reference methods, for the preparation of compounds **1** and **8** (including two methods for the preparation of **1** [19]), and for IR and EPR spectroscopic experiments are given in the ESI.†

All calculations were performed with the ORCA program package, version 4.1.1 and 4.2.[56]

The spectroscopic experiments were carried out at the VUV beamline of the Swiss Light Source (SLS) at the Paul-Scherrer Institute, Villigen/CH. In most experiments the photon energy was scanned in 5 meV steps and calibrated using autoionization resonances in Ar. The ionization energies reported in the main paper are accurate to within ±20 meV and were corrected for the Stark-shift by the extraction field (8–9 meV). Note that in some experiments 10 meV steps were used. A detailed description of the beamline is given in the literature.[47]

$[MeBi(SPh)_2]$ (8).[39]

Neat trimethyl bismuth (100 mg, 0.394 mmol) and diphenyl disulfide (85.9 mg, 0.393 mmol) were heated to 120 °C for 3 d. After cooling to ambient temperature, a green solid was obtained, which was dissolved in benzene (1.5 mL) and layered with *n*-pentane (1.5 mL). After 16 h at ambient temperature, the product could be isolated by filtration and dried *in vacuo* as yellow needles. Yield: 70.8 mg, 0.160 mmol, 41%.

^{1}H NMR (500 MHz, C_6D_6): δ = 0.94 (s, 3H, CH_3), 6.86 (dd, 2H, $^3J_{HH}$ = 7.4 Hz, $^3J_{HH}$ = 7.5 Hz, *p*-C_6H_5), 7.03 (t, 4H, $^3J_{HH}$ = 7.6 Hz, *m*-C_6H_5), 7.48 (d, 4H, $^3J_{HH}$ = 7.8 Hz, *o*-C_6H_5) ppm.

^{13}C NMR (126 MHz, C_6D_6): δ = 40.40 (br, CH_3), 127.29 (s, *p*-C_6H_5), 128.60 (s, *m*-C_6H_5), 135.62 (s, *o*-C_6H_5), 136.06 (s, *ipso*-C_6H_5) ppm.

Elemental analysis: anal. calc. for: $[C_{13}H_{13}BiS_2]$ (442.35 g mol^{-1}): C 35.30, H 2.96, S 14.50; found: C: 35.12, H 2.90, S 14.40.

Conflicts of interest

There are no conflicts to declare.

Author contributions

DPM, DS, ER and PH carried out the synchrotron radiation experiments, JR carried out all synthetic work, SW and DK performed the computations, IK performed the ESR and TP the IR spectroscopy. IF, BE and CL planned the project, contributed to the interpretation of the results and wrote the manuscript.

Acknowledgements

Funding by the DFG (funding to CL, IF (FI575/13-1) and through GRK2112), by the Swiss Federal Office for Energy (BFE Contract Number SI/501269-01), and the FCI (PhD and Liebig scholarships to DK and CL) are gratefully acknowledged. CL thanks Prof. Holger Braunschweig for continuous support. The spectroscopic experiments were performed at the VUV beamline of the Swiss Light Source, located at the Paul Scherrer Institute (PSI).

Notes and references

1 L. Dostál, *Coord. Chem. Rev.*, 2017, **353**, 142–158.
2 F. Dielmann, O. Back, M. Henry-Ellinger, P. Jerabek, G. Frenking and G. Bertrand, *Science*, 2012, **337**, 1526–1528.
3 L. Liu, D. A. Ruiz, D. Munz and G. Bertrand, *Chem*, 2016, **1**, 147–153.
4 P. Šimon, F. de Proft, R. Jambor, A. Růžička and L. Dostál, *Angew. Chem., Int. Ed.*, 2010, **49**, 5468–5471.
5 I. Vranova, M. Alonso, R. Lo, R. Sedlak, R. Jambor, A. Ruzicka, F. De Proft, P. Hobza and L. Dostál, *Chem.–Eur. J.*, 2015, **21**, 16917–16928.

6 I. Vranova, M. Alonso, R. Jambor, A. Ruzicka, M. Erben and L. Dostál, *Chem.–Eur. J.*, 2016, **22**, 7376–7380.
7 G. C. Wang, L. A. Freeman, D. A. Dickie, R. Mokrai, Z. Benkő and R. J. Gilliard, *Chem.–Eur. J.*, 2019, **25**, 4335–4339.
8 C. Lichtenberg, *Angew. Chem., Int. Ed.*, 2016, **55**, 484–486.
9 A. M. Arif, A. H. Cowley, N. C. Norman and M. Pakulski, *J. Am. Chem. Soc.*, 1985, **107**, 1062–1063.
10 F. Wang, O. Planas and J. Cornella, *J. Am. Chem. Soc.*, 2019, **141**, 4235–4240.
11 M. C. Thompson, J. Ramsay and J. M. Weber, *Angew. Chem., Int. Ed.*, 2016, **55**, 15171–15174.
12 H. T. Sun, Y. Matsushita, Y. Sakka, N. Shirahata, M. Tanaka, Y. Katsuya, H. Gao and K. Kobayashi, *J. Am. Chem. Soc.*, 2012, **134**, 2918–2921.
13 H. T. Sun, Y. Sakka, N. Shirahata, Y. Matsushita, K. Deguchi and T. Shimizu, *J. Phys. Chem. C*, 2013, **117**, 6399–6408.
14 E. H. Fink, K. D. Setzer, D. A. Ramsay, M. Vervloet and J. M. Brown, *J. Mol. Spectrosc.*, 1990, **142**, 108–116.
15 J. D. Corbett, *J. Am. Chem. Soc.*, 1958, **80**, 4257–4260.
16 P. Kuijpers and A. Dymanus, *Chem. Phys. Lett.*, 1976, **39**, 217–220.
17 E. H. Fink, K. D. Setzer, D. A. Ramsay and M. Vervloet, *Chem. Phys. Lett.*, 1991, **179**, 95–102.
18 R. A. Lynde and J. D. Corbett, *Inorg. Chem.*, 1971, **10**, 1746–1749.
19 K. Schäfer and F. Hein, *Z. Anorg. Allg. Chem.*, 1917, **100**, 249–303.
20 S. Schulz, A. Kuczkowski, D. Bläser, C. Wolper, G. Jansen and R. Haack, *Organometallics*, 2013, **32**, 5445–5450.
21 J. M. Herbelin, R. Klingberg, D. J. Spencer, M. A. Kwok, H. Bixler, R. Ueunten, R. Cook and W. Hansen, *Opt. Commun.*, 1981, **36**, 475–476.
22 S. W. Kang, K. M. Jeon, J. S. Shin, J. R. Chun, Y. H. Kim, S. J. Lee and J. Y. Yun, *Chem. Vap. Deposition*, 2013, **19**, 61–67.
23 B. Hornung, A. Bodi, C. I. Pongor, Z. Gengeliczki, T. Baer and B. Sztáray, *J. Phys. Chem. A*, 2009, **113**, 8091–8098.
24 T. Baer and R. P. Tuckett, *Phys. Chem. Chem. Phys.*, 2017, **19**, 9698–9723.
25 B. K. Cunha de Miranda, C. Alcaraz, M. Elhanine, B. Noller, P. Hemberger, I. Fischer, G. Garcia, H. Soldi-Lose, B. Gans, L. A. Viera Mendez, S. Boye-Peronne, S. Douin, J. Zabka and P. Botschwina, *J. Phys. Chem. A*, 2010, **114**, 4818–4830.
26 A. M. Schulenburg, C. Alcaraz, G. Grassi and F. Merkt, *J. Chem. Phys.*, 2006, **125**, 104310.
27 H. Bock and R. Dammel, *Chem. Ber.*, 1987, **120**, 1961–1970.
28 F. Holzmeier, M. Lang, K. Hader, P. Hemberger and I. Fischer, *J. Chem. Phys.*, 2013, **138**, 214310.
29 S.-J. Kim, T. P. Hamilton and H. F. Schaefer III, *J. Phys. Chem.*, 1993, **97**, 1872–1877.
30 S. Lacombe, D. Gonbeau, J.-L. Cabioch, B. Pellerin, J.-M. Denis and G. Pfister-Guillouzo, *J. Am. Chem. Soc.*, 1988, **110**, 6964–6967.
31 S. Y. Liang, P. Hemberger, J. Levalois-Grützmacher, H. Grützmacher and S. Gaan, *Chem.–Eur. J.*, 2017, **23**, 5595–5601.
32 S. Y. Liang, P. Hemberger, N. M. Neisius, A. Bodi, H. Grützmacher, J. Levalois-Grützmacher and S. Gaan, *Chem.–Eur. J.*, 2015, **21**, 1073–1080.
33 G. Herzberg, *Molecular Spectra and Molecular Structure*, Krieger, Malabar/FL, 1966.
34 S. J. W. Price and A. F. Trotman-Dickenson, *Trans. Faraday Soc.*, 1958, **54**, 1630–1637.
35 L. H. Long and J. F. Sackman, *Trans. Faraday Soc.*, 1954, **50**, 1177–1182.
36 S. J. W. Price, in *Comprehensive Chemical Kinetics*, ed. C. H. Bamford and C. F. H. Tipper, Elsevier, 1972, vol. 4, pp. 197–257.
37 The average bond dissociation energy for a Bi–CH_3 bond in **1** has been reported to be 33.8 kcal mol^{-1} (141 kJ mol^{-1}) (ref. 35). The sum of the bond dissociation energies associated with the cleavage of the second and the third Bi–CH_3 bond in **1** (BDE(MeBi–CH_3) plus BDE(Bi–CH_3)) was estimated to be at least 57.8 kcal mol^{-1} (242 kJ mol^{-1}) (ref. 34). This gives a maximum value of 43.6 kcal mol^{-1} (182 kJ mol^{-1}) for the bond dissociation energy of the first Bi–CH_3 bond in **1**.
38 D. L. Haire, U. M. Oehler, P. H. Krygsman and E. G. Janzen, *J. Org. Chem.*, 1988, **53**, 4535–4542.
39 In a different synthetic approach, compound **8** has previously been obtained from reaction of *in situ* generated [MeBi$(OEt)_2$] with two equiv. HSPh: M. Wieber and U. Baudis, *Z. Anorg. Allg. Chem.*, 1976, **423**, 40–46.
40 A. G. Davies and S. C. W. Hook, *J. Chem. Soc. B*, 1970, 735–737.
41 M. Wieber and I. Sauer, *Z. Naturforsch., B: Anorg. Chem., Org. Chem.*, 1984, **39**, 1668–1670.
42 P. Simon, R. Jambor, A. Ruzicka and L. Dostál, *Organometallics*, 2013, **32**, 239–248.
43 M. Dräger and B. M. Schmidt, *J. Organomet. Chem.*, 1985, **290**, 133–145.
44 K. M. Anderson, C. J. Baylies, A. H. M. Monowar Jahan, N. C. Norman, A. G. Orpen and J. Starbuck, *Dalton Trans.*, 2003, 3270–3277.
45 P. Šimon, R. Jambor, A. Růžička and L. Dostál, *J. Organomet. Chem.*, 2013, **740**, 98–103.
46 For reactions of the related precursor Sb_2Me_4 under near-chemical vapor deposition conditions see: N. Bahlawane, F. Reilmann, S. Schulz, D. Schuchmann and K. Kohse-Höinghaus, *J. Am. Soc. Mass Spectrom.*, 2008, **19**, 1336–1342.
47 M. Johnson, A. Bodi, L. Schulz and T. Gerber, *Nucl. Instrum. Methods Phys. Res., Sect. A*, 2009, **610**, 597–603.
48 (*a*) E. Welz, J. Böhnke, R. D. Dewhurst, H. Braunschweig and B. Engels, *J. Am. Chem. Soc.*, 2018, **140**, 12580–12591; (*b*) J. Böhnke, T. Dellermann, M. A. Celik, I. Krummenacher, R. D. Dewhurst, S. Demeshko, W. C. Ewing, K. Hammond, M. Heß, E. Bill, E. Welz, M. I. S. Röhr, R. Mitrić, B. Engels, F. Meyer and H. Braunschweig, *Nat. Commun.*, 2018, **9**, 1197.
49 V. Settels, W. Liu, J. Pflaum, R. F. Fink and B. Engels, *J. Comput. Chem.*, 2012, **33**, 1544–1553.
50 (*a*) J.-D. Chai and M. Head-Gordon, *J. Chem. Phys.*, 2008, **128**, 084106; (*b*) S. Grimme, J. Antony, S. Ehrlich and H. Krieg, *J. Chem. Phys.*, 2010, **132**, 154104.

51 (*a*) C. Angeli, R. Cimiraglia, S. Evangelisti, T. Leininger and J.-P. Malrieu, *J. Chem. Phys.*, 2001, **114**, 10252–10264; (*b*) C. Angeli, R. Cimiraglia and J.-P. Malrieu, *Chem. Phys. Lett.*, 2001, **350**, 297–305; (*c*) C. Angeli, R. Cimiraglia and J.-P. Malrieu, *J. Chem. Phys.*, 2002, **117**, 9138–9153.

52 D. A. Pantazis and F. Neese, *Theor. Chem. Acc.*, 2012, **131**, 1292.

53 It should be noted that methyl nitrene (N–CH_3) and methyl phosphinidene (P–CH_3) also have triplet ground states. But the structures with methylene (rather than methyl) functional groups, *i.e.* HN=CH_2 and HP=CH_2, are energetically favored over N–CH_3 and P–CH_3. See ref. 27–32 and A. G. Kutateladze, *Computational Methods in Photochemistry*, CSC Press Taylor and Francis Group, 2019.

54 Bismuth-containing radical species were not detected under these conditions. It has been reported that even persistent dialkyl bismuth radicals may not be detectable by EPR spectroscopy, which has been ascribed to fast relaxation as a result of spin orbit coupling: S. Ishida, F. Hirakawa, K. Furukawa, K. Yoza and T. Iwamoto, *Angew. Chem., Int. Ed.*, 2014, **53**, 11172–11176.

55 Trapping of alkyl radical species in reactions of bismuth compounds has been reported: J. Ramler, I. Krummenacher and C. Lichtenberg, *Angew. Chem., Int. Ed.*, 2019, **58**, 12924–12929.

56 (*a*) F. Neese, *Wiley Interdiscip. Rev.: Comput. Mol. Sci.*, 2012, **2**, 73–78; (*b*) F. Neese, *Wiley Interdiscip. Rev.: Comput. Mol. Sci.*, 2018, **8**, e1327.

XIV Bismuthinidenes

Recently, in cooperation with the research groups of Prof. FISCHER and Prof. ENGELS, we have demonstrated the generation of the free organometallic bismuthinidene BiMe from $BiMe_3$ via thermal homolysis in the gas phase.[236] Bismuthinidenes are bismuth species with the metal atom in the oxidation state +I. Organometallic bismuthinidenes are, to date, only isolable by stabilization as Lewis base adducts (Scheme 34).[64–66] For non-stabilized organometallic bismuthinidenes singlet and triplet ground states are theoretically conceivable (Scheme 34).

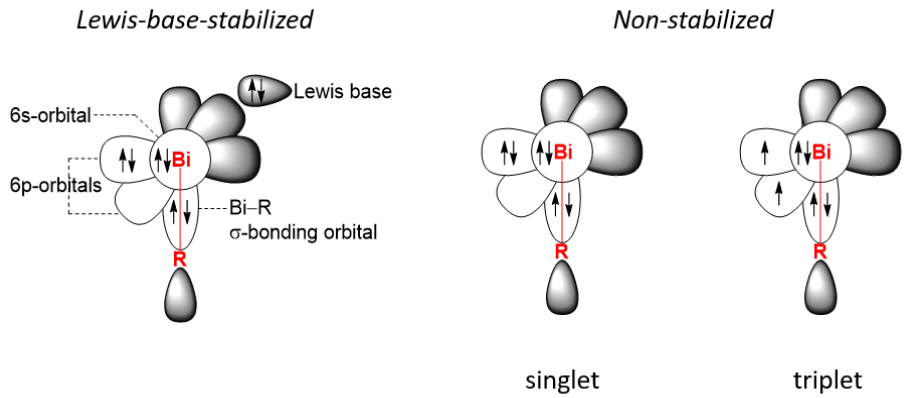

Scheme 34. Lewis-base-stabilized and non-stabilized bismuthinidenes with their corresponding valence orbitals.

Spectroscopic characterization and theoretical calculations supported a triplet biradical ground state for the first Lewis base-free organometallic bismuthinidene, BiMe.[236]

1 Trimethylbismuth: Precursor for BiMe and Trapping Reactions

As mentioned above, BiMe was generated via thermal homolysis from $BiMe_3$ in the gas phase and described as a biradical. Additionally, a trapping reaction with Ph_2S_2 in the condensed phase yielding $MeBi(SPh)_2$ suggested that BiMe may be formed as a transient intermediate upon thermolysis of $BiMe_3$, which was further supported by EPR experiments (see Chapter XIII).[236] Additional attempted trapping reactions are summarized in Table 5.

Table 5. Attempted trapping reactions for the *in situ* generated bismuthinidene BiMe.

Entry	trapping reagent[a]	reaction conditions	result
1	phenanthrene-9,10-dione	120 °C, toluene, 4 d	selective formation of a new species, no isolation
2	3,5-di-*tert*-butyl-*ortho*-benzoquinone	120 °C, neat, 7 h	unselective reaction, no product isolated
3	3,6-di-*tert*-butyl-*ortho*-benzoquinone	120 °C, neat, 7 h	no reaction
4	2,5-di-*tert*-butyl-*para*-benzoquinone	i) benzene, 60 °C, 1 h ii) benzene, 455 nm, 3 d	i) no reaction ii) unselective reaction, small amounts of 2,5-di-*tert*-butyl-*para*-hydro-quinone
5	2,6-di-*tert*-butyl-*para*-benzoquinone	i) benzene, 60 °C, 1 h ii) 455 nm, 3 d	i) no reaction ii) unselective reaction
6	*o*-chloranil	120 °C, neat, 16 h	unselective reaction (see text)
7	diphenylacetylene	i) 120 °C, neat, 16 h ii) *hν*, benzene, 24 h	color change to green, but no significant conversions (<10%)
8	*para*-tolylacetylene	130 °C, neat, 16 h	color change to yellow, but no significant conversions (<10%)
9	1,4-bis(trimethylsilyl)buta-1,3-diyne	i) 120 °C, neat, 16 h, ii) *hν*, benzene, 2 h,	no reaction
10	1,4-diphenylbuta-1,3-diyne	i) 120 °C, toluene, 3 d ii) 120 °C, neat, 3 d	no reaction
11	benzil	120 °C, neat, 16 h	no reaction
12	Se_2Ph_2	120 °C, neat, 20 h	$MeBi(SePh)_2$ (see text)
13	$cAAC^{Me}$	*hν*, benzene, 3 h	color change to faintly pink, decoloration after 5 min

a The trapping reagents were all used in excess (≥5 eq.), with the exception of *o*-chloranil and Se_2Ph_2, which were used in equimolar amounts. *o*-chloranil = tetrachloro-*ortho*-benzoquinone. benzil = 1,2-diphenylethane-1,2-dione.

At this point, only the most promising conversions will be discussed. Based upon these results, it is clear that harsh conditions are required to achieve significant conversions. For example, heating a mixture of phenanthrene-9,10-dione and $BiMe_3$ to 120 °C in toluene solution for 4 d led to a new species, as well as stoichiometric amounts of unreacted phenanthrene-9,10-dione and $BiMe_3$ (entry 1). The new species shows a singlet at $\delta(^1H)$ = 1.35 ppm in its ^1H NMR spectrum, likely corresponding to a methyl group bound to a bismuth center. An additional singlet at $\delta(^1H)$ = 4.01 ppm indicates the formation of an ether moiety. The resonance pattern in the aromatic region indicates an unsymmetrically substituted phenanthrene moiety. However,

crystallization attempts only led to the isolation of phenanthrene-9,10-dione, or yielded amorphous material in quantities that were so small that further analyses were not possible.

The reaction of neat $BiMe_3$ with *o*-chloranil led to full consumption of $BiMe_3$ after 16 h at 120 °C (Table 5, entry 6). Upon dissolving the resulting dark red-brown residue in C_6D_6 a single ^1H NMR-spectroscopic resonance (singlet) was found at $\delta(^1H)$ = 2.33 ppm, which argues for the formation of an O_2BiMe moiety as in compound **28** (Scheme 35).

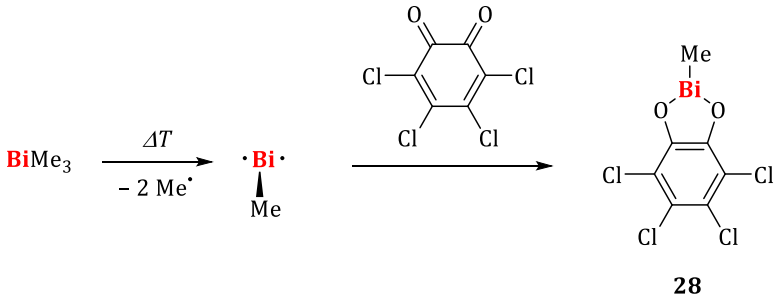

28

Scheme 35. Reaction of $BiMe_3$ with *o*-chloranil and proposed product **28** according to ^1H NMR spectroscopy.

Evaporation of the solvent and subsequent washing with *n*-pentane and methylene chloride yielded a brown powder, which was recrystallized from THF and *n*-pentane. Small amounts of crystalline material were obtained after storage at –30 °C for 30 d. Single-crystal X-ray diffraction analysis revealed the formation of $[(C_6Cl_4O_2)Bi(thf)_2Cl]_2$, (**29**) which crystallized in the monoclinic space group $P2_1/n$ with Z = 2 (Figure 59).

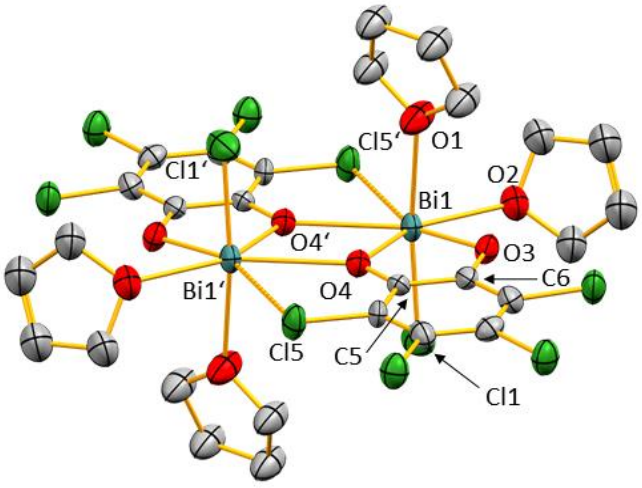

Figure 59. Molecular structure of $[(C_6Cl_4O_2)Bi(thf)_2Cl]_2$ (**29**) in the solid state. Displacement ellipsoids are drawn at the 50% probability level. Hydrogen atoms and split positions of disordered thf molecules are omitted for clarity. Selected bond lengths (Å) and angles (°): Bi1–Cl1, 2.522(4); Bi1–O1, 2.579(7); Bi1–O2, 2.503(10); Bi1–O3, 2.129(8); Bi1–O4, 2.217(9); Bi1–O4', 2.637(8); Bi1···Cl5', 3.324; O3–C6, 1.350(15); O4–C5, 1.350(15); Cl1–Bi1–O1, 171.0(2); Cl1–Bi1–O2-4, 87.4(3)–90.4(2); O2–Bi1–O3, 76.5(3); O3–Bi1–O4, 75.7(3); O4–Bi1–O4', 68.5(3); O2–Bi1–Cl5', 80.30.

The solid-state structure shows the bismuth atom bound to *o*-chloranil through two O–Bi interactions. One chlorine atom acts as a third ligand, and two thf molecules additionally stabilize the Lewis-acidic bismuth center. The coordination sphere is completed by the formation of a dimer, with one oxygen atom of the *o*-chloranil ligand bridging between two bismuth centers. Based on distance criteria, weak Bi1···Cl5' (ca. 3.32 Å, 13% under the sum of the van-der-Waals radii of 3.82 Å) interactions are also present. The bismuth atoms in $[(C_6Cl_4O_2)Bi(thf)_2Cl]_2$ adopt a distorted pentagonal bipyramidal coordination geometry with the chlorine atom and one thf ligand in axial positions (171.0(2)°). The Bi–O bonds involving the thf ligands (2.522(4)–2.579(7) Å), as well as the Bi1–O4' bond (2.637(8) Å), which is the longest Bi–O bond in this compound, are significantly longer than the Bi–O3/4 distances, which involve oxygen atoms of a *o*-chloranil ligand that acts as a chelating ligand towards Bi1 (2.129(8)–2.217(9) Å). These results reflect the differences in the dative vs. covalent nature of the Bi–O interactions in **29**. The bond lengths of the dative Bi–O interactions,[237,238] as well as the bond lengths of the covalent bismuth oxygen interactions,[239,240] are in the expected range compared to related neutral, Lewis-acidic bismuth species such as $BiCl_3(thf)_2$ and bismuth alkoxides. The reduction of *o*-chloranil to a dianionic chelating ligand is confirmed by the elongated C–O bonds in **29** (1.350(15) Å), as compared to those in the free starting material (1.208(4) Å),[241] as well as to *o*-chloranil coordinating as a neutral donor in compounds as Cr(0)(*o*-chloranil)$_2$ (ca. 1.251–1.342 Å),[242,243]. Interestingly, the bismuth atoms in **29** bear chloride ligands instead of a methyl group as expected for **28**. Due to the absence of other chlorine sources, the source of the chlorine atoms is likely to be *o*-chloranil itself. Due to the small amounts of material collected, a yield of **27** could not be determined. To gain further insights into the course of the reaction, a high-resolution mass spectrum of the reaction mixture in pyridine was acquired. A peak at *m/z* = 467.8703 was found (ASAP, negative mode), which corresponds to **28** plus one electron ($[C_7H_3BiCl_4O_2]^{\bullet-}$, *m/z* = 467.8969). However, the signal was very weak in intensity (<5%). No peak indicating the presence of **29** (or a thf-free analog) was detected. The fact that **29** could not be detected by mass spectrometry, suggests that it is formed as a minor side product.

As mentioned above, the reaction of $BiMe_3$ with S_2Ph_2 at 120 °C yielded $MeBi(SPh)_2$ in 41% yield.[236] The analog reaction with Se_2Ph_2 as a trapping reagent led to the isolation of $MeBi(SePh)_2$ in 20% yield as a light-yellow solid, characterized by ^{1}H, ^{13}C and ^{77}Se NMR spectroscopy (Table 5, entry 13). To clearly demonstrate that the reactions of $BiMe_3$ with E_2Ph_2 (E = S, Se) at elevated temperatures proceed via the generation of a bismuthinidene, spectroscopic yields above 50%, or isolated yields close to 50%, would be required, otherwise a polar mechanism for the formation of $MeBi(EPh)_2$ cannot be ruled out. Since the reaction with Se_2Ph_2 was also inconclusive in this respect, this approach was not pursued further.

In conclusion, the trapping reactions attempted thus far have not provided unambiguous proof of the generation of BiMe from the thermolysis of $BiMe_3$. The reasons for this might be that BiMe is not formed in sufficient quantities under the conditions employed, that any BiMe that is generated decomposes too rapidly to undergo selective trapping reactions, or that the trapping reactions are not sufficiently selective. In the future, the use of (sterically demanding) Lewis bases could be useful to trap the desired bismuthinidene. If the generation of BiMe from $BiMe_3$ by thermolysis under standard laboratory conditions could be demonstrated, it would enable the facile introduction of the "BiMe" building block into organic and inorganic substrates.

2 Lighter Congeners: $AsMe_3$ and $SbMe_3$

In light of the results obtained for $BiMe_3$ as a precursor for BiMe, the lighter congeners $AsMe_3$ and $SbMe_3$ were synthesized and their potential as precursors for EMe species (E = As, Sb) was investigated in the condensed phase.

For that, in analogy to $BiMe_3$,[236] toluene solutions of EMe_3 and the radical trap PBN were heated to 60 °C for 2 h 20 min and subsequently analyzed by EPR spectroscopy (E = As, Sb; PBN = *N*-*t*Bu-α-phenylnitrone) (Scheme 36).

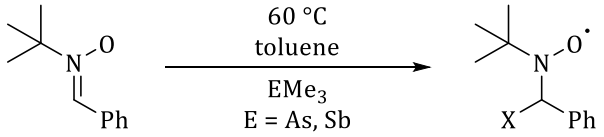

30

X = unknown fragment

Scheme 36. Spin trapping reaction of unknown radical species from EMe_3. E = As, Sb.

For both reactions, a resonance with intensities ca. ten times weaker than for the analog reaction with $BiMe_3$ were detected. However, the signals that were detected for E = As, Sb show only a partial overlap with the spectrum simulated for radical **30** with X = Me. A closer analysis shows that the experimentally detected weak resonances are more complex, suggesting that more than one radical species is present (Figure 60). Nonetheless, this indicates the formation of radicals upon heating $AsMe_3$ and $SbMe_3$ at moderate reaction temperatures in the condensed phase. Importantly, the formation of radicals occurs to lesser extents and with lower selectivities than in the case of $BiMe_3$.

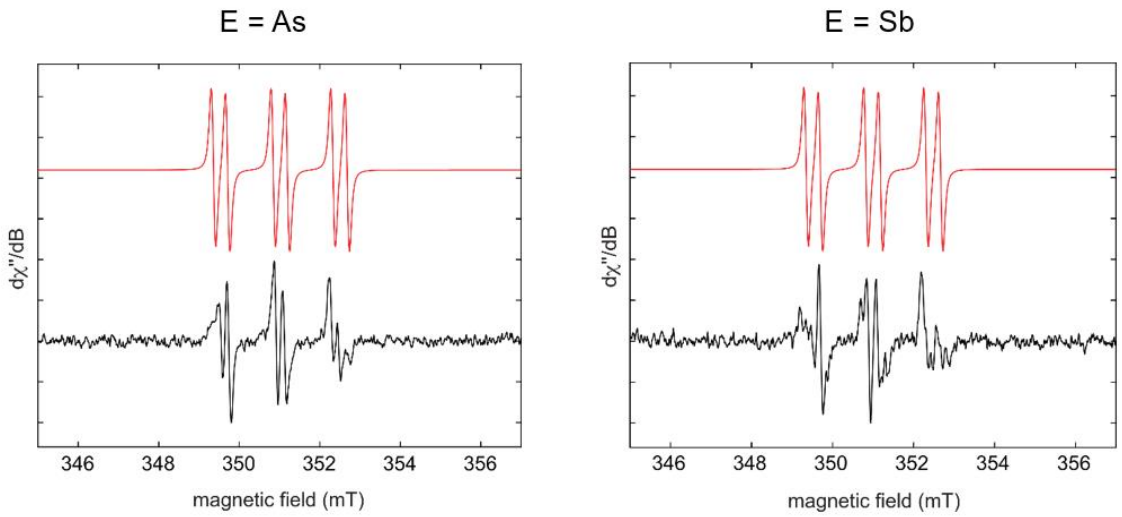

Figure 60. Abstraction and spin trapping of an unknown fragment from EMe_3 (black spectrum, E = As, Sb). The red spectra represent the simulated spectrum for the methyl radical abstraction product **30** (X = Me, see Scheme 36).

Accordingly, in analogy to the synthesis of $MeBi(SPh)_2$, neat EMe_3 (E = As, Sb) was reacted with one equivalent of S_2Ph_2 at 120 °C for 4 d (Scheme 37).

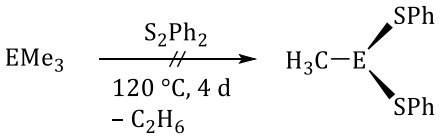

Scheme 37. Attempted reactions of EMe_3 with S_2Ph_2. E = As, Sb.

^1H NMR spectroscopic analyses of the reaction mixtures in C_6D_6 showed no ($AsMe_3$), or very low conversions (<5%, $SbMe_3$) of the starting materials, which is in accordance with the EPR spectroscopic results. This indicates that the selective homolytic E–Me bond dissociation is more difficult to address for E = As, Sb, than was observed for $BiMe_3$ under standard laboratory conditions.

The potential formation of EMe from EMe_3 (E = As, Sb) should further be investigated by synchrotron radiation experiments. Their electronic structures should then be characterized by computational analyses and photoelectron spectroscopic investigations, in order to elaborate on the differences between the $AsMe_3$, $SbMe_3$ and $BiMe_3$.

3 Bi(allyl)$_3$: Potential Precursor for an Organometallic Bismuthinidene

Tris(allyl)bismuth (**31**) was chosen in order to investigate the influence of electronic factors on the generation of bismuthinidenes starting from BiR_3 species (allyl = C_3H_5). The decomposition of $Bi(allyl)_3$ by formation of 1,5-hexadiene has already been described,[22] therefore a stepwise

homolytic Bi–C bond cleavage can be postulated, similar to the stepwise methyl-radical loss for $BiMe_3$. The Bi(I) species thus formed could again theoretically adopt two different electronic structures and one additional tautomer (Scheme 38).[236]

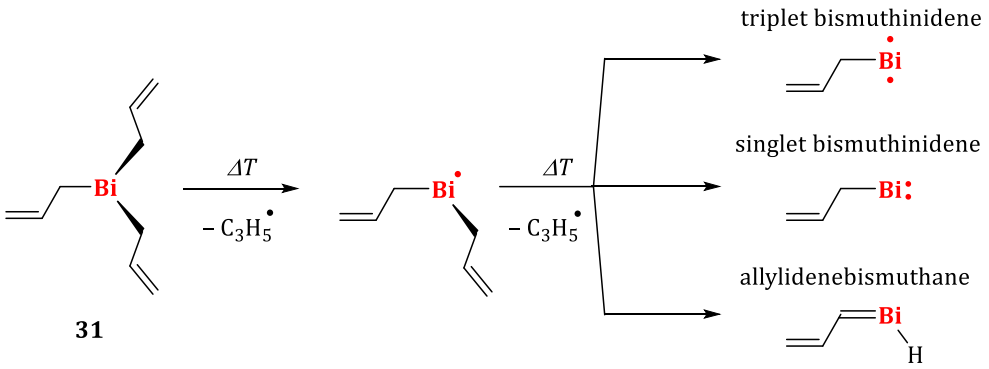

Scheme 38. Postulated stepwise abstraction of allyl-radicals from **31** in the gas phase by flash pyrolysis.

In cooperation with the research group of Prof. FISCHER, photoelectron spectroscopic experiments were carried out. However, the conditions chosen resulted only in the detection of signals of unidentified species, or Bi(0). Nonetheless, in analogy to $BiMe_3$, **31** was reacted with stoichiometric amounts of S_2Ph_2 in the condensed phase (Scheme 39).

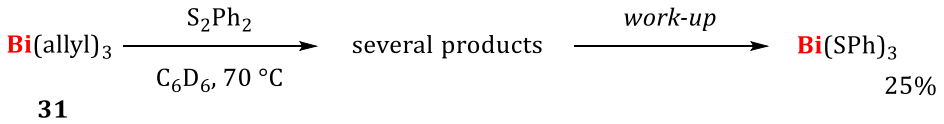

Scheme 39. Reaction of **31** with S_2Ph_2 leading to several products, and the isolation of $Bi(SPh)_3$ after work-up.

The reaction of **31** with S_2Ph_2 was monitored by ^1H NMR spectroscopy, revealing the incomplete conversion (~70%) of $Bi(allyl)_3$ to four new species after 6 h at 70 °C. The formation of 1,5-hexadiene (29%) and (allyl)SPh (14%) was unambiguously identified by comparison with the ^1H NMR spectra of the pure substances. The remaining resonance patterns and integral ratios suggested the presence of species of the chemical composition $(allyl)_2Bi(SPh)$ (51%) and $(allyl)Bi(SPh)_2$ (**32**, 6%). Unexpectedly, after filtration of the reaction mixture, layering the filtrate with *n*-pentane and storage at ambient temperature, a red crystalline solid was obtained after 16 h by filtration, which was identified as $Bi(SPh)_3$ by single-crystal X-ray diffraction analysis and ^1H NMR spectroscopy,[244] and isolated in 25% yield.

In order to synthesize $(allyl)Bi(SPh)_2$ to confirm its formation in the above-mentioned reaction, $Bi(allyl)_3$ was comproportionated with two equivalents of $BiCl_3$ in dichlormethane solution at ambient temperature. Instead of the desired $Bi(allyl)Cl_2$, $Bi(allyl)_2Cl$ was isolated in 51% yield as a yellow solid (Scheme 40a,b).

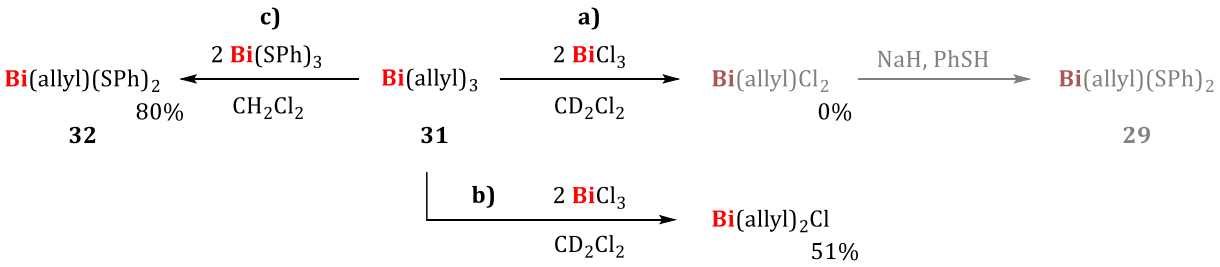

Scheme 40. a) Failed synthesis of $Bi(allyl)(SPh)_2$ by generation of $Bi(allyl)Cl_2$ and subsequent salt elimination , and b) product $Bi(allyl)_2Cl$ isolated instead. c) Reaction of $Bi(allyl)_3$ with $Bi(SPh)_3$ to generate the desired $Bi(allyl)(SPh)_2$.

Combining **31** with two equivalents of $BiCl_3$ in CD_2Cl_2 led to the formation of a black solid, and a ^1H NMR spectrum of the reaction mixture revealed the formation of one new species with two multiplets at $\delta(^1H)$ = 3.62 and 6.43 ppm in a 4:1 ratio. This indicates a fluxional behavior for the allyl groups as described for the $Bi(allyl)_2^+$ cation.[22] Filtration and crystallization from the filtrate at –30 °C yielded a yellow crystalline solid, which decomposed to a black material after 1 h at ambient temperature. However, a ^1H NMR-spectroscopic analysis of the black residue showed the same resonance pattern as the reaction mixture. Crystallization from the mother liquor yielded yellow crystals suitable for X-ray diffraction analysis, which started decomposing within a few minutes at ambient temperature. X-ray diffraction analysis revealed the formation of $Bi(allyl)_2Cl$ (monoclinic space group $P2_1/c$ with Z = 4, Figure 61).

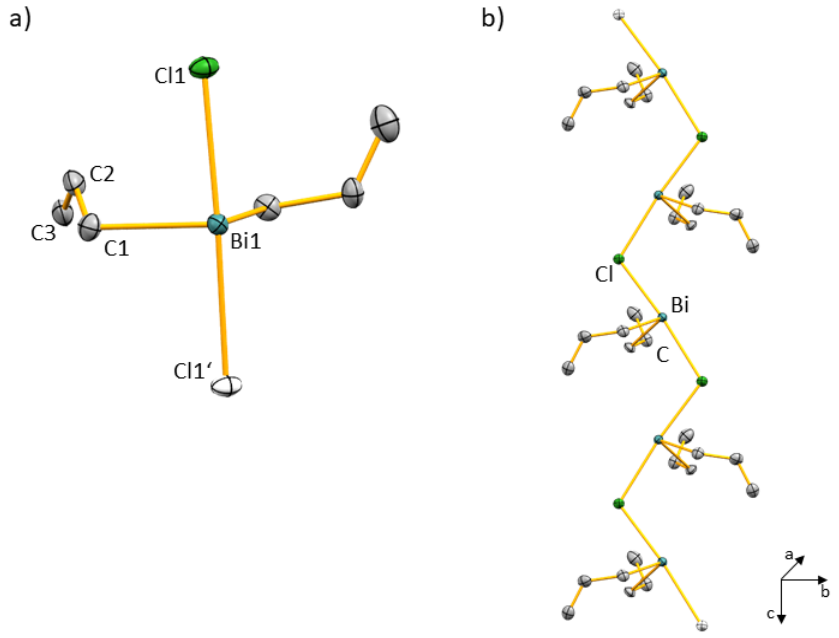

Figure 61. a) Molecular structure of $[Bi(C_3H_5)_2Cl]$. Displacement ellipsoids are drawn at the 50% probability level. Hydrogen atoms are omitted for clarity. Atoms exceeding one formula unit are shown as white ellipsoids. b) Representation of the coordination polymer $[Bi(C_3H_5)_2Cl]_\infty$. Selected bond lengths (Å), and angles (°): Bi1–C1, 2.287(5); Bi1–C4, 2.279(4); Bi1–Cl1, 2.7237(11); Bi1···Cl1', 2.8179(11); C1–C2, 1.481(7); C2–C3, 1.311(7); Cl1–Bi1–Cl1', 175.11(2); C4–Bi1–C1, 95.28(17); C1–Bi1–Cl1, 87.30(12); C1–Bi1–Cl1', 89.52(13); C4–Bi1–Cl1, 86.94(13); C4–Bi1–Cl1', 89.66(12).

The bismuth atom in $Bi(allyl)_2Cl$ adopts a bisphenoidal coordination geometry with the chlorine atoms in axial positions and the carbon based substituents in equatorial positions, and shows bonding parameters similar to $Bi(allyl)_2I$.[22] As observed for $Bi(allyl)_2I$, the chlorido derivative forms a linear polymeric structure in the solid state by intermolecular Cl–Bi interactions (2.8179(11) Å), which are slightly elongated compared to the intramolecular Bi–Cl distances (2.7237(11) Å). The Bi–C bonds in $Bi(allyl)_2Cl$ (2.279(4)–2.287(5) Å) are shortened compared to $Bi(allyl)_2I$ (2.299(10)–2.301(11) Å),[22] which can be ascribed to the more electronegative chlorido ligand. The decomposition of $Bi(allyl)_2Cl$ into a black solid at ambient temperature indicates poor stability of the compound.

Since the synthesis of **32** via route a) in Scheme 40 failed, a different approach was pursued: $Bi(SPh)_3$ was synthesized according to the literature procedure[244] and reacted with 0.5 equivalents of $Bi(allyl)_3$ (**31**) to generate **32** by comproportionation (Scheme 40c). After 3 h at ambient temperature in methylene chloride the reaction mixture was filtered and layered with *n*-pentane. **32** was isolated as yellow needles by filtration in 80% yield and fully characterized. The first coordination sphere of the solid-state structure of **32** shows the bismuth atom in a trigonal pyramidal coordination geometry with an angular sum of 274.9° (triclinic space group $\bar{P}1$ with $Z = 2$, Figure 62).

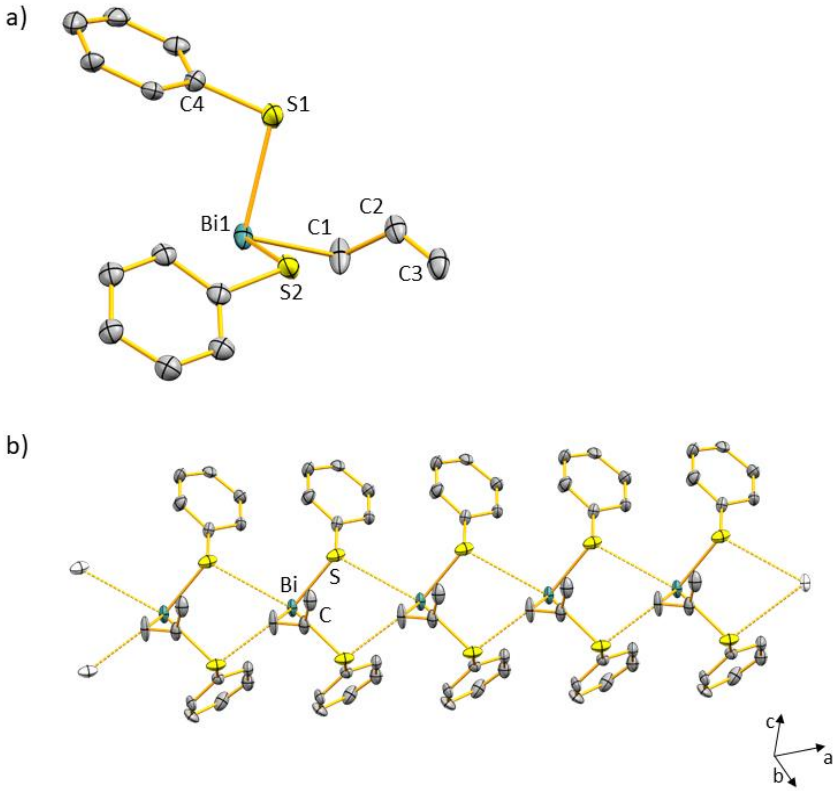

Figure 62. a) Molecular structure of $[Bi(SPh)_2(C_3H_5)]$ (**32**). Displacement ellipsoids are drawn at the 50% probability level. Hydrogen atoms and disordered phenyl-groups are omitted for clarity. b) Cut out of coordination polymer $[Bi(SPh)_2(C_3H_5)]_\infty$. Selected bond lengths (Å) and bond angles (°): Bi1–S1, 2.5873(12); Bi1–S2, 2.5828(11); Bi1–C1, 2.274(4); C1–C2, 1.475(6); C2–C3, 1.320(7); S1–C4, 1.779(4); S1'···Bi1, 3.411; S2'···Bi1, 3.444; C1–Bi1–S1, 90.74(13); C1–Bi1–S2, 91.12(13); S1–Bi1–S2, 93.00(4); C4–S1–Bi1; 99.84(13).

Similarly to $BiMe(SPh)_2$,[236] **32** forms a one-dimensional coordination polymer via intermolecular bismuth sulfur interactions in the solid state, which expands through translation along the crystallographic a-axis. The intramolecular Bi–S bonds (2.5873(12), 2.5828(11) Å) are significantly shorter than in the methyl analog $BiMe(SPh)_2$ (2.699(2)–2.756(2) Å), and at the same time, the intermolecular Bi–S bonds (ca. 3.41–3.44 Å) in **32** are elongated compared to those in $BiMe(SPh)_2$ (ca. 2.97–3.01 Å). These findings indicate a less pronounced intermolecular interaction between two molecular units, resulting in stronger intramolecular bismuth-sulfur interactions. In the coordination polymer, the bismuth atom adopts a square pyramidal coordination geometry with the allyl substituents in the apical positions ($\tau = 0.01$). The C–Bi bond length (2.274(4) Å) is similar to those in $Bi(allyl)_2Cl$ (2.279(4)–2.287(5) Å), but significantly shorter than in $Bi(allyl)_2I$ (2.200(10)–2.301(11) Å). A small number of related compounds $BiR(SR')_2$ have been reported in the literature (R = aryl, alkyl, R' = aryl, alkyl).[245–248] However, only one species with R = alkyl is known, namely the methyl analog $BiMe(SPh)_2$ synthesized by our group.[236] Known species with R = aryl contain additional donor functional groups at the aryl substituent or additional donor ligands.

32 does not show any fluxional behavior of the allyl group on the NMR time scale. First signs of decomposition are detected immediately upon solvation as a new set of ^{1}H NMR spectroscopic resonances, attributable to Bi(allyl)$_2$(SPh) according to the resonance pattern and integral ratio. The degradation of **32** seems to be temperature dependent: after 24 h at ambient temperature, the formation of a black solid, as well as (allyl)SPh (according to ^{1}H NMR spectroscopy) is observed. However, after 20 min at 70 °C the selective formation of Bi(SPh)$_3$ and 1,5-hexadiene, accompanied by the formation of a black solid, are observed.

The independent synthesis of **32** unambiguously confirmed its formation during the reaction of Bi(allyl)$_3$ with S_2Ph_2 by comparison of ^{1}H NMR-spectroscopic data of the isolated compound. Nonetheless, since the conversion to **32** only occurred in minor amounts (6%), it does not confirm the selective formation of a bismuthinidene by heating Bi(allyl)$_3$.

The reactivity of **31** towards Se_2Ph_2 and Te_2Ph_2 was also investigated. To this end, **31** was combined with E_2Ph_2 (E = Se, Te) in C_6D_6, and the reaction was monitored by ^{1}H NMR spectroscopy (Scheme 41).

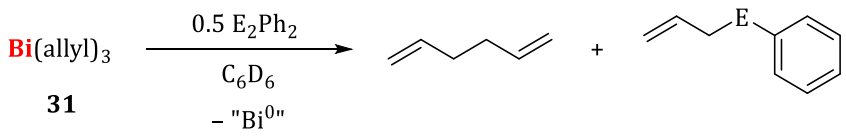

Scheme 41. Reaction of Bi(allyl)$_3$ with E_2Ph_2. E = Se, Te.

Reaction of **31** with Se_2Ph_2 was carried out at 60 °C and full conversion was reached after 4 h according to ^{1}H NMR spectroscopy. 1,5-Hexadiene and (allyl)SePh were identified as the sole products in solution.[249] An isolation of these products was not carried out. The analog reaction with Te_2Ph_2 showed full conversion of the starting materials after 1 h at ambient temperature to 1,5-hexadiene and (allyl)TePh. (Allyl)TePh was characterized by ^{1}H and ^{13}C NMR data. With the heavier E_2Ph_2 (E = Se, Te) homologs, **31** therefore acts as an allyl-transfer reagent. In conlusion, it is apparent that allyl radicals are formed upon heating Bi(allyl)$_3$. However, it seems that the PhE radicals (E = S, Se, Te) react with the allyl radicals preferentially to a potential transient bismuth based radical. This might be due to the relatively long life-time of the allyl radical compared to bismuth radicals, which result in the formation of (allyl)EPh and the degradation of the bismuth radical species, which is why the reactions performed in this chapter are accompanied by the formation of black solids.

XV Summary and Outlook

In this work, neutral and cationic diorganobismuth species have been studied, focusing on the rationalization of their Lewis acidity, their use as ligands in complexes of main group and transition metals and the identification of active catalysts.

Well-defined bismuth compounds in radical catalysis. Transition metal bismuthanes, i.e. molecular complexes with a Bi–TM bond (TM = transition metal), have been demonstrated to undergo highly selective, stoichiometric reactions that are likely to proceed via radical pathways (Scheme 42).

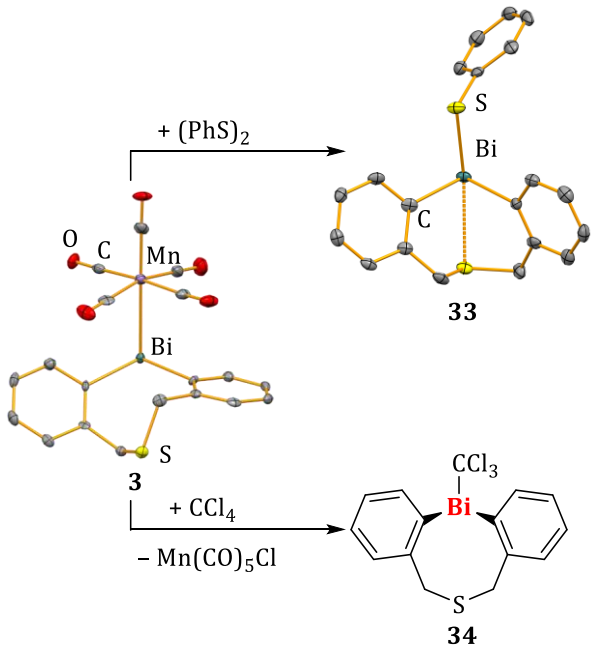

Scheme 42. Selective reactions of **3** with $(PhS)_2$, and CCl_4, respectively, to form **33** and **34**.

Following these results, representatives of this class of compounds were used as (pre-)catalysts in the cyclo-isomerization of δ-iodo-olefins. For the first time, the parent compound 6-iodo-1-hexene was successfully cyclized under thermal conditions in a catalyzed reaction via radical intermediates. Especially in comparison to traditional catalysts for the cyclo-isomerization of δ-iodo-olefins, which involve polar reaction pathways, the high group tolerance of the transition metal bismuthanes is apparent: the cyclo-isomerization of substrates that were previously subject to (polar) degradation reactions was successfully achieved with the bismuth-based catalysts.

In addition to thermally-induced radical catalysis, it was shown for the first time that molecular bismuth compounds can also be used in photochemically induced homogeneous catalysis. To this end, diarylbismuth chalcogenides were used as catalysts in the dehydrocoupling of silanes with TEMPO ((2,2,6,6-tetramethylpiperidin-1-yl)oxyl) (Scheme 43).

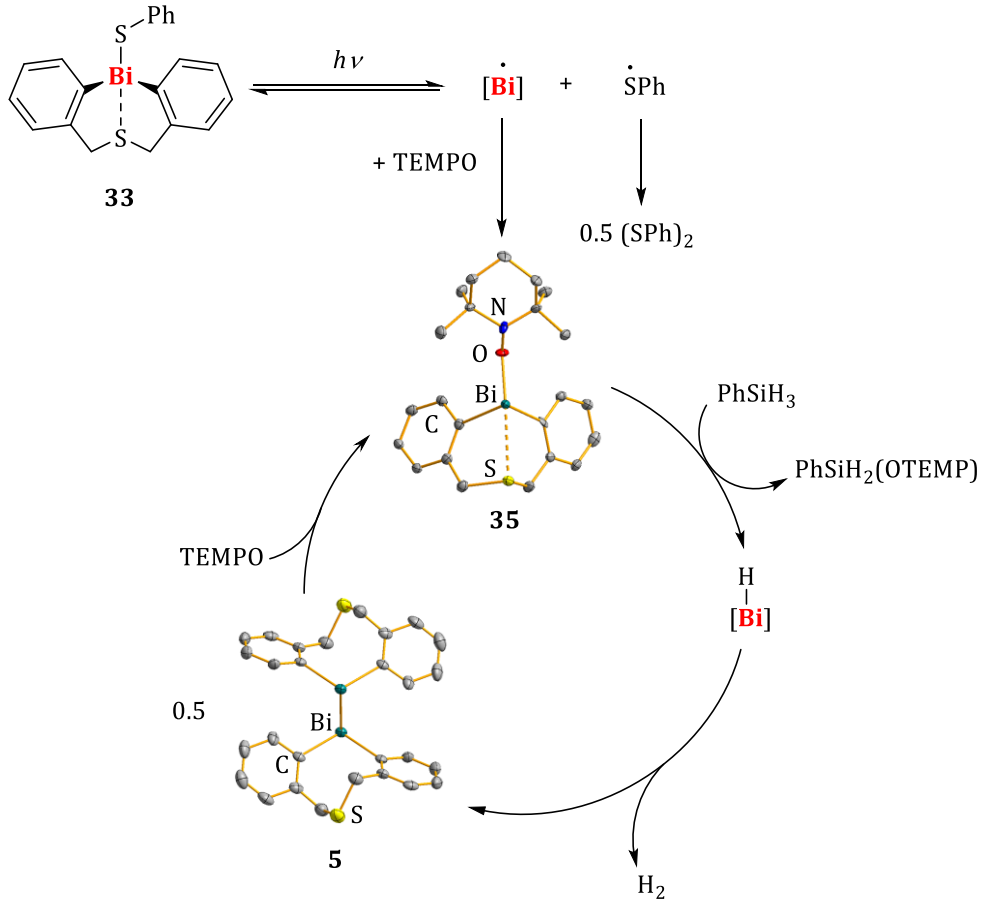

Scheme 43. Proposed catalytic cycle for the dehydrocoupling of phenylsilane with TEMPO catalyzed by **33** under photochemical conditions.

Compared to the bismuth compounds previously used as catalysts in this reaction, in particular the sulfur-containing compound **33** showed a considerably higher catalytic activity. Intermediate species **35** and **5** were identified by mass spectrometric studies and were prepared and fully characterized by rational syntheses. The catalytic activity of these species was demonstrated in independent reactions. (TD-)DFT calculations suggest the formation of a bismuth-centered radical by homolysis of the Bi–S bond as an initiation step. Future studies will address the question of whether the dehydrocoupling of silanes with TEMPO or other substrates such as alcohols can also be catalyzed under thermal conditions by the same class of compounds, and which mechanism underlies such a thermally-induced reaction.

Neutral and cationic dibenzobismepines. The synthesis of a dinuclear dibenzobismepine species (**7**), as well as the first representatives of halobismepines (**8-X**, X = Cl, Br, I) have been successfully established in this work (Scheme 44).

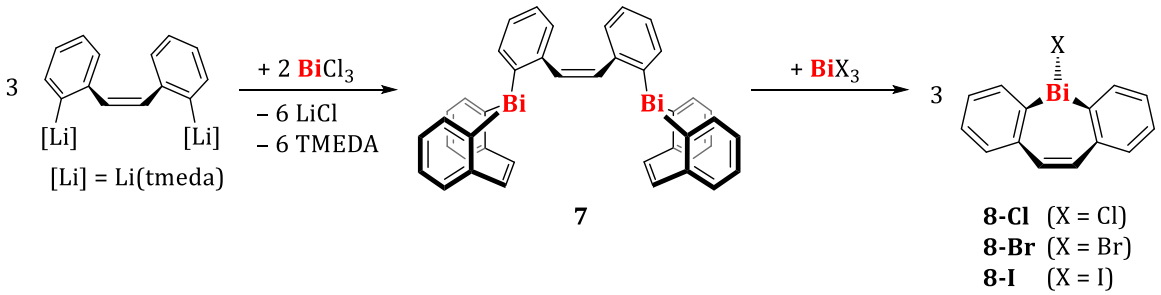

Scheme 44. Synthesis of a dinuclear dibenzobismepine via salt elimination, and subsequent comproportionation to give halogen-substituted derivatives. tmeda = *N*,*N*,*N*‘,*N*‘-etramethylethane-1,2-diamine.

Additionally, starting from the halobismepines **8-Cl** and **8-Br**, the first examples of cationic derivatives were synthesized, which were obtained by salt eliminations with silver salts or halide abstraction with aluminum trihalides (Scheme 45).

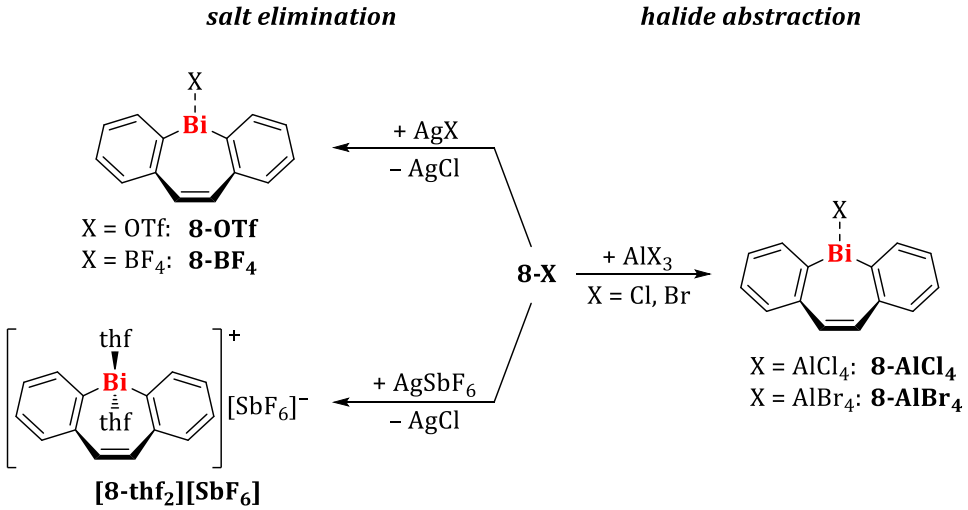

Scheme 45. Synthesis of cationic dibenzobismepines by metathesis or halide abstraction.

The solid-state structures of the dibenzobismepines show boat conformations of the central heterocycle in each case, with bending occurring to a more pronounced extent in neutral representatives compared to cationic derivatives. The first description of an olefin-bismuth interaction was achieved for **8-X** (X = Cl, Br, I), since in these compounds the structural parameters, as well as performed NBO analyses, indicate a weak, intramolecular interaction between the olefin backbone of the ligand and the bismuth center in the form of a π(C=C)→σ*(Bi–X) interaction. The HOMO–9 molcular orbital revealed an overlap between the π(C=C) and σ(Bi–X)-orbitals (Figure 63).

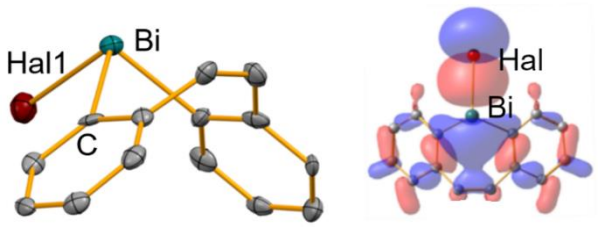

Figure 63. Molecular structure of **8-Br** in the solid state (left) and orbital interaction between π(C=C)-orbital and σ(Bi–X)-orbital (isovalue of 0.024). The results obtained for **8-Cl** and **8-I** are visually identical.

The cationic bismepines crystallized either as contact ion pairs (**8-BF_4**, **8-OTf**, **8-$AlBr_4$**), or as solvent-separated ion pairs (**[8-thf_2][SbF_6]**). The less pronounced boat conformation, as well as the fact that these species carry 14π-electrons in a cyclic-conjugated π-electron-system motivated DFT calculations regarding possible aromaticity. For both the thf-stabilized bismepine cation and the calculated (so far not isolable) donor-free cation, an experimentally found bent conformation as well as a planar structure at the energetic minimum were found. In both cases, the thf adducts as well as the donor-free compounds, the conformational conversion proceeds via an energetically low-lying transition state, with the planar geometry representing the energetic minimum for the Lewis base-free species. An aromaticity of the central seven-membered ring was demonstrated for the donor-free cation by calculating NICS values. Although the adduct formation with THF is exothermic and exergonic according to DFT calculations, these results clearly show that the synthesis of donor-free bismepine cations with weak cation-anion interactions is a worthwhile goal for the future.

Furthermore, the Lewis acidity of a series of bismuth compounds was quantified by the Gutmann-Beckett (GB) method. Thus, for the first time, the Lewis acidity of triorganyl bismuthanes, diorganobismuth halides, bismuth salts of the type BiX_3 (X = Cl, Br, I, OTf) and cationic bismuth organyls have been evaluated and compared with one another. Commercially available bismuth triflate showed an exceptionally high acceptor number, which is in ranges of the extremely Lewis acidic compounds BBr_3 and $SbCl_5$. Further investigations regarding a particularly "soft" Lewis acidity of bismuth compounds resulted in an extension of the GB method. Whereas the original GB method is based on the use of the hard Lewis base $OPEt_3$, the use of the softer Lewis bases $SPMe_3$ and $SePMe_3$ allowed the introduction of a method which includes the softness/hardness of the Lewis acids to quantify the Lewis acid strength. Thus, it was demonstrated that the Lewis acidity of soft, cationic diorganobismuthanes can exceed that of classic, hard Lewis acids, so that despite the presence of hard ligands such as THF, the activation of soft donors proceeds preferentially (Figure 64a).

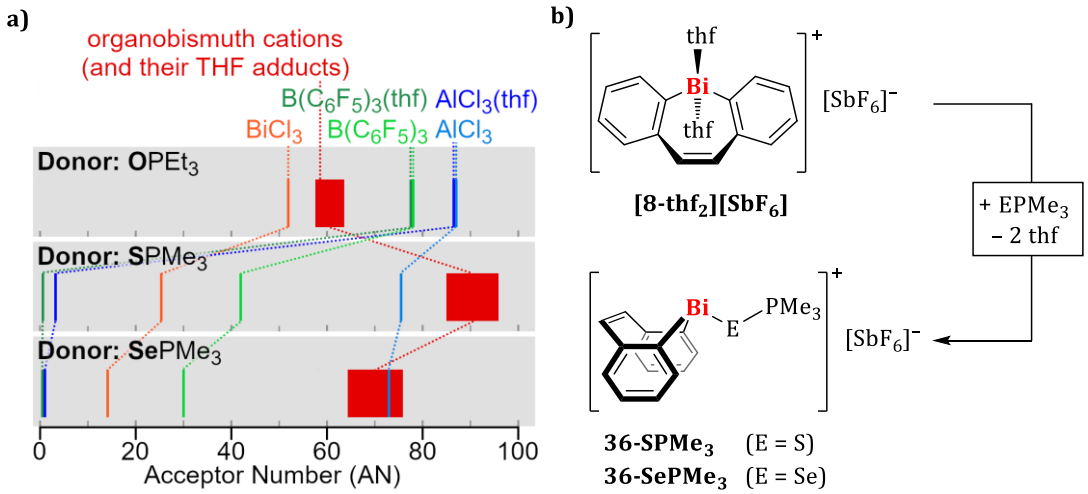

Figure 64. a) Comparison of acceptor numbers for selected Lewis acids determined by the Gutmann-Beckett, as well as the modified Gutmann-Beckett method. b) Synthesis of **36-EPMe$_3$** (E = S, Se).

In the course of this work, very rare representatives of diorganobismuth cations with a coordination number of three were obtained and fully characterized (Figure 64b). Experimental and theoretical analyses of both Lewis acid/base adducts **36-EPMe$_3$** (E = S, Se) indicate a high covalent contribution to the Bi–E interaction.

Dibenzobismepines as ligands. It was possible to introduce the dibenzobismepine framework as a monoanionic ligand into transition metal complexes. This was achieved through salt elimination reactions starting from transition metallates and **8-Cl** (Scheme 46).

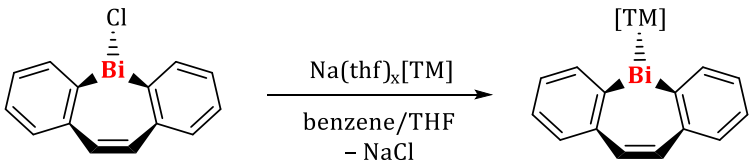

8-Cl

9 ([TM] = Mn(CO)$_5$)
10 ([TM] = Fe(CO)$_2$Cp)
13 ([TM] = Co(CO)$_4$)
13-L ([TM] = Co(CO)$_3$L, L = PPh$_3$, PCy$_3$, *t*BuNC)
15 ([TM] = Co(CO)$_2$(PCy$_3$)(*t*BuNC))

Scheme 46. Synthesis of transition metal complexes with a dibenzobismepine ligand starting from **8-Cl**. Na(thf)$_x$(TM) = Na[Co(CO)$_4$], Na(thf)[Fe(CO)$_2$Cp], Na(thf)$_3$[Mn(CO)$_5$), x = 0, 1, 3.

Of those complexes presented, **10**, **13-L** (L = PPh$_3$, PCy$_3$, *t*BuNC) and **15** showed sufficiently high stability in solution and in the solid state to allow for isolation and full characterization. The prepared transition metal bismuthanes are of yellow to red color, and UV-vis spectroscopic studies in combination with TD-DFT calculations indicated a population of σ*(Co–C$_{CO}$)-orbitals upon irradiation. Consequently, an olefin-transition metal interaction was realized by

photochemically-induced CO elimination, and the synthesis of chiral cobalt complexes was investigated by utilizing the hemilabile olefin functionality in the ligand backbone via olefin coordination/olefin dissociation reactions (Scheme 47).

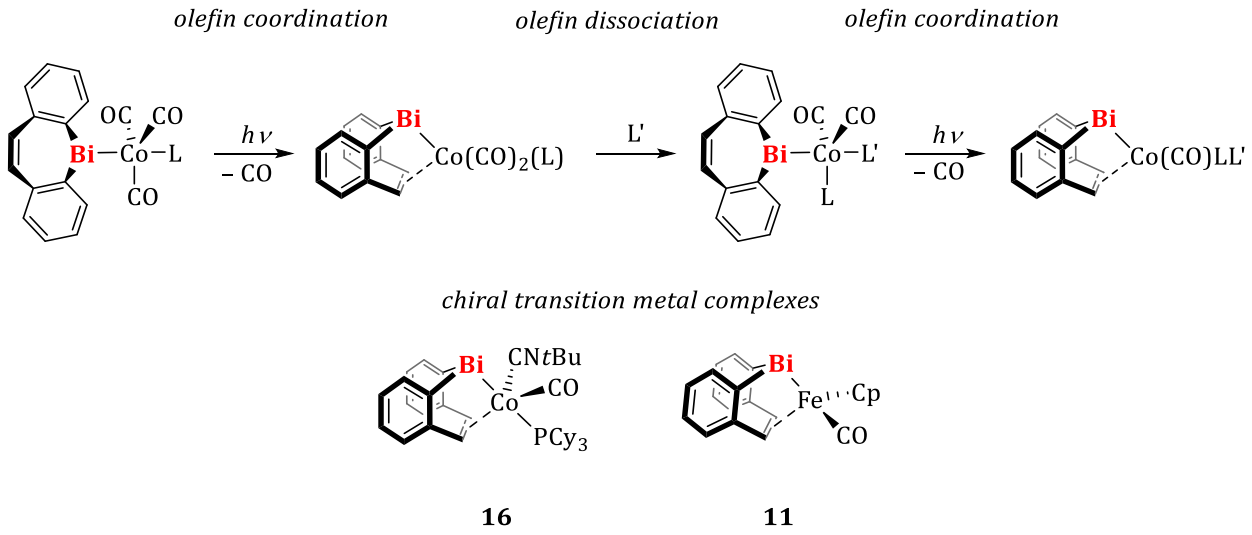

Scheme 47. Alternating olefin coordination/olefin dissociation reactions lead to the stepwise introduction of different ligands so that chiral cobalt complexes are obtained.

Synthetic efforts regarding the cobalt complexes yielded first promising results, including the preparation of chiral complex **16**. Still, the separation of mixtures of enantiomers, as well as the separation of by-products formed during the synthesis, requires further investigation. The photochemically induced CO elimination from the iron complex **10** led to the formation of the chiral complex **11** as a racemic mixture.

In addition to the olefin moiety, dibenzobismepines contain further donor functionalities with the arene groups, so that it was possible to introduce **7** and **8-I** as rigid, ditopic arene donors towards soft Lewis acids, specifically as ligands for Tl^+. Thus, either a coordination polymer in the solid state (**37[BArF^{24}]**) or a molecular Lewis acid/base pair (**38[BArF^{24}]**) was obtained (Scheme 48).

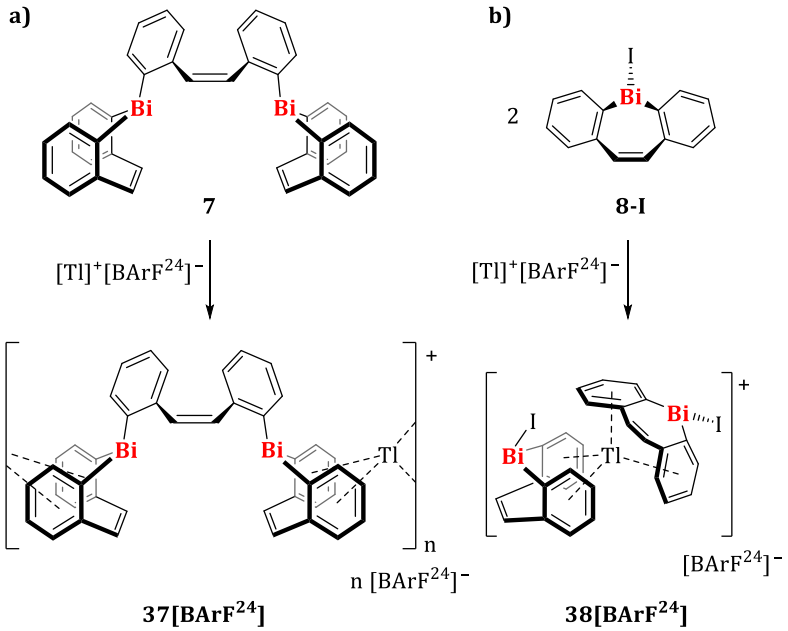

Scheme 48. Successful introduction of dibenzobismepines into the coordination sphere of Tl^+.

The solid-state structures of both compounds revealed a previously unknown tetra-arene coordination of the thallium(I) cations. Additional quantum chemical calculations demonstrated that unprecedented olefin→Tl^+ interactions also occur in compounds of this type. DOSY NMR spectroscopic and mass spectrometric studies demonstrated that the interaction between bismepines and thallium is maintained in solution. Incorporation of Bi into the ligand framework (instead of the lighter homologs N–Sb) is accompanied by electronic and geometrical modifications, which together with strong dispersion interactions significantly contributes to the stabilities of compounds **37[BArF24]** and **38[BArF24]** according to DFT calculations performed. This results in increasing strength of ligation in the N < P < As < Sb < Bi series.

Starting from the cationic dibenzobismepine **[8-thf$_2$][SbF$_6$]**, it was possible to prepare two platinum complexes with different ligand environments (Figure 65).

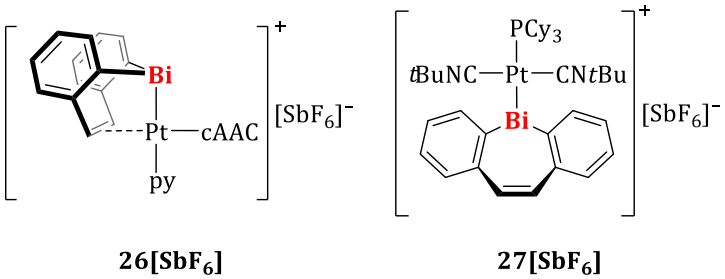

Figure 65. Bismuth-platinum complexes synthesized in this work.

The structural parameters of both compounds in the solid state, as well as the results obtained by DFT calculations, suggest a covalent Bi–Pt interaction in both complexes, although both Bi→Pt and Bi←Pt donor/acceptor interactions are possible in principle.

Upon reaction of **[8-thf$_2$][SbF$_6$]** and related cationic diarylbismuth species with an Os(II) complex, it was revealed that the formation of Lewis acid/base adducts with Bi–Os interactions is hampered by steric hindrance of the ligands. According to quantum chemical calculations, Os–Bi interactions become feasible by lowering the steric demand, thus obtaining complexes (*in silico*) that show not only a Os→Bi interaction, which would be expected due to the cationic bismuth fragment, but also pronounced Os←Bi bonding interactions (Scheme 49). In summary, these results highlight the wide variety of coordination modes and electronic structures that dibenzobismepine species can adopt in (transition) metal complexes.

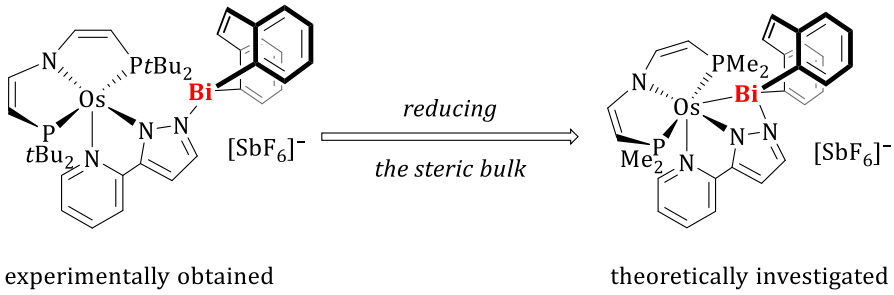

Scheme 49. Reduction of the steric demand on an osmium(II) complex leads to the formation of compounds with Os–Bi donor/acceptor interactions.

Dimethyl bismuth cations. The synthesis of the first mononuclear alkyl bismuth cation species was achieved by metathesis of BiMe$_2$Cl with AgSbF$_6$ in good yields. The yellow compound shows absorptions in the visible light region, with excitations leading to a population of the bismuth-centered molecular orbital of p-orbital character originating from a σ(Bi–C)-orbital. The synthesis of Lewis base adducts starting from **21** was successful with a range of neutral donor ligands, with only the pyridine adduct showing sufficiently high stability for isolation and full characterization (Scheme 50).

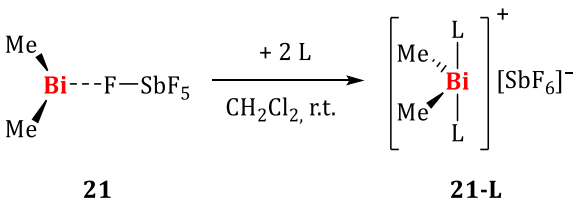

Scheme 50. Synthesis of Lewis base adducts of **21**.

In addition to the hexafluoroantimonate salt, first representatives of bismuth cations with cyanoborate anions were prepared and characterized. In contrast to the SbF_6 salt, sufficiently volatile neutral donors can be removed from the colorless cyanoborate compounds by drying *in vacuo* yielding the solvent-free contact ion pairs regardless of the initially employed solvent. According to DFT calculations, the strength of the cation-anion interaction can be precisely controlled by appropriate choice of the $[BH_n(CN)_{4-n}]$ anion.

Starting from **21**, reaction with $BiMe_3$ led to the synthesis of **39**, the first dinuclear bismuth species with a dative Bi→Bi interaction (Scheme 51).

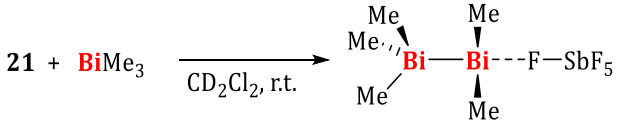

39

Scheme 51. Realization of the first dinuclear bismuth compound with a dative Bi→Bi interaction.

In solution, **39** shows rapid exchange of the methyl ligands on the NMR time scale. Low-temperature NMR spectroscopic studies and line-shape analysis provided the thermodynamic parameters for the methyl exchange, which were confirmed by DFT calculations. For the mechanism of the methyl exchange it is assumed that the two bismuth complex fragments in **39** first dissociate, and in the subsequent electrophilic attack of a $[BiMe_2]^+$ unit on a methyl group of a $BiMe_3$ molecule, a structural motif of the type Bi–(μ_2-CH_3)–Bi with a bridging trigonal-planar methyl group is formed. According to DFT calculations, the bridging methyl moiety shows sp^2 hybridization, rendering this reaction the first example of a methyl exchange in a homoleptic main group metal complex proceeding via an S_E2 (back) reaction, the electrophilic counterpart of a S_N2 reaction.

Analog experiments with the phenyl derivatives $[Ph_2Bi(SbF_6)]$ and $BiPh_3$ also resulted in a compound exhibiting rapid phenyl exchange in solution, however, this compound could not be isolated to date. Low-temperature NMR spectroscopic studies on the *in situ* generated compound showed that phenyl exchange was not sufficiently hindered even at temperatures of –80 °C for ^1H NMR spectroscopic signal separation. However, further studies concerning the electronic and steric influence of the ligands regarding the formation and stability of species with dative Bi→Bi interactions should be undertaken in order to elucidate the properties of this new class of compounds.

CO insertion into a cationic bismuth amide. In the course of studies on cationic bismuth amides within our group, a representative of a previously unknown substance class, a cationic bismuth carbamoyl (**41**), was prepared by CO insertion upon reaction of **40** with CO (Scheme 52).

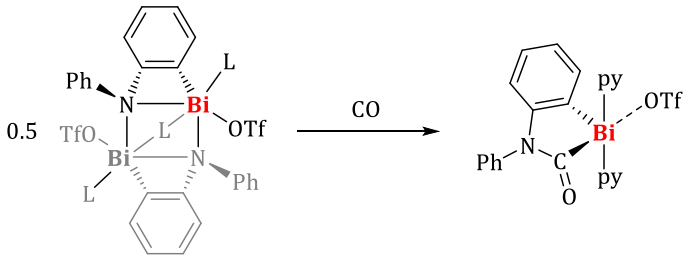

40 **41**

Scheme 52. CO insertion into a cationic bismuth amide (**40**).

Upon release of ring tension, **40** reacts with CO and isoelectronic isocyanides under mild reaction conditions. The calculated mechanism for CO insertion indicates a stepwise CO association to the bismuth center to form a Lewis acid/base adduct, with subsequent insertion. IR spectroscopic reaction monitoring was in agreement with the theoretical findings. The insertion product **41** exhibits a chemically reversible redox process under cyclic voltammetry conditions, resulting in the *in situ* (reversible) formation of a bismuth radical.

Lewis base-free organometallic bismuthinidene. Starting from $BiMe_3$, controlled thermal homolysis resulted in the formation of Bi(I)Me, which was detected spectroscopically and mass spectrometrically in the gas phase. The compound BiMe generated under these conditions is the first Lewis base-free organometallic bismuthinidene known to date and exhibits a triplet ground state according to DFT and multi-reference calculations. Furthermore, within the scope of this work, the homolytic bond dissociation energy of $Me_2Bi–CH_3$ was determined to be 210 ± 7 kJ · mol^{-1}, which exceeds the value previously assumed in the literature by 15%. Reactivity studies also suggested that transient BiMe can be used in preparative chemistry under standard laboratory conditions, so that in the future $BiMe_3$ could serve as a suitable precursor for the introduction of "BiMe" fragments into organic and inorganic substrates. EPR spectroscopic studies confirmed the liberation of radical intermediate species from $BiMe_3$ at 60 °C in solution. Suitable BiR_3 precursors will facilitate investigations of the electronic and steric influence of substituents R on the formation of organometallic Lewis base-free bismuthinidenes and their electronic structure. EPR spectroscopic and preparative studies with the lighter pnictogen compounds $AsMe_3$ and $SbMe_3$ indicate a lower reactivity with respect to homolytic $Me_2E–CH_3$ (E = As, Sb) bond cleavage. Further spectroscopic and theoretical studies on the lighter homologs are ongoing.

XVI Zusammenfassung und Ausblick

In dieser Arbeit wurden neutrale und kationische Diorganobismutspezies untersucht, wobei der Fokus auf dem Verständnis ihrer Lewis-Azidität, ihrem Einsatz als Liganden in Komplexen von Hauptgruppen- und Übergangsmetallen und der Identifikation aktiver Katalysatoren lag.

Wohl-definierte Bismutverbindungen in der Radikalkatalyse. Es konnte gezeigt werden, dass Übergangsmetallbismutane, also molekulare Komplexe mit einer Bi–ÜM Bindung (ÜM = Übergangsmetall), hochselektive, stöchiometrische Radikalreaktionen eingehen (Schema 1).

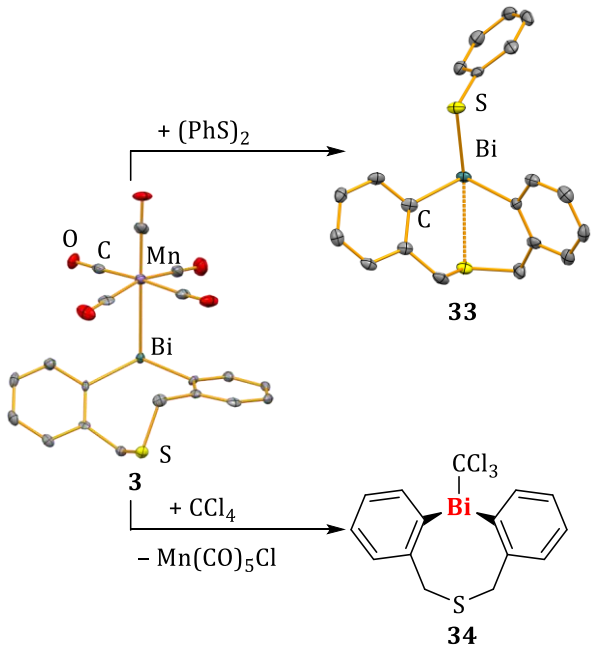

Schema 1. Selektive Umsetzungen von **3** mit $(PhS)_2$, beziehungsweise CCl_4 unter Bildung von **33** und **34.**

Auf diesen Ergebnissen aufbauend konnten Vertreter dieser Substanzklasse als (Prä-)Katalysatoren in der Zyklo-Isomerisierung von δ-Iod-olefinen eingesetzt werden, wobei es erstmalig gelang die Stammverbindung 6-Iod-1-hexen unter thermischen Bedingungen radikalisch katalysiert zu zyklisieren. Gerade im Vergleich zu traditionellen Katalysatoren für die Zyklo-Isomerisierung von *δ*-Iod-olefinen, wobei polare Reaktionspfade durchlaufen werden, zeigt sich die große Gruppentoleranz der Übergangsmetallbismutane, sodass auch die Zyklo-Isomerisierung von Substraten gelang, die bisher (polaren) Degradationsreaktionen unterlagen.

Neben der thermisch-induzierten Radikalkatalyse konnte erstmals gezeigt werden, dass molekulare Bismutverbindungen auch in der photochemisch-induzierten Homogenkatalyse eingesetzt werden können. Dazu wurden Diarylbismutchalkogenide als Katalysatoren in der

Dehydrokupplung von Silanen mit TEMPO ((2,2,6,6-Tetramethylpiperidin-1-yl)oxyl) eingesetzt (Schema 2).

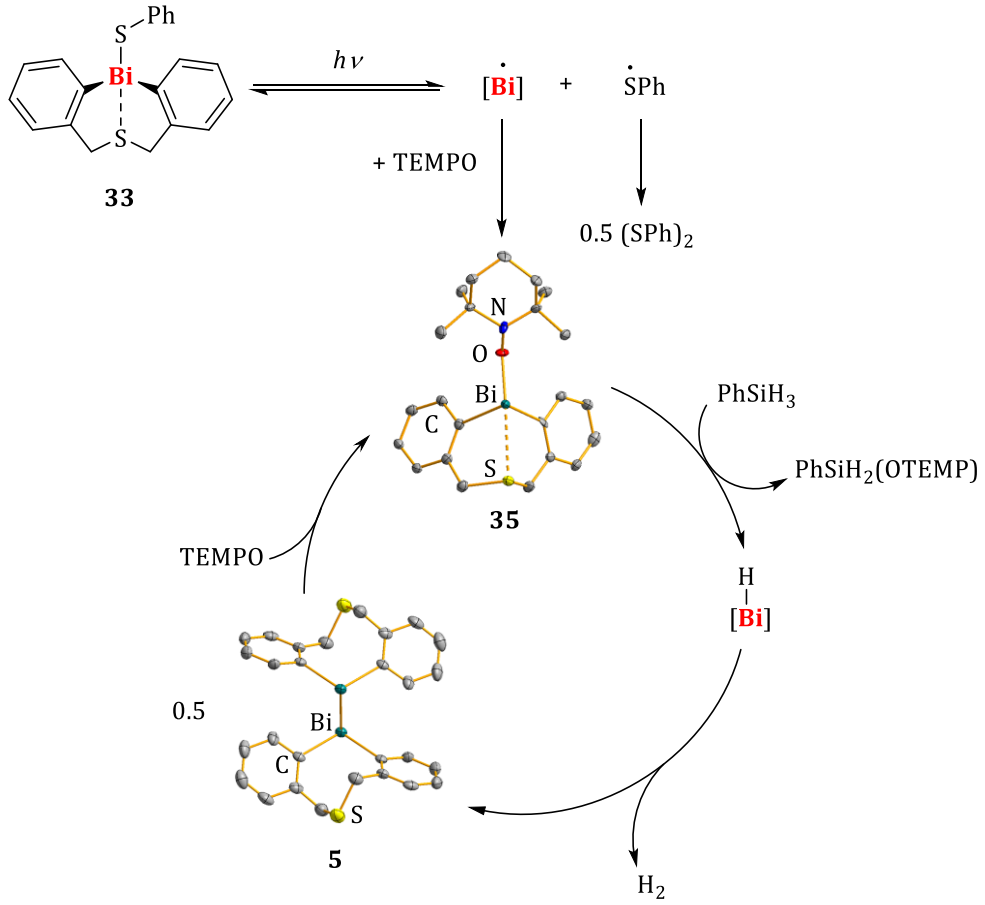

Schema 2. Vorgeschlagener Katalysezyklus für die durch **33** katalysierte Dehydrokupplung von Phenylsilan mit TEMPO unter photochemischen Bedingungen.

Im Vergleich zu den bisher in dieser Reaktion als Katalysatoren eingesetzten Bismutverbindungen zeigte insbesondere die schwefelhaltige Verbindung **33** eine wesentlich höhere katalytische Aktivität. Intermediär auftretende Spezies **35** und **5** konnten durch massenspektrometrische Untersuchungen identifiziert, und durch rationale Synthesen hergestellt und vollständig charakterisiert werden. Die katalytische Aktivität dieser Spezies wurde in Testreaktionen nachgewiesen. TD-DFT Berechnungen legen die Bildung eines bismut-zentrierten Radikals durch Homolyse der Bi–S Bindung als Initiationsschritt nahe. Zukünftige Untersuchungen sollen sich mit der Frage beschäftigen, ob die Dehydrokupplung von Silanen mit TEMPO oder anderen Substraten wie Alkoholen auch unter thermischen Bedingungen durch die gleiche Substanzklasse katalysiert werden kann, und welcher Mechanismus einer solchen thermisch-induzierten Reaktion zugrunde liegt.

Neutrale und kationische Dibenzobismepine. Die Synthese einer dinuklearen Dibenzobismepinspezies (**7**), sowie der ersten Vertreter von Halobismepinen (**8-X**, X = Cl, Br, I), wurde im Rahmen dieser Arbeit etabliert (Schema 3).

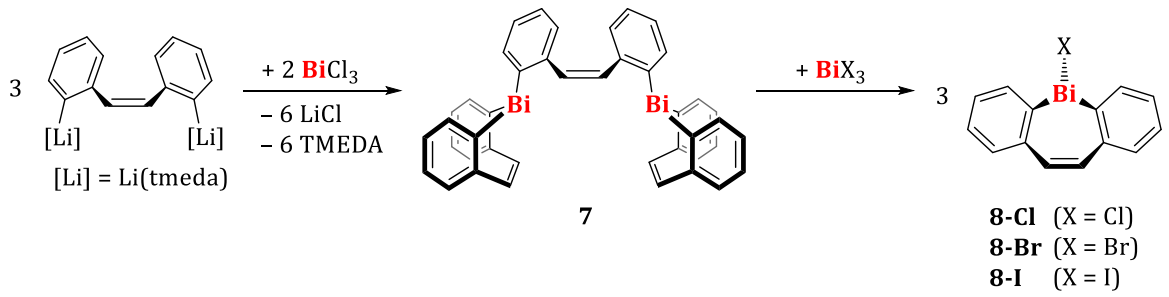

Schema 3. Darstellung eines dinuklearen Dibenzobismepins über eine Salzeliminierung, und nachfolgende Komproportionierung zu halogen-substituierten Derivaten. tmeda = *N*,*N*,*N*‘,*N*‘-Tetramethylethan-1,2-diamin.

Außerdem konnten ausgehend von den Halobismepinen **8-Cl** und **8-Br** die ersten Beispiele von kationischen Derivaten dargestellt werden, wobei der Zugang zu diesen über Salzeliminierungen mit Silbersalzen oder der Halogenidabstraktion mit Aluminiumtrihalogeniden erfolgte (Schema 4).

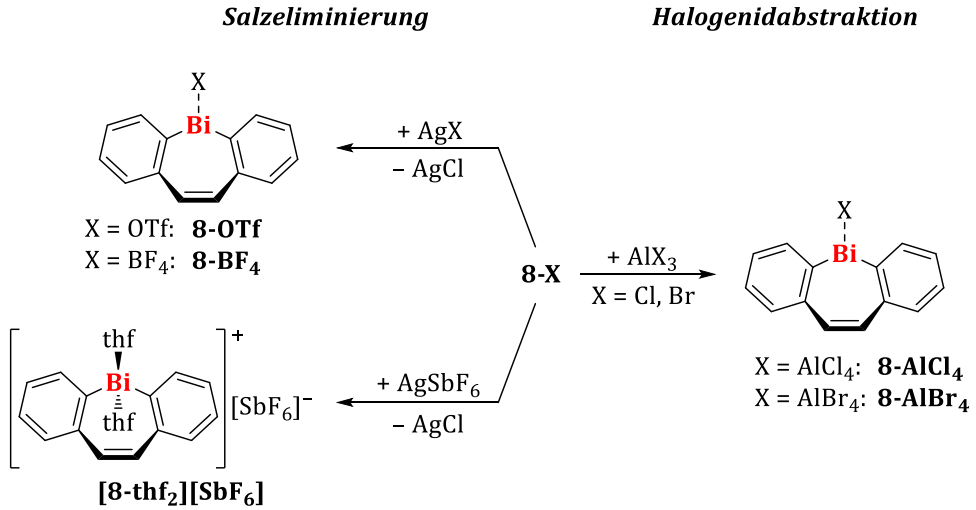

Schema 4. Synthese von kationischen Dibenzobismepinen über Metathese oder Halogenidabstraktion.

Die Festkörperstrukturen der erhaltenen Dibenzobismepine zeigen in allen Fällen eine Bootkonformation des zentralen Heterozyklus, wobei die Abwinkelung bei neutralen Vertretern im Vergleich mit kationischen Derivaten in deutlicherem Maße auftritt. Die erstmalige Beschreibung einer Olefin-Bismut Wechselwirkung gelang für **8-X** (X = Cl, Br, I), da in diesen Verbindungen die strukturellen Parameter, sowie durchgeführte NBO Analysen, auf eine schwache, intramolekulare, Wechselwirkung zwischen dem Olefinrückgrat des Liganden und dem

Bismutzentrum in Form einer π(C=C)→σ*(Bi–X) Interaktion hindeuten. Zusätzlich zeigt das HOMO–9 einen Überlapp von π(C=C) und σ(Bi–X)-Orbitalen (Abbildung 1).

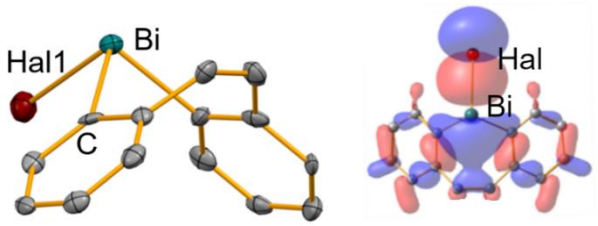

Abbildung 1. Molekulare Struktur von **8-Br** im Festkörper (links) und Orbitalwechselwirkung zwischen besetztem π(C=C)-Orbital und σ(Bi–X)-Orbital. Die Ergebnisse für **8-Cl** und **8-I** sind optisch identisch.

Die kationischen Bismepine kristallisierten entweder als Kontaktionenpaare (**8-BF_4**, **8-OTf**, **8-$AlBr_4$**) oder als Lösungsmittel-separiertes Ionenpaar (**[8-thf_2][SbF_6]**). Die weniger stark ausgeprägte Bootkonformation, sowie die Eigenschaft, dass diese Spezies 14π-Elektronen in einem zyklisch-konjugierten π-Elektronensystem tragen, motivierten zu DFT Rechnungen hinsichtlich einer möglichen Aromatizität. Sowohl für das zweifach THF-stabilisierte Bismepinkation als auch für das berechnete (bisher nicht isolierbare) donor-freie Kation konnte jeweils eine experimentell vorgefundene abgewinkelte, als auch eine planare Minimumstruktur gefunden werden. Die Konformationsänderung verläuft in beiden Fällen, in den THF-Addukten sowie in den donor-freien Verbindungen, über einen energetisch niedrig liegenden Übergangszustand, wobei die planare Geometrie das Minimium für die Lewis-basen-freien Spezies darstellt. Durch die Berechnung von NICS-Werten konnte für das donor-freie, planare Kation eine Aromatizität des zentralen Siebenrings nachgewiesen werden. Zwar ist die Adduktbildung mit THF laut quantenchemischen Berechnungen exotherm und exergon, nichtsdestotrotz zeigen diese Ergebnisse deutlich, dass die Synthese von donor-freien Bismepinkationen mit möglichst schwacher Kation-Anion Wechselwirkung ein lohnendes Ziel für die Zukunft darstellt.

Des Weiteren wurde die Lewis-Azidität von einer Reihe an Bismutverbindungen mittels der Gutmann-Beckett (GB) Methode quantifiziert. So konnten erstmals die Lewis-Aziditäten von Triorganylbismutanen, Diorganobismuthalogeniden, Bismutsalzen des Typs BiX_3 (X = Cl, Br, I, OTf) und kationischen Bismutorganylen evaluiert und untereinander verglichen werden. Käufliches Bismuttriflat zeigte eine außergewöhnlich hohe Akzeptornummer, welche in Bereichen der äußerst Lewis-aziden Verbindungen BBr_3 und $SbCl_5$ liegt. Weiterführende Untersuchungen hinsichtlich einer besonders „weichen“ Lewis-Azidität von Bismutverbindungen resultierten in einer Erweiterung der GB Methode. Basiert die ursprüngliche GB Methode auf der Nutzung der harten Lewis-Base $OPEt_3$, so konnte durch Einsatz der weicheren Lewis-Basen $SPMe_3$

und $SePMe_3$ eine Methode eingeführt werden, in der die Weichheit/Härte der untersuchten Lewis-Säuren zur Quantifizierung der Lewis-Säure-Stärke mit einbezogen wird. So wurde gezeigt, dass die Lewis-Azidität weicher, kationischer Diorganobismutane die von klassischen, harten Lewis-Säuren übersteigen kann, sodass trotz Anwesenheit harter Liganden wie THF die Aktivierung weicher Donoren bevorzugt abläuft (Abbildung 2a).

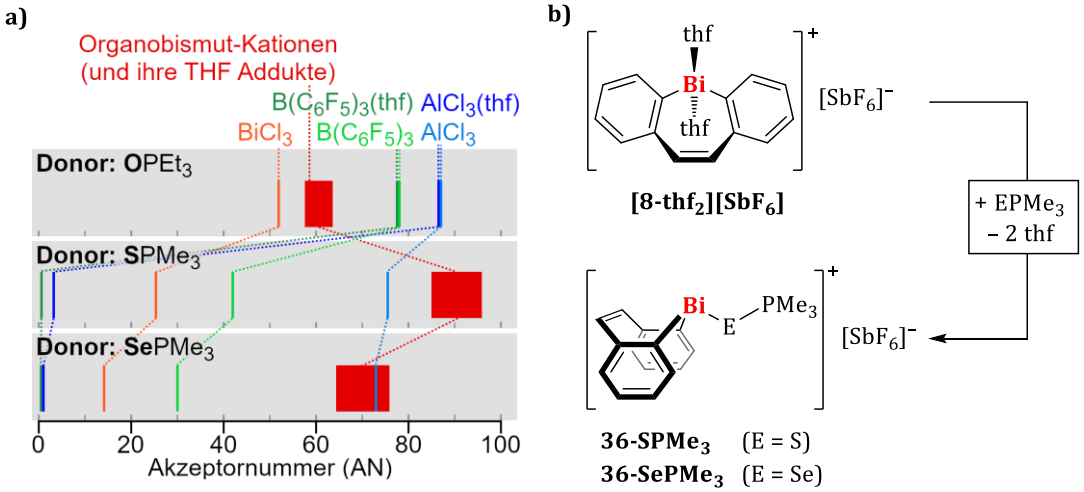

Abbildung 2. a) Vergleich von Akzeptornummern für ausgewählte Lewis-Säuren, die mit der Gutmann-Beckett, sowie der modifizierten Gutmann-Beckett Methode, bestimmt wurden. b) Synthese von **36-EPMe$_3$** (E = S, Se).

Im Rahmen dieser Arbeiten konnten sehr seltene Vertreter von Diorganobismutkationen mit einer Koordinationszahl von drei erhalten und vollständig charakterisiert werden (Abbildung 2b). Experimentelle und theoretische Analysen beider Lewis-Säure/Base-Addukte **36-EPMe$_3$** (E = S, Se) deuten auf einen hohen kovalenten Anteil der Bi–E Wechselwirkung hin.

Dibenzobismepine als Liganden. Es war möglich das Dibenzobismepin-Grundgerüst als monoanionischen Liganden in Übergangsmetallkomplexe einzuführen. Dies gelang über Salzeliminierungen ausgehend von Metallat-Komplexen und **8-Cl** (Schema 5).

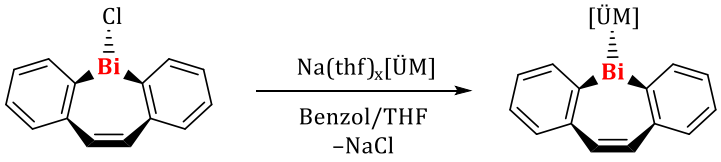

8-Cl

9 ([ÜM] = $Mn(CO)_5$)
10 ([ÜM] = $Fe(CO)_2Cp$)
13 ([ÜM] = $Co(CO)_4$)
13-L ([ÜM] = $Co(CO)_3L$, L = PPh_3, PCy_3, tBuNC)
15 ([ÜM] = $Co(CO)_2(PCy_3)(t$BuNC))

Schema 5. Synthese von Übergangsmetallkomplexen mit einem Dibenzobismepin-Liganden ausgehend von **8-Cl**. $Na(thf)_x[ÜM]$ = $Na[Co(CO)_4]$, $Na(thf)[Fe(CO)_2Cp]$, $Na(thf)_3[Mn(CO)_5]$. x = 0, 1, 3.

Von den dargestellten Komplexen zeigten **10**, **13-L** (L = PPh_3, PCy_3, *t*BuNC) und **15** eine ausreichend hohe Stabilität in Lösung und im Festkörper, sodass diese in moderaten bis guten Ausbeuten isoliert und vollständig charakterisiert werden konnten. Die dargestellten Übergangsmetallbismutane sind gelb bis rot gefärbte Verbindungen, und UV-vis spektroskopische Untersuchungen in Verbindung mit TD-DFT Berechnungen wiesen auf eine Population von σ*(Co–C_{CO})-Orbitalen durch Bestrahlung hin. Eine Olefin-Übergangsmetall-Wechselwirkung wurde folglich durch photochemisch induzierte CO-Eliminierung realisiert, wobei die Synthese chiraler Cobaltkomplexe durch Nutzung der hemilabilen Olefinfunktionalität im Ligandrückgrat über Olefin-Koordination/Olefin-Dissoziations-Reaktionen untersucht wurde (Schema 6).

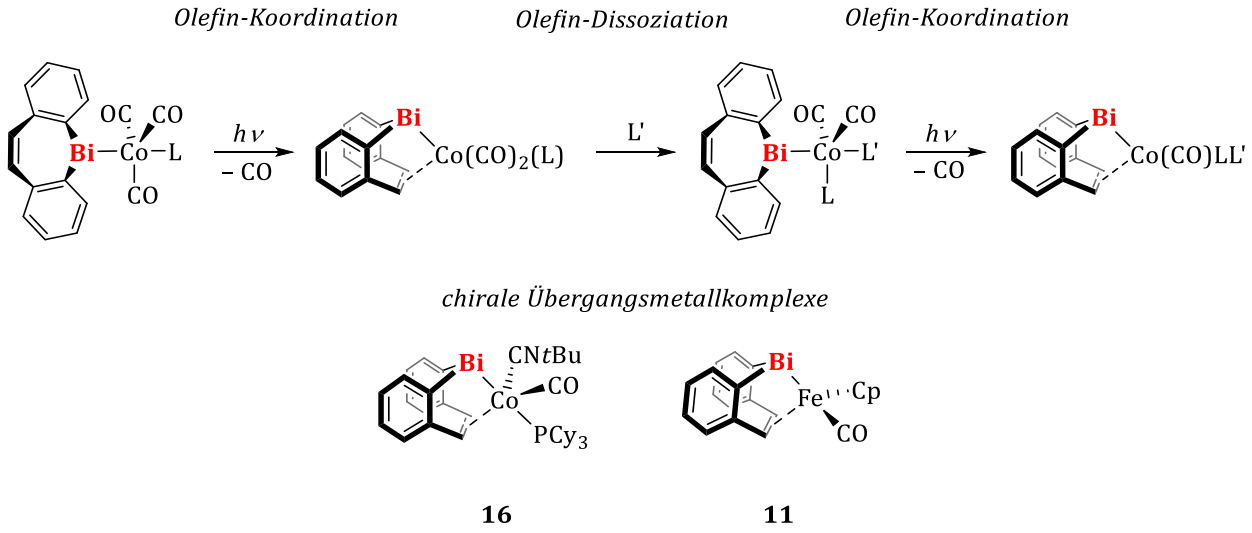

Schema 6. Alternierende Olefin-Koordination/Olefin-Dissoziations-Reaktionen führen zur schrittweisen Einführung unterschiedlicher Liganden, sodass chirale Cobaltkomplexe erhalten werden.

Erste vielversprechende Ergebnisse, unter anderem der Erhalt von **16**, wurden für die cobalt-basierten Komplexe erhalten. Insbesondere die Auftrennung von Enantiomerengemischen, sowie die Abtrennung von bei der Synthese entstehenden Nebenprodukten, bedarf weiterer Untersuchungen. Die photochemisch induzierte CO-Eliminierung am Eisenkomplex **10** führten zum Erhalt des chiralen Komplexes **11** als racemisches Gemisch.

Mit den Arengruppen enthalten Dibenzobismepine weitere Donorfunktionalitäten neben der Olefineinheit, sodass es möglich war **7** und **8-I** als rigide, ditope Aren-Donoren für weiche Lewis-Säuren, im Speziellen als Liganden für Tl^+, einzuführen. So wurde entweder ein Koordinationspolymer im Festkörper (**37[BArF^{24}]**) oder ein molekulares Lewis-Säure/Base-Paar (**38[BArF^{24}]**) erhalten (Schema 7).

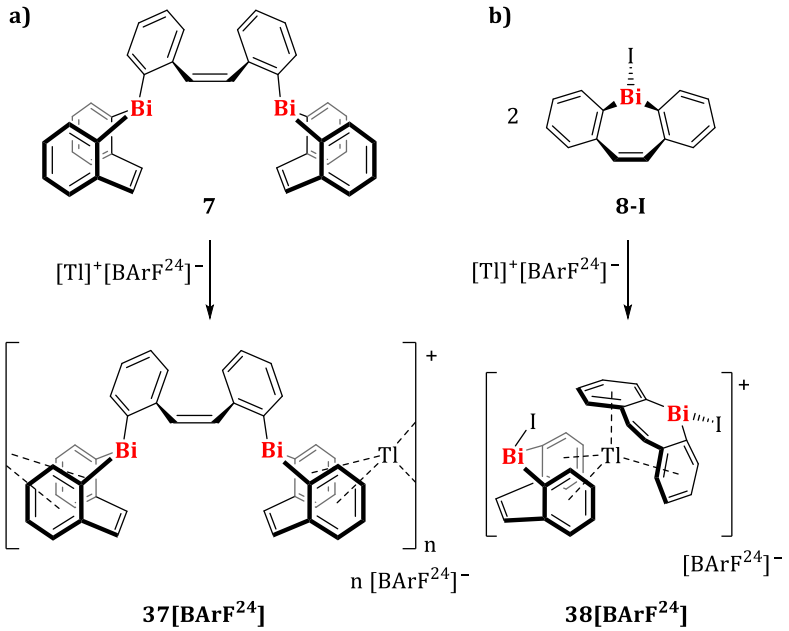

Schema 7. Erfolgreiche Einführung von Dibenzobismepinen in die Koordinationssphäre von Tl^+.

Die Festkörperstrukturen beider Verbindungen zeigen eine bisher unbeschriebene, tetra-Aren Koordination der Thallium(I)-Kationen. Zusätzliche quantenchemische Berechnungen offenbarten, dass auch bisher beispiellose Olefin→Tl^+ Wechselwirkungen in Verbindungen dieser Art auftreten. Durch DOSY-NMR-spektroskopische und massenspektrometrische Untersuchungen konnte gezeigt werden, dass die Wechselwirkung zwischen Bismepinen und Thallium in Lösung aufrechterhalten wird. Laut durchgeführten DFT Rechnungen wird die Inkorporation von Bi in das Ligandgerüst (statt der leichteren Homologen N–Sb) begleitet von elektronischen und geometrischen Veränderungen, was zusammen mit starken Dispersionswechselwirkungen zu der Stabilität der Verbindungen **37[BArF^{24}]** und **38[BArF^{24}]** signifikant beiträgt. Dies resultiert in steigender Stärke der Ligand-Thallium Wechselwirkung in der Reihe N < P < As < Sb < Bi.

Ausgehend von dem kationischen Dibenzobismepin **[8-thf$_2$][SbF$_6$]** war es möglich zwei Platinkomplexe mit unterschiedlicher Ligandenumgebung herzustellen (Abbildung 3).

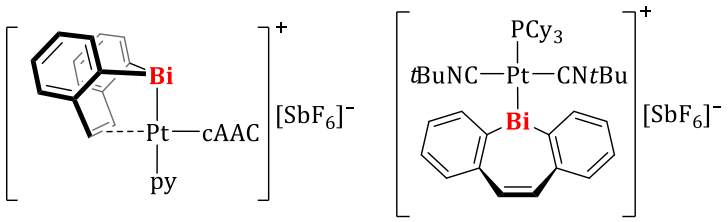

26[SbF$_6$] **27[SbF$_6$]**

Abbildung 3. Im Rahmen dieser Arbeit synthetisierte Bismut-Platin Komplexe.

Die strukturellen Parameter beider Verbindungen im Festkörper, sowie durch DFT Rechnungen erhaltene Ergebnisse, sprechen für eine kovalente Bi–Pt Wechselwirkung in beiden Komplexen, wobei sowohl Bi→Pt, als auch Bi←Pt Donor/Akzeptor-Wechselwirkungen prinzipiell möglich sind.

Bei Umsetzung von **[8-thf$_2$][SbF$_6$]** und einer weiteren kationischen Bismutspezies mit einem Os(II)-Komplex wurde deutlich, dass die Bildung von Lewis-Säure/Base-Addukten mit Bi–Os Wechselwirkung durch sterische Hinderung am Ligandgerüst erschwert wird. Os–Bi Wechselwirkungen werden quantenchemischen Berechnungen zufolge durch Erniedrigung des sterischen Anspruchs zugänglich, sodass (*in silico*) Komplexe erhalten werden, die nicht nur eine Os→Bi Wechselwirkung, was aufgrund des kationischen Bismutfragments zu erwarten wäre, sondern auch ausgeprägte Os←Bi Bindungswechselwirkungen zeigen (Schema 8). Dies und die zuvor dargestellten Ergebnisse unterstreichen die breite Vielfalt an Koordinationsmodi und elektronischer Struktur, die Dibenzobismepin-Spezies in (Übergangsmetall-)Komplexen einnehmen können.

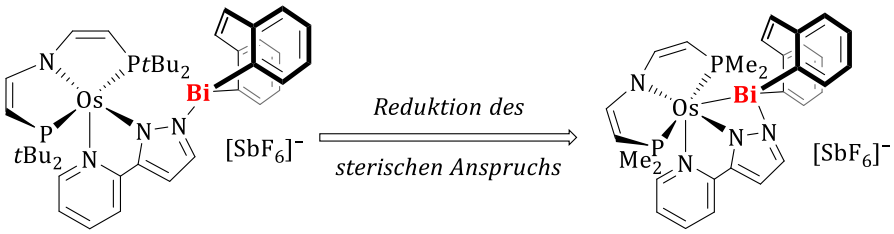

experimentell erhalten theoretisch untersucht

Schema 8. Reduktion des sterischen Anspruchs an einem Osmium(II)-Komplex führt zur Ausbildung von Os–Bi Donor/Akzeptorwechselwirkungen.

Dimethylbismut-Kationen. Die Synthese der ersten mononuklearen Alkylbismut-Kation Spezies gelang durch Metathese von $BiMe_2Cl$ mit $AgSbF_6$ in guten Ausbeuten. Die gelbe Verbindung zeigt Absorptionen im Bereich des sichtbaren Lichts, wobei die Anregungen zu einer Population eines bismut-zentrierten Molekülorbitals mit starkem p-Orbitalcharakter ausgehend von einem σ(Bi–C)-Orbitals führen. Die Synthese von Lewis-Basen-Addukten ausgehend von **21** gelang mit einer

Reihe an neutralen Donor-Liganden, wobei lediglich das Pyridin-Addukt eine ausreichend hohe Stabilität für eine Isolierung und vollständige Charakterisierung zeigte (Schema 9).

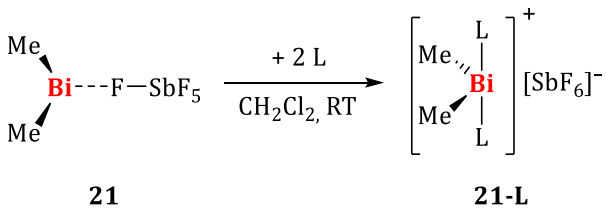

21 **21-L**

L = Pyridin, thf, Benzaldehyd

Schema 9. Synthese von Lewis-Basen-Addukten von **21**.

Neben dem Hexafluoroantimonat-Salz konnten die ersten Vertreter von Bismut-Kationen mit Cyanoborat-Anionen hergestellt und charakterisiert werden. Im Gegensatz zum SbF_6-Salz können in den farblosen Cyanoborat-Verbindungen hinreichend flüchtige neutrale Donoren durch Trocknung im Vakuum entfernt werden, sodass, trotz der Synthese in THF oder Pyridin, die Lösungsmittel-freien Kontaktionenpaare erhalten werden. Durch geeignete Wahl des $[BH_n(CN)_{4-n}]$-Anions kann die Stärke der Kation-Anion-Wechselwirkung laut DFT Rechnungen gesteuert werden.

Ausgehend von **21** gelang durch Umsetzung mit $BiMe_3$ die Synthese von **39**, der ersten dinuklearen Bismutspezies mit dativer Bi→Bi Wechselwirkung (Schema 10).

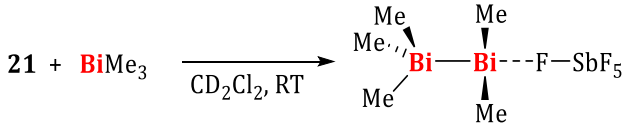

39

Schema 10. Darstellung der ersten dinuklearen Bismutverbindung mit dativer Bi→Bi Wechselwirkung.

39 zeigt in Lösung einen auf der NMR Zeitskala schnellen Austausch der Methylliganden. Durch Tieftemperatur-NMR-spektroskopischen Untersuchungen und Linienformanalyse konnten die thermodynamischen Parameter für den Methylaustausch erhalten werden, welche durch DFT Rechnungen bestätigt werden konnten. Mechanistisch wird angenommen, dass die beiden Bismutfragmente in **39** zunächst dissoziieren, und im nachfolgenden elektrophilen Angriff einer $[BiMe_2]^+$-Einheit an einer Methylgruppe eines $BiMe_3$-Moleküls ein Strukturmotiv der Art Bi–(μ_2-CH_3)–Bi mit verbrückender trigonal-planarer Methyleinheit gebildet wird. Die verbrückende Methyleinheit ist nach den erhaltenen DFT Ergebnissen sp^2-hybridisiert, wodurch diese Reaktion das erste Beispiel darstellt, in dem der Methylaustausch in einem homoleptischen

Hauptgruppenmetallkomplex über eine S_E2-(Rück)Reaktion, das elektrophile Pendant einer S_N2-Reaktion, verläuft.

Analoge Versuche mit den Phenylderivaten [$Ph_2Bi(SbF_6)$] und $BiPh_3$ führten ebenfalls zum Erhalt einer Verbindung, die einen schnellen Phenylaustausch in Lösung zeigt, allerdings konnte diese nicht isoliert und weiter charakterisiert werden. Tieftemperatur-NMR-spektroskopische Untersuchungen an dieser Verbindung zeigten, dass der Phenylaustausch auch bei Temperaturen von –80 °C für eine ^{1}H NMR-spektroskopische Signalseparierung nicht ausreichend gehemmt wurde. Weitere Untersuchungen zum elektronischen und sterischen Einfluss der Liganden auf die Bildung und Stabilität von Spezies mit dativer Bi→Bi-Wechselwirkung sind jedoch sinnvoll und lohnenswert.

CO-Insertion an einem kationischen Bismutamid. Im Rahmen von Untersuchungen an kationischen Bismutamiden innerhalb unserer Arbeitsgruppe gelang es bei Umsetzung von **40** mit CO einen Vertreter einer bisher nicht bekannten Substanzklasse, ein kationisches Bismutcarbamoyl (**41**), durch CO Insertion darzustellen (Schema 11).

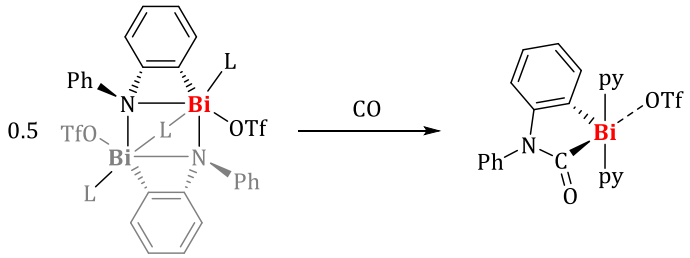

40 **41**

Schema 11. CO-Insertion an einem kationischen Bismutamid (**40**). L = thf

Unter Freisetzung von Ringspannung reagiert **40** unter milden Reaktionsbedingungen mit CO und zu CO isoelektronischen Isocyaniden, wobei beim berechneten Mechanismus für die CO-Insertion von einer schrittweisen CO-Assoziation an das Bismutzentrum unter Bildung eines Lewis-Säure/Base-Addukts, mit nachfolgender Insertion, ausgegangen wird. Die IR-spektroskopische Reaktionsverfolgung stimmte mit den theoretischen Ergebnissen überein. Das Insertionsprodukt **41** zeigt unter cyclovoltammetrischen Bedingungen einen chemisch reversiblen Redoxprozess, wodurch *in situ* (reversibel) ein Bismutradikal gebildet wird.

Lewis-basen-freies, organometallisches Bismutiniden. Durch kontrollierte thermische Homolyse ausgehend von $BiMe_3$ konnte die Spezies Bi(I)Me spektroskopisch und massenspektrometrisch in der Gasphase nachgewiesen werden. Das so generierte BiMe zeigt, als erstes bisher bekanntes metallorganisches Bismutiniden, laut DFT und Multi-Referenz Berechnungen einen Triplett-Grundzustand. Außerdem konnte im Rahmen dieser Arbeit die homolytische Bindungsdissoziationsenergie von $Me_2Bi–CH_3$ auf 210 ± 7 kJ · mol^{-1} beziffert

werden, was den in der Literatur bis dato angenommenen Wert um 15% übersteigt. Es konnte außerdem gezeigt werden, dass transient auftretendes BiMe in der präparativen Chemie unter Standardlaborbedingungen eine Rolle spielen kann, sodass in Zukunft $BiMe_3$ als geeignetes Substrat zur Einführung von „BiMe“-Fragmenten dienen könnte. EPR-spektroskopische Untersuchungen bestätigten die Freisetzung von radikalischen Spezies aus $BiMe_3$ bei 60 °C in Lösung. In Zukunft sollen geeignete Vorläufermoleküle BiR_3 gewählt werden, um den elektronischen und sterischen Einfluss der Substituenten R auf die Bildung von organometallischen Lewis-basen-freien Bismutinidenen und deren elektronischer Struktur zu untersuchen. EPR-spektroskopische und präparative Untersuchungen mit den leichteren Pnictogenverbindungen $AsMe_3$ und $SbMe_3$ deuten auf eine geringere Reaktivität hinsichtlich einer homolytischen $Me_2E–CH_3$ (E = As, Sb) Bindungsspaltung hin. Weitere spektroskopische und theoretische Untersuchungen an den leichteren Homologen stehen aus.

XVII Experimental

1 General Considerations

Due to the air- and moisture-sensitive nature of the compounds used and synthesized, all experiments were carried out using standard Schlenk techniques under a dry argon atmosphere (Argon 5.0) or in gloveboxes from *MBraun*, *Inert* or *GS Glovebox Systemtechnik*, unless specified otherwise. Due to the high toxicity of thallium and mercury compounds, reactions involving these were carried out in the glovebox whenever possible, and contaminated consumables were collected and disposed separately. Contaminated glassware was washed with aqueous HCl prior to the standard cleaning procedure. Experiments with SbF_5 were carried out in a glovebox and all equipment used was subsequently quenched in an aqueous $Ca(OH)_2$ ice bath. All solvents were dried over suitable drying agents (*n*-pentane and *n*-hexane over NaK-alloys, ethanol over sodium/diethyl phthalate, difluorobenzene and acetonitrile over molecular sieves 4 Å or 3 Å, benzene and toluene over sodium, diethyl ether and tetrahydrofuran over Na/benzophenone or K/benzophenone, dichloromethane and chloroform over P_2O_5), distilled under an argon atmosphere and stored over molecular sieves. Deuterated solvents (tetrahydrofuran-d_8, benzene-d_6, dichloromethane-d_2, chloroform-d_1, pyridine-d_5, acetonitrile-d_3) were degassed in three freeze-pump-thaw cycles and stored over 4 Å or 3 Å molecular sieves.

1.1 Analytical Methods

Unless stated otherwise, **NMR spectra** were recorded at room temperature (approximately 23 °C) on the following Bruker devices: *Avance 300* spectrometer, an *Avance 400* spectrometer or an *Avance 500* spectrometer. Either the residual proton signal of the solvent or the solvent signal itself was used for locking ^{1}H and $^{13}C\{^{1}H\}$ NMR spectra. The chemical shifts are provided in ppm using the following external standards: $SiMe_4$ (^{1}H, ^{13}C), $[BF_3 \cdot OEt_2]$ (^{11}B), $CFCl_3$ (^{19}F), $Al(NO_3)_3$ (^{27}Al), $SiMe_4$ in $CDCl_3$ (^{29}Si), 85% H_3PO_4 (^{31}P), $SeMe_2$ plus 5% C_6D_6 (^{77}Se) and $TeMe_2$ plus 5% C_6D_6 (^{125}Te). NMR resonances were assigned using standard 2D NMR experiments, and unless stated otherwise, ^{13}C and ^{31}P NMR spectra were recorded ^{1}H decoupled.

Elemental analyses (C, H, N, S) were obtained by means of combustion and gas chromatographic analysis on a *Carlo-Erba* or *Leco* instrument.

UV-vis measurements were performed under an inert gas atmosphere (glovebox) in quartz glass cuvettes (10 mm) on a *UV5 Mettler Toledo UV-vis Excellence* or a *JASCO-V600* spectrometer.

EPR spectroscopic experiments were carried out on a Bruker X-band spectrometer (9.38 GHz; *ELEXSYS E580 CW/FT*), which is equipped with an *Oxford Instruments* helium cryostat (*ESR900*) and a *MercuryiTC* temperature controller. Spectra were recorded using 0.2 mW or 0.4 mW

microwave power and 0.5 G field modulation at 100 kHz. The softwares *MATLAB 8.0* and *EasySpin 4.5.1 toolbox* were used for simulations.

IR spectra were recorded either in solution or in pure substance on *a JASCO FT/IR-6200 type A spectrometer* using a cuvette equipped with a KBr window.

Photochemical experiments were carried out under a mercury vapor lamp of the type *LOT Quantum Design LSB740* (I = 19 A, U = 26 V, 400–500 W) with IR filters irradiating at 210–600 nm, in a *MPDSBasic photonCABINET* photoreactor from *KARLBIEDEN*, equipped with *photoLAB LED* radiation sources of wavelengths 365 (Φ_e = 43.2 W), 460 (Φ_e = 26.6–45.0 W), 525 (Φ_e = 9.0–15.2 W) and 625 nm (Φ_e = 12.2–20.0 W). *thermoCONTROL 100* functions as the cooling unit. All experiments were carried out using borosilicate glassware. Further experiments were carried out with *Avance* LED lamps (P = 3 W) at wavelength maxima of 400 nm, 455 nm or 525 nm.

Cyclic voltammetry was performed on a *Gamry Instruments Reference 600* potentiostat. For this purpose, a standard three-electrode construction was employed using a platinum disk working electrode, a platinum wire counter electrode, and a silver wire, separated by a *Vycor* membrane, serving as the reference electrode. The ferrocene/ferrocenium redox couple was used as an internal standard for referencing the measured potential. Tetra-*n*-butylammonium hexafluorophosphate ([nBu$_4$N][PF$_6$], 0.1 M) was used as the electrolyte. Experiments were carried out under an argon atmosphere in a glovebox at ambient temperature.

Melting points were determined on an *OptiMelt* apparatus from *SRS* with a heating rate of 10 °C · min^{-1}.

GCMS data were recorded on an *Agilent 7890A* gas chromatograph (column: HP-5MS 5% methylphenylsiloxane, 27 cm, Ø 0.25 mm, film: 0.25 µm; injector: 250 °C; oven: 40 °C (8 min), 20 °C to 280 °C (5 min); He (1.5 mL · min^{-1})) equipped with an *Agilent 5975C* mass detector with triple-axis detector and a FID detector in EI mode.

High-resolution mass spectrometry was carried out on an *Exactive Plus* HRMS device with an Orbitrap detector from *Thermo-Scientific* using the ionization method specified.

Crystal data were collected either with a *Bruker Apex II* diffractometer with CCD area detector and a multi-mirror monochromator or with a *Bruker D8-QUEST* diffractometer with CCD area detector and multi-mirror monochromator using Mo$_{K\alpha}$ radiation (λ = 0.71073 Å). The respective solid-state structures were solved using intrinsic phase methods (*ShelXT*), refined with the *ShelX* software package and developed using Fourier techniques.[250–252] All non-hydrogen atoms were refined anisotropically. Hydrogen atoms were assigned to idealized positions or, if possible, found directly. The crystallographic data used in the publications were deposited with the Cambridge Crystallographic Data Center (CCDC) and are available at

https://www.ccdc.cam.ac.uk/structures. The images of the solid-state structures were created with the *Mercury* software.

DFT calculations were carried out with the *Gaussian* program,[103] with 6-31G(d, p)[78] (H, B, C, N, O, F, P, S, Cl) or LanL2DZ[108–110] (Co, Se, Sb, Te, Os, Tl, Bi) as the basis sets used, as well as the B3LYP and CAM-B3LYP functionals.[104] The D3 version of the Grimme dispersion model with the original D3 damping function was used.[106] Frequency analyses of the reported structures showed no imaginary frequencies for ground states and exactly one imaginary frequency for transition states. Thermodynamic parameters were calculated at a temperature of 298.15 K and a pressure of 1.00 atm. NBO analyses were carried out with the *NBO 7* program version.[177]

2 Synthesis and Characterization

The following numbering scheme was used for reporting NMR chemical shifts for bismepine compounds:

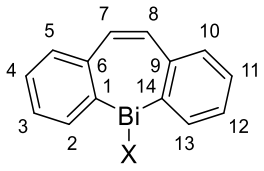

2.1 Experimental Part for Chapter V

Reaction of 2-iodo-2-methyl-6-heptene with 1 or 10 mol% [$Ph_2Bi\{Mn(CO)_5\}$] (1) as catalyst.

The reaction was carried out as described in the literature.[72]

10 mol%: After 5 h at ambient temperature the consumption of the starting material and the formation of 2-(iodomethyl)-1,1-dimethylcyclopentane was observed with a yield of 91% (determined by GCMS analysis).

1 mol%: After 2 d at ambient temperature the full consumption of the starting material was observed. ^{1}H and ^{13}C NMR spectroscopic analyses of the reaction mixture indicate the formation of 3-iodo-1,1-dimethylcyclohexane as the main product with a yield of 90%, besides the formation of 2-(iodomethyl)-1,1-dimethylcyclopentane (10%, determined by GCMS and ^{1}H NMR spectroscopic analyses).

^{1}H and ^{13}C NMR spectroscopic analyses of the main product:

^{1}H NMR (500 MHz, $CDCl_3$): δ = 0.91 (s, 3H, 8-CH_3), 0.91 (s, 3H, 9-CH_3), 1.20 (m, 1H, 5-CH_2), 1.45–1.51 (m, 3H, 4,5-CH_2), 1.82 (m, 1H, 6-CH_2), 1.87 (m, 1H, 2-CH_2), 2.14 (m, 1H, 2-CH_2), 2.41 (m, 1H, 6-CH_2), 4.36 (m, 1H, 1-CHI) ppm.

^{13}C NMR (126 MHz, $CDCl_3$): δ = 24.09 (s, 8/9-CH_3), 24.95 (s, 4-CH_2), 28.55 (s, 1-CHI), 32.99 (s, 8/9-CH_3), 35.22 (s, 3-$C(CH_3)_2$), 37.91 (s, 5-CH_2), 40.67 (s, 6-CH_2), 53.64 (s, 2-CH_2) ppm.

Reaction of 3 with 2,5-di-*tert*-butyl-1,4-benzoquinone. 2,5-Di-*tert*-butyl-1,4-benzoquinone (3.10 mg, 14.0 µmol) was added to a solution of **3** (8.60 mg, 14.0 µmol) in benzene-d_6 (0.5 mL). The orange solution turned yellow. After 3.5 h at 60 °C the reaction mixture was stirred at ambient temperature for 2 d. The obtained green suspension was filtered, leading to a colorless filtrate. The filtrate was layered with *n*-pentane (0.5 mL). After 2 d at ambient temperature small amounts of a crystalline solid of **4** were obtained by filtration and characterized by X-ray diffraction analysis.

Reaction of 3 with Ph_4Bi_2. Ph_4Bi_2 (11.7 mg, 16.0 µmol) was added to a solution of **3** (10.0 mg, 16.0 µmol) in toluene (0.5 mL). The reaction mixture was stirred for 30 min, filtered and the filtrate was layered with *n*-pentane (1 mL). After 1 d at –30 °C a red crystalline solid was obtained by filtration and dried *in vacuo*. The product was identified as **5** by X-ray diffraction analysis.[77] A yield was not determined.

[($C_{14}H_{10}$)Bi{$Mn(CO)_5$}] (9). In a J. Young NMR tube **8-Cl** (15.0 mg, 35.5 µmol) and $Na(thf)_3[Mn(CO)_5]$ (15.4 mg, 35.5 µmol) were dissolved in benzene-d_6 (0.5 mL). The brown suspension was frozen at 0 °C and after the addition of THF-d_8 (0.1 mL) the suspension was allowed to warm to ambient temperature. Insoluble materials were removed by filtration and the brownish-red filtrate was analyzed by ^{1}H and ^{13}C NMR spectroscopy, revealing the selective formation of one new species. Isolation of **9** did not succeed due to decomposition during work-up.

^{1}H NMR (300 MHz, C_6D_6/THF-d_8, 5:1): δ = 6.61 (s, 2H, 7,8-CH), 6.97 (ddd, 2H, $^4J_{HH}$ = 1.4 Hz, $^3J_{HH}$ = 7.2 Hz, $^3J_{HH}$ = 7.3 Hz, 4,11-C_6H_4), 7.07 (ddd, 2H, $^4J_{HH}$ = 1.4 Hz, $^3J_{HH}$ = 7.4 Hz, $^3J_{HH}$ = 7.6 Hz, 3,12-C_6H_4), 7.27 (dd, 2H, $^4J_{HH}$ = 1.4 Hz, $^3J_{HH}$ = 7.4 Hz, 2,13-C_6H_4), 7.58 (dd, 2H, $^4J_{HH}$ = 1.4 Hz, $^3J_{HH}$ = 7.3 Hz, 5,10-C_6H_4) ppm.

^{13}C NMR (75 MHz, C_6D_6): δ = 128.06 (s, 3,12-C_6H_4, overlap with solvent resonance), 128.57 (s, 4,11-C_6H_4), 133.85 (s, 2,13-C_6H_4), 134.44 (s, 7,8-CH), 137.63 (s, 5,10-C_6H_4), 146.20 (s, 6,9-C_6H_4), 203.99 (s, br, CO) ppm.

Note: The ^{13}C resonance for the C-1 and C-14 atoms was neither detected in the ^{13}C NMR spectrum, nor in ^{1}H, ^{13}C HMBC experiments. This was ascribed to the high quadrupole moment of the ^{209}Bi nucleus (100%, I = 9/2, quadrupole moment Q = $-0.4 \cdot 10^{-28} \cdot m^{-2}$), which broadens the

resonances of atoms bonded to the Bi center to such an extent that they may not be observable under standard conditions.

[($C_{14}H_{10}$)Bi{$Fe(CO)_2Cp$}] (10). A solution of Na(thf)[$FeCp(CO)_3$] (35.6 mg, 130 µmol) in THF (2.5 ml) was added to a solution of **8-Cl** (54.9 mg, 130 µmol) in THF (2.5 ml) at –78 °C in small portions. After stirring for 30 min at –78 °C the reaction mixture was allowed to warm up to ambient temperature and stirred for a further 30 min. All volatiles were removed under reduced pressure and the residue was extracted with toluene (6 mL) and filtered. The filtrate was layered with *n*-pentane (7 mL). After 3 d at –30 °C **10** was obtained as a dark red solid by filtration and dried *in vacuo*. Yield: 46.0 mg, 80.0 µmol, 63%.

^{1}H NMR (400 MHz, C_6D_6): δ = 4.06 (s, 5H, Cp), 6.91 (s, 2H, 7,8-CH), 7.09–7.13 (m, 4H, 3,12-C_6H_4, 4,11-C_6H_4), 7.25–7.28 (m, 2H, 5,10-C_6H_4), 8.13 (dd, 2H, $^4J_{HH}$ = 1.8 Hz, $^3J_{HH}$ = 7.1 Hz, 2,13-C_6H_4) ppm.

^{13}C NMR (101 MHz, C_6D_6): δ = 83.30 (s, Cp), 127.30 (s, 4,11-C_6H_4), 129.72 (s, 3,12-C_6H_4), 130.65 (s, 5,10-C_6H_4), 134.56 (s, 7,8-CH), 135.41 (s, br, 1,14-C_6H_4), 139.04 (s, 2,13-C_6H_4), 144.72 (s, 6,9-C_6H_4), 212.49 (s, CO) ppm.

IR (neat): $\tilde{\nu}_{CO}$ = 1972 (s), 1926 (s) cm^{-1}.

UV-vis (THF): λ_{max} = 362 nm, onset at 450 nm.

Elemental analysis: Anal. calc. (%) for $C_{21}H_{15}BiFeO_2$ (564.17 g · mol^{-1}): C 44.71, H 2.68; found: C 45.10, H 2.73.

[{κ^2*C*,κ^1*Bi*-($C_{14}H_{10}$)Bi}Fe(CO)Cp] (11). A solution of **10** (20.0 mg, 34.5 µmol) in benzene-d_6 (0.5 mL) was irradiated (525 nm) for 5 h. Small amounts of black, insoluble solid were removed by filtration and the obtained dark red solution was layered with *n*-pentane (1 mL). After 16 h at –30 °C **11** was obtained as a dark red, crystalline solid by filtration and dried *in vacuo*. Yield: 11.0 mg, 19.9 µmol, 58%.

^{1}H NMR (400 MHz, C_6D_6): δ = 3.88 (s, 5H, Cp), 4.66 (d, 1H, $^3J_{HH}$ = 10.5 Hz, 7-CH), 5.03 (d, 1H, $^3J_{HH}$ = 10.5 Hz, 8-CH), 6.77 (dd, 1H, $^3J_{HH}$ = 7.2 Hz, $^3J_{HH}$ = 7.3 Hz, 12-C_6H_4), 6.75–7.00 (m, 3H, 3-C_6H_4, 4,11-C_6H_4), 7.16 (m, 1H, 5-C_6H_4, overlap with solvent signal), 7.48 (d, 1H, $^3J_{HH}$ = 7.6 Hz, 10-C_6H_4), 7.76 (d, 1H, $^3J_{HH}$ = 7.2 Hz, 13-C_6H_4), 7.87 (d, 1H, $^3J_{HH}$ = 7.3 Hz, 2-C_6H_4) ppm.

^{13}C NMR (101 MHz, C_6D_6): δ = 69.66 (s, 7-CH), 73.53 (s, 8-CH), 81.30 (s, Cp), 125.27 (s, 4-C_6H_4), 125.85 (s, 12-C_6H_4), 126.00 (s, 3-C_6H_4), 126.29 (s, 11-C_6H_4), 128.73 (s, 10-C_6H_4), 130.31 (s, br, 1-C_6H_4), 132.08 (s, 5-C_6H_4), 132.48 (s, br, 14-C_6H_4) 135.41 (s, 2-C_6H_4), 137.00 (s, 13-C_6H_4), 153.34 (s, 6-C_6H_4), 158.43 (s, 9-C_6H_4), 220.22 (s, CO) ppm.

IR (neat): $\tilde{\nu}_{CO}$ = 1930 (s) cm^{-1}.

UV-vis (THF): λ_{max} = 353 nm.

Elemental analysis: Anal. calc. (%) for $C_{20}H_{15}BiFeO$ (536.16 g · mol^{-1}): C 44.80, H 2.82; found: C 44.60, H 2.71.

[{($C_{14}H_{10}$)Bi}$_2$Fe(CO)$_4$] (12). A suspension of $Na_2Fe(CO)_4$ (5.1 mg, 23.7 µmol) in THF (2 mL) was added dropwise to a solution of chloro-bismepine **8-Cl** (20.0 mg, 47.4 µmol) in THF (2 mL). The reaction mixture was stirred for 2 h at ambient temperature, after which all volatiles were removed under reduced pressure. The residue was extracted with toluene (3 x 1 mL) and filtered. The filtrate was layered with *n*-pentane and stored at –30 °C. After 16 h **12** was isolated as a red, crystalline solid by filtration and dried *in vacuo*. Yield: 11.8 mg, 12.5 µmol, 53%.

^{1}H NMR (400 MHz, C_6D_6): δ = 6.66 (s, 4H, 7,8-C_2H_2), 7.00 (dd, 4H, $^3J_{HH}$ = 7.6 Hz, $^3J_{HH}$ = 7.5 Hz, 4,11-C_6H_4), 7.07 (dd, 4H, $^3J_{HH}$ = 7.5 Hz, $^3J_{HH}$ = 7.1 Hz, 3,12-C_6H_4), 7.30 (d, 4H, $^3J_{HH}$ = 7.6 Hz, 5,10-C_6H_4), 7.55 (d, 4H, $^3J_{HH}$ = 7.1 Hz, 2,13-C_6H_4) ppm.

^{13}C NMR (101 MHz, C_6D_6): δ = 127.70 (s, 3,12-C_6H_4), 133.98 (s, 2,13-C_6H_4), 134.34 (s, 5,10-C_6H_4), 137.45 (s, 4,11-C_6H_4), 139.56 (s, 7,8-C_2H_2), 146.09 (s, 6,9-C_6H_4), 152.57 (s, 1,14-C_6H_4), 244.56 (s, CO) ppm.

Elemental analysis: Anal. calc. (%) for [$C_{32}H_{20}Bi_2FeO_4$] (942.31 g · mol^{-1}): C 40.79, H 2.14; found: C 40.92, H 2.19.

IR (neat): $\tilde{\nu}_{CO}$ = 2040 (s), 1981 (w), 1961 (s), 1933 (w) cm^{-1}.

UV-vis (THF): λ_{max} = 362 nm, onset at ca. 450 nm.

[($C_{14}H_{10}$)Bi{Co(CO)$_4$}] (13). 8-Cl (15.0 mg, 35.5 µmol) and Na[Co(CO)$_4$] (6.90 mg, 35.5 µmol) were dissolved in benzene-d_6 (0.5 mL) and THF-d_8 (0.1 mL). The obtained suspension was filtered. Due to decomposition during work-up, **13** was only characterized in solution.

^{1}H NMR (500 MHz, C_6D_6/THF-d_8, 5:1): δ = 6.72 (s, 2H, 7,8-CH), 7.06 (dd, 2H, $^3J_{HH}$ = 7.7 Hz, $^3J_{HH}$ = 7.3 Hz, 4,11-C_6H_4), 7.20 (d, 2H, $^3J_{HH}$ = 7.5 Hz, 5,10-C_6H_4), 7.27 (dd, 2H, $^3J_{HH}$ = 7.3 Hz, $^3J_{HH}$ = 7.5 Hz, 3,12-C_6H_4), 8.47 (d, 2H, $^3J_{HH}$ = 7.7 Hz, 2,13-C_6H_4) ppm.

^{13}C NMR (126 MHz, C_6D_6/THF-d_8, 5:1): δ = 131.17 (s, 3,12-C_6H_4), 132.25 (s, 7,8-C_6H_4), 133.10 (s, 5,10-C_6H_4), 138.66 (s, 4,11-C_6H_4), 142.43 (s, 2,13-CH), 151.40 (s, 6,9-C_6H_4), 200.99 (s, CO) ppm.

The carbon atoms corresponding to 1,14-C_6H_4 were not observed in the ^{13}C NMR spectrum due to quadrupole broadening caused by the ^{209}Bi nucleus.

IR (THF): $\tilde{\nu}_{CO}$ = 2075 (s), 2036 (w), 2019 (s), 1989 (s) cm^{-1}.

UV-vis (THF): λ_{max} = 369 nm, onset at 510 nm.

[{κ²*C*,κ¹*Bi*-($C_{14}H_{10}$)Bi}$Co(CO)_3$] (14). A suspension of **8-Cl** (20.0 mg, 47.3 µmol) and Na[$Co(CO)_4$] (9.20 mg, 47.3 µmol) in a mixture of toluene/THF (0.7 mL, 1:0.05) was irradiated (525 nm) for 45 h. The suspension was filtered and the filtrate was layered with *n*-pentane (1.5 mL). After 16 h at –30 °C **14** was obtained by filtration and dried *in vacuo*. Yield: 10.0 mg, 18.3 µmol, 39%.

^{1}H NMR (500 MHz, C_6D_6): δ = 5.11 (s, 2H, 7,8-CH), 6.95 (m, 4H, 3,12-C_6H_4, 4,11-C_6H_4), 7.31 (d, 2H, $^3J_{HH}$ = 7.5 Hz, 5,10-C_6H_4), 7.39 (d, 2H, $^3J_{HH}$ = 7.1 Hz, 2,13-C_6H_4) ppm.

^{13}C NMR (126 MHz, C_6D_6): δ = 75.60 (s, 7,8-CH), 126.50 (s, 4,11-C_6H_4), 127.55 (s, 3,12-C_6H_4), 131.64 (s, 5,10-C_6H_4), 134.08 (s, 2,13-C_6H_4), 147.66 (s, br, 1,14-C_6H_4), 154.64 (s, 6,9-C_6H_4), 207.00 (s, br, CO) ppm.

Elemental analysis: Anal. calc. (%) for $C_{17}H_{10}O_3CoBi$ (530.17 g · mol^{-1}): C 38.51, H 1.90; found: C 38.41, H 2.05.

IR (neat): $\tilde{\nu}_{CO}$ = 2003 (s) cm^{-1}.

UV-vis (THF): λ_{max} = 346 nm, onset at 420 nm.

[($C_{14}H_{10}$)Bi{$Co(CO)_3$(PPh_3)}] (13-PPh_3). A solution of PPh_3 (10.6 mg, 0.04 mmol) and Na[$Co(CO)_4$] (7.8 mg, 40.3 µmol) in THF (2.0 mL) was added dropwise to a solution of **8-Cl** (17.0 mg, 40.3 µmol) in THF (1 mL) at –78 °C. After 30 min at –78 °C the reaction mixture was stirred for a further 15 min at ambient temperature. All volatiles were removed under reduced pressure and the residue was extracted with toluene (6 mL) and filtered. The filtrate was layered with *n*-pentane (6 mL). After 3 d at –30 °C **13-PPh_3** was isolated by filtration as an orange solid and dried *in vacuo*. Yield: 18.4 mg, 22.8 µmol, 58%.

^{1}H NMR (400 MHz, C_6D_6): δ = 6.87 (s, 2H, 7,8-CH), 6.99–7.07 (m, 9H, *para*-PPh_3, *meta*-PPh_3), 7.09 (ddd, 2H, $^4J_{HH}$ = 1.2 Hz, $^3J_{HH}$ = 7.3 Hz, $^3J_{HH}$ = 7.6 Hz, 4,11-C_6H_4), 7.24 (d, 2H, $^3J_{HH}$ = 7.6 Hz, 5,10-C_6H_4), 7.32 (ddd, 2H, $^4J_{HH}$ = 1.2 Hz, $^3J_{HH}$ = 7.3 Hz, $^3J_{HH}$ = 7.9 Hz, 3,12-C_6H_4), 7.64–7.72 (m, 6H, *ortho*-PPh_3), 8.92 (d, 2H, $^3J_{HH}$ = 7.9 Hz, 2,13-C_6H_4) ppm.

^{13}C NMR (101 MHz, C_6D_6): δ = 127.22 (s, 4,11-C_6H_4), 128.99 (d, $^3J_{PC}$ = 10.2 Hz, *meta*-PPh_3), 130.36 (s, 5,10-C_6H_4), 130.74 (d, $^4J_{PC}$ = 3.0 Hz, *para*-PPh_3), 131.45 (s, 3,12-C_6H_4), 133.55 (d, $^2J_{PC}$ = 11.3 Hz, *ortho*-PPh_3), 133.98 (s, 7,8-CH), 135.13 (d, $^1J_{PC}$ = 44.3 Hz, *ipso*-PPh_3), 139.54 (s, 2,13-C_6H_4), 143.36 (s, 6,9-C_6H_4), 145.38 (s, br, 1,14-C_6H_4) 201.61 (d, $^2J_{PC}$ = 16.9 Hz, CO) ppm.

^{31}P NMR (121 MHz, C_6D_6): δ = 68.22 (s, PPh_3) ppm.

IR (neat): $\tilde{\nu}_{CO}$ = 1927 (s), 1944 (s), 2010 (w) cm^{-1}.

UV-vis (THF): λ_{max} = 382 nm, onset at 480 nm.

Elemental analysis: Anal. calc. (%) for $C_{35}H_{25}BiCoO_3P$ (792.47 g · mol^{-1}): C 53.05, H 3.18; found: C 53.05, H 3.09.

[{κ²*C*,κ¹*Bi*-($C_{14}H_{10}$)Bi}Co(CO)$_2$(PPh$_3$)] (14-PPh$_3$). A solution of **13-PPh$_3$** (34.8 mg, 40.0 µmol) in benzene-d_6 was irradiated (455 nm) for 5 h. Small amounts of a black, insoluble precipitate were removed by filtration and the yellow filtrate was layered with *n*-pentane (2 mL) and stored at ambient temperature. After 16 h **14-PPh$_3$** was isolated as an orange solid by filtration and dried *in vacuo*. Yield: 16.3 mg, 20.0 µmol, 50%.

^{1}H NMR (300 MHz, C_6D_6): δ = 4.60 (d, 2H, $^3J_{HP}$ = 7.0 Hz, 5,6-CH), 6.94–7.01 (m, 13H, *para*-PPh_3, 3,8-C_6H_4, 2,9-C_6H_4, *meta*-PPh_3), 7.33–7.36 (m, 2H, 4,7-C_6H_4), 7.59–7.66 (m, 6H, *ortho*-PPh_3), 7.70–7.73 (m, 2H, 1,10-C_6H_4) ppm.

^{13}C NMR (126 MHz, C_6D_6): δ = 76.24 (s, 7,8-CH), 126.35 (d, $^4J_{PC}$ = 12.1 Hz, 4,11-C_6H_4), 128.62 (s, 3,12-C_6H_4) 128.94 (d, $^3J_{PC}$ = 9.4 Hz, *meta*-PPh_3), 130.18 (s, 5,10-C_6H_4), 130.51 (d, $^4J_{PC}$ = 2.2 Hz, *para*-PPh_3), 133.51 (s, 2,13-C_6H_4), 133.94 (d, $^2J_{PC}$ = 10.7 Hz, *ortho*-PPh_3), 135.09 (d, $^1J_{PC}$ = 1.2 Hz, *ipso*-PPh_3), 143,11 (s, br, 1,14-C_6H_4), 156.79 (d, $^3J_{PC}$ = 5.7 Hz, 6,9-C_6H_4), 205.15 (s, br, CO) ppm.

^{31}P NMR (121 MHz, C_6D_6): δ = 73.94 (s) ppm.

Elemental analysis: Anal. calc. (%) for $H_{25}CoBiC_{34}O_2P$ (764.45 g · mol^{-1}): C 53.42, H 3.30; found: C 53.71, H 3.34.

IR (neat): $\tilde{\nu}_{CO}$ = 1975 (s), 1923 (s) cm^{-1}.

UV-vis (THF): λ_{max} = 360 nm, 435 nm.

[($C_{14}H_{10}$)Bi{Co(CO)$_3$(PCy$_3$)}] (13-PCy$_3$). A brown solution of PCy_3 (28.4 mg, 100 µmol) and Na[Co(CO)$_4$] (18.3 mg, 94.6 µmol) in THF (1.5 mL) was added to a colorless solution of **8-Cl** (40.0 mg, 94.6 µmol) in THF (1.5 mL) at –78 °C. The dark red suspension was stirred for 2 h at –78 °C, then for 15 h at ambient temperature. All volatiles were removed under reduced pressure. The residue was extracted with toluene (3.0 mL), filtered and the filtrate was layered with *n*-pentane (3 mL). **13-PCy$_3$** was obtained as an orange solid after 16 h at –30 °C, filtered and dried *in vacuo*. Yield: 25.0 mg, 30.8 µmol, 32%.

^{1}H NMR (400 MHz, C_6D_6): δ = 1.08–1.20 (m, 9H, PCy_3), 1.49–1.57 (m, 9H, PCy_3), 1.71 (m, 6H, PCy_3), 2.01–2.10 (m, 9H, PCy_3), 6.89 (s, 2H, 7,8-C_2H_2), 7.11 (dd, 2H, $^3J_{HH}$ = 7.6 Hz, $^3J_{HH}$ = 8.1 Hz, 4,11-C_6H_4), 7.25 (d, 2H, $^3J_{HH}$ = 7.6 Hz, 5,10-C_6H_4), 7.39 (dd, 2H, $^3J_{HH}$ = 7.4 Hz, $^3J_{HH}$ = 8.1 Hz, 3,12-C_6H_4), 8.90 (d, 2H, $^3J_{HH}$ = 7.4 Hz, 2,13-C_6H_4) ppm.

^{13}C NMR (101 MHz, C_6D_6): δ = 26.57 (d, $^4J_{PC}$ = 1.2 Hz, 4-CH_2, PCy_3), 27.78 (d, $^2J_{PC}$ = 10.2 Hz, 2,6-CH_2, PCy_3), 30.46 (s, 3,5-CH_2, PCy_3), 37.74 (d, $^1J_{PC}$ = 18.6 Hz, 1-CH, PCy_3), 127.18 (s, 3,12-C_6H_4), 130.23 (s, 2,13-C_6H_4), 131.23 (s, 5,10-C_6H_4), 134.08 (s, 4,11-C_6H_4), 139.22 (s, 7,8-C_2H_2), 143.48 (d, $^4J_{PC}$ = 1.0 Hz, 6,9-C_6H_4), 144.09 (s, 1,14-C_6H_4), 202.95 (s, CO) ppm.

^{31}P NMR (162 MHz, C_6D_6): δ = 78.55 (s, PCy_3) ppm.

IR (neat): $\tilde{\nu}_{CO}$ = 1998 (w), 1932 (s), 1913 (s) cm^{-1}.

UV-vis (THF): λ_{max} = 369 nm, onset at ca. 430 nm.

Elemental analysis: Anal. calc. (%) for $C_{35}H_{43}BiCoO_3P$ (810.61 g · mol^{-1}): C 51.86, H 5.35; found: C 50.60, H 6.48.[8]

[{κ^2*C*,κ^1*Bi*-($C_{14}H_{10}$)Bi}Co(CO)$_2$(PCy_3)] (14-PCy_3). A solution of **13-PCy_3** (13.0 mg, 16.0 µmol) in benzene-d_6 (1 mL) was irradiated (360 nm) for 7.5 h. The suspension was filtered. **14-PCy_3** was obtained as yellow needles after 16 h at ambient temperature by slow evaporation of the solvent and dried *in vacuo*. Yield: 10.0 mg, 12.7 µmol, 79%.

^{1}H NMR (400 MHz, C_6D_6): δ = 0.98–1.19 (m, 9H, PCy_3), 1.35–1.50 (m, 6H, PCy_3), 1.49–1.55 (m, 3H, PCy_3), 1.60–1.72 (m, 6H, PCy_3), 1.77–1.89 (m, 3H, PCy_3), 2.01 (m, 6H, PCy_3), 5.24 (d, 2H, $^3J_{HP}$ = 5.6 Hz, 7,8-C_2H_2), 6.98 (dd, $^3J_{HH}$ = 6.9 Hz, 2H, $^3J_{HH}$ = 7.3 Hz, 4,11-C_6H_4), 7.08 (dd, 2H, $^3J_{HH}$ = 6.9 Hz, $^3J_{HH}$ = 7.3 Hz, 3,12-C_6H_4), 7.63 (d, 2H, $^3J_{HH}$ = 7.3 Hz, 5,10-C_6H_4), 7.74 (d, 2H, $^3J_{HH}$ = 6.9 Hz, 2,13-C_6H_4) ppm.

^{1}H NMR (400 MHz, $CDCl_3$): δ = 1.29 (m, 9H, PCy_3), 1.46 (m, 6H, PCy_3), 1.76 (s, br, 3H), 1.90 (m, 9H, PCy_3), 2.02 (m, 6H, PCy_3), 4.96 (d, 2H, $^3J_{HP}$ = 5.7 Hz, 7,8-C_2H_2), 7.03 (ddd, 2H, $^4J_{HH}$ = 1.3 Hz, $^3J_{HH}$ = 7.2 Hz, $^3J_{HH}$ = 7.3 Hz, 4,11-C_6H_4), 7.09 (ddd, 2H, $^4J_{HH}$ = 1.3 Hz, $^3J_{HH}$ = 7.5 Hz, $^3J_{HH}$ = 6.9 Hz, 3,12-C_6H_4), 7.42 (dd, 2H, $^4J_{HH}$ = 0.7 Hz, $^3J_{HH}$ = 6.4 Hz, 5,10-C_6H_4), 7.73 (dd, 2H, $^4J_{HH}$ = 1.1 Hz, $^3J_{HH}$ = 6.9 Hz, 2,13-C_6H_4) ppm.

^{13}C NMR (101 MHz, C_6D_6): δ = 26.52 (s, 4-CH_2, PCy_3), 28.00 (d, $^2J_{PC}$ = 9.4 Hz, 2,6-CH_2, PCy_3), 30.07 (s, 3,5-CH_2, PCy_3), 36.27 (d, $^1J_{PC}$ = 13.4 Hz, 1-CH, PCy_3), 72.57 (s, 7,8-C_2H_2), 125.59 (s, 4,11-C_6H_4), 125.92 (s, 3,12-C_6H_4), 129.31 (s, 5,10-C_6H_4), 134.80 (s, 2,13-C_6H_4), 143.17 (s, 1,14-C_6H_4), 157.37 (s, 6,9-C_6H_4), 205.83 (s, CO) ppm.

^{13}C NMR (101 MHz, $CDCl_3$): δ = 26.60 (s, 4-CH_2, PCy_3), 27.99 (d, $^2J_{PC}$ = 9.5 Hz, 2,6-CH_2, PCy_3), 30.37 (s, 3,5-CH_2, PCy_3), 36.53 (d, $^1J_{PC}$ = 13.1 Hz, 1-CH, PCy_3), 73.36 (s, 7,8-C_2H_2), 126.16 (s, 4,11-C_6H_4), 126.41 (s, 3,12-C_6H_4), 129.57 (s, 5,10-C_6H_4), 135.28 (s, 2,13-C_6H_4), 143.79 (s, 1,14-C_6H_4), 157.69 (s, 6,9-C_6H_4), 205.83 (s, CO) ppm.

[8] The elemental analysis obtained does not conform to scientific requirements.

^{31}P NMR (162 MHz, C_6D_6): δ = 68.49 (s, PCy_3) ppm.

^{31}P NMR (162 MHz, $CDCl_3$): δ = 68.11 (s, PCy_3) ppm.

IR (neat): $\tilde{\nu}_{CO}$ = 1969 (s), 1933 (s) cm^{-1}.

UV-vis (THF): λ_{max} = 350 nm, 430 nm.

Elemental analysis: Anal. calc. (%) for $C_{34}H_{43}BiCoO_2P$ (782.60 g · mol^{-1}): C 52.18, H 5.54; found: C 53.69, H 5.59.[9]

[($C_{14}H_{10}$)Bi{Co(CO)(*t*BuNC)}] (13-*t*BuNC). To a suspension of **8-Cl** (72.0 mg, 170 µmol) and Na[$Co(CO)_4$] (32.7 mg, 170 µmol) in a mixture of toluene (3 mL) and THF (0.5 mL) was added *tert*-butylisonitrile (14.1 mg, 19.1 µL, 170 µmol). After 1 h the dark red suspension was filtered and the filtrate was layered with *n*-pentane (3 mL). After 16 h at –30 °C **13-*t*BuNC** was obtained as a red solid by filtration and dried *in vacuo*. Yield: 64.3 mg, 105 µmol, 62%.

^{1}H NMR (400 MHz, C_6D_6): δ = 0.59 (s, 9H, CH_3), 6.78 (s, 2H, 7,8-C_2H_2), 7.06 (dd, 2H, $^3J_{HH}$ = 7.1 Hz, $^3J_{HH}$ = 7.8 Hz, 4,11-C_6H_4), 7.16–7.24 (m, 4H, 3,12-C_6H_4, 5,10-C_6H_4), 8.82 (d, 2H, $^3J_{HH}$ = 7.3 Hz, 2,13-C_6H_4) ppm.

^{13}C NMR (101 MHz, C_6D_6): δ = 29.39 (s, CH_3), 57.20 (s, $C(CH_3)_3$), 127.22 (s, 3,12-C_6H_4), 130.28 (s, 2,13-C_6H_4), 131.59 (s, 5,10-C_6H_4), 133.66 (s, 4,11-C_6H_4), 139.58 (s, 7,8-C_2H_2), 142.86 (s, 6,9-C_6H_4), 146.70 (s, 1,14-C_6H_4), 150.80 (s, NC), 203.67 (s, CO) ppm.

IR (neat): $\tilde{\nu}_{CO/NC}$ = 2167 (s, NC), 1984 (w, CO), 1934 (s, CO), 1923 (s, CO) cm^{-1}.

UV-vis (THF): λ_{max} = 362 nm, onset at ca. 450 nm.

Elemental analysis: Anal. calc. (%) for $C_{22}H_{19}BiCoNO_3$ (613.31 g · mol^{-1}): C 43.08, H 3.12, N 2.28; found: C 43.13, H 3.09, N 2.24.

[{κ^2*C*,κ^1*Bi*-($C_{14}H_{10}$)Bi}$Co(CO)_2$(*t*BuNC)] (14-*t*BuNC). A solution of **13-*t*BuNC** (30.0 mg, 48.9 µmol) in benzene-d_6 (1 mL) was irradiated (360 nm) for 2.5 h. The suspension was filtered and the filtrate was layered with *n*-pentane (1 mL). **14-*t*BuNC** was obtained as yellow needles after 16 h at ambient temperature by filtration and dried *in vacuo*. Yield: 21.2 mg, 36.2 µmol, 74%.

^{1}H NMR (400 MHz, C_6D_6): δ = 0.70 (s, 9H, CH_3), 5.44 (s, 2H, 7,8-C_2H_2), 6.93–7.02 (m, 4H, 4,11-C_6H_4; 3,12-C_6H_4), 7.55 (s, br, 2H, 5,10-C_6H_4), 7.63 (d, 2H, $^3J_{HH}$ = 6.3 Hz, 2,13-C_6H_4) ppm.

[9] The elemental analysis obtained does not conform to scientific requirements.

^{13}C NMR (101 MHz, C_6D_6): δ = 29.80 (s, CH_3), 57.19 (s, $C(CH_3)_3$), 74.53 (s, 7,8-C_2H_2), 126.15 (s, 3,12-C_6H_4), 126.42 (s, 4,10-C_6H_4), 130.48 (s, 5,10-C_6H_4), 134.81 (s, 2,13-C_6H_4), 142.71 (s, 1,14-C_6H_4), 156.68 (s, 6,9-C_6H_4), 162.21 (s, br, NC), 203.35 (s, CO) ppm.

IR (neat): $\tilde{\nu}_{CO/NC}$ = 2163 (s, NC), 1983 (s, CO), 1930 (s, CO) cm^{-1}.

UV-vis (THF): λ_{max} = 338 nm, onset at ca. 450 nm.

Elemental analysis: Anal. calc. (%) for $C_{21}H_{19}BiCoNO_2$ (585.30 g · mol^{-1}): C 43.09, H 3.27, N 2.3; found: C 43.22, H 3.43, N 2.17.

[($C_{14}H_{10}$)Bi{Co(CO)$_2$(*t*BuNC)(PCy_3)}] (15). Neat PCy_3 (7.19 mg, 25.6 µmol) was added to a solution of **14-*t*BuNC** (15.0 mg, 25.6 µmol) in benzene-d_6 (0.7 mL). After 3 h at 60 °C the obtained dark red suspension was filtered and the filtrate was layered with hexamethyldisiloxane (1.0 mL). After 16 h at ambient temperature **15** was obtained by filtration and dried *in vacuo*. Yield: 15.0 mg, 17.3 µmol, 68%.

^{1}H NMR (400 MHz, C_6D_6): δ = 0.50 (s, 9H, CH_3), 1.18–1.30 (m, 9H, PCy_3), 1.65–1.71 (m, 9H, PCy_3), 1.81 (m, 6H, PCy_3), 2.10–2.15 (m, 3H, PCy_3), 2.19–2.24 (m, 6H, PCy_3), 6.90 (s, 2H, 7,8-C_2H_2), 7.14 (ddd, 2H, $^4J_{HH}$ = 1.3 Hz, $^3J_{HH}$ = 7.4 Hz, $^3J_{HH}$ = 7.7 Hz, 4,11-C_6H_4), 7.24 (dd, 2H, $^4J_{HH}$ = 1.3 Hz, $^3J_{HH}$ = 7.7 Hz, 5,10-C_6H_4), 7.30 (ddd, 2H, $^4J_{HH}$ = 1.3 Hz, $^3J_{HH}$ = 7.3 Hz, $^3J_{HH}$ = 7.4 Hz, 3,12-C_6H_4), 8.95 (dd, 2H, $^4J_{HH}$ = 1.2 Hz, $^3J_{HH}$ = 7.4 Hz, 2,13-C_6H_4) ppm.

^{13}C NMR (101 MHz, C_6D_6): δ = 26.48 (s, 4-CH_2, PCy_3), 27.70 (d, $^2J_{PC}$ = 10.1 Hz, 2,6-CH_2, PCy_3), 29.02 (s, CH_3), 30.21 (s, 3,5-CH_2, PCy_3), 37.25 (d, $^1J_{PC}$ = 17.0 Hz, 1-CH, PCy_3), 54.98 (s, $C(CH_3)_3$), 126.13 (s, 3,12-C_6H_4), 29.05 (s, 2,13-C_6H_4), 130.11 (s, 5,10-C_6H_4), 134.12 (s, 4,11-C_6H_4), 139.95 (s, 7,8-C_2H_2), 142.63 (s, br, 1,14-C_6H_4), 143.51 (s, 6,9-C_6H_4), 154.83 (s, br, NC), 204.24 (d, $^2J_{PC}$ = 14.6 Hz, CO) ppm.

^{31}P NMR (162 MHz, C_6D_6): δ = 83.60 (s, PCy_3) ppm.

IR (neat): $\tilde{\nu}_{CO/NC}$ = 2116 (s, NC), 1932 (s, CO), 1881 (s, CO) cm^{-1}.

UV-vis (THF): λ_{max} = 340 nm, onset at ca. 430 nm.

Elemental analysis: Anal. calc. (%) for $C_{39}H_{52}BiCoNO_2P$ (865.74 g · mol^{-1}): C 54.11, H 6.05, N 1.62; found: C 54.14, H 5.84, N 1.49.

[{κ^2*C*,κ^1*Bi*-($C_{14}H_{10}$)Bi}Co(CO)(*t*BuNC)(PCy_3)] (16). A solution of **15** (15.0 mg, 17.3 µmol) in benzene-d_6 (0.5 mL) was irradiated at a wavelength of 365 nm for 12 h. The reaction mixture was analyzed by ^{1}H and ^{31}P NMR spectroscopy. All volatiles were removed under reduced pressure and the residue was dissolved in 1,2-difluorobenzene (0.5 mL) and layered with *n*-pentane (0.5 mL). After 3 d at –30 °C small amounts of a crystalline solid were obtained by filtration, with

crystals suitable for X-ray diffraction analysis. Since it was not possible to isolate **16** completely, a yield was not determined.

[{κ²*C*,κ¹*Bi*-($C_{14}H_{10}$)Bi}Co(CO)(*t*BuNC)((*S*)-Monophos)] (17). (*S*)-Monophos (17.7 mg, 48.9 µmol) and THF (0.1 mL) were added to a solution of **13-*t*BuNC** (30.0 mg, 48.9 µmol) in benzene (1.0 mL). After the end of gas evolution (1 h), the reaction mixture was irradiated at a wavelength of 365 nm for 7 h. The reaction mixture was filtered and the filtrate was layered with *n*-pentane. After 16 d at ambient temperature small amounts of a crystalline, yellow solid were obtained by filtration, which were suitable for X-ray diffraction analysis. Since it was not possible to isolate **17** completely, a yield was not determined.

Reaction of 11 with HOTf. Iron complex **11** (10.0 mg, 18.6 µmol) was dissolved in benzene (0.5 mL). A large amount of dark solid instantly precipitated after the addition of HOTf (2.8 mg, 18.6 µmol). The suspension was filtered and the solid was re-dissolved in THF (1 mL), whereby small amounts of black solid remained insoluble. The THF phase was layered with *n*-pentane (1 mL) and after 16 h at –30 °C $[Fe(thf)_4(OTf)_2]$ was obtained by filtration and dried *in vacuo*. Yield: 5.1 mg, 8.0 µmol, 86%.

Reaction of 11 with MeOTf. Iron complex **11** (10.0 mg, 18.6 µmol) was dissolved in benzene-d_6 (0.5 mL) and MeOTf (3.1 mg, 18.6 µmol) was added. After 4 h at ambient temperature a precipitate formed and the ^{1}H NMR spectrum showed an incomplete conversion of starting material **11**. The reaction mixture was heated to 60 °C for 5.5 h, after which an almost complete consumption (90%) of **11** was observed by ^{1}H NMR spectroscopy. The suspension was filtered and the solid was re-dissolved in THF (1 mL), whereby small amounts of black solid remained insoluble. The filtrate was layered with *n*-pentane and after 16 h at ambient temperature a crystalline solid was obtained, which was identified as **11** by single-crystal X-ray diffraction analysis. The mother liquor was layered with *n*-pentane (1 mL) and after 16 h at–30 °C a dark solid was obtained by filtration, which could not be analyzed due to the small amount of material.

Reaction of 14-PPh_3 with I_2. 14-PPh_3 (8.0 mg, 10.2 µmol) was dissolved in toluene (3 mL) and cooled to −78 °C. I_2 (0.01 M in toluene, 1.0 mL, 10.0 µmol) was added to the solution and the reaction mixture was slowly warmed up to ambient temperature. The suspension was filtered and the filtrate was layered with *n*-pentane (3 mL). After 16 h at –30 °C a yellow solid had precipitated, which was identified as **8-I** by ^{1}H NMR spectroscopy.[82]

Reaction of 14 with $CoCp_2^*$. Cobalt complex **14** (10.0 mg, 19.0 µmol) and $CoCp_2^*$ (6.2 mg, 19.0 µmol) were dissolved in benzene (0.5 mL) and the reaction mixture stirred at ambient temperature for 2 h. The reaction mixture was filtered and the filtrate was layered with *n*-pentane (1 mL). The residue was extracted with THF, filtered and the filtrate was layered with *n*-pentane (1 mL). After 16 h at −30 °C black crystals were isolated from the THF phase by filtration and drying the solid *in vacuo*. X-ray diffraction analysis revealed the formation of $[CoCp_2^*][Co(CO)_4]$. Yield: 11.0 mg, 21.0 µmol, quantitative.

Reaction of 14 with AgOTf. Cobalt complex **14** (4.2 mg, 7.9 µmol) and AgOTf (2.1 mg, 7.9 µmol) were dissolved in benzene (0.5 mL). A gray precipitate formed instantly. The reaction mixture was filtered after 1 h at ambient temperature and the filtrate was layered with *n*-pentane (1 mL). The residue was extracted with THF, filtered, whereby small amounts of black solid remained insoluble and the filtrate layered with *n*-pentane (1 mL). After 16 h at −30 °C a yellow-gray solid crystallized out from both phases, which was identified as a mixture of phenanthrene and compound **14** in a 2:1 molar ratio in both cases according to ^{1}H NMR spectroscopy.

Reaction of 14-PPh_3 with S_8. Cobalt complex **14-PPh_3** (5.0 mg, 6.50 µmol) and S_8 (0.1 mg, 0.81 µmol) were dissolved in benzene-d_6 (0.5 mL) and the reaction mixture was heated to 60 °C for 16 h. The black insoluble precipitate was removed by filtration from the green suspension. The filtrate was layered with *n*-pentane (1.5 mL) and stored at ambient temperature. After 3 d an orange solid (**18**) had precipitated, which was isolated by filtration and dried *in vacuo*. A yield was not determined.

^{1}H NMR (400 MHz, C_6D_6): δ = 6.64 (s, 4H, 7,8-CH), 7.25–7.28 (m, 4H, C_6H_4), 7.25–7.28 (m, 4H, C_6H_4), 8.98 (d, 4H, $^3J_{HH}$ = 8.0 Hz, C_6H_4) ppm.

One resonance in the ^{1}H NMR spectroscopic experiment was not visible because of the presence of overlapping resonances from at least two by-products, one of which is non-coordinating PPh_3 according to ^{1}H NMR spectroscopy.

Reaction of 17 with S_8. The chelate complex **17** (10 mg, 12 µmol) was dissolved in benzene (0.5 mL). 100 µL of a S_8 solution (0.12 M in benzene, 0.30 mg, 12 µmol) were added to this solution, the reaction mixture turning black after two minutes. 50% conversion to an unknown product was determined by ^{31}P NMR spectroscopy. Another 150 µL of the S_8 solution (0.12 M in benzene, 0.45 mg, 18 µmol) were added. Complete conversion was determined by ^{31}P NMR spectroscopy,

so that the reaction mixture was filtered and the filtrate was layered with *n*-pentane (1 mL). The isolation of a product did not succeed.

Table 6. Summary of other attempts to synthesize **7**.

Entry	starting material	reagents	reaction conditions	result
1	(*Z*)-1,2-bis-(2-bromphenyl)ethene	Zn (6.5 eq.), $CoBr_2$(0.14 eq.), allylchloride (0.34 eq.), $BiCl_3$ (0.67 eq.)	THf, r.t.	phenanthrene
2	(*Z*)-1,2-bis-(2-bromphenyl)ethene	Zn (6.5 eq.), $CoBr_2$(0.14 eq.), allylchloride (0.34 eq.), $BiCl_3$ (0.67 eq.)	MeCN, –40 °C	phenanthrene
3	(*Z*)-1,2-bis-(2-bromphenyl)ethene	Bi metal, TMSCl (5%), LiI (0.13 eq.)	THF, r.t.	no reaction
4	(*Z*)-1,2-bis-(2-bromphenyl)ethene	Bi metal, TMSCl (5%), LiI (0.13 eq.)	THF, 70 °C	no reaction

Table 7. Reactions of bismepine species with transition metal complexes.

Entry	precursor	transition metal complex	reaction conditions	result
1	**7**	$[Cr(CH_3CN)_3(CO)_3]$	benzene, r.t.	no reaction
2	**7**	$[Cr(C_6H_6)(CO)_3]$	400 nm, r.t.	broad ^{1}H NMR spectrum, no products isolated
3	**7**	$[W(CO)_6]$	THF/MeCN, *hν*	conversion to unknown compound
4	**7**	$[W(CO)_3(CH_3CN)_3]$	several[a]	recovery of **7**
5	**7**	$[Fe(CO)_5]$	a) *hν*, 1 h, THF b) 7, THF, r.t.	recovery of **7**
6	**7**	$[FeCp_2Cl]$	benzene/THF, r.t.	**8-Cl**
7	**7**	$[ClRh(CO)_2]_2$	benzene, 60 °C, 5 d	recovery of **7**
8	**7**	$[Rh(coe)_2Cl]_2$	several[a]	recovery of **7**
9	**7**	$[Rh(P\textit{i}Pr_3)_2(N_2)Cl]$	benzene, r.t.	recovery of **7,** $Rh(Cl)_2(PiPr_3)_2$
10	**7**	$[Ni(cod)_2]$	benzene/THF, r.t.	recovery of **7**
11	**7**	Pd(II)acetate	benzene, r.t.	phenanthrene
12	**7**	$[Pd(CH_3CN)_4][BF_4]$	DCM, 50 min, 60 °C	**8-Cl**
13	**7**	$[Pt(nbe)_3]$	several[a]	recovery of **7**
14	**7**	$[Pt(PCy_3)_2]$	toluene, –78 °C	color change, decomposition
15	**7**	CuCl	several[a]	recovery of **7**
16	**7**	AgOTf	benzene, 80 °C, 5 d	phenanthrene, **8-OTf**
17	**7**	$AuCl(SMe_2)$	benzene, r.t.	phenanthrene, **8-Cl**
18	**7**	$AuCl(PPh_3)$	benzene, 60 °C	recovery of **7**
19	**8-Cl**	$Mo(CO)_3(CH_3CN)_3$	benzene, r.t.	**7**
20	**8-Cl**	$[W(CO)_6]$	a) *hν*, 1 h, THF b) THF, r.t.	phenanthrene, recovery of **8-Cl**
21	**8-Cl**	$[Mn(CO)_5]_2$	several[a]	recovery of **8-Cl**
22	**8-Cl**	$[Fe(CO)_2Cp]_2$	several[a]	phenanthrene, **7**
23	**8-Cl**	$[Co(CO)_4]_2$	several[a]	phenanthrene, **7**
24	**8-Cl**	$[Rh(P\textit{i}Pr_3)_2(N_2)Cl]$	benzene, r.t.	recovery of **8-Cl**
25	**8-Cl**	$[Pt(PCy_3)_2]$	benzene, r.t.	decomposition
26	**8-Cl**	$AuCl(SMe_2)$	benzene, r.t.	phenanthrene
27	**8-Cl**	$AuCl(PPh_3)$	benzene/THF, 60 °C	gold mirror, recovery of **8-Cl**

hν: irradiation with a mercury vapor lamp. a. If no reaction was observed at ambient temperature, several conditions were applied one after another: 60 °C, 80 °C, *hν* (400 nm), *hν* (Hg vapor lamp).

2.2 Experimental Part for Chapter VIII

19-Cl. Route A. $MeBiCl_2$ (10 mg, 33.9 µmol) and Tl[BArF^{24}] (72.4 mg, 67.8 µmol) were dissolved in pyridine (1.5 mL). A precipitate formed and was removed by filtration. The filtrate was layered with toluene (2 mL) and after 3 d at –30 °C a colorless crystalline solid had precipitated, which was isolated by filtration and dried *in vacuo*. Yield: 26 mg, 16.8 µmol, 50%.

Route B. $BiCl_3$ (50.0 mg, 0.16 mmol) was added to a solution of Tl[BArF^{24}] (0.16 g, 0.16 mmol) in pyridine (1.5 mL). The precipitate was removed by filtration and the filtrate was layered with *n*-pentane (2 mL). After 16 h at –30 °C a colorless solid was isolated by filtration and dried *in vacuo*. Yield: 0.17 g, 0.11 mmol, 70%.

^{1}H NMR (400 MHz, CD_2Cl_2): δ = 7.48 (m, 10H, *meta*-C_5H_5N), 7.55 (s, br, 4H, *para*-BArF^{24}), 7.72 (s, br, 8H, *ortho*-BArF^{24}), 7.93 (t, 5H, $^3J_{HH}$ = 6.1 Hz, *para*-C_5H_5N), 8.76 (d, 10H, $^3J_{HH}$ = 4.8 Hz, *ortho*-C_5H_5N) ppm.

^{11}B NMR (128 MHz, CD_2Cl_2): δ = –6.6 (s, BArF^{24}) ppm.

^{13}C NMR (100 MHz, CD_2Cl_2): δ = 117.87 (m, *para*-$C_6H_3(CF_3)_2$), 124.98 (q, $^3J_{CF}$ = 272.2 Hz, CF_3), 125.96 (s, *meta*-C_5H_5N), 129.27 (quartquart, $^2J_{CF}$ = 31.6 Hz, $^4J_{CF}$ = 2.7 Hz, *meta*-(3,5-$C_6H_3(CF_3)_2$), 135.18 (s, br, *ortho*-$C_6H_3(CF_3)_2$), 139.77 (s, *para*-C_5H_5N), 147.84 (s, *ortho*-C_5H_5N), 162.20 (q, $^1J_{BC}$ = 49.9 Hz, *ipso*-$C_6H_3(CF_3)_2$) ppm.

^{19}F NMR (376 MHz, CD_2Cl_2): δ = –62.9 (s, CF_3) ppm.

Elemental analysis: Anal. calc. for $C_{32}H_{12}BBiCl_2F_{24}(py)_{4.5}$ (1497.67 g · mol^{-1}): C 43.67, H 2.32, N 4.20; found: C 43.35, H 2.52, N 4.36.[10]

19-Br. $BiBr_3$ (50.0 mg, 0.11 mmol) was added to a solution of Tl[BArF^{24}] (0.11 g, 0.11 mmol) in pyridine (1.5 mL). The precipitate was removed by filtration and the filtrate was layered with *n*-pentane (2 mL). After 16 h at –30 °C a colorless solid was isolated by filtration and dried *in vacuo*. Yield: 0.12 g, 98.3 µmol, 86%.

^{1}H NMR (400 MHz, CD_2Cl_2): δ = 7.45 (m, 10H, *meta*-C_5H_5N), 7.55 (s, br, 4H, *para*-BArF^{24}), 7.72 (s, br, 8H, *ortho*-BArF^{24}), 7.91 (t, 5H, $^3J_{HH}$ = 6.1 Hz, *para*-C_5H_5N), 8.95 (d, 10H, $^3J_{HH}$ = 4.9 Hz, *ortho*-C_5H_5N) ppm.

^{11}B NMR (128 MHz, CD_2Cl_2): δ = –6.6 (s, BArF^{24}) ppm.

[10] The pyridine donor ligands can be partially removed *in vacuo*.

^{13}C NMR (100 MHz, CD_2Cl_2): δ = 117.82 (m, *para*-$C_6H_3(CF_3)_2$), 124.95 (q, $^3J_{CF}$ = 271.8 Hz, CF_3), 126.37 (s, *meta*-C_5H_5N), 129.27 (quartquart, $^2J_{CF}$ = 31.5 Hz, $^4J_{CF}$ = 2.8 Hz, *meta*-(3,5-$C_6H_3(CF_3)_2$), 135.15 (s, br, *ortho*-$C_6H_3(CF_3)_2$), 140.10 (s, *para*-C_5H_5N), 148.42 (s, *ortho*-C_5H_5N), 162.11 (q, $^1J_{BC}$ = 48.9 Hz, *ipso*-$C_6H_3(CF_3)_2$) ppm.

^{19}F NMR (376 MHz, CD_2Cl_2): δ = −62.9 (s, CF_3) ppm.

Elemental analysis: Anal. calc. for $C_{32}H_{12}BBiBr_2F_{24}(py)_{4.0}$ (1546.42 g · mol^{-1}): C 40.34, H 2.08, N 3.62; found: C 40.69, H 1.82, N 3.50.[11]

19-I. BiI_3 (50.0 mg, 84.7 µmol) was added to a solution of Tl[BArF^{24}] (87.5 mg, 84.7 µmol) in pyridine (1.0 mL). The precipitate was removed by filtration and the filtrate was layered with *n*-pentane (2 mL). After 16 h at –30 °C an orange solid was isolated by filtration and dried *in vacuo*. Yield: 0.12 g, 72.0 µmol, 85%.

^{1}H NMR (400 MHz, CD_2Cl_2): δ = 7.36 (m, 10H, *meta*-C_5H_5N), 7.55 (s, br, 4H, *para*-BArF^{24}), 7.72 (s, br, 8H, *ortho*-BArF^{24}), 7.87 (t, 5H, $^3J_{HH}$ = 7.7 Hz, *para*-C_5H_5N), 8.88 (d, 10H, $^3J_{HH}$ = 3.4 Hz, *ortho*-C_5H_5N) ppm.

^{11}B NMR (128 MHz, CD_2Cl_2): δ = −6.6 (s, BArF^{24}) ppm.

^{13}C NMR (100 MHz, CD_2Cl_2): δ = 117.86 (m, *para*-$C_6H_3(CF_3)_2$), 124.97 (q, $^3J_{CF}$ = 272.5 Hz, CF_3), 126.05 (s, *meta*-C_5H_5N), 129.25 (quartquart, $^4J_{CF}$ = 2.3 Hz, $^2J_{CF}$ = 29.2 Hz, *meta*-(3,5-$C_6H_3(CF_3)_2$), 135.18 (s, br, *ortho*-$C_6H_3(CF_3)_2$), 139.02 (s, *para*-C_5H_5N), 150.41 (s, *ortho*-C_5H_5N), 162.64 (q, $^1J_{BC}$ = 50.6 Hz, *ipso*-$C_6H_3(CF_3)_2$) ppm.

^{19}F NMR (376 MHz, CD_2Cl_2): δ = −62.9 (s, CF_3) ppm.

Elemental analysis: Anal. calc. (%) for $C_{32}H_{12}BBiI_2F_{24}(py)_{3.5}$ (1602.87 g · mol^{-1}): C 37.09, H 1.86, N 3.06; found: C 37.33, H 2.12, N 2.91.[12]

Reaction of $BiCl_3$ with $SePMe_3$. $BiCl_3$ (54.2 mg, 0.17 mmol) and $SePMe_3$ (40.0 mg, 0.26 mmol) were suspended in methanol (3 mL) and stored at ambient temperature for 16 h without stirring. The black precipitate was removed by filtration and the yellow filtrate dried *in vacuo*. The residue was extracted with THF (4 mL) to give a colorless solution after filtration. Layering the solution with *n*-pentane (4 mL) led to a yellow coloration at the interface. Yellow crystals of $BiCl_3(SePMe_3)_n$

[11] The pyridine donor ligands can be partially removed *in vacuo*.

[12] The pyridine donor ligands can be partially removed *in vacuo*.

(n = 2, 3) were obtained after 1 d at –30 °C, which were isolated by filtration and dried *in vacuo*. Yield: 58 mg, 92.9 µmol, 72%.[13]

Material suitable for single-crystal X-ray diffraction analyses of several samples revealed the formation of $BiCl_3(SePMe_3)_2$ and $BiCl_3(SePMe_3)_3$. A composition ratio was not determined.

In methylene chloride solution, the product decomposes completely after 2 d at 60 °C.

^{1}H NMR (500 MHz, CD_2Cl_2): δ = 1.94 (d, 9H, $^2J_{PH}$ = 13.3 Hz, PMe_3) ppm.

^{1}H{^{31}P} NMR (500 MHz, CD_2Cl_2): δ = 1.90 (s with satellites, 9H, $^3J_{SeH}$ = 65.0 Hz, PMe_3) ppm.

^{13}C NMR (126 MHz, CD_2Cl_2): δ = 1.90 (d, 9H, $^1J_{CP}$ = 49.2 Hz, PMe_3) ppm.

^{31}P{^{1}H} NMR (202 MHz, CD_2Cl_2): δ = 9.43 (d, $^1J_{SeP}$ = 338.1 Hz, $SePMe_3$) ppm.

^{77}Se NMR (100 MHz, CD_2Cl_2): δ = –44.2 (s, br, detected via ^{1}H, ^{77}Se HMBC experiments) ppm.

21-benzaldehyde. 21 (85.6 mg, 180 µmol) was dissolved in DCM (2 mL) and benzaldehyde (38.2 mg, 360 µmol, 36.4 µl) was added. The colorless solution was layered with *n*-pentane (2 mL). After 1 d at –30 °C **21-benzaldehyde** was obtained as a colorless crystalline solid by filtration and dried *in vacuo*. Yield: 79 mg, 0.12 mmol, 63%.

^{1}H NMR (500 MHz, CD_2Cl_2): δ = 2.03 (s, 6H, CH_3), 7.63 (t, 4H, $^3J_{HH}$ = 7.87 Hz, H3/H5), 7.82 (t, 2H, $^3J_{HH}$ = 7.47 Hz, H4), 8.00 (d, 4H, $^3J_{HH}$ = 7.01 Hz, H2/C6), 9.96 (s, 2H, CHO) ppm.

^{13}C NMR (126 MHz, CD_2Cl_2): δ = 53.14 (CH_3), 129.56 (s, C3/C5), 131.57 (s, C2/C6), 135.42 (s, C4), 136.99 (s, C1), 198.47 (s, CHO) ppm.

^{19}F NMR (470 MHz, CD_2Cl_2): δ = –121.9 (s, SbF_6) ppm.

Elemental analysis: Anal. calc. (%) for $C_{16}H_{18}BiF_6O_2Sb$ (687.05 g · mol^{-1}): C 27.97, H 2.62, found: C 27.99, H 2.62.

Melting point: 115 °C.

21-MeCN. **21** (20.0 mg, 42.1 µmol) was dissolved in DCM (2 mL) and MeCN (3.40 mg, 84.2 µmol, 4.43 µl) was added. The colorless solution was layered with *n*-pentane (2 mL). After 1 d at –30 °C **21-MeCN** was obtained as a colorless crystalline solid by filtration. The solid started to melt after 5 min at ambient temperature. Yield: 14 mg, 27.1 µmol 64%.

^{1}H NMR (400 MHz, CD_2Cl_2): δ = 1.75 (s, 6H, MeCN), 2.25 (s, br, 6H, $BiMe_2$) ppm.

[13] The yield is based on the assumption that only $BiCl_3(SePMe_3)_2$ was present.

21-thf. **21** (20.0 mg, 42.1 µmol) was dissolved in DCM (2 mL) and THF (6.10 mg, 84.2 µmol, 6.86 µl) was added. The colorless solution was layered with *n*-pentane (2 mL). After 1 d at –30 °C **21-thf** was obtained as a colorless crystalline solid by filtration. The solid started to melt after 5 min at ambient temperature. Yield: 10.0 mg, 16.2 µmol 38%.

^{1}H NMR (400 MHz, CD_2Cl_2): δ = 1.87 (s, 6H, CH_3), 1.97(m, 4H, β-thf), 3.89 (m, 4H, α-thf) ppm.

^{13}C NMR (101 MHz, CD_2Cl_2): δ = 26.11 (s, β-thf), 48.73 (s, br, $BiMe_2$), 72.11 (s, α-thf) ppm.

^{19}F NMR (376 MHz, CD_2Cl_2): δ = –132.0 ppm.

ESI-MS (THF): positive mode (%): calc. for $[Me_2Bi]^+$, *m/z* = 239.0268; found *m/z* = 239.0268 (20), negative mode, calculated for $[SbF_6]^-$: *m/z* = 239.8948, found *m/z* = 239.8942 (100).

$[BiMeF(py)_3]_2[SbF_6]_2$ (22). Storing the contact ion pair **21** as a solid at ambient temperature for several days led to a discoloration. Dissolving this solid with pyridine and layering the colorless solution with *n*-pentane led to the formation of small amounts of a crystalline material, which was suitable for single-crystal X-ray diffraction analysis and revealed the formation of **22**. A yield was not determined due to insufficient amounts of material. However, several repeats of this experiment led to the isolation of **21-py** in nearly quantitative yield.

Dimethylbismuth dicyanodihydridoborate (23-DHB). A solution of $Cs[BH_2(CN)_2]$ (10.8 mg, 54.6 µmol) in THF (1.5 mL) was added to a solution of $BiMe_2Cl$ (15.0 mg, 54.6 µmol) in THF (1 mL). After the addition of methylene chloride (0.5 mL) the precipitate was removed by filtration and the filtrate was layered with *n*-pentane (2 mL). After 16 h at –30 °C colorless crystals of **23-DHB** were obtained by filtration and dried *in vacuo*. Yield: 16.0 mg, 52.5 µmol, 96%.

^{1}H{^{11}B} NMR (500 MHz, THF-d_8): δ = 1.22 (s, 2H, $BH_2(CN)_2$), 1.51 (s, 6H, CH_3) ppm.

^{1}H NMR (500 MHz, THF-d_8): δ = 1.22 (q, br, 2H, $^{2}J_{BH}$ = 97.9 Hz, $BH_2(CN)_2$), 1.51 (s, 6H, CH_3) ppm.

^{11}B NMR (160 MHz, THF-d_8): δ = –42.1 (t, $^{2}J_{BH}$ = 97.9 Hz, $BH_2(CN)_2$) ppm.

^{11}B{^{1}H} NMR (160 MHz, THF-d_8): δ = –42.1 (s, $BH_2(CN)_2$) ppm.

^{13}C NMR (126 MHz, THF-d_8): δ = 36.46 (s, CH_3), 135.26 (s, br, CN) ppm.

IR (neat): $\tilde{\nu}_{CN/BH}$ = 2393 (s, BH), 2195 (s, CN) cm^{-1}.

Dimethylbismuth tricyanohydridoborate (23-MHB). A solution of $Ag[BH(CN)_3]$ (10.8 mg, 54.6 µmol) in a mixture of THF (1.5 mL) and pyridine (0.2 mL) was added to a solution of $BiMe_2Cl$ (15.0 mg, 54.6 µmol) in THF (1 mL). The precipitate was removed by filtration and the filtrate was

layered with *n*-pentane (2 mL). After 16 h at –30 °C colorless crystals of **23-MHB** were obtained by filtration and dried *in vacuo*. Yield: 13.0 mg, 39.5 µmol, 72%.

^{1}H{^{11}B} NMR (400 MHz, THF-d_8): δ = 1.58 (s, 6H, CH_3), 1.88 (s, 1H, $BH(CN)_3$) ppm.

^{1}H NMR (400 MHz, THF-d_8): δ = 1.58 (s, 6H, CH_3), 1.88 (q, br, 1H, $^{2}J_{BH}$ = 98.0 Hz, $BH(CN)_3$) ppm.

^{11}B NMR (128 MHz, THF-d_8): δ = –39.8 (d, $^{2}J_{BH}$ = 98.0 Hz, $BH(CN)_3$) ppm.

^{11}B{^{1}H} NMR (128 MHz, THF-d_8): δ = –39.8 (s, $BH(CN)_3$) ppm.

^{13}C NMR (100 MHz, THF-d_8): δ = 40.35 (s, CH_3), 127.49 (q, $^{1}J_{BC}$ = 68.4 Hz, CN) ppm.

Table 8. Reactions of organometallic bismuth halides BiR_nX_{3-n} (n = 1, 2) with cyanohydridoborate salts that did not lead to the desired product. Standard work-up: Filtration, layering with *n*-pentane and storage at –30 °C.

Entry	Ct[$BH_n(CN)_{4-n}$]	$R_{3-n}BiX_n$	reaction conditions	result
1	$Ag[BH(CN)_3]$	Ph_2BiCl	i) DCM ii) Et_2O/THF iii) 1,2-DFB, 90 °C	recovery of Ph_2BiCl
2	$Ag[BH(CN)_3]$	Ph_2BiI	DCM, 1,2-DFB, THF, pyridine r.t., 60 °C, 80 °C	no reaction[a,b]
3	$K[BH_2(CN)_2]$	Me_2BiCl	THF, r.t.	no reaction[a,b]
4	$Na[BH_3(CN)]$	Me_2BiCl	1,2-DFB, r.t.	black suspension, unselective reaction[a]
5	$Na[B(CN)_4]$	Me_2BiCl	i) DCM, r.t. ii) THF, r.t.	no reaction[a,b]
6	$Ag[B(CN)_4]$	Me_2BiCl	pyridine, Et_2O, r.t.	formation of a precipitate, isolation of a colorless solid which decomposes after 5 h at r.t. to a black material
7	$Cs[BH_2(CN)_2]$	$MeBiBr_2$	THF, r.t.	yellow precipitate, isolation of yellow solid: containing no methyl group[a]
4	$Ag[BH(CN)_3]$	$MeBiBr_2$	THF/pyridine, r.t.	isolation of a colorless oil, containing no methyl group[a]

Ct = cation. 1,2-DFB = 1,2-difluorobenzene. a: according to ^{1}H NMR spectroscopy. b: the formation of a precipitate (probably CtX, X = Cl, I) did not occur.

[$BiPh_2(SbF_6)$] (25). A solution of $AgSbF_6$ (43.1 mg, 126 µmol) in 1,2-difluorobenzene (2 mL) was added to a solution of $BiPh_2Cl$ (50.0 mg, 126 µmol) in 1,2-difluorobenzene (2 mL). The reaction mixture was stirred for 2 h, then the precipitate was removed by filtration and the light yellow solution was layered with *n*-pentane (5 mL). After 16 h at –30 °C **25** was obtained as a yellow solid by filtration and dried *in vacuo*. Yield: 57.0 g, 95.3 µmol, 76%.

Single crystals of **25** suitable for X-ray diffraction analysis were obtained by layering a solution of **25** in DCM with *n*-pentane and storage at –30 °C for 16 h. Due to the crystals melting at ambient temperature during crystal picking, the X-ray diffraction data obtained is not of a quality sufficient for the discussion of bonding parameters.

The compound decomposes with the formation of benzene when exposed to vacuum for longer periods of time (>2 h, even in silanized glassware). In solution, when exposed to light, the compound decomposes with the formation of biphenyl (~20% decomposition after 6 h). In the dark, a solution of **25** in CD_2Cl_2 is stable for several days.

^{1}H NMR (400 MHz, CD_2Cl_2): δ = 7.63 (t, 2H, $^3J_{HH}$ = 7.3 Hz, *para*-C_6H_5), 8.08 (t, 4H, $^3J_{HH}$ = 7.4 Hz, *meta*-C_6H_5), 8.55 (d, 4H, $^3J_{HH}$ = 7.5 Hz, *ortho*-C_6H_5) ppm.

^{13}C NMR (101 MHz, CD_2Cl_2): δ = 131.34 (s, *para*-C_6H_5), 134.79 (s, *meta*-C_6H_5), 138.76 (s, *ortho*-C_6H_5), 214.76 (s, *ipso*-C_6H_5, detected by ^{1}H, ^{13}C HMBC experiments) ppm.

^{19}F NMR (376 MHz, CD_2Cl_2): δ = –122.2 (s) ppm.

Elemental analysis: Anal. calc. (%) for $C_{12}H_{10}BiSbF_6$ (597.95 g · mol^{-1}): C 24.06, H 1.68, found: C 23.98, H 1.75.

Melting point: 58 °C.

5*H*-Dibenzo[*b,f*]bismepine-5-yl tetrachloroaluminate (8-AlCl$_4$). 8-Cl (6.0 mg, 14.2 µmol) was dissolved in benzene-d_6 (0.4 mL) and aluminum(III)chloride (1.9 mg, 14.3 µmol) was added, yielding a yellow solution. Multinuclear NMR spectroscopic analyses of the reaction mixture showed a complete conversion to **8-AlCl$_4$**. Due to decomposition in the solid state, the product was not isolated.

^{1}H NMR (400 MHz, C_6D_6): δ = 6.31 (s, 2H, 7,8-C_2H_4), 7.01 (dd, 2H, $^3J_{HH}$ = 7.5 Hz, $^3J_{HH}$ = 7.6 Hz, 4,11-C_6H_4), 7.48 (dd, 2H, $^3J_{HH}$ = 7.5 Hz, $^3J_{HH}$ = 7.6 Hz, 3,12-C_6H_4), 7.65 (d, 2H, $^3J_{HH}$ = 7.6 Hz, 5,10-C_6H_4), 8.58 (d, 2H, $^3J_{HH}$ = 7.5 Hz, 2,13-C_6H_4) ppm.

^{13}C NMR (400 MHz, C_6D_6): δ = 129.78 (s, 4,9-C_6H_4), 131.27 (s, 7,8-C_2H_4), 133.97 (s, 3,12-C_6H_4), 136.78 (s, 2,13-C_6H_4), 137.72 (s, 5,10-C_6H_4), 143.24 (s, 6,9-C_6H_4), 204.30 (s, br, 1,14-C_6H_4, only detected via ^{1}H, ^{13}C HMBC NMR experiments) ppm.

^{27}Al NMR (104 MHz, C_6D_6): δ = 103.1 (br, $AlCl_4^-$) ppm.

5*H*-Dibenzo[*b,f*]bismepine-5-yl tetrabromoaluminate (8-AlBr$_4$). 8-Br (10.0 mg, 21.4 µmol) was dissolved in benzene-d_6 (0.4 mL) and aluminum(III)bromide (5.70 mg, 21.4 µmol) was added at ambient temperature. After 4 h the resulting solution was layered with *n*-pentane (2 mL) and

stored for 20 h at ambient temperature. The brown precipitate of **8-AlBr$_4$** was isolated by filtration, washed with *n*-pentane (2 mL) and dried *in vacuo*. Yield: 10.0 mg, 13.6 µmol, 64%.

^{1}H NMR (400 MHz, C_6D_6): δ = 6.36 (s, 2H, 7,8-C_2H_2), 7.01 (dd, 2H, $^3J_{HH}$ = 7.6 Hz, $^3J_{HH}$ = 7.6 Hz, C_6H_4), 7.42 (dd, 2H, $^3J_{HH}$ = 7.5 Hz, $^3J_{HH}$ = 7.5 Hz, C_6H_4), 7.57 (d, 2H, $^3J_{HH}$ = 7.8 Hz, C_6H_4), 8.69 (d, 2H, $^3J_{HH}$ = 7.6 Hz, C_6H_4) ppm.

^{27}Al NMR (104 MHz, C_6D_6): δ = 84.5 (br, $AlBr_4^-$), 94.2 (br, $AlBr_3$) ppm.

26[SbF$_6$]. A solution of [Pt(cAAC^{Me})(PCy$_3$)] (8.0 mg, 10.5 µmol) in pyridine (1.5 ml) was added to a solution of **[8-thf$_2$][SbF$_6$]** (10.0 mg, 13.04 µmol) in pyridine (1.5 mL). The obtained yellow solution was layered with *n*-pentane (3 mL). After 2 d at –30 °C **26[SbF$_6$]** was obtained as a yellow solid by filtration and dried *in vacuo*. Yield: 10.0 mg, 8.46 µmol, 80% in 70% purity.

^{1}H NMR (400 MHz, pyridine-d$_5$): δ = 0.43 (s, 6H, CH_3), 1.11 (s, 3H, CH_3), 1.12 (s, 3H, CH_3), 1.46 (s, 12H, CH_3), 2.64–2.76 (m, 2H, CH), 5.59 (s, 2H, H-7, H-8), 7.14–7.20 (m, 3H, CH), 7.20–7.24 (m, 2H, C_5H_5N, overlap with solvent signal), 7.29 (dd, 2H, $^3J_{HH}$ = 7.3 Hz, $^3J_{HH}$ = 7.9 Hz, H-3, H-12), 7.33 (d, 2H, $^3J_{HH}$ = 7.6 Hz, H-5,H-10), 7.52 (dd, 2H, $^3J_{HH}$ = 7.3 Hz, $^3J_{HH}$ = 7.9 Hz, H-2, H-13), 7.56–7.61 (m, 1H, C_5H_5N, overlap with solvent signal), 8.04 (d, 2H, $^3J_{HH}$ = 7.2 Hz, H-2, H-13), 8.72–8.73 (m, 2H, C_5H_5N) ppm.

The ^{1}H NMR spectroscopic resonances for the CH_2 groups of the cAAC^{Me} ligand could not be separated from resonances of the impurities present in the sample.

27[SbF$_6$]. A colorless solution of **[8-thf$_2$][SbF$_6$]** (10 mg, 13 µmol) in THF (1 ml) was combined with a solution of [Pt(PCy$_3$)$_2$] (10 mg, 13 µmol) in THF (1 ml) yielding a dark red solution. An excess of *t*BuNC was added to the solution resulting in a color change to yellow. The solution was layered with *n*-pentane (2.5 mL) and after 16 h at –30 °C **27[SbF$_6$]** was obtained as a yellow solid by filtration and dried *in vacuo.* Yield: 10 mg, 7.9 µmol, 61%.

^{1}H NMR (500 MHz, THF-d$_8$): δ = 1.71 (s, 18H, C(CH_3)$_3$), 1.31–1.42 (m, 9H, $H_{ax.}$-22., $H_{ax.}$-23, $H_{ax.}$-24), 1.56–1.67 (m, 6H, $H_{ax.}$-21, $H_{ax.}$-25), 1.74–1.85 (m, 7H, β-thf, $H_{eq.}$-23) 1.88–1.97 (s, br, 6H, $H_{eq.}$-22, $H_{eq.}$-24), 1.98–2.08 (s, br, 6H, $H_{eq.}$-21, $H_{eq.}$-25), 2.43–2.52 (m, 3H, H-20), 3.59–3.66 (m, 4H, α-thf) 6.93 (s, 2H, H-7, H-8), 7.17 (ddd, 2H, $^4J_{HH}$ = 1.4 Hz, $^3J_{HH}$ = 7.3 Hz, $^3J_{HH}$ = 7.3 Hz, H-4, H-11), 7.23 (ddd, 2H, $^4J_{HH}$ = 1.5 Hz, $^3J_{HH}$ = 7.3 Hz, $^3J_{HH}$ = 7.5 Hz, H-3, H-12), 7.40 (dd, 2H, $^4J_{HH}$ = 1.2 Hz, $^3J_{HH}$ = 7.6 Hz, H-5, H-10), 8.11 (dd, 2H, $^4J_{HH}$ = 1.2 Hz, $^3J_{HH}$ = 7.3 Hz, H-2, H-13) ppm.

^{13}C NMR (126 MHz, THF-d$_8$): δ = 26.19 (s, THF, β-CH_2), 26.80 (s, C-23), 28.00 (d, $^1J_{CP}$ = 11.0 Hz, C-22, C-24), 29.49 (s, C-17, C-18, C-19), 30.65 (dd, $^2J_{CP}$ = 15.6 Hz, $^3J_{CPt}$ = 15.6 Hz, C-21, C-25), 36.57 (dd, $^1J_{CP}$ = 20.9 Hz, $^2J_{CPt}$ = 19.7 Hz, C-20), 60.71, (s, C-16), 68.02 (s, THF, α-CH_2), 128.05 (s, C-3,

C-12), 128.97 (s, C-4, C-11), 130.44 (s, C-5, C-10), 137.54 (s, C-7, C-8), 140.32 (s, C-2, C-13), 141.20 (s, C-6, C-9), 146.10 (s, C-1, C-14) ppm.

Reaction of Ph_2Bi-OTf with XeF_2. Benzene-d_6 (0.5 mL) was added to $Ph_2Bi(OTf)$ (15.0 mg, 29.0 µmol) and XeF_2 (4.9 mg, 29.0 µmol). After 20 min at ambient temperature gas evolution has ceased and a ^1H NMR spectroscopic analysis indicated an incomplete reaction. The reaction mixture was stirred for 2 d at ambient temperature. After filtration and layering the filtrate with *n*-pentane (0.7 mL) the colorless solution was stored at –30 °C. After 2 d at –30 °C $[BiPh_3][OTF]_2$ was isolated as a crystalline, colorless solid by filtration and dried *in vacuo*. Yield: 8.0 mg, 10.8 µmol, 37%.

The compound was analyzed by single-crystal X-ray diffraction analysis and by comparison to spectral data available in the literature.[232]

Reaction of 21 with XeF_2. To a solution of **21** (10.0 mg, 21.1 µmol) in CD_2Cl_2, XeF_2 (3.6 mg, 21.1 µmol) was added at ambient temperature. After 20 min at ambient temperature gas evolution has ceased and multinuclear NMR spectroscopic analyses indicated an incomplete conversion of **21** to at least four new species containing fluorine atoms according to ^{19}F NMR spectroscopy. Since an isolation of one of these species did not succeed, this approach was discarded.

Reaction of SbF_3 with 8-Cl. SbF_3 (4.2 mg, 23.7 µmol) was added to a solution of **8-Cl** (10.0 mg, 23.7 µmol) in benzene-d_6 (0.5 mL) and the suspension was heated to 60 °C for 2 d. A new heteropine species was detected via ^1H NMR spectroscopic analysis in a 1:1 ration with the starting material **8-Cl**. An excess of SbF_3 (14.0 mg, 78.8 µmol) was added and the reaction mixture was heated to 60 °C for another 16 h. The ratio of new heteropine species to starting material rose to 2.6:1 as determined by ^1H NMR spectroscopic analysis and the reaction mixture was stirred at 60 °C for a further 16 h. At this point the ^1H NMR spectroscopic analysis indicated a 8.9:1 ratio of the new species versus starting material. The suspension was filtered and the filtrate was layered with *n*-pentane (1 mL). After 16 h at ambient temperature colorless crystals were obtained by filtration, which were identified as starting material **8-Cl** by single-crystal X-ray diffraction analysis. The mother liquor was layered with *n*-pentane (0.5 mL) and after 16 h at ambient temperature colorless crystals were obtained by filtration. X-ray diffraction analysis identified the crystals as the stibepine $\{C_{14}H_{10}\}SbCl$. The mother liquor was then dried *in vacuo* and ^1H and ^{19}F NMR spectroscopic analyses indicated the selective formation of $\{C_{14}H_{10}\}SbCl$. A yield was not determined.

Table 9. Summary of reactions of **[8-thf$_2$][SbF$_6$]** with transition metal complexes.

Entry	transition metal complex	reaction conditions	result
1	$[Mn_2(CO)_{10}]$	DCM, 525 nm, 19 h	formation of **8-Cl**
2	$[Fe_2(CO)_9]$	DCM, 30 min, 60 °C	formation of black precipitate, partial recovery of **[8-thf$_2$][SbF$_6$]**
3	$[Fe(CO)_2Cp]_2$	DCM, r.t.	unselective reaction, formation of phenanthrene
4	$[Os_3(CO)_{12}]$	DCM, 19 h, 60 °C	phenanthrene, reaction mixture became viscous
5	$[Rh(cod)Cl]_2$	THF, r.t.	unselective reaction, formation of phenanthrene, black precipitate
6	$Ni(cod)_2$	THF, r.t.	unselective reaction, formation of phenanthrene, black precipitate
7	$AuCl(PPh_3)$	THF, r.t.	$[Au(PPh_3)_2][SbF_6]$, recovery of **[8-thf$_2$][SbF$_6$]**
8	[Pt(IMes)(PCy$_3$)]	THF, r.t.	decomposition
9	$[Pt(PCy_3)_2Cl_2]$	THF, r.t.	polymerization of THF
10	$[Pt(nbe)_3]$	THF, r.t.	polymerization of THF

IMes = 1,3-dimesitylimidazol-2-ylidene.

2.3 Experimental Part for Chapter XIV

Reaction of BiMe$_3$ with *o*-chloranil. $BiMe_3$ (13.0 mg, 51.2 µmol) and *o*-chloranil (12.6 mg, 51.2 µmol) were heated to 120 °C for 16 h. The resulting dark red-brown residue was extracted with pyridine (5 mL) and filtered. All volatiles in the filtrate were removed under reduced pressure and the residue was washed with *n*-pentane (1.5 mL), benzene (1.5 mL) and methylene chloride (2 mL) and dried *in vacuo*. The brown powder was dissolved in THF (2 mL) and layered with *n*-pentane. After 30 d at –30 °C small amounts of a crystalline solid, by-product **29**, were obtained by filtration, which were sufficient for an X-ray crystallographic analysis but for no other analysis or yield determination.

A repeat of the experiment with subsequent mass spectrometric analysis suggests an unselective reaction, the desired product **28** being present in traces.

ASAP-MS (negative mode)**:** Calcd. for $[C_7H_3BiCl_4O_2]^{\bullet-}$, *m/z* = 467.8969; found: 467.8703 (5%).

(SePh)$_2$BiMe. Neat $BiMe_3$ (17.0 mg, 66.4 µmol) and Se_2Ph_2 (20.7 mg, 66.4 µmol) were combined in a J. Young NMR tube. The mixture was heated to 120 °C for 20 h. After cooling to ambient temperature benzene (0.5 mL) was added resulting in a red suspension. Filtration and storage of

the filtrate yielded $(SePh)_2BiMe$ as a light yellow solid after 2 d at ambient temperature. $(SePh)_2BiMe$ was isolated by filtration and dried *in vacuo*. Yield: 7.0 mg, 13.1 μmol, 20%.

^{1}H NMR (400 MHz, C_6D_6): δ = 1.09 (s, 3H, CH_3), 6.89 (t, 2H, $^3J_{HH}$ = 7.4 Hz, *para*-C_6H_5), 6.98 (t, 4H, $^3J_{HH}$ = 7.4 Hz, *meta*-C_6H_5), 7.48 (d, 2H, $^3J_{HH}$ = 7.4 Hz, *ortho*-C_6H_5) ppm.

^{13}C NMR (100 MHz, C_6D_6): δ = 30.80 (s, CH_3, detected via ^{1}H, ^{13}C HSQC experiments), 127.68 (s, *para*-C_6H_5), 128.78 (s, *meta*-C_6H_5), 137.24 (s, *ortho*-C_6H_5), 137.79 (s, *ipso*-C_6H_5) ppm.

^{77}Se NMR (76 MHz, C_6D_6): δ = 223.1 (s, SePh) ppm.

$AsMe_3$. To a three-necked flask equipped with a dropping funnel with pressure compensation and an adapter for inert gas/vacuum, methylmagnesium bromide (1.0 M in nBu$_2$O, 95.3 mL, 95.3 mmol) was added. A solution of $AsBr_3$ (10.0 g, 31.8 mmol) in nBu$_2$O (20 mL) was added dropwise over 2 h at 0 °C. After complete addition the reaction mixture was stirred for a further 2 h at 0 °C then for 16 h at ambient temperature. The dropping funnel was removed and a Vigreux column (h = 19 cm, $Ø$ = 3 cm) equipped with a distillation apparatus and a Schlenk tube was added to the three-necked flask. The reaction mixture was distilled at atmospheric pressure and an oil bath temperature of 90 °C. The receiver Schlenk tube was cooled with liquid nitrogen to collect the $AsMe_3$ distillate. Yield: 3.26 g, 27.2 mmol, 85% (containing <3 mol% nBu$_2$O). Boiling point: 53–55 °C.[253]

^{1}H NMR (400 MHz, C_6D_6): δ = 0.76 (s, 9H, CH_3) ppm.

$SbMe_3$. Methylmagnesium bromide (3.0 M in Et_2O, 86.6 mmol, 29.8 mL) was added to a suspension of $SbCl_3$ (6.82 g, 29.9 mmol) in diethyl ether (100 mL) at 0 °C. The reaction mixture was stirred at 0 °C for 15 min, then 1.5 h at ambient temperature. The suspension was filtered and diethyl ether was removed partially by distillation at 50 °C (oil bath temperature). The residue was distilled at 90 °C and $5 \cdot 10^{-3}$ mbar to give $SbMe_3$ as a colorless oil. Yield: 1.40 g, 8.07 mmol, 27% (containing 10 mol% Et_2O).

^{1}H NMR (400 MHz, C_6D_6): δ = 0.60 (s, 9H, CH_3) ppm.

$Bi(allyl)_3$ (31). A suspension of $BiCl_3$ (5.04 g, 16.0 mmol) in diethylether (60 mL) was cooled with a water bath. Allylmagnesium chloride (2 M in THF, 24.0 mL, 48.0 mmol) was added portionwise resulting in a coloration to yellow. After 1 h at ambient temperature the resulting grey suspension was filtered and the yellow filtrate was distilled at 1.4 mbar at ambient temperature. The oily

residue was extracted with *n*-pentane (20 mL) and filtered. The solvent was removed at 1.3 mbar yielding **31** as a yellow liquid after another filtration. Yield: 1.98 g, 5.96 mmol, 37%.

Reaction of Bi(allyl)$_3$ with BiCl$_3$. $BiCl_3$ (37.9 mg, 120 µmol) was added to a solution of $Bi(allyl)_3$ (20.0 mg, 60.2 µmol) in CD_2Cl_2 (0.5 mL). The reaction mixture was filtered and the filtrate layered with *n*-pentane (0.5 mL) and stored at –30 °C. After 5 d at –30 °C yellow crystalline $Bi(allyl)_2Cl$ was obtained by filtration and dried *in vacuo*. Yield: 10.0 mg, 30.6 µmol, 51%.

^{1}H NMR (500 MHz, C_6D_6): δ = 3.62 (d, 4H, $^3J_{HH}$ = 10.9 Hz, CH_2), 6.43 (m, 1H, CH) ppm.

Bi(SPh)$_2$(C$_3$H$_5$) (32). Neat $Bi(C_3H_5)_3$ (6.2 mg, 18.6 µmol) was added to a solution of $Bi(SPh)_3$ (20 mg, 37.3 µmol) in CD_2Cl_2 (0.5 mL). After 3 h at ambient temperature the yellow suspension was filtered and layered with *n*-pentane (0.5 mL). The first fraction of **32** was obtained after 1 d at –30 °C as yellow, crystalline needles by filtration and dried *in vacuo*. The mother liquor was stored at –30 °C for a further 1 d, enabling the isolation of a second fraction of crystalline **32**, which was dried *in vacuo*. Yield of combined fractions: 21 mg, 44.8 µmol, 80%.

^{1}H NMR (500 MHz, C_6D_6): δ = 2.17 (dd, 2H, $^4J_{HH}$ = 0.7 Hz, $^3J_{HH}$ = 6.8 Hz, 1-CH_2), 4.26 (dm, 1H, $^3J_{HH}$ = 8.1 Hz, *cis*-3-CH_2CH=CH_2), 4.28 (dm, 1H, $^3J_{HH}$ = 16.9 Hz, *trans*-CH_2CH=CH_2), 6.19 (ddt, 1H, $^3J_{HH}$ = 6.8 Hz, $^3J_{HH}$ = 8.1 Hz, $^3J_{HH}$ = 16.9 Hz, CH_2CH=CH_2), 6.85 (tt, 2H, $^4J_{HH}$ = 1.3 Hz, $^3J_{HH}$ = 7.4 Hz, *para*-C_6H_5), 7.01 (m, 4H, *meta*-C_6H_5), 7.46 (m, 4H, *ortho*-C_6H_5) ppm.

^{13}C NMR (100 MHz, C_6D_6): δ = 64.31 (s, br, CH_2CH=CH_2), 119.90 (s, CH_2CH=CH_2), 127.38 (s, *para*-C_6H_5), 128.62 (s, *meta*-C_6H_5), 131.10 (s, CH_2CH=CH_2), 135.35 (s, *ipso*-C_6H_5), 135.87 (s, *ortho*-C_6H_5) ppm.

32 decomposes to $Bi(SPh)_3$ and probably $Bi(SPh)(C_3H_5)_2$ within a short period of time (~10% decomposition in 8 h).

Elemental analysis: Anal. calc. for $C_{15}H_{15}BiS_2$ (468.39 g · mol^{-1}): C 38.47, H 3.23, S 13.69; found: C 38.24, H 3.62, S 13.41.

Reaction of Bi(C$_3$H$_5$)$_3$ with S$_2$Ph$_2$. In a Schlenk flask neat $Bi(C_3H_5)_3$ (50.0 mg, 0.15 mmol) and S_2Ph_2 (32.9 mg, 0.15 mmol) were combined and the mixture was first heated to 50 °C for 16 h, then to 100 °C for 1 h. After the mixture had cooled to ambient temperature it was extracted with toluene (2 mL) and filtered. The yellow filtrate was layered with *n*-pentane (2 mL). After 2 d at –30 °C a crystalline solid was obtained by filtration and dried *in vacuo*. The mother liquor was stored at –30 °C for a further 16 h and a second fraction of a red crystalline solid was obtained by

filtration and dried *in vacuo*. The product was identified as $Bi(SPh)_3$ by X-ray diffraction analysis and comparison to spectral data available in the literature.[244] Yield of combined fractions: 20.0 mg, 0.04 mmol, 25%.

Reaction of $Bi(C_3H_5)_3$ with Se_2Ph_2. Se_2Ph_2 (13.8 mg, 44.1 µmol) was added to a solution of $Bi(C_3H_5)_3$ (12.8 mg, 44.1 µmol) in benzene-d_6 (0.5 mL). After 4 h at 60 °C the clear yellow solution turned to a green suspension with a dark precipitate (probably "bismuth black").[16] ^{1}H NMR spectroscopic analysis indicated full conversion of the starting materials to 1,5-hexadiene and $PhSe(C_3H_5)$.

^{1}H NMR spectroscopic data of $PhSe(C_3H_5)$[14]:

^{1}H NMR (400 MHz, C_6D_6): δ = 3.18 (d, 2H, $^3J_{HH}$ = 7.5 Hz, CH_2), 4.73 (m, 2H, $CH_2CH{=}CH_2$), 5.78 (ddt, 1H, $^3J_{HH}$ = 7.5 Hz, $^3J_{HH}$ = 9.8 Hz, $^3J_{HH}$ = 16.9 Hz, $CH_2CH{=}CH_2$), 6.96 (m, 3H, *meta*-C_6H_5, *para*-C_6H_5), 7.41 (m, 2H, *ortho*-C_6H_5) ppm.

Reaction of $Bi(C_3H_5)_3$ with Te_2Ph_2. To a solution of $Bi(C_3H_5)_3$ (10.0 mg, 34.5 µmol) in C_6D_6 (0.5 mL) Te_2Ph_2 (14.1 mg, 34.5 µmol) was added. A black solid precipitated instantly (probably "bismuth black").[16] After 1 h at ambient temperature, ^{1}H NMR spectroscopic analysis indicated the full conversion of the starting materials to 1,5-hexadiene and $PhTe(C_3H_5)$.

^{1}H and ^{13}C NMR spectroscopic data of $PhTe(C_3H_5)$:

^{1}H NMR (400 MHz, C_6D_6): δ = 3.25 (d, 2H, $^3J_{HH}$ = 8.0 Hz, CH_2), 4.57 (dm, 1H, $^3J_{HH}$ = 9.9 Hz, *cis*-$CH_2CH{=}CH_2$), 4.60 (dm, 1H, $^3J_{HH}$ = 16.8 Hz, *trans*-$CH_2CH{=}CH_2$), 5.87 (m, 1H, $CH_2CH{=}CH_2$), 6.92 (t, 2H, $^3J_{HH}$ = 7.0 Hz, *meta*-C_6H_5), 6.99 (t, 1H, $^3J_{HH}$ = 7.0 Hz, *para*-C_6H_5), 7.64 (d, 2H, $^3J_{HH}$ = 6.8 Hz, *ortho*-C_6H_5) ppm.

^{13}C NMR (100 MHz, C_6D_6): δ = 11.04 (s, $CH_2CH{=}CH_2$), 112.92 (s, *ipso*-C_6H_5), 114.86 (s, $CH_2CH{=}CH_2$), 127.80 (s, *meta*-C_6H_5) 129.34 (s, *para*-C_6H_5), 136.59 (s, $CH_2CH{=}CH_2$), 139.39 (s, *ortho*-C_6H_5) ppm.

[14] The ^{1}H NMR spectrum contains 0.2 equivalents of 1,5-hexadiene.

XVIII List of Compounds

1	$[Ph_2Bi\{Mn(CO)_5\}]$
2	$[(HC(C\{Me\}N(Dip))_2(Cl)Ga]_2Sb^{\bullet}$
3	$[\{(C_{14}H_{12})S\}Bi\{Mn(CO)_5\}]$
4	$[(\{(C_{14}H_{12})S\}Bi)_2C_6H_4O_2]$
5	$[\{(C_{14}H_{12})S\}Bi]_2$
6	$\{(C_{14}H_{12})S\}BiCl$
7	$(C_{14}H_{10})_3Bi_2$
8-Cl	$(C_{14}H_{10})BiCl$
8-Br	$(C_{14}H_{10})BiBr$
8-I	$(C_{14}H_{10})BiI$
8-BF_4	$[(C_{14}H_{10})Bi(BF_4)]$
8-OTf	$[(C_{14}H_{10})Bi(OTf)]$
8-$AlCl_4$	$[(C_{14}H_{10})Bi(AlCl_4)]$
8-$AlBr_4$	$[(C_{14}H_{10})Bi(AlBr_4)]$
[8-thf_2][SbF_6]	$[(C_{14}H_{10})Bi(thf)_2][SbF_6]$
9	$[(C_{14}H_{10})Bi\{Mn(CO)_5\}]$
10	$[(C_{14}H_{10})Bi\{Fe(CO)_2Cp\}]$
11	$[\{\kappa^2C,\kappa^1Bi\text{-}(C_{14}H_{10})Bi\}Fe(CO)Cp]$
12	$[\{(C_{14}H_{10})Bi\}_2Fe(CO)_4]$
13	$[(C_{14}H_{10})Bi\{Co(CO)_4\}]$
13-PPh_3	$[(C_{14}H_{10})Bi\{Co(CO)_3(PPh_3)\}]$
13-PCy_3	$[(C_{14}H_{10})Bi\{Co(CO)_3(PCy_3)\}]$
13-*t*BuNC	$[(C_{14}H_{10})Bi\{Co(CO)_3(t\text{BuNC})\}]$
14	$[\{\kappa^2C,\kappa^1Bi\text{-}(C_{14}H_{10})Bi\}Co(CO)_3]$
14-PPh_3	$[\{\kappa^2C,\kappa^1Bi\text{-}(C_{14}H_{10})Bi\}Co(CO)_2(PPh_3)]$
14-PCy_3	$[\{\kappa^2C,\kappa^1Bi\text{-}(C_{14}H_{10})Bi\}Co(CO)_2(PCy_3)]$

14-*t*BuNC	[{κ²*C*,κ¹*Bi*-($C_{14}H_{10}$)Bi}Co(CO)$_2$(*t*BuNC)]
15	[($C_{14}H_{10}$)Bi{Co(CO)$_2$(*t*BuNC)(PCy_3)}]
16	[{κ²*C*,κ¹*Bi*-($C_{14}H_{10}$)Bi}Co(CO)(*t*BuNC)(PCy_3)]
17	[{κ²*C*,κ¹*Bi*-($C_{14}H_{10}$)Bi}Co(CO)(*t*BuNC)(*S*-Monophos)]
18	[{($C_{14}H_{12}$)S}Bi]$_2$S
19-Cl	[$BiCl_2(py)_5$][$BArF^{24}$]
19-Br	[$BiBr_2(py)_5$][$BArF^{24}$]
19-I	[$BiI_2(py)_5$][$BArF^{24}$]
20	$BiCl_3(py)_2$
21	[$BiMe_2(SbF_6)$]
21-py	[$BiMe_2(py)_2$][SbF_6]
21-benzaldehyde	[$BiMe_2(C_7H_6O)_2$][SbF_6]
21-thf	[$BiMe_2(thf)_2$][SbF_6]
21-thf$_1$	[$BiMe_2(thf)(SbF_6)$]
21-MeCN	[$BiMe_2(MeCN)_2$][SbF_6]
22	[$BiMeF(py)_3]_2$·2[SbF_6]
23-DHB	[$BiMe_2$(DHB)]
23-MHB	[$BiMe_2$(MHB)]
24	*t*BuNB*t*Bu
25	[$BiPh_2(SbF_6)$]
25-BiPh$_2$Cl	[$BiPh_2(BiPh_2Cl)(SbF_6)$]
26	[{κ²*C*,κ¹*Bi*-($C_{14}H_{10}$)Bi}Pt(cAAC)(py)][SbF_6]
27	[{($C_{14}H_{10}$)Bi}Pt(*t*BuNC)$_2$(PCy_3)][SbF_6]
28	($C_6Cl_4O_2$)BiMe
29	[($C_6Cl_4O_2$)Bi(thf)$_2$Cl]$_2$
30	$C_{12}H_{18}NO^{\bullet}$
31	Bi(allyl)$_3$
32	(allyl)Bi(SPh)$_2$

33	{($C_{14}H_{12}$)S}Bi(SPh)
34	{($C_{14}H_{12}$)S}Bi(CCl_3)
35	{($C_{14}H_{12}$)S}Bi(OTEMP)
36-SPMe$_3$	[($C_{14}H_{10}$)Bi($SPMe_3$)][SbF_6]
36-SePMe$_3$	[($C_{14}H_{10}$)Bi($SePMe_3$)][SbF_6]
37[BArF^{24}]	[{($C_{14}H_{10}$)$_3$$Bi_2$}Tl][$BArF^{24}$]
38[BArF^{24}]	[{($C_{14}H_{10}$)BiI}$_2$Tl][$BArF^{24}$]
39	[$BiMe_2$($BiMe_3$)][SbF_6]
40	[Bi_2(N(C_6H_4)Ph)$_2$(OTf)$_2$(thf)$_3$]
41	[Bi(CONPh(C_6H_4))(NC_5H_5)$_2$][OTf]

XIX References

[1] P. de Marcillac, N. Coron, G. Dambier, J. Leblanc, J.-P. Moalic, *Nature* **2003**, *422*, 876.
[2] R. Mohan, *Nat. Chem.* **2010**, *2*, 336.
[3] A. Kuczkowski, S. Fahrenholz, S. Schulz, M. Nieger, *Organometallics* **2004**, *23*, 3615.
[4] A. Kuczkowski, S. Schulz, M. Nieger, *Chem. Ber.* **2001**, 2605.
[5] A. Kuczkowski, S. Schulz, M. Nieger, P. R. Schreiner, *Organometallics* **2002**, *21*, 1408.
[6] A. Kuczkowski, F. Thomas, S. Schulz, M. Nieger, *Organometallics* **2000**, *19*, 5758.
[7] N. J. Holmes, W. Levason, M. Webster, *J. Organomet. Chem.* **1997**, *545-546*, 111.
[8] P. Pyykkö, *Chem. Rev.* **1988**, *88*, 563.
[9] P. Pyykkö, *Annu. Rev. Phys. Chem.* **2012**, *63*, 45.
[10] A. J. Plajer, A. L. Colebatch, F. J. Rizzuto, P. Pröhm, A. D. Bond, R. García-Rodríguez, D. S. Wright, *Angew. Chem. Int. Ed.* **2018**, *57*, 6648.
[11] E. Becker, C. Slugovc, E. Rüba, C. Standfest-Hauser, K. Mereiter, R. Schmid, K. Kirchner, *J. Organomet. Chem.* **2002**, *649*, 55.
[12] H. J. Breunig, T. Borrmann, E. Lork, O. Moldovan, C. I. Raț, R. P. Wagner, *J. Organomet. Chem.* **2009**, *694*, 427.
[13] H. Schumann, H. J. Breunig, *J. Organomet. Chem.* **1975**, *87*, 83.
[14] T.-P. Lin, I.-S. Ke, F. P. Gabbaï, *Angew. Chem. Int. Ed.* **2012**, *51*, 4985.
[15] R. J. Schwamm, C. M. Fitchett, M. P. Coles, *Chem. Asian J.* **2019**, *14*, 1204.
[16] J. Bresien, A. Schulz, M. Thomas, A. Villinger, *Eur. J. Inorg. Chem.* **2019**, 1279.
[17] A. Hanft, C. Lichtenberg, *Dalton Trans.* **2018**, *47*, 10578.
[18] C. Tschersich, S. Hoof, N. Frank, C. Herwig, C. Limberg, *Inorg. Chem.* **2016**, 1837.
[19] R. J. Schwamm, B. M. Day, M. P. Coles, C. M. Fitchett, *Inorg. Chem.* **2014**, *53*, 3778.
[20] H. Dengel, C. Lichtenberg, *Chem. Eur. J.* **2016**, *22*, 18465.
[21] B. Ritschel, J. Poater, H. Dengel, F. M. Bickelhaupt, C. Lichtenberg, *Angew. Chem. Int. Ed.* **2018**, *57*, 3825.
[22] C. Lichtenberg, F. Pan, T. P. Spaniol, U. Englert, J. Okuda, *Angew. Chem. Int. Ed.* **2012**, *51*, 13011.
[23] C. J. Carmalt, L. J. Farrugia, N. C. Norman, *J. Chem. Soc., Dalton Trans.* **1996**, 443.
[24] N. W. Alcock, M. Ravindran, G. R. Willey, *J. Chem. Soc., Chem. Commun.* **1989**, 1063.
[25] R. D. Rogers, A. H. Bond, S. Aguinaga, A. Reyes, *J. Am. Chem. Soc.* **1992**, *114*, 2967.
[26] J. E. Walley, L. S. Warring, G. Wang, D. A. Dickie, S. Pan, G. Frenking, R. J. Gilliard, *Angew. Chem. Int. Ed.* **2021**, *60*, 6682.
[27] M. Lehmann, A. Schulz, A. Villinger, *Angew. Chem. Int. Ed.* **2012**, *51*, 8087.
[28] M. Veith, B. Bertsch, V. Huch, *Z. Anorg. Allg. Chem.* **1988**, *559*, 73.
[29] K. M. Marczenko, S. Jee, S. S. Chitnis, *Organometallics* **2020**, *39*, 4287.
[30] A. Hanft, K. Radacki, C. Lichtenberg, *Chem. Eur. J.* **2020**.
[31] R. F. Childs, D. L. Mulholland, A. Nixon, *Can. J. Chem.* **1982**, *60*, 809.
[32] J. C. Haartz, D. H. McDaniel, *J. Am. Chem. Soc.* **1973**, *95*, 8562.
[33] U. Mayer, V. Gutmann, W. Gerger, *Monatsh. Chem.* **1975**, *106*, 1235.
[34] M. A. Beckett, G. C. Strickland, J. R. Holland, K. S. Varma, *Polymer* **1996**, *37*, 4629.
[35] R. Kannan, S. Kumar, A. P. Andrews, E. D. Jemmis, A. Venugopal, *Inorg. Chem.* **2017**, *56*, 9391.
[36] S. Balasubramaniam, S. Kumar, A. P. Andrews, B. Varghese, E. D. Jemmis, A. Venugopal, *Eur. J. Inorg. Chem.* **2019**, 3265.
[37] Y. Soltani, S. J. Adams, J. Börger, L. C. Wilkins, P. D. Newman, S. J. A. Pope, R. L. Melen, *Dalton Trans.* **2018**, *47*, 12656.
[38] M. Olaru, D. Duvinage, E. Lork, S. Mebs, J. Beckmann, *Angew. Chem. Int. Ed.* **2018**, *57*, 10080.
[39] T. A. Engesser, M. R. Lichtenthaler, M. Schleep, I. Krossing, *Chem. Soc. Rev.* **2016**, *45*, 789.

[40] I. Krossing, I. Raabe, *Angew. Chem. Int. Ed.* **2004**, *43*, 2066.
[41] I. M. Riddlestone, A. Kraft, J. Schaefer, I. Krossing, *Angew. Chem. Int. Ed.* **2018**, *57*, 13982.
[42] S. H. Strauss, *Chem. Rev.* **1993**, *93*, 927.
[43] H. Qin, N. Yamagiwa, S. Matsunaga, M. Shibasaki, *J. Am. Chem. Soc.* **2006**, *128*, 1611.
[44] G. Sabitha, E. Venkata Reddy, C. Maruthi, J. Yadav, *Tetrahedron Lett.* **2002**, *43*, 1573.
[45] J. M. Bothwell, S. W. Krabbe, R. S. Mohan, *Chem. Soc. Rev.* **2011**, *40*, 4649.
[46] T. Ollevier, *Org. Biomol. Chem.* **2013**, *11*, 2740.
[47] R. Qiu, S. Yin, X. Zhang, J. Xia, X. Xu, S. Luo, *Chem. Commun.* **2009**, 4759.
[48] R. Qiu, Y. Qiu, S. Yin, X. Song, Z. Meng, X. Xu, X. Zhang, S. Luo, C.-T. Au, W.-Y. Wong, *Green Chem.* **2010**, *12*, 1767.
[49] R. Qiu, S. Yin, X. Song, Z. Meng, Y. Qiu, N. Tan, X. Xu, S. Luo, F.-R. Dai, C.-T. Au, W.-Y. Wong, *Dalton Trans.* **2011**, 9482.
[50] S.-F. Yin, S. Shimada, *Chem. Commun.* **2009**, 1136.
[51] X. Zhang, R. Qiu, N. Tan, S. Yin, J. Xia, S. Luo, C.-T. Au, *Tetrahedron Lett.* **2010**, *51*, 153.
[52] R. Kannan, S. Balasubramaniam, S. Kumar, R. Chambenahalli, E. D. Jemmis, A. Venugopal, *Chem. Eur. J.* **2020**, *26*, 12717.
[53] S. Ishida, F. Hirakawa, K. Furukawa, K. Yoza, T. Iwamoto, *Angew. Chem. Int. Ed.* **2014**, *53*, 11172.
[54] R. J. Schwamm, J. R. Harmer, M. Lein, C. M. Fitchett, S. Granville, M. P. Coles, *Angew. Chem. Int. Ed.* **2015**, *54*, 10630.
[55] C. Ganesamoorthy, C. Helling, C. Wölper, W. Frank, E. Bill, G. E. Cutsail, S. Schulz, *Nat. Commun.* **2018**, *9*, 87.
[56] S. Ishida, F. Hirakawa, T. Iwamoto, *Bull. Chem. Soc. Jpn.* **2018**, *91*, 1168.
[57] G. E. Cutsail, *Dalton Trans.* **2020**, *49*, 12128.
[58] R. J. Schwamm, M. Lein, M. P. Coles, C. M. Fitchett, *Chem. Commun.* **2018**, *54*, 916.
[59] J. D. Corbett, *J. Am. Chem. Soc.* **1958**, *80*, 4757.
[60] J. D. Corbett, R. A. Lynde, *Inorg. Chem.* **1971**, *10*, 1746.
[61] P. Kuijpers, A. Dymanus, *Chem. Phys. Lett.* **1976**, *39*, 217.
[62] E. Fink, K. Setzer, D. Ramsay, M. Vervloet, J. Brown, *J. Mol. Spectrosc.* **1990**, *142*, 108.
[63] E. H. Fink, K. D. Setzer, D. A. Ramsay, M. Vervloet, *Chem. Phys. Lett.* **1991**, *179*, 95.
[64] G. Wang, L. A. Freeman, D. A. Dickie, R. Mokrai, Z. Benkő, R. J. Gilliard, *Chem. Eur. J.* **2019**, *25*, 4335.
[65] P. Šimon, F. de Proft, R. Jambor, A. Růžička, L. Dostál, *Angew. Chem. Int. Ed.* **2010**, *49*, 5468.
[66] I. Vránová, M. Alonso, R. Lo, R. Sedlák, R. Jambor, A. Růžička, F. de Proft, P. Hobza, L. Dostál, *Chem. Eur. J.* **2015**, *21*, 16917.
[67] M. M. Siddiqui, S. K. Sarkar, M. Nazish, M. Morganti, C. Köhler, J. Cai, L. Zhao, R. Herbst-Irmer, D. Stalke, G. Frenking, H. W. Roesky, *J. Am. Chem. Soc.* **2021**, *143*, 1301.
[68] F. Wang, O. Planas, J. Cornella, *J. Am. Chem. Soc.* **2019**, *141*, 4235.
[69] D. H. R. Barton, W. B. Motherwell, A. Stobie, *J. Chem. Soc., Chem. Commun.* **1981**, 1232.
[70] D. H. Barton, J.-P. Finet, W. B. Motherwell, C. Pichon, *Tetrahedron* **1986**, *42*, 5627.
[71] O. Planas, F. Wang, M. Leutzsch, J. Cornella, Catalytic Fluorination of Boron Compounds at a Bismuth Redox Platform, ChemRxiv. Preprint, **2019**.
[72] J. Ramler, I. Krummenacher, C. Lichtenberg, *Angew. Chem. Int. Ed.* **2019**, *58*, 12924.
[73] A. L. Beckwith, *Tetrahedron* **1981**, *37*, 3073.
[74] A. L. Beckwith, C. J. Easton, T. Lawrence, A. K. Serelis, *Aust. J. Chem.* **1983**, *36*, 545.
[75] D. P. Curran, N. A. Porter, B. Giese, Stereochemistry of radical reactions: concepts, guidelines, and synthetic applications, John Wiley & Sons, Hoboken, NJ, **2008**.
[76] A. Toma, C. I. Raț, A. Silvestru, T. Rüffer, H. Lang, M. Mehring, *J. Organomet. Chem.* **2016**, *806*, 5.
[77] J. Ramler, I. Krummenacher, C. Lichtenberg, *Chem. Eur. J.* **2020**.
[78] W. Hieber, J. G. Floss, *Z. Anorg. Allg. Chem.* **1957**, *291*, 314.

[79] A. J. Ashe III, E. G. Ludwig Jr, J. Oleksyszyn, *Organometallics* **1983**, *2*, 1859.
[80] J. Ramler, *master thesis*, Institute of Inorganic Chemistry, Julius-Maximilians-University, Würzburg, **2017**.
[81] H. J. Breunig, *Z. Anorg. Allg. Chem.* **2005**, *631*, 621.
[82] J. Ramler, K. Hofmann, C. Lichtenberg, *Inorg. Chem.* **2020**, *59*, 3367.
[83] J. M. Cassidy, K. H. Whitmire, *Inorg. Chem.* **1991**, *30*, 2788.
[84] F. Calderazzo, R. Poli, G. Pelizzi, *J. Chem. Soc., Dalton Trans.* **1984**, 2535.
[85] A. J. Ashe III, J. W. Kampf, D. B. Puranik, *J. Organomet. Chem.* **1993**, *447*, 197.
[86] P. Panster, W. Malisch, *J. Organomet. Chem.* **1977**, *134*, C32-C36.
[87] C. Mihm, *bachelor thesis*, Institute of Inorganic Chemistry, Julius-Maximilians-University, Würzburg, **2018**.
[88] J. M. Wallis, G. Müller, H. Schmidbaur, *Inorg. Chem.* **1987**, *26*, 458.
[89] M. R. Churchill, K. N. Amoh, H. J. Wasserman, *Inorg. Chem.* **1981**, *20*, 1609.
[90] R. E. Bachman, K. H. Whitmire, *Inorg. Chem.* **1995**, *34*, 1542.
[91] J. M. Wallis, G. Müller, H. Schmidbaur, *J. Organomet. Chem.* **1987**, *325*, 159.
[92] R. Schiwon, R. Metzinger, C. Pfirrmann, C. Limberg, *Z. Naturforsch. B* **2013**, *68*, 561.
[93] T. Gröer, M. Scheer, *J. Chem. Soc., Dalton Trans.* **2000**, 647.
[94] G. Bendt, R. Schiwon, S. Salamon, J. Landers, U. Hagemann, C. Limberg, H. Wende, S. Schulz, *Inorg. Chem.* **2016**, *55*, 7542.
[95] T. Gröer, M. Scheer, *Organometallics* **2000**, *19*, 3683.
[96] R. Schiwon, F. Schax, B. Braun, C. Limberg, *J. Organomet. Chem.* **2016**, *821*, 71.
[97] R. Schiwon, B. Braun, R. Metzinger, C. Limberg, *Z. Anorg. Allg. Chem.* **2016**, *642*, 1198.
[98] M. Shieh, Y. Liou, M.-H. Hsu, R.-T. Chen, S.-J. Yeh, S.-M. Peng, G.-H. Lee, *Angew. Chem. Int. Ed.* **2002**, *41*, 2384.
[99] M. A. Fox, J. K. Whitesell, Organische Chemie, Akademischer Verlag, Heidelberg, **1995**.
[100] S. Martinengo, G. Ciani, *J. Chem. Soc., Chem. Commun.* **1987**, *0*, 1589.
[101] G. Ciani, M. Moret, A. Fumagalli, S. Martinengo, *J. Organomet. Chem.* **1989**, *362*, 291.
[102] T. Ziegler, A. Rauk, *Inorg. Chem.* **1979**, *18*, 1755.
[103] Gaussian 16, Revision B.01, M. J. Frisch, G. W. Trucks, H. B. Schlegel, G. E. Scuseria, M. A. Robb, J. R. Cheeseman, G. Scalmani, V. Barone, G. A. Petersson, H. Nakatsuji, X. Li, M. Caricato, A. V. Marenich, J. Bloino, B. G. Janesko, R. Gomperts, B. Mennucci, H. P. Hratchian, J. V. Ortiz, A. F. Izmaylov, J. L. Sonnenberg, Williams, F. Ding, F. Lipparini, F. Egidi, J. Goings, B. Peng, A. Petrone, T. Henderson, D. Ranasinghe, V. G. Zakrzewski, J. Gao, N. Rega, G. Zheng, W. Liang, M. Hada, M. Ehara, K. Toyota, R. Fukuda, J. Hasegawa, M. Ishida, T. Nakajima, Y. Honda, O. Kitao, H. Nakai, T. Vreven, K. Throssell, J. A. Montgomery Jr., J. E. Peralta, F. Ogliaro, M. J. Bearpark, J. J. Heyd, E. N. Brothers, K. N. Kudin, V. N. Staroverov, T. A. Keith, R. Kobayashi, J. Normand, K. Raghavachari, A. P. Rendell, J. C. Burant, S. S. Iyengar, J. Tomasi, M. Cossi, J. M. Millam, M. Klene, C. Adamo, R. Cammi, J. W. Ochterski, R. L. Martin, K. Morokuma, O. Farkas, J. B. Foresman, D. J. Fox, Gaussian, Inc., Wallingford CT, **2016**.
[104] A. D. Becke, *J. Chem. Phys.* **1993**, *98*, 5648.
[105] T. Yanai, D. P. Tew, N. C. Handy, *Chem. Phys. Lett.* **2004**, *393*, 51.
[106] S. Grimme, J. Antony, S. Ehrlich, H. Krieg, *J. Chem. Phys.* **2010**, *132*, 154104.
[107] P. C. Hariharan, J. A. Pople, *Theoret. Chim. Acta* **1973**, *28*, 213.
[108] P. J. Hay, W. R. Wadt, *J. Chem. Phys.* **1985**, *82*, 299.
[109] P. J. Hay, W. R. Wadt, *J. Chem. Phys.* **1985**, *82*, 270.
[110] T. H. Dunning, P. J. Hay, Methods of electronic structure theory, Springer, Boston, MA, **1977**.
[111] C. Chen, T. R. Dugan, W. W. Brennessel, D. J. Weix, P. L. Holland, *J. Am. Chem. Soc.* **2014**, *136*, 945.
[112] A. Gutnov, H.-J. Drexler, A. Spannenberg, G. Oehme, B. Heller, *Organometallics* **2004**, *23*, 1002.

[113] I. Thiel, M. Lamač, H. Jiao, A. Spannenberg, M. Hapke, *Organometallics* **2013**, *32*, 3415.
[114] L. Lubczyk, *bachelor thesis*, Institute of Inorganic Chemistry, Julius-Maximilians-University, Würzburg, **2020**.
[115] C. Elschenbroich, Organometallchemie, Teubner, Wiesbaden, **2005**.
[116] National Institute of Advanced Industrial Science and Technology (AIST), can be found under https://sdbs.db.aist.go.jp/sdbs/cgi-bin/landingpage?sdbsno=18516, last checked 04.01.2021, 10:18.
[117] F. A. Cotton, F. Zingales, *J. Am. Chem. Soc.* **1961**, *83*, 351.
[118] P. M. Boorman, P. J. Craig, T. W. Swaddle, *Can. J. Chem.* **1970**, *48*, 838.
[119] X. Jiang, L. Chen, X. Wang, Li Long, Z. Xiao, X. Liu, *Chem. Eur. J.* **2015**, 13065.
[120] M. Elstner, Physikalische Chemie I: Thermodynamik und Kinetik, Springer-Verlag, **2017**.
[121] T. M. Bockman, J. K. Kochi, *J. Am. Chem. Soc.* **1988**, *110*, 1294.
[122] T. M. Bockman, J. K. Kochi, *J. Am. Chem. Soc.* **1989**, *111*, 4669.
[123] C. Tschersich, C. Limberg, S. Roggan, C. Herwig, N. Ernsting, S. Kovalenko, S. Mebs, *Angew. Chem. Int. Ed.* **2012**, 4989.
[124] K. Materne, S. Hoof, N. Frank, C. Herwig, C. Limberg, *Organometallics* **2017**, *36*, 4891.
[125] C. Tschersich, B. Braun, C. Herwig, C. Limberg, *Organometallics* **2015**, *34*, 3782.
[126] C. F. Riemersma, E. C. Monkcom, R. J. M. Klein Gebbink, M. Lutz, *Acta Cryst. E* **2019**, 1548.
[127] M. Wieber, I. Sauer, *Z. Naturforsch. B* **1987**, *42*, 695.
[128] J. E. McDonough, A. Mendiratta, J. J. Curley, G. C. Fortman, S. Fantasia, C. C. Cummins, E. V. Rybak-Akimova, S. P. Nolan, C. D. Hoff, *Inorg. Chem.* **2008**, 2133.
[129] T. Ollevier, Bismuth-mediated organic reactions, Springer Science & Business Media, **2012**.
[130] T. Ollevier, V. Desyroy, E. Nadeau, *Arkivoc* **2007**, *10*, 10.
[131] P. A. Evans, A. Grisin, M. J. Lawler, *J. Am. Chem. Soc.* **2012**, *134*, 2856.
[132] N. C. Norman, *Phosphorus, Sulfur, Silicon Relat. Elem.* **1994**, *87*, 167.
[133] M. Krasowska, A.-M. Fritzsche, M. Mehring, A. A. Auer, *ChemPhysChem* **2019**, *20*, 2539.
[134] M. Krasowska, W. B. Schneider, M. Mehring, A. A. Auer, *Chem. Eur. J.* **2018**, *24*, 10238.
[135] S. Müller-Becker, W. Frank, J. Schneider, *Z. Anorg. Allg. Chem.* **1993**, *619*, 1073.
[136] W. Frank, J. Schneider, S. Müller-Becker, *J. Chem. Soc., Chem. Commun.* **1993**, 799.
[137] J. Ramler, C. Lichtenberg, *Chem. Eur. J.* **2020**, *26*, 10250.
[138] H. Schumann, L. Eguren, *J. Organomet. Chem.* **1991**, *403*, 183.
[139] A. J. Carty, N. J. Taylor, A. W. Coleman, M. F. Lappert, *J. Chem. Soc., Chem. Commun.* **1979**, 639.
[140] H. Braunschweig, P. Cogswell, K. Schwab, *Coord. Chem. Rev.* **2011**, *255*, 101.
[141] N. C. Norman, Chemistry of arsenic, antimony and bismuth, Springer Science & Business Media, **1997**.
[142] G. A. Bowmaker, F. M. M. Hannaway, P. C. Junk, A. M. Lee, B. W. Skelton, A. H. White, *Aust. J. Chem.* **1998**, *51*, 325.
[143] S. L. Benjamin, W. Levason, G. Reid, M. C. Rogers, R. P. Warr, *J. Organomet. Chem.* **2012**, *708-709*, 106.
[144] J. N. Murphy, F. M. Kerton, L. N. Dawe, *J. Chem. Crystallogr.* **2014**, *44*, 108.
[145] C. Silvestru, H. J. Breunig, H. Althaus, *Chem. Rev.* **1999**, *99*, 3277.
[146] S. C. James, N. C. Norman, A. G. Orpen, *J. Chem. Soc., Dalton Trans.* **1999**, 2837.
[147] B. Wagner, J. Heine, *Z. Anorg. Allg. Chem.* **2020**.
[148] G. R. Willey, D. R. Aris, W. Errington, *Inorg. Chim. Acta* **2000**, *300*, 1004.
[149] M. G. B. Drew, D. G. Nicholson, I. Sylte, A. Vasudevan, *Inorg. Chim. Acta* **1990**, *171*, 11.
[150] L. Liu, L. N. Zakharov, J. A. Golen, A. L. Rheingold, T. A. Hanna, *Inorg. Chem.* **2008**, *47*, 11143.
[151] H.-J. Drexler, I. Starke, M. Grotjahn, H. Reinke, E. Kleinpeter, H.-J. Holdt, *Z. Naturforsch. B* **1999**, *54*, 799.
[152] W. Frank, G. J. Reiss, J. Schneider, *Angew. Chem. Int. Ed.* **1995**, *34*, 2416.

[153] J. Näslund, I. Persson, M. Sandström, *Inorg. Chem.* **2000**, *39*, 4012.
[154] P. Nørby, M. R. V. Jørgensen, S. Johnsen, B. Brummerstedt Iversen, *Eur. J. Inorg. Chem.* **2016**, 1389.
[155] G. A. Bowmaker, J. M. Harrowfield, P. C. Junk, B. W. Skelton, A. H. White, *Aust. J. Chem.* **1998**, *51*, 285.
[156] U. H. Hamdeh, R. D. Nelson, B. J. Ryan, U. Bhattacharjee, J. W. Petrich, M. G. Panthani, *Chem. Mater.* **2016**, *28*, 6567.
[157] R. Rajasekharan-Nair, D. Moore, A. R. Kennedy, J. Reglinski, M. D. Spicer, *Inorg. Chem.* **2014**, *53*, 10276.
[158] S. Mazières, C. Le Roux, M. Peyronneau, H. Gornitzka, N. Roques, *Eur. J. Inorg. Chem.* **2004**, 2823.
[159] M. Schäfer, G. Frenzen, B. Neumüller, K. Dehnicke, *Angew. Chem. Int. Ed.* **1992**, *31*, 334.
[160] W. Frank, J. Weber, E. Fuchs, *Angew. Chem. Int. Ed.* **1987**, *26*, 74.
[161] R. D. Rogers, A. H. Bond, S. Aguinaga, *J. Am. Chem. Soc.* **1992**, *114*, 2960.
[162] J.-F. Morfin, R. Tripier, M. Le Baccon, H. Handel, *Inorg. Chim. Acta* **2009**, *362*, 1781.
[163] I. P. Ferreira, E. D. L. Piló, A. A. Recio-Despaigne, J. G. Da Silva, J. P. Ramos, L. B. Marques, P. H. D. M. Prazeres, J. A. Takahashi, E. M. Souza-Fagundes, W. Rocha, H. Beraldo, *Bioorg. Med. Chem.* **2016**, 2988.
[164] O. Toma, N. Mercier, M. Allain, A. Forni, F. Meinardi, C. Botta, *Dalton Trans.* **2015**, *44*, 14589.
[165] C. L. Raston, G. L. Rowbottom, A. H. White, *J. Chem. Soc., Dalton Trans.* **1981**, 1383.
[166] L. P. Battaglia, A. B. Corradi, G. Pelosi, P. Tarasconi, C. Pelizzi, *J. Chem. Soc., Dalton Trans.* **1989**, 671.
[167] E. Conrad, N. Burford, R. McDonald, M. J. Ferguson, *Chem. Commun.* **2010**, *46*, 4598.
[168] D. Mansfeld, M. Mehring, *Z. Anorg. Allg. Chem.* **2005**, *631*, 2429.
[169] M. Mehring, *Coord. Chem. Rev.* **2007**, *251*, 974.
[170] A. Døssing, A. Kadziola, P. Gawryszewska, A. Watras, A. Melchior, *Inorg. Chim. Acta* **2017**, *467*, 93.
[171] A. Døssing, H. Toftlund, A. Hazell, J. Bourassa, P. C. Ford, *J. Chem. Soc., Dalton Trans.* **1997**, 335.
[172] I. Bkouche-Waksman, J. Guilhem, C. Pascard, B. Alpha, R. Deschenaux, J.-M. Lehn, *Helv. Chim. Acta* **1991**, *74*, 1163.
[173] Y. V. Prokudina, E. I. Davydova, A. Virovets, B. Stöger, E. Peresypkina, A. V. Pomogaeva, A. Y. Timoshkin, *Chem. Eur. J.* **2020**, 16338.
[174] D. J. Williams, J. T. Anderton, E. A. Armstrong, M. H. Bowen, R. E. Hart, S. K. Tata, D. R. Smith, K. M. White, D. Vanderveer, *Main Group Chem.* **2007**, *6*, 263.
[175] A. J. Barton, A. R. J. Genge, W. Levason, G. Reid, *J. Chem. Soc., Dalton Trans.* **2000**, 2163.
[176] G. R. Willey, L. T. Daly, M. G. B. Drew, *J. Chem. Soc., Dalton Trans.* **1996**, 1063.
[177] NBO 7.0, E. D. Glendening, J. K. Badenhoop, A. E. Reed, J. E. Carpenter, J. A. Bohmann, C. M. Morales, P. Karafiloglou, C. R. Landis, F. Weinhold, Theoretical Chemistry Institute, University of Wisconsin, Madison, **2018**.
[178] R. Hua, *Curr. Org. Synth.* **2008**, *5*, 1.
[179] H. R. Kricheldorf, *Chem. Rev.* **2009**, *109*, 5579.
[180] D. Tiwari, D. Alibhai, D. J. Fermin, *ACS Energy Lett.* **2018**, *3*, 1882.
[181] S. L. Benjamin, *PhD thesis*, Faculty of Natural and Environmental Sciences, University of Southampton, Southampton, **2012**.
[182] G. A. Bowmaker, F. M. M. Hannaway, P. C. Junk, A. M. Lee, B. W. Skelton, A. H. White, *Aust. J. Chem.* **1998**, *51*, 331.
[183] H. Althaus, H. J. Breunig, E. Lork, *Organometallics* **2001**, *20*, 586.
[184] H. J. Breunig, H. Althaus, *Phosphorus, Sulfur, Silicon Relat. Elem.* **2001**, *168*, 123.
[185] J. Ramler, F. Fantuzzi, F. Geist, A. Hanft, H. Braunschweig, B. Engels, C. Lichtenberg, *submitted* **2021**.

[186] can be found under http://www.periodensystem-online.de/index.php?show=list&id=acid&prop=pKb-Werte&sel=oz&el=92, last checked 23.02.2021, 11:43.
[187] AAT Bioquest, can be found under https://www.aatbio.com/data-sets/pka-and-pkb-reference-table, **2019**, last checked 09.04.2021, 9:30.
[188] I. Kumar, P. Bhattacharya, K. H. Whitmire, *J. Organomet. Chem.* **2015**, *794*, 153.
[189] V. Stavila, E. V. Dikarev, *J. Organomet. Chem.* **2009**, *694*, 2956.
[190] V. Stavila, J. C. Fettinger, K. H. Whitmire, *Organometallics* **2007**, *26*, 3321.
[191] T. Dunaj, K. Dollberg, C. Ritter, F. Dankert, C. von Hänisch., *Eur. J. Inorg. Chem.* **2021**, 870.
[192] S. Shimada, O. Yamazaki, T. Tanaka, Y. Suzuki, M. Tanaka, *J. Organomet. Chem.* **2004**, *689*, 3012.
[193] S. Solyntjes, J. Bader, B. Neumann, H.-G. Stammler, N. Ignat'ev, B. Hoge, *Chem. Eur. J.* **2017**, 1557.
[194] A. M. Toma, A. Pop, A. Silvestru, T. Rüffer, H. Lang, M. Mehring, *Dalton Trans.* **2017**, *46*, 3953.
[195] Z. Xie, Z. Liu, F. Xue, T. C. Mak, *J. Organomet. Chem.* **1997**, *539*, 127.
[196] T. C. Devore, L. Brock, R. Kahlscheuer, K. Dulaney, J. L. Gole, *Chem. Phys.* **1991**, *155*, 423.
[197] E. Y. Chen, T. J. Marks, *Chem. Rev.* **2000**, *100*, 1391.
[198] C.-C. Chang, B.-S. Liao, S.-T. Liu, *Synlett* **2007**, 283.
[199] G. Wittig, P. Raff, *Justus Liebigs Ann. Chem.* **1951**, *573*, 195.
[200] G. Wittig, P. Raff, *Z. Naturforsch. B* **1951**, *6*, 225.
[201] E. Bernhardt, G. Henkel, H. Willner, *Z. Anorg. Allg. Chem.* **2000**, *626*, 560.
[202] D. Williams, B. Pleune, J. Kouvetakis, M. D. Williams, R. A. Andersen, *J. Am. Chem. Soc.* **2000**, *122*, 7735.
[203] N. V. Ignat'ev, M. Finze, *Eur. J. Inorg. Chem.* **2019**, 3539.
[204] S. Arlt, J. Harloff, A. Schulz, A. Stoffers, A. Villinger, *Inorg. Chem.* **2016**, *55*, 12321.
[205] S. Balasubramaniam, S. Kumar, A. P. Andrews, E. D. Jemmis, A. Venugopal, *Eur. J. Inorg. Chem.* **2020**, 2530.
[206] S. S. Chitnis, N. Burford, A. Decken, M. J. Ferguson, *Inorg. Chem.* **2013**, *52*, 7242.
[207] K. Rosenstengel, A. Schulz, A. Villinger, *Inorg. Chem.* **2013**, *52*, 6110.
[208] C. Kerpen, J. A. P. Sprenger, L. Herkert, M. Schäfer, L. A. Bischoff, P. Zeides, M. Grüne, R. Bertermann, F. A. Brede, K. Müller-Buschbaum, N. V. Ignat'ev, M. Finze, *Angew. Chem. Int. Ed.* **2017**, *56*, 2800.
[209] K. W. Morse, D. G. Holah, M. Shimoi, *Inorg. Chem.* **1986**, *25*, 3113.
[210] S. H. Zottnick, W. G. Daul, C. Kerpen, M. Finze, K. Müller-Buschbaum, *Chem. Eur. J.* **2018**, *24*, 15287.
[211] J. Bresien, C. Hering-Junghans, A. Schulz, M. Thomas, A. Villinger, *Organometallics* **2018**, *37*, 2571.
[212] L. A. Bischoff, M. Drisch, C. Kerpen, P. T. Hennig, J. Landmann, J. A. P. Sprenger, R. Bertermann, M. Grüne, Q. Yuan, J. Warneke, X.-B. Wang, N. V. Ignat'ev, M. Finze, *Chem. Eur. J.* **2019**, *25*, 3560.
[213] K. Delpy, H.-U. Meier, P. Paetzold, C. von Plotho, *Z. Naturforsch. B* **1984**, *39*, 1696.
[214] K. Delpy, D. Schmitz, P. Paetzold, *Chem. Ber.* **1983**, *116*, 2994.
[215] H. Braunschweig, M. Burzler, K. Radacki, F. Seeler, *Angew. Chem. Int. Ed.* **2007**, *46*, 8071.
[216] P. Schreyer, P. Paetzold, R. Boese, *Chem. Ber.* **1988**, *121*, 195.
[217] P. Paetzold, C. von Plotho, G. Schmid, R. Boese, B. Schrader, D. Bougeard, U. Pfeiffer, R. Gleiter, W. Schüfer, *Chem. Ber.* **1984**, *117*, 1089.
[218] F. Dahcheh, D. Martin, D. W. Stephan, G. Bertrand, *Angew. Chem.* **2014**, *126*, 13375.
[219] R. Boese, N. Niederprm, D. Blser, *Struct. Chem.* **1992**, *3*, 399.
[220] M. Bao, T. Hayashi, S. Shimada, *Organometallics* **2007**, *26*, 1816.
[221] J. Ramler, K. Radacki, J. Abbenseth, C. Lichtenberg, *Dalton Trans.* **2020**, *49*, 9024.

[222] C. J. Carmalt, N. C. Norman, A. Orpen, S. E. Stratford, *J. Organomet. Chem.* **1993**, *460*, C22-C24.
[223] C. J. Carmalt, D. Walsh, A. H. Cowley, N. C. Norman, *Organometallics* **1997**, *16*, 3597.
[224] J. Beckmann, J. Bolsinger, A. Duthie, P. Finke, E. Lork, C. Lüdtke, O. Mallow, S. Mebs, *Inorg. Chem.* **2012**, *51*, 12395.
[225] R. Hillwig, F. Kunkel, K. Harms, B. Neumüller, K. Dehnicke, *Z. Naturforsch. B* **1997**, *52*, 149.
[226] D. M. Hawley, G. Ferguson, *J. Chem. Soc., A* **1968**, 2059.
[227] L. O. Müller, D. Himmel, J. Stauffer, G. Steinfeld, J. Slattery, G. Santiso-Quiñones, V. Brecht, I. Krossing, *Angew. Chem. Int. Ed.* **2008**, *47*, 7659.
[228] H. Braunschweig, P. Brenner, P. Cogswell, K. Kraft, K. Schwab, *Chem. Commun.* **2010**, *46*, 7894.
[229] R. D. Adams, W. C. Pearl, *J. Organomet. Chem.* **2011**, *696*, 1198.
[230] M. N. Bochkarev, G. A. Razuvaev, L. N. Zakharov, Y. Struchkov, *J. Organomet. Chem.* **1980**, *199*, 205.
[231] O. Planas, F. Wang, M. Leutzsch, J. Cornella, *Science* **2020**, *367*, 313.
[232] A. P. M. Robertson, N. Burford, R. McDonald, M. J. Ferguson, *Angew. Chem. Int. Ed.* **2014**, *53*, 3480.
[233] A. J. Ashe III, L. Goossen, J. W. Kampf, H. Konishi, *Angew. Chem. Int. Ed.* **1992**, *31*, 1642.
[234] H. Sashida, *J. Chem. Soc., Chem. Commun.* **1998**, 767.
[235] S. Yasuike, H. Ohta, S. Shiratori, J. Kurita, T. Tsuchiya, *J. Chem. Soc., Chem. Commun.* **1993**, 1817.
[236] D. P. Mukhopadhyay, D. Schleier, S. Wirsing, J. Ramler, D. Kaiser, E. Reusch, P. Hemberger, T. Preitschopf, I. Krummenacher, B. Engels, I. Fischer, C. Lichtenberg, *Chem. Sci.* **2020**, *11*, 7562.
[237] T. J. Boyle, D. M. Pedrotty, B. Scott, J. W. Zillere, *Polyhedron* **1998**, *17*, 1959.
[238] J. R. Eveland, K. H. Whitmire, *Inorg. Chim. Acta* **1996**, *249*, 41.
[239] V. Balasanthiran, M. H. Chisholm, C. B. Durr, J. C. Gallucci, *Dalton Trans.* **2013**, *42*, 11234.
[240] S. H. Chikkali, D. Gudat, F. Lissner, M. Niemeyer, T. Schleid, M. Nieger, *Chem. Eur. J.* **2009**, *15*, 482.
[241] G. Zanotti, A. Del Pra, *Acta Cryst. B* **1978**, *34*, 2997.
[242] H. C. Chang, H. Miyasaka, S. Kitagawa, *Inorg. Chem.* **2001**, *40*, 146.
[243] C. G. Pierpont, H. H. Downs, *J. Am. Chem. Soc.* **1976**, *98*, 4834.
[244] H. Sommer, A. Eichhöfer, D. Fenske, *Z. Anorg. Allg. Chem.* **2008**, *634*, 436.
[245] M. Dräger, B. M. Schmidt, *J. Organomet. Chem.* **1985**, *290*, 133.
[246] P. Šimon, R. Jambor, A. Růžička, L. Dostál, *Organometallics* **2013**, *32*, 239.
[247] K. M. Anderson, C. J. Baylies, A. H. M. Monowar Jahan, N. C. Norman, A. G. Orpen, J. Starbuck, *Dalton Trans.* **2003**, 3270.
[248] P. Šimon, R. Jambor, A. Růžička, L. Dostál, *J. Organomet. Chem.* **2013**, *740*, 98.
[249] M. R. Binns, R. K. Haynes, *J. Org. Chem.* **1981**, *46*, 3790.
[250] G. M. Sheldrick, *Acta Cryst. A* **2015**, *71*, 3.
[251] G. M. Sheldrick, *Acta Cryst. A* **2008**, *64*, 112.
[252] G. Sheldrick, *Acta Cryst. A* **2014**, *70*, C1437-C1437.
[253] R. B. King, Organometallic Syntheses, Elsevier Science, Burlington, **1988**.
[254] J. Ramler, J. Poater, F. Hirsch, B. Ritschel, I. Fischer, F. M. Bickelhaupt, C. Lichtenberg, *Chem. Sci.* **2019**, *10*, 4169.
[255] J. Ramler, L. Wüst, L. Wolz, C. Lichtenberg, *Organometallics* **2021**, *40*, 832.

XX Appendix

1 Supporting Information

1.1 Chapter III

Supporting Information for chapter III can be found under https://doi.org/10.1002/anie.201904365.

1.2 Chapter IV

Supporting Information for chapter IV can be found under https://doi.org/10.1002/chem.202002219.

1.3 Chapter VI

Supporting Information for chapter VI can be found under https://doi.org/10.1021/acs.inorgchem.9b03189.

1.4 Chapter VII

Supporting Information for chapter VII can be found under https://doi.org/10.1002/chem.202001674.

1.5 Chapter VIII

The Dimethylbismuth Cation: Entry into Dative Bi–Bi Bonding and Unconventional Methyl Exchange

Jacqueline Ramler,[1] Felipe Fantuzzi,[1,2] Felix Geist,[1] Anna Hanft,[1] Holger Braunschweig,[1] Bernd Engels,[1] and Crispin Lichtenberg[1,]*

1 Institute of Inorganic Chemistry, Julius-Maximilians-University Würzburg, Am Hubland, 97074 Würzburg, Germany.

2 Institute of Physical and Theoretical Chemistry, Julius-Maximilians-University Würzburg, Emil-Fischer-Str. 42, 97074, Würzburg, Germany.

Table of Contents

Experimental

General considerations. All air- and moisture-sensitive manipulations were carried out using standard vacuum line Schlenk techniques or in gloveboxes containing an atmosphere of purified argon. Solvents were degassed and purified according to standard laboratory procedures. NMR spectra were recorded on Bruker instruments operating at 300, 400 or 500 MHz with respect to ^{1}H. ^{1}H and ^{13}C NMR chemical shifts are reported relative to $SiMe_4$ using the residual ^{1}H and ^{13}C chemical shifts of the solvent as a secondary standard. ^{19}F NMR chemical shifts are reported relative to $CFCl_3$ as external standards. NMR spectra were recorded at ambient temperature (typically 23 °C), if not otherwise noted. UV-vis spectra were recorded with a UV5 Mettler Toledo UV-vis-Excellence spectrometer. Elemental analyses was obtained using a Leco, or a Carlo Erba instrument. Single crystals suitable for X-ray diffraction analysis were coated with polyisobutylene or perfluorinated polyether oil in a glovebox, transferred to a nylon loop and then to the goniometer of a diffractometer equipped with a molybdenum X-ray tube (λ = 0.71073 Å). The data obtained were integrated with SAINT and a semi-empirical absorption correction from equivalents with SADABS was applied. The structure was solved and refined using the Bruker SHELX 2014 software package. All non-hydrogen atoms were refined with anisotropic displacement parameters. All hydrogen atoms were refined isotropically on calculated positions by using a riding model with their U_{iso} values constrained to 1.5 U_{eq} of their pivot atoms for terminal sp^3 carbon atoms and 1.2 times for all other atoms. Crystallographic data have been deposited with the Cambridge Crystallographic Data Centre as supplementary publication numbers. 2080851-2080853. These data can be obtained free of charge from The Cambridge Crystallographic Data Centre.

For comparison with compounds **1**-**3**, NMR spectroscopic data in the solvent CD_2Cl_2 was collected for literature-known $BiMe_3$.

^{1}H NMR (500 MHz, CD_2Cl_2): δ = 1.11 (s, 9H, CH_3) ppm.
^{13}C NMR (125 MHz, CD_2Cl_2): δ = –6.82 (br, CH_3) ppm.

[$BiMe_2(SbF_6)$](1). A solution of $AgSbF_6$ (0.22 g, 0.63 mmol) in methylene chloride (DCM) (3 mL) was added to a solution of $BiMe_2Cl$ (0.17 g, 0.63 mmol) in DCM (2 mL). The precipitate was filtered off. All volatiles were removed from the yellow filtrate under reduced pressure to give a yellow powder, which was dried in vacuo. Yield: 0.22 g, 0.47 mmol, 75%.

Single crystals suitable for X-ray diffraction analysis of **1** were obtained by layering a solution of **1** in DCM with *n*-pentane and storage at –30 °C for 16 h.

^{1}H NMR (400 MHz, C_6D_6): δ = 1.47 (s, 6H, CH_3) ppm.
^{1}H NMR (400 MHz, CD_2Cl_2): δ = 2.28 (s, 6H, CH_3) ppm.
^{13}C NMR (101 MHz, C_6D_6): δ = 66.72 (br, CH_3) ppm.
^{13}C NMR (101 MHz, CD_2Cl_2): δ = 64.38 (br, CH_3) ppm.
^{19}F NMR (376 MHz, C_6D_6): δ = –123.02 (s, SbF_6) ppm.
^{19}F NMR (376 MHz, CD_2Cl_2): δ = –128.44 (s, SbF_6) ppm.

Elemental analysis: Anal. calc. for: $C_2H_6BiSbF_6$ (474.84 g/mol): C 5.06, H 1.27, found: C 5.45, H 1.40.

The NMR spectra obtained in C_6D_6 are likely represent the benzene adduct in solution instead of the contact ion pair. This is indicated by a color change from yellow to colorless when dissolving

1 in benzene. Unfortunately, attempts to crystallize the benzene adduct only lead in the precipitation of the contact ion pair as yellow crystals. However, reaction of **1** (20.0 mg, 42.1 µmol) with two equivalents of hexamethyl benzene (12.8 mg, 78.8 µmol) in CD_2Cl_2 (0.5 mL) resulted in a highfield shift of the methyl protons of **1** in the ^{1}H NMR spectrum obtained from the reaction solution ($\Delta\delta$ = 0.5 ppm), which is in line with the results obtained for the pyridine adduct **2** (data for compound $[BiMe_2(C_6Me_6)_n][SbF_6]$: ^{1}H NMR (400 MHz, CD_2Cl_2): δ = 1.81 (s, 6H, $BiMe_2$), 2.26 (s, 36H, C_6Me_6) ppm.).

$[BiMe_2(py)_2][SbF_6]$ (2). $[BiMe_2(SbF_6)]$ (**1**) (85.6 mg, 0.18 mmol) was dissolved in DCM (2 mL), and pyridine (28.5 mg, 0.36 mmol, 30 µl) was added. The colorless solution was layered with *n*-pentane (2 mL). After 1 d at –30 °C a colorless crystalline solid had precipitated, was isolated by filtration, and dried in vacuo. Yield: 97 mg, 0.15 mmol, 84%.

^{1}H NMR (400 MHz, CD_2Cl_2): δ = 1.79 (s, 6H, CH_3), 7.60 (t, 4H, $^3J_{HH}$ = 6.92 Hz, H2/H6), 8.05 (t, 2H, $^3J_{HH}$ = 7.75 Hz, H4), 8.64 (d, 4H, $^3J_{HH}$ = 4.67 Hz, H3/H5) ppm.
^{13}C NMR (125 MHz, CD_2Cl_2): δ = 33.86 (CH_3), 126.86 (s, C2/C6), 140.58 (s, C4), 149.75 (s, C3/C5) ppm.

A signal for the $[SbF_6]^-$ anion in a ^{19}F NMR experiment could not be detected due to signal broadening.

Elemental analysis: Anal. calc. for: $C_2H_6BiF_6Sb(C_5H_5N)_2$ (633.00 g/mol): C 22.77, H 2.55, N 4.43 found: C 22.96, H 2.32, N 4.77.

$[BiMe_2(BiMe_3)(SbF_6)]$ (3). [$BiMe_2(SbF_6)]$ (**1**) (20 mg, 42.2 µmol) was dissolved in DCM (2 mL) and a solution of $BiMe_3$ (11.2 mg, 42.2 µmol) in DCM (1 mL) was added. The light yellow solution was stored at –30 °C. After 1 d light yellow crystals were obtained, isolated by filtration, and dried in vacuo. Yield: 27 mg, 37.0 µmol, 88%.

^{1}H NMR (500 MHz, 298.15 K, CD_2Cl_2): δ = 2.05 (br, 15H, CH_3) ppm.
^{1}H NMR (300 MHz, 298.15 K, CD_2Cl_2): δ = 2.05 (br, 15H, CH_3) ppm.
^{1}H NMR (300 MHz, 233.15 K, CD_2Cl_2): δ = 1.97 (s, 9H, $Bi(CH_3)_3$), 2.21 (s, 6H, $Bi(CH_3)_2$) ppm.
^{13}C NMR (126 MHz, 233.15 K, CD_2Cl_2): δ = 26.07 (s, CH_3), 73.46 (s, CH_3) ppm.
^{19}F NMR (470 MHz, 233.15 K, CD_2Cl_2): δ = –124.39 (SbF_6) ppm.

Elemental analysis: Anal. calc. for: $C_5H_{15}Bi_2F_6Sb$ (728.89 g/mol): C 8.24, H 2.07, found: C 8.39, H 1.89.

Reaction of $Bi_2Me_5SbF_6$ with two equivalents of pyridine. Pyridine (3.3 µL, 41 µmol) was added to a light yellow solution of $Bi_2Me_5SbF_6$ (**3**) (15.0 mg, 20.6 µmol) in CD_2Cl_2 (0.5 mL). A ^{1}H NMR spectroscopic analysis of the obtained colorless solution showed the quantitative formation of $BiMe_3$ and $BiMe_2(py)_2SbF_6$ (**2**).

Single Crystal X-ray Diffraction Analysis

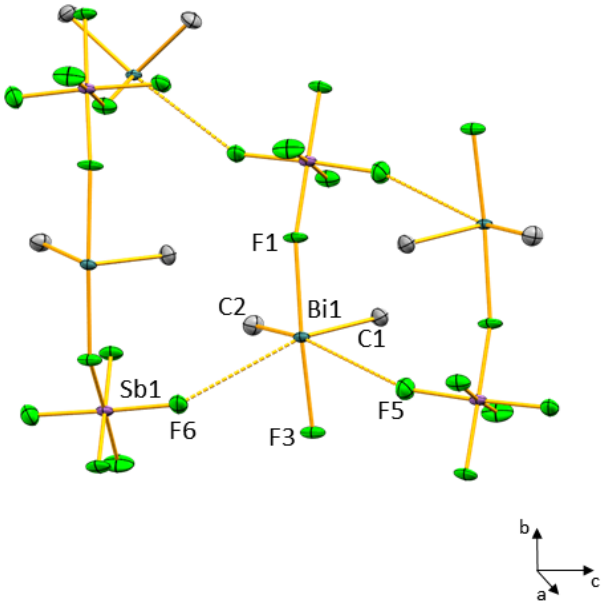

Figure S1. Cutout of the solid-state structure of $[BiMe_2(SbF_6)]$ (**1**) (including weak intermolecular contacts). Displacement ellipsoids are represented at the 50% probability level. Hydrogen atoms are omitted for clarity. Selected bond length (Å) and angles (°): Bi1–C1, 2.215(5); Bi1–C2, 2.223(5); Bi1–F1, 2.451(3); Bi1–F3, 2.452(3); Bi1···F5, 3.272; Bi1···F6, 3.452; C1–Bi1–C2, 93.0(2); C1–Bi1–F1, 83.91(17); C2–Bi1–F1, 87.20(17); C1–Bi1–F3, 88.60(17); C2–Bi1–F3, 86.18(17); F1–Bi1–F3, 169.73(11); Sb1–F1–Bi1, 160.53(17).

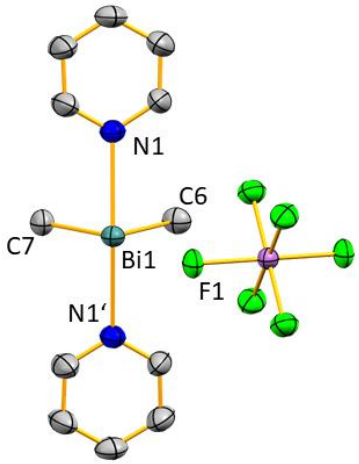

Figure S2. Molecular structure of $[BiMe_2(py)_2][SbF_6]$ (**2**) in the solid state. Displacement ellipsoids are shown at the 50% probability level. Hydrogen atoms and second, crystallographically independent $[SbF_6]^-$ anion which is present in the unit cell are omitted for clarity (the overall occupancy of each $[SbF_6]^-$ moiety is 0.5). Selected bond length (Å) and angles (°): Bi1–C7, 2.223(12); Bi1–C6, 2.235(12); Bi1–N1, 2.519(7); Bi1–N1', 2.519(7); Bi1···F1, 3.483(7); C7–Bi1–C6, 92.3(5); C7–Bi1–N1, 86.35(16); C6–Bi1–N1, 86.08(16); C7–Bi1–N1, 86.35(16); C6–Bi1–N1, 86.08(16); N1–Bi1–N1', 169.1(3).

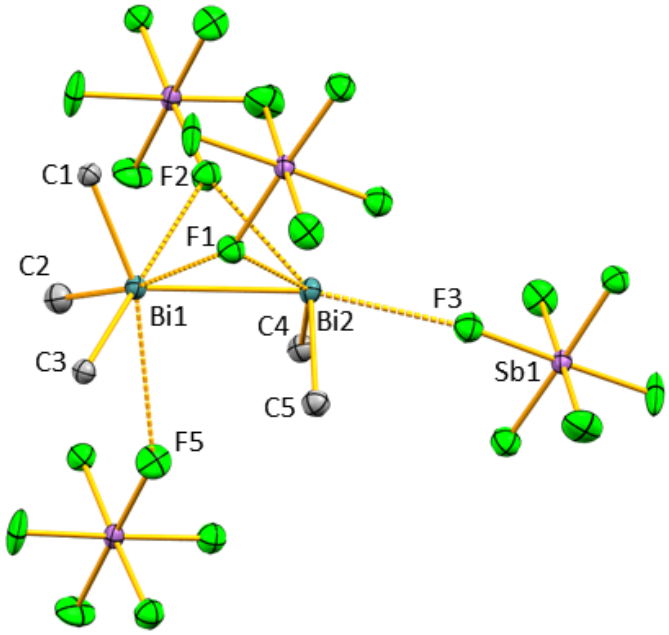

Figure S3. Cutout of the solid state structure of $[Bi_2Me_5(SbF_6)]$ (**3**) (including weak intermolecular interactions). Displacement ellipsoids are shown at the 50% probability level. Hydrogen atoms are omitted for clarity. Three of the four $[SbF_6]^-$ anions exceed one formula unit and belong to neighboring $Bi_2Me_5SbF_6$ units. Selected bond length (Å) and angles (°): C4–Bi2, 2.24(2); C5–Bi2, 2.24(2); C1–Bi1, 2.219(18); Bi1–C2, 2.21(2); Bi1–C3, 2.223(18); Bi1–Bi2, 3.0005(11); Bi2···F3, 2.809(12); Bi1···F1, 3.212; Bi1–F2, 3.177; Bi2···F1, 3.366; Bi2···F2, 3.275; Bi1···F5, 3.274; C2–Bi1–C1, 97.7(7); C2–Bi1–C3, 103.1(8); C1–Bi1–C3, 101.6(7); C2–Bi1–Bi2, 120.6 (6); C1–Bi1–Bi2, 113.9(5); C3–Bi1–Bi2, 116.8(5); C5–Bi2–C4, 94.2(8); C5–Bi2–Bi1, 90.3(5); C4–Bi2–Bi1, 91.8(5).

$[BiMe_2(BiMe_3)(SbF_6)]$ (**3**) crystallizes in the monoclinic space group $P2_1/c$ with $Z = 4$ as a two-component twin with the two components in a ratio of 99:1 that are related by a 180° rotation about the reciprocal [100] axis.

Variable Temperature NMR Spectroscopic Experiments

Variable temperature ^{1}H NMR spectroscopic experiments on CD_2Cl_2 solutions of compound **3** were carried out in the temperature range of –50 °C to +25 °C. For line shape analyses the program TopSpin 4.0.4 of Bruker was used. At room temperature, **3** shows only one broad resonance, which splits into two resonances with the integral ratio 2:3 in the low-temperature scenario. The coalescence temperature is 16 °C.

Since the Bruker software *DNMR Lineshape Analysis* has limited capabilities when exchange reactions are considered, the following intermolecular exchange model was used (Figure S4). The activation parameters were obtained from the Eyring plot (Figure S5) and are summarized in Table S1.

An alternative approach, in which line shape analysis with intermolecular exchange reactions between two methyl groups and three equivalent methyl groups was examined, gave very similar results ($\Delta G^{\ddagger}$ (298 K) = 13.3 kcal · mol^{-1}).

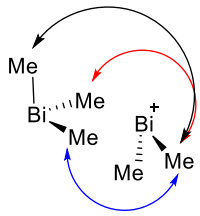

Figure S4. Exchange reactions which form the basis for the line shape analysis.

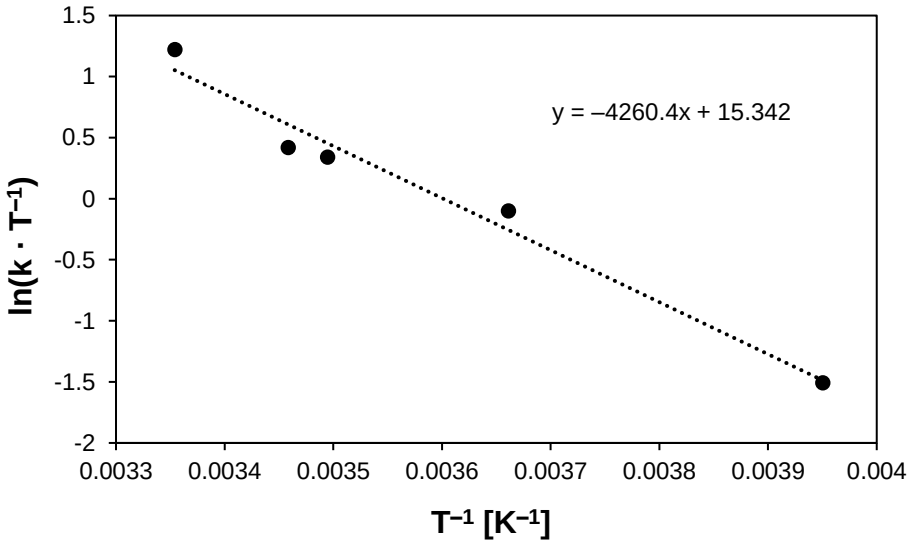

Figure S5. Eyring plot of the reaction rate for the methyl exchange in $Bi_2Me_5SbF_6$ (3) determined by line shape analysis.

Table S1. Activation parameters determined by line shape analysis of VT ^{1}H NMR spectra of $Bi_2Me_5SbF_6$ (**3**).

Compound	***ΔG*‡ (298 K)** [kcal · mol^{-1}]	***ΔH*‡** [kcal · mol^{-1}]	***ΔS*‡** [cal · mol^{-1}]	***k* (298 K)** [s^{-1}]
$Bi_2Me_5SbF_6$	13.5	8.5	–16.7	1010

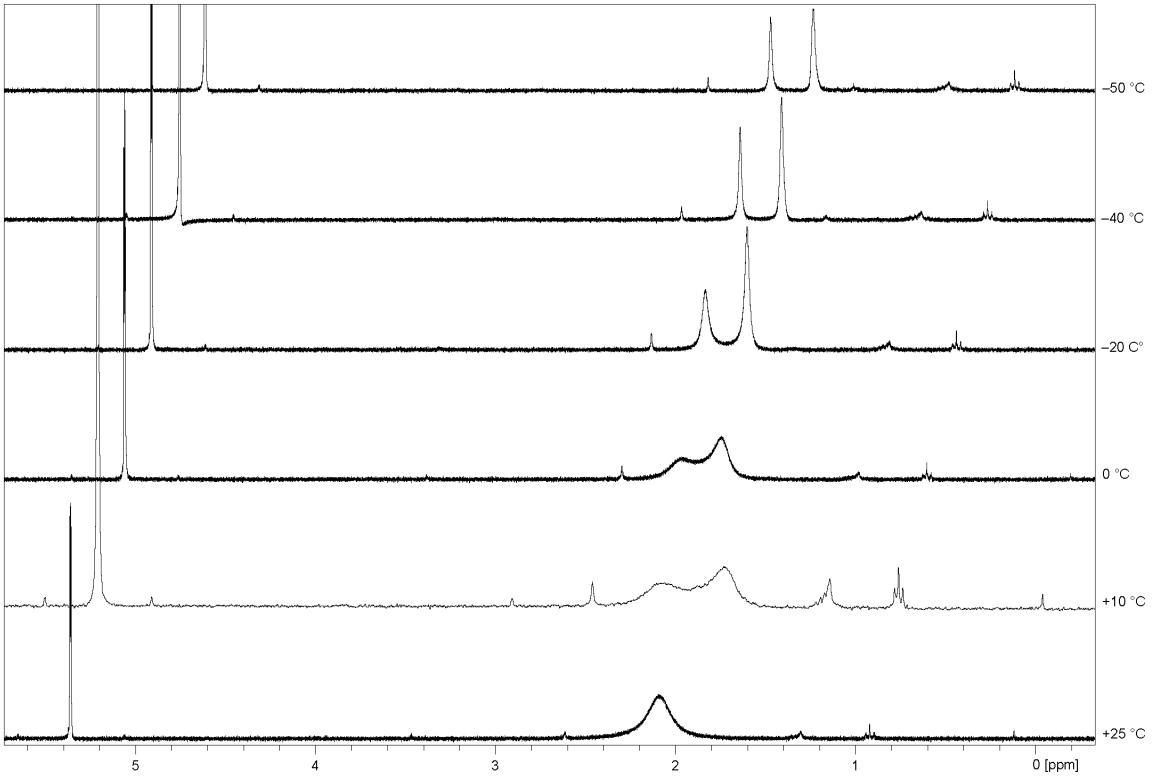

Figure S6. VT ^{1}H NMR spectra of [$Bi_2Me_5(SbF_6)$] (**3**) in a temperature range of +25 °C to –50 °C. The coalescence temperature is 289.15 K (16 °C). Beginning decomposition of [$Bi_2Me_5(SbF_6)$] (**3**) can be observed during the VT ^{1}H NMR spectroscopic measurements.

UV/vis Spectroscopy and TD-DFT Calculations

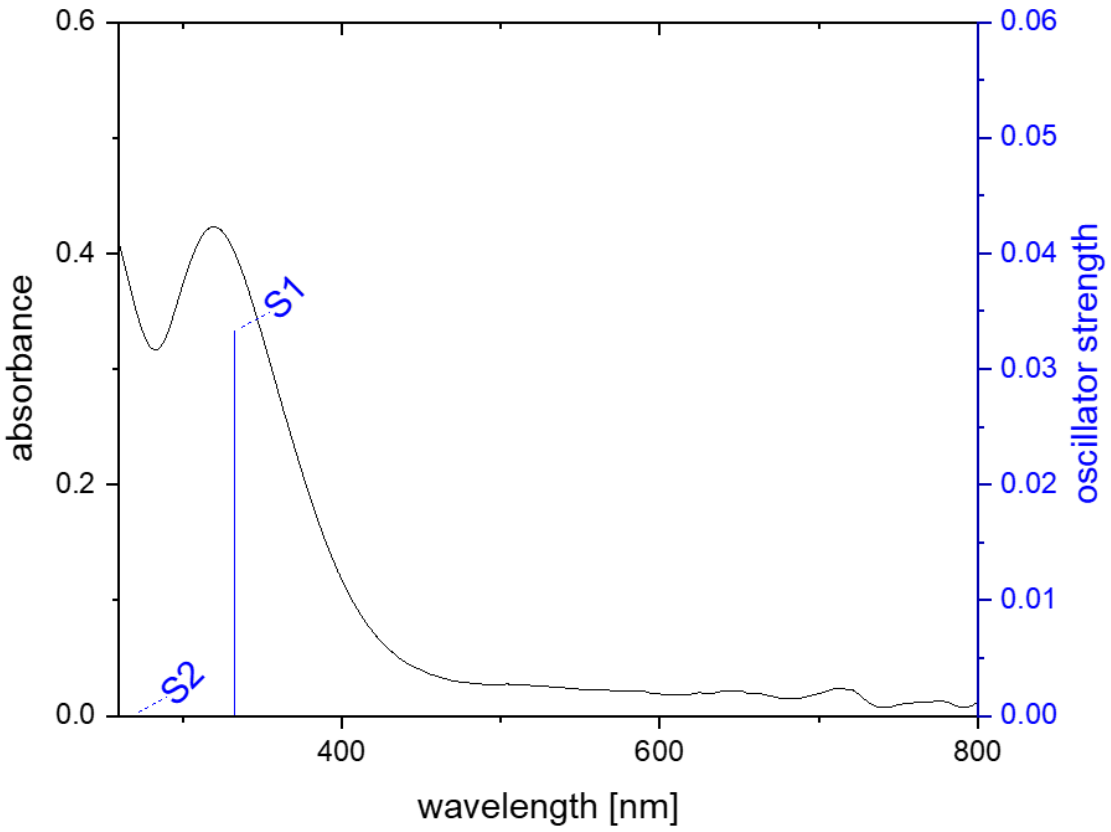

Figure S7. Experimental UV/vis spectrum of [$BiMe_2(SbF_6)$] (**1**) (3.4 mM) in DCM (black, absorption maximum at 321 nm) and calculated transitions (blue).

Table S2. Details on lowest energy UV/vis transitions relevant to the experimental absorption spectrum of $BiMe_2SbF_6$ (**1**) as determined by TD-DFT calculations.

Excitation	**λ [nm]**	**f**	**Main MO contributions**	
			type	**%**
$S_0 \rightarrow S_1$	332.7	0.0333	HOMO → LUMO	72
			HOMO → LUMO+1	27
$S_0 \rightarrow S_2$	268.0	0.0000	HOMO-1 → LUMO	27
			HOMO-1 → LUMO+1	72
$S_0 \rightarrow S_3$	236.2	0.0079	HOMO → LUMO	27
			HOMO → LUMO+1	71

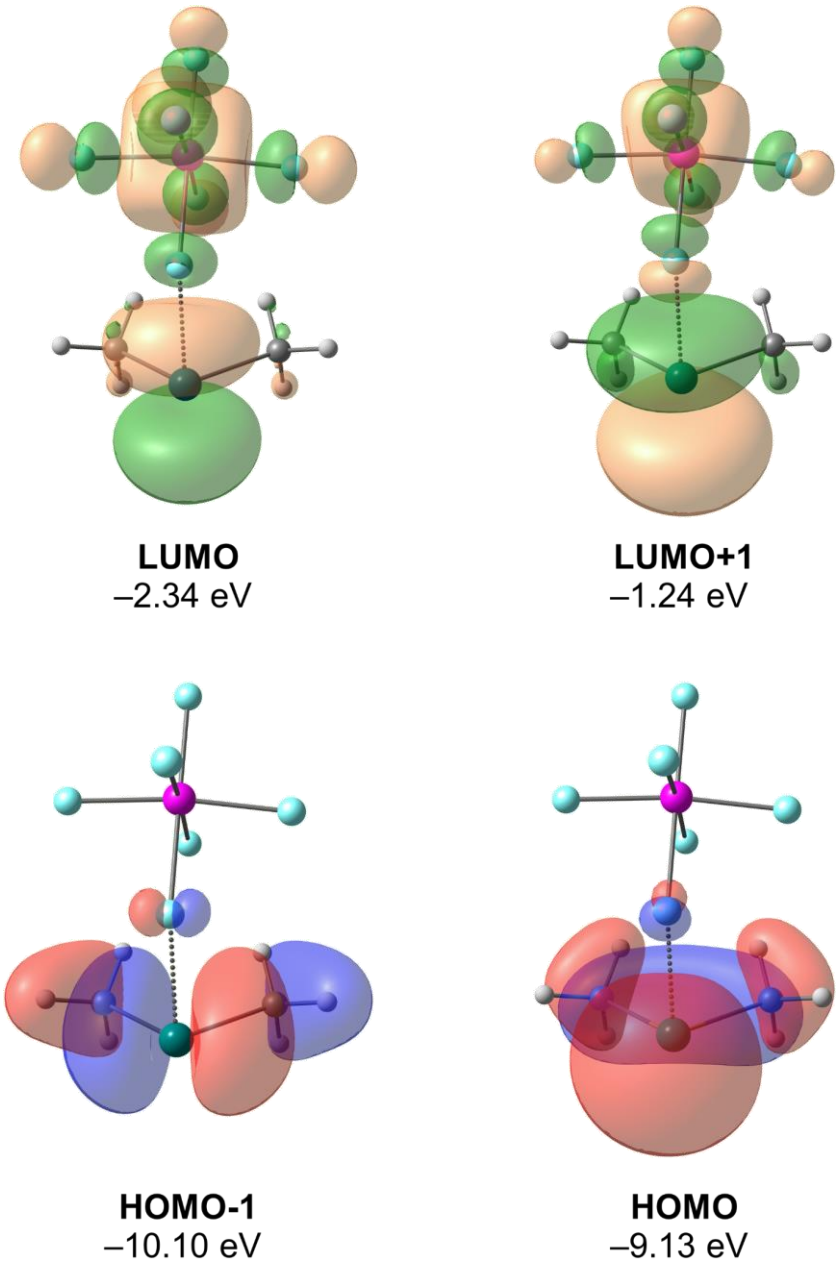

Figure S8. Selected molecular orbitals of compound [$BiMe_2(SbF_6)$] (**1**) (isovalues = 0.03) with main contributions to transitions listed in Table S2.

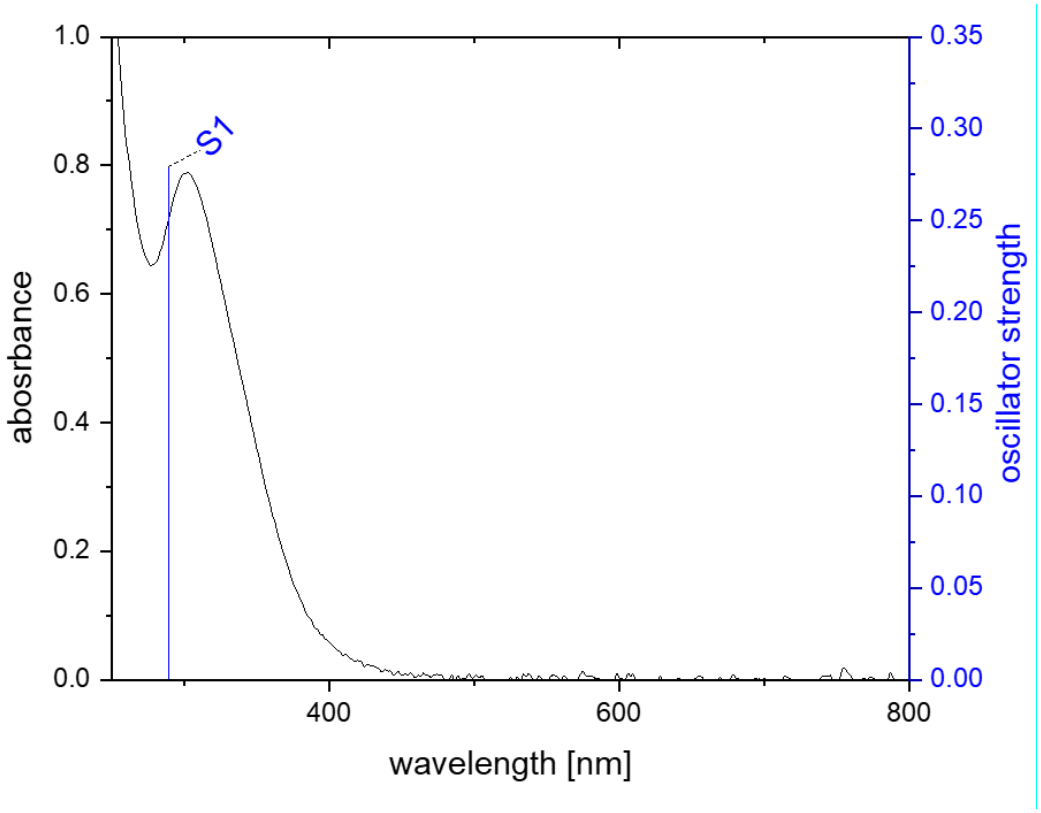

Figure S9. Experimental UV/vis spectrum of $[Bi_2Me_5(SbF_6)]$ (**3**) (4.2 mM) in DCM (black, absorption maximum at 302 nm) and calculated transition (blue).

Table S3. Details on lowest energy UV/vis transitions relevant to the experimental absorption spectrum of $Bi_2Me_5SbF_6$ (**3**) as determined by TD-DFT calculations.

Excitation	**λ [nm]**	**f**	**Main MO contributions**	
			type	**%**
$S_0 \rightarrow S_1$	288.8	0.2792	HOMO → LUMO	56
			HOMO → LUMO+1	21
			HOMO-1 → LUMO	14
			HOMO-1 → LUMO+1	6

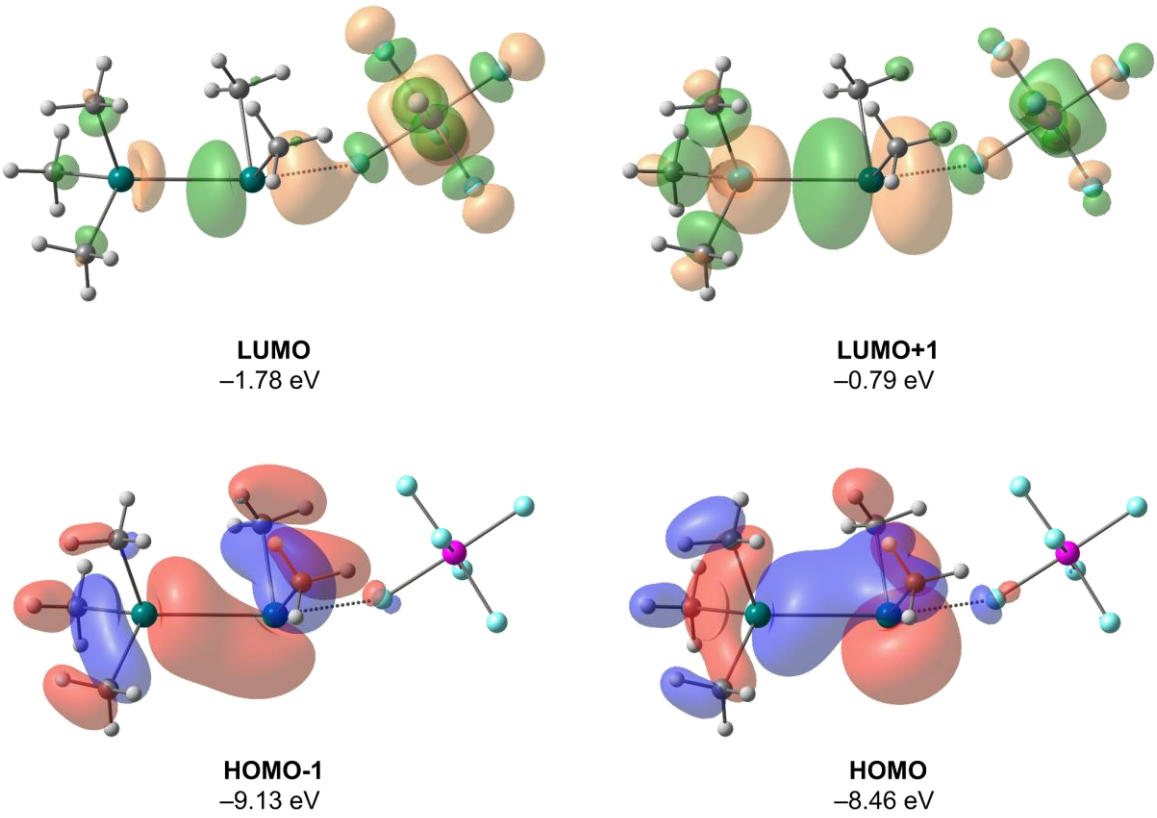

Figure S10. Selected molecular orbitals of compound $[Bi_2Me_5(SbF_6)]$ (**3**) (isovalues = 0.03) with main contributions to transition $S_0 \rightarrow S_1$ listed in Table S3.

DFT Calculations

Energies of Compounds Investigated by DFT Calculations

The energies of compounds investigated by DFT calculations are given in Table S4 (concentration corrections not added). Their Cartesian coordinates are given in a separate .xyz file.

Table S4. Energies of calculated species.

Entry	Compound	ΔG [hartree]	Imaginary frequencies
1	$BiMe_2SbF_6$ (**1**)	–690.0794	none
2	$BiMe_2(py)_2SbF_6$ (**2**)	–1186.7053	none
3	$BiMe_3$	–125.1482	none
4	$Bi_2Me_5SbF_6$ (**3**)	–815.227712	none
5	$Bi_2Me_5SbF_6$ (**4**)	–815.194804	none
6	$Bi_2Me_5SbF_6$ (**5**)	–815.216688	none
7	$Bi_2Me_5SbF_6$ (**TS1**)	–815.205027	1
8	$Bi_2Me_5SbF_6$ (**6**)	–815.216337	none
9	Bi_2Me_4	–170.514824	none
10	$N_2Me_5^+$ (**7-N**)	–308.714929	none
11	$P_2Me_5^+$ (**7-P**)	–882.027852	none
12	$As_2Me_5^+$ (**7-As**)	–211.53249	none
13	$Sb_2Me_5^+$ (**7-Sb**)	–210.094591	none
14	$Bi_2Me_5^+$ (**7-Bi**)	–210.172091	none
15	$Me_2Pn–(\mu_2\text{-}sp^2\text{-}CH_3)–PnMe_2^+$ (**8-P**)	–881.932491	1
16	$Me_2Pn–(\mu_2\text{-}sp^2\text{-}CH_3)–PnMe_2^+$ (**8-As**)	–211.475067	none
17	$Me_2Pn–(\mu_2\text{-}sp^2\text{-}CH_3)–PnMe_2^+$ (**8-Sb**)	–210.061389	none
18	$Me_2Pn–(\mu_2\text{-}sp^2\text{-}CH_3)–PnMe_2^+$ (**8-Bi**)	–210.160652	none
19	$N_2Me_5^+$ (**9-N**)	–308.754084	none

NBO Calculations

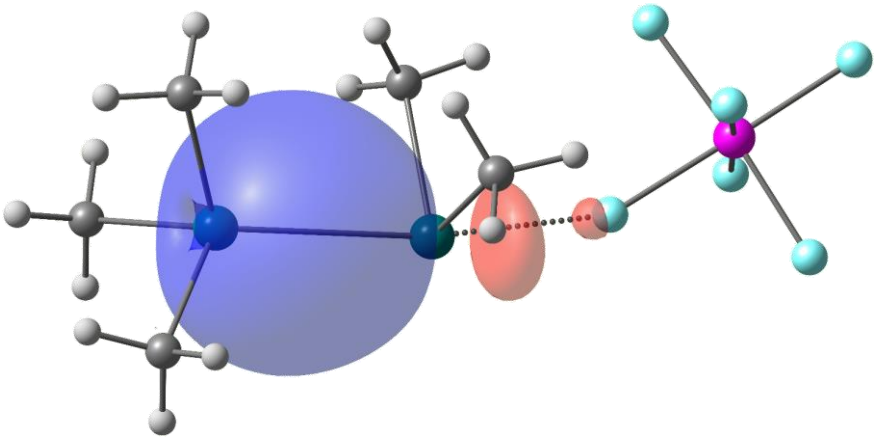

Figure S11. NBO of **3** depicting the Bi→Bi bond.

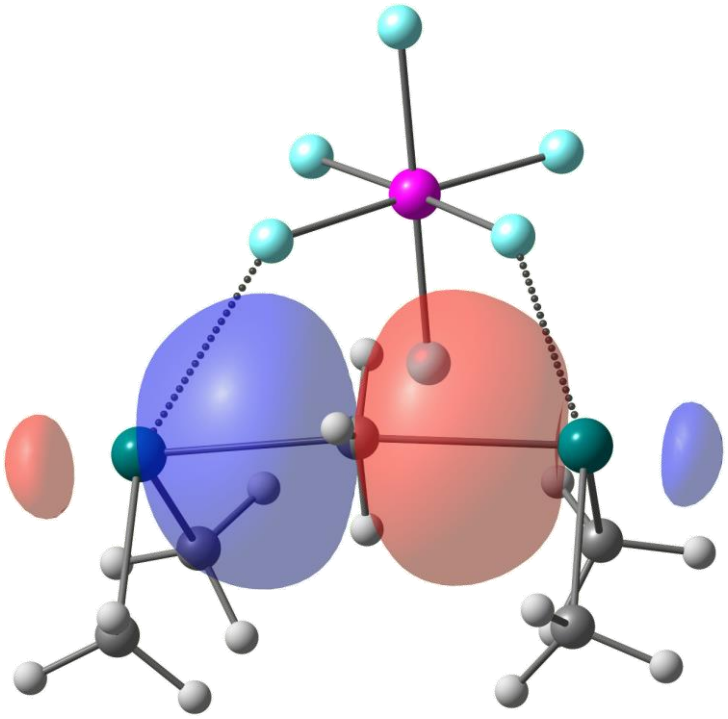

Figure S12. NBO of **6** depicting the Bi–(μ_2-sp^2-CH_3)–Bi three-center-two-electron bond.

IBO Calculations

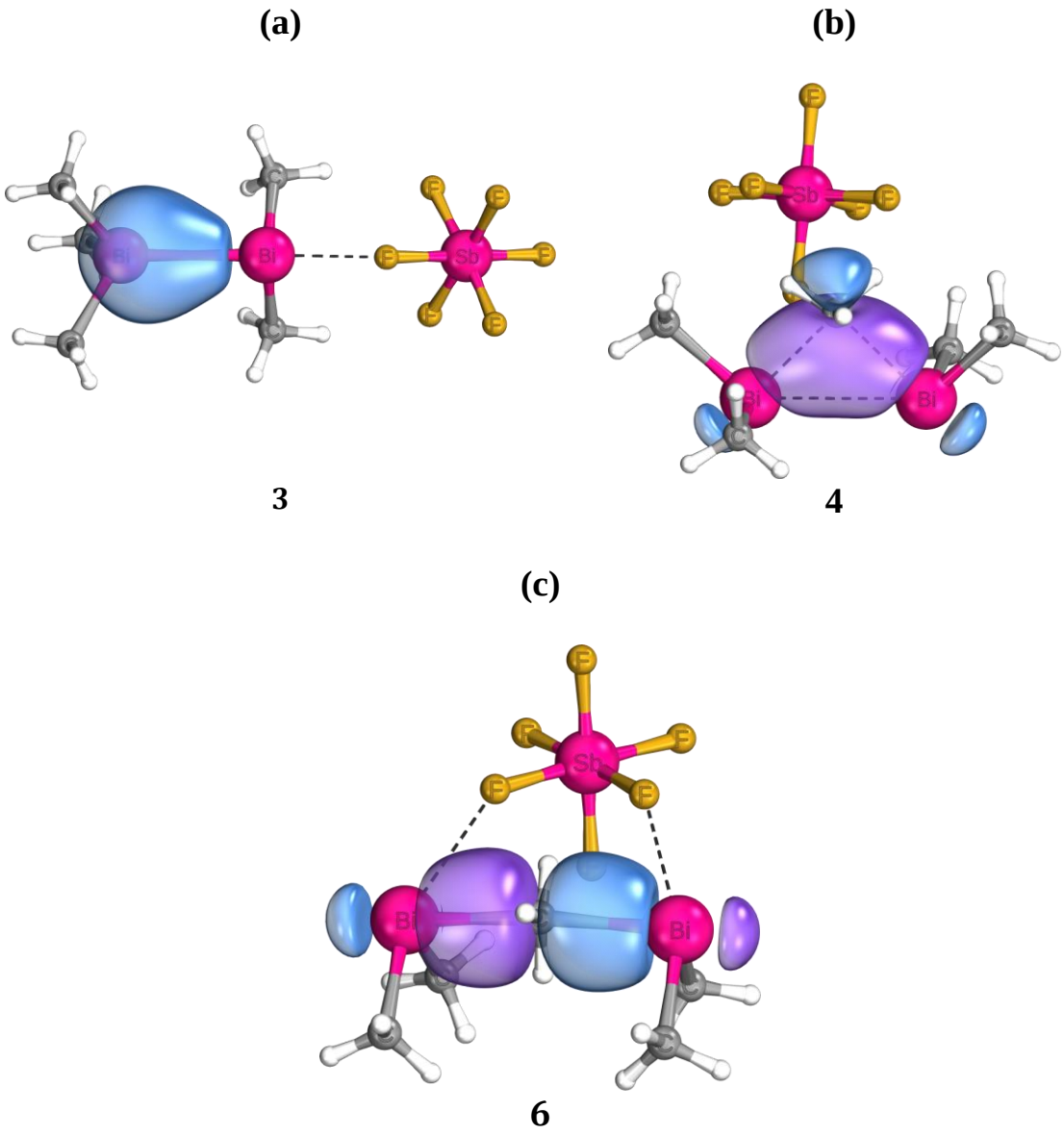

Figure S13. NBOs of depicting the (a) Bi→Bi bond of **3**, (b) the three-center-two-electron bond of **4**, and (c) the Bi–(μ_2-sp^2-CH_3)–Bi three-center-two-electron bond of **6**.

EDA-NOCV Calculations

Table S5. EDA-NOCV results (B3LYP-D3/QZ4P) for **3**. The donor-acceptor and the electron-sharing bond scenarios for the fragments $BiMe_3$ and **1** are considered. Energy terms are given in kcal mol^{-1}. For ΔE_{disp}, ΔE_{elstat}, and ΔE_{orb}, the values in parentheses show the weight of each contribution with respect to the total attractive interaction. For $\Delta E_{orb(1)}$ and $\Delta E_{orb(rest)}$, the values in parentheses show the weight of each contribution with respect to the total orbital interaction, ΔE_{orb}.

Energy terms	**$BiMe_3$ + 1** **Donor-acceptor bond**	**$[BiMe_3]^+ + 1^-$** **Electron-sharing bond**
ΔE_{int}	–20.9	–137.1
ΔE_{pauli}	53.4	90.9
ΔE_{elstat}	–35.9 (48.4%)	–123.8
ΔE_{disp}	–3.9 (5.3%)	–3.9
ΔE_{orb}	–34.4 (46.4%)	–100.3
$\Delta E_{orb(1)}$	–29.8 (86.7%)	-
$\Delta E_{orb-rest}$	–4.6 (13.3%)	-

NMR Spectra of Isolated Complexes and Reaction Mixtures

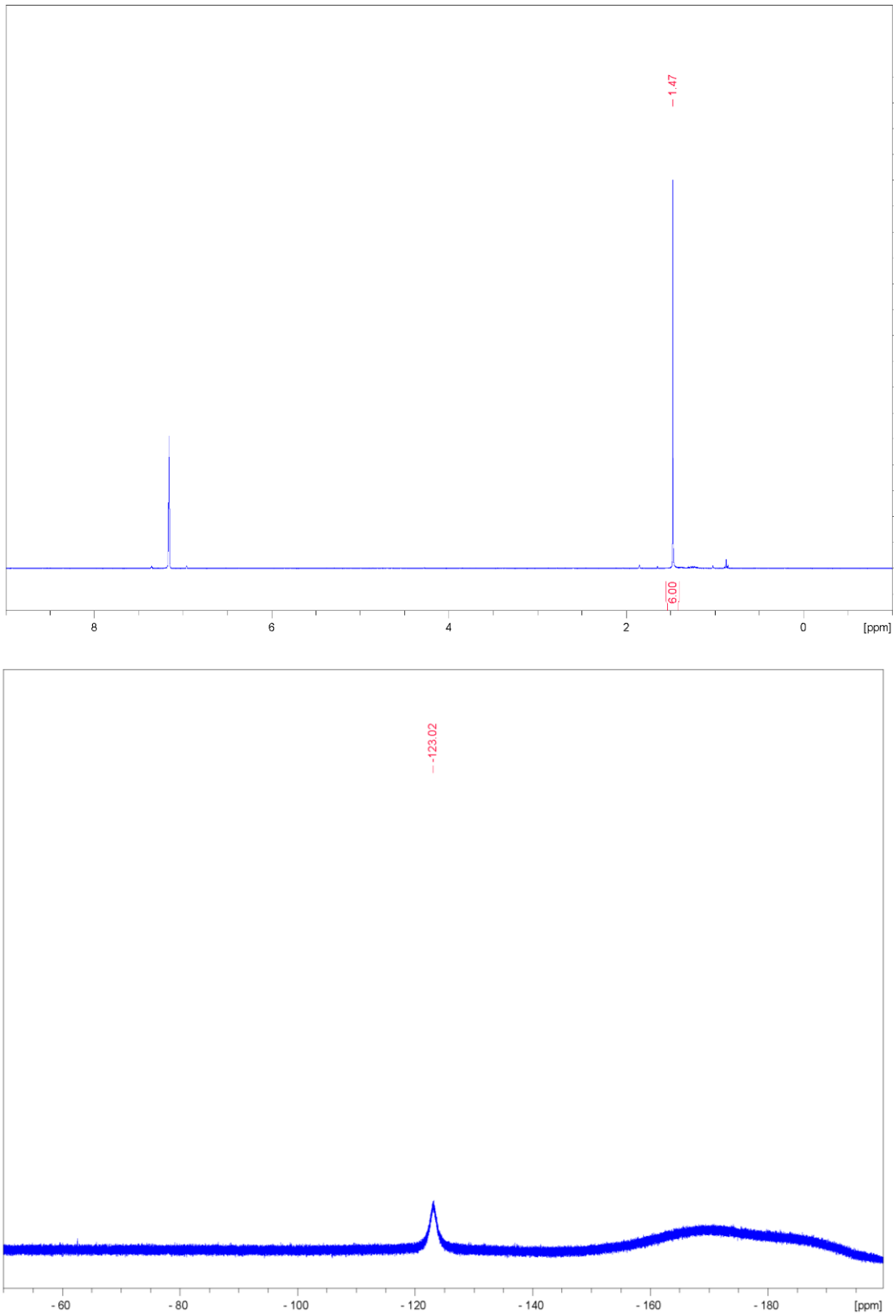

Figure S14. ^{1}H and ^{19}F NMR spectra of $[BiMe_2(SbF_6)]$ (**1**) in C_6D_6.

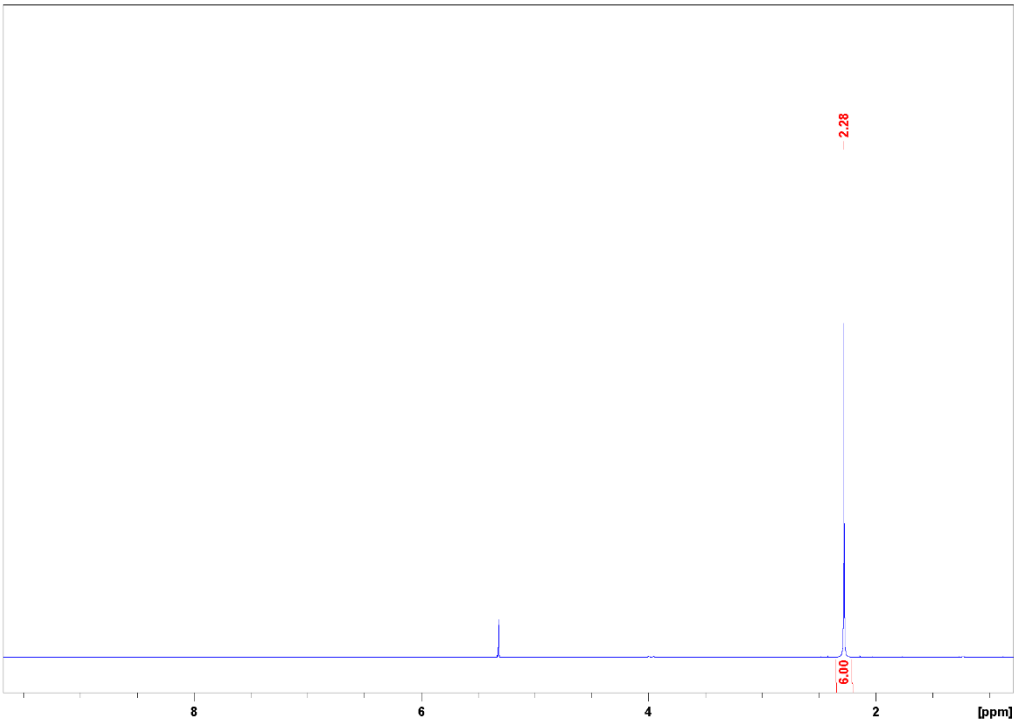

Figure S15. ^{1}H NMR spectrum $[BiMe_2(SbF_6)]$ (**1**) in CD_2Cl_2.

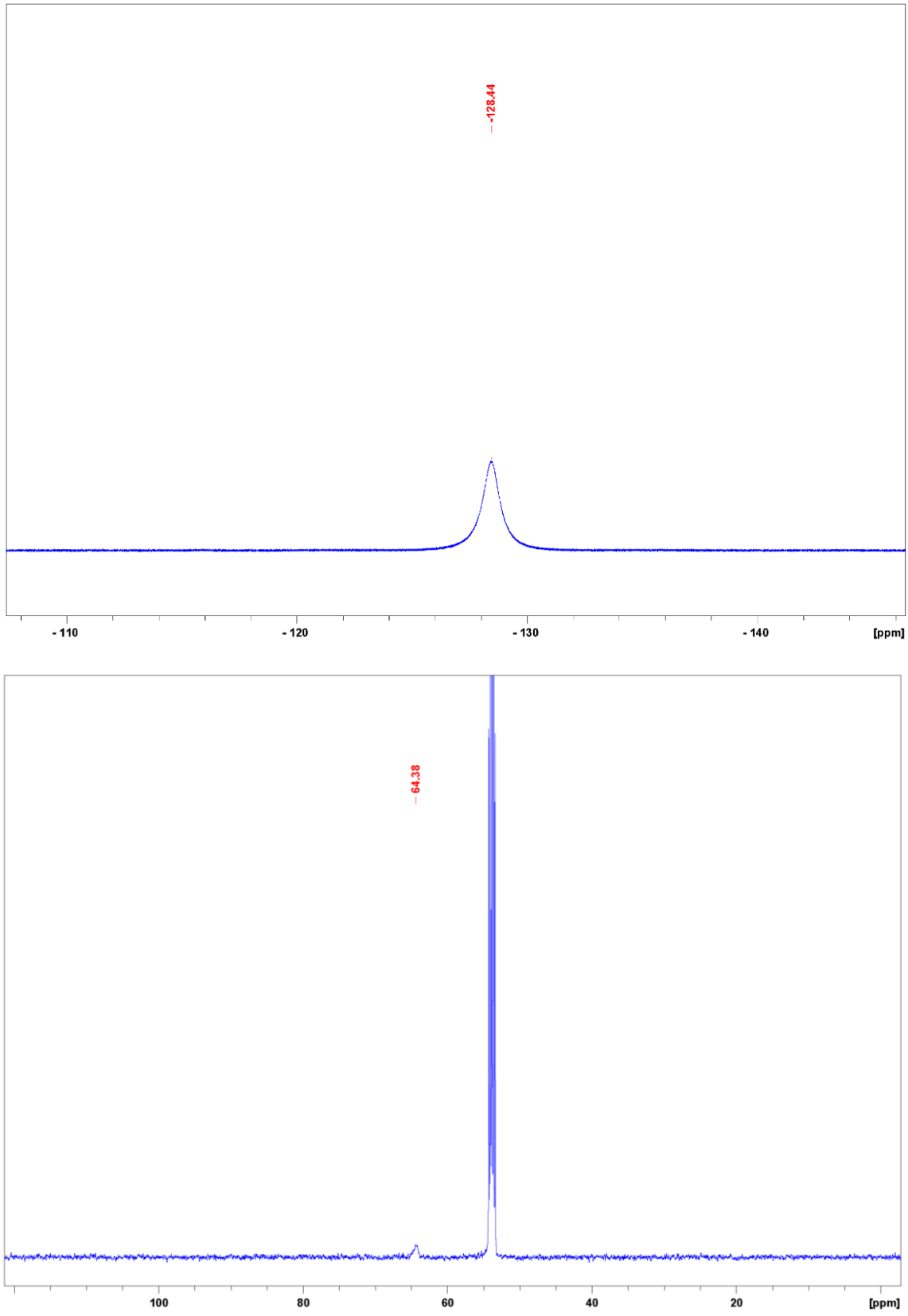

Figure S16. ^{19}F and ^{13}C NMR spectra of $[BiMe_2(SbF_6)]$ (**1**) in CD_2Cl_2.

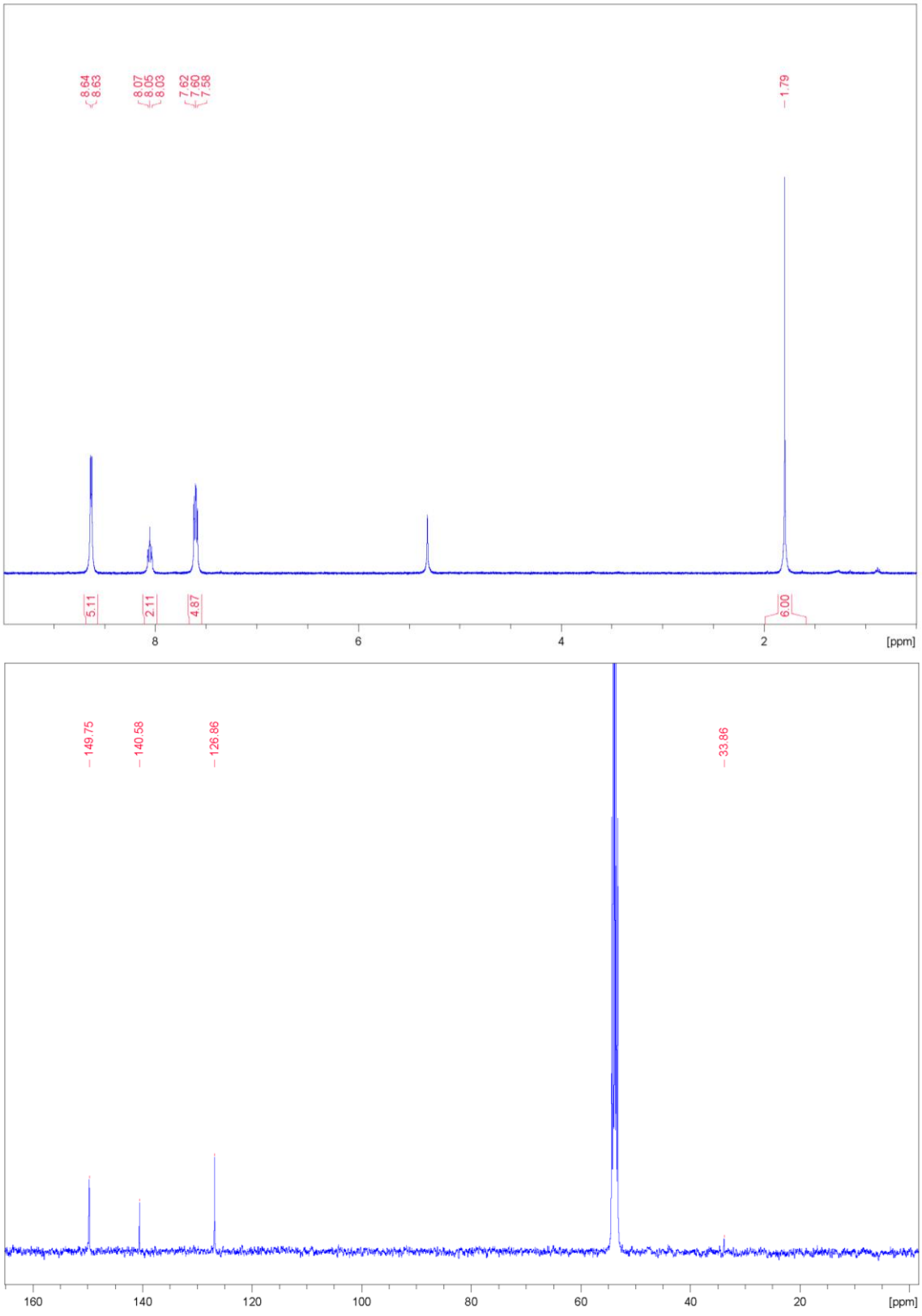

Figure S17. ^{1}H and ^{13}C NMR spectra of $[BiMe_2(py)_2][SbF_6]$ (**2**) in CD_2Cl_2.

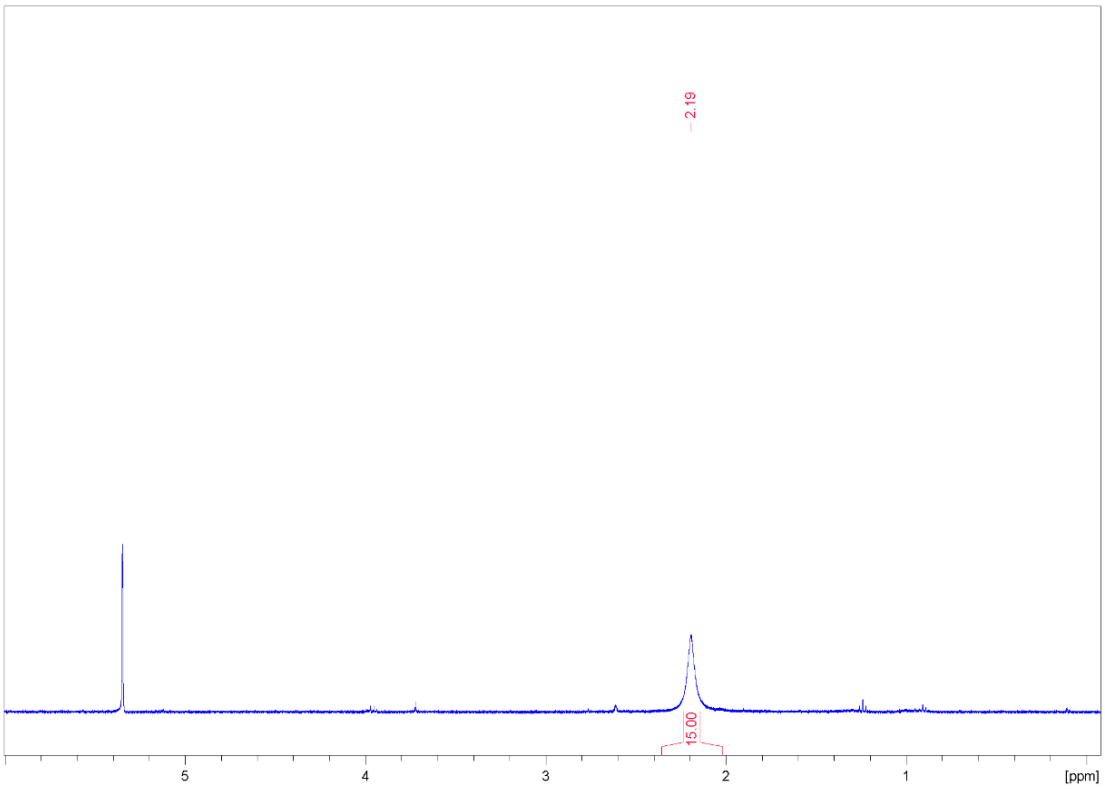

Figure S18. ^{1}H NMR spectrum of $[BiMe_2(BiMe_3)(SbF_6)]$ (**3**) in CD_2Cl_2.

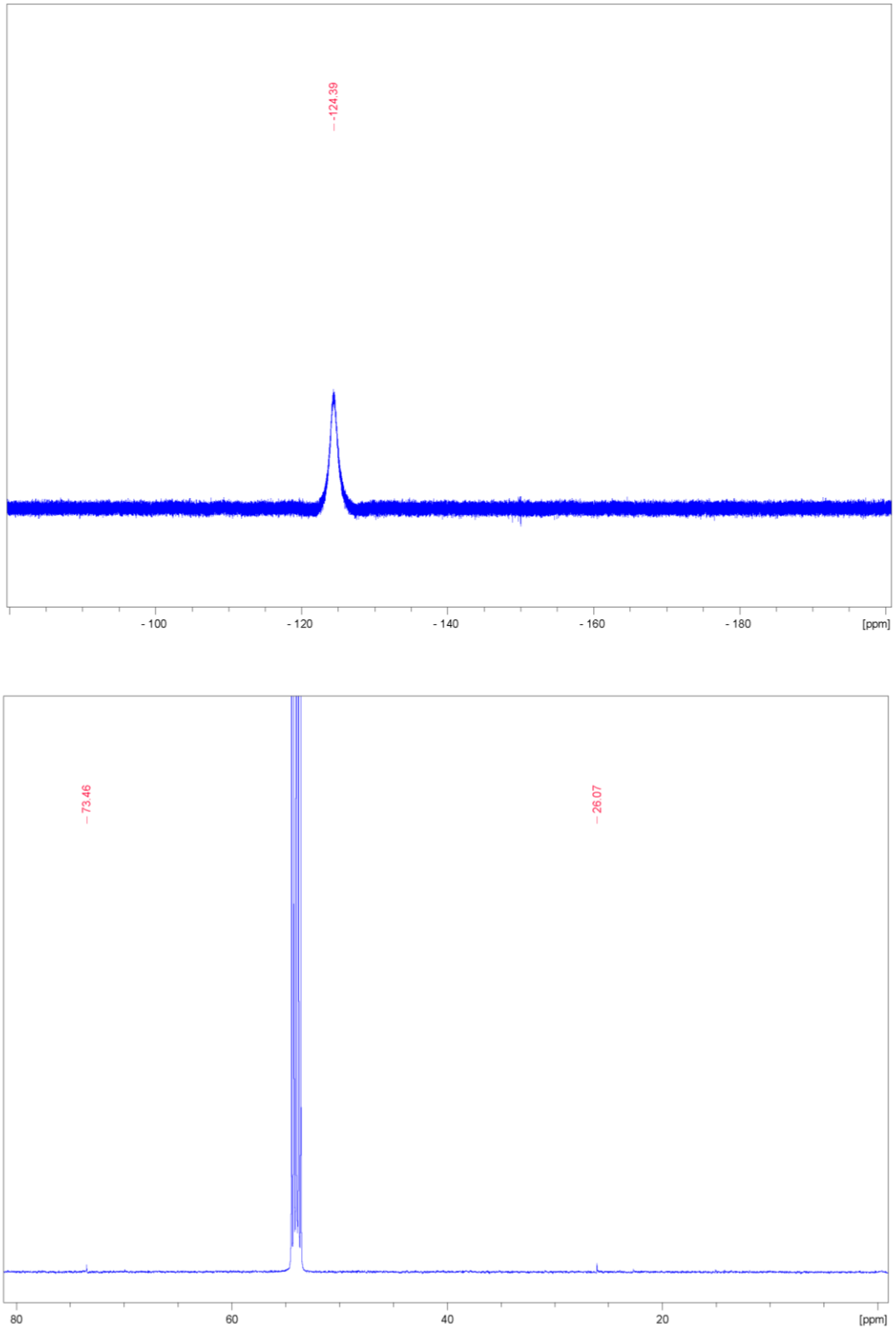

Figure S19. ^{19}F and ^{13}C NMR spectra of $[BiMe_2(BiMe_3)(SbF_6)]$ (**3**) in CD_2Cl_2.

1.6 Chapter X

Supporting Information for chapter X can be found under ttps://doi.org/10.1021/acs.organomet.1c00020.

1.7 Chapter XI

Supporting Information for chapter XI can be found under https://doi.org/10.1039/D0DT01663B.

1.8 Chapter XII

Supporting Information for chapter XII can be found under https://doi.org/10.1039/C9SC00278B.

1.9 Chapter XIII

Supporting Information for chapter XIII can be found under https://doi.org/10.1039/D0SC02410D.